

# Aquaporins - from Ion Channels to Human Cancers

By

SAEED NOURMOHAMMADI



THE UNIVERSITY  
*of* ADELAIDE

The Discipline of Physiology  
Faculty of Health and Medical Sciences  
The University of Adelaide

A thesis submitted in fulfilment for the degree of  
DOCTOR OF PHILOSOPHY

JANUARY 2023

## Abstract

Despite advances in diagnostic techniques and cancer care management, cancer continues to be one of the leading causes of death worldwide. This thesis used two different approaches to advance cancer treatments: i) In the first approach, we used natural compounds as promising sources of new agents for controlling cancer proliferation and metastasis, and ii) second, we developed a mass-throughput technique for exploring the role and significance of aquaporins in cancer development.

In phase 1A (chapter 2), using computational and experimental biology approaches, we identified candidate mechanisms of action of a traditional Chinese medicine, Compound Kushen Injection (CKI), in a breast cancer cell line. CKI disrupts the cell cycle and induces apoptosis in breast cancer cells; however, the exact mechanism of its single compounds and their effects on cancer proliferation, migration and invasion remained unknown. High-performance liquid chromatography (HPLC) fractionation and molecular biology techniques were used to define chemical fractions required for CKI to induce apoptosis. Bioinformatic analysis of RNA-seq data revealed correlations between different compounds and gene expression and phenotype.

In phase 1B (chapter 3), CKI, fractionated mixtures, and isolated components were tested on migration assays with colon (HT-29, SW-480, DLD-1), brain (U87-MG, U251-MG), and breast (MDA-MB-231) cancer cell lines. Human embryonic kidney (HEK-293) and human foreskin fibroblast (HFF) served as non-cancerous controls. Wound closure, transwell invasion, and live cell imaging showed CKI reduced motility in all eight lines. Fractionation and reconstitution of CKI study on cancer cell lines demonstrated that combinations of compounds were required for activity. Live cell imaging confirmed that whole CKI strongly reduced migration of HT-29 and MDA-MB-231 cells, moderately slowed brain cancer cells, and had no effect on HEK-293. CKI uniformly blocked invasiveness through extracellular matrix. Apoptosis was increased by CKI in breast cancer but not in non-cancerous lines. Cell viability was not affected by CKI in all cell lines. Transcriptomic analyses of MDA-MB-231 indicated down-regulation of actin cytoskeletal and focal adhesion genes with CKI, consistent with the observed impairment of cell migration. As a result, we found the pharmacological complexity of CKI is important for effective blockade of cancer proliferation, cell migration and invasion.

In phase 2 (chapter 4-5), our aim was to investigate the primary dogma that aquaporins

(AQP) are only permeable to water and glycerol. Aquaporins are of interest internationally as therapeutic targets for treatment strategies in diverse classes of cancers, but understanding of their full range of substrate permeabilities remains incomplete. Our primary aim was to discover new classes of aquaporins that serve as dual water and ion channels and then provide better insights into the novel function of aquaporins, their mechanism of gating and signaling networks in human-related diseases such as cancer. Using a combination of molecular biology, electrophysiology, and computational biology, we introduced the first unbiased screening method for ion channel activity across all 13 classes of human aquaporins, addressing a major gap in knowledge. Using known AQP ion channel, hAQP1, we optimized an assay which, unlike traditional electrophysiology methods, provides 1- an unbiased high-throughput screen of ion channel functionality of diverse phyla, 2- screening a large number of intracellular signals that might govern their activity and function, 3- mass-screening of drugs, and 4- a broad range of mutagenesis study of AQP ion channels shorter time frame. Strikingly, we found all hAQPs appear to have cation permeability, though to some different degree. Moreover, we noted that ion functionality of hAQPs, unlike most of other ion channels, is active from acidic to neutral pH values ( pH 5.0-7.4).

Finally, following our study in chapter 4, we used a combination of wet and dry lab approaches to investigate the potential significance of hAQPs in cancer development. Using transcriptome analysis, we identified an association between AQP mRNA expression and cancer severity and their translational importance in patient tissue samples. As a result, we found AQP9, -7, -5 and -3 as the most promising prognostic marker among other hAQPs in common cancers. This was followed by unveiling these four AQP ion permeability modulatory mechanism using our optimised yeast screening.

In summary, this work augmented our understanding of the fundamental properties of natural compounds for cancer treatment and introduced a novel approach to dissecting their downstream targets in different hallmarks of cancer. Moreover, we further discovered a new set of AQP ion channels and revealed their potential prognostic values in cancer. Outcomes from this dissertation are likely to serve as a strong foundation for the future basic research and clinical innovation and shed more light on the significance of ion channels in cancer development and paved the way for developing an AQP-based therapy.

**Keywords:** *Systems biology, Natural Compounds, TCM, CKI, Multi-target medicine, Anticancer, Pathway/ network research, Cell Migration, Cell Invasion, Cell cycle, Cancer metabolism, Aquaporin, Ion channels, Yeast, High-throughput screening, Bioinformatics*

## Acknowledgements

First and foremost, I would like to praise and thank God, the almighty, who has granted me countless blessings and strength throughout all the challenging moments of completing this dissertation. I am truly grateful for his unconditional and endless love, mercy and grace.

I am extremely grateful to my esteemed supervisor Prof. Andrea Yool. It truly has been an honour to be her PhD student. Her immense knowledge and enthusiasm for research have been motivational for both my academic research and daily life. I am also grateful for the freedom she has given me to pursue my own ideas and for always believing in me. It meant the world. I have been very fortunate to have Andrea as my supervisor. Without her effort, help and guidance, I would have been nowhere. THANK YOU VERY MUCH, ANDREA!

I also would like to thank my co-supervisor, Prof. David Adelson, for his guidance and expert advice in the bioinformatics section of my PhD study. His valuable suggestions have significantly contributed to the improvement of my PhD work. Dave, Äôs guidance has navigated me between bench research and computer programming. THANK YOU SO MUCH, DAVE!

Thank you to my secondary co-supervisor, a true friend, Dr Sam Henderson. I truly appreciate your support and guidance throughout my candidature. I am so grateful for all the time you contributed to helping me, for advice and support whenever I am in need throughout my PhD. Although more importantly, you made the journey fun. THANK YOU, SAM!

I would also like to thank Dr Sunita Ramesh for the hours she donated to help me with my progress. You are a brilliant and humble scientist; I was very fortunate to know you not as a colleague but also as a kind friend. THANK YOU, SUNITA!

Many thanks to all the past and present members of the Yool group for assisting in every aspect of my PhD, especially: Dr Mohamad Kourghi and Dr Michael Lucio De Ieso, for all the support and for always making me feel welcome at the beginning of my journey at Yool lab. THANK YOU, my friends.

This work would not have been possible without the scholarship from The University of Adelaide. I am very grateful for the Beacon of Enlightenment Ph.D. scholarship, that enabled me to complete my Ph.D. study and assist my future endeavours.

I would especially like to thank my family for all their love and encouragement. To my lovely mum and sister, you gave me the strength I would never have had on my own. My beloved Papa, who is unfortunately not here to see the end of my PhD journey, Papa, I did my best to make you proud. I would not be here if it were not for your encouragement to aim high and never give up! THANKS!

And finally, to my gorgeous, supportive, encouraging, and loving partner, Thazin, whose faithful support throughout all the stages of my journey, particularly during challenging times. I would not be standing here without you! THANKS!

## Declaration

I certify that this work contains no material which has been accepted for the award of any other degree or diploma in my name in any university or other tertiary institution and, to the best of my knowledge and belief, contains no material previously published or written by another person, except where due reference has been made in the text. In addition, I certify that no part of this work will, in the future, be used in a submission in my name for any other degree or diploma in any university or other tertiary institution without the prior approval of the University of Adelaide and where applicable, any partner institution responsible for the joint award of this degree.

I give consent to this copy of my thesis when deposited in the University Library, being made available for loan and photocopying, subject to the provisions of the Copyright Act 1968.

The author acknowledges that copyright of published works contained within this thesis resides with the copyright holder(s) of those works.

I also give permission for the digital version of my thesis to be made available on the web, via the University's digital research repository, the Library Search and also through web search engines, unless permission has been granted by the University to restrict access for a period of time.

SIGNED: ..... DATE: 11/07/2022 .....

## Publications arising from this Thesis

### *First author (published):*

1- Aung TN\*, **Nourmohammadi S\***, Qu Z, Harata-Lee Y, Cui j, Shen H, Zhang J, Yool AJ, Du H, Kortchak DR and Adelson DL. Fractional Deletion of Compound Kushen Injection, A Natural Compound Mixture, Indicates Cytokine Signaling Pathways Are Critical for Its Perturbation of The Cell Cycle. *Scientific Reports-Nature*, 9(1), pp.1-16 (2019). \*Co-first author, (chapter 2).

2- **Nourmohammadi S**, Aung TN, Cui j, Pei JV, Kourghi M, De leso ML, Harata-Lee Y, Qu Z, Adelson DL and Yool AJ. Effect of Compound Kushen Injection, a natural compound mixture, and its identified chemical components on migration and invasion of colon, brain and breast cancer cell lines. *Frontiers in Oncology*, 9, p.314 (2019), (chapter 3).

### *First author (manuscript in preparation):*

3- **Nourmohammadi S**, Ramesh SA, Henderson SW, Muita BK, Yool AJ. Overview of Aquaporins Channel Function and Classification . 2022 (Manuscript format, chapter 1).

4- **Nourmohammadi S**, Henderson SW, Ramesh SA, Yool AJ. The Secret Code Behind the Aquaporin families; Discovery of New Subset of Ion Channels, 2022 (Manuscript format, chapter 4).

5- **Nourmohammadi S**, Aung TN, Henderson SW, Adelson DL, Yool AJ. Investigating the Role of Aquaporin Ion Channels in Cancer; is beneficial or detrimental, that is the question, 2022 (Manuscript format, chapter 5).

### *Co-author (published):*

1- Aung TN, Shafi S, Wilmott JS, **Nourmohammadi S**, Vathiotis I, Gavrielatou N, Fernandez A, Yaghoobi V, Sinnberg T, Amaral T, Khosrotehrani K, Osman I, Acs B, Bai Y, Martinez-Morilla S, Moutafi M, Thompson JF, Scolyer RA, Rimm DL. Objective Assessment of Tumor Infiltrating Lymphocytes as a Prognostic Marker in Melanoma using Machine Learning Algorithms. *eBioMedicine* (2022).



2- Crame E, **Nourmohammadi S**, Wardill HR, Coller JK, Bowen JM. Contribution of TLR4 to Colorectal Tumor Microenvironment, Etiology and Prognosis (*accepted*, Journal of Cancer Research and Clinical Oncology, Submission ID c830cb10-2c64-48c7-bdf8-a2636c233954) (2022).

3- Henderson SW, **Nourmohammadi S**, Ramesh SA, Yool AJ. Aquaporin ion conductance properties defined by membrane environment, protein structure, and cell physiology. Biophysical Reviews, pp.1-18 (2022).

4- Chow PH, Cox CD, Pei JV, Anabaraonye N, **Nourmohammadi S**, Henderson SW, Martinac B, Abdulmalik O, Yool AY. Inhibition of the Aquaporin-1 cation conductance by selected furan compounds reduces red blood cell sickling. Frontiers in Pharmacology, 12 (2022).

5- Chow PH, Kourghi M, Pei JV, **Nourmohammadi S**, Yool AJ. "5-hydroxymethyl-furfural and structurally related compounds block the ion conductance in human aquaporin-1 channels and slow cancer cell migration and invasion. Molecular Pharmacology, 98(1), pp.38-48 (2020).

6- De Ieso ML, Pei JV, **Nourmohammadi S**, Smit E, Chow PH, Kourghi M, Hardingham JE and Yool AJ. Combined pharmacological administration of AQP1 ion channel blocker AqB011 and water channel blocker Bacopaside II amplifies inhibition of colon cancer cell migration. Scientific Reports-Nature, 9(1), pp.1-17 (2019).

7- Pei JV, Heng S, De Ieso ML, Kourghi M, **Nourmohammadi S**, Abell AD, Yool AJ. Development of a photoswitchable lithium-sensitive probe to analyze nonselective cation channel activity in migrating cancer cells. Molecular Pharmacology, 95(5), pp.573-583 (2019).

8- M Kourghi, ML De Ieso, Nourmohammadi S, JV Pei, AJ Yool. Identification of loop D domain amino acids in the human Aquaporin-1 channel involved in activation of the ionic conductance and inhibition by AqB011. Frontiers in chemistry, 6, p.142 (2018).

*PDFs of above publications can be found in Appendix section.*

# Table of Contents

	<b>Page</b>
<b>1 Introduction: Overview of aquaporin (AQP) channel function and classifications</b>	<b>1</b>
<b>2 Fractional deletion of Compound Kushen Injection, a natural compound mixture, indicates cytokine signaling pathways are critical for its perturbation of the cell cycle</b>	<b>56</b>
<b>3 Effect of Compound Kushen Injection, a Natural Compound Mixture, and its identified Chemical Components on Migration and Invasion of Colon, Brain, and Breast Cancer Cell Lines</b>	<b>74</b>
<b>4 The Secret Code Behind the Aquaporin Families; Discovery of New Subset of Ion Channels</b>	<b>90</b>
<b>5 Investigating the Role of Aquaporin Ion Channels in Cancer; is Beneficial or Detrimental, that is the Question.</b>	<b>135</b>
<b>6 General discussion and future directions</b>	<b>180</b>
<b>A Co-author Publications as PDFs Arising from This Thesis</b>	<b>190</b>

# Chapter 1

## Introduction: Overview of aquaporin (AQP) channel function and classifications

The work of this dissertation is two-fold. First, I have implemented a yeast screening method through which I explore the selective permeability of ion and water via aquaporin channels. I have also applied cellular bioassays to complement the screening assays. For the second part of the dissertation, I have performed transcriptome analysis of several human cancers to study the prognostic importance of aquaporin channels and disease severity in incremental stages. This chapter provides an overview of aquaporins as dual water and gated ion channels with complex mechanisms of regulation and diverse repertoires of substrate permeabilities with their translational relevance in the context of cancer. This chapter is in the format of the manuscript that was submitted to *Journal Name* as a review article.



Name of Co-Author	Mr. Biko Kahare Muita		
Contribution to the Paper	Wrote the manuscript.		
Signature		Date	8 Jul 2022

Name of Co-Author	Professor Andrea J. Yool		
Contribution to the Paper	Formulation of primary draft, provided crucial feedback and edited the manuscript.		
Signature		Date	8 Jul 2022

# Overview of aquaporins (AQP) channels: from classifications to regulation and function

**Nourmohammadi S**<sup>1</sup>, Ramesh SA<sup>2</sup>, Henderson SW<sup>1</sup>, Muita BK<sup>3</sup>, Yool AJ<sup>1</sup>.

1- School of Biomedicine, University of Adelaide, Adelaide, SA 5005, Australia

2- College of Science and Engineering, Flinders University, Bedford Park, SA 5042, Australia

3- Department of Molecular and Biomedical Science, School of Biological Sciences, University of Adelaide, Adelaide, South Australia 5005 Australia

## 1- Aquaporins are multifunctional channels, found across different phyla

### 1.1 Conserved features of the Aquaporin superfamily

About 50-65% of body mass is water and maintaining water balance is essential for all living creatures. The existence of water pores was first proposed in 1896 by Overton who observed that hydrophilic solutes showed an inverse relationship between movement across cell membrane and their molecular size, suggesting the possibility of lipid and aqueous pore-like combination on the cell membrane (1). In 1956-7, Stein and Danielli (3), in parallel with Sidel and Solomon (4), further elaborated on the concept of "aqueous pores" with the proposal that the movement of water and other ions could be due to the presence of hydrophilic pores.

It was not until the mid-1980s when the first aquaporin channel, isolated from calf and rat lenses, was sequenced and structurally analyzed by Gorin and colleagues, and named the major intrinsic polypeptide (MIP) (5). They speculated that the primary function of MIP in lens might be as a gap junction polypeptide.

In 1986 Benga and colleagues identified a protein proposed to mediate the rapid water movement across human red blood cell membranes (6). Agre and colleagues subsequently cloned the channel and confirmed water permeability using the *Xenopus laevis* oocyte expression system. This water channel initially known as CHIP28 and later renamed aquaporin-1 (AQP1) (7). With advances in sequencing technology, genome and transcriptome sequencing approaches have uncovered a vast array of orthologous channels across diverse kingdoms.

AQPs across phyla show homology in the primary amino acid sequences and the presence of two signature sequence motifs: i) asparagine-proline-alanine (NPA) motifs in both loops B and E which form the water pores (8); and ii) a major selectivity filter, usually consisting of aromatic residues and an arginine (ar/R), at which the molecular selectivity of permeant

substrates is controlled (9). AQPs assemble primarily as homotetramers, or occasionally as heterotetramers (10-12). Each monomer (~30 kDa) is composed of six bilayer-spanning  $\alpha$ -helical domains and intracellular amino and carboxyl termini (13). Two folded loops (B and E) that meet within the transmembrane region of each monomer create the intrasubunit pore, well characterised in the bidirectional, single-file transport of water (14) (Figure 1). The monomer is thought to have evolved from an internal gene duplication of a three transmembrane domain and inversion of the internal repeat resulting in the mature protein (15). These four monomers assemble as a right-handed bundle surrounding a central pore which has been shown to have ion conductivity in some aquaporins such as AQP1 (16).

Cytosolic and extracellular loops have been associated with gating mechanisms, subcellular trafficking, and sites of post-translational modification including glycosylation (17, 18), phosphorylation (19, 20) and pH-sensitivity (21-23).

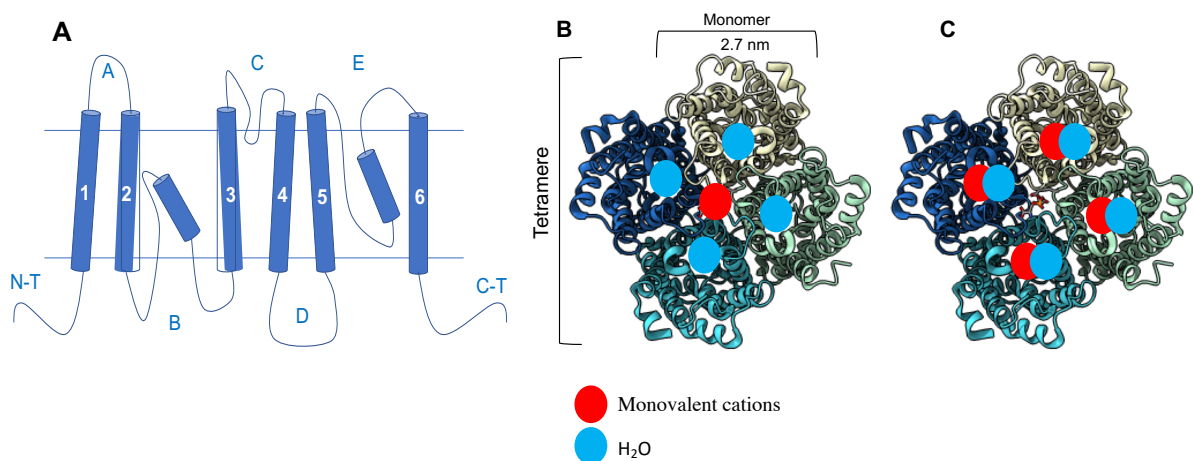


**Figure 1: Diagram illustrating the structure of AQP1, adapted from Yool and Campbell (2012).** A) Transmembrane topology of the AQP1 monomer, with six transmembrane domains (labelled 1 to 6) and 5 loops labelled A to E. Two folded loops (B and E) that meet within the transmembrane region of each monomer create the water pore. N-T = Amino terminus, C-T = Carboxyl terminus. (B) Representation of an archetypal AQP homotetramer (hAQP1) from the top view depicting the pathways for water conductivity (blue circles) and ion conductivity (red circles). These pathways are predicted to be shared with AtPIP2;1 from plants (24). (C) Depiction of the putative pathways for water and ion conductivity in mammalian AQPs 6 (23) and 0 (25).

## 1.2 AQP channel classes across phyla

### 1.2.1 Comparison of AQPs in vertebrates and invertebrates

Although the structural architecture shared between AQPs from different forms of life is the same, there are some unique structural features in the amino, carboxyl-termini and loops, suggesting different roles in modulatory and gating of these protein channels (26, 27). Traditional classifications of AQPs that have been founded on solute permeability require reconsideration as the number of AQP classes found to be permeable to multiple solutes is growing (28).

Based on sequence similarities, 17 aquaporin isoform genes have been classified in vertebrates (AQP0-AQP16) with higher mammals express AQP0-12. Based on both sequences and functions, AQPs are divided into three categories: classical or orthodox aquaporins (AQP0, 1, 2, 4, 5, 6 and 14; aquaglyceroporins (AQP3, 7, 9, 10 and 13); and unorthodox or supraaquaporins (AQP11 and 12) with about 20% of amino acid sequence homology to others. The aqua-ammoniaporin-like (AQP8) is often placed in the classical AQP category (29-33).

Whole-genome duplication events through vertebrate evolution have added to the diversity of AQP classes (34). For instance, while human AQP3 and 7 isoforms have been speculated to be produced by local gene duplication as they are located on the same chromosome, AQP10 has been lost (30) or turned to a pseudogene in other vertebrates (35). Among all living organisms, the most diverse AQP gene families are found in plants and fish with up to 70 and at least 40 paralogs in upland cotton and Atlantic salmon respectively (36).

### 1.2.2 Plants

Planta show the broadest range of aquaporin channel types, divided into seven categories (37, 38). The classes of plasma membrane intrinsic proteins (PIPs), tonoplast intrinsic proteins (TIPs), and nodulin26-like intrinsic proteins (NIPs), have been well studied (39-42). Two other groups, the small basic intrinsic proteins (SIPs) (43) and the uncategorized (X) intrinsic proteins (XIPs) (44), have been discovered more recently. The last two groups, GLpF-like intrinsic proteins (GIPs) and Hybrid intrinsic proteins (HIPs), are only found in non-vascular plants (mosses) (45). NIPs and GIPs are capable of transporting polyols such as glycerol in plants, and are thought to have evolved from horizontal gene transfer of bacterial aqpN



channels. PIPs, XIPs and SIPs are speculated to be derived from unicellular eukaryotes and vertically transferred to plants and green algae. On the other hand, TIPs and HIPs are thought to have evolved from ancient ancestors of Embryophyta, which encodes all seven subfamilies (45).

### 1.2.3 Insects

Insect AQPs have been divided into three subfamilies: water selective, glycerol-permeable and cation permeable (46, 47). However phylogenetic analyses of predicted insect AQPs suggest the presence of six major subfamilies; big brain proteins (BIB) permeable to cations; *Drosophila* intrinsic protein (DRIP) which is water-specific; aquaglyceroporin which mediates water and glycerol; *Pyrocoelia rufa* integral proteins (PRIP) which channel water and urea; entomoglyceroporin (EgIp) which is glycerol permeable; and unorthodox aquaporin (AQP12L) whose function remains to be defined (48). It has been suggested that insect AQPs may play a role in anhydrobiosis and cryoprotection while DRIP and PRIP are involved in maintaining water hemostasis in high-volume liquid diets (49). While all subfamilies of AQPs express in early arthropods, higher insects such as winged insects, lack AQP. The loss of AQPs in advanced insects probably is due to the gain of glycerol and urea permeability by classical AQPs called entomoglyceroporin (EgIp) (48).

### 1.2.4 Prokaryotic and archaea

Prokaryotes (eubacteria, archaea, and fungi) have been assumed to encode one class of each AQP (29). However, using a different phylogenetic analysis, Finn and colleagues proposed that prokaryotic AQPs can be separated into four groups (AqpZ, AqpN, AqpM, and GlpF) (30). While some bacteria such as *E.coli* express one aquaporin and one aquaglyceroporin (AQPZ and GlpF) other strains encode multiple AQPs (33). In some cases, especially high temperature growing eukaryotes such as thermophilic archaea (*Methanothermobacter marburgensis* aquaporin, MmAqpM), relatively low number of AQPs has been reported, perhaps reflecting independent options for water permeation directly through the plasma membrane at high temperatures (50).

### 1.2.5 Unicellular eukaryotic and protozoa

Eukaryotes appear to need high numbers of water and solute transporters due to their more complex metabolic activity as compared to ancestral eubacteria and archaea. AQP occurrence in protozoa ranges from no AQPs in *Cryptosporidium parvum*, to only one AQP in *Plasmodium falciparum*, to four AQP in *Trypanosoma cruzi*. The number of AQP classes could reflect the need to adapt to environmental stresses such as nutrient shortage or exposure to toxins, in addition to basic water transport (51, 52).

### 1.2.6 Fungal

Fungi consist of both uni- and multicellular organisms that carry genes for both aquaporin and aquaglyceroporin. Some fungi only encode one AQP (*S. pombe*), while others (*Trichoderma harzianum*) express up to eight AQPs (33). Baker's yeast, *Saccharomyces cerevisiae*, has two AQPs that appear to be involved in spore formation and cell wall hydrophobicity (53), and two glycerol permeable AQPs mainly involved in osmoregulation in response to environmental stress, during the mating process (54), and in protection from toxic compounds such as metalloids (55).

## 1.3 Solute permeabilities and regulation

Phylogenetic studies suggest the early gene duplication event that launched the separation of AQP channels into water and glycerol transporters occurred during the evolution of Prokaryota (56). In fact, the view that aquaporins are only permeable to water and glycerol has been changing due to the growing array of techniques and expanding knowledge of aquaporin functions (see Figure 2). A study combining high-resolution crystallography and molecular dynamic simulation suggested hydrogen bond interactions between water molecules and the ar/R selectivity filter and the NPA motifs prevented protons or ions from passing through the monomeric pores (57); the arrangement of residues in the ar/R filter has been associated with the functional properties of the channels (58-60). For instance, the selectivity filter in human classical AQPs displays a narrowed limiting pore size, about 1.5 Angstroms (Å), to that seen in AGQPs (Verma et al., 2015), consistent with the exclusion of glycerol from passage through the monomeric pores of orthodox AQPs (Ho et al., 2009).

Modulation mechanisms of these channels can depend on microenvironmental pH or ion concentration, post-translational modifications, and mechanical stress that alter the channel conformation and modulate the heights of electrochemical barriers (28, 61, 62).

Properties of aquaporins are commonly investigated using heterologous expression of the channels in *Xenopus* oocytes, cell lines, yeast, bacterial cells, or liposomes with purified reconstituted aquaporins (62). Nearly all aquaporins have been shown to be permeable to water, while many are emerging as more complex multifunctional channels (Figure 2 and Supplementary S1).

One of the novel substrates for transport by eukaryotic AQPs that is gaining attention is hydrogen peroxide ( $H_2O_2$ ), which mediates cell signaling and responses to oxidative stress (63). Vertebrate and plant AQPs have been proposed to transport gases such as  $NH_3$  (64, 65),  $CO_2$  (66) and  $O_2$  (66), and others,, although their physiological significance has been considered controversial.

The AQP ion conductance capability has been one of the most hotly debated features of these channels. Nevertheless, several studies have shown that a subset of these channels are permeable to ions (28, 62). The list of additional AQP ion channels is likely to be expanded.

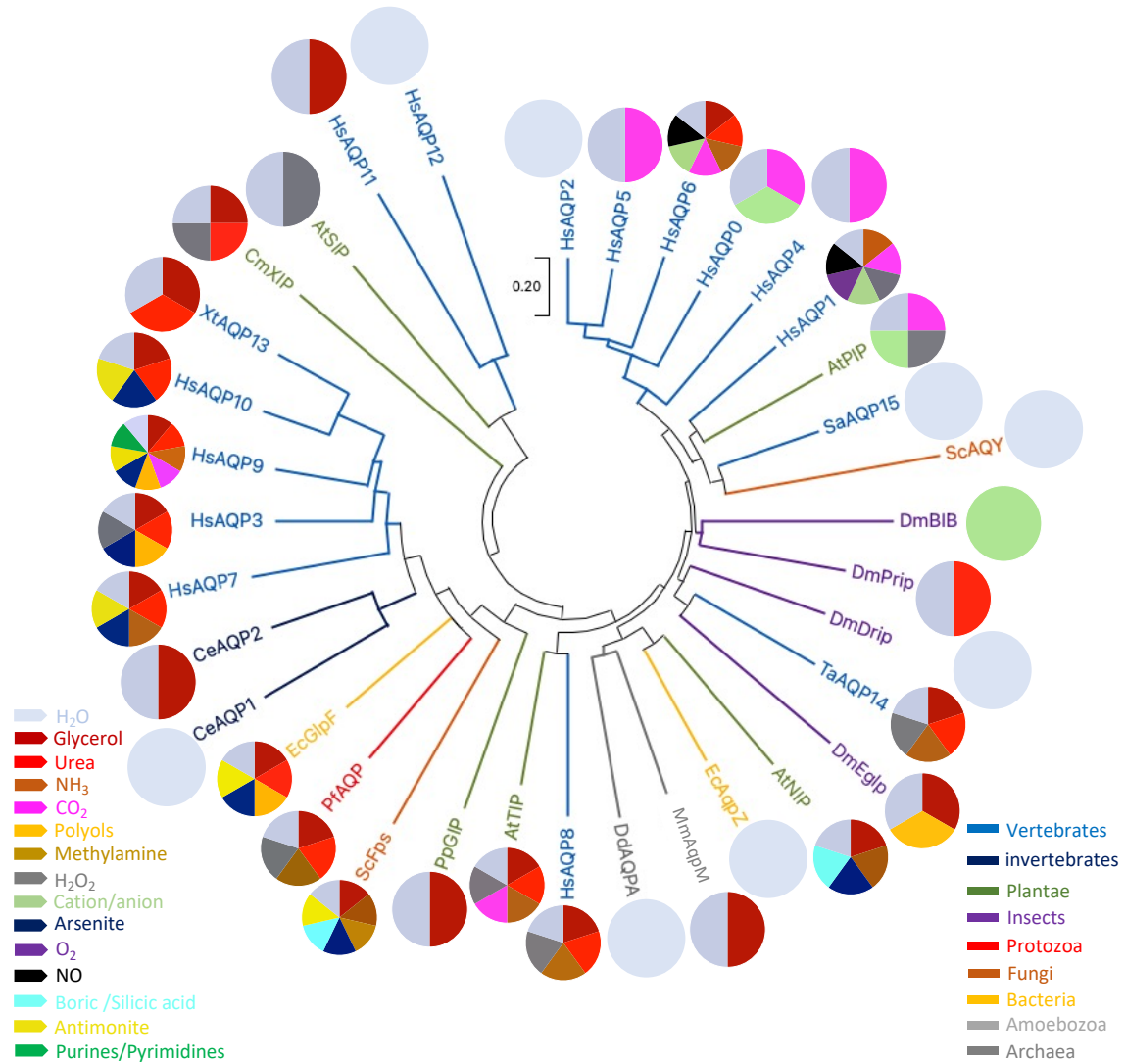


**Figure 2: phylogenetic tree of AQPs across different phyla and summary of their permeability to solutes.** Phylogenetic tree illustrating the level of sequence similarities across phyla, and a summary of solute permeabilities of aquaporins across different phyla. The sequencing alignment and phylogenetic tree was generated using MEGA v11 software (see Supplementary S1 for more details).

#### 1.4 Physiological Functions of AQPs

AQPs found in nearly all tissues are involved in the basic functions of most organs. This is especially true in the renal system; in human kidneys AQP2 is the main target of action for antidiuretic hormone (AVP) (67). AVP drives the recruitment of AQP2 to the plasma membrane from subapical intracellular vesicles to increase water permeability in the collecting duct. AQP4 is also found in the kidney and is regulated by phosphorylation by phosphokinase C to reduce water permeability. In *Drosophila melanogaster*, the aquaporins Drip and Prip are

expressed in the malphigian tubules (functionally analogous to mammalian kidneys); altering the expression of AQPs directly affected organ functionality (68). The renal system primarily leverages the water channel functionality of AQPs; however, the additional ion channel function contributed by renal AQPs such as AQP1 in proximal tubule might also exhibit utility in regulating rates of Na<sup>+</sup> and water uptake from the urine.

In the human brain, AQP1, AQP4, and AQP9 are expressed in different cell types. AQP1 in normal conditions is exclusively expressed in the choroid plexuses (69) with a major role in CSF secretion. AQP1 also is atypically expressed in reactive glia in response to brain injury (70). AQP4 and AQP9 are both expressed in astrocytes (71). AQP4 is the most extensively studied brain AQP and plays a protective role by facilitating perisynaptic fluid clearance after intense neuronal stimulation (72, 73). AQP9 is weakly expressed and its function is yet to be resolved however it is thought to be involved in energy metabolism (74). Despite knowledge gaps regarding the full range of AQP involvement in the nervous system, they are of interest as potential targets for therapeutics for conditions such as brain tumours, epilepsy, stroke and neuroinflammation (75).

AQPs in the lungs (AQP1-4) are believed to be important for lung water clearance at birth and maintenance of airway liquid composition (76). In the eye, AQP0, AQP1, AQP3, AQP4 and AQP5 are believed to be involved in intraocular pressure regulation, lens and corneal transparency, and corneal and conjunctival barrier functions (77). In the digestive system, at least six aquaporin isoforms, i.e., AQP1, AQP3, AQP4, AQP5, AQP8, and AQP9, have been reported to be expressed in the digestive system for fluid transfer in the digestive tract.

AQPs play pivotal roles in a broad range of fundamental physiological processes; thus, their dysfunction due to mutations or impaired regulation is a leading area of research on understanding underlying mechanisms for numerous pathophysiological problems (27, 78, 79). There is now compelling evidence that aquaporins herald as a new class of attractive targets for drug discovery in both non-infectious and Infectious diseases (80).

## 2- Strategies for assessing novel AQP functions

### 2.1 Overview of mass-throughput screening tools

Assessment of AQP water channel activity using *Xenopus laevis* oocytes as a heterologous expression system was first demonstrated by Preston and colleagues who observed volume changes in response to an osmotic gradient for oocytes expressing AQP1 (7). Swelling of oocytes due to aquaporin-mediated water influx is relatively simple to measure using

videography; in contrast, oocytes have been more challenging for screening of novel functions such as ion conductance, modulation by signaling networks, or defining AQP-selective pharmacological tools, given the technical and labour-intensive methods required. Oocytes have been used for single-channel patch clamp analyses of AQP ion channel activity, as demonstrated by Anthony and colleagues (81). Parallel automated recording arrays for oocyte and single cell electrophysiology offer a method for upscaling throughput rates, but the cost can be prohibitive. Comparison of common methods to study ion channels summarized in Table 1.

Since ion channels have relevance to a broad range of diseases, identifying agonists and antagonists to modulate ion channels also has been a great area of interest to academic and industrial researchers, a goal that would benefit from HTS methods (82-84) that incorporate good understanding of both the biology of the channels of interest and the theoretical basis of methodologies. Assays that mimic natural membrane environments of channels would be expected to provide better insight into gating mechanisms and pharmacology. Automated electrophysiology, fluorescent probes, and plate readers provide options; nonetheless, caveats are that most assays don't combine features of mass-throughput and high sensitivity with a low cost.

**Table 1: Comparison of different methods used for ion channel screening.**

Protocol	Cost	Information content	Ease of operation	High throughput
Yeast Growth	+	+	+++	+++
LFA	+	++	+++	++
Auto EP	+++	+++	+	+
Membrane Potential	++	+	++	+
Ligand binding	+	+	+++	+
MDS	+	++	++	+++

+++, High; ++, Medium; +, Low. LFA (Liposome Flux Assay), EP (Electrophysiology), MDS (Molecular Dynamics Simulation), Table modified from (85).

## 2.2 Yeast based studies of established ion channels

Over the past two decades, genetic methods and heterologous expression systems such as yeast or bacteria have been powerful approaches for the biological investigation of exogenous ion channels (86-89). Yeast as a heterologous system to study ion channels was developed by Gaber and colleagues (90, 91). In 1992, two plant channels, AtKAT1 and AtAKT1, (92, 93) were characterised using a yeast uptake-deficient strain; subsequent characterisation of a mammalian ion channel (94) used the same approach.

Yeast and bacteria have developed unique transport systems that harvest or exclude sodium (95, 96), allowing adaptive responses to a range of environmental stresses. Deletion of these genes creates an impaired phenotype that can be tested for rescue by introduced genes for channels or transporters of interest. For instance, deletion or inactivation of  $K^+$  uptake genes in *S. cerevisiae*  $\Delta trk1\Delta trk2$  (93) and *E. coli* TK2420 (97), yielded strains that survive only when supplemented with high  $K^+$  concentrations, unless introduced exogenous genes are able to provide a substitute pathway for  $K^+$  entry into the yeast cells and complement the genetic deficit (98) (see Figure 3 for more details on ion channels express in yeast). This method offers an efficient system for probing functions of ion-conducting channels. While there are many advantages of using a high-throughput expression system for ion channels and aquaporins, It is also important to consider that heterologous expression of genes in yeast or bacteria also has several shortcomings (details discussed in chapter

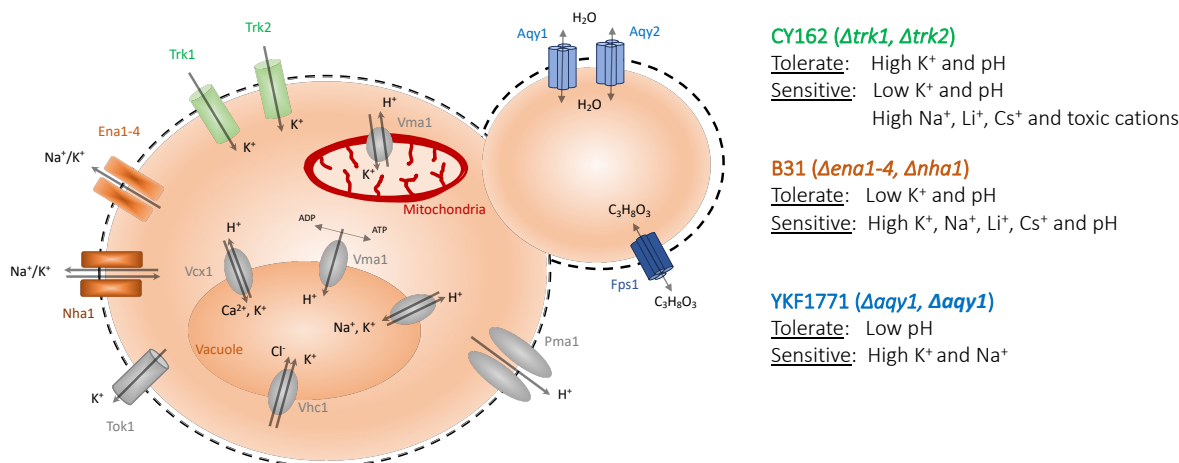


**Figure 3:** A summary of the major contributors to ion channels in *Saccharomyces cerevisiae* and mutant strains lacking  $K^+$ ,  $Na^+$  or water channels used in this thesis. Modified from (87, 99)

### 2.3 Computational modelling for novel channel discovery

Computational biophysics take advantage of multidisciplinary fields from physics and computer sciences to chemistry and biology to investigate the physical principles underlying biomolecular systems. Molecular Dynamics (MD) is a computational tool that uses the principal regime of physics to predict the motion of every atom in molecular systems.

The journey of Molecular Dynamic (MD) simulation initiated back in 1957 when a group of theoretical physicists, Alder and Wainwright, proposed a method in which the atoms interacted only through perfect collisions (100). Later in the late 1960s, as computer science became more widespread, MD simulations were developed for more biological complex systems and the groundwork by Levitt (101) and Warshel (102) that enabled these simulations were later awarded Nobel Prize in Chemistry, 2013. The first atomistic MD simulation of a protein containing 58 amino acids was performed in the late 1970s (103).

Since then, MD simulations have been used to investigate a variety of protein channels questions that maybe slow or difficult to be answered by experiments, including conformational flexibility and stability, mutational study, drug screening, protein-protein interaction, pH, voltage and mechanical simulation and the effect of microenvironmental changes on protein channel modulation and gating mechanisms, for more details see (104).

The impact of MD simulation in membrane biology has expanded exponentially, mainly because of two key developments. First, due to recent breakthroughs in crystallography (awarded Nobel prizes in 2003 and 2012), and cryo-EM (awarded a Noble prize in 2017), numerous high resolution protein channel structures are now available. This has dramatically expanded membrane biology studies which relied, for many decades, predominantly on experimental functional characterization of these channels (104). Second, the development of graphics processing units (GPUs) enabled MD and its software packages to be conducted locally at a lower cost than the supercomputers in the past (105, 106). For more details on some of the most common software packages that perform MD computations, see (107-109) and methodologies, see (110, 111). K. R. Wilson and his group were the first to use MD simulation of an ion channel system in early 1980 (112). However, they could not observe conduction events directly due to the short timescale.

Having increased computer power in recent years, attention has moved to fully unbiased exploration of ion motion in a broader time scale (113) from microsecond scale (114) to millisecond scales (115). In 1998, using experimental structural biology techniques, R. MacKinnon and his group provided the first glimpse of an ion channel molecular architecture, KcsA, pivotal for structural modelling studies. Because of the fast motion of water and ions ( $10^9$  waters and  $10^8$  ions per second), Aquaporins (AQPs) and ion channels have become an ideal candidates for *in silico* studies (116).

Structures of various states of many (~50) aquaporins have been determined by X-ray diffraction and cryo-electron microscopy, which provide invaluable insights into atomistic molecular architecture in aquaporins. However, one major concern with protein structures



obtained from these kinds of studies is that they may not represent the physiological structure due to the effect of various experimental conditions from low temperature and radiation damage (used in Cryo-EM) to reagent and atom staining (used in X-ray) (117, 118).

Shortcomings of current experimental methods at the 3D modelling study of AQPs in the molecular level could be addressed by MD simulation by providing comprehensive progression into the physio-chemical mechanisms and time evolution of the AQP gating mechanisms at atomic resolution. Solving the structural architecture of AQP1 (57, 119) and bacterial aquaglyceroporin (GlpF) (120) allowed full permeation events analysis of AQPs at atomistic real-time MD simulations (121). Since then, MD simulations of aquaporins have been providing precious visions into other potential features of AQPs such as selectivity (60), kinetics and channel permeabilities (122), proton exclusion (123), gating mechanisms (61, 124), conduction of various gas species and signalling molecules (125, 126), mutational study (127), post-translational modification (128) and drug screening (129) and even voltage-dependence of these channels (130, 131) and many more. We will not discuss them all but shall rather focus on the future potential role of MD simulation studies for discovering novel functions of these channels that have been remained relatively poorly explored compared to properties mentioned above.

The possibility of coupling between water and ion transport by some ion channels (e.g, K<sup>+</sup> channels, KcsA) (132) and their general structural similarity with AQPs (16) did raise the speculation of a possible ancestral evolution of these channels and potential dual water and ion channels functionality for aquaporins (28, 133).

The first AQP, hAQP1, confirmed to be permeable to ions by MD simulation study was conducted by Tajkhorshid, Yool and colleagues (134) which suggested a potential contribution of MD for the structure-function investigation of the ion transport features of AQPs. With hAQP4 simulated electroporation by MD, M. Brandi and colleagues suggested the possibility of sodium and chloride transport via its monomeric and central pores (135). More crystal structures of AQPs in various states could facilitate utilizing computational techniques to simulate the physiological behaviour, particularly the permeation of ions and the possibility of coupled water and ion transport, via these channels. However, the challenge in studying ion motion is to create even more accurate and realistic MD models that capture ion-ion or ion-ligands interaction energies. We must consider the possibility of artifacts and misinterpretation from MD studies when assigning AQPs as ion channels, but, the impact on the field could be profound.

There are only a few examples of AQP ion channels, with some remaining speculative (28), requiring further validation. Improved computer simulations could broaden our understanding of conformational details of all relevant pathways and states in AQP ion channels. Atomistic MD simulations have the potential to support future AQP ion channel discovery by improving the length of simulation time scales and enhancing realistic physiological assemblies of proteins and lipids (136), identifying candidates to be validated experimentally.

Lipid and protein interactions impact protein functions (137, 138), and modelling these levels of complexity would deliver deeper insights into the dynamic function of aquaporins in natural environments and responses to microenvironmental changes (139, 140). Simulations could inform new drug discovery of modulators, from synthetic (141-143) or natural product compounds (144), which could prove useful in slowing AQP-facilitated cancer progression and other disease processes.

Experimental methods in combination with MD simulations represent a synergistic opportunity to study AQP ion channels and their physiological roles. As molecular simulations become faster, less expensive and more accessible, we should expect more candidate AQP ion channels to be identified.

## 2.5 Classes of known AQP ion channels

Aquaporins have been thought to function primarily as a water channel and aquaglyceroporins are known to transport water, glycerol and small solute across the cell membrane in all kingdoms of life (145). To date, mammalian AQPs 0, 1, 6, 8, 9, *Drosophila* Big Brain (BIB), some isoforms of plants PIPs, TIPs and soybean nodulin 26 have been shown to have ion channel activity (81, 146-149). More classes are likely to be discovered. AQP1 and AtPIP2;1 channels are predicted to conduct ions via the central pore of the tetramer while AQP0, 6 and BIB is permeable to ions through individual monomer pores (Figure 1 B and C).

### 2.5.1 AQP0

Gorin and colleagues were the first to clone bovine lens cell membrane major intrinsic protein (MIP), later called AQP0, though the protein's function was unclear (5). Later in 1991, Pisano and colleagues isolated the human AQP0 gene and reported on its genomic structure (150). Lens-specific AQP0 is the most abundant protein of lens junctions, and has been shown to conduct ions when reconstituted in bilayers (146, 151). However, Kushmerick and colleagues have reported the lack of ion conductivity of AQP0 when expressed in the *Xenopus* oocyte

expression system (152). In black lipid membranes, the ion channel activity of AQP0 was found to be voltage- and pH-sensitive, activated at acidic pH and closed at neutral pH (153). Volume regulation is one of the suggested roles for AQP0 in lens, where the accumulation of extracellular fluid is reduced by transporting the water into fiber cells in order to reduce light scattering by minimizing the extracellular space and maintain optimal transparency (25). AQP0 dual water and ion function could be involved in the optimization of lens transparency.

### 2.5.2 AQP1

Mammalian AQP1 ion channel activity has been well investigated in terms of physiological significance and structural and functional properties (154). Primarily, AQP1 was recognized as a channel that permeates only water; however, Yool and colleagues later revealed that it also carries ions through the membrane (133) and that the AQP1 ion channel does transport monovalent cations such as  $\text{Na}^+$  and  $\text{K}^+$  but not anions or divalent cations  $\text{Ca}^{2+}$  and  $\text{Mg}^{2+}$  (133). In *Xenopus* oocytes, electrophysiological studies have shown that AQP1 functions as a cyclic nucleotide-gated cation channel with a unitary conductance of about 150 picosiemens (pS) when activated by cGMP (81, 133, 155). Upon cGMP activation, the cytoplasmic Loop D undergoes a conformational change, that leads to the opening of the ion pore (134). Hence, the cGMP-induced conformational change is suggested to be the gating mechanisms of the AQP1 central ion pore (134). The function of AQP1 as a cGMP gated ion channel has been supported by subsequent experiments that employed electrophysiological techniques (156-158). The structure of AQP1 with the central ion pore in its tetramer structure has been well discussed (134). Further, Campbell and colleagues showed that substituting the amino acid alanine into the hydrophobic barrier residues allows the transport of a monovalent cation, tetraethylammonium, through the ion central pore (159). This further confirms the capability of dual water and ion transport by the AQP1 channel.

### 2.5.3 AQP6

The mechanism of action of a mammalian dual water and anionic channel AQP6 differs from many other types of AQP channels. The channel was rather activated than blocked by the treatment of mercuric chloride ( $\text{HgCl}_2$ ) (148). This was demonstrated in *Xenopus* oocytes where the introduction of up to 300  $\mu\text{mol/l}$  of  $\text{HgCl}_2$  to AQP6 increased the water conductivity five-fold, and the ion conductivity six-fold (160). Using site-directed mutagenesis, cysteine residues, C155 and C190, were identified as the sites of activation of AQP6 by  $\text{HgCl}_2$  (148,

161). Research showed the similar structural and dual ion and water function activity between AQP1- and AQP6 in *Xenopus laevis* oocytes indicating many classes of AQP channels could have common functional activities (159). High AQP6 expression was also shown in some ovarian cancers (162) but the contribution of AQP6 dual functionality has yet to be fully illuminated. Due to its significant activation to exposure to HgCl<sub>2</sub>, the physiological relevance of AQP6 merits further investigation in AQP6-related diseases such as cancer (see chapter 5).

#### 2.5.4 hAQPs permeable to ammonium cation

Using the oocyte expression system, Holm et al. 2005, investigated the permeability of mammalian AQP1, -3, -8, -9 and plant TaTIP2;1 to ammonia (NH<sub>3</sub>) and ammonium (NH<sub>4</sub><sup>+</sup>). The inward current carried by ammonium (NH<sub>4</sub><sup>+</sup>) was evident in oocytes expressing AQP3, -8, -9, and TIP2;1, but not AQP1. Interestingly, a positive association of NH<sub>4</sub><sup>+</sup> conductance and lowering pH was observed at bath pH of 6.5 which was progressively abolished at pH <7.4. As a result, they suggested that AQP3, -8, -9 and TIP2;1 could be ammonium permeable (163). Their prior work in a yeast strain deficient in ammonia transport suggested the potential permeability of hAQP8 and TaTIP2;1 to ammonia and possibly ammonium (164). Comparing the diameter of ar/R constriction domain between AQP8, TIP2;1 and AQP1 revealed histidine-180 is replaced to phenylalanine results in narrower diameter in AQP1 ar/R constriction. This explained why AQP1 showed no permeability to NH<sub>4</sub><sup>+</sup> (a bulky cation compared to Na<sup>+</sup> and K<sup>+</sup>) in the previous study by Holm et al., 2005. Mutagenesis study of AQP1 suggested ar/R constriction filter is playing role for ammonium cation permeability in AQPs (9).

In our study (see chapter 3 and 4), using both the yeast and oocyte expression systems, we showed a possibility of Na<sup>+</sup> and K<sup>+</sup> permeability of other AQPs which can be stimulated by pH and voltage. In agreement with the above studies, we speculated that ar/R region could be one of the potential regions that can contribute towards AQP ion permeability in response to pH and voltage. The potential K<sup>+</sup>/Na<sup>+</sup> permeability observed for all AQPs in our study could be via ar/R conformational changes associated under pH and/or cell membrane hyperpolarization/depolarization changes which in turn may lead to either widening the central pore (i.e., responsible for AQP1 ion permeability) or ar/R diameter and facilitate the passing of cations through the monomeric pores.

### 2.5.5 AQP9

A study by Yuliya and colleagues in 2012, showed AQP9  $-/-$  mouse erythrocyte had significant lower cation conductance when compared with wild type mouse erythrocyte. Using whole-cell patch-clamp on mouse erythrocyte, they found the cation conductance was induced by oxidative stress (165). This result was indeed very interesting for us, as our optimized yeast screening model revealed PfAQP as a potential non-selective cation channel (data not shown).

### 2.5.6 PIP subfamilies

AtPIP2;1 is one of thirteen plasma membrane intrinsic proteins (PIP) in *Arabidopsis* (41). AtPIP2;1 is highly expressed in roots and stomata, which supports a major function of AtPIP2;1 to maintain water homeostasis during transpiration (166). AtPIP2;1 ion conductivity was first demonstrated using two-electrode voltage clamping of *Xenopus* oocytes that expressed the protein (149). The cation conductance, which was mainly attributed to  $\text{Na}^+$ , was sensitive to divalent cations,  $\text{Ca}^{2+}$  and  $\text{Cd}^{2+}$ , and low pH with an  $\text{IC}_{50}$  of 6.8 (149). A G103W mutation in the AtPIP2;1 water pore impaired both the ion permeability and water transport of the channel and co-expression of AtPIP2;1 with AtPIP2;2, which is 93% identical to AtPIP2;1, or AtPIP1;2, enhanced water permeability but completely abolished the ion conductivity (149). This suggested that ion currents observed in AtPIP2;1-expressing oocytes was not an indirect effect of endogenous oocyte channels in response to swelling. These results together provide evidence that AtPIP2;1 is yet another example of dual water and ion conducting aquaporins. The AtPIP2;1 ion conductance and modulatory mechanisms yet to be fully explored. One possible signalling cascade to be explored is phosphorylation state that has been recently suggested by Qiu et al, (167).

Two other closely related isoforms of the AtPIP2;1 (AtPIP2;2 and HvPIP2;8) displayed cation permeability when expressed in *Xenopus laevis* oocytes (168, 169).

Compared to AtPIP2;1, the cation conductance of AtPIP2;2 showed less sensitivity for  $\text{Ca}^{2+}$ . Our prior study showed higher sensitivity of AtPIP2;1 compared to AtPIP2;2 cation conductance for  $\text{Ca}^{2+}$ . We further indicated the voltage-dependent block of both channels ion conductance by different divalent cations (169).

A survey of screening of the barley PIP1 and PIP2 subtypes in *Xenopus* oocytes, Tran and colleagues found barley HvPIP2;8 as the only subclass permeable to monovalent cations (168). Similar to *Arabidopsis thaliana* PIPs the ion current was inhibited by divalent cations.

However, compared to AtPIP2;1, barely PIP2;8 showed opposite selectivity preference for Na<sup>+</sup> and K<sup>+</sup> (167).

### 2.5.7 TIPs subfamilies

Some TIP subfamilies serve as NH<sub>4</sub><sup>+</sup> when expressed in *Xenopus laevis* oocytes. AtTIP2;1 and wheat homolog TaTIP2;1 displayed inward ion currents when NH<sub>4</sub><sup>+</sup> was present in the external saline (163). It was suggested that NH<sub>3</sub>-gated NH<sub>4</sub><sup>+</sup> conductance by initially binding to intersubunit pore in which proton associated with NH<sub>3</sub> follows as NH<sub>4</sub><sup>+</sup> form (28).

### 2.5.8 Drosophila Big Brain

Drosophila BIB protein, a member of the aquaporin channel family, was shown to transport monovalent cations but not water, and was shown to be modulated by endogenous tyrosine kinase signalling pathways when expressed in *Xenopus* oocytes. This activation was impaired in the presence of insulin and reversibly activated with lavendustin A, a known tyrosine kinase inhibitor (47). Divalent cations Ca<sup>2+</sup> and Ba<sup>2+</sup>, were shown to block the BIB channel, and a highly conserved glutamate residue in the first transmembrane domain was demonstrated as a binding site for divalent cations (170). Unraveling the role of BIB ion channel activity in early development of *Drosophila* neurogenesis would help to gain better insight into the functional relevance of ion conductance (171).

### 2.5.9 Soybean nodulin 26

Nod26 is the major membrane aquaporin superfamily protein component in root nodules in which nitrogen-fixing bacteroids are enclosed. Although only water and glycerol transport of nod26 was previously recognised, the selective ion permeability of Nod26 channels was then discovered and reported by Weaver and colleagues in 1994. The group showed both cations and anions permeate nod26, with anions selectively being weak (147). Phosphorylation at position ser-262 in Nod26 by calmodulin-like domain protein kinase amplified the voltage-dependent gating activity of nod26 (172). Ion transporting ability of nod26 was further confirmed by Hwang and colleagues demonstrating the flow of NH<sub>3</sub> out of the symbiosome (64) indicating the ion conductance activity of the AQP channel

Phylogenetic tree (Figure 4) and Clustal alignment (Figure 5) depicting the level similarities between known aquaporin ion channel proteins from different phyla versus previously uncharacterized hAQP ion channels (AQP3, 5, 7, 9 and 12s). Human aquaporin 0, 1, 3, 5, 6, 7, 9, 12A and 12B, rat AQP8, *Oryza sativa Japonica* PIP1;1, *Arabidopsis thaliana* PIP2;1 and PIP2;2, *Hordeum vulgare* PIP2;8, *Triticum aestivum* TIP2;1, *Glycine max* NOD26 and *Drosophila melanogaster* BIB were used for sequencing alignment (accession number Supplementary S2). Residues with at least 70% similarity are highlighted.

In AtPIP2;1 (RDSHVPVL at loop D) which is conserved for some of other PIP2s isoforms (highlighted in the alignment as a green box) shown to be a cytosolic pH-sensor for water transport regulation (173). Potential residues for binding of direct cGMP or phosphorylation induced ion permeability by PKG pathway in AQP5, 6 and 9 also suggested based on our yeast screening work, chapter 3. (red box, loop D). Our results (chapter 5, Figure 7-8) from hAQP3, 5, 7 and -9 treated with PK stimuli, suggested PKC and G as a potential modulator of hAQP ion functionality.

Therefore, using NetPhos website (<https://services.healthtech.dtu.dk/service.php?NetPhos-3.1>), we predicted PKC phosphorylation/binding site for AQP9; (S11 at N-terminal, and T33 at domain 1), for AQP3; (T242 at C-terminal) and AQP7 (S10 at N-terminal, and S216 at end of domain 5 facing toward loop E and T299 at C-terminal); as potential for future mutagenesis study (highlighted as a yellow box). Predicted PKG phosphorylation/binding site for AQP9 (R164 at loop D, and AQP5 (R153 at loop D); highlighted in red.

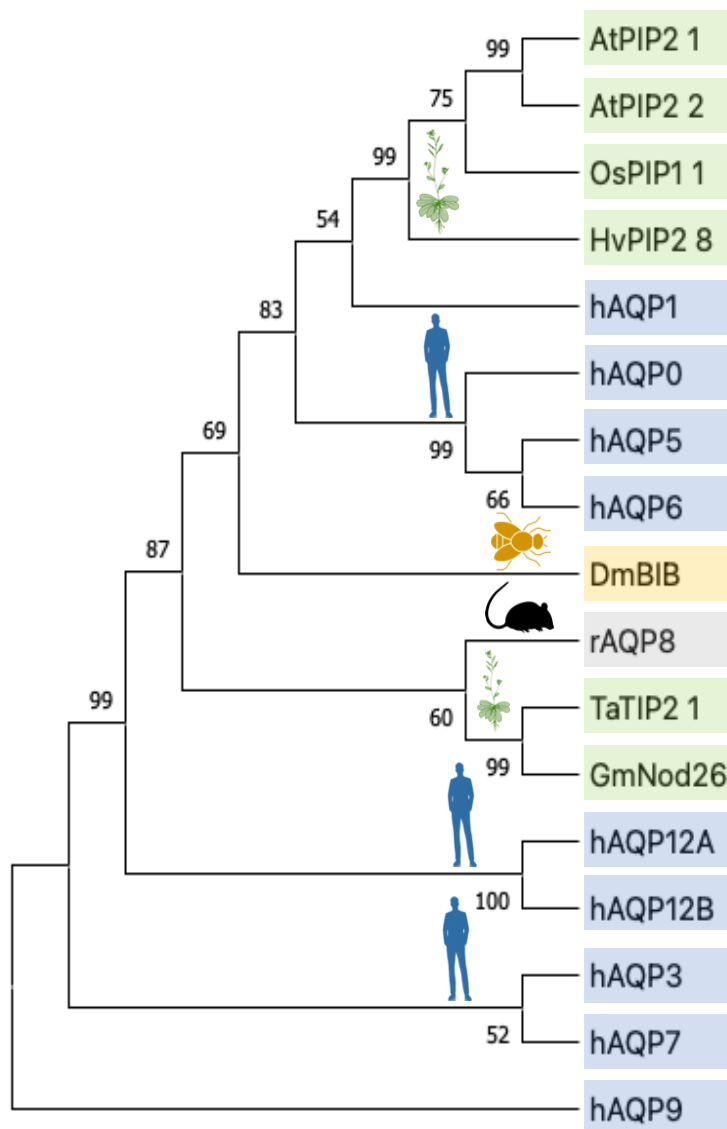


**Figure 4: Phylogenetic tree depicting the level similarities between known aquaporin ion channel proteins from different phyla versus previously uncharacterized hAQP ion channels (AQP3, 5, 7, 9 and 12s).**

Phylogenetic analysis and sequencing alignment depicting the level of sequence similarities (+70% similarities regions where highlighted) of AQP ion channels across different phyla. Protein sequences were compared (some of the newly found hAQP ion channels, hAQP3, 5, 7, 9 and 12s included). The evolutionary history was inferred using unweighted

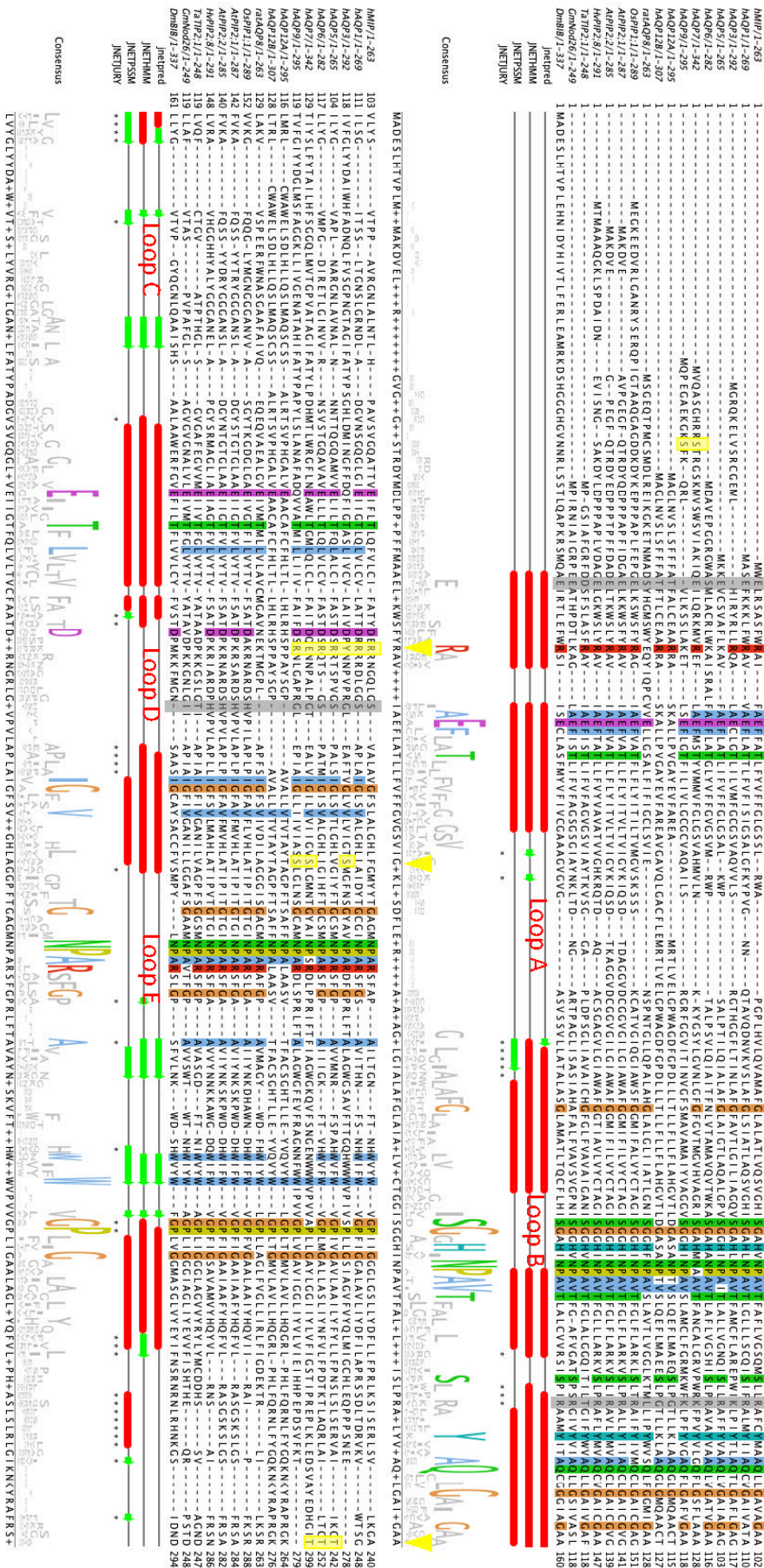
pair group method with arithmetic mean (UPGMA) method in MEGA11. The bootstrap consensus tree concluded from 10,000 replicate. The percentage of the associated taxa are shown next to the branches. The evolutionary distances were computed using the Poisson correction method. The analysis involved 17 amino acid sequences. Estimated transmembrane domains, loops are shown under the sequencing alignments. Level of conservation of amino acids in the sequences illustrated under the transmembrane and loop domains. The C-terminal of BIB AQP containing extra amino acids were eliminated. Potential residues involved in AQP ion functionality were highlighted in yellow at loop D, E and N- or C-terminus.



**Figure 5: Clustal alignment comparison between unknow AQP ion channels and some novel hAQP ion channels.**

### 3- AQP pharmacology

Aquaporins are expressed in diverse tissues and cell types and have crucial roles in various physiological processes such as renal water absorption (174, 175), cell motility, production of cerebral spinal fluid (157, 176, 177), skin hydration (178) and fat metabolism (179, 180). The functional role of aquaporins in pathophysiology has been widely studied in transgenic mice lacking these proteins. Aquaporins have been shown to have a role in pathologies such as congenital bilateral cataracts (181), diabetes insipidus



(182, 183), oedema (184, 185) and cancers where in their expression may correlate with overall survival (75, 143, 186-188).

Numerous pharmacological modulators of aquaporins (AQPs 1,2, 3 and 4) have been identified that act on the water transport through the monomeric pores in aquaporins. Some of these modulators include tetraethylammonium – TEA<sup>+</sup> (189-191), bumetanide and its derivatives (192, 193), arylsulfonamide derivatives (142), methylurea compounds (194), inorganic metal compounds (195-197) and natural extracts such bacopsides (198). Modulators such as TEA, some bumetanide derivatives (AqB013) and arylsulfonamide derivatives (142) were shown to inhibit water channel activity of aquaporins such as AQP1 and AQP4.

Tetraethylammonium (concentrations ranging from 100  $\mu$ M to 10 mM) reduces water permeability of different aquaporins (AQP1, 2 and 4) expressed in *Xenopus* oocytes and is thought to act by binding to a tyrosine residue on the extracellular side of transmembrane helix (189, 199). However, studies by another group in erythrocytes that natively express AQP1, and epithelial cells stably transfected with AQP1 failed to confirm TEA<sup>+</sup> mediated inhibition at concentrations of up to 100  $\mu$ M (200). Discrepancy in results was attributed to expression in oocytes leading to non-specific effects such as block of K<sup>+</sup> channels leading to basal volume change and/or lower density of protein expression in the plasma membrane rendering the cells more sensitive to low affinity inhibitors in the micro or millimolar range.

Arylsulfonamide derivative acetazolamide at a concentration of 10  $\mu$ M inhibited water transport from oocytes expressing AQP1 (201) and HEK293 cells expressing AQP1 (202). However, this compound did not inhibit endogenous AQPs in human cells (203). Several anti-epileptic drugs and arylsulfonamides were reported to inhibit water transport activity in AQP4 expressing *Xenopus* oocytes with IC<sub>50</sub> <1  $\mu$ M (142). Interestingly in follow up studies using stopped-flow water permeability assays, Yang et al., (2008) reported a lack of water transport inhibition by arylsulfonamide derivatives in AQP4 stably expressed in Fisher rat thyroid epithelial (FRT) cells at concentrations up to 100  $\mu$ M (204). The authors attributed the *Xenopus* oocyte system as probably unsuitable for such characterisation as change in oocyte volume (sampled every minute) after exposure to hypotonic solution depended on factors such as volume regulatory mechanisms, proteins expressed, unstirred layers and viability.

Inorganic metals such nickel chloride (hAQP3 in bronchial epithelial cells, 1 mM) (205), copper sulphate (hAQP3 in Swan 71 cells, 100  $\mu$ M) (206), silver nitrate (hAQP3 in erythrocytes, 10  $\mu$ M) (207), mercury chloride (hAQP1 in *Xenopus* oocytes – 1mM) (208, 209) inhibit water channel activity at varying concentrations. AuPhen a gold containing compound

inhibits water channel activity of hAQP3 in erythrocytes (50  $\mu\text{M}$ ) and hAQP7 in adipocytes (15  $\mu\text{M}$ ) (210, 211).

Furosemide, a loop diuretic medication used to treat fluid build-up due to heart failure inhibits hAQP1 at 10  $\mu\text{M}$  in *Xenopus* oocytes while bumetanide used to reduce excess fluid build-up or oedema in the body has been shown to inhibit rat AQP4 expressed in *Xenopus* oocytes at a concentration of 100  $\mu\text{M}$  (212). Bumetanide derivative analog AqB013 inhibited rAQP4 and hAQP1 when expressed in *Xenopus* oocytes ( $\text{IC}_{50} \sim 20 \mu\text{M}$ ) (192). The efficacy of the block was enhanced when a valine (189) residue was mutated to alanine in AQP4 confirming that inhibition was specific to the aquaporin.

Many small molecules such as Phloretin, DFP00173 and Z433927330 have been shown to inhibit aquaglyceroporins AQP3, 7 and 9 when the aquaporins were expressed in either *Xenopus* oocytes (213), proteoliposomes (214), CHO cell lines (194) with  $\text{IC}_{50}$  ranging from  $\sim 0.2 \mu\text{M}$  to 1.1  $\mu\text{M}$ .

In addition, those described above, studies have screened libraries of diverse drugs in primary astrocytes, cells expressing AQP4 (215); AQP1-expressing CHO cells (216) and AQP1-expressing *S. cerevisiae* cells (217) to identify compounds that modulate AQP water channel function. Study by Mola et al., (2009) identified 4 compounds that modulated both AQP4 and AQP1 activity with  $\text{EC}_{50}$  values ranging from 20  $\mu\text{M}$  to 50  $\mu\text{M}$  (215). Two classes of compounds from sulfonamides and dihydrobenzofurans were found to inhibit AQP1 mediated water channel activity (216). Freeze-thaw method used by To et al., (2015) for preliminary screening followed by validation of the selected compounds by surface plasmon resonance analysis and in rat erythrocytes led to identification of 2 compounds that inhibited water transport activity with  $\text{EC}_{50}$  ranging between 20  $\mu\text{M}$  to 48  $\mu\text{M}$  (217).

Interestingly in another study conducted by Esteva-Font et al., (2016), small molecule modulators of water transport via AQPs reported in various studies (192, 193, 203, 215-217) were tested in different cellular systems and compared against  $\text{HgCl}_2$  (218). None of the 13 compounds tested (well above reported  $\text{IC}_{50}$  values – 50  $\mu\text{M}$ ) were observed to significantly effect water transport in rat and human erythrocytes, haemoglobin free ghost membranes and in haemoglobin release assays when compared to the inhibition observed with  $\text{HgCl}_2$  (218). The study concluded that any apparent small inhibition of water transport observed in their study was likely an artifact due to the tested compounds causing erythrocyte crenation and aggregation and none of the previously reported small molecule modulators of AQP water transport inhibit water channel activity significantly.

In summary these findings suggest that studies conducted in different expression systems may lead to varied results and are likely to be confounded by either the sensitivity of the assays carried out in these systems, or the fact that a subset of the AQPs transport solutes, small molecules, and ions in addition to water. These transport capabilities of AQPs might result in changed membrane permeability leading to conflicting results in different expression systems and assays.

### 3.2 Limited array of pharmacological agents for AQP ion channels

The discovery that hAQP1 has the capacity to transport both water and cations (81, 133) caused a paradigm shift in the functional role of aquaporins and their importance in physiological processes. Since then, a subset of AQPs (human AQPs 0, 1 and 6, BIB, plant aquaporins AtPIP2;1, AtPIP2;2 and Nod26) have been shown to have ion channel activity along with facilitating water movement (47, 81, 147, 149, 160, 219). It has been suggested that in hAQP1 and AtPIP2;1, water moves along the individual monomeric pores (13, 220) while ions move through the central pore created by assembly of 4 subunits as tetramers in the plasma membrane (16, 134, 149). In BIB, hAQP0 and hAQP6, ion and water permeation are thought to occur through the individual monomeric pores (23, 171, 221). Though the initial discovery of ion channel function of aquaporins was disputed (154), given the importance of aquaporins in various physiological processes and increasing evidence of their roles in diverse pathophysiological processes, this concept is gaining acceptance.

Current research indicates that ion channel activity of aquaporins may play a key role in physiological processes in mammals such as cerebrospinal fluid production (222, 223), maintaining optimal lens transparency (hAQP0) (25) and possible roles in acid-base regulation (hAQP6) (162, 224, 225) and in plants regulating Na<sup>+</sup> entry into cells when exposed to salinity (AtPIP2;1) (149). The ion channel activity of AQPs has been shown to have important function in diseases such as cancer metastasis (hAQP1, hAQP5, hAQP3) (226-228) and brain oedema (hAQP4) resulting from gliomas or traumatic injuries (229).

Despite this emerging evidence, there are very few modulators or inhibitors of AQP ion channel activity currently known. Derivatives of Bumetanide AqB007 and AqB011 are inhibitors of hAQP1 ion channel activity with an IC<sub>50</sub> of 170 μM and 14 μM respectively (230) and have no effect on osmotic water permeability. Compound isolated from medicinal plant *Bacopa monnieri* bacopaside I blocked both water (IC<sub>50</sub> 117 μM) and ion channel activity (IC<sub>50</sub> 18 μM)

in AQP1 expressing colon cancer cell line HT29 and impaired migration (198). Recently, 5-Hydroxymethyl-2-furfural (5HMF), a natural component of honeys and two structurally related compounds 5-nitro-2-furoic acid (5NFA) and 5-acetoxymethyl-2-furaldehyde were shown to effectively inhibit AQP1 mediated ion currents in *Xenopus* oocytes with  $IC_{50}$  ranging from 0.43 mM to 3 mM (141). All the three compounds impaired cell motility and migration in high AQP1 expressing colon cancer cell line (HT29) and breast cancer cell line (MDA) with minimal cytotoxicity. Apart from the mentioned compounds, no other inhibitors have been identified that effectively block AQP mediated ion channel activity.

### 3.3 Roles of AQP channels in cancer progression (candidate therapeutic targets)

Cancer remains one of the leading causes of death worldwide, with numbers expected to increase unless effective treatments are identified that can limit or cure the disease and improve prognosis and survival. Along with other ion channels, AQPs have been implicated in cancer cell invasion and metastasis. The expression AQP1 is highly upregulated in gliomas (231), glioblastoma (232, 233) carcinomas of mammary glands (232), colorectal and lungs and even in multiple myeloma (234).

AQP1 is expressed in brain microvessel endothelium in contrast to normal brain where there is little or no expression of AQP1 (235), however the signals that induce change in expression are unknown. It has been suggested that AQP1 expression is upregulated in response to hypoxia in the tumour cells and facilitates endothelial cell migration and angiogenesis (236), crucial to supply of nutrients, energy for growth and excretion of waste (237). AQP1 knockdown in chick embryo and AQP1 deficient mice resulted in reduced angiogenesis and tumour growth (238, 239). Angiogenesis is a key factor in tumour growth stimulated by vascular endothelial growth factor (VEGF) in response to hypoxia (240). In endometrial adenocarcinoma, a positive correlation was observed between AQP1 expression, VEGF and intratumoral microvascular density (241). Knockdown of AQP1 expression combined with VEGF inhibition led to additive inhibition of hypoxia induced angiogenesis in human retinal vascular endothelial cells (242). However, AQP1 expression wasn't altered when VEGF neutralising antibodies were applied to these lines. Further, in primary breast tumours, there were no differences in the VEGF levels between wild type mice and AQP1 null mice (218) suggesting that VEGF maybe regulated independently of AQP1 expression. The AQP1 gene expression is induced under hypoxic conditions in the tumours by other factors such as hypoxia-inducible factor (HIF-1 $\alpha$ ) (243) and

the AQP1 promoter has a binding site for HIF<sub>1</sub> $\alpha$  which drives AQP1 expression in cultured human retinal vascular endothelial cells (244). Thus, it is evident that the expression of AQP1 is upregulated by hypoxia in tumour cells and may lead to endothelial cell migration and angiogenesis. Pharmacological agents that impair increased AQP1 expression and activity have the potential to impede angiogenesis crucial for tumour cell survival.

Epithelial-mesenchymal transition (EMT) in which the epithelial cells lose polarity, cell-cell adhesion, gain migratory and invasive capabilities and show downregulation of epithelial cadherin is a hallmark of cancer (245-249). The EMT transition in the cells is induced in response to signals from tumour-associated stroma and growth factors such as the epidermal growth factor (EGF), hepatocyte derived growth factor (HGF) and transforming growth factor beta (TGF- $\beta$ ) (250-253). These factors in turn induce other transcription factors that repress transcription of E-cadherin (254, 255). Different AQPs have been implicated in EMT process. Expression of AQP3 is upregulated in colorectal, pancreatic, and gastric cancers (256-258) and has been shown to aid in increased cell migration and invasion. In gastric cancer, cells with high levels of AQP3 expression had higher levels of mesenchymal phenotype markers such as vimentin and fibronectin compared to AQP3 deficient cells (228). Conversely in cells with higher expression of AQP3, E-cadherin levels were lower. The mechanisms that govern AQP3 mediated cell migration in pancreatic and colorectal cancer cells are yet unknown.

In lung adenocarcinoma, AQP1 overexpression correlated with increased migration, invasion and downregulation of E-cadherin that enables tight adhesions between epithelial cells and links to cytoskeleton (259). The role of AQP4 in cell migration and metastases is not yet clear as knock down of AQP4 expression in breast cancer cells resulted in increased expression of E-cadherin and  $\beta$ -catenin and knockdown in glioma cells increased expression of connexin-43 (260, 261). Interestingly, in primary astrocytes the knockdown of AQP4 resulted in down regulation of connexin-43 and increased adhesion in glioma cells transfected with wild type AQP4 (262, 263). The expression of AQP5 in non-small lung carcinomas is associated with increased invasion, and overexpression leads to reduction in epithelial cell markers such as E-cadherin,  $\alpha$  and  $\gamma$ -catenin and increased expression of EMT markers such as vimentin and fibronectin (264). In hepatocellular carcinoma, expression of AQP9 is down regulated and increased expression is associated with reduced tumour growth due to cell cycle arrest at G1 phase and increased apoptosis and decreased EMT, leading to reduced invasion and metastasis (265). Most studies investigating the role of AQPs in disease and pathology compare the expression levels in normal vs cancerous tissues and effect of knockdown or mutations in

residues affecting key pathways. Emerging evidence suggests that expression levels of different AQPs may have unique effects in influencing the progression of different cancers and influence various processes and signalling pathways depending on the type of cancer.

### **Cell motility**

In normal healthy individuals, cell migration is common during development but decreases at later stages, but in pathological conditions such as cancers cell migration is activated leading to invasion and metastasis. Numerous AQPs are emerging as players that contribute to migration and metastasis in numerous cancers. AQPs 1, 4, 5 and 9 have been shown to have polarised localisation at the leading edges of migrating cells co-localising with numerous ion transporters facilitating the exchange of  $\text{Na}^+$ ,  $\text{H}^+$ ,  $\text{Cl}^-$  and  $\text{K}^+$  (266-271). Migration of cells is complex involving processes such as formation of protrusions (272) into the extracellular matrix (ECM), cytoskeleton interactions such as actin polymerisation and depolymerisation (273-275) and increased expression of matrix metalloproteinases (MMP9, MMP2) to degrade ECM (276-278) to make space for migrating cells and cell adhesion (279).

The AQP permeability to water, solutes and other ions and expression of a subset of these proteins (AQP1, 4, 5 and 9) at the leading edges of migrating cells indicates that they are well positioned to facilitate changes in shape, size and cell volume enabling migration and invasion in cancer cells. At the leading edges of migrating cells, high AQP1 expression enables rapid protrusion formation, cytoskeletal modifications, cell volume and shape changes that allow tumour cells to migrate and invade rapidly (280, 281). In melanoma cells (B16F10) and mammary gland tumours cells (4T1) AQP1 was observed to increase cell migration and lamellipodial width (282) while in melanoma and endothelial cell lines, AQP1 knockdown was observed to impede cytoskeleton reorganisation via interaction with Lin-7/ $\beta$  catenin (283). In HT20 colon cancer cells knockdown of AQP1 led to re-localisation of actin in migrating cells suggesting that AQP1 acts as a scaffolding protein (284). Further, permeability to ions in addition to water is suggested to be important for migration in colon cancer cells (230). Interestingly, high AQP1 expression has been correlated with low cell migration in cholangiocarcinoma while downregulation of expression is associated with mucin production and aggressive invasion of cells (285, 286).

Expression of AQP3 increases invasion and metastases in colorectal carcinoma cells via modulation of epidermal growth factor (257, 258) and is differentially expressed along with

AQP1 and AQP8 in cervical carcinoma impacting tumour progression in a study conducted in Uygur women (287). However, whether the expression of these AQPs impacted cell shape and volume regulation and interactions with cytoskeleton remains to be defined. In samples from patients with triple negative breast cancer, AQP3 and 5 were observed to be primarily expressed in the membrane and cytoplasm of cancer cells and overexpression of these AQPs was associated with size, lymph node status and metastasis (288). In a study that analysed the tissue microarray from 486 colon cancer patients, AQP1, 3 and 5 were overexpressed and expression strongly correlated with metastasis (289). However, these studies did not define whether these AQPs were involved in cell shape and volume regulation.

In gliomas, expression of AQP4 is suggested to have a role in cell migration via cell volume regulation and interactions with cytoskeleton. The phosphorylation status of AQP has been shown to play an important role with protein kinase C mediated phosphorylation (S180) of AQP4 protein leading to decreased invasion in glioma cells (290). Interaction of the protein syntrophin with the C-terminus of AQP4 is suggested to induce effects on changes in actin cytoskeleton (291). Reduced AQP4 expression correlates with change in shape, impaired F-actin polymerisation and reduced invasion in gliomas and primary astrocytes (260, 262). Further, expression of AQP4 facilitated glioma invasion was shown to be dependent on co-expression of chloride channels (ClC2) and -chloride transporter (KCC1) in invadopodia which are formed in migrating cells (290, 292). Flux of ions through these transporters could provide driving force for water efflux leading to cell shape and volume change.

Expression of AQP5 leads to changes in cell volume regulation, formation of protrusions, migration and metastasis. Interaction of AQP5 with growth factor receptor (ERK1/2) directly or indirectly is suggested to influence cancer cell migration and invasion (293, 294). In human prostate cancer, lung cancer and colon cancer, expression of AQP5 correlates with metastasis and invasion (268, 295). Combination of AQP5 activity and other ion channels such as Na<sup>+</sup>/H<sup>+</sup> exchanger is suggested to facilitate cell motility and cell volume regulation (296).

Overexpression of AQP8 in colorectal cancer cell lines (CRC SW480 and HT29) decreased proliferation, invasion and metastasis and has been suggested to act by inactivating P13K/AKT signalling pathways and inhibiting PCDH7 expression (297). In the human oesophageal cancer cells (Eca-109), cell migration and AQP8 expression was observed to be induced by epidermal



growth factor (EGF) (298). In colorectal cancer tissues analysed from 40 patients, AQP8 was observed to have very low expression in contrast to AQP5 (299).

Formation of filipodial protrusions is dependent on water flux mediated by AQP9 in fibroblasts and AQP induced actin polymerisation is via the activation of CDC42 pathway and protein kinase C mediated phosphorylation (300). In breast cancer, higher expression of AQP9 was associated with worst relapse free survival (301). In hepatocellular carcinoma, expression of the AQP9 and associated protein levels are downregulated and aid in increased migration and invasion (265). Overexpression of AQP9 in hepatoma cell line (SMMC7721) led to inhibition of cell proliferation, increased apoptosis and similar results were obtained in subcutaneously xenografted liver tumours in nude mice (265). Overexpression of AQP9 in the cell line induced increase in protein levels of forkhead box protein, down regulation of proliferating cell nuclear antigen and upregulation of caspase-3 expression. In clear cell renal cell carcinoma, enhanced expression of AQP9 correlated with increased invasion and poor patient survival (302).

Thus, different classes of AQPs have important roles in cell migration and invasion and many of the AQPs (AQP1, 2, 4, 5) facilitate these processes via changes in cell shape and volume and interactions and modulation of actin cytoskeleton. However more research is needed to understand whether the role of these AQPs and the processes they modulate, and influence is cancer specific.

### **ECM degradation and cell adhesion**

The degradation of extracellular matrix is essential for creating space into and through which the cancer cells can migrate and invade. The AQPs 1, 3, 4 and 9 have been shown to interact with MMPs (2, 9) to induce ECM degradation in cancers such as lung (303, 304), gastric (305), prostate (306) and glioma cells (260). The mechanism underpinning increased migration and invasion is suggested to be via increased ERK1/2 signalling and that AQPs are one of the key players in regulating the MMP proteases required for degradation of the ECM facilitating invasion.

During cell movement, interactions between the ECM and actin cytoskeleton are critical to facilitate anchoring, extension, and detachment to allow for forward progress (307). Cell polarity and organisation of the cytoskeleton regulate the generation and positions of focal adhesions that induce cell movement (308, 309). Expression of AQPs 1-4 have been shown to interact with cell adhesion molecules in migrating cells. Interaction of  $\beta$ -catenin, focal adhesion kinase and integrin with AQP1 in mesenchymal cells is suggested to be important for migration of normal cells but whether this interaction occurs in cancer cells is yet to be defined (310-

312). AQP2 facilitated migration is thought to occur via regulating integrin  $\beta$ 1 at the focal adhesion sites involving a motif (arginine, glycine, aspartate) in the second extracellular loop (269). In the absence of AQP2, integrin  $\beta$ 1 remains at the focal adhesion sites, slowing down migration of cells. In endometrial carcinoma, expression of AQP2 enables annexin-2 mediated adhesion, reorganisation of F-actin filaments and estradiol -induced cell migration (313). In oesophageal and oral squamous carcinoma, siRNA mediated knockdown of AQP3 correlated with decreased phosphorylation of focal adhesion kinase, diminished cell adhesion and cell death (314). In glioma cells from patient biopsies, AQP1 and AQP4 were highly expressed however in six glioma cell lines studied (D54, D65, STTG1, U87, U251, GBM62), only 3 cell lines (D65, U251, GBM62) retained AQP1 expression when cultured (263). Reintroduction of either AQPs restored water permeability, however only the presence of AQP1 increased cell growth and migration while the AQP4 expression was linked to cell adhesion but not migration (263).

In summary, a subset of AQPs play an important role in ECM degradation and cell adhesion, critical components of cell migration and invasion. However, the role of different AQPs seems to be cancer specific and the molecular mechanism that determines processes such as ECM degradation and cell adhesion is still needs more research.

### 3.4 Alternative medicines as sources of new AQP blocking agents (Bacopaside, 5HMF)

Current cancer treatments mainly target apoptosis and cell proliferation to halt cancer progression and treatment regimens involve a combination of chemotherapeutic drugs, surgery and radiotherapy. However, in many patients, tumours develop mutations and become resistant to the drugs used (315, 316), rendering treatments less effective and impacting overall survival. Further nonselective toxicity and undesirable side effects of many of the drugs are a limiting factor in cancer treatments. Thus, drugs that are effective and halt progression of tumours via chemo sensitisation are urgently needed.

Natural plant products used in traditional medicine since dawn of time are a valuable repository for identifying therapeutic compounds that maybe effective in limiting cell migration, invasion, halting proliferation and promoting apoptosis without the associated side effects. Many alkaloids such as quercetin, tetrandrine in various cancers have been shown to be effective in inducing apoptosis and re-establishing drug sensitivity in tumour cells by reversing efflux of drugs from the cells (317-320). Several studies have looked at plant derived products targeting

different pathways in addition to apoptosis for treatments of various cancers, however these are out of scope for this review. In this review the focus is instead on natural products that are known to act on limiting migration and invasion via modulating AQP activity.

Bacopasides derived from medicinal plant *B. monnieri* have been shown to selectively alter either the water channel activity or water and ion channel activity mediated by AQP1 (198). Bacopaside 1 blocks water and ion permeability mediated by AQP1 in colon cancer cells (HT29) but not AQP4 while bacopaside II only acts on water permeation through AQP1. The degree of inhibition of water and ion transport was dependent on expression levels of AQP1 in the cells as there were minimal effects of these compounds on SW480 cells that have very low levels of AQP1 expression (see more information in section 3.2). Bacopaside II has been shown to reduce endothelial cell migration, tube formation and induced apoptosis in colorectal cell lines (198, 226, 321, 322). Combined treatment with bacopasides I and II in triple negative breast cancer cell line (MDA-MB-231) with subpar IC<sub>50</sub> doses showed a synergistic effect and reduced proliferation with minimal cytotoxicity (323).

Thus, the classes of compounds i.e., bacopasides and 5HMF are new pharmacological antagonists of AQP1 activity, with minimal cytotoxicity, effective in impeding cell migration and invasion and should be tested further as therapeutic agents in regulating cancer metastasis and progression.

### 3.5 Compound Kushing Injection (CKI) therapeutic effects in limiting cancer progression

A mixture, compound Kushen injection (CKI) derived from two medicinal plants *Radix Sophora flavescens* and *Rhizoma smilacis* has been used in traditional Chinese medicine to treat solid tumours. Treatment of human breast cancer cell line (MCF-7) with CKI (1 and 2 mg/ml) inhibited cell proliferation and increased apoptosis in a dose dependent manner (324). Further, the number of genes differentially expressed between different treatments was observed to dose dependent with twice as many genes down regulated in high dose treatment compared to treatment with low dose. The treatment with CKI is suggested to suppress regulatory proteins involved in the cell cycle and DNA repair pathway while increasing the expression of genes important for DNA double strand breaks (325). The treatment with CKI also induced reduced glucose consumption and increased energy charge measured as ADP/ATP ratio suggesting that pathways for energy production were impaired.

In another study, effect of CKI, fractionated mixtures and isolated components were studied in colon (HT-29, SW480), brain (U87-MG, U251-MG) and breast (MDA-MB 231) cancer cell lines (326). This study revealed that combinations of fractionated mixture were more effective than single fractions or isolated compounds (matrine and oxymatrine) in reducing cell motility in all cell lines but the degree of inhibition of migration was dependent on the cancer cell line. A strong inhibition of migration was observed in HT29 and MDA-MB-231 cells while a smaller reduction was observed in brain cancer cell lines but had no effect on non-cancerous HEK293 cell line (326). Increased apoptosis was evident in breast cancer cell line in comparison to other cell lines. Transcriptomic analysis (RNASeq) of breast cancer cell line showed down regulation of genes relating to actin and focal adhesion supporting impaired migration in cells treated with CKI. These studies suggest that multiple bioactive compounds present in the mixtures derived from plants and may act on different pathways to limit cancer progression.

Numerous natural plant products that contain alkaloids, flavonoids, terpenoids, polyphenols, quinones, saponins and epigallocatechin gallate have been used in traditional medicine as treatments for brain cancer or glioblastoma (75). Most of these products have been reported to act on apoptosis, cell cycle, matrix metalloproteases, cytoskeleton and signalling pathways such as ERK, AKT/mTOR and JAK/STAT3 (see Table 2 and references within) (75). In GBM, the expression of AQPs 1 and 4 are highly upregulated and levels correlate with poor overall survival. However, current treatments for GBM don't focus on the AQPs as potential targets to limit cell migration and invasion.

In summary, as many AQPs such as 1, 4 are highly expressed in diverse cancer cells especially at the leading edges of migrating cells, involved in protrusion formation, ECM degradation and inducing changes in cytoskeleton, it is imperative that future research identifies products that can act on these AQPs to limit cell migration and invasion. Carcinogenesis is a complex process involving multiple pathways, genes and transport proteins; thus, it is essential that new treatment protocols focus on more than a single target to achieve successful outcomes.

#### 4- Summary and significance

Aquaporins are found in all kingdoms of life and are involved in multiple cellular functions, as such their study and characterization has led to elucidation of previously unresolved processes. Despite the ubiquity and importance of aquaporins there is limited knowledge about them, however, there is growing interest in clarifying their function and linkage to different

pathophysiological states. Understanding the multifunctional roles of aquaporins opens the door to new application in physiological and pathological processes across all forms of life. To date aquaporins have been implicated in a range of physiological conditions. For instance, in cancer, aquaporins are involved in the growth, invasion, migration and angiogenesis of cancer cells facilitating cancer progression. They are believed to be involved in tissue inflammation and edema. Aquaporins are also thought to be involved in the mode of action of toxins produced by *Bacillus thuringiensis* bacteria known as Bt toxins. Their involvement in abnormal physiological conditions has also made them a target for pharmacological treatments. Pharmacological blockers of aquaporins are being investigated as tools for cancer treatment to slow cancer progression in reproductive cancer and other cancer that are being discovered to be AQP related. Although promising further study to investigate pharmacological agents and their effect on cancer progression and growth is needed.

Characterization of AQP function is important however it has proven to be complicated. Recent identification of AQPs as gated channels, requiring phosphorylation or glycosylation activation, suggests they may have dual functions in different cells or require specific conditions. Human AQP1 has been shown to be a cGMP-gated cation channel and may have a physiologically relevant function. The redundancy of having dedicated ion channels and aquaporins with ion channel function is a matter of speculation however the exploration of pharmacological agents for ion channels may enable the development of therapies

## 5- References

1. Overton E. Ueber die osmotischen Eigenschaften der Zelle in ihrer Bedeutung für die Toxicologie und Pharmakologie. Vierteljahrsschr Naturforsch Ges Zuerich. 1896;41:383.
2. Benga G. Birth of water channel proteins—the aquaporins. Cell biology international. 2003;27(9):701-9.
3. Stein W, Danielli J. Structure and function in red cell permeability. Discussions of the Faraday Society. 1956;21:238-51.
4. Sidel VW, Solomon A. Entrance of water into human red cells under an osmotic pressure gradient. The Journal of general physiology. 1957;41(2):243-57.
5. Gorin MB, Yancey SB, Cline J, Revel J-P, Horwitz J. The major intrinsic protein (MIP) of the bovine lens fiber membrane: characterization and structure based on cDNA cloning. Cell. 1984;39(1):49-59.
6. Kuchel P. The story of the discovery of aquaporins: convergent evolution of ideas—but who got there first. Cell Mol Biol. 2006;52(7):2-5.
7. Preston GM, Carroll TP, Guggino WB, Agre P. Appearance of water channels in *Xenopus* oocytes expressing red cell CHIP28 protein. Science. 1992;256(5055):385-7.
8. Ishibashi K, Morishita Y, Tanaka Y. The evolutionary aspects of aquaporin family. Aquaporins: Springer; 2017. p. 35-50.

9. Beitz E, Wu B, Holm LM, Schultz JE, Zeuthen T. Point mutations in the aromatic/arginine region in aquaporin 1 allow passage of urea, glycerol, ammonia, and protons. *Proceedings of the National Academy of Sciences*. 2006;103(2):269-74.
10. Neely JD, Christensen BM, Nielsen S, Agre P. Heterotetrameric composition of aquaporin-4 water channels. *Biochemistry*. 1999;38(34):11156-63.
11. Fetter K, Van Wilder V, Moshelion M, Chaumont F. Interactions between plasma membrane aquaporins modulate their water channel activity. *The Plant Cell*. 2004;16(1):215-28.
12. Bienert MD, Diehn TA, Richet N, Chaumont F, Bienert GP. Heterotetramerization of plant PIP1 and PIP2 aquaporins is an evolutionary ancient feature to guide PIP1 plasma membrane localization and function. *Frontiers in plant science*. 2018;9:382.
13. Jung JS, Preston GM, Smith BL, Guggino WB, Agre P. Molecular structure of the water channel through aquaporin CHIP. The hourglass model. *Journal of Biological Chemistry*. 1994;269(20):14648-54.
14. Murata K, Mitsuoka K, Hirai T, Walz T, Agre P, Heymann JB, et al. Structural determinants of water permeation through aquaporin-1. *Nature*. 2000;407(6804):599.
15. Pao G, Wu LF, Johnson K, Höfte H, Chrispeels M, Sweet G, et al. Evolution of the MIP family of integral membrane transport proteins. *Molecular microbiology*. 1991;5(1):33-7.
16. Yool AJ, Weinstein AM. New roles for old holes: ion channel function in aquaporin-1. *Physiology*. 2002;17(2):68-72.
17. Buck TM, Eledge J, Skach WR. Evidence for stabilization of aquaporin-2 folding mutants by N-linked glycosylation in endoplasmic reticulum. *American Journal of Physiology-Cell Physiology*. 2004;287(5):C1292-C9.
18. Hendriks G, Koudijs M, van Balkom BW, Oorschot V, Klumperman J, Deen PM, et al. Glycosylation is important for cell surface expression of the water channel aquaporin-2 but is not essential for tetramerization in the endoplasmic reticulum. *Journal of Biological Chemistry*. 2004;279(4):2975-83.
19. Zwang NA, Hoffert JD, Pisitkun T, Moeller HB, Fenton RA, Knepper MA. Identification of phosphorylation-dependent binding partners of aquaporin-2 using protein mass spectrometry. *Journal of proteome research*. 2009;8(3):1540-54.
20. Németh-Cahalan KL, Clemens DM, Hall JE. Regulation of AQP0 water permeability is enhanced by cooperativity. *Journal of General Physiology*. 2013;141(3):287-95.
21. Freitas JA, Németh-Cahalan KL, Hall JE, Tobias DJ. Cooperativity and allostery in aquaporin 0 regulation by Ca<sup>2+</sup>. *Biochimica et Biophysica Acta (BBA)-Biomembranes*. 2019;1861(5):988-96.
22. Gotfryd K, Móscsa AF, Missel JW, Truelsen SF, Wang K, Spulber M, et al. Human adipose glycerol flux is regulated by a pH gate in AQP10. *Nature communications*. 2018;9(1):1-11.
23. Yasui M, Hazama A, Kwon T-H, Nielsen S, Guggino WB, Agre P. Rapid gating and anion permeability of an intracellular aquaporin. *Nature*. 1999;402(6758):184-7.
24. Kourghi M, Pei JV, De Ieso ML, Nourmohammadi S, Chow PH, Yool AJ. Fundamental structural and functional properties of Aquaporin ion channels found across the kingdoms of life. *Clinical and Experimental Pharmacology and Physiology*. 2018;45(4):401-9.
25. Ehring GR, Zampighi G, Horwitz J, Bok D, Hall JE. Properties of channels reconstituted from the major intrinsic protein of lens fiber membranes. *The Journal of general physiology*. 1990;96(3):631-64.
26. Gonen T, Walz T. The structure of aquaporins. *Quarterly reviews of biophysics*. 2006;39(4):361-96.

27. Azad AK, Raihan T, Ahmed J, Hakim A, Emon TH, Chowdhury PA. Human aquaporins: functional diversity and potential roles in infectious and non-infectious diseases. *Frontiers in Genetics*. 2021;12:654865.
28. Tyerman SD, McGaughey SA, Qiu J, Yool AJ, Byrt CS. Adaptable and multifunctional ion-conducting aquaporins. *Annual review of plant biology*. 2021;72:703-36.
29. Abascal F, Irisarri I, Zardoya R. Diversity and evolution of membrane intrinsic proteins. *Biochimica et Biophysica Acta (BBA)-General Subjects*. 2014;1840(5):1468-81.
30. Finn RN, Chauvigné F, Hlidberg JB, Cutler CP, Cerdà J. The lineage-specific evolution of aquaporin gene clusters facilitated tetrapod terrestrial adaptation. *PloS one*. 2014;9(11):e113686.
31. Chauvigné F, Yilmaz O, Ferré A, Fjellidal PG, Finn RN, Cerdà J. The vertebrate Aqp14 water channel is a neuropeptide-regulated polytransporter. *Communications biology*. 2019;2(1):1-13.
32. King LS, Kozono D, Agre P. From structure to disease: the evolving tale of aquaporin biology. *Nature reviews Molecular cell biology*. 2004;5(9):687-98.
33. Ishibashi K, Tanaka Y, Morishita Y. Perspectives on the evolution of aquaporin superfamily. *Vitamins and hormones*. 2020;112:1-27.
34. Dehal P, Boore JL. Two rounds of whole genome duplication in the ancestral vertebrate. *PLoS biology*. 2005;3(10):e314.
35. Tanaka Y, Morishita Y, Ishibashi K. Aquaporin10 is a pseudogene in cattle and their relatives. *Biochemistry and biophysics reports*. 2015;1:16-21.
36. Finn R, Cerdà J. Aquaporin. *Encyclopedia of Signaling Molecules*. 2018:1-18.
37. Maurel C, Boursiac Y, Luu D-T, Santoni V, Shahzad Z, Verdoucq L. Aquaporins in plants. *Physiological reviews*. 2015;95(4):1321-58.
38. Laloux T, Junqueira B, Maistriaux LC, Ahmed J, Jurkiewicz A, Chaumont F. Plant and mammal aquaporins: same but different. *International journal of molecular sciences*. 2018;19(2):521.
39. Kammerloher W, Fischer U, Piechottka GP, Schäffner AR. Water channels in the plant plasma membrane cloned by immunoselection from a mammalian expression system. *The Plant Journal*. 1994;6(2):187-99.
40. Chaumont F, Barrieu F, Wojcik E, Chrispeels MJ, Jung R. Aquaporins constitute a large and highly divergent protein family in maize. *Plant physiology*. 2001;125(3):1206-15.
41. Johanson U, Karlsson M, Johansson I, Gustavsson S, Sjövall S, Fraysse L, et al. The complete set of genes encoding major intrinsic proteins in *Arabidopsis* provides a framework for a new nomenclature for major intrinsic proteins in plants. *Plant physiology*. 2001;126(4):1358-69.
42. Grondin A, Rodrigues O, Verdoucq L, Merlot S, Leonhardt N, Maurel C. Aquaporins contribute to ABA-triggered stomatal closure through OST1-mediated phosphorylation. *The Plant Cell*. 2015:tpc. 15.00421.
43. Johanson U, Gustavsson S. A new subfamily of major intrinsic proteins in plants. *Molecular Biology and Evolution*. 2002;19(4):456-61.
44. Danielson JÅ, Johanson U. Unexpected complexity of the aquaporin gene family in the moss *Physcomitrella patens*. *BMC Plant Biology*. 2008;8(1):45.
45. Danielson JÅ, Johanson U. Unexpected complexity of the aquaporin gene family in the moss *Physcomitrella patens*. *BMC plant biology*. 2008;8(1):1-15.
46. Xia W, Zhao P, Yi Z, Cui Y. Phylogenetic and specific sequence analysis of four paralogs in insect aquaporins. *Molecular medicine reports*. 2017;16(4):4903-8.
47. Yanochko GM, Yool AJ. Regulated Cationic Channel Function in *Xenopus* Oocytes Expressing *Drosophila* Big Brain. *Journal of Neuroscience*. 2002;22(7):2530-40.

48. Finn RN, Chauvigné F, Stavang JA, Belles X, Cerda J. Insect glycerol transporters evolved by functional co-option and gene replacement. *Nature communications*. 2015;6(1):1-7.
49. Maruyama M, Kambara K, Naka H, Azuma M. Insect water-specific aquaporins in developing ovarian follicles of the silk moth *Bombyx mori*: role in hydration during egg maturation. *The Biological Bulletin*. 2015;229(1):58-69.
50. Kozono D, Ding X, Iwasaki I, Meng X, Kamagata Y, Agre P, et al. Functional expression and characterization of an archaeal aquaporin: AqpM from *Methanothermobacter marburgensis*. *Journal of Biological Chemistry*. 2003;278(12):10649-56.
51. Von Bülow J, Beitz E. Number and regulation of protozoan aquaporins reflect environmental complexity. *The Biological Bulletin*. 2015;229(1):38-46.
52. Uzcátegui NL, Figarella K, Segnini A, Marsiccobetre S, Lang F, Beitz E, et al. *Trypanosoma brucei* aquaglyceroporins mediate the transport of metabolic end-products: Methylglyoxal, D-lactate, L-lactate and acetate. *Biochimica et Biophysica Acta (BBA)-Biomembranes*. 2018;1860(11):2252-61.
53. Hohmann S. Osmotic adaptation in yeast-control of the yeast osmolyte system. *International review of cytology*. 2002;215:149-87.
54. Tamás MJ, Luyten K, Sutherland FCW, Hernandez A, Albertyn J, Valadi H, et al. Fps1p controls the accumulation and release of the compatible solute glycerol in yeast osmoregulation. *Molecular microbiology*. 1999;31(4):1087-104.
55. Wysocki R, Chéry CC, Wawrzycka D, Van Hulle M, Cornelis R, Thevelein JM, et al. The glycerol channel Fps1p mediates the uptake of arsenite and antimonite in *Saccharomyces cerevisiae*. *Molecular microbiology*. 2001;40(6):1391-401.
56. Zardoya R. Phylogeny and evolution of the major intrinsic protein family. *Biology of the Cell*. 2005;97(6):397-414.
57. Murata K, Mitsuoka K, Hirai T, Walz T, Agre P, Heymann JB, et al. Structural determinants of water permeation through aquaporin-1. *Nature*. 2000;407(6804):599-605.
58. de Groot BL, Grubmüller H. The dynamics and energetics of water permeation and proton exclusion in aquaporins. *Current opinion in structural biology*. 2005;15(2):176-83.
59. Froger A, Thomas D, Delamarche C, Tallur B. Prediction of functional residues in water channels and related proteins. *Protein Science*. 1998;7(6):1458-68.
60. Hub JS, De Groot BL. Mechanism of selectivity in aquaporins and aquaglyceroporins. *Proceedings of the National Academy of Sciences*. 2008;105(4):1198-203.
61. Törnroth-Horsefield S, Wang Y, Hedfalk K, Johanson U, Karlsson M, Tajkhorshid E, et al. Structural mechanism of plant aquaporin gating. *Nature*. 2006;439(7077):688-94.
62. Henderson SW, Nourmohammadi S, Ramesh SA, Yool AJ. Aquaporin ion conductance properties defined by membrane environment, protein structure, and cell physiology. *Biophysical Reviews*. 2022:1-18.
63. Bienert GP, Chaumont F. Aquaporin-facilitated transmembrane diffusion of hydrogen peroxide. *Biochimica et Biophysica Acta (BBA)-General Subjects*. 2014;1840(5):1596-604.
64. Hwang JH, Ellingson SR, Roberts DM. Ammonia permeability of the soybean nodulin 26 channel. *FEBS letters*. 2010;584(20):4339-43.
65. Loqué D, Ludewig U, Yuan L, von Wirén N. Tonoplast intrinsic proteins AtTIP2; 1 and AtTIP2; 3 facilitate NH<sub>3</sub> transport into the vacuole. *Plant physiology*. 2005;137(2):671-80.
66. Uehlein N, Lovisolo C, Siefritz F, Kaldenhoff R. The tobacco aquaporin NtAQP1 is a membrane CO<sub>2</sub> pore with physiological functions. *Nature*. 2003;425(6959):734-7.
67. van Os CH, Deen PM. Aquaporin-2 water channel mutations causing nephrogenic diabetes insipidus. *Proc Assoc Am Physicians*. 1998;110(5):395-400.



68. Cabrero P, Terhzaz S, Dornan AJ, Ghimire S, Holmes HL, Turin DR, et al. Specialized stellate cells offer a privileged route for rapid water flux in *Drosophila* renal tubule. *Proceedings of the National Academy of Sciences*. 2020;117(3):1779-87.
69. Nielsen S, Smith BL, Christensen EI, Agre P. Distribution of the aquaporin CHIP in secretory and resorptive epithelia and capillary endothelia. *Proc Natl Acad Sci U S A*. 1993;90(15):7275-9.
70. Badaut J, Fukuda AM, Jullienne A, Petry KG. Aquaporin and brain diseases. *Biochimica et Biophysica Acta (BBA)-General Subjects*. 2014;1840(5):1554-65.
71. Cavazzin C, Ferrari D, Facchetti F, Russignan A, Vescovi AL, La Porta CA, et al. Unique expression and localization of aquaporin-4 and aquaporin-9 in murine and human neural stem cells and in their glial progeny. *Glia*. 2006;53(2):167-81.
72. Nagelhus EA, Horio Y, Inanobe A, Fujita A, Haug FM, Nielsen S, et al. Immunogold evidence suggests that coupling of K<sup>+</sup> siphoning and water transport in rat retinal Müller cells is mediated by a coenrichment of Kir4.1 and AQP4 in specific membrane domains. *Glia*. 1999;26(1):47-54.
73. Amiry-Moghaddam M, Williamson A, Palomba M, Eid T, de Lanerolle NC, Nagelhus EA, et al. Delayed K<sup>+</sup> clearance associated with aquaporin-4 mislocalization: phenotypic defects in brains of alpha-syntrophin-null mice. *Proc Natl Acad Sci U S A*. 2003;100(23):13615-20.
74. Badaut J, Regli L. Distribution and possible roles of aquaporin 9 in the brain. *Neuroscience*. 2004;129(4):971-81.
75. Yool AJ, Ramesh S. Molecular targets for combined therapeutic strategies to limit glioblastoma cell migration and invasion. *Frontiers in pharmacology*. 2020;11:358.
76. Kreda SM, Gynn MC, Fenstermacher DA, Boucher RC, Gabriel SE. Expression and localization of epithelial aquaporins in the adult human lung. *Am J Respir Cell Mol Biol*. 2001;24(3):224-34.
77. Verkman A, Ruiz-Ederra J, Levin MH. Functions of aquaporins in the eye. *Progress in retinal and eye research*. 2008;27(4):420-33.
78. Salman MM, Kitchen P, Yool AJ, Bill RM. Recent breakthroughs and future directions in drugging aquaporins. *Trends in Pharmacological Sciences*. 2022;43(1):30-42.
79. Verkman A. Aquaporins in clinical medicine. *Annual review of medicine*. 2012;63:303.
80. Azad AK, Raihan T, Ahmed J, Hakim A, Emon TH, Chowdhury PA. Human Aquaporins: Functional Diversity and Potential Roles in Infectious and Non-infectious Diseases. *Frontiers in Genetics*. 2021;12:344.
81. Anthony TL, Brooks HL, Boassa D, Leonov S, Yanochko GM, Regan JW, et al. Cloned human aquaporin-1 is a cyclic GMP-gated ion channel. *Molecular Pharmacology*. 2000;57(3):576-88.
82. Denyer J, Worley J, Cox B, Allenby G, Banks M. HTS approaches to voltage-gated ion channel drug discovery. *Drug discovery today*. 1998;3(7):323-32.
83. Gill S, Gill R, Lee SS, Hesketh JC, Fedida D, Rezazadeh S, et al. Flux assays in high throughput screening of ion channels in drug discovery. *Assay and drug development technologies*. 2003;1(5):709-17.
84. Yu H-b, Li M, Wang W-p, Wang X-l. High throughput screening technologies for ion channels. *Acta Pharmacologica Sinica*. 2016;37(1):34-43.
85. Garcia ML, Kaczorowski GJ. Ion channels find a pathway for therapeutic success. *Proceedings of the National Academy of Sciences*. 2016;113(20):5472-4.
86. Mackie TD, Brodsky JL. Investigating potassium channels in budding yeast: A genetic sandbox. *Genetics*. 2018;209(3):637-50.

87. Locascio A, Andrés-Colás N, Mulet JM, Yenush L. *Saccharomyces cerevisiae* as a tool to investigate plant potassium and sodium transporters. *International Journal of Molecular Sciences*. 2019;20(9):2133.
88. Qu Y, Guan R, Bose J, Henderson SW, Wege S, Qiu L-J, et al. GmSALT3 confers shoot Na<sup>+</sup> and Cl<sup>-</sup> exclusion in soybean via two distinct processes. *bioRxiv*. 2020.
89. Tomar PPS, Arkin IT. SARS-CoV-2 E protein is a potential ion channel that can be inhibited by Gliclazide and Memantine. *Biochemical and biophysical research communications*. 2020;530(1):10-4.
90. Ko CH, Gaber RF. TRK1 and TRK2 encode structurally related K<sup>+</sup> transporters in *Saccharomyces cerevisiae*. *Molecular and Cellular Biology*. 1991;11(8):4266-73.
91. Nakamura RL, Gaber RF. [6] Studying ion channels using yeast genetics. *Methods in enzymology*. 1998;293:89-104.
92. Anderson JA, Huprikar SS, Kochian LV, Lucas WJ, Gaber RF. Functional expression of a probable *Arabidopsis thaliana* potassium channel in *Saccharomyces cerevisiae*. *Proceedings of the National Academy of Sciences*. 1992;89(9):3736-40.
93. Sentenac H, Bonneaud N, Minet M, Lacroute F, Salmon J-M, Gaymard F, et al. Cloning and expression in yeast of a plant potassium ion transport system. *Science*. 1992;256(5057):663-5.
94. Tang W, Ruknudin A, Yang WP, Shaw S-Y, Knickerbocker A, Kurtz S. Functional expression of a vertebrate inwardly rectifying K<sup>+</sup> channel in yeast. *Molecular biology of the cell*. 1995;6(9):1231-40.
95. Yenush L. Potassium and sodium transport in yeast. *Yeast Membrane Transport*. 2016:187-228.
96. Stautz J, Hellmich Y, Fuss MF, Silberberg JM, Devlin JR, Stockbridge RB, et al. Molecular mechanisms for bacterial potassium homeostasis. *Journal of Molecular Biology*. 2021:166968.
97. Epstein W, Buurman E, McLaggan D, Naprstek J. Multiple mechanisms, roles and controls of K<sup>+</sup> transport in *Escherichia coli*. *Biochemical Society Transactions*. 1993;21(4):1006-10.
98. Leng Q, Mercier RW, Yao W, Berkowitz GA. Cloning and first functional characterization of a plant cyclic nucleotide-gated cation channel. *Plant Physiology*. 1999;121(3):753-61.
99. Pettersson N, Filipsson C, Becit E, Brive L, Hohmann S. Aquaporins in yeasts and filamentous fungi. *Biology of the Cell*. 2005;97(7):487-500.
100. Alder BJ, Wainwright TE. Phase transition for a hard sphere system. *The Journal of chemical physics*. 1957;27(5):1208-9.
101. Levitt M, Lifson S. Refinement of protein conformations using a macromolecular energy minimization procedure. *Journal of molecular biology*. 1969;46(2):269-79.
102. Lifson S, Warshel A. Consistent force field for calculations of conformations, vibrational spectra, and enthalpies of cycloalkane and n-alkane molecules. *The Journal of Chemical Physics*. 1968;49(11):5116-29.
103. McCammon JA, Gelin BR, Karplus M. Dynamics of folded proteins. *Nature*. 1977;267(5612):585-90.
104. Hollingsworth SA, Dror RO. Molecular dynamics simulation for all. *Neuron*. 2018;99(6):1129-43.
105. Salomon-Ferrer R, Gotz AW, Poole D, Le Grand S, Walker RC. Routine microsecond molecular dynamics simulations with AMBER on GPUs. 2. Explicit solvent particle mesh Ewald. *Journal of chemical theory and computation*. 2013;9(9):3878-88.
106. Stone JE, Hallock MJ, Phillips JC, Peterson JR, Luthey-Schulten Z, Schulten K, editors. Evaluation of emerging energy-efficient heterogeneous computing platforms for biomolecular

and cellular simulation workloads. 2016 IEEE International Parallel and Distributed Processing Symposium Workshops (IPDPSW); 2016: IEEE.

107. Van Der Spoel D, Lindahl E, Hess B, Groenhof G, Mark AE, Berendsen HJ. GROMACS: fast, flexible, and free. *Journal of computational chemistry*. 2005;26(16):1701-18.

108. Kalé L, Skeel R, Bhandarkar M, Brunner R, Gursoy A, Krawetz N, et al. NAMD2: greater scalability for parallel molecular dynamics. *Journal of Computational Physics*. 1999;151(1):283-312.

109. Case DA, Cheatham III TE, Darden T, Gohlke H, Luo R, Merz Jr KM, et al. The Amber biomolecular simulation programs. *Journal of computational chemistry*. 2005;26(16):1668-88.

110. De Levie R, Seidah NG, Moreira H. Transport of ions of one kind through thin membranes. *The Journal of membrane biology*. 1972;10(1):171-92.

111. Kurnikova MG, Coalson RD, Graf P, Nitzan A. A lattice relaxation algorithm for three-dimensional Poisson-Nernst-Planck theory with application to ion transport through the gramicidin A channel. *Biophysical Journal*. 1999;76(2):642-56.

112. Mackay D, Berens PH, Wilson KR, Hagler A. Structure and dynamics of ion transport through gramicidin A. *Biophysical journal*. 1984;46(2):229-48.

113. Köpfer DA, Song C, Gruene T, Sheldrick GM, Zachariae U, de Groot BL. Ion permeation in K<sup>+</sup> channels occurs by direct Coulomb knock-on. *Science*. 2014;346(6207):352-5.

114. Boiteux C, Vorobyov I, Allen TW. Ion conduction and conformational flexibility of a bacterial voltage-gated sodium channel. *Proceedings of the National Academy of Sciences*. 2014;111(9):3454-9.

115. Dror RO, Jensen MØ, Borhani DW, Shaw DE. Exploring atomic resolution physiology on a femtosecond to millisecond timescale using molecular dynamics simulations. *Journal of General Physiology*. 2010;135(6):555-62.

116. Janosi L, Ceccarelli M. The gating mechanism of the human aquaporin 5 revealed by molecular dynamics simulations. *PLoS One*. 2013;8(4):e59897.

117. Ubarretxena-Belandia I, Stokes DL. Present and future of membrane protein structure determination by electron crystallography. *Advances in protein chemistry and structural biology*. 2010;81:33-60.

118. Rawson S, Davies S, Lippiat JD, Muench SP. The changing landscape of membrane protein structural biology through developments in electron microscopy. *Molecular membrane biology*. 2016;33(1-2):12-22.

119. de Groot BL, Grubmüller H. Water permeation across biological membranes: mechanism and dynamics of aquaporin-1 and GlpF. *Science*. 2001;294(5550):2353-7.

120. Fu D, Libson A, Miercke LJ, Weitzman C, Nollert P, Krucinski J, et al. Structure of a glycerol-conducting channel and the basis for its selectivity. *science*. 2000;290(5491):481-6.

121. Tajkhorshid E, Nollert P, Jensen MØ, Miercke LJ, O'Connell J, Stroud RM, et al. Control of the selectivity of the aquaporin water channel family by global orientational tuning. *Science*. 2002;296(5567):525-30.

122. Jensen MØ, Dror RO, Xu H, Borhani DW, Arkin IT, Eastwood MP, et al. Dynamic control of slow water transport by aquaporin 0: implications for hydration and junction stability in the eye lens. *Proceedings of the National Academy of Sciences*. 2008;105(38):14430-5.

123. Chakrabarti N, Tajkhorshid E, Roux Bt, Pomès R. Molecular basis of proton blockage in aquaporins. *Structure*. 2004;12(1):65-74.

124. Fischer G, Kosinska-Eriksson U, Aponte-Santamaría C, Palmgren M, Geijer C, Hedfalk K, et al. Crystal structure of a yeast aquaporin at 1.15 Å reveals a novel gating mechanism. *PLoS biology*. 2009;7(6):e1000130.

125. Wang Y, Cohen J, Boron WF, Schulten K, Tajkhorshid E. Exploring gas permeability of cellular membranes and membrane channels with molecular dynamics. *Journal of structural biology*. 2007;157(3):534-44.
126. Yusupov M, Yan D, Cordeiro RM, Bogaerts A. Atomic scale simulation of H<sub>2</sub>O<sub>2</sub> permeation through aquaporin: toward the understanding of plasma cancer treatment. *Journal of Physics D: Applied Physics*. 2018;51(12):125401.
127. Hadidi H, Kamali R. Molecular dynamics study of water transport through AQP5-R188C mutant causing palmoplantar keratoderma (PPK) using the gating mechanism concept. *Biophysical Chemistry*. 2021;277:106655.
128. Sachdeva R, Singh B. Phosphorylation of Ser-180 of rat aquaporin-4 shows marginal affect on regulation of water permeability: molecular dynamics study. *Journal of Biomolecular Structure and Dynamics*. 2014;32(4):555-66.
129. De Almeida A, Mósca AF, Wragg D, Wenzel M, Kavanagh P, Barone G, et al. The mechanism of aquaporin inhibition by gold compounds elucidated by biophysical and computational methods. *Chemical communications*. 2017;53(27):3830-3.
130. Hub JS, Aponte-Santamaría C, Grubmüller H, de Groot BL. Voltage-regulated water flux through aquaporin channels in silico. *Biophysical journal*. 2010;99(12):L97-L9.
131. Mom R, Muries B, Benoit P, Robert-Paganin J, Réty S, Venisse Js, et al. Voltage-gating of aquaporins, a putative conserved safety mechanism during ionic stresses. *FEBS letters*. 2021;595(1):41-57.
132. Lynch CI, Rao S, Sansom MS. Water in nanopores and biological channels: A molecular simulation perspective. *Chemical Reviews*. 2020;120(18):10298-335.
133. Yool AJ, Stamer WD, Regan JW. Forskolin stimulation of water and cation permeability in aquaporin1 water channels. *Science*. 1996;273(5279):1216-8.
134. Yu J, Yool AJ, Schulten K, Tajkhorshid E. Mechanism of gating and ion conductivity of a possible tetrameric pore in aquaporin-1. *Structure*. 2006;14(9):1411-23.
135. Bernardi M, Marracino P, Liberti M, Gárate J-A, Burnham CJ, Apollonio F, et al. Controlling ionic conductivity through transprotein electropores in human aquaporin 4: a non-equilibrium molecular-dynamics study. *Physical Chemistry Chemical Physics*. 2019;21(6):3339-46.
136. Flood E, Boiteux C, Lev B, Vorobyov I, Allen TW. Atomistic simulations of membrane ion channel conduction, gating, and modulation. *Chemical Reviews*. 2019;119(13):7737-832.
137. Aponte-Santamaría C, Briones R, Schenk AD, Walz T, de Groot BL. Molecular driving forces defining lipid positions around aquaporin-0. *Proceedings of the National Academy of Sciences*. 2012;109(25):9887-92.
138. Gu R-X, Ingólfsson HI, De Vries AH, Marrink SJ, Tieleman DP. Ganglioside-lipid and ganglioside-protein interactions revealed by coarse-grained and atomistic molecular dynamics simulations. *The Journal of Physical Chemistry B*. 2017;121(15):3262-75.
139. Pei JV, Heng S, De Ieso ML, Sylvia G, Kourghi M, Nourmohammadi S, et al. Development of a photoswitchable lithium-sensitive probe to analyze nonselective cation channel activity in migrating cancer cells. *Molecular pharmacology*. 2019;95(5):573-83.
140. Kapilan R, Vaziri M, Zwiazek JJ. Regulation of aquaporins in plants under stress. *Biological research*. 2018;51(1):1-11.
141. Chow PH, Kourghi M, Pei JV, Nourmohammadi S, Yool AJ. 5-hydroxymethyl-furfural and structurally related compounds block the ion conductance in human aquaporin-1 channels and slow cancer cell migration and invasion. *Molecular Pharmacology*. 2020;98(1):38-48.
142. Huber VJ, Tsujita M, Yamazaki M, Sakimura K, Nakada T. Identification of arylsulfonamides as Aquaporin 4 inhibitors. *Bioorganic & medicinal chemistry letters*. 2007;17(5):1270-3.

143. De Ieso ML, Pei JV, Nourmohammadi S, Smith E, Chow PH, Kourghi M, et al. Combined pharmacological administration of AQP1 ion channel blocker AqB011 and water channel blocker Bacopaside II amplifies inhibition of colon cancer cell migration. *Scientific reports*. 2019;9(1):1-17.
144. Aung T, Nourmohammadi S, Qu Z, Harata-Lee Y, Cui J, Shen H, et al. Fractional Deletion of compound Kushen injection indicates cytokine Signaling pathways are critical for its perturbation of the cell cycle. *Scientific reports*. 2019;9(1):1-16.
145. King LS, Kozono D, Agre P. From structure to disease: the evolving tale of aquaporin biology. *Nature reviews Molecular cell biology*. 2004;5(9):687.
146. Modesto E, Barcellos L, Campos-de-Carvalho A. MIP 28 forms channels in planar lipid bilayers. *Brazilian Journal of Medical and Biological Research*. 1990;23(10):1029-32.
147. Weaver CD, Shomer NH, Louis CF, Roberts DM. Nodulin 26, a nodule-specific symbiosome membrane protein from soybean, is an ion channel. *Journal of Biological Chemistry*. 1994;269(27):17858-62.
148. Hazama A, Kozono D, Guggino WB, Agre P, Yasui M. Ion permeation of AQP6 water channel protein single-channel recordings after Hg<sup>2+</sup> activation. *Journal of Biological Chemistry*. 2002;277(32):29224-30.
149. Byrt CS, Zhao M, Kourghi M, Bose J, Henderson SW, Qiu J, et al. Non-selective cation channel activity of aquaporin AtPIP2; 1 regulated by Ca<sup>2+</sup> and pH. *Plant, cell & environment*. 2017;40(6):802-15.
150. Pisano MM, Chepelinsky AB. Genomic cloning, complete nucleotide sequence, and structure of the human gene encoding the major intrinsic protein (MIP) of the lens. *Genomics*. 1991;11(4):981-90.
151. Shen L, Shrager P, Girsch SJ, Donaldson PJ, Peracchia C. Channel reconstitution in liposomes and planar bilayers with HPLC-purified MIP26 of bovine lens. *The Journal of membrane biology*. 1991;124(1):21-32.
152. Kushmerick C, Rice S, Baldo G, Haspel H, Mathias R. Ion, water and neutral solute transport in *Xenopus* oocytes expressing frog lens MIP. *Experimental eye research*. 1995;61(3):351-62.
153. Zampighi GA, Hall JE, Kreman M. Purified lens junctional protein forms channels in planar lipid films. *Proceedings of the National Academy of Sciences*. 1985;82(24):8468-72.
154. Agre P, Lee MD, Devidas S, Guggino WB. Aquaporins and ion conductance. *Science*. 1997;275(5305):1490-2.
155. Boassa D, Yool AJ. Single amino acids in the carboxyl terminal domain of aquaporin-1 contribute to cGMP-dependent ion channel activation. *BMC physiology*. 2003;3(1):12.
156. Saparov SM, Kozono D, Rothe U, Agre P, Pohl P. Water and ion permeation of aquaporin-1 in planar lipid bilayers: major differences in structural determinants and stoichiometry. *Journal of Biological Chemistry*. 2001;276(34):31515-20.
157. Boassa D, Stamer WD, Yool AJ. Ion channel function of aquaporin-1 natively expressed in choroid plexus. *Journal of Neuroscience*. 2006;26(30):7811-9.
158. Kourghi M, De Ieso ML, Nourmohammadi S, Pei JV, Yool AJ. Identification of loop D domain amino acids in the human Aquaporin-1 channel involved in activation of the ionic conductance and inhibition by AqB011. *Frontiers in chemistry*. 2018;6:142.
159. Yool AJ, Campbell EM. Structure, function and translational relevance of aquaporin dual water and ion channels. *Molecular aspects of medicine*. 2012;33(5-6):553-61.
160. Hazama A, Kozono D, Guggino WB, Agre P, Yasui M. Ion permeation of AQP6 water channel protein: single-channel recordings after Hg<sup>2+</sup> activation. *Journal of Biological Chemistry*. 2002;277(32):29224-30.
161. Yasui M, Hazama A, Kwon T-H, Nielsen S, Guggino WB, Agre P. Rapid gating and anion permeability of an intracellular aquaporin. *Nature*. 1999;402(6758):184.

162. Ma J, Zhou C, Yang J, Ding X, Zhu Y, Chen X. Expression of AQP6 and AQP8 in epithelial ovarian tumor. *Journal of molecular histology*. 2016;47(2):129-34.
163. Holm LM, Jahn TP, Møller AL, Schjoerring JK, Ferri D, Klaerke DA, et al. NH<sub>3</sub> and NH<sub>4</sub><sup>+</sup> permeability in aquaporin-expressing *Xenopus* oocytes. *Pflügers Archiv*. 2005;450(6):415-28.
164. Jahn TP, Møller AL, Zeuthen T, Holm LM, Klærke DA, Mohsin B, et al. Aquaporin homologues in plants and mammals transport ammonia. *FEBS letters*. 2004;574(1-3):31-6.
165. Kucherenko YV, Huber SM, Nielsen S, Lang F. Decreased redox-sensitive erythrocyte cation channel activity in aquaporin 9-deficient mice. *The Journal of membrane biology*. 2012;245(12):797-805.
166. Alexandersson E, Fraysse L, Sjövall-Larsen S, Gustavsson S, Fellert M, Karlsson M, et al. Whole gene family expression and drought stress regulation of aquaporins. *Plant molecular biology*. 2005;59(3):469-84.
167. Qiu J, McGaughey SA, Groszmann M, Tyerman SD, Byrt CS. Phosphorylation influences water and ion channel function of AtPIP2; 1. *Plant, cell & environment*. 2020;43(10):2428-42.
168. Tran STH, Horie T, Imran S, Qiu J, McGaughey S, Byrt CS, et al. A survey of barley PIP aquaporin ionic conductance reveals Ca<sup>2+</sup>-sensitive HvPIP2; 8 Na<sup>+</sup> and K<sup>+</sup> conductance. *International journal of molecular sciences*. 2020;21(19):7135.
169. Kourghi M, Nourmohammadi S, Pei JV, Qiu J, McGaughey S, Tyerman SD, et al. Divalent cations regulate the ion conductance properties of diverse classes of aquaporins. *International journal of molecular sciences*. 2017;18(11):2323.
170. Yanochko GM, Yool AJ. Block by extracellular divalent cations of *Drosophila* big brain channels expressed in *Xenopus* oocytes. *Biophysical journal*. 2004;86(3):1470-8.
171. Yool AJ. Dominant-negative suppression of big brain ion channel activity by mutation of a conserved glutamate in the first transmembrane domain. *Gene Expression The Journal of Liver Research*. 2006;13(6):329-37.
172. Lee JW, Zhang Y, Weaver CD, Shomer NH, Louis CF, Roberts DM. Phosphorylation of nodulin 26 on serine 262 affects its voltage-sensitive channel activity in planar lipid bilayers. *Journal of Biological Chemistry*. 1995;270(45):27051-7.
173. Rodrigues C, Mósca AF, Martins AP, Nobre T, Prista C, Antunes F, et al. Rat aquaporin-5 is pH-gated induced by phosphorylation and is implicated in oxidative stress. *International Journal of Molecular Sciences*. 2016;17(12):2090.
174. Su W, Cao R, Zhang X-y, Guan Y. Aquaporins in the kidney: physiology and pathophysiology. *American Journal of Physiology-Renal Physiology*. 2020;318(1):F193-F203.
175. Deen PM, Verdijk MA, Knoers NV, Wieringa B, Monnens LA, van Os CH, et al. Requirement of human renal water channel aquaporin-2 for vasopressin-dependent concentration of urine. *Science*. 1994;264(5155):92-5.
176. Brown P, Davies S, Speake T, Millar I. Molecular mechanisms of cerebrospinal fluid production. *Neuroscience*. 2004;129(4):955-68.
177. Boassa D, Yool AJ. Physiological roles of aquaporins in the choroid plexus. *Current topics in developmental biology*. 2005;67:181-206.
178. Blaydon DC, Kelsell DP. Defective channels lead to an impaired skin barrier. *Journal of cell science*. 2014;127(20):4343-50.
179. Maeda N. Implications of aquaglyceroporins 7 and 9 in glycerol metabolism and metabolic syndrome. *Molecular Aspects of Medicine*. 2012;33(5-6):665-75.
180. Silva IVd, Soveral G. Aquaporins in obesity. *Aquaporins*. 2017:227-38.
181. Berry V, Francis P, Kaushal S, Moore A, Bhattacharya S. Missense mutations in MIP underlie autosomal dominant 'polymorphic' and lamellar cataracts linked to 12q. *Nature genetics*. 2000;25(1):15-7.

182. Sands JM, Klein JD. Physiological insights into novel therapies for nephrogenic diabetes insipidus. *American Journal of Physiology-Renal Physiology*. 2016;311(6):F1149-F52.
183. Saglar Ozer E, Moeller HB, Karaduman T, Fenton RA, Mergen H. Molecular characterization of an aquaporin-2 mutation causing a severe form of nephrogenic diabetes insipidus. *Cellular and Molecular Life Sciences*. 2020;77(5):953-62.
184. Oliva Jr A, Kang Y, Truettner J, Sanchez-Molano J, Furones C, Yool A, et al. Fluid-percussion brain injury induces changes in aquaporin channel expression. *Neuroscience*. 2011;180:272-9.
185. Kitchen P, Salman MM, Halsey AM, Clarke-Bland C, MacDonald JA, Ishida H, et al. Targeting aquaporin-4 subcellular localization to treat central nervous system edema. *Cell*. 2020;181(4):784-99. e19.
186. Yool AJ. Functional domains of aquaporin-1: keys to physiology, and targets for drug discovery. *Current pharmaceutical design*. 2007;13(31):3212-21.
187. Tomita Y, Palethorpe HM, Smith E, Nakhjavani M, Townsend AR, Price TJ, et al. Bumetanide-derived aquaporin 1 inhibitors, AqB013 and AqB050 inhibit tube formation of endothelial cells through induction of apoptosis and impaired migration in vitro. *International Journal of Molecular Sciences*. 2019;20(8):1818.
188. Varricchio A, Ramesh SA, Yool AJ. Novel ion channel targets and drug delivery tools for controlling glioblastoma cell invasiveness. *International Journal of Molecular Sciences*. 2021;22(21):11909.
189. Brooks HL, Regan JW, Yool AJ. Inhibition of aquaporin-1 water permeability by tetraethylammonium: involvement of the loop E pore region. *Molecular pharmacology*. 2000;57(5):1021-6.
190. Yool AJ, Brokl OH, Pannabecker TL, Dantzer WH, Stamer WD. Tetraethylammonium block of water flux in Aquaporin-1 channels expressed in kidney thin limbs of Henle's loop and a kidney-derived cell line. *BMC physiology*. 2002;2(1):1-8.
191. Liu K, Tsujimoto H, Cha S-J, Agre P, Rasgon JL. Aquaporin water channel AqAQP1 in the malaria vector mosquito *Anopheles gambiae* during blood feeding and humidity adaptation. *Proceedings of the National Academy of Sciences*. 2011;108(15):6062-6.
192. Migliati E, Meurice N, DuBois P, Fang JS, Somasekharan S, Beckett E, et al. Inhibition of aquaporin-1 and aquaporin-4 water permeability by a derivative of the loop diuretic bumetanide acting at an internal pore-occluding binding site. *Molecular pharmacology*. 2009;76(1):105-12.
193. Yool AJ, Morelle J, Cnops Y, Verbavatz J-M, Campbell EM, Beckett EA, et al. AqF026 is a pharmacologic agonist of the water channel aquaporin-1. *Journal of the American Society of Nephrology*. 2013;24(7):1045-52.
194. Sonntag Y, Gena P, Maggio A, Singh T, Artner I, Oklinski MK, et al. Identification and characterization of potent and selective aquaporin-3 and aquaporin-7 inhibitors. *Journal of Biological Chemistry*. 2019;294(18):7377-87.
195. Aikman B, De Almeida A, Meier-Menches SM, Casini A. Aquaporins in cancer development: Opportunities for bioinorganic chemistry to contribute novel chemical probes and therapeutic agents. *Metallomics*. 2018;10(5):696-712.
196. Serna A, Galán-Cobo A, Rodrigues C, Sánchez-Gomar I, Toledo-Aral JJ, Moura TF, et al. Functional inhibition of aquaporin-3 with a gold-based compound induces blockage of cell proliferation. *Journal of cellular physiology*. 2014;229(11):1787-801.
197. Martins AP, Ciancetta A, De Almeida A, Marrone A, Re N, Soveral G, et al. Aquaporin inhibition by gold (III) compounds: new insights. *ChemMedChem*. 2013;8(7):1086-92.
198. Pei JV, Kourghi M, De Ieso ML, Campbell EM, Dorward HS, Hardingham JE, et al. Differential inhibition of water and ion channel activities of mammalian aquaporin-1 by two

- structurally related bacopaside compounds derived from the medicinal plant bacopa monnieri. *Molecular pharmacology*. 2016;90(4):496-507.
199. Detmers FJ, De Groot BL, Müller EM, Hinton A, Konings IB, Sze M, et al. Quaternary ammonium compounds as water channel blockers: specificity, potency, and site of action. *Journal of Biological Chemistry*. 2006;281(20):14207-14.
200. Seeliger D, Zapater C, Krenc D, Haddoub R, Flitsch S, Beitz E, et al. Discovery of novel human aquaporin-1 blockers. *ACS chemical biology*. 2013;8(1):249-56.
201. Ma B, Xiang Y, Mu S-M, Li T, Yu H-M, Li X-J. Effects of acetazolamide and anordiol on osmotic water permeability in AQP1-cRNA injected *Xenopus* oocyte. *Acta Pharmacol Sin*. 2004;25(1):90-7.
202. Gao J, Wang X, Chang Y, Zhang J, Song Q, Yu H, et al. Acetazolamide inhibits osmotic water permeability by interaction with aquaporin-1. *Analytical biochemistry*. 2006;350(2):165-70.
203. Søgaard R, Zeuthen T. Test of blockers of AQP1 water permeability by a high-resolution method: no effects of tetraethylammonium ions or acetazolamide. *Pflügers Archiv - European Journal of Physiology*. 2008;456(2):285-92.
204. Yang B, Zhang H, Verkman A. Lack of aquaporin-4 water transport inhibition by antiepileptics and arylsulfonamides. *Bioorganic & medicinal chemistry*. 2008;16(15):7489-93.
205. Zelenina M, Bondar AA, Zelenin S, Aperia A. Nickel and extracellular acidification inhibit the water permeability of human aquaporin-3 in lung epithelial cells. *Journal of Biological Chemistry*. 2003;278(32):30037-43.
206. Alejandra R, Natalia S, Alicia E D. The blocking of aquaporin-3 (AQP3) impairs extravillous trophoblast cell migration. *Biochemical and Biophysical Research Communications*. 2018;499(2):227-32.
207. Niemietz CM, Tyerman SD. New potent inhibitors of aquaporins: silver and gold compounds inhibit aquaporins of plant and human origin. *FEBS Letters*. 2002;531(3):443-7.
208. Preston GM, Carroll TP, Guggino WB, Agre P. Appearance of Water Channels in *Xenopus* Oocytes Expressing Red Cell CHIP28 Protein. *Science*. 1992;256(5055):385-7.
209. Preston GM, Jung JS, Guggino W, Agre P. The mercury-sensitive residue at cysteine 189 in the CHIP28 water channel. *Journal of Biological Chemistry*. 1993;268(1):17-20.
210. Martins AP, Marrone A, Ciancetta A, Galán Cobo A, Echevarría M, Moura TF, et al. Targeting Aquaporin Function: Potent Inhibition of Aquaglyceroporin-3 by a Gold-Based Compound. *PLOS ONE*. 2012;7(5):e37435.
211. de Almeida A, Soveral G, Casini A. Gold compounds as aquaporin inhibitors: new opportunities for therapy and imaging. *MedChemComm*. 2014;5(10):1444-53.
212. Ozu M, Dorr RA, Teresa Politi M, Parisi M, Toriano R. Water flux through human aquaporin 1: inhibition by intracellular furosemide and maximal response with high osmotic gradients. *European Biophysics Journal*. 2011;40(6):737-46.
213. Tsukaguchi H, Shayakul C, Berger UV, Mackenzie B, Devidas S, Guggino WB, et al. Molecular characterization of a broad selectivity neutral solute channel. *Journal of Biological Chemistry*. 1998;273(38):24737-43.
214. Müller-Lucks A, Gena P, Frascaria D, Altamura N, Svelto M, Beitz E, et al. Preparative scale production and functional reconstitution of a human aquaglyceroporin (AQP3) using a cell free expression system. *New biotechnology*. 2013;30(5):545-51.
215. Mola MG, Nicchia GP, Svelto M, Spray DC, Frigeri A. Automated cell-based assay for screening of aquaporin inhibitors. *Anal Chem*. 2009;81(19):8219-29.
216. Patil RV, Xu S, van Hoek AN, Rusinko A, Feng Z, May J, et al. Rapid Identification of Novel Inhibitors of the Human Aquaporin-1 Water Channel. *Chem Biol Drug Des*. 2016;87(5):794-805.



217. To J, Yeo CY, Soon CH, Torres J. A generic high-throughput assay to detect aquaporin functional mutants: Potential application to discovery of aquaporin inhibitors. *Biochim Biophys Acta*. 2015;1850(9):1869-76.
218. Esteva-Font C, Jin B-J, Lee S, Phuan P-W, Anderson MO, Verkman AS. Experimental evaluation of proposed small-molecule inhibitors of water channel aquaporin-1. *Molecular Pharmacology*. 2016;89(6):686-93.
219. Modesto E, Barcellos L, Campos-de-Carvalho A. MIP 28 forms channels in planar lipid bilayers. *Brazilian Journal of Medical and Biological Research= Revista Brasileira de Pesquisas Medicas e Biologicas*. 1990;23(10):1029-32.
220. Preston GM, Jung JS, Guggino WB, Agre P. Membrane topology of aquaporin CHIP. Analysis of functional epitope-scanning mutants by vectorial proteolysis. *Journal of Biological Chemistry*. 1994;269(3):1668-73.
221. Ikeda M, Beitz E, Kozono D, Guggino WB, Agre P, Yasui M. Characterization of aquaporin-6 as a nitrate channel in mammalian cells: requirement of pore-lining residue threonine 63. *Journal of Biological Chemistry*. 2002;277(42):39873-9.
222. Wright EM, Saito Y. The Choroid Plexus as a Route from Blood to Brain a. *Annals of the New York Academy of Sciences*. 1986;481(1):214-20.
223. Speake T, Brown PD. Ion channels in epithelial cells of the choroid plexus isolated from the lateral ventricle of rat brain. *Brain research*. 2004;1005(1-2):60-6.
224. Matsuki-Fukushima M, Hashimoto S, Shimono M, Satoh K, Fujita-Yoshigaki J, Sugiya H. Presence and localization of aquaporin-6 in rat parotid acinar cells. *Cell and Tissue Research*. 2008;332(1):73-80.
225. Laforenza U, Gastaldi G, Polimeni M, Tritto S, Tosco M, Ventura U, et al. Aquaporin-6 is expressed along the rat gastrointestinal tract and upregulated by feeding in the small intestine. *BMC physiology*. 2009;9(1):1-12.
226. Dorward HS, Du A, Bruhn MA, Wrin J, Pei JV, Evdokiou A, et al. Pharmacological blockade of aquaporin-1 water channel by AqB013 restricts migration and invasiveness of colon cancer cells and prevents endothelial tube formation in vitro. *Journal of Experimental & Clinical Cancer Research*. 2016;35(1):1-9.
227. Jung HJ, Park J-Y, Jeon H-S, Kwon T-H. Aquaporin-5: a marker protein for proliferation and migration of human breast cancer cells. *PloS one*. 2011;6(12):e28492.
228. Chen J, Wang T, Zhou Y-C, Gao F, Zhang Z-H, Xu H, et al. Aquaporin 3 promotes epithelial-mesenchymal transition in gastric cancer. *Journal of Experimental & Clinical Cancer Research*. 2014;33(1):1-10.
229. Yang L, Wang X, Zhen S, Zhang S, Kang D, Lin Z. Aquaporin-4 upregulated expression in glioma tissue is a reaction to glioma-associated edema induced by vascular endothelial growth factor. *Oncology reports*. 2012;28(5):1633-8.
230. Kourghi M, Pei JV, De Ieso ML, Flynn G, Yool AJ. Bumetanide derivatives AqB007 and AqB011 selectively block the aquaporin-1 ion channel conductance and slow cancer cell migration. *Molecular pharmacology*. 2016;89(1):133-40.
231. Saadoun S, Papadopoulos M, Davies D, Bell B, Krishna S. Increased aquaporin 1 water channel expression in human brain tumours. *British journal of cancer*. 2002;87(6):621-3.
232. Endo M, Jain RK, Witwer B, Brown D. Water channel (aquaporin 1) expression and distribution in mammary carcinomas and glioblastomas. *Microvascular research*. 1999;58(2):89-98.
233. Markert JM, Fuller CM, Gillespie GY, Bubien JK, McLEAN LA, Hong RL, et al. Differential gene expression profiling in human brain tumors. *Physiological genomics*. 2001;5(1):21-33.

234. Vacca A, Frigeri A, Ribatti D, Nicchia GP, Nico B, Ria R, et al. Microvessel overexpression of aquaporin 1 parallels bone marrow angiogenesis in patients with active multiple myeloma. *British journal of haematology*. 2001;113(2):415-21.
235. Papadopoulos M, Saadoun S, Binder D, Manley G, Krishna S, Verkman A. Molecular mechanisms of brain tumor edema. *Neuroscience*. 2004;129(4):1009-18.
236. Clapp C, de la Escalera GM. Aquaporin-1: a novel promoter of tumor angiogenesis. *Trends in Endocrinology & Metabolism*. 2006;17(1):1-2.
237. Nishida N, Yano H, Nishida T, Kamura T, Kojiro M. Angiogenesis in cancer. *Vascular health and risk management*. 2006;2(3):213.
238. Camerino G, Nicchia G, Dinardo M, Ribatti D, Svelto M, Frigeri A. In vivo silencing of aquaporin-1 by RNA interference inhibits angiogenesis in the chick embryo chorioallantoic membrane assay. *Cell Mol Biol (Noisy-le-grand)*. 2006;52(7):51-6.
239. Saadoun S, Papadopoulos MC, Hara-Chikuma M, Verkman A. Impairment of angiogenesis and cell migration by targeted aquaporin-1 gene disruption. *Nature*. 2005;434(7034):786-92.
240. Suzuki R, Okuda M, Asai J, Nagashima G, Itokawa H, Matsunaga A, et al. Astrocytes co-express aquaporin-1,-4, and vascular endothelial growth factor in brain edema tissue associated with brain contusion. *Brain Edema XIII: Springer*; 2006. p. 398-401.
241. Pan H, Sun C-C, Zhou C-Y, Huang H-F. Expression of aquaporin-1 in normal, hyperplastic, and carcinomatous endometria. *International Journal of Gynecology & Obstetrics*. 2008;101(3):239-44.
242. Kaneko K, Yagui K, Tanaka A, Yoshihara K, Ishikawa K, Takahashi K, et al. Aquaporin 1 is required for hypoxia-inducible angiogenesis in human retinal vascular endothelial cells. *Microvascular research*. 2008;75(3):297-301.
243. Abreu-Rodríguez I, Sánchez Silva R, Martins AP, Soveral G, Toledo-Aral JJ, López-Barneo J, et al. Functional and transcriptional induction of aquaporin-1 gene by hypoxia; analysis of promoter and role of Hif-1 $\alpha$ . *PloS one*. 2011;6(12):e28385.
244. Tanaka A, Sakurai K, Kaneko K, Ogino J, Yagui K, Ishikawa K, et al. The role of the hypoxia-inducible factor 1 binding site in the induction of aquaporin-1 mRNA expression by hypoxia. *DNA and cell biology*. 2011;30(8):539-44.
245. Thiery JP. Epithelial–mesenchymal transitions in tumour progression. *Nature reviews cancer*. 2002;2(6):442-54.
246. Thiery JP. Epithelial–mesenchymal transitions in development and pathologies. *Current opinion in cell biology*. 2003;15(6):740-6.
247. Cavallaro U, Christofori G. Cell adhesion and signalling by cadherins and Ig-CAMs in cancer. *Nature Reviews Cancer*. 2004;4(2):118-32.
248. Kalluri R, Weinberg RA. The basics of epithelial-mesenchymal transition. *The Journal of clinical investigation*. 2009;119(6):1420-8.
249. van Zijl F, Krupitza G, Mikulits W. Initial steps of metastasis: cell invasion and endothelial transmigration. *Mutation Research/Reviews in Mutation Research*. 2011;728(1-2):23-34.
250. Miettinen PJ, Ebner R, Lopez AR, Derynck R. TGF-beta induced transdifferentiation of mammary epithelial cells to mesenchymal cells: involvement of type I receptors. *The Journal of cell biology*. 1994;127(6):2021-36.
251. Lo H-W, Hsu S-C, Xia W, Cao X, Shih J-Y, Wei Y, et al. Epidermal growth factor receptor cooperates with signal transducer and activator of transcription 3 to induce epithelial-mesenchymal transition in cancer cells via up-regulation of TWIST gene expression. *Cancer research*. 2007;67(19):9066-76.

252. Pagan R, Sánchez A, Martin I, Llobera M, Fabregat I, Vilaró S. Effects of growth and differentiation factors on the epithelial-mesenchymal transition in cultured neonatal rat hepatocytes. *Journal of hepatology*. 1999;31(5):895-904.
253. Xu J, Lamouille S, Derynck R. TGF- $\beta$ -induced epithelial to mesenchymal transition. *Cell research*. 2009;19(2):156-72.
254. Yang J, Mani SA, Donaher JL, Ramaswamy S, Itzykson RA, Come C, et al. Twist, a master regulator of morphogenesis, plays an essential role in tumor metastasis. *cell*. 2004;117(7):927-39.
255. Medici D, Hay ED, Olsen BR. Snail and Slug promote epithelial-mesenchymal transition through  $\beta$ -catenin-T-cell factor-4-dependent expression of transforming growth factor- $\beta$ 3. *Molecular biology of the cell*. 2008;19(11):4875-87.
256. Huang Y, Zhu Z, Sun M, Wang J, Guo R, Shen L, et al. Critical role of aquaporin-3 in the human epidermal growth factor-induced migration and proliferation in the human gastric adenocarcinoma cells. *Cancer biology & therapy*. 2010;9(12):1000-7.
257. Liu W, Wang K, Gong K, Li X, Luo K. Epidermal growth factor enhances MPC-83 pancreatic cancer cell migration through the upregulation of aquaporin 3. *Molecular medicine reports*. 2012;6(3):607-10.
258. Li A, Lu D, Zhang Y, Li J, Fang Y, Li F, et al. Critical role of aquaporin-3 in epidermal growth factor-induced migration of colorectal carcinoma cells and its clinical significance. *Oncology Reports*. 2013;29(2):535-40.
259. Yun S, Sun P-L, Jin Y, Kim H, Park E, Park SY, et al. Aquaporin 1 is an independent marker of poor prognosis in lung adenocarcinoma. *Journal of pathology and translational medicine*. 2016;50(4):251-7.
260. Ding T, Ma Y, Li W, Liu X, Ying G, Fu L, et al. Role of aquaporin-4 in the regulation of migration and invasion of human glioma cells. *International journal of oncology*. 2011;38(6):1521-31.
261. Li Y, Sun S, Han X. Down-regulation of AQP4 inhibits proliferation, migration and invasion of human breast cancer cells. *Folia Biol (Praha)*. 2016;62(3):131-7.
262. Nicchia GP, Srinivas M, Li W, Brosnan CF, Frigeri A, Spray DC. New possible roles for aquaporin-4 in astrocytes: cell cytoskeleton and functional relationship with connexin43. *The FASEB journal*. 2005;19(12):1674-6.
263. McCoy E, Sontheimer H. Expression and function of water channels (aquaporins) in migrating malignant astrocytes. *Glia*. 2007;55(10):1034-43.
264. Chae YK, Woo J, Kim M-J, Kang SK, Kim MS, Lee J, et al. Expression of aquaporin 5 (AQP5) promotes tumor invasion in human non small cell lung cancer. *PLoS One*. 2008;3(5):e2162.
265. Li C-F, Zhang W-G, Liu M, Qiu L-W, Chen X-F, Lv L, et al. Aquaporin 9 inhibits hepatocellular carcinoma through up-regulating FOXO1 expression. *Oncotarget*. 2016;7(28):44161.
266. Hu J, Verkman AS. Increased migration and metastatic potential of tumor cells expressing aquaporin water channels *FASEB J*. 2006;20:1892-4.
267. Shi Y-H, Rehemu N, Ma H, Tuokan T, Chen R, Suzuke L. Increased migration and local invasion potential of SiHa cervical cancer cells expressing Aquaporin 8. *Asian Pacific Journal of Cancer Prevention*. 2013;14(3):1825-8.
268. Li J, Wang Z, Chong T, Chen H, Li H, Li G, et al. Over-expression of a poor prognostic marker in prostate cancer: AQP5 promotes cells growth and local invasion. *World Journal of Surgical Oncology*. 2014;12(1):1-9.
269. Chen Y, Rice W, Gu Z, Li J, Huang J, Brenner MB, et al. Aquaporin 2 promotes cell migration and epithelial morphogenesis. *Journal of the American Society of Nephrology*. 2012;23(9):1506-17.

270. Zhang W-g, Li C-f, Liu M, Chen X-f, Shuai K, Kong X, et al. Aquaporin 9 is down-regulated in hepatocellular carcinoma and its over-expression suppresses hepatoma cell invasion through inhibiting epithelial-to-mesenchymal transition. *Cancer Letters*. 2016;378(2):111-9.
271. Verkman A. More than just water channels: unexpected cellular roles of aquaporins. *Journal of cell science*. 2005;118(15):3225-32.
272. Cramer LP, Siebert M, Mitchison TJ. Identification of novel graded polarity actin filament bundles in locomoting heart fibroblasts: implications for the generation of motile force. *The Journal of cell biology*. 1997;136(6):1287-305.
273. Pollard T, Borisy G. Cellular motility driven by assembly and disassembly of filaments. *Cell*. 2003;112(4):453-60.
274. Theriot JA, Mitchison TJ. Actin microfilament dynamics in locomoting cells. *Nature*. 1991;352(6331):126-31.
275. Wang Y-L. Exchange of actin subunits at the leading edge of living fibroblasts: possible role of treadmilling. *The Journal of cell biology*. 1985;101(2):597-602.
276. Diez S, Gerisch G, Anderson K, Müller-Taubenberger A, Bretschneider T. Subsecond reorganization of the actin network in cell motility and chemotaxis. *Proceedings of the National Academy of Sciences*. 2005;102(21):7601-6.
277. Frittoli E, Rottner K, Scita G. Actin polymerization machinery: the finish line of signaling networks, the starting point of cellular movement. *Cellular and Molecular Life Sciences CMLS*. 2005;62(9):955-70.
278. Schwab A, Nechyporuk-Zloy V, Fabian A, Stock C. Cells move when ions and water flow *Pflügers Arch*. 2007;453:421-32.
279. Weaver AM. Invadopodia: specialized cell structures for cancer invasion. *Clinical & experimental metastasis*. 2006;23(2):97-105.
280. De Ieso ML, Yool AJ. Mechanisms of Aquaporin-Facilitated Cancer Invasion and Metastasis. *Frontiers in Chemistry*. 2018;6.
281. Tomita Y, Dorward H, Yool AJ, Smith E, Townsend AR, Price TJ, et al. Role of aquaporin 1 signalling in cancer development and progression. *International journal of molecular sciences*. 2017;18(2):299.
282. Papadopoulos M, Saadoun S, Verkman A. Aquaporins and cell migration. *Pflügers Archiv-European Journal of Physiology*. 2008;456(4):693-700.
283. Monzani E, Bazzotti R, Perego C, La Porta CA. AQP1 is not only a water channel: it contributes to cell migration through Lin7/beta-catenin. *PloS one*. 2009;4(7):e6167.
284. Jiang Y. Aquaporin-1 activity of plasma membrane affects HT20 colon cancer cell migration. *IUBMB life*. 2009;61(10):1001-9.
285. Aishima S, Kuroda Y, Nishihara Y, Taguchi K, Iguchi T, Taketomi A, et al. Down-regulation of aquaporin-1 in intrahepatic cholangiocarcinoma is related to tumor progression and mucin expression. *Human pathology*. 2007;38(12):1819-25.
286. Sekine S, Okumura T, Nagata T, Shibuya K, Yoshioka I, Matsui K, et al. Expression analysis of aquaporin-1 (AQP-1) in human biliary tract carcinoma. *Journal of Cancer Therapy*. 2016;7(1):17-23.
287. Shi Y-H, Chen R, Talafu T, Nijati R, Lalai S. Significance and expression of aquaporin 1, 3, 8 in cervical carcinoma in Xinjiang Uygur women of China. *Asian Pacific Journal of Cancer Prevention*. 2012;13(5):1971-5.
288. Zhu Z, Jiao L, Li T, Wang H, Wei W, Qian H. Expression of AQP3 and AQP5 as a prognostic marker in triple-negative breast cancer. *Oncology letters*. 2018;16(2):2661-7.
289. Kang BW, Kim JG, Lee SJ, Chae YS, Jeong JY, Yoon GS, et al. Expression of aquaporin-1, aquaporin-3, and aquaporin-5 correlates with nodal metastasis in colon cancer. *Oncology*. 2015;88(6):369-76.

290. McCoy ES, Haas BR, Sontheimer H. Water permeability through aquaporin-4 is regulated by protein kinase C and becomes rate-limiting for glioma invasion. *Neuroscience*. 2010;168(4):971-81.
291. Neely JD, Amiry-Moghaddam M, Ottersen OP, Froehner SC, Agre P, Adams ME. Syntrophin-dependent expression and localization of Aquaporin-4 water channel protein. *Proceedings of the National Academy of Sciences*. 2001;98(24):14108-13.
292. McFerrin MB, Sontheimer H. A role for ion channels in glioma cell invasion. *Neuron glia biology*. 2006;2(1):39-49.
293. Kang SK, Chae YK, Woo J, Kim MS, Park JC, Lee J, et al. Role of human aquaporin 5 in colorectal carcinogenesis. *The American journal of pathology*. 2008;173(2):518-25.
294. Zhang H, Verkman A. Aquaporin-1 tunes pain perception by interaction with Nav1.8 Na<sup>+</sup> channels in dorsal root ganglion neurons. *Journal of Biological Chemistry*. 2010;285(8):5896-906.
295. Zhang Z, Chen Z, Song Y, Zhang P, Hu J, Bai C. Expression of aquaporin 5 increases proliferation and metastasis potential of lung cancer. *The Journal of pathology*. 2010;221(2):210-20.
296. Stroka KM, Jiang H, Chen S-H, Tong Z, Wirtz D, Sun SX, et al. Water permeation drives tumor cell migration in confined microenvironments. *Cell*. 2014;157(3):611-23.
297. Wu DQ, Yang ZF, Wang KJ, Feng XY, Lv ZJ, Li Y, et al. AQP8 inhibits colorectal cancer growth and metastasis by down-regulating PI3K/AKT signaling and PCDH7 expression. *American journal of cancer research*. 2018;8(2):266.
298. Chang H, Shi Y-H, Talaf T-K, Lin C. Aquaporin-8 mediates human esophageal cancer Eca-109 cell migration via the EGFR-Erk1/2 pathway. *International Journal of Clinical and Experimental Pathology*. 2014;7(11):7663.
299. Wang W, Li Q, Yang T, Bai G, Li D, Li Q, et al. Expression of AQP5 and AQP8 in human colorectal carcinoma and their clinical significance. *World Journal of Surgical Oncology*. 2012;10(1):1-5.
300. Loitto VM, Huang C, Sigal YJ, Jacobson K. Filopodia are induced by aquaporin-9 expression. *Experimental cell research*. 2007;313(7):1295-306.
301. Zhu L, Ma N, Wang B, Wang L, Zhou C, Yan Y, et al. Significant prognostic values of aquaporin mRNA expression in breast cancer. *Cancer management and research*. 2019;11:1503.
302. Xu W-H, Shi S-N, Xu Y, Wang J, Wang H-K, Cao D-L, et al. Prognostic implications of Aquaporin 9 expression in clear cell renal cell carcinoma. *Journal of Translational Medicine*. 2019;17(1):1-14.
303. Wei X, Dong J. Aquaporin 1 promotes the proliferation and migration of lung cancer cell in vitro. *Oncology reports*. 2015;34(3):1440-8.
304. Xia H, Ma YF, Yu CH, Li YJ, Tang J, Li JB, et al. Aquaporin 3 knockdown suppresses tumour growth and angiogenesis in experimental non-small cell lung cancer. *Experimental physiology*. 2014;99(7):974-84.
305. Xu H, Xu Y, Zhang W, Shen L, Yang L, Xu Z. Aquaporin-3 positively regulates matrix metalloproteinases via PI3K/AKT signal pathway in human gastric carcinoma SGC7901 cells. *Journal of Experimental & Clinical Cancer Research*. 2011;30(1):1-6.
306. Chen J, Wang Z, Xu D, Liu Y, Gao Y. Aquaporin 3 promotes prostate cancer cell motility and invasion via extracellular signal-regulated kinase 1/2-mediated matrix metalloproteinase-3 secretion. *Molecular medicine reports*. 2015;11(4):2882-8.
307. Curtis A. The adhesion of cells to glass: a study by interference reflection microscopy. *J Cell Biol*. 1964;19(199).
308. Geiger B BA, Pankov R, Yamada K. Transmembrane crosstalk between the extracellular matrix-cytoskeleton crosstalk. *Nat Rev Mol Cell Biol*. 2001;2:793-805.

309. Martin K, Slack JK, Boerner SA, Martin CC, and Parsons JT. Integrin connections map: to infinity and beyond *Science*. 2002;296:1652-3.
310. Meng F, Rui Y, Xu L, Wan C, Jiang X, Li G. Aqp1 enhances migration of bone marrow mesenchymal stem cells through regulation of FAK and  $\beta$ -catenin. *Stem cells and development*. 2014;23(1):66-75.
311. Schaller MD, Borgman CA, Cobb BS, Vines RR, Reynolds AB, Parsons JT. pp125FAK a structurally distinctive protein-tyrosine kinase associated with focal adhesions. *Proceedings of the National Academy of Sciences*. 1992;89(11):5192-6.
312. McLean GW, Carragher NO, Avizienyte E, Evans J, Brunton VG, Frame MC. The role of focal-adhesion kinase in cancer—a new therapeutic opportunity. *Nature Reviews Cancer*. 2005;5(7):505-15.
313. Zou L-B, Zhang R-J, Tan Y-J, Ding G-L, Shi S, Zhang D, et al. Identification of estrogen response element in the aquaporin-2 gene that mediates estrogen-induced cell migration and invasion in human endometrial carcinoma. *The Journal of Clinical Endocrinology & Metabolism*. 2011;96(9):E1399-E408.
314. Kusayama M, Wada K, Nagata M, Ishimoto S, Takahashi H, Yoneda M, et al. Critical role of aquaporin 3 on growth of human esophageal and oral squamous cell carcinoma. *Cancer science*. 2011;102(6):1128-36.
315. Schmitt CA, McCurrach ME, de Stanchina E, Wallace-Brodeur RR, Lowe SW. INK4a/ARF mutations accelerate lymphomagenesis and promote chemoresistance by disabling p53. *Genes & development*. 1999;13(20):2670-7.
316. Dive C, Hickman J. Drug-target interactions: only the first step in the commitment to a programmed cell death? *British journal of cancer*. 1991;64(1):192-6.
317. Tian H, Pan Q. A comparative study on effect of two bisbenzylisoquinolines, tetrandrine and berbamine, on reversal of multidrug resistance. *Yao xue xue bao= Acta Pharmaceutica Sinica*. 1997;32(4):245-50.
318. Choi S-U, Park S-H, Kim K-H, Choi E-J, Kim S, Park W-K, et al. The bisbenzylisoquinoline alkaloids, tetrandrine and fangchinoline, enhance the cytotoxicity of multidrug resistance-related drugs via modulation of P-glycoprotein. *Anti-cancer drugs*. 1998;9(3):255-61.
319. Chai S, To KK, Lin G. Circumvention of multi-drug resistance of cancer cells by Chinese herbal medicines. *Chinese medicine*. 2010;5(1):1-9.
320. Kang J, Kim E, Kim W, Seong KM, Youn H, Kim JW, et al. Rhamnetin and cirsiolol induce radiosensitization and inhibition of epithelial-mesenchymal transition (EMT) by miR-34a-mediated suppression of Notch-1 expression in non-small cell lung cancer cell lines. *Journal of Biological Chemistry*. 2013;288(38):27343-57.
321. Palethorpe HM, Tomita Y, Smith E, Pei JV, Townsend AR, Price TJ, et al. The aquaporin 1 inhibitor bacopaside II reduces endothelial cell migration and tubulogenesis and induces apoptosis. *International journal of molecular sciences*. 2018;19(3):653.
322. Smith E, Palethorpe HM, Tomita Y, Pei JV, Townsend AR, Price TJ, et al. The purified extract from the medicinal plant *Bacopa monnieri*, bacopaside II, inhibits growth of colon cancer cells in vitro by inducing cell cycle arrest and apoptosis. *Cells*. 2018;7(7):81.
323. Palethorpe HM, Smith E, Tomita Y, Nakhjavani M, Yool AJ, Price TJ, et al. Bacopasides I and II act in synergy to inhibit the growth, migration and invasion of breast cancer cell lines. *Molecules*. 2019;24(19):3539.
324. Qu Z, Cui J, Harata-Lee Y, Aung TN, Feng Q, Raison JM, et al. Identification of candidate anti-cancer molecular mechanisms of compound kushen injection using functional genomics. *Oncotarget*. 2016;7(40):66003.

325. Cui J, Qu Z, Harata-Lee Y, Nwe Aung T, Shen H, Wang W, et al. Cell cycle, energy metabolism and DNA repair pathways in cancer cells are suppressed by Compound Kushen Injection. *BMC cancer*. 2019;19(1):1-10.
326. Nourmohammadi S, Aung TN, Cui J, Pei JV, De Ieso ML, Harata-Lee Y, et al. Effect of Compound Kushen Injection, a Natural Compound Mixture, and Its Identified Chemical Components on Migration and Invasion of Colon, Brain, and Breast Cancer Cell Lines. *Front Oncol*. 2019;9:314.
327. Campbell EM, Ball A, Hoppler S, Bowman AS. Invertebrate aquaporins: a review. *Journal of Comparative Physiology B*. 2008;178(8):935-55.
328. Ishibashi K, Tanaka Y, Morishita Y. The role of mammalian supraaquaporins inside the cell: An update. *Biochimica et Biophysica Acta (BBA)-Biomembranes*. 2021;1863(7):183617.
329. Beitz E, Becker D, Bülow Jv, Conrad C, Fricke N, Geadkaew A, et al. In vitro analysis and modification of aquaporin pore selectivity. *Aquaporins*. 2009:77-92.
330. Finn RN, Cerda J. Evolution and functional diversity of aquaporins. *The Biological Bulletin*. 2015;229(1):6-23.
331. Laizé V, Gobin R, Rousselet G, Badier C, Hohmann S, Ripoche P, et al. Molecular and Functional Study of AqY1 from *Saccharomyces cerevisiae*: Role of the C-Terminal Domain. *Biochemical and biophysical research communications*. 1999;257(1):139-44.
332. Calamita G, Bishai WR, Preston GM, Guggino WB, Agre P. Molecular cloning and characterization of AqpZ, a water channel from *Escherichia coli*. *Journal of Biological Chemistry*. 1995;270(49):29063-6.
333. Almasalmeh A, Krenc D, Wu B, Beitz E. Structural determinants of the hydrogen peroxide permeability of aquaporins. *Wiley Online Library*; 2014. p. 647-56.
334. Song J, Almasalmeh A, Krenc D, Beitz E. Molar concentrations of sorbitol and polyethylene glycol inhibit the *Plasmodium aquaglyceroporin* but not that of *E. coli*: involvement of the channel vestibules. *Biochimica et Biophysica Acta (BBA)-Biomembranes*. 2012;1818(5):1218-24.
335. Zeuthen T, Wu B, Pavlovic-Djuranovic S, Holm LM, Uzcategui NL, Duszenko M, et al. Ammonia permeability of the aquaglyceroporins from *Plasmodium falciparum*, *Toxoplasma gondii* and *Trypanosoma brucei*. *Molecular microbiology*. 2006;61(6):1598-608.
336. Le Caherec F, Bron P, Verbavatz J, Garret A, Morel G, Cavalier A, et al. Incorporation of proteins into (*Xenopus*) oocytes by proteoliposome microinjection: functional characterization of a novel aquaporin. *Journal of cell science*. 1996;109(6):1285-95.
337. Herraiz A, Chauvigné F, Cerdà J, Bellés X, Piulachs M-D. Identification and functional characterization of an ovarian aquaporin from the cockroach *Blattella germanica* L. (Dictyoptera, Blattellidae). *Journal of Experimental Biology*. 2011;214(21):3630-8.
338. Drake LL, Rodriguez SD, Hansen IA. Functional characterization of aquaporins and aquaglyceroporins of the yellow fever mosquito, *Aedes aegypti*. *Scientific reports*. 2015;5(1):1-7.

## 6- Supplementary tables

### Supplementary S1: Functional properties of aquaporins (AQPs) across different phyla.

Vertebrate aquaporins																
	H <sub>2</sub> O	Gly	CO <sub>2</sub>	Urea	NH <sub>3</sub>	H <sub>2</sub> O <sub>2</sub>	As	Si	Ions	L A	Se	O <sub>2</sub>	Polyol s	Purines	Antim onite (Sb)	carbamides
AQP0	+		+						+							
AQP1	+		+		+	+			+			+				
AQP2	+															

AQP3	+	+		+						+								+
AQP4	+			+														
AQP5	+			+														
AQP6	+	+	+	+	+								+					
AQP7	+	+		+	+					+								+
AQP8	+	+		+	+	+												
AQP9	+	+	+	+	+					+				+	+		+	+
AQP10	+	+		+						+								+
AQP11	+	±																
AQP12s	+																	
AQP13	+	+		+														
AQP14	+	+		+	+	+												
AQP15	+																	
AQP16	+																	

Plant aquaporins																			
	H <sub>2</sub> O	H <sub>2</sub> O <sub>2</sub>	CO <sub>2</sub>	Urea	NH <sub>3</sub>	Gly	As	Sb	Si	Ions	NO	LA	Se	O <sub>2</sub>	metalloids	Silicic acid	formamide	Boric acid	
PIPs	+	+	+							+									
TIPs	+	+	+	+	+	+													
NIPs	+				+	+	+										+	+	+
SIPs	+	+														+			
XIPs	+	+		+		+													+

Microbial aquaporins																		
	H <sub>2</sub> O	H <sub>2</sub> O <sub>2</sub>	CO <sub>2</sub>	Urea	NH <sub>3</sub>	Gly	As	methylamine	Ions	NO	LA	Se	O <sub>2</sub>	Polyols	Purines	Antimonite (Sb)	Boric acid	
FpsI	+				+	+	+	+								+	+	
Aqy	+																	
GlpF	+			+		+	+					+		+		+		
AqpZ	+																	
AqpM	+					+												

Invertebrate (insects) & Protozoa aquaporins																		
	H <sub>2</sub> O	H <sub>2</sub> O <sub>2</sub>	CO <sub>2</sub>	Urea	NH <sub>3</sub>	Gly	As	Sb	Si	Ions	NO	LA	Se	O <sub>2</sub>	Polyols	Purines	trehalose	
PfAQP	+	+		+	+	+												
Drip	+																	
Prip	+			+														
EGLPs	+	+														+		+
BIB										+								

Supplementary S1 References: (38, 47, 50, 63, 327-338)

**Supplementary S2. Amino acid sequences details**



<b>Protein name</b>	<b>Accession number</b>
hMIP	NP_036196.1
hAQP1	NP_932766.1
hAQP3	NP_004916.1
hAQP5	NP_001642.1
hAQP6	NP_001643.2
hAQP7	NP_001161.1
hAQP9	NP_066190.2
hAQP12A	NP_945349.1
hAQP12B	NP_001095937.1
rAQP8	NM_019158.2
DmBIB	NM_057489
AtPIP2;1	NM_115202
AtPIP2;2	NP_181254.1
OsPIP1;1	NM_001401917.1
HvPIP2;8	AB808658.1
TaTIP2;1	AAS19468.1
GmNod26	AAA02946.1

## Chapter 2

### **Fractional deletion of Compound Kushen Injection, a natural compound mixture, indicates cytokine signaling pathways are critical for its perturbation of the cell cycle**

CKI is a mixture of compounds containing several major and minor components. Accumulating evidence suggests that CKI has anti-cancer activity. However, the exact molecular mechanism by which each or a group of single compounds exerts its anti-cancer activity remains poorly understood. The work for this chapter addressed this question by using analytical chemistry coupled with cellular and molecular assays. Results here indicate that the experimental approach for this work has enabled the association of specific compounds with alterations in specific pathway gene expression. This novel approach of depleting components from a mixture and observing the effects using both phenotypic and gene expression studies is likely to be a powerful tool for future research on the mechanism of action of complex mixtures of compounds. This chapter is published in *Scientific Reports*. Specific Aim1: To fractionate and reconstitute CKI in order to examine the functions and interactions of reconstituted compounds in MDA-MB-231 breast cancer cell line. Specific Aim2: To determine how specific compounds are responsible for specific aspects of CKI's effects on cancer cell gene expression in order to identify genes/pathways that are associated with specific fractions/components of CKI.

# Statement of Authorship

Title of Paper	Fractional Deletion of Compound Kushen Injection, A Natural Compound Mixture, Indicates Cytokine Signaling Pathways Are Critical for Its Perturbation of The Cell Cycle
Publication Status	<input checked="" type="checkbox"/> Published <input type="checkbox"/> Accepted for Publication <input type="checkbox"/> Submitted for Publication <input type="checkbox"/> Unpublished and Unsubmitted work, written in manuscript style
Publication Details	Nwe Aung T*, Nourmohammadi S*, Qu Z, Harata-Lee Y, Cui j, Shen H, Zhang J, Yool AJ, Du H, Kortchak DR and Adelson DL.

## Principal Author

Name of Principal Author (Candidate)	Mr. Saeed Nourmohammadi and Dr. Thazin Nwe Aung				
Contribution to the Paper	Co-first author. Designed and carried out the experiments, analysed data and wrote the manuscript. *Other co-authors signed the statement of authorship in the previous version. Please see Dr Aung's Thesis, titled: Molecular Mechanisms of Natural Compounds: Compound Kushen Injection (CKI) in Cancer, Chapter 2*.				
Overall percentage (%)	40%				
Certification:	This paper reports on original research I conducted during the period of my Higher Degree by Research candidature and is not subject to any obligations or contractual agreements with a third party that would constrain its inclusion in this thesis. I am the primary author of this paper.				
Signature	<table border="1" style="width: 100%;"> <tr> <td style="width: 80%;"></td> <td style="width: 20%; text-align: center;">Date</td> </tr> <tr> <td></td> <td style="text-align: center;">07/07/2022</td> </tr> </table>		Date		07/07/2022
	Date				
	07/07/2022				

10/07/2022

## Co-Author Contributions

By signing the Statement of Authorship, each author certifies that:

- i. the candidate's stated contribution to the publication is accurate (as detailed above);
- ii. permission is granted for the candidate to include the publication in the thesis; and
- iii. the sum of all co-author contributions is equal to 100% less the candidate's stated contribution.

Name of Co-Author	Professor Andrea J. Yool				
Contribution to the Paper	Assisted with experiments and manuscript writing.				
Signature	<table border="1" style="width: 100%;"> <tr> <td style="width: 80%;"></td> <td style="width: 20%; text-align: center;">Date</td> </tr> <tr> <td></td> <td style="text-align: center;">8 Jul 2022</td> </tr> </table>		Date		8 Jul 2022
	Date				
	8 Jul 2022				

Name of Co-Author	Professor David L. Adelson				
Contribution to the Paper	Supervised the research, assisted the research with funding, experimental design and wrote the manuscript.				
Signature	<table border="1" style="width: 100%;"> <tr> <td style="width: 80%;"></td> <td style="width: 20%; text-align: center;">Date</td> </tr> <tr> <td></td> <td style="text-align: center;">13/07/2022</td> </tr> </table>		Date		13/07/2022
	Date				
	13/07/2022				

OPEN

# Fractional Deletion of Compound Kushen Injection Indicates Cytokine Signaling Pathways are Critical for its Perturbation of the Cell Cycle

T. N. Aung<sup>1</sup>, S. Nourmohammadi<sup>2</sup>, Z. Qu<sup>1</sup>, Y. Harata-Lee<sup>1</sup>, J. Cui<sup>1</sup>, H. Y. Shen<sup>1</sup>, A. J. Yool<sup>2</sup>, T. Pukala<sup>3</sup>, Hong Du<sup>4</sup>, R. D. Kortschak<sup>1</sup>, W. Wei<sup>5</sup> & D. L. Adelson<sup>1</sup>

We used computational and experimental biology approaches to identify candidate mechanisms of action of a Traditional Chinese Medicine, Compound Kushen Injection (CKI), in a breast cancer cell line (MDA-MB-231). Because CKI is a complex mixture of plant secondary metabolites, we used a high-performance liquid chromatography (HPLC) fractionation and reconstitution approach to define chemical fractions required for CKI to induce apoptosis. The initial fractionation separated major from minor compounds, and it showed that major compounds accounted for little of the activity of CKI. Furthermore, removal of no single major compound altered the effect of CKI on cell viability and apoptosis. However, simultaneous removal of two major compounds identified oxymatrine and oxysophocarpine as critical with respect to CKI activity. Transcriptome analysis was used to correlate compound removal with gene expression and phenotype data. Many compounds in CKI are required to trigger apoptosis but significant modulation of its activity is conferred by a small number of compounds. In conclusion, CKI may be typical of many plant based extracts that contain many compounds in that no single compound is responsible for all of the bioactivity of the mixture and that many compounds interact in a complex fashion to influence a network containing many targets.

Natural compounds are chemically diverse and have long served as resources for the identification of drugs<sup>1</sup>. However, the standard approach of fractionating natural product extracts to identify a single compound's biological activity can fail because the original activity of the mixture is not present in single compounds after fractionation. This failure to identify single compounds implies that some natural product mixtures derive their activity from the interaction of several bioactive compounds within the mixture. Characterising the mode of action of natural product mixtures has remained a difficult task as the combinatorial complexity of such mixtures makes it unfeasible to screen all combinations of the compounds in the mixture.

We introduce here a “subtractive fractionation approach” using high performance liquid chromatography (HPLC) that can pinpoint significant interacting compounds within a mixture when coupled with a suitable bioassay. We combined this approach with RNA sequencing (RNAseq) characterisation of our bioassay, correlating the removal of interacting compounds with concomitant alterations in gene expression. This combination allowed us to identify specific combinations of compounds associated with specific pathways and regulatory interactions. In this report, we have applied this approach for the first time to a particular Traditional Chinese Medicine formulation: CKI, which is used to treat approximately 30,000 cancer patients/day in China in conjunction with Western chemotherapy.

CKI is composed primarily of alkaloids and flavonoids extracted from two herbal medicinal plants: Kushen (*Sophora flavescens*) and Baituling (*Heterosmilax chinensis*). Twenty-one chromatographic peaks have been

<sup>1</sup>Department of Molecular and Biomedical Science, School of Biological Sciences, University of Adelaide, Adelaide, South Australia, 5005, Australia. <sup>2</sup>Adelaide Medical School, University of Adelaide, Adelaide, South Australia, 5005, Australia. <sup>3</sup>School of Physical Sciences, University of Adelaide, Adelaide, South Australia, 5005, Australia. <sup>4</sup>School of Chinese Materia Medica, Beijing University of Chinese Medicine, Beijing, 100029, P.R. China. <sup>5</sup>Beijing Zhendong Guangming Pharmaceutical Research Institute, Shanxi – Zhendong Pharmaceutical Co Ltd, Beijing, P.R. China. T. N. Aung and S. Nourmohammadi contributed equally. Correspondence and requests for materials should be addressed to D.L.A. (email: [david.adelson@adelaide.edu.au](mailto:david.adelson@adelaide.edu.au))

Received: 16 January 2019

Accepted: 5 September 2019

Published online: 02 October 2019

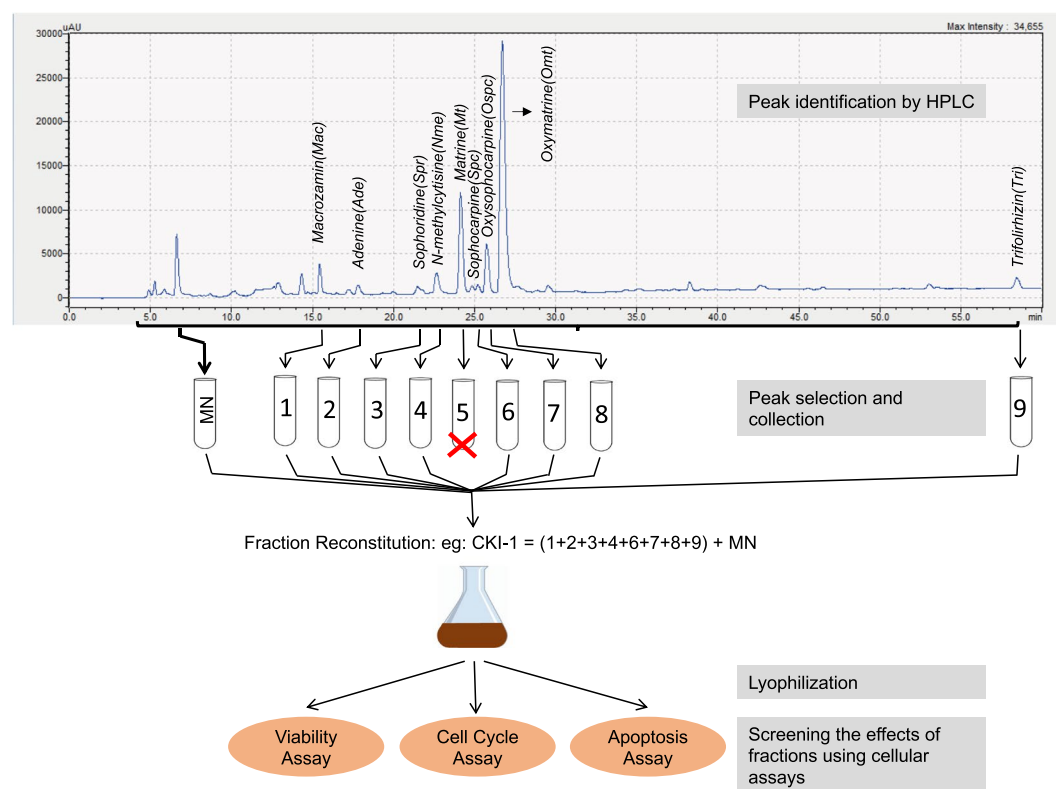


**Figure 1.** Fractionation of CKI. Diagram illustrating the process of subtractive fractionation, reconstitution, and screening of fractionated compounds using three cell-based assays.

identified from CKI with eight compounds being recognised as major components on the basis of their abundance<sup>2</sup>. The extract containing the most abundant compounds in CKI is derived from Kushen herb which has a long history in the treatment of patients suffering immune function disorders<sup>3,4</sup>. The main component of CKI, macrozamin, is a derivative of baituling which has been a suggested therapeutic agent for the treatment of inflammatory disease<sup>5</sup>. Gao and colleagues showed that treatment with each of four of the main compounds of CKI (oxymatrine, matrine, sophoridine and N-methylcytisine) at 4 mg/ml significantly decreased cell viability<sup>6</sup>. However, these concentrations are relatively high when compared to the contributing concentration of these four main compounds in CKI<sup>2</sup>. The two main components of CKI, matrine and oxymatrine, may have significant anti-cancer activities in various types of solid tumors including breast cancer, non-small cell lung cancer, cervical cancer, prostate cancer, synovial sarcoma, and hepatocellular carcinoma<sup>7-13</sup>. In contrast, the toxicity of medicinal herbs containing matrine and oxymatrine as main components has also been reported<sup>14</sup>. Administration of matrine 150 mg/kg and oxymatrine 360 mg/kg significantly increased cytochrome P450 family protein CYPB1/2 in rats demonstrating a potential therapeutic drawback of these two compounds<sup>15</sup>. Overall, understanding the effects of CKI based on the effects of single compounds present in CKI has been at best partially successful.

Alternatively, by removing one, two or three compounds, we have been able to map the effects of these compounds and their interactions to effects on specific pathways based on altered gene expression profiles in a cell-based assay. This has illuminated the roles of several major compounds of CKI, which on their own have little or no activity in our bioassay. This approach can be used to dissect the roles and interactions of individual compounds from complex natural compound mixtures whose biological activity cannot be attributed to single purified compounds.

## Results

**Subtractive fractionation overview.** Well-resolved chromatographic separation of CKI was used to collect all of the major components of CKI as individual fractions (Fig. 1). We then reconstituted all of the separated fractions except for those we wished to subtract. We tested the reconstituted combination of compounds/peaks to see if removal of a single (CKI-1) or multiple compounds, (CKI-2 or CKI-3), or removal of all major peaks (minor, MN) or depletion of all minor peaks (major, MJ) significantly altered the effect of CKI in our cell based assays. Our cell based assays<sup>16</sup> measured MDA-MB-231 (human breast adenocarcinoma) cell viability, cell-cycle phase and cell apoptosis. A summary of the subtractive fractions used in the cell-based assays is shown in Table 1. We then carried out RNA isolation of cells treated with CKI, individual compounds or CKI deletions for RNAseq. Differentially expressed (DE) genes in these samples allowed the association of specific compounds with cell phenotype and underlying alterations in gene regulation. By comparing DE genes across treatment combinations, we identified specific candidate pathways that were altered by removal of single or multiple compounds, as detailed below.

HPLC Fractionation	Treatments	Proliferation Assay (MDA-MB-213)	Cell-Cycle Assay (MDA-MB-213)	Apoptosis Assay in Three Cell Lines		
				MDA-MB-231	HEK-293	HFF
9 known + small unknown	Original CKI	***	****	**	**	
9 known major compounds	MJ					
Small unknown minor compounds	MN	***				
CKI-1	CKI-Mac					
	CKI-Ade					
	CKI-Tri					
	CKI-Nme					
	CKI-Spr					
	CKI-Mt					
	CKI-Omt					
	CKI-Ospc					
CKI-3	CKI-MacAdeTri					
	CKI-MtNmeSpr					
	CKI-OmtOspcSpc					
	CKI-MacOmtOspc	*	****	****	****	*
CKI-2	CKI-MacAde					
	CKI-MacTri					
	CKI-AdeTri					
	CKI-MtNme					
	CKI-MtSpr					
	CKI-NmeSpr					
	CKI-OmtOspc	*	****	****	****	**
	CKI-OmtSpc					
3 compounds	MacAdeTri					
	MtNmeSpr					
	OmtOspcSpc					
	MacOmtOspc					
2 compounds	MacAde					
	MacTri					
	AdeTri					
	MtNme					
	MtSpr					
	NmeSpr					
	OmtOspc					
	OmtSpc					
OspcSpc						

**Table 1.** Summarised results of HPLC fractionation and treatments using three cell-based assays at 48-hour from Figs 2 and 3 and Supplementary Fig. 2. Statistically significant results of CKI treatment were calculated based on comparison against UT whereas those of other treatments were calculated based on comparison against corresponding CKI treatments. Statistically significant results were represented as (\*) $P < 0.05$  or (\*\*)  $P < 0.01$  or (\*\*\*) $P < 0.001$  or (\*\*\*\*) $P < 0.0001$ .

**HPLC fractions and content identification using LC-MS/MS.** HPLC fractionation and reconstitution was used to generate a number of CKI-1, CKI-2, CKI-3, MJ and MN mixtures, (Fig. 1 and Supplementary Fig. 1) with specific combinations and their components shown in Table 1. The concentrations of known compounds in CKI and reconstituted subtractive fractions were determined from standard curves (Supplementary Data 1) for nine available reference compounds, using cytosine as an internal standard (Table 2). The combined concentration of nine reference compounds from CKI was approximately 10.8 mg/ml, whereas subtractive fractions CKI-OmtOspc and CKI-MacOmtOspc had concentrations of reference compounds of 3.8 mg/ml and 2.1 mg/ml which were equivalent to the concentrations of these compounds in unfractionated CKI. The depleted OmtOspc and MacOmtOspc were not observed in the CKI-OmtOspc and CKI-MacOmtOspc respectively. Based on the concentrations of nine measurable major compounds from CKI, CKI-OmtOspc and CKI-MacOmtOspc (Table 2), the observed final concentration of nine reference compounds in 1/13.25 dilution of CKI, CKI-OmtOspc and CKI-MacOmtOspc that cells were exposed to was 0.82 mg/ml, 0.29 mg/ml and 0.16 mg/ml respectively. These collectively suggested any effects observed after the treatments of CKI-OmtOspc and CKI-MacOmtOspc were not influenced by the concentrations. A total of 9 (CKI-1), 4 (CKI-3) and 9 (CKI-2) combinations, along with MJ and MN deletions were tested in our cell-based assays (Table 1).

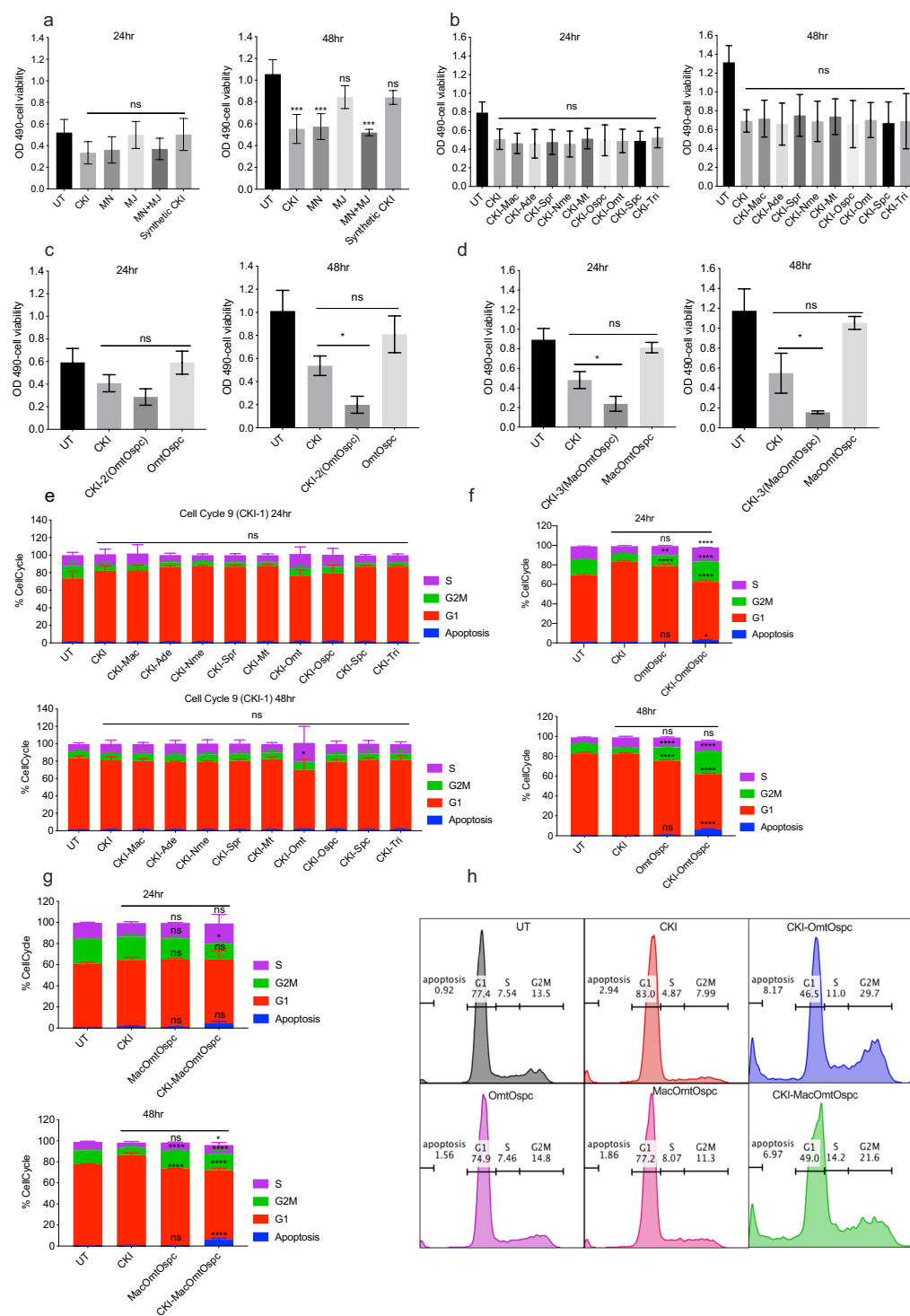


**Figure 2.** XTT cell viability assay and cell-cycle assay of subtractive fractions at 24- and 48-hour timepoint treatments in MDA-MB-231 cells treated with 2 mg/ml of CKI and 2 mg/ml equivalent concentrations of all other treating agents. **(a)** Suppression of cell viability from the following fractions: UT (untreated), MJ, MN, MJ + MN (combination of MJ and MN) and Syn\_CKI (synthetic CKI generated using nine major compounds). **(b)** Effect of 9 (CKI-1) subtractive fractions compared to CKI. **(c)** Effect of CKI-OmtOspc subtractive fraction and OmtOspc compared to CKI. **(d)** Effect of CKI-MacOmtOspc subtractive fraction and MacOmtOspc, compared to CKI. Statistically significant results relative to CKI treatment shown as (\*) $P < 0.05$  or ns (not significant), all data were shown as mean  $\pm$  SD. **(e)** Effect of 9 (CKI-1) subtractive fractions on cell-cycle in MDA-MB-231 cells as determined by PI staining assay. **(f)** Effect of CKI-OmtOspc subtractive fraction and OmtOspc on cell-cycle in MDA-MB-231 cells as determined by PI staining assay. **(g)** Effect of CKI-MacOmtOspc subtractive fraction and MOO on cell-cycle in MDA-MB-231 cells as determined by PI staining assay. **(h)** The representative histograms of cell-cycle analysis for the treatments as compared to UT. Statistically significant results shown as (\*) $P < 0.05$  or (\*\*) $P < 0.01$  or (\*\*\*) $P < 0.001$  or (\*\*\*\*) $P < 0.0001$ . All data were shown as mean  $\pm$  SD.

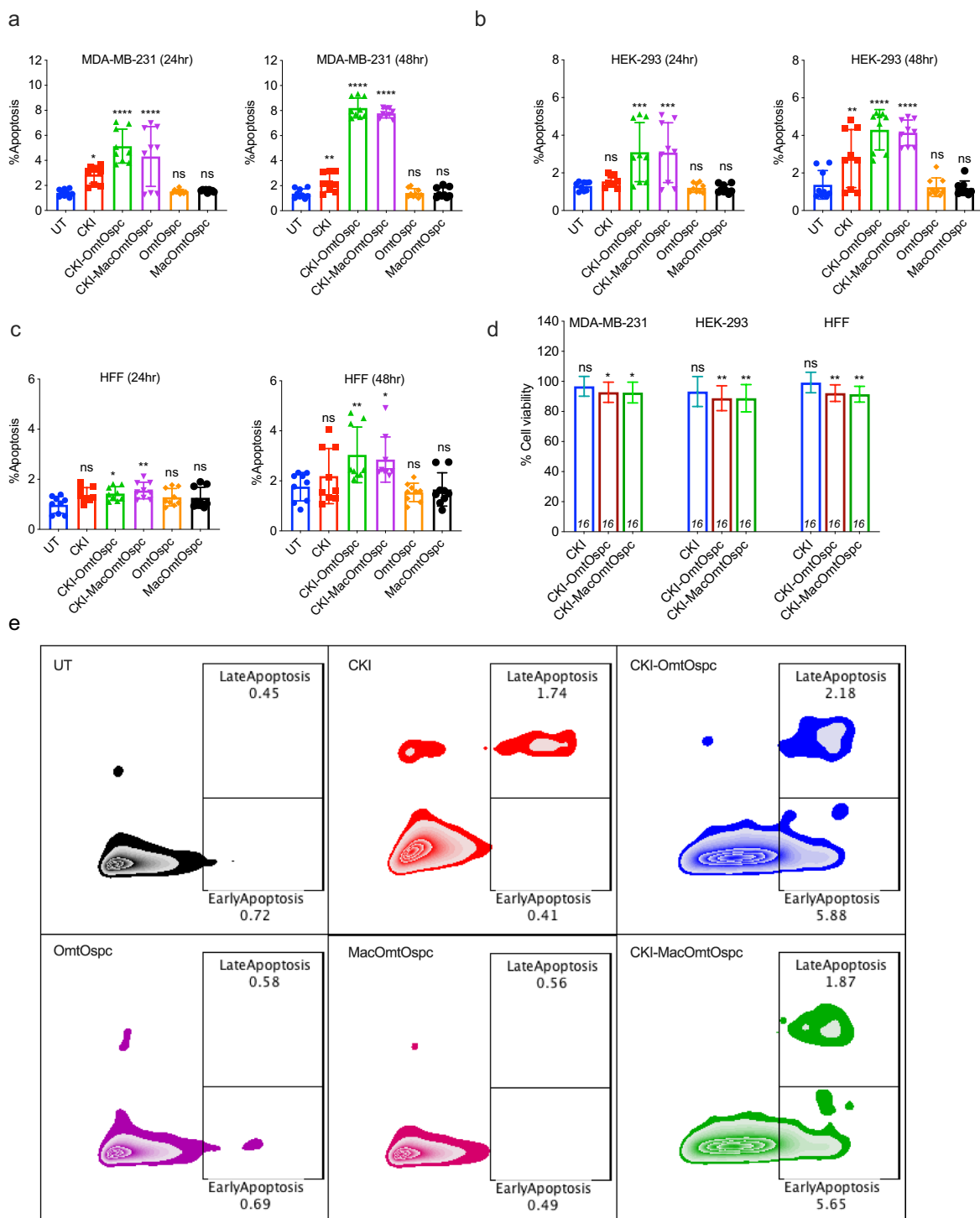


**Figure 3.** Apoptosis and cytotoxicity assays of subtractive fractions at 24- and 48-hour time point treatments. Apoptotic effect of CKI-OmtOspc, CKI-MacOmtOspc subtractive fractions, OmtOspc and MacOmtOspc in (a) MDA-MB-231 cells, (b) HEK-293 cells, and (c) HFF cells as determined by Annexin V/PI assay. (d) Cytotoxic effect of CKI, CKI-OmtOspc and CKI-MacOmtOspc subtractive fractions was determined using Alamar Blue cytotoxicity assay. All treatments were compared against UT. (e) Representative plots of Annexin V and PI staining in MDA-MB-231. Statistically significant results shown as (\*) $P < 0.05$  or (\*\*) $P < 0.01$  or (\*\*\*) $P < 0.001$  or (\*\*\*\*) $P < 0.0001$ ; ns (not significant). All data were shown as mean  $\pm$  SD.

**Phenotypic changes associated with compound deletion.** Fractionation and full reconstitution of WRCKI-H (reconstitution using milliQ H<sub>2</sub>O buffered with 10 mM HEPES) or WRCKI-B (reconstitution using buffer/vehicle control) caused no changes in cell viability compared to original CKI (see methods) at either 24- or 48-hour in MDA-MB-231 cells (Supplementary Fig. 2a). As a result, original CKI was used as a basis for



Mixtures	Compounds	Regression	Coefficient of Determination	Concentration (mg/ml) (n = 2)
CKI	Macrozamin	$y = 6E-05x + 6E-05$	0.996	$1.1 \pm 0.03$
	Adenine	$y = 0.021x + 0.0074$	0.994	$0.09 \pm 0.09$
	N-methylcytosine	$y = 0.0937x + 0.042$	0.9895	$0.17 \pm 0.02$
	Sophoridine	$y = 0.1443x + 0.2679$	0.987	$0.4 \pm 0.08$
	Matrine	$y = 0.0132x + 0.7512$	0.993	$1.26 \pm 0.06$
	Sophocarpine	$y = 0.0343x + 0.3974$	0.994	$0.54 \pm 0.02$
	Oxysophocarpine	$y = 0.0371x - 0.0108$	0.999	$1.1 \pm 0.1$
	Oxymatrine	$y = 0.0132x + 0.6226$	0.992	$6.1 \pm 0.09$
	Trifolirhizin	$y = 0.0026x - 0.0002$	0.990	$0.08 \pm 0.002$
	<b>Total</b>			<b>10.8</b>
CKI-OmtOspc	Macrozamin	$y = 6E-05x + 6E-05$	0.996	$1.1 \pm 0.04$
	Adenine	$y = 0.021x + 0.0074$	0.994	$0.3 \pm 0.5$
	N-methylcytosine	$y = 0.0937x + 0.042$	0.9895	$0.03 \pm 0.03$
	Sophoridine	$y = 0.1443x + 0.2679$	0.987	$0.3 \pm 0.07$
	Matrine	$y = 0.0132x + 0.7512$	0.993	$1.7 \pm 0.1$
	Sophocarpine	$y = 0.0343x + 0.3974$	0.994	$0.3 \pm 0.01$
	Trifolirhizin	$y = 0.0026x - 0.0002$	0.990	$0.07 \pm 0.01$
	<b>Total</b>			<b>3.8</b>
CKI-MacOmtOspc	Adenine	$y = 0.021x + 0.0074$	0.994	$0.06 \pm 0.09$
	N-methylcytosine	$y = 0.0937x + 0.042$	0.9895	$0.02 \pm 0.01$
	Sophoridine	$y = 0.1443x + 0.2679$	0.987	$0.04 \pm 0.02$
	Matrine	$y = 0.0132x + 0.7512$	0.993	$1.7 \pm 0.06$
	Sophocarpine	$y = 0.0343x + 0.3974$	0.994	$0.2 \pm 0.02$
	Trifolirhizin	$y = 0.0026x - 0.0002$	0.990	$0.08 \pm 0.003$
	<b>Total</b>			<b>2.1</b>

**Table 2.** Concentration of nine major compounds in CKI (Batch No: 20170322), remaining major compounds in CKI-OmtOspc, and remaining major compounds in CKI-MacOmtOspc. \*Total alkaloid content in CKI = 26.5 mg/ml based on manufacturer's assay.

comparison for further fractionation experiments. Our results in Supplementary Fig. 2a showed that several cycles of lyophilisation yielded WRCKI mixtures that were indistinguishable from CKI in our bioassay, indicating the complete elimination of the solvents used in HPLC fractionation process. Both CKI and reconstituted WRCKI caused significantly reduced viability compared to untreated (UT) cells at 48-hour after treatment. The MJ subtractive fraction contained a total of nine compounds, including eight previously identified MJ peaks<sup>3</sup> and adenine, and the MN fraction contained the remaining peaks (Supplementary Fig. 1). MJ had no effect on cell viability, while MN reduced cell viability to the same extent as CKI compared to UT (Fig. 2a). The nine major compounds were individually depleted from CKI and tested as 9 (CKI-1) subtractive fractions, with no significant alterations in cell viability compared to CKI (Fig. 2b). We then assessed the interaction effects of single MJ compounds by adding them back to the MN subtractive fraction. No change in cell viability compared to MN was observed (Supplementary Fig. 2b). Sets of three compounds from the nine major/standard compounds of CKI were depleted to generate 3 (CKI-3) subtractive fractions. The nine reference compounds were allocated into three groups, one of which contained structurally similar compounds (Omt, Ospc, Spc) and two other groups ([Mac, Ade, Tri] and [Nme, Mt, Spr]) that contained structurally different compounds. Of these three groups, only CKI-OmtOspcSpc decreased cell viability (albeit not statistically significantly) compared to CKI after 48 hours (Supplementary Fig. 2c), and none of the sets of three compounds on their own had any effect on cell viability (Supplementary Fig. 2c–e). In order to follow up the suggestion of decreased cell viability from CKI-OmtOspcSpc depletion, we then generated 9 (CKI-2) subtractive fractions based on the CKI-3 subtractive fractions (Table 1). Out of 9 (CKI-2) subtractive fractions (Supplementary Fig. 2), only CKI-OmtOspc significantly decreased cell viability compared to CKI ( $P < 0.05$ ) (Fig. 2c). We then depleted macrozamin, the only major compound derived from Baituling, together with OmtOspc as CKI-3 (CKI-MacOmtOspc) in order to determine if there was an additional effect when compared to CKI-OmtOspc. CKI-OmtOspc and CKI-MacOmtOspc both decreased cell viability to the same extent (Fig. 2c,d).

While no change in cell viability was found across all CKI-1 treatments, cell-cycle assay was performed to identify more subtle differences. There was no statistically significant difference in phases of the cell-cycle of MDA-MB-231 cells for many of the CKI-1 treatments compared to CKI except for a statistically significant change in G1 phase by CKI-Omt after 48 hours (Fig. 2e). On the other hand, CKI-OmtOspc treatment significantly altered the cell-cycle for MDA-MB-231 cells and induced significantly higher apoptosis from 0.25 mg/ml through 2 mg/ml treatments as compared to CKI at both timepoints (Fig. 2f and Supplementary Fig. 3). CKI-MacOmtOspc treatment also significantly altered the cell-cycle at both timepoints with generally similar effects to CKI-OmtOspc (Fig. 2g,h).

Annexin V/PI apoptosis assays were performed using subtractive fractions on MDA-MB-231, HEK-293 (human embryonic kidney cells) and HFF (primary human foreskin fibroblasts) cell lines. While CKI at 2 mg/ml caused increased apoptosis in MDA-MB-231 cells at both 24- and 48-hour after treatment, CKI-OmtOspc and CKI-MacOmtOspc subtractive fractions at concentrations equivalent to CKI 2 mg/ml significantly increased the percentage of apoptotic cells at 24-hour with increasing apoptosis at the 48-hour timepoint, indicating that CKI-OmtOspc and CKI-MacOmtOspc significantly enhanced apoptosis compared to CKI (Fig. 3a,e and Supplementary Fig. 4a). Although CKI did not generally cause apoptosis in HEK-293 or HFF cells, CKI-OmtOspc and CKI-MacOmtOspc subtractive fractions significantly induced apoptosis in HEK-293 cells ( $***P < 0.001$ ) at 24-hour and 48-hour ( $****P < 0.0001$ ) and in HFF cells ( $*P < 0.05$  and  $**P < 0.01$ ) at 24-hour and at 48-hour ( $**P < 0.01$  and  $*P < 0.05$ ). CKI only induced apoptosis of HEK-293 at 48-hour ( $**P < 0.01$ ) and showed no significant apoptotic induction in HFF (Fig. 3b,c and Supplementary Fig. 4b,c). These results indicated that the CKI-OmtOspc and CKI-MacOmtOspc subtractive fractions induced apoptosis not only in cancerous cells but also in non-cancerous cell lines. In contrast, no significant apoptosis was triggered by CKI on HFF cells. A small but significant apoptotic induction was observed for HEK-293 cells.

Because of the significantly decreased viability accompanied by increased apoptosis triggered by subtractive fractions, cytotoxicity tests were carried out for all three cell lines using CKI (2 mg/ml) and CKI-OmtOspc and CKI-MacOmtOspc subtractive fractions at concentrations equivalent to CKI 2 mg/ml. CKI-OmtOspc and CKI-MacOmtOspc at equivalent concentration to CKI 2 mg/ml were significantly cytotoxic to both non-cancerous cell lines (Fig. 3d).

Overall, these results indicated that removal of combinations of specific compounds from CKI had unpredictable effects on the ability of CKI to kill cells. While removal of all major compounds from CKI caused no loss of activity and removal of all minor compounds caused total loss of activity, removal of selected major compounds (CKI-OmtOspc) paradoxically caused major, significant increases in the ability of CKI to reduce cell viability and kill cells.

**Differential gene expression.** In order to understand the interactions of the components in CKI as a result of depletion, we carried out RNAseq of MDA-MB-231 cells treated with CKI and subtractive fractions. Four out of nine (CKI-1) subtractive fractions, namely CKI-Omt, CKI-Mac, CKI-Tri and CKI-Nme, were selected due to their structural differences, and transcriptomes of cells treated with these fractions for 48-hours were sequenced. CKI-OmtOspc and CKI-MacOmtOspc, OmtOspc, MacOmtOspc and CKI treated cells were sequenced at 24 and 48-hour timepoints. A summary of the samples, number of samples, RNA-Seq sample names, processed sample names and treatments are shown in Supplementary Table 1.

Two batches of RNAseq results were merged in order to compare CKI-1 to CKI-OmtOspc (CKI-2) and CKI-MacOmtOspc (CKI-3) fractions. After removing batch effects with the R package RUV from the merged dataset, CKI treated replicates between the two batches clustered together (Fig. 4a), indicating that gene expression patterns of the samples treated by CKI were similar regardless of the batches. We also examined the correlation between the samples with the same treatments from two batches. The Pearson correlation coefficient of untreated samples was 0.95 and of CKI treated samples was 0.94 at 48-hour between the two sequencing batches (Supplementary Fig. 5), indicating a small batch effect. In addition, clear clustering of all 4 (CKI-1) treated samples (Fig. 4a and Supplementary Figs 6–9), showed that these replicates share comparable gene expression patterns. Likewise, OmtOspc and MacOmtOspc groups and CKI-OmtOspc and CKI-MacOmtOspc groups showed similar changes in gene expression, except for one replicate (CKI-MacOmtOspc, 24-hour) that clustered with UT, OmtOspc and MacOmtOspc.

The number of DE genes associated with each treatment was calculated using pairwise comparative analysis. CKI treatment was used as a baseline to compare all other treatments in order to emphasize the effect of depleted compounds and CKI treatment was compared to UT.

There were thousands of upregulated and downregulated genes at 24- and 48-hours in most pairwise comparisons (Fig. 4b). However DE genes between OmtOspc and MacOmtOspc treatments were not observed and there were almost no DE genes between CKI-Mac, CKI-Nme and CKI-Tri treatments (Fig. 4b) indicating that these three subtractive fractions had very similar effects on gene expression.

When we compared the DE genes found between treatments, there were a large number of DE genes (~71.3%) shared between all four (CKI-1) treatments (Supplementary Fig. 10 and Supplementary Table 2). A similar number of shared DE genes (~24.6%) between four (CKI-1), OmtOspc and MacOmtOspc and between four (CKI-1), CKI-OmtOspc and CKI-MacOmtOspc as compared to CKI at 48-hour indicated that gene expression patterns from CKI-1 treatments were mostly different from CKI-OmtOspc, CKI-MacOmtOspc, OmtOspc and MacOmtOspc treated cells. 55% of the DE genes between UT, OmtOspc and MacOmtOspc were shared. When the four (CKI-1) treatments were compared to CKI treatment, 42.8% of DE genes were shared, and when CKI-OmtOspc and CKI-MacOmtOspc treatments were compared to CKI, 50.1% DE genes were shared, indicating that CKI-OmtOspc and CKI-MacOmtOspc treatments appeared to be more similar to CKI than CKI-1 treatments.

The overall levels of similarity in DE genes were as follows: 1) All CKI-1 treatments had approximately 70% similar gene expression patterns, 2) OmtOspc and MacOmtOspc treatments were approximately 50% similar to UT and 33% similar to CKI-1 treatments, 3) gene expression patterns between CKI-1, CKI-OmtOspc and CKI-MacOmtOspc were approximately 37% similar.

**Gene ontology and pathway annotation of DE genes.** DE genes were analysed for over-representation in our data sets with respect to biological function using Gene Ontology (GO) annotation. We looked for shared DE genes between treatments and identified over-represented functional terms in these shared genes. The only

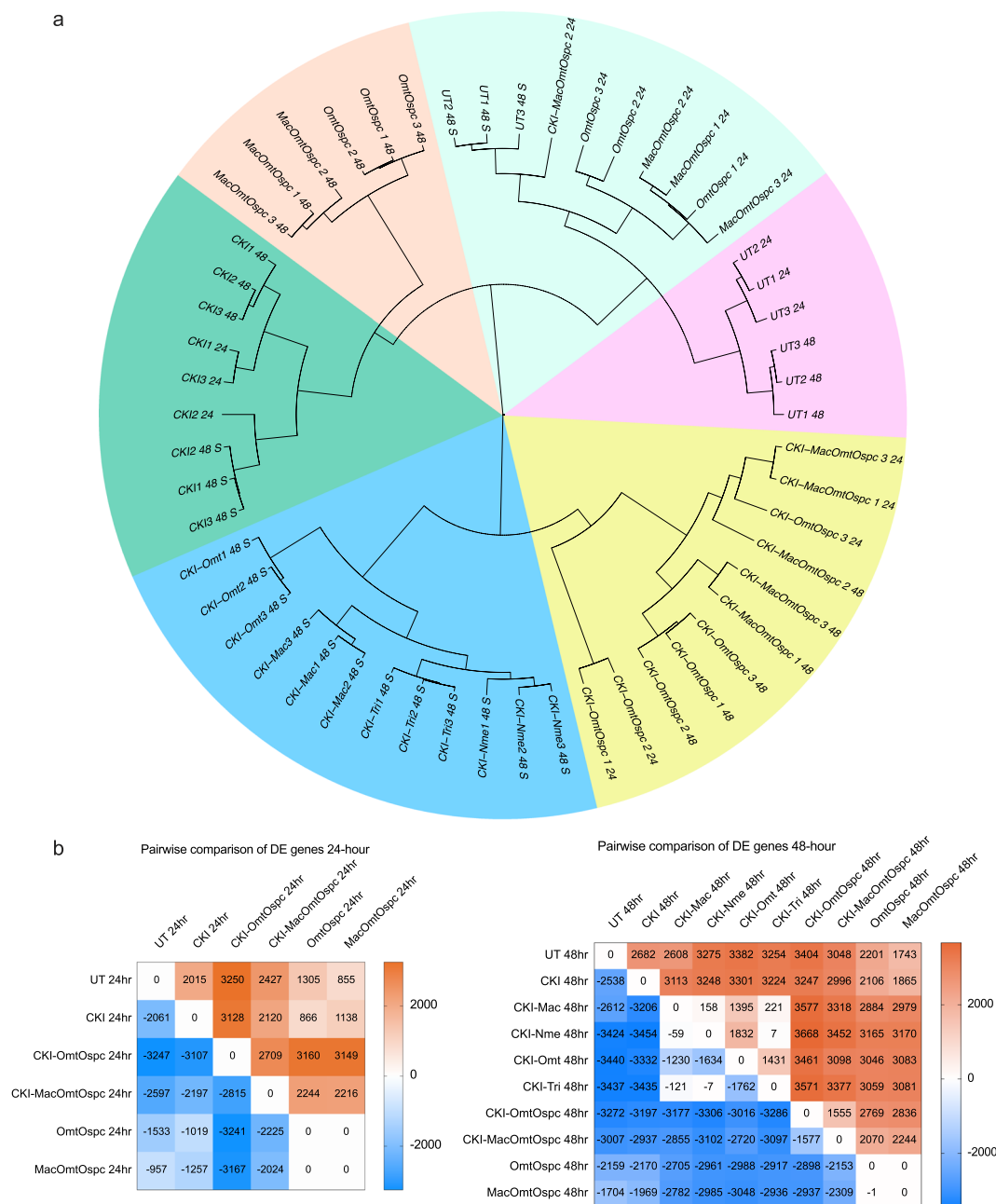


**Figure 4.** Gene expression clustering and summary of differential gene expression. **(a)** Clustering of treated samples based on gene expression, calculated as transcripts per million using Ward’s hierarchical cluster analysis (Ward.D2) method. Number of DE genes (FDR < 0.05 according to edgeR) associated with each treatment was calculated using pairwise comparison at **(b)** 24-hour and 48-hour timepoints. Treatments were compared column versus row. Up-regulated genes are shown in shades of red and down-regulated genes are shown in shades of blue.

common function enriched across all comparisons was for “cell-cycle checkpoint” (Fig. 5a). This confirmed earlier results<sup>16</sup> and was consistent with the phenotype data for CKI.

**Subtracted fractionation altered pathways.** We also performed pathway-based analysis to look for pathway level perturbation by comparing DE genes within Kyoto Encyclopedia of Genes and Genomes (KEGG) pathways between treatments. We used Signaling Pathway Impact Analysis (SPIA) to identify pathways with statistically significant perturbation values expected to alter pathway flux. We identified 86 pathways (Supplementary Fig. 11) with statistically significant ( $P < 0.05$ ) perturbations of gene expression and of these, 15 pathways were most obviously linked to our phenotypes of cell viability, cell-cycle and apoptosis (Fig. 5b). By comparing the pathway gene expression global perturbation scores (pG) between treatments, three specific observations could be made: (1) CKI-1 fractional deletions vs CKI had significant effects on flux in some pathways

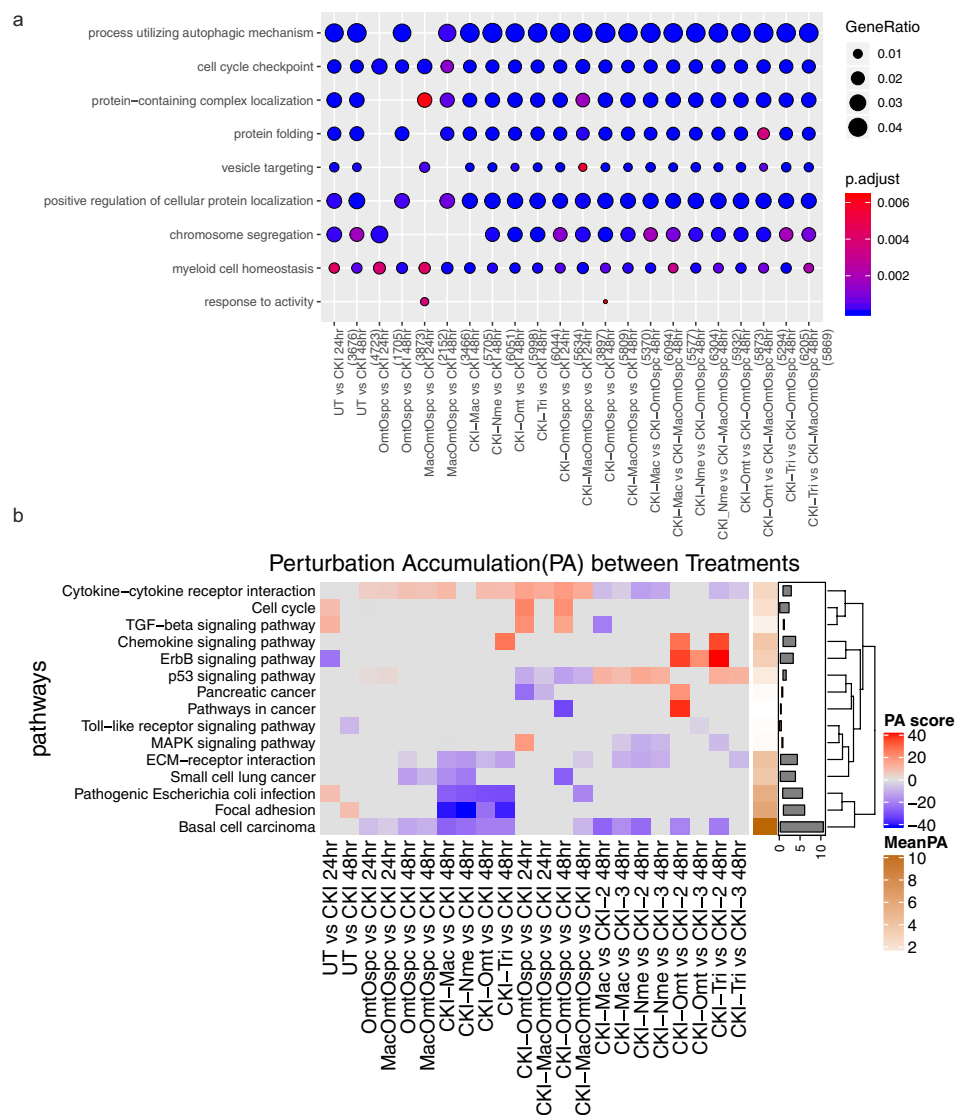


**Figure 5.** Over-representation analysis of GO functional annotation and KEGG pathway perturbation analysis. **(a)** Over-represented terms (Biological Process at level 3) for DE genes identified from comparison of subtractive fraction-treated cells against CKI treatment in order to show the relative change from depleting compounds. Gene ratio of each term calculated from clusterProfiler was plotted based on the adjusted p-values. The top 5 most statistically significantly over-represented categories of GO terms were plotted by default. Colour gradient of adjusted p-values ranging from red to blue in order of increasing p-values (high to low significance). Number of identified genes in each treatment (numbers in parentheses) were shown in the bottom and the sizes of the dots correspond to the ratio of genes out of all significant DE gene from each treatment involved in the particular terms. **(b)** Identification of significantly perturbed pathways using SPIA ( $pG < 0.05$ ) analysis. Eighty-nine significantly perturbed pathways from twenty-two comparisons were found (Supplementary Fig. 10). Only the 15 pathways most obviously linked to our phenotypes of cell viability, cell-cycle and apoptosis were shown here. Positive (overall increase in gene expression for pathway) and negative (overall decrease in gene expression for pathway) perturbation accumulation values of the pathways were shown in red and blue, respectively. Mean perturbation values of each pathway were shown in bar plot.

without phenotypic effects, (2) CKI-OmtOspc vs CKI, which had a pronounced phenotypic effect at both 24- and 48-hours, had a significant effect on reducing estimated pathway flux for Cytokine-Cytokine Receptor, Cell-Cycle and TGF-Beta signaling pathways (Figs 6 and 7 and Supplementary Figs 12–21), (3) comparison of CKI-1 fractional deletions vs fractional deletions of CKI-OmtOspc/CKI-MacOmtOspc showed consistent pathway perturbations for Cytokine-Cytokine Receptor and p53 signaling pathways. On this basis, we inferred that different major compounds could be deleted with very similar effects, indicating that they may have similar targets. In contrast, deleting Omt and Ospc simultaneously caused a significant shift in phenotype and was accompanied by specific perturbations in pathways that regulate inflammation, cell-cycle and apoptosis. The combined deletion of Omt and Ospc had a synergistic effect on cell viability, cell-cycle and apoptosis and a synergistic effect on gene expression, consistent with the observed changes in pathway specific perturbation of gene expression. Because

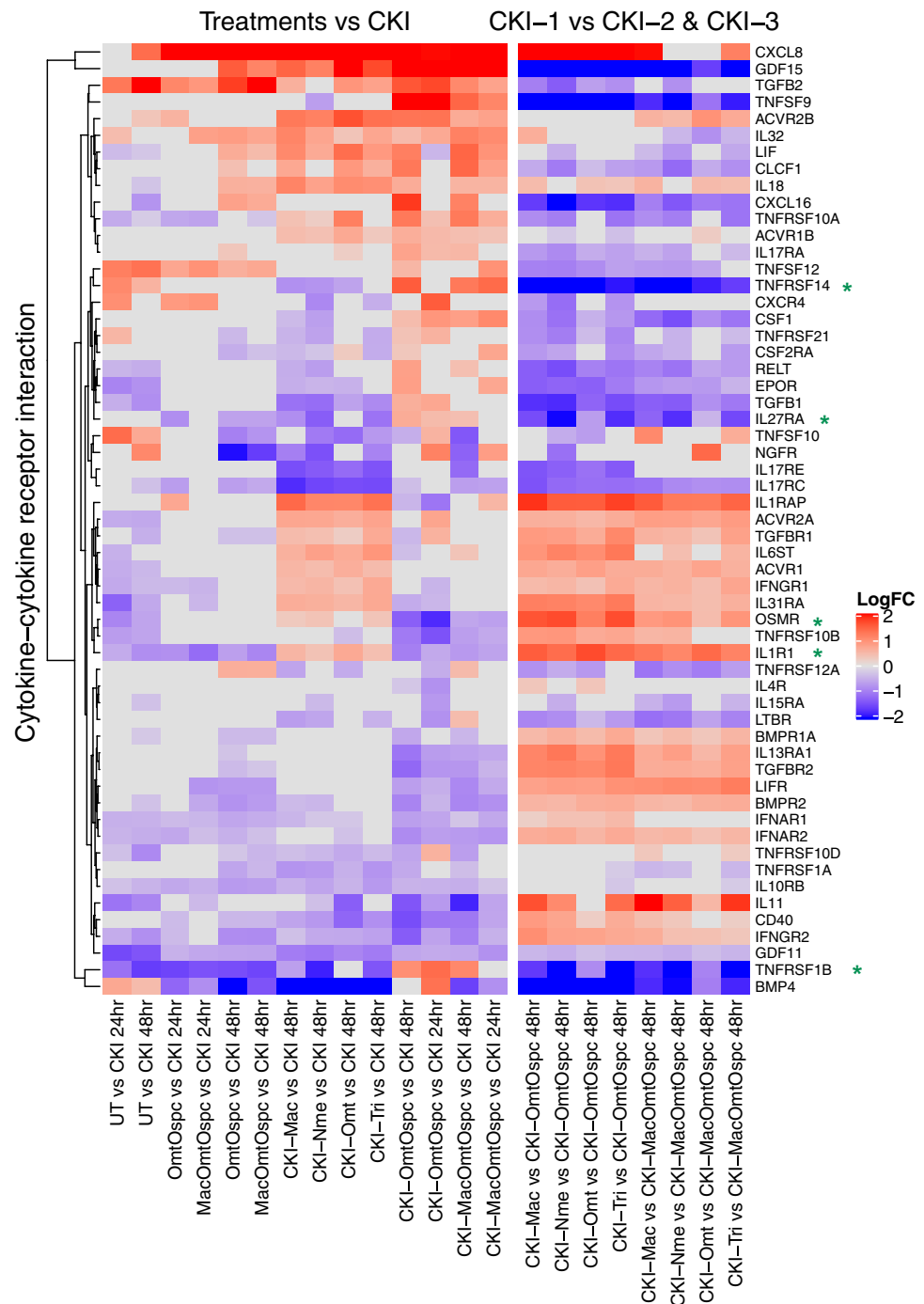


**Figure 6.** Differential gene expression profiles of all treatments for Cytokine-Cytokine Receptor pathway. The left panel shows comparison of subtractive fraction treated cells against CKI treatment and the right panel shows comparison of single compound subtractive fraction treated cells against the treatments for two and three compound subtractive fractions. Asterisks in green show a subset of genes that had opposite changes in gene expression across treatments.

this double compound deletion potentiated the cell killing effect of CKI we hypothesised that the compounds in CKI have multiple targets leading to a phenotypic effect that reflects the integration of stimulation and inhibition across all those targets. Removal of Omt and Ospc alters the balance of stimulation and inhibition leading to an integrated effect for the remaining compounds in the mixture that caused more cell death than CKI.

More detailed examination of some of these interactions within significantly perturbed pathways highlighted the gene-specific changes in expression for some key regulators of inflammation and the cell-cycle. Most effects on gene expression from deletion of single versus two compounds were similar, suggesting that the enhanced cell killing by CKI-OmtOspc was due to additive effects of the compound deletions. However, by comparing differences in pairwise comparisons between treatments at the gene level within the Cytokine-Cytokine Receptor

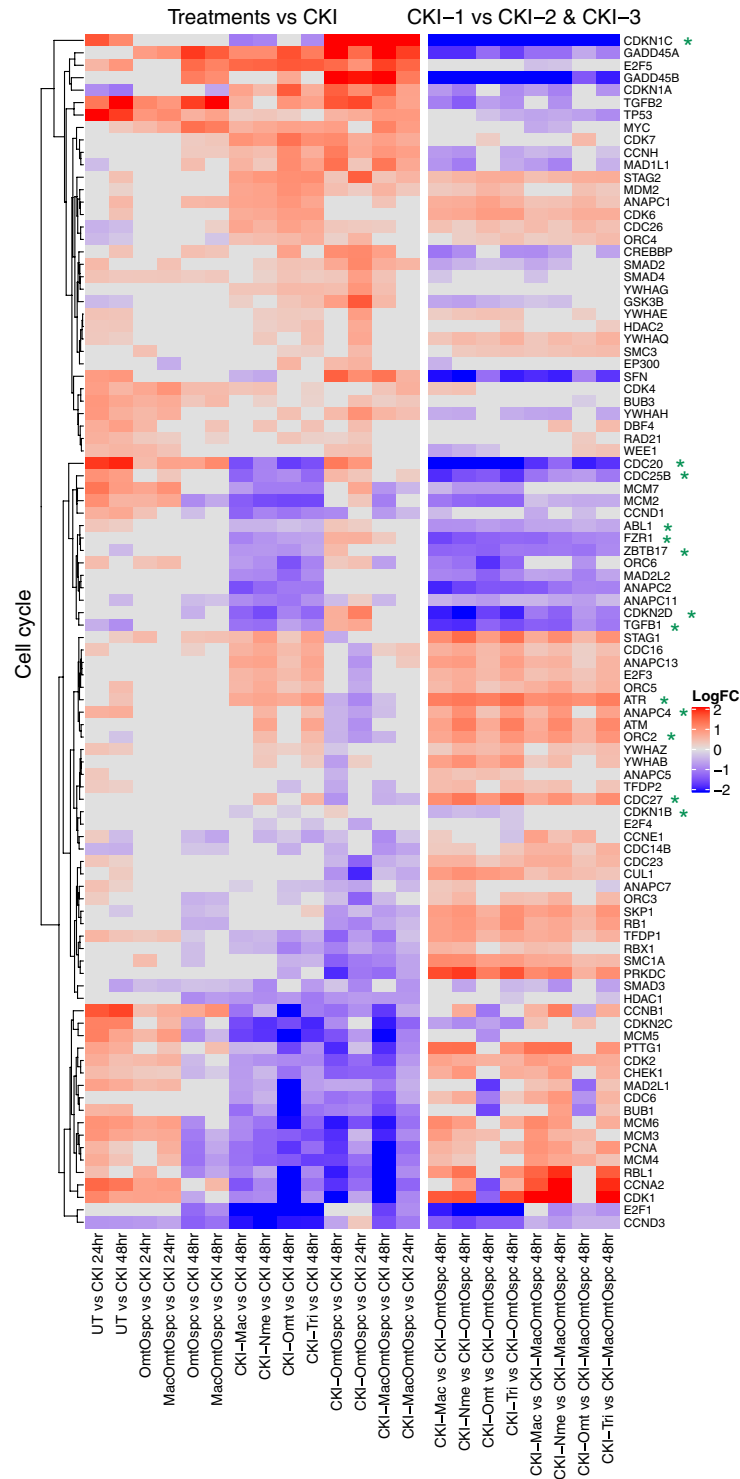


**Figure 7.** Differential gene expression profiles of all treatments for Cell-Cycle pathway. The left panel shows comparison of subtractive fraction treated cells against CKI treatment and the right panel shows comparison of single compound subtractive fraction treated cells against the treatments for two and three compound subtractive fractions. Asterisks in green show a subset of genes that have opposite changes in gene expression across treatments.

Interaction and Cell-Cycle pathways we identified a subset of genes that had opposite changes in gene expression when comparing single compound deletions to CKI-OmtOspc deletion. In the Cytokine-Cytokine Receptor Interaction pathway (Fig. 6 and Supplementary Figs 12–14), these genes are *IL1-R1* (Interleukin-1 Receptor), *IL-27RA* (Interleukin-27 Receptor alpha subunit), *TNFRSF1B* (Tumor Necrosis Factor Receptor Superfamily Member 1B), *TNFRSF14* (Tumor Necrosis Factor Receptor Superfamily, Member 14) and *OSMR* (Oncostatin M

Receptor/IL-31 Receptor Subunit Beta), and they all transduce inflammatory ligand signals to the NF- $\kappa$ B pathway and/or the apoptosis pathway. In the Cell-Cycle pathway (Fig. 7 and Supplementary Figs 15–17), these genes are *CDKN1C* (Cyclin-Dependent Kinase Inhibitor 1C (P57, Kip2)), *CDC25B* (Cell Division Cycle 25B), *ATR* (ATR Serine/Threonine Kinase), *CDKN1B* (Cyclin-Dependent Kinase Inhibitor 1B (P27, Kip1)), *CDKN2D* (Cyclin-Dependent Kinase Inhibitor 2D (P19, Inhibits CDK4)), *TGFBI* (Transforming Growth Factor Beta 1), *FZRI* (Fizzy And Cell Division Cycle 20 Related 1), *CDC20* (Cell Division Cycle 20), *CDC27* (Cell Division Cycle 27), *ORC2* (Origin Recognition Complex Subunit 2), *ANAPC4* (Anaphase Promoting Complex Subunit 4), *ZBTB17* (Zinc Finger And BTB Domain Containing 17) and, *ABL1* (ABL Proto-Oncogene 1, Non-Receptor Tyrosine Kinase). The opposite changes in gene expression stimulated by CKI-OmtOspc compared to CKI-1 subfractions provide support for the idea that multiple major compounds can have similar effects on specific genes but that the combination of Omt and Ospc can have synergistic and opposite effects on those same genes. This means that multiple compounds with overlapping targets (based on their structural similarities) can either reinforce a single outcome or exhibit unpredictable and opposite effects when combined.

Overall our results support the concept of multi-compound/multi-target interactions for plant extract-based drugs that contain many plant secondary metabolites. Biological effects of complex plant extracts may result from interactions of multiple compounds, with negligible effects from single compounds alone. This has implications for how we assess the functional evidence for such extracts.

## Discussion

Previous studies have demonstrated that CKI can alter the cell-cycle, induce apoptosis and reduce proliferation and migration in various cancer cell lines<sup>6,16–18</sup>. CKI also killed leukaemia cells via the Prdxs/ROS/Trx1 signalling pathway in an acute myeloid leukaemia patient-derived xenograft model and caused cell-cycle arrest in U937 leukaemia-derived cells<sup>19</sup>. Cell-cycle arrest by CKI at checkpoints is correlated with the induction of double strand breaks by CKI treatment<sup>20</sup>. In contrast to our experiments reported above, oxymatrine was previously shown to arrest the cell-cycle and induce apoptosis in human glioblastoma cells through EGFR/PI3K/Akt/mTOR signaling pathway<sup>21</sup> and inhibit the proliferation of laryngeal squamous cell carcinoma Hep-2 cells<sup>22</sup>. As shown in this report, oxymatrine or oxysophocarpine or combined OmtOspc treatment caused no significant change in cell viability, the cell-cycle or apoptosis, in agreement with prior work that showed oxymatrine and oxysophocarpine exerting no significant effect on apoptosis, cell-cycle or cell proliferation in HCT116 human colon cancer cells<sup>23</sup>.

The paradoxical result that removal of OmtOspc caused a striking increase in apoptosis is most simply explained by a model based on integrating effects of multiple compounds on many targets. The interactions between compounds in the mixture can be synergistic and antagonistic such that if two compounds are removed that have a synergistic effect that is antagonistic to the remainder of the mixture, the resulting depleted mixture will be dis-inhibited compared to CKI. This is illustrated by our studies and others that show single compounds alone had no or little effect compared to CKI. For instance, while CKI treatment resulted in increased DNA double strand breaks and affected the cell-cycle resulting in decreased cancer cell proliferation, oxymatrine alone exhibited only a small effect in the same assay<sup>20</sup>. Gao and colleagues also reported that oxysophocarpine at 4 mg/ml had no effect, oxymatrine at 4 mg/ml (\*P < 0.05) and CKI at 2 mg/ml (\*\*\*P < 0.001) significantly reduced the proliferation of hepatocellular carcinoma SMMC-7721 cells *in vitro*<sup>6</sup>. Although significant inhibition of proliferation by oxymatrine occurred, the concentration used in this experiment was ~8 times higher than that of oxymatrine in 2 mg/ml of CKI. These studies agree with our experimental outcomes that oxymatrine and oxysophocarpine individually had no or little effect compared to CKI treatment.

At the level of gene expression in our study, GO analysis indicated that genes for “cell-cycle checkpoint” were significantly enriched in cells treated with all fractionated mixtures or mixtures of Omt and Ospc. Consistent with other studies, our results also demonstrated that these compounds had little or no phenotypic effect on their own, but that when both were deleted, the remaining compounds unexpectedly had significantly greater effects on phenotype and gene expression. When examined in the context of specific pathways, treatment with OmtOspc or CKI-OmtOspc which had strikingly different effects on phenotype, had similar effects on the perturbation of the “Cytokine-Cytokine Receptor Interaction” pathway, the most commonly perturbed pathway seen in our analysis that CKI induced cytokines IL4 and IL10 in cancer patients with acute leukaemia<sup>24</sup> and administration of CKI significantly increased the levels of IgA, IgG, IgM, IL2, IL4 and IL10, and decreased the levels of IL6 and TNF- $\alpha$  in rats with induced gastric cancer<sup>25</sup>. In contrast to this observation, IL4 and IL10 levels were significantly decreased in transgenic mice treated with oxymatrine at a dose of 200 mg/kg<sup>26</sup>. In our experiment, we also observed that while CKI and many of the depleted fractions had significant effects on the genes in the “Cytokine-Cytokine Receptor Interaction” pathway, OmtOspc and MacOmtOspc had little effect on the genes in that pathway. The observation that many genes in the “Cytokine-Cytokine Receptor Interaction” pathway were not affected by OmtOspc and MacOmtOspc compared to deletion fractions confirmed that removal of compounds rather than treatment with single or a few compounds can be more informative of the role and significance of individual compounds as part of mixtures/extracts.

In summary, our approach allowed the identification of both synergistic and antagonistic interactions within the drug mixture. Viewed as a network where the compounds and the targets are nodes and the interactions between compounds and targets, and between targets are edges, it is clear that the edges (interactions) determine the overall effect of the compound mixture. By removing one or two compounds from a mixture, we can potentially perturb the target network(s) to either reduce the effect of the mixture for some outcome or potentiate it for another. We believe this approach may be of general use for the study of herbal medicines/extracts, avoiding failures that stem from exclusive reliance on the identification of a single compound that accounts for most of the biological activity in mixtures.

## Methods

**Cell lines.** MDA-MB-231 cells were purchased from the American Type Culture Collection (ATCC, VA, USA). HEK-293 and HFF were kindly provided by Prof. Andrea Yool (Medical School, University of Adelaide). Cells were cultured in Dulbecco's Modified Eagle's Medium (Thermo Fisher Scientific) with 10% Fetal bovine serum (Thermo Fisher Scientific) at 37 °C with 5% CO<sub>2</sub>.

**Compound fractionation by HPLC.** CKI (Batch No: 20170322, total alkaloid concentration of 26.5 mg/ml) was provided by Zhendong Pharmaceutical Co.Ltd (China). HPLC separation for CKI was achieved using a Shimadzu HPLC instrument (Japan) equipped with a photodiode-array UV-Vis detector with preparative C<sub>18</sub> column (5 µm, 250 × 10 mm) (CA, USA). The following mobile phase was used to fractionate the CKI mixture: 0.01 M ammonium acetate (adjusted to pH 8.0, solvent A) and acetonitrile + 0.09% trifluoroacetic acid (solvent B). The flow rate was 2 ml/min and a linear gradient was used as follows: 0 min, 100% A; 60 min, 65% A; 70 min, 100% A. The chromatogram was recorded from 200 nm to 280 nm, with monitoring at 215 nm. Samples were frozen and lyophilised using a Christ Alpha 1-2 LD lyophiliser (Martin Christ Gefriertrocknungsanlagen GmbH, Germany). CKI 1 ml was fractionated on HPLC column and whole reconstituted CKI (WRCKI) was generated by collecting all fractions. Three rounds of lyophilisation were performed to remove the solvents used during the HPLC fractionation process and final reconstitution for all samples was carried out using vehicle control buffer [MilliQ H<sub>2</sub>O containing 0.25% Tween 80 and 10 mM HEPES (Gibco, Life technologies, USA)] or MilliQ H<sub>2</sub>O buffered with 10 mM HEPES and adjusted to pH 6.8–7.0. For example, WRCKI-H was resuspended with equivalent volume 1 ml using MilliQ H<sub>2</sub>O buffered with 10 mM HEPES and adjusted to pH 6.8–7.0.

CKI was then processed to deplete single (CKI-1), double (CKI-2) and triple (CKI-3) compounds using HPLC by standardizing using nine compounds, namely Oxymatrine (Omt), Oxysophocarpine (Ospc), N-methylcytisine (Nme), Matrine (Mt), Sophocarpine (Spc), Trifolirhizin (Tri), Adenine (Ade), Sophoridine (Spr) (Beina Biotechnology Institute Co., Ltd, China), and Macrozamin (Mac) (Zhendong Pharmaceutical Co.Ltd, China) which were previously reported to be found in CKI. In single compound depletions (CKI-1), CKI-Omt for example, Oxymatrine peak between 26–28 minutes was removed and the remaining HPLC fractions were collected, lyophilised three times and reconstituted for further experiments. This procedure was applied to all CKI-1, CKI-2 and CKI-3 fractions. HPLC fractionation separated Minor (MN) and Major (MJ) peaks to determine the principal and secondary components. The MJ mixture contained the nine standard compounds mentioned above and MN contained the remaining CKI components. In addition, nine CKI-1 fractional deletions, nine CKI-2 fractional deletions and three CKI-3 fractional deletions were produced.

**Identification of reconstituted mixtures by liquid chromatography/mass spectrometry (LC-MS/MS).** Agilent 6230 TOF mass spectrometer was used to determine the concentration of the known compounds from the CKI and reconstituted CKI-OmtOspc and CKI-MacOmtOspc mixtures. 10 µl sample was injected with a flow rate of 0.8 ml/min, a gradient program of 0 min, 100% A; 25 min, 40% B; 35 min, 60% B; and solvents MilliQ H<sub>2</sub>O + 0.1% formic acid (solvent A) and acetonitrile + 0.1% formic acid (solvent B). The column used was C<sub>18</sub> (5 µm, 150 × 4.6 mm, Diamosnil, Dkimatech, China). The recovered contents of the samples were measured by spike-in compound cytosine. Gas phase ions were generated with an electrospray source, with key instrument parameters: gas temperature, 325; sheath gas temperature, 350; vCap, 3500; fragmentor, 175; acquisition range (m/z) 60–17000. Calibration curves for nine standard compounds containing various concentrations were shown in Supplementary Data.

**Cell viability assay.** 2,3-bis-(2-methoxy-4-nitro-5-sulfophenyl)-2H-tetrazolium-5-carboxanilide (XTT) and N-methyl dibenzopyrazine methyl sulfate (PMS) (50: 1, Sigma-Aldrich, St. Louis, MO, USA) assay was used to assess cell viability as described in Qu *et al.*<sup>16</sup>. Briefly, 8,000 cells in 50 µl of medium were plated in 96-well trays overnight prior to drug treatments in triplicate. On the following day, CKI (at a final concentration of 0.25, 0.5, 1 and 2 mg/ml total alkaloid) and fractionated mixtures (equivalent dilutions of CKI) were added. For example, dilution 1/13.25 is equal to CKI 2 mg/ml and equivalent 1/13.25 dilution was performed for all fractionated mixtures to achieve 2 mg/ml equivalent dilutions of CKI. Cells were subsequently treated with 50 µl of drug mixtures to provide final concentrations of 0.25, 0.5, 1 and 2 mg/ml of total alkaloids in 100 µl. Cell viability was then measured at 24- and 48-hour after drug treatment by the addition of 50 µl of XTT:PMS mixture (50: 1 ratio). An equal volume of medium and treating agents plus XTT: PMS was used to subtract the background optical density. The absorbance of each well was recorded using a Biotrack II microplate reader at 492 nm. The experiments were performed twice by each of three different operators and each experiment had three technical replicates.

**Annexin V/PI apoptosis assay.** Apoptosis resulting from treatment was determined using an Annexin V-FITC apoptosis detection kit (ThermoFisher Scientific) according to the manufacturer's protocol. Briefly, 4 × 10<sup>5</sup> cells were seeded in 6-well plates in triplicate overnight prior to treatment. On the following day, cells were treated with the agents as described for 24 and 48 hours. Data were acquired with a BD LSR Fortessa X20 (BD BioSciences, NJ, USA) flow cytometer, and FlowJo software (TreeStar Inc., OR, USA) was used to analyse the acquired data and produce percent apoptosis values.

**Cell-cycle assay.** Cell culture and drug treatments were performed as described above for cell-cycle analysis. A Propidium Iodide (PI) staining protocol<sup>27</sup> was used to detect the changes in cell-cycle as a result of treatment after 24 and 48 hours. The characteristics of stained cells were measured using a BD LSR Fortessa flow cytometer, and acquired data were analysed using FlowJo software. The experiments were performed twice by each of three different operators and each experiment had three technical replicates.



**Cytotoxicity assay.** Cells were seeded in 96-well plates at a density of  $2.5 \times 10^3$  cells per well in triplicate. CKI and fractionated mixtures at final concentrations of 1 mg/ml and 2 mg/ml were added to each well and after 24 hours of incubation and viable cells were measured using the Alamar Blue assay (Thermo Fisher Scientific).  $5 \mu\text{M}$  of Mercuric chloride (Sigma-Aldrich) was used as a positive control and wells without cells were set as a negative control in the same plate. The experiments were performed twice and each experiment had three technical replicates.

**Sample preparation and RNA sequencing.** Cells were plated in 6-well plates with a density of  $2 \times 10^5$  cells/well overnight prior to drug treatments. On the following day, CKI (at a final concentration of 2 mg/ml) and fractionated mixtures (equivalent dilutions of CKI) were added. Two batches of samples were prepared. In the first batch, cells were treated with CKI, CKI-OmtOspc and CKI-MacOmtOspc at 24- and 48-hour time-points in triplicates and in the second batch, cells were treated with CKI, CKI-Mac, CKI-Nme, CKI-Omt and CKI-Tri at 48-hour timepoint in triplicates along with 3 UT replicates in both batches. Total RNA was isolated by using PureLink™ RNA mini kit (Thermo Fisher Scientific) according to the manufacturer's instructions and the quantity and quality of RNA samples were determined using a Bioanalyzer at the Cancer Genome Facility of the Australian Cancer Research Foundation (Australia). RNA samples with RNA integrity number (RINs)  $> 7.0$  were sent to be sequenced at Novogene (China). Briefly, after QC were performed, mRNA was isolated using oligo (dT) beads and randomly fragmented by adding fragmentation buffer, followed by cDNA synthesis primed with random hexamers. Next, a custom second-strand synthesis buffer (Illumina), dNTPs, RNase H and DNA polymerase I were added for second-strand synthesis. After end repair, barcode ligation and sequencing adaptor ligation, the double-stranded cDNA library was size selected and PCR amplified. Sequencing was carried out on an Illumina HiSeq X platform with paired-end 150 bp reads.

**Transcriptome data processing.** FastQC (v0.11.4, Babraham Bioinformatics) was used to check the quality of raw reads before proceeding with downstream analysis. Trim\_galore (v0.3.7, Babraham Bioinformatics) with the parameters: `-stringency 5 -paired -fastqc_args` was used to trim adaptors and low-quality sequences. STAR (v2.5.3a) was then applied to align the trimmed reads to the reference genome (hg19, UCSC) with the parameters: `-outSAMstrandField intronMotif -outSAMattributes All -outFilterMismatchNmax 10 -seedSearch-StartLmax 30 -outSAMtype BAM SortedByCoordinate`<sup>28</sup>. Then, subread (v1.5.2) was used to generate read counts data with the following parameters `featureCounts -p -t exon -g gene_id`<sup>29</sup>. Significantly differentially expressed genes between all treatments and CKI were analysed and selected using edgeR (v3.22.3) with false discovery rate (FDR)  $< 0.05$ <sup>30</sup>.

Removal of unwanted variance (RUVs) package in R was applied to two different batches of transcriptome datasets to eliminate batch variance<sup>31</sup>. Pearson correlation coefficient between samples with the same treatments (CKI and UT at 48-hour) of two batches were analysed to confirm the variances were minimal between two batches. Three replicates of UT from each batch (UT 48; Batch1 and UT 48S; Batch2) and CKI treated samples from each batch (CKI 48; Batch1 and CKI 48S; Batch2) at 48-hour time point were combined in order for the two batches of RNA-Seq samples to be processed in one single analysis. CKI treatment was used as a baseline to compare with all other treatments in order to emphasize the effect of depleted compounds. Analyses of Phylogenetics and Evolution (APE) was used to cluster the treatments<sup>32</sup> followed by RUV. GO and KEGG over-representation analyses were performed using clusterProfiler with the parameters `ont = "BP" (Biological Process)`, `pAdjust-Method = "BH"`, `pvalueCutoff = 0.01`, and `qvalueCutoff = 0.05`<sup>33,34</sup>. Signalling Pathway Impact Analysis (SPIA) was carried out to identify the commonly perturbed pathways within the treatments using the SPIA R package<sup>35</sup>. KEGG database used is the public domain version (KEGG data for SPIA analysis was downloaded from KEGG's website on: 09/07/2012) that is released as part of SPIA. Significantly perturbed pathways were visualised using Pathview package in R<sup>36</sup>.

**Statistical analysis.** Statistical analyses were carried out using GraphPad Prism 8.0 (GraphPad Software Inc., CA, USA). Student's t-test or ANOVA (one-way or two-way) was used when there were two or three groups to compare respectively. Post hoc "Bonferroni's multiple comparisons test" was performed when ANOVA results were significant. Statistically significant results were represented as (\*)  $P < 0.05$  or (\*\*)  $P < 0.01$  or (\*\*\*)  $P < 0.001$  or (\*\*\*\*)  $P < 0.0001$ ; ns (not significant). All data were shown as mean  $\pm$  standard deviation (SD).

**Declaration of transparency and scientific rigour.** This declaration acknowledges that this paper adheres to the principles for transparent reporting and scientific rigour of preclinical research recommended by funding agencies, publishers and other organisations engaged with supporting research.

### Data Availability

All raw data and the processed data (gene row count (logCPM)) obtained in this study were deposited in the National Center for Biotechnology Information (NCBI) Gene Expression Omnibus (GEO) with the Superseries accession number GSE125743, available at <https://www.ncbi.nlm.nih.gov/geo/query/acc.cgi?acc=GSE125743>.

### References

1. Harvey, A. L., Edrada-Ebel, R. & Quinn, R. J. The re-emergence of natural products for drug discovery in the genomics era. *Nature Reviews Drug Discovery* **14**, 111 (2015).
2. Ma, Y. *et al.* Identification and determination of the chemical constituents in a herbal preparation, Compound Kushen injection, by HPLC and LC-DAD-MS/MS. *Journal of Liquid Chromatography & Related Technologies* **37**, 207–220 (2014).
3. Xu, G. *et al.* Attenuation of acute lung injury in mice by oxymatrine is associated with inhibition of phosphorylated p38 mitogen-activated protein kinase. *Journal of ethnopharmacology* **98**, 177–183 (2005).

4. Cheng, H. *et al.* Matrine improves 2,4,6-trinitrobenzene sulfonic acid-induced colitis in mice. *Pharmacological research* **53**, 202–208 (2006).
5. Jiang, J., Wu, F., Lu, J., Lu, Z. & Xu, Q. Anti-inflammatory activity of the aqueous extract from rhizoma smilacis glabrae. *Pharmacological research* **36**, 309–314 (1997).
6. Gao, L. *et al.* Uncovering the anticancer mechanism of Compound Kushen Injection against HCC by integrating quantitative analysis, network analysis and experimental validation. *Scientific reports* **8**, 624 (2018).
7. Wu, C. *et al.* Oxymatrine inhibits the proliferation of prostate cancer cells *in vitro* and *in vivo*. *Molecular medicine reports* **11**, 4129–4134 (2015).
8. Cai, Y. *et al.* HMGB1-mediated autophagy decreases sensitivity to oxymatrine in SW982 human synovial sarcoma cells. *Scientific reports* **6**, 37845 (2016).
9. Zhou, Y. J., Guo, Y. J., Yang, X. L. & Ou, Z. L. Anti-Cervical Cancer Role of Matrine, Oxymatrine and Sophora Flavescens Alkaloid Gels and its Mechanism. *Journal of Cancer* **9**, 1357 (2018).
10. Aung, T. N., Qu, Z., Kortschak, R. D. & Adelson, D. L. Understanding the effectiveness of natural compound mixtures in cancer through their molecular mode of action. *International journal of molecular sciences* **18**, 656 (2017).
11. Wu, L. *et al.* Synthesis and biological evaluation of matrine derivatives containing benzo- $\alpha$ -pyrone structure as potent anti-lung cancer agents. *Scientific reports* **6**, 35918 (2016).
12. Li, H. *et al.* Matrine inhibited proliferation and increased apoptosis in human breast cancer MCF-7 cells via upregulation of Bax and downregulation of Bcl-2. *International Journal of Clinical and Experimental Pathology* **8**, 14793 (2015).
13. Yu, P. *et al.* Matrine suppresses breast cancer cell proliferation and invasion via VEGF-Akt-NF- $\kappa$ B signaling. *Cytotechnology* **59**, 219–229 (2009).
14. Wang, X. & Yang, R. Movement disorders possibly induced by traditional Chinese herbs. *European neurology* **50**, 153–159 (2003).
15. Yuan, F. *et al.* Effects of matrine and oxymatrine on catalytic activity of cytochrome P450s in rats. *Basic & clinical pharmacology & toxicology* **107**, 906–913 (2010).
16. Qu, Z. *et al.* Identification of candidate anti-cancer molecular mechanisms of compound kushen injection using functional genomics. *Oncotarget* **7**, 66003 (2016).
17. Xu, W. *et al.* Compound Kushen Injection suppresses human breast cancer stem-like cells by down-regulating the canonical Wnt/ $\beta$ -catenin pathway. *J Exp Clin Cancer Res* **30**, 103 (2011).
18. Nourmohammadi, S. *et al.* Effect of Compound Kushen Injection, a natural compound mixture, and its identified chemical components on migration and invasion of colon, brain and breast cancer cell lines. *Frontiers in oncology* **9**, 314 (2019).
19. Jin, Y. *et al.* Compound kushen injection suppresses human acute myeloid leukaemia by regulating the Prdxs/ROS/Trx1 signalling pathway. *Journal of Experimental & Clinical Cancer Research* **37**, 277 (2018).
20. Cui, J. *et al.* Cell cycle, energy metabolism and DNA repair pathways in cancer cells are suppressed by Compound Kushen Injection. *BMC cancer* **19**, 103 (2019).
21. Dai, Z. *et al.* Oxymatrine induces cell cycle arrest and apoptosis and suppresses the invasion of human glioblastoma cells through the EGFR/PI3K/Akt/mTOR signaling pathway and STAT3. *Oncology reports* **40**, 867–876 (2018).
22. Ying, X.-J. *et al.* Oxymatrine downregulates HPV16E7 expression and inhibits cell proliferation in laryngeal squamous cell carcinoma Hep-2 cells *in vitro*. *BioMed research international* **2015** (2015).
23. Zhang, L., Zheng, Y., Deng, H., Liang, L. & Peng, J. Aloperine induces G2/M phase cell cycle arrest and apoptosis in HCT116 human colon cancer cells. *International journal of molecular medicine* **33**, 1613–1620 (2014).
24. Tu, H. *et al.* Efficacy of compound kushen injection in combination with induction chemotherapy for treating adult patients newly diagnosed with acute leukemia. *Evidence-Based Complementary and Alternative Medicine* **2016** (2016).
25. Zhou, S.-K., Zhang, R.-L., Xu, Y.-F. & Bi, T.-N. Antioxidant and immunity activities of fufang kushen injection liquid. *Molecules* **17**, 6481–6490 (2012).
26. DONG, Y. *et al.* Effects of oxymatrine on the serum levels of T helper cell 1 and 2 cytokines and the expression of the S gene in hepatitis B virus S gene transgenic mice: A study on the anti-hepatitis B virus mechanism of oxymatrine. *Journal of gastroenterology and hepatology* **17**, 1299–1306 (2002).
27. Riccardi, C. & Nicoletti, I. Analysis of apoptosis by propidium iodide staining and flow cytometry. *Nature protocols* **1**, 1458 (2006).
28. Dobin, A. *et al.* STAR: ultrafast universal RNA-seq aligner. *Bioinformatics* **29**, 15–21 (2013).
29. Liao, Y., Smyth, G. K. & Shi, W. featureCounts: an efficient general purpose program for assigning sequence reads to genomic features. *Bioinformatics* **30**, 923–930 (2013).
30. Robinson, M. D., McCarthy, D. J. & Smyth, G. K. edgeR: a Bioconductor package for differential expression analysis of digital gene expression data. *Bioinformatics* **26**, 139–140 (2010).
31. Risso, D., Ngai, J., Speed, T. P. & Dudoit, S. Normalization of RNA-seq data using factor analysis of control genes or samples. *Nature biotechnology* **32**, 896 (2014).
32. Paradis, E., Claude, J. & Strimmer, K. APE: analyses of phylogenetics and evolution in R language. *Bioinformatics* **20**, 289–290 (2004).
33. Yu, G., Wang, L.-G., Han, Y. & He, Q.-Y. clusterProfiler: an R package for comparing biological themes among gene clusters. *OmicS: a journal of integrative biology* **16**, 284–287 (2012).
34. Kanehisa, M., Sato, Y., Furumichi, M., Morishima, K. & Tanabe, M. New approach for understanding genome variations in KEGG. *Nucleic acids research* **47**, D590–D595 (2018).
35. Tarca, A., Kathri, P. & Draghici, S. SPIA: Signaling Pathway Impact Analysis (SPIA) using combined evidence of pathway over-representation and unusual signaling perturbations. *R package version 2.36.0* (2019).
36. Luo, W. & Brouwer, C. Pathview: an R/Bioconductor package for pathway-based data integration and visualization. *Bioinformatics* **29**, 1830–1831 (2013).

## Acknowledgements

This work was supported by the special international corporation project of Traditional Chinese Medicine (GZYYGJ2017035) and The University of Adelaide, Zhendong Australia China Centre for Molecular Chinese Medicine. T.N.A. would like to thank Dr. Denis Scanlon and Associate Prof. Stephen Bell for assistance with HPLC usage, Jue Zhang for valuable discussions and Tyler MacNeil for proof reading and suggestions.

## Author Contributions

T.N.A., S.N., Z.Q. and D.L.A. designed the study, analysed the data and wrote the manuscript. T.N.A. and S.N. conducted the experiments. Y.H.-L., J.C., H.S., A.J.Y., T.P. and H.D. assisted with the experiments and analysed the data. A.J.Y. and R.D.K. assisted in writing the manuscript. W.W. provided CKI and essential information and characterisation of CKI composition.

## Additional Information

**Supplementary information** accompanies this paper at <https://doi.org/10.1038/s41598-019-50271-4>.

**Competing Interests:** The authors declare no conflicts of interest. We wish to draw the attention of the Editor to the following facts which may be considered as apparent conflicts of interest and to significant financial contributions to this work. While a generous donation was used to set up the Zhendong Centre by Shanxi - Zhendong Pharmaceutical Co Ltd, they did not determine the research direction for this work, influence the analysis of the data or influence the writing of the paper. T.N.A: no competing interests, S.N. no competing interests, Z.Q. no competing interests, Y.H.L. no competing interests, J.C. no competing interests, H.Y.S. no competing interests, A.J.Y. no competing interests, T.P. no competing interests, H.D. no competing interests, R.D.K. no competing interests, W.W. is an employee of the Zhendong Research Institute seconded to Zhendong Centre to learn bioinformatics methods and provide technical advice regarding CKI., D.L.A. Director of the Zhendong Centre which was set up with a generous donation from the Zhendong Pharmaceutical Co Ltd. Zhendong Pharmaceutical has had no control over these experiments, their design or analysis and have not exercised any editorial control over the manuscript.

**Publisher's note** Springer Nature remains neutral with regard to jurisdictional claims in published maps and institutional affiliations.



**Open Access** This article is licensed under a Creative Commons Attribution 4.0 International License, which permits use, sharing, adaptation, distribution and reproduction in any medium or format, as long as you give appropriate credit to the original author(s) and the source, provide a link to the Creative Commons license, and indicate if changes were made. The images or other third party material in this article are included in the article's Creative Commons license, unless indicated otherwise in a credit line to the material. If material is not included in the article's Creative Commons license and your intended use is not permitted by statutory regulation or exceeds the permitted use, you will need to obtain permission directly from the copyright holder. To view a copy of this license, visit <http://creativecommons.org/licenses/by/4.0/>.

© The Author(s) 2019

# Chapter 3


## Effect of Compound Kushen Injection, a Natural Compound Mixture, and its identified Chemical Components on Migration and Invasion of Colon, Brain, and Breast Cancer Cell Lines

As a result of previous work that showed that CKI significantly disrupted the cell cycle and induced apoptosis in breast cancer cells, I hypothesized that CKI might also cause a previously unrecognized inhibition of cancer cell migration and invasion. Effects of CKI on migration were tested using the complete mixture, fractionated subsets, and single identified chemical components in various cell lines. Fractionation and reconstitution experiments showed that multiple compounds in CKI are required to inhibit cell migration. Transcriptomic analyses of the cancer cells after CKI-treatment indicated down-regulation of gene expression for actin cytoskeleton and focal adhesion pathways, consistent with the observed impairment of cell migration by CKI. Work here identifies the pharmacological complexity of CKI as an important feature of its effectiveness in blocking migration and invasion of cancer cells. This chapter is published in *Frontiers in Oncology*. Specific Aim1: To fractionate and reconstitute CKI in order to determine the effects on cell migration of reconstituted mixtures as compared to complete CKI in various cancer and non-cancer cell lines. Specific Aim2: To identify the molecular pathways associated with the inhibition of cell migration by CKI and CKI fractions.

# Statement of Authorship

Title of Paper	Effect of Compound Kushen Injection, a natural compound mixture, and its identified chemical components on migration and invasion of colon, brain and breast cancer cell lines
Publication Status	<input checked="" type="checkbox"/> Published <input type="checkbox"/> Accepted for Publication <input type="checkbox"/> Submitted for Publication <input type="checkbox"/> Unpublished and Unsubmitted work, written in manuscript style
Publication Details	Nourmohammadi S, Nwe Aung T, Cui j, Pei JV, Kourghi M, De Ieso ML, Harata-Lee Y, Qu Z, Adelson DL and Yool AJ.

## Principal Author


Name of Principal Author (Candidate)	Mr. Saeed Nourmohammadi and Dr. Thazin Nwe Aung	
Contribution to the Paper	First author. Designed and carried out the experiments, analysed data and wrote the manuscript. *Other co-authors signed the statement of authorship in the previous version. Please see Dr Aung's Thesis, titled: Molecular Mechanisms of Natural Compounds: Compound Kushen Injection (CKI) in Cancer, Chapter 3".	
Overall percentage (%)	75%	
Certification:	This paper reports on original research I conducted during the period of my Higher Degree by Research candidature and is not subject to any obligations or contractual agreements with a third party that would constrain its inclusion in this thesis. I am the primary author of this paper.	
Signature		Date 07/07/2022


10/07/2022

## Co-Author Contributions

By signing the Statement of Authorship, each author certifies that:

- the candidate's stated contribution to the publication is accurate (as detailed above);
- permission is granted for the candidate to include the publication in the thesis; and
- the sum of all co-author contributions is equal to 100% less the candidate's stated contribution.

Name of Co-Author	Professor David L. Adelson	
Contribution to the Paper	Supervised the research, assisted the research with funding, experimental design and wrote the manuscript.	
Signature		Date 13/07/2022

Name of Co-Author	Professor Andrea J. Yool	
Contribution to the Paper	Supervised the research, assisted the research with funding, experimental design and wrote the manuscript.	
Signature		Date 8 Jul 2022

Please cut and paste additional co-author panels here as required.



# Effect of Compound Kushen Injection, a Natural Compound Mixture, and Its Identified Chemical Components on Migration and Invasion of Colon, Brain, and Breast Cancer Cell Lines

## OPEN ACCESS

### Edited by:

Jiangjiang Qin,  
Zhejiang Chinese Medical  
University, China

### Reviewed by:

Ying Wang,  
University of Macau, China  
Gang Cao,  
Zhejiang Chinese Medical  
University, China  
Songwei Duan,  
Harvard University, United States

### \*Correspondence:

David L. Adelson  
david.adelson@adelaide.edu.au  
Andrea J. Yool  
andrea.yool@adelaide.edu.au

<sup>†</sup> These authors have contributed  
equally to this work and are co-first  
authors

### Specialty section:

This article was submitted to  
Pharmacology of Anti-Cancer Drugs,  
a section of the journal  
Frontiers in Oncology

**Received:** 14 February 2019

**Accepted:** 08 April 2019

**Published:** 26 April 2019

### Citation:

Nourmohammadi S, Aung TN, Cui J,  
Pei JV, De Ieso ML, Harata-Lee Y,  
Qu Z, Adelson DL and Yool AJ (2019)  
Effect of Compound Kushen Injection,  
a Natural Compound Mixture, and Its  
Identified Chemical Components on  
Migration and Invasion of Colon,  
Brain, and Breast Cancer Cell Lines.  
*Front. Oncol.* 9:314.  
doi: 10.3389/fonc.2019.00314

Saeed Nourmohammadi<sup>1†</sup>, Thazin Nwe Aung<sup>2†</sup>, Jian Cui<sup>2</sup>, Jinxin V. Pei<sup>1</sup>,  
Michael Lucio De Ieso<sup>1</sup>, Yuka Harata-Lee<sup>2</sup>, Zhipeng Qu<sup>2</sup>, David L. Adelson<sup>2\*</sup> and  
Andrea J. Yool<sup>1\*</sup>

<sup>1</sup> Adelaide Medical School, The University of Adelaide, Adelaide, SA, Australia, <sup>2</sup> Department of Molecular and Biomedical Science, School of Biological Sciences, The University of Adelaide, Adelaide, SA, Australia

Traditional Chinese Medicines are promising sources of new agents for controlling cancer metastasis. Compound Kushen Injection (CKI), prepared from medicinal plants *Sophora flavescens* and *Heterosmilax chinensis*, disrupts cell cycle and induces apoptosis in breast cancer; however, effects on migration and invasion remained unknown. CKI, fractionated mixtures, and isolated components were tested in migration assays with colon (HT-29, SW-480, DLD-1), brain (U87-MG, U251-MG), and breast (MDA-MB-231) cancer cell lines. Human embryonic kidney (HEK-293) and human foreskin fibroblast (HFF) served as non-cancerous controls. Wound closure, transwell invasion, and live cell imaging showed CKI reduced motility in all eight lines. Fractionation and reconstitution of CKI demonstrated combinations of compounds were required for activity. Live cell imaging confirmed CKI strongly reduced migration of HT-29 and MDA-MB-231 cells, moderately slowed brain cancer cells, and had a small effect on HEK-293. CKI uniformly blocked invasiveness through extracellular matrix. Apoptosis was increased by CKI in breast cancer but not in non-cancerous lines. Cell viability was unaffected by CKI in all cell lines. Transcriptomic analyses of MDA-MB-231 indicated down-regulation of actin cytoskeletal and focal adhesion genes with CKI treatment, consistent with observed impairment of cell migration. The pharmacological complexity of CKI is important for effective blockade of cancer migration and invasion.

**Keywords:** traditional chinese medicine (TCM), compound kushen injection (CKI), cell migration, invasion, cancer, gene regulatory networks, alternative medicine

## INTRODUCTION

Cancer progression results from uncontrolled migration of cells away from the primary tumor, intravasation into lymphatic or vascular circulation, invasion into secondary tissues and the formation of metastasized tumors (1, 2) which are the main cause of cancer-related deaths (3–5). Migrating cells generate a driving force for cell motility based on the extension of filipodia and

lamellipodia using actin polymerization at the leading edges of the cell (6). New approaches for enhancing cancer treatment by impairing cell migration and metastasis might offer promise for curing patients with malignancies. Combinations of anticancer therapeutic regimens that not only reduce cell proliferation but also limit metastasis would be advantageous (7–9).

Herbal medicines are used in complementary and traditional medicines (10–12). Traditional Chinese medicine (TCM) relies on natural product extracts containing complex mixtures of components, suggested to deliver therapeutic benefit to individuals suffering from non-small cell lung cancer, liver, breast, and colorectal cancers (10, 13, 14). The inherent complexity of TCM suggests principle components might act in concert with adjuvant components, explaining an apparent synergy in therapeutic benefits seen from the whole extract as compared to individual compounds (15). Modulation of multiple regulatory signaling targets has been proposed as essential for the anti-proliferative, anti-migratory and anti-metastatic properties of TCMs (16, 17).

Compound Kushen Injection (CKI) has been used in combination with chemotherapies such as oxaliplatin and 5-fluorouracil in China since 1995 for the treatment of gastric, liver and non-small cell lung carcinomas (18). Composed of alkaloids, flavonoids, organic acids and saccharides (19), CKI has been reported to boost immunity, decrease inflammation, and decrease metastasis (20), for example by repressing RNA markers associated with tumor metastasis in MCF-7 cells (17, 18), and impairing migration in hepatocellular carcinoma cells (21). The challenge for defining mechanisms of action of TCMs such as CKI is to understand the differential activities of chemical components not only singly but in combination, recognizing the likely involvement of multiple gene expression and signaling pathways in the beneficial outcomes (22).

Work here is the first to show that CKI and defined chemical fractions slow cancer cell migration and invasion, and to use systems biology to identify sets of genes linked to cell migration that are regulated by CKI treatment. Differential expression of genes in the actin cytoskeleton and focal adhesion pathways supports the idea that the therapeutic activity of CKI in humans involves a serendipitous combination of effects on cancer cell properties.

## MATERIALS AND METHODS

### Cell Lines

MDA-MB-231, HT-29, SW-480, DLD-1, U-87 MG, U-251 MG, and HEK-293 were purchased from the American Type Culture Collection (ATCC, Manassas, VA) and human foreskin fibroblast (HFF) was kindly provided by Dr. Eric Smith (Basil Hetzel Institute, The Queen Elizabeth Hospital, SA, Australia). DLD-1 cells were grown in RPMI (Roswell Park Memorial Institute) culture medium (Thermo Fisher Scientific, MA, USA) with 10 % fetal bovine serum (FBS, Thermo Fisher Scientific). All other cell lines were cultured in Dulbecco Modified Eagle Medium (DMEM, Thermo Fisher Scientific) with 10 % FBS, except for HFF (which contained 15 % FBS), at 37°C in 5 % CO<sub>2</sub>.

### CKI Preparation and Other Chemicals

CKI (Batch No: 20170322, total alkaloid concentration of 25 mg/ml) was obtained from Zhendong Pharmaceutical Co. Ltd (Shanxi, China). High performance liquid chromatography (HPLC) fractionation and liquid chromatography-mass spectrometry (LC-MS/MS) were used to analyse single compounds and confirm their concentrations in CKI. Fractionation of CKI was done by using Shimadzu HPLC SPC-M20A photodiode-array UV-Vis detector (Japan) equipped with a C<sub>18</sub> column (5 μm, 250 × 10 mm; Phenomenex, CA, USA), with methods for fractionation and concentration determinations as described previously (23) (**Supplementary Images 2, 3**). The nine compounds comprising the major fraction (MJ): oxymatrine, oxysophocarpine, n-methylcytisine, matrine, sophocarpine, trifolirhizin, adenine, and sophoridine were purchased as isolated compounds from Beina Biotechnology Institute Co., Ltd (Shanxi, China), and macrozamin was obtained from Zhendong Pharmaceutical Co. Ltd (Beijing, China). Two-fold serial dilutions from 2 mg/ml through to 0.25 mg/ml of total alkaloids in CKI, as well as equivalent dilutions of the MJ and minor (MN) fractions were used for bioassay experiments on the cancer and non-cancerous cell lines and compared with effects of vehicle control treatments; 0.25% Tween 80 (Sigma-Aldrich, MO, USA) and 10 mM HEPES (Thermo Fisher Scientific) in the same cell lines.

### Circular Wound Closure Assay

Two-dimensional (2D) cell migration was measured using circular wound closure rates (24). CKI-based and vehicle control treatments were applied in low serum DMEM, with the mitotic inhibitor 5-fluoro-2'-deoxyuridine (FUDR). Initial wound areas were imaged at 0 h (10x objective) with a Canon EOS 6D camera (Canon, Tokyo, Japan) on an Olympus inverted microscope (Olympus Corp., Tokyo, Japan); XnConvert software was used to standardize the images. NIH ImageJ software (U.S. National Institutes of Health, MD, USA) was used to quantify wound areas at 0 h and at a second timepoint (18–24 h), set for each cell line to ensure wounds were not completely closed. Experiments were independently repeated three times, with four to eight replicates.

### Transwell Invasion Assay

Invasion assays were performed in 24-well transwell inserts (6.5 mm, 8 μm pore size; Corning® Transwell polycarbonate; Sigma-Aldrich). The upper surface of the filter was layered with extracellular matrix (ECM) gel from Sigma-Aldrich (at dilutions empirically optimized for each cell line; **Supplementary Table 2**), allowed to dry overnight, and rehydrated with 50 μl of serum-free media per insert for 1 h prior to cell seeding. Cultures were grown to 40% confluence and then starved in medium with 2% FBS serum for 24 h prior to seeding. Cells were detached (at ≤ 80% confluency) and resuspended in serum-free culture media (**Supplementary Table 2**). Cells were then seeded in transwell inserts (total 150 μl of cell suspension per transwell, including 50 μl of rehydration medium added earlier) at appropriate number of cells per well in the presence of CKI, MN or MJ at 2 mg/ml, or vehicle control medium. The chemoattractant gradient was created with 700 μl of culture medium (containing the

relevant CKI-based or vehicle treatment), with 5, 10, or 15% FBS for HEK-293, cancerous cells, or HFF, respectively. Depending on invasion characteristics, cells from each line were incubated for an optimized time period ranging from 5 to 24 h at 37°C in 5% CO<sub>2</sub>. Non-invasive cells were scraped from the upper surface of the filter with a cotton swab; migrated cells on the bottom surface were counted after staining with crystal violet (Sigma-Aldrich). The average number of invasive cells was calculated from four randomly selected fields (x100 magnification). Cell counts were normalized to numbers in the vehicle control treatment. Three independent experiments were carried out with two replicates.

### Cytotoxicity Assay

Cell viability was measured with the Alamar Blue assay (25) according to the manufacturer's instructions (Thermo Fisher Scientific). Cells were seeded in 96-well plates in media with 2% FBS and FUDR. After overnight incubation, treatments were applied, and cultures were incubated for 24 h. After application of 10% Alamar Blue solution (30–90 min), fluorescence was measured by using FLUOstar Optima microplate reader. Mercuric chloride (2.5 mM) served as a positive control, inducing cytotoxic cell death. A control sample with medium and treatment agent only (no cells) was included for background color subtraction.

### Apoptosis Assay

Apoptosis assays based on annexin V and propidium iodide staining were performed as described previously (17). Briefly, MDA-MB-231, HEK-293 and HFF cells were seeded in 6-well trays and treated with 2 mg/ml of CKI. After 24 h of treatment, cells were harvested, and levels of apoptotic cells were measured using the Annexin V-FITC detection kit (Thermo Fisher Scientific) according to the manufacturer's guidelines. Cells were acquired on a LSRFortessa X-20 (BD Biosciences, NJ, USA) and data were analyzed using FlowJo software (TreeStar Inc., OR, USA).

### Live Cell Imaging

Cells in 96 well-plates were cultured to 80 % confluency, then serum-starved for 12–18 h in optimal culture media with 2% FBS and 400 nM FUDR. Wounds were created as circular lesions in the confluent monolayers, and treatments were added as described for the circular wound closure assay above. Plates were placed in an enclosed humidified chamber at 37°C with 5% CO<sub>2</sub> for 20 h, and images were acquired at 10-min intervals with a Nikon Ti E Live Cell Microscope (Nikon, Tokyo, Japan) using Nikon NIS-Elements software. Time-lapse movies as AVI files were exported from NIS-Elements. ImageJ (U.S. National Institutes of Health) was used to convert the exported files into TIFF files and converted files were then analyzed using Fiji software (26).

### Immunofluorescence Labeling and Confocal Microscopy

Cells were plated in  $\mu$ -Plate 8 Well dishes (Ibidi, Munich, Germany), in 2 % FBS with FUDR 400 nM in optimal culture media and incubated 12–18 h at 37°C in 5% CO<sub>2</sub>. The following

day, 2 mg/ml of CKI, MN, MJ or vehicle control treatments were applied, and cells were incubated for 24 h. After washing with phosphate-buffered saline (PBS), cells were fixed in 4 % paraformaldehyde (at room temperature for 10–30 min), rinsed 2–3 times with PBS, and permeabilized with 200  $\mu$ l of 0.1% Triton X-100 in PBS (3–5 min at room temperature). After 2–3 washes with PBS, Phalloidin-iFluor 488 Reagent CytoPainter (ab176753; Abcam, MA, USA) at 200  $\mu$ l per well was used to stain F-actin cytoskeleton (room temperature in the dark for 1–2 h) and washed again 2–3 times with PBS. Cell nuclei were labeled with 200  $\mu$ l of 1:1,000 Hoechst stain (cat # 861405; Sigma-Aldrich) for 5–10 min. Cells were visualized using a SP5 laser scanning confocal microscope (Leica, Germany).

### Pathway Enrichment Analysis of Migratory Genes Affected by CKI

RNA-seq (RNA-sequencing) data (23) of MDA-MB-231 cells treated with CKI were used to identify cell migration genes affected by CKI. Gene Ontology (GO) enrichment analyses were carried out with R package clusterProfiler 3.8.0 (10). The following parameters for GO enrichment analysis were used: biological process at the third level; right-sided hypergeometric test; and Benjamini-Hochberg method to correct *p*-values. *P*-value cutoff 0.05 and FDR (false discovery rate) 0.1 values were used to identify significantly over-represented GO terms. Pathways that were significantly perturbed by CKI treatment were identified with Signaling Pathway Impact Analysis (SPIA) (27), and visualized using the pathview package in R (28). KEGG (Kyoto Encyclopedia of Genes and Genomes) functional analysis was performed with R package clusterProfiler 3.8.0 (10) and OmicCircos v 1.18.0 (29). Venn diagrams were generated using an online tool (<http://bioinformatics.psb.ugent.be/webtools/Venn/>).

### Intracellular Protein Staining and Quantification by Flow Cytometry

Cells cultured in 6-well trays were treated with CKI, MN or MJ as described above, harvested after 24 h, fixed and permeabilized using Nuclear Factor Fixation and Permeabilization Buffer Set (Biolegend, CA, USA) according to the manufacturer's instructions.  $2 \times 10^5$  cells were labeled with rabbit anti-Cyclin D1 (CCND1) (92G2, Cell Signaling Technologies, MA USA), rabbit anti- $\beta$ -actin (ACTB) (D6A8, Cell Signaling Technologies), rabbit anti-protein kinase B (AKT1, 2, 3) (Ab32505, Abcam) or rabbit IgG isotype control (Cell Signaling Technologies), and these antibodies were detected with anti-rabbit IgG-PE (Cell Signaling Technologies). For detection of  $\beta$ -catenin, rabbit anti- $\beta$ -catenin (CTNNB1)-Alexa Fluor 647 and isotype control for CTNNB1 rabbit IgG-Alexa Fluor 647 (Abcam) were used. The cells were then sorted, and the data were acquired on a BD LSRFortessa X-20. Sorting parameters were set to gate and exclude small particles such as cell debris and large duplex cells. The data were analyzed using FlowJo software.

### Statistical Tests

Statistical analyses were carried out using GraphPad Prism 8 software (San Diego, CA, USA) with one-way ANOVA.



Statistically significant results were represented as \* $p < 0.05$  or \*\* $p < 0.01$ ; \*\*\* $p < 0.001$  or \*\*\*\* $p < 0.0001$ ; ns (not significant). All data are shown as mean  $\pm$  standard deviation (SD); *n* values for independent samples are indicated in italics above the x-axes in histogram figures, unless otherwise stated.

## RESULTS

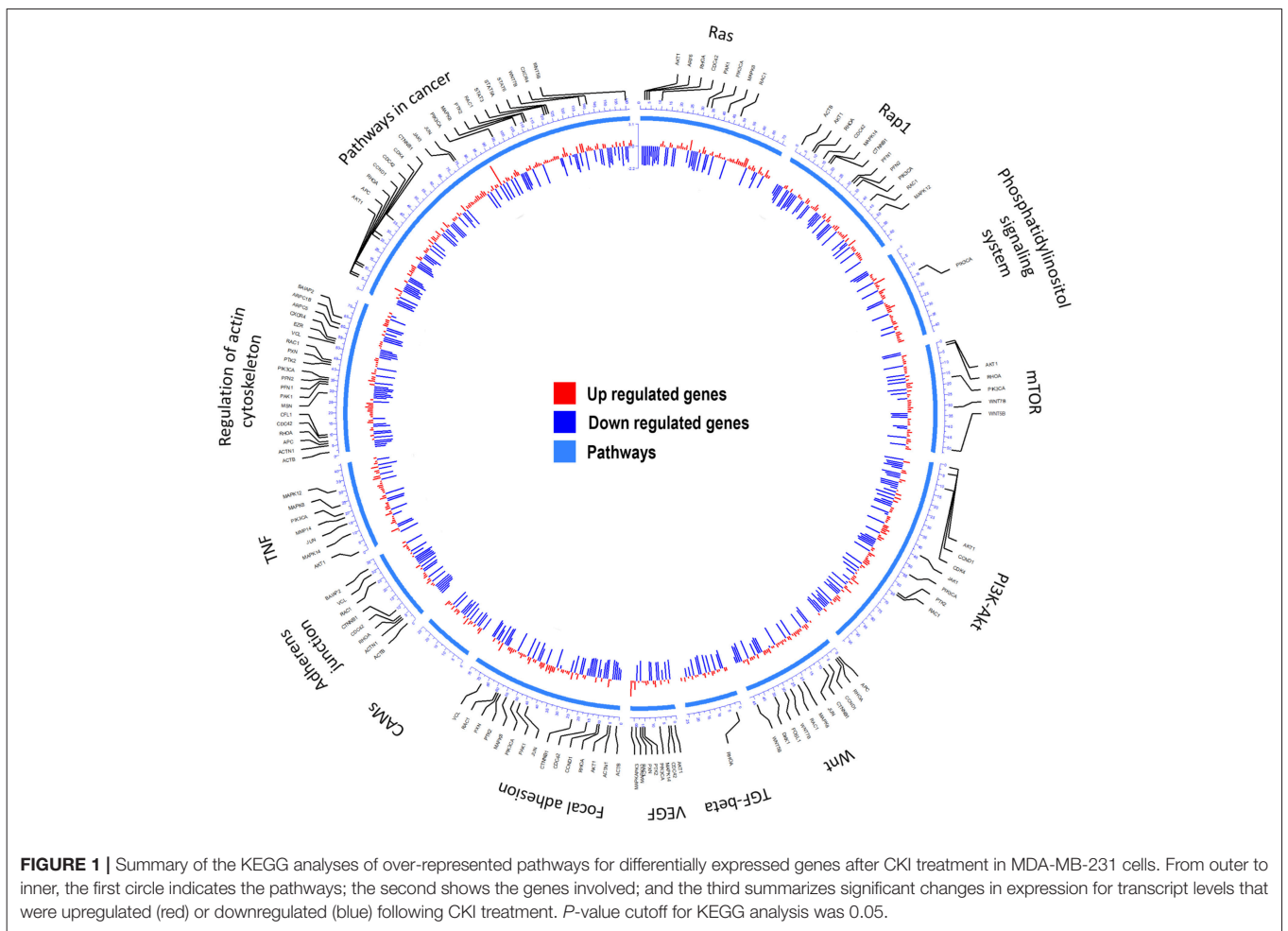
### Functional Annotation of MDA-MB-231 Transcriptome Treated by CKI

Transcriptome (23) analyses were performed to identify over-represented Gene Ontology (GO) terms and Kyoto Encyclopedia of Genes and Genomes (KEGG) for all differentially expressed (DE) genes by comparing MDA-MB-231 gene expression profiles with and without CKI treatment (Figure 1 and Supplementary Image 1). Differences in gene expression levels were used to identify migration related GO terms and pathways of interest, which were classified by functional roles via GO and KEGG over-representation analyses. Enriched GO terms connected to cell migration such as “positive regulation of locomotion,” “tissue migration,” and “leucocyte migration” emerged from analyses of DE genes

in CKI-treated MDA-MB-231 cells (Supplementary Image 1 and Supplementary Data Sheet 1). Integration of DE genes associated with CKI treatment into KEGG pathways showed that some of the most over-represented pathways were “focal adhesion,” “regulation of actin cytoskeleton,” “pathways in cancer,” “TGF- $\beta$  signaling pathway,” and “adherens junction” (Figure 1). These results indicated that many of the genes affected by CKI treatment were involved in cell migration-related pathways.

### Identification of CKI Components

CKI was fractionated and components were selectively recombined to create MJ and MN fractions (Supplementary Image 2) as treatments for bioassays on cultured cells. Concentrations of the nine major compounds in CKI were measured using LC-MS/MS (see Materials and Methods). The concentrations of MJ components were determined (Supplementary Images 3, 4) from calibration curves of nine standard compounds as previously described (23) and summarized in Supplementary Table 1. The total concentration of the nine major compounds in CKI was 9.99 mg/ml which accounted for approximately 40 % of the dry mass of CKI, and the total concentration of the nine compounds in



MJ was 8.62 mg/ml, indicating that the major compounds were clearly fractionated from CKI, and that MJ and MN components were well-separated.

## Impairment of Cell Migration by CKI and Fractionated Mixtures

Effects of CKI on two-dimensional cell migration were assessed using a circular wound healing assay (Figure 2A). Percent wound closure after 20 h was calculated based on the initial wound area. CKI-based treatments were tested on six different cancer cell lines (HT-29, SW-480, DLD-1, U-87 MG, U-251 MG and MDA-MB-231) and two non-cancerous cell lines (HEK-293 and HFF), at five doses ranging from 0 to 2 mg/ml (Figure 2B). In all cell lines, net migration rates were inhibited more by CKI than by MN or MJ treatments alone, except in HEK-293 which showed low sensitivity to CKI. The retention of biological activity in the fractionated MJ and MN treatments was confirmed by demonstrating reconstituted CKI (in which MN and MJ were mixed together) was equally effective as CKI for blocking cell migration (Figure 2B). The most sensitive cell lines were breast cancer (MDA-MB-231) and colon cancer (HT-29). DLD-1 and HEK-293 cell lines were the least sensitive.

In all the CKI-sensitive cell lines, the inhibition of migration by MN alone was greater than that seen with MJ alone except in HEK-293 and U-251 MG (Figure 2B), but neither treatment was as potent as CKI in any cell line. To determine if a single compound in MJ accounted for the enhanced inhibition seen with co-application of MJ and MN, each of the isolated major compounds alone was added in turn to 1 mg/ml MN, at a final concentration equal to its original concentration in 2 mg/ml CKI. Wound healing assays showed certain compounds added to MN produced a significantly greater inhibition than MN alone, but the effective compounds and levels of potency differed between cell lines (Figure 2C and Supplementary Image 5). Matrine was effective in MDA-MB-231, HT-29 and U-251 MG cell lines; sophocarpine was effective in HEK-293; trifolirhizin was effective in HT-29, SW-480 and U-251 MG; and adenine was effective in HT-29 cells, as determined by a significant decrease in migration as compared to MN alone. More than one compound in MJ appeared to contribute to the activity of CKI in blocking cell migration.

None of the CKI-based treatments induced significant cytotoxicity at 1 or 2 mg/ml, as assessed by Alamar Blue assays (Figures 3A–C). The lack of cytotoxicity suggested that the observed impairment of the two-dimensional cell migration was not an indirect consequence of reduced cell viability. However, CKI at 2 mg/ml substantially increased apoptosis in MDA-MB-231, without a significant effect on HEK-293 or HFF cell lines (Figures 3D–G). These data extend prior work which showed CKI increased apoptosis in MCF-7 breast cancer cells (17), and support the idea that multiple responses induced by CKI could contribute to its overall anti-cancer effects.

To quantify the effects of CKI on two-dimensional cell motility *in vitro* in more detail, trajectories of individual cells were monitored in real time using live cell imaging (Figure 4). Vehicle-treated cells were compared with those treated with 2 mg/ml CKI, or 1 mg/ml MN or MJ (doses equal to their concentration in CKI). Data were compiled for representative

cells from six cancer and two non-cancerous cell lines. Positions of individual cells as a function of time over 20 h were determined by the location of the cell nucleus (Figure 4A). Distances moved per unit time interval showed a Gaussian distribution; the peak position illustrates the mean distance traveled per increment. Significant displacement of the curve to the left (representing a decreased mean distance traveled per time interval) was evident for CKI treatment in all cell lines as compared to vehicle-treated controls (Figure 4B and Supplementary Video). Significant reductions in mean distance by either MN or MJ were observed in HT-29 and SW-480 cells. Reductions in mean distance by MN but not MJ were seen in U-87 MG, MDA-MB-231 and HFF cells. U-251 MG and DLD-1 cancer cells responded only to whole CKI. The effectiveness of CKI in blocking migration depended on the simultaneous presence of multiple minor and major compounds, but the specific agents conferring anti-migration activity appeared to depend on the cell line.

## Impairment of Invasiveness by CKI Treatments in Cancer and Non-cancer Cell Lines

A transwell Boyden chamber assay with ECM-coated filters was used to measure the invasiveness of cells in response to a serum chemoattractant gradient in vehicle control, CKI, MN, and MJ treatment conditions (Figure 5). CKI treatment and the combined MN+MJ treatment (i.e., reconstituted CKI) both significantly reduced invasiveness in all cell types. Smaller but significant decreases in invasiveness were seen with MN alone in all cell types except SW-480 and were seen with MJ alone in all but SW-480 and MDA-MB-231 cell lines. These results suggested that a combination of major and minor components of CKI was required for maximal inhibition of invasiveness through extracellular matrix barriers.

## Transcriptome Analysis of MDA-MB-231 Cells Treated With CKI

Functional enrichment analysis was used to narrow the field of candidate mechanisms potentially associated with the effects of CKI. The main finding was that the major pathways affected by CKI treatment were cell migration-related. Perturbations of KEGG Pathways that were significantly over-represented in DE genes with CKI treatment were further analyzed using SPIA (Figure 6A and Supplementary Data Sheet 2). “Melanogenesis,” “TGF- $\beta$  signaling pathway,” “focal adhesion,” “regulation of actin cytoskeleton,” “ErbB signaling pathway,” and “GnRH signaling pathway” were significantly perturbed based on “global perturbation values” ( $pG < 0.05$ ), consistent with the results of the KEGG analysis. CKI appears to impair cell migration by altering both adhesion and motility (Figures 6B,C). Genes from two strongly affected pathways (“focal adhesion” and “actin cytoskeleton”) were characterized by comparing three independent gene datasets: (i) a set containing 135 Tumor Alterations Relevant for Genomics driven Therapy (TARGET) genes; (ii) a set containing 140 migration related genes collected from published articles; and (iii) a set containing 1,381 genes from KEGG pathways. We identified 14 clinically relevant

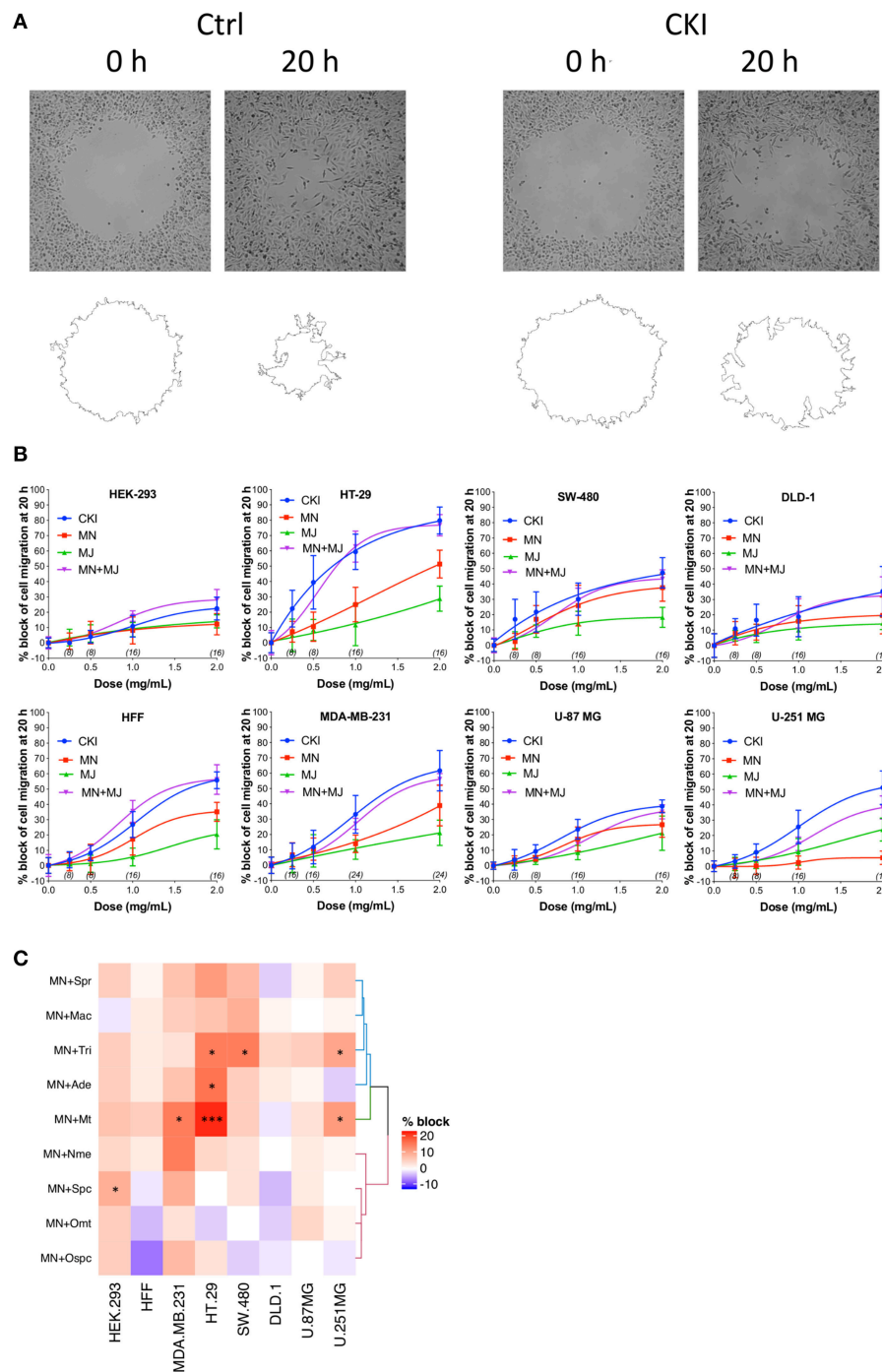
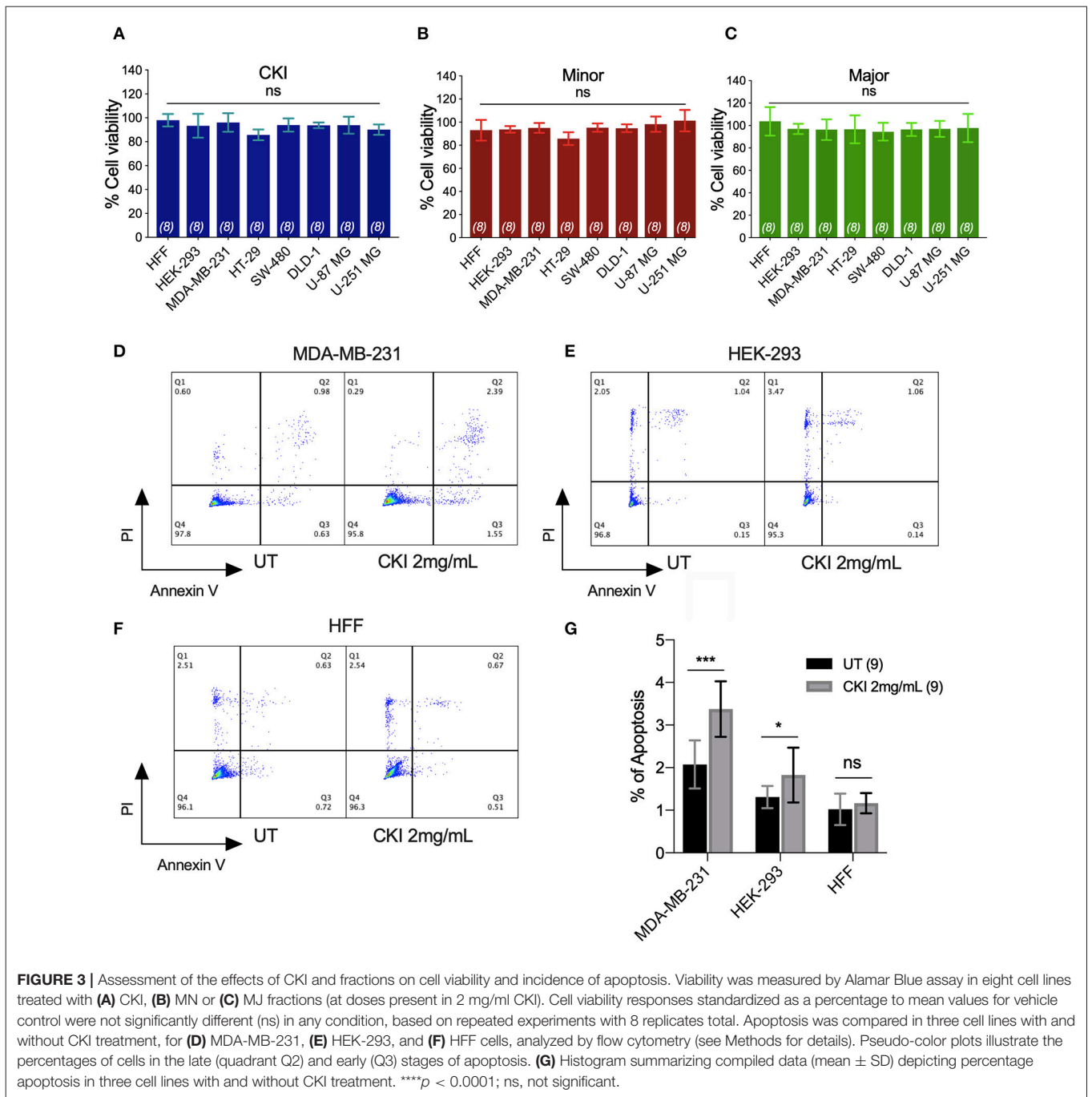


**FIGURE 2 |** Dose-dependent inhibition of cell migration by CKI, MJ and MN fractions in eight cell lines, measured by wound closure assays. **(A)** Wound areas were imaged at 0 h (initial) and after 20 h of treatment. **(B)** Graphs show percent inhibition of cell migration standardized to the initial wound area, as a function of dose for treatments with CKI (blue), MJ (green), MN (red), and reconstituted CKI with major and minor fractions combined (MN+ MJ; purple). **(C)** Combinatorial analysis of effects on wound closure for the MN fraction tested in combination with each of nine individual major compounds of CKI, summarized as a heatmap. Data were normalized to values for percentage of migration blocked with MN alone at 0.5 mg/ml. Boxes display the net effects of added single major compounds, as no change (white), increased percentage block (red), or reduced percentage of migration blocked (blue). Statistically significant differences are shown as \* $p < 0.05$  and \*\*\* $p < 0.001$ . No symbol in a box indicates the response was not significantly different from that with MN alone.



DE genes, which were: *CTNNB1*, *CDH1*, *AKT1*, *AKT2*, *AKT3*, *CCND1*, *MAPK1*, *JAK2*, *APC*, *CDK4*, *RB1*, *PIK3CA*, and *PTEN*, all of which have been shown to affect cell migration (Figure 6D, Supplementary Table 3, and Supplementary Data Sheet 3), suggesting that the slowing of cell migration could be clinically relevant to CKI treatment outcomes.

### CKI Interrupts F-actin Polymerization

The results of functional enrichment analysis highlighted the actin cytoskeleton and focal adhesion pathways as potential targets of CKI. As a result, we decided to examine the

effect of CKI on F-actin polymerization, filopodia formation and lamellipodia extension using confocal microscopy in all eight cell lines (Figure 7). Cells in all lines treated with CKI, MN and MJ (at doses equal to those in 2 mg/ml CKI) at 24h were smaller and lacked cellular processes such as lamellipodia as compared to vehicle control treated. Abundant lamellipodia seen in the control treatment were visibly diminished in the treatment groups. Comparing responses within the treatment groups, CKI disrupted the lamellipodia extensions more than was seen with MN or MJ alone. The impairment of F-actin polymerization was consistent with

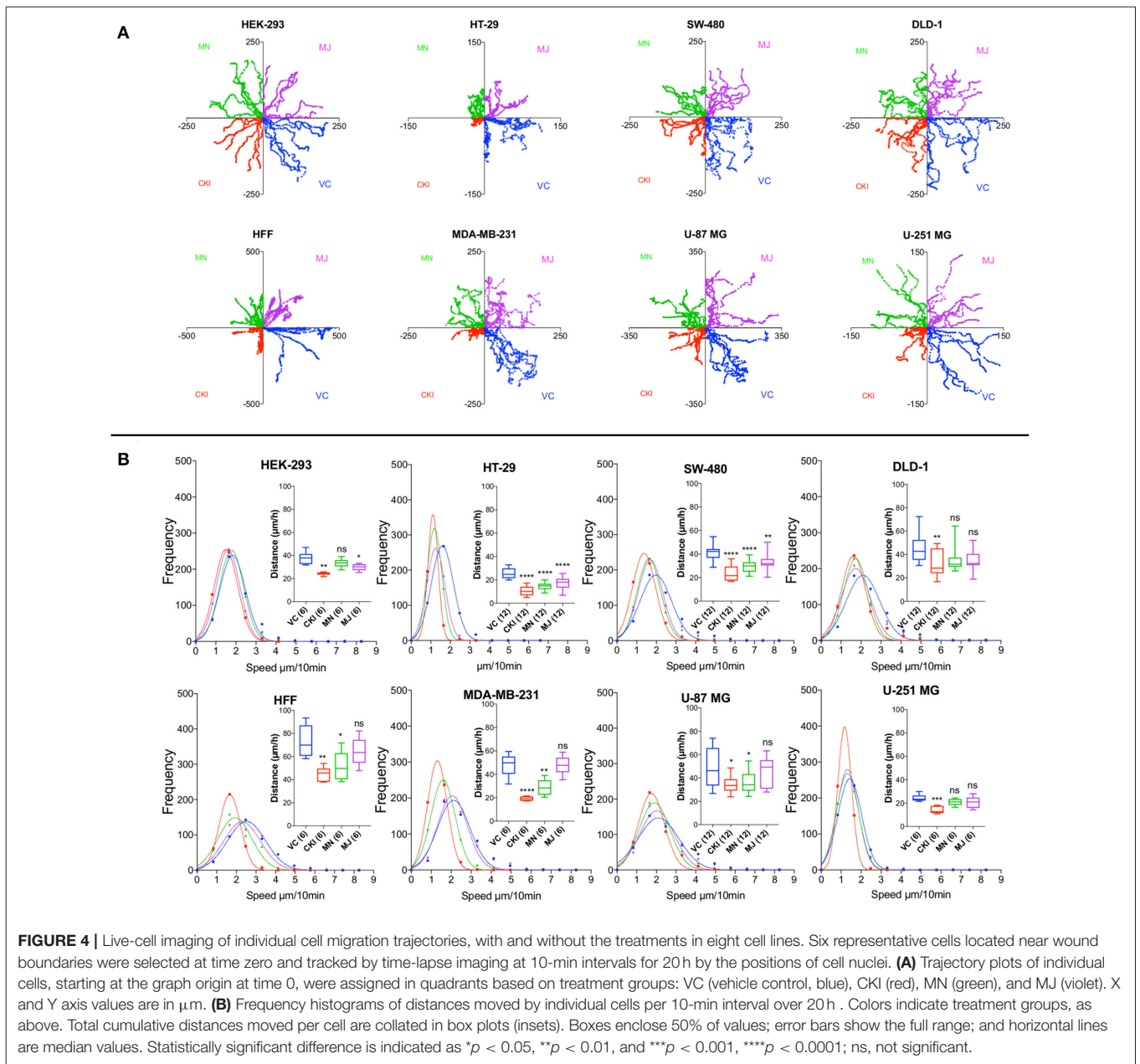


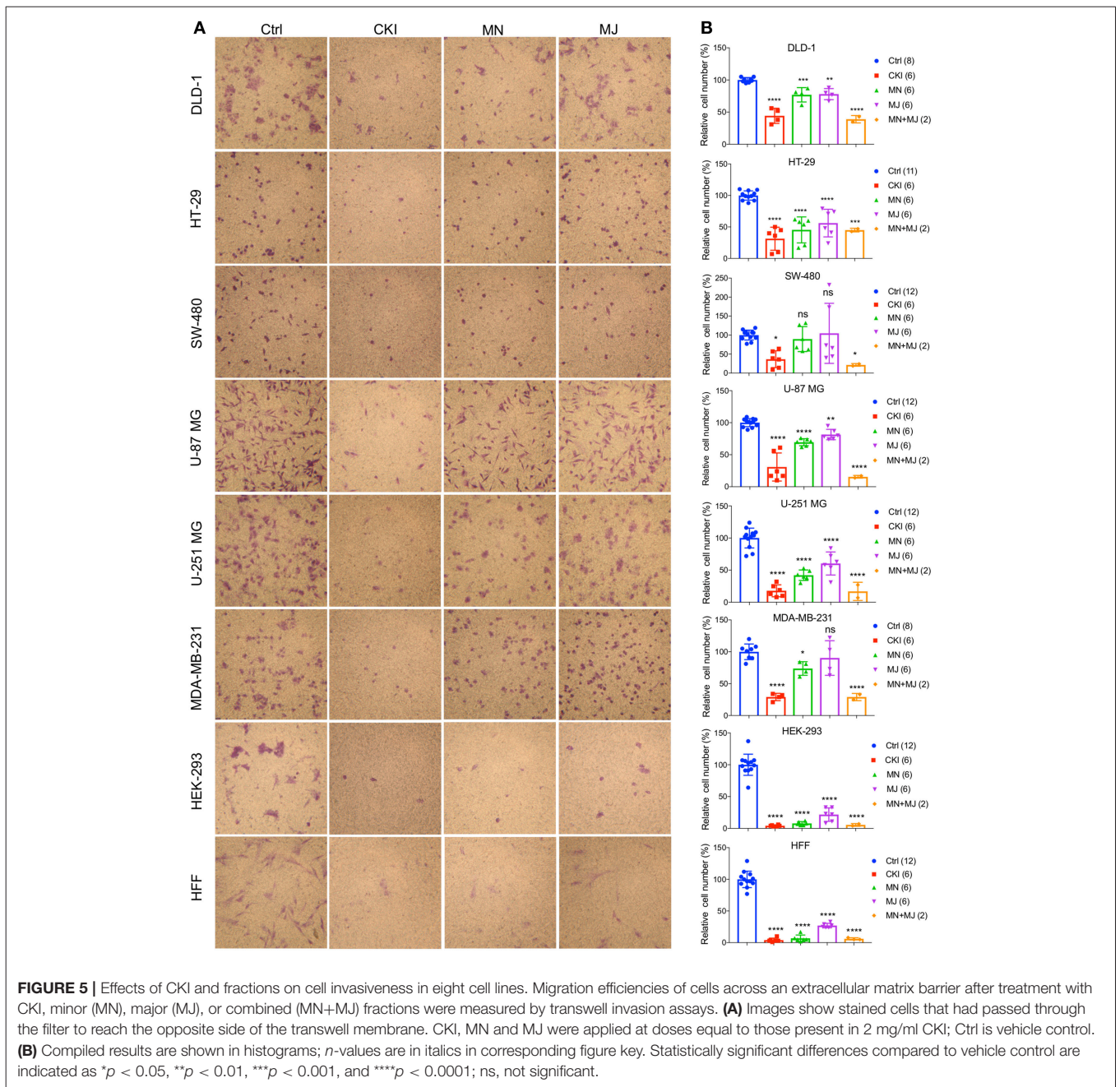
**FIGURE 4 |** Live-cell imaging of individual cell migration trajectories, with and without the treatments in eight cell lines. Six representative cells located near wound boundaries were selected at time zero and tracked by time-lapse imaging at 10-min intervals for 20 h by the positions of cell nuclei. **(A)** Trajectory plots of individual cells, starting at the graph origin at time 0, were assigned in quadrants based on treatment groups: VC (vehicle control, blue), CKI (red), MN (green), and MJ (violet). X and Y axis values are in  $\mu\text{m}$ . **(B)** Frequency histograms of distances moved by individual cells per 10-min interval over 20 h. Colors indicate treatment groups, as above. Total cumulative distances moved per cell are collated in box plots (insets). Boxes enclose 50% of values; error bars show the full range; and horizontal lines are median values. Statistically significant difference is indicated as \* $p < 0.05$ , \*\* $p < 0.01$ , \*\*\* $p < 0.001$ , \*\*\*\* $p < 0.0001$ ; ns, not significant.

the idea that MN and MJ fractions both contribute slowing cell migration.

### CKI and Fractionated Mixtures Perturb the Actin Cytoskeleton

To validate the gene expression changes at the protein level, we performed flow cytometry analyses of four proteins; CTNNB1, AKT (1–3), CCND1, and ACTB, selected for their significant contributions in actin cytoskeleton and focal adhesion pathways in MDA-MB-231, HEK-293, and HFF cell lines. Results shown in **Figure 8** indicated that CKI, MN and MJ significantly downregulated the protein expression, confirming the gene expression data. While there was prominent down-regulation of CTNNB1, CCND1, and ACTB expression in MDA-MB-231 by all treatments, AKT (1–3) was downregulated by CKI

and MN but not MJ treatments. In HFF cells, all treatments downregulated ACTB and CCND1 significantly; CKI and MN significantly reduced AKT (1–3) expression whereas MJ caused significant increase. In contrast, in the HFF cell line, CTNNB1 protein expression was significantly increased by CKI and MN, but significantly downregulated by MJ. In HEK-293 cells, CKI upregulated ACTB, AKT and CCND1, whereas MN upregulated ACTB and downregulated CTNNB1 with no significant effect on AKT (1,2,3) or CCND1; MJ had no significant impact on these four proteins (**Figure 8**). These results showed that CKI, MN and MJ significantly downregulated the four proteins in MDA-MB-231 cells, with similar although not identical results in the two non-cancer cell lines, providing additional support for the idea that CKI affects cancer cell migration by altering cytoskeletal structure.



## DISCUSSION

Natural compounds with anti-cancer activities have been suggested to include potential anti-metastatic agents (17, 21, 30, 31). Clinical chemotherapeutics for cancers are targeted mainly at killing rapidly dividing cells (32), but cause serious side effects including immunosuppression, hair loss and infertility, without eliminating risks of secondary neoplasms (33). Non-toxic treatments to reduce metastasis as adjuncts to primary cancer therapies are greatly needed. CKI increased apoptotic activity in breast cancer MCF-7 and hepatocellular carcinoma

HCC cell lines (17, 21). Results here showed that CKI also significantly slowed cell migration and invasion, an outcome consistent with its beneficial clinical effects. CKI is a mixture of natural compounds containing nine major and numerous unidentified minor compounds. The complexity of TCM presents a challenge for identifying single active compounds. By separating components of CKI into major and minor groups, and by adding novel screens for migration and invasion into the analyses of CKI biological activity, we have shown that co-application of multiple compounds was far more effective in blocking cell migration than single agents alone, and that

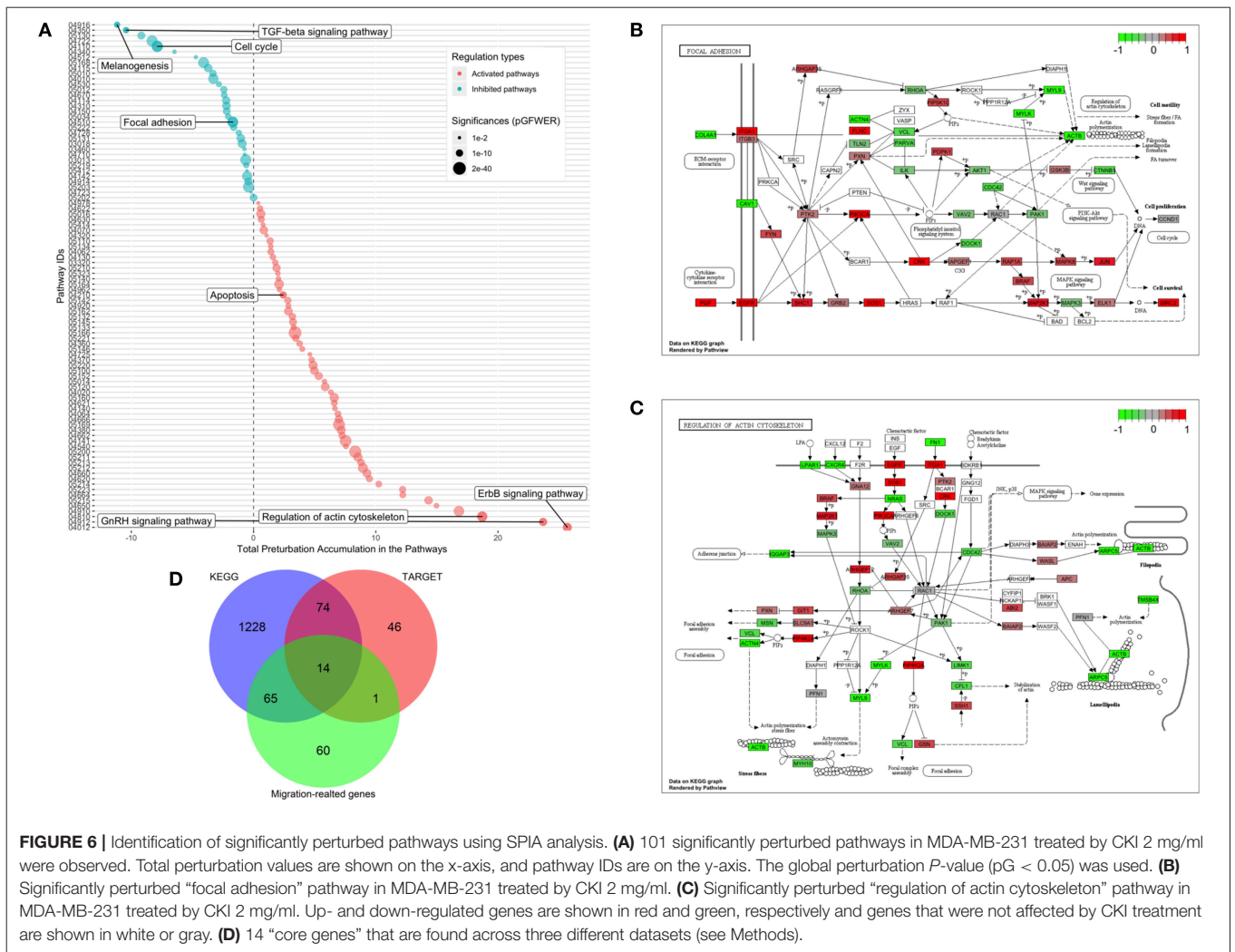
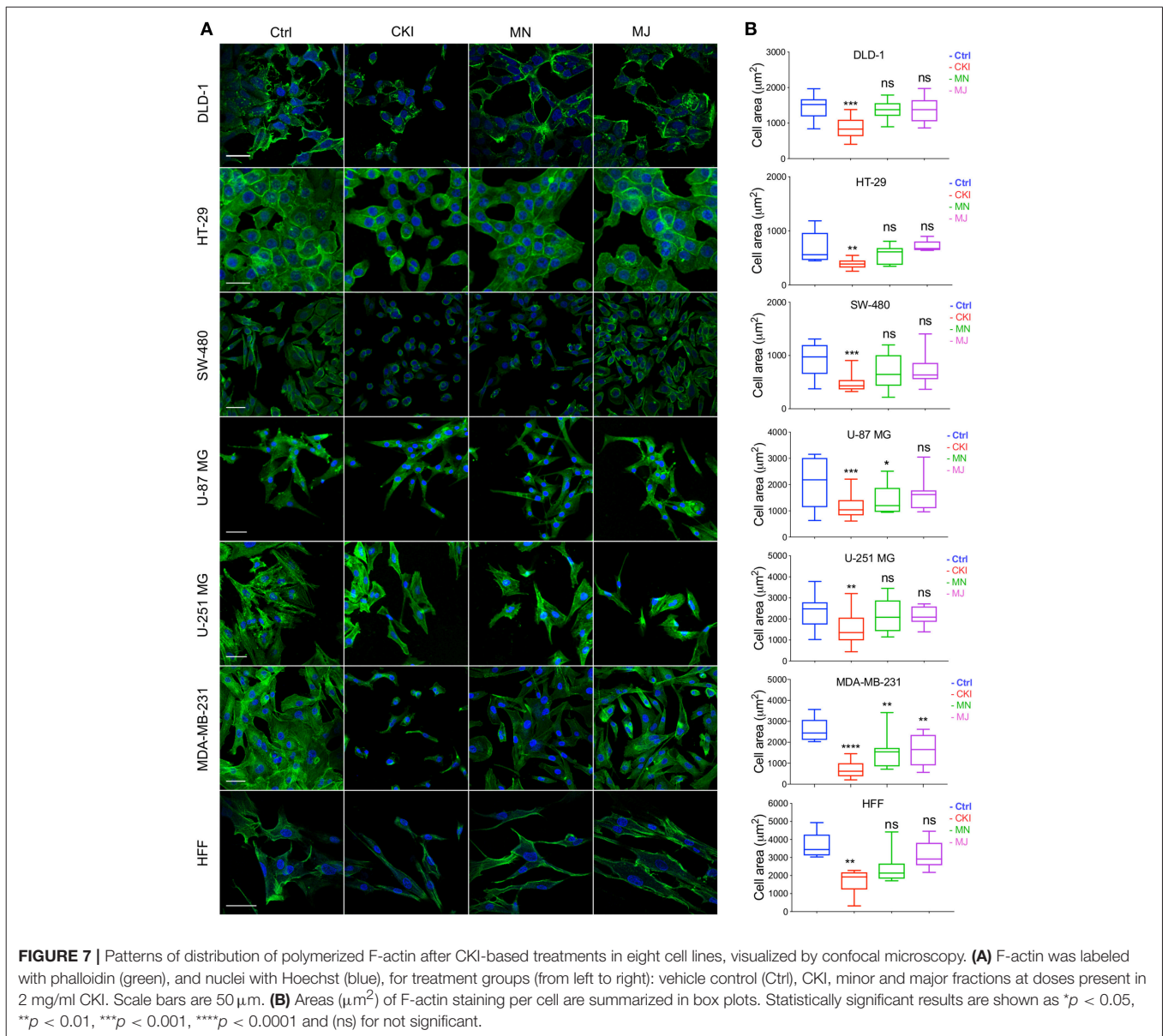


**FIGURE 6 |** Identification of significantly perturbed pathways using SPIA analysis. **(A)** 101 significantly perturbed pathways in MDA-MB-231 treated by CKI 2 mg/ml were observed. Total perturbation values are shown on the x-axis, and pathway IDs are on the y-axis. The global perturbation *P*-value ( $pG < 0.05$ ) was used. **(B)** Significantly perturbed “focal adhesion” pathway in MDA-MB-231 treated by CKI 2 mg/ml. **(C)** Significantly perturbed “regulation of actin cytoskeleton” pathway in MDA-MB-231 treated by CKI 2 mg/ml. Up- and down-regulated genes are shown in red and green, respectively and genes that were not affected by CKI treatment are shown in white or gray. **(D)** 14 “core genes” that are found across three different datasets (see Methods).

different compounds (serendipitously combined in CKI) are required for activity across diverse cell types. We showed the inhibition of migration by the major fraction alone was not as potent as whole CKI in any of the cell lines tested, demonstrating one or more minor compounds were necessary for the full effect. Each of the single compounds in the major fraction was coapplied with the minor fraction to test for a dominant modulator, but interestingly the most effective combinations of compounds differed between cell lines (Figure 2C and Supplementary Image 5). More than one major compound contributes to the activity of CKI in blocking cell migration.

Components of CKI have both anti-proliferation and anti-migration activities which differ between cell lines, suggesting that refinement of the TCM composition could enable customized management for different cancer types. A subset of the major compounds in CKI have been investigated previously. For example, oxymatrine impaired angiogenesis in mouse breast cancer *in vitro* and *in vivo*, by altering NF- $\kappa$ B pathway and VEGF signaling (34). Matrine inhibited migration and proliferation of mouse lung adenocarcinoma *in vitro* and

slowed xenograft growth *in vivo*, by reducing expression of a calcium-dependent chloride channel shown to be upregulated in multiple cancer types (35, 36). Consistent with these findings, we found matrine added to the CKI minor fraction further impaired cancer cell migration (Figure 2C); however, in contrast, addition of oxymatrine to the CKI minor fraction did not affect the control of migration in any of the cell lines we tested. Oxysophocarpine slowed metastasis of oral squamous cell carcinoma *in vitro* and *in vivo*, by altering transcription factor Nrf2 and stress protein signaling pathways (37). In contrast, our results showed oxysophocarpine partially reversed the inhibition of migration observed with the CKI minor fraction. Work here showed that the major components trifolirhizin and adenine, not previously characterized, when added to CKI minor fraction further slowed cell migration, suggesting these agents merit further study as potential therapeutics, singly and in combination. Not all components of CKI enhance its anti-cancer activities; for example, depletion of three compounds (oxymatrine, oxysophocarpine and macrozamin) increased the anti-proliferative activity of CKI (23).

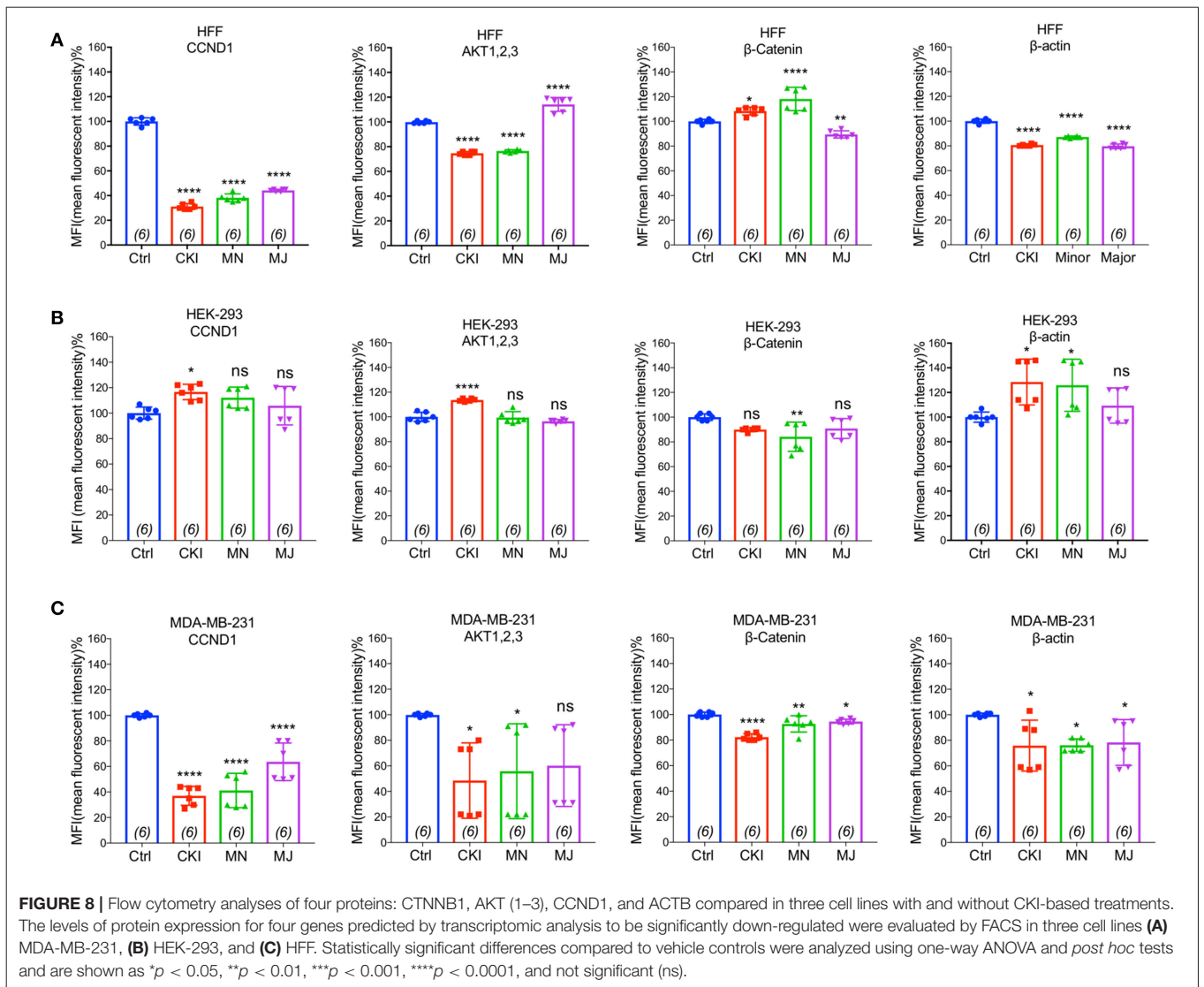


Rational analysis of the differential effects of agents in a TCM mixture can benefit from quantitative systems biology approaches. Transcriptomics has proven valuable for identifying altered patterns of global gene expression in response to complex agents such as CKI (18). Our pathway analysis of the transcriptome of CKI-treated MDA-MB-231 cells revealed a strong association with genes linked to “TGF- $\beta$  signaling,” “focal adhesion,” “GnRH signaling,” and “regulation of actin cytoskeleton.” These pathways are linked with migratory phenotype, actin polymerization and lamellipodia protrusion (38–40). Focal adhesion sites are points of contact with extracellular matrix, anchoring actin filaments via protein complexes with transmembrane integrin receptors (41). Matrine has been reported to disrupt actin filament organization in DLD-1 colorectal adenocarcinoma cells (42). Work here is

the first to show that treatment with whole CKI significantly perturbed “focal adhesion” and “regulation of actin cytoskeleton” pathways, and to confirm predictions of the transcriptomic results by showing CKI reduced lamellipodial abundance, length of extension, and area of F-actin polymerization.

Two striking outcomes of our pathway analyses were the significant negative perturbation of the cytokine TGF- $\beta$  (transforming growth factor beta) and positive perturbation of GnRH (Gonadotropin-releasing hormone) signaling pathways by CKI treatment. Multifunctional TGF- $\beta$  promotes the process of epithelial-mesenchymal transition, which facilitates cell migration, invasion and metastasis (43, 44). Reduced TGF- $\beta$  signaling would be consistent with our findings of impaired invasion and migration with CKI treatment. Conversely, GnRH activity has been associated with attenuating migration of





DU145 human prostatic carcinoma cells by remodeling the actin cytoskeleton (45). Increased GnRH signaling would be consistent with beneficial effects of CKI treatment. Further work is needed to fully understand the mechanisms of action of CKI on cell migration and invasion, the signaling pathways involved, the synergistic effects of combined therapeutic agents, and the translational potential by extending these analyses to metastatic cancer cells *in vivo*. Our results showed not only that more than one component of CKI is necessary for a beneficial effect in slowing migration, but that the optimal combinations of coapplied agents are not universal across all types of cancers. This work suggests future opportunities exist to refine CKI composition to target different classes of cancers differentially.

## CONCLUSION

The primary outcome of this study is the demonstration that cancer cell migration and invasion rates are significantly reduced

by CKI, suggesting that therapeutic activity of CKI in human cancer patients may arise in part from downregulation of a panel of key molecular targets necessary for adhesion and motility in metastasis. The secondary outcome of this study is that multiple compounds in CKI, acting together, are responsible for this effect.

## DATA AVAILABILITY

Data were submitted to NCBI Gene Expression Omnibus (GEO), with RNA\_Seq. Accession Number GSE125743, available at <https://www.ncbi.nlm.nih.gov/geo/query/acc.cgi?acc=GSE125743>.

## AUTHOR CONTRIBUTIONS

SN, TA, DA, and AY designed the study, analyzed the data and wrote the manuscript. SN and TA conducted the experiments and JC, JP, MD, YH-L, and ZQ assisted with experiments and analysis.

## FUNDING

This work was supported by the Australian Research Council (grants DP160104641 and DP190101745); special international corporation project of traditional Chinese medicine (GZYYGJ2017035); the Chinese National Project for Standardization of Chinese Materia Medica (ZYBZH-C-JIN-43); and The University of Adelaide Zengdong Australia China Centre for Molecular Chinese Medicine.

## ACKNOWLEDGMENTS

The authors thank Dr. Eric Smith for providing the HFF cell line, Dr. Mohamad Kourghi and Pak Hin Chow for valuable discussions, and Dr. Agatha Labrinidis and Dr. Jane Sibbons at Adelaide Microscopy for training and assistance. This manuscript has been released as a BioRxiv pre-print (MS ID #BIORXIV/2018/500124) at: <https://www.biorxiv.org/content/10.1101/500124v1> (46).

## SUPPLEMENTARY MATERIAL

The Supplementary Material for this article can be found online at: <https://www.frontiersin.org/articles/10.3389/fonc.2019.00314/full#supplementary-material>

**Supplementary Image 1 |** Functional classification of genes by GO over-representation analyses. Over-represented GO terms (Biological Process, BP = 3) for differentially expressed (DE) genes were identified from MDA-MB-231 cells treated by CKI. Upregulated and downregulated genes contained in each term were shown in red and green, respectively. GO terms shown above the blue line were significant terms related to migration.

**Supplementary Image 2 |** HPLC profiles of the components present in (A) CKI, (B) MJ, and (C) MN fractions. Samples (50  $\mu$ l at 1 mg/ml) were run through a C<sub>18</sub> semi-preparative column. Numbers indicate the nine major compounds; 1: macrozamin, 2: adenine, 3: n-methylcytosine, 4: sophoridine, 5: matrine, 6: sophocarpine, 7: oxysophocarpine, 8: oxymatrine, and 9: trifolirhizin.

**Supplementary Image 3 |** (A) Total ion chromatogram (TIC) for CKI in 1 in 100 dilution from 25 mg/ml of stock concentration. Single peaks were extracted based

on the molecular mass. (B) cytosine (spike in control), (C) macrozamin, (D) adenine, (E) n-methylcytosine, (F) sophoridine and matrine (similar molecular mass with different retention time) (G) oxysophocarpine, (H) oxymatrine, (I) sophocarpine, and (J) trifolirhizin.

**Supplementary Image 4 |** (A) Total ion chromatogram (TIC) for MJ in 1 in 100 dilution from 25 mg/ml of stock concentration. Single peaks were extracted based on the molecular mass. (B) adenine, (C) cytosine (spike in control), (D) macrozamin, (E) n-methylcytosine, (F) sophoridine, and matrine (similar molecular mass with different retention time) (G) oxysophocarpine, (H) oxymatrine, (I) sophocarpine, and (J) trifolirhizin.

**Supplementary Image 5 |** Combinatorial analysis of the effects of MN with each of the nine major individual compounds, analyzed in eight cell lines with wound closure assays. Data were normalized to results with 0.5 mg/ml minor (MN) alone. Significantly increased or decreased percent block of migration resulting from the addition of major compounds is shown as \* $p < 0.05$ , \*\* $p < 0.01$ , \*\*\* $p < 0.001$ , and not significant (ns). Data are mean  $\pm$  SD.

**Supplementary Video |** Live-cell imaging of the migration blocking effect of CKI in MDA-MB-231 cells in the wound closure migration assay. Videos show cell motility and wound closure rate in CKI at 2 mg/ml was reduced as compared to untreated control. Images were captured at 10-min intervals for 20 h.

**Supplementary Data Sheet 1 |** Significantly over-represented functional GO terms, as determined by GO analysis of the transcriptome from CKI treated MDA-MB-231 cells ( $P < 0.05$ ).

**Supplementary Data Sheet 2 |** Significantly perturbed pathways, as determined by SPIA analysis of the transcriptome from CKI treated MDA-MB-231 cells. ( $pG < 0.05$ ).

**Supplementary Data Sheet 3 |** Matching of genes in two strongly affected pathways ("focal adhesion" and "actin cytoskeleton") against three independent gene datasets containing: (i) a set TARGET gene and (ii) migration related genes from published articles. 14 core DE genes from three datasets including *CTNNB1*, *CDH1*, *AKT1*, *AKT2*, *AKT3*, *CCND1*, *MAPK1*, *JAK2*, *APC*, *CDK4*, *RB1*, *PIK3CA*, and *PTEN*, are known to have effects on cell migration.

**Supplementary Table 1 |** Concentration of 9 major compounds in CKI (Batch No:20151139) and MJ. Total alkaloid content in CKI (Batch No:20151139) = 25 mg/ml based on manufacturer's assay. Regression line for the calculation of compounds has previously been described (23).

**Supplementary Table 2 |** Concentrations of Matrigel and number of cells used for each cell line in transwell invasion assay.

**Supplementary Table 3 |** Fourteen clinically relevant DE genes from three independent gene datasets.

## REFERENCES

- Hanahan D, Weinberg RA. Hallmarks of cancer: the next generation. *Cell*. (2011) 144:646–74. doi: 10.1016/j.cell.2011.02.013
- Steege PS. Targeting metastasis. *Nat Rev Cancer*. (2016) 16:201. doi: 10.1038/nrc.2016.25
- Weigelt B, Peterse JL, Van't Veer LJ. Breast cancer metastasis: markers and models. *Nat Rev Cancer*. (2005) 5:591. doi: 10.1038/nrc1670
- Chaffer CL, Weinberg RA. A perspective on cancer cell metastasis. *Science*. (2011) 331:1559–64. doi: 10.1126/science.1203543
- Riihimäki M, Hemminki A, Sundquist J, Hemminki K. Patterns of metastasis in colon and rectal cancer. *Sci Rep*. (2016) 6:29765. doi: 10.1038/srep29765
- Fife C, Mccarroll J, Kavallaris M. Movers and shakers: cell cytoskeleton in cancer metastasis. *Br J Pharmacol*. (2014) 171:5507–23. doi: 10.1111/bph.12704
- Roth P, Weller M. Challenges to targeting epidermal growth factor receptor in glioblastoma: escape mechanisms and combinatorial treatment strategies. *NeuroOncology*. (2014) 16:viii14–9. doi: 10.1093/neuonc/nou222
- Ratajczak MZ, Suszynska M, Kucia M. Does it make sense to target one tumor cell chemotactic factor or its receptor when several chemotactic axes are involved in metastasis of the same cancer? *Clin Transl Med*. (2016) 5:28. doi: 10.1186/s40169-016-0113-6
- Chowdhury FA, Hossain MK, Mostofa A, Akbor MM, Sayeed B, Shahdaat M. Therapeutic potential of thymoquinone in glioblastoma treatment: targeting major gliomagenesis signaling pathways. *BioMed Res. Int*. (2018) 2018:4010629. doi: 10.1155/2018/4010629
- Xu R, Lin L, Li Y, Li Y. ShenQi FuZheng Injection combined with chemotherapy in the treatment of colorectal cancer: a meta-analysis. *PLoS ONE* (2017) 12:e0185254. doi: 10.1371/journal.pone.0185254
- Reid R, Steel A, Wardle J, Trubody A, Adams J. Complementary medicine use by the Australian population: a critical mixed studies systematic review of utilisation, perceptions and factors associated with use. *BMC Complement Alternat Med*. (2016) 16:176. doi: 10.1186/s12906-016-1143-8
- Gall A, Leske S, Adams J, Matthews V, Anderson K, Lawler S, et al. Traditional and complementary medicine use among indigenous cancer patients in Australia, Canada, New Zealand, and the United States: a systematic review. *Integr Cancer Therap*. (2018) 17:568–81 doi: 10.1177/1534735418775821
- Li X, Yang G, Li X, Zhang Y, Yang J, Chang J, et al. Traditional Chinese medicine in cancer care: a review of controlled clinical studies published in Chinese. *PloS One*. (2013) 8:e60338. doi: 10.1371/journal.pone.0060338

14. Chung VC, Wu X, Hui EP, Ziea ET, Ng BF, Ho RS, et al. Effectiveness of Chinese herbal medicine for cancer palliative care: overview of systematic reviews with meta-analyses. *Sci Rep.* (2015) 5:18111. doi: 10.1038/srep18111
15. Wang L, Zhou G-B, Liu P, Song J-H, Liang Y, Yan X-J, et al. Dissection of mechanisms of Chinese medicinal formula Realgar-Indigo naturalis as an effective treatment for promyelocytic leukemia. *Proc Natl Acad Sci USA.* (2008) 105:4826–31. doi: 10.1073/pnas.0712365105
16. Pan X, Han H, Wang L, Yang L, Li R, Li Z, et al. Nitidine chloride inhibits breast cancer cells migration and invasion by suppressing c-Src/FAK associated signaling pathway. *Cancer Lett.* (2011) 313:181–91. doi: 10.1016/j.canlet.2011.09.001
17. Qu Z, Cui J, Harata-Lee Y, Aung TN, Feng Q, Raison JM, et al. Identification of candidate anti-cancer molecular mechanisms of compound kushen injection using functional genomics. *Oncotarget.* (2016) 7:66003. doi: 10.18632/oncotarget.11788
18. Aung TN, Qu Z, Kortschak RD, Adelson DL. Understanding the effectiveness of natural compound mixtures in cancer through their molecular mode of action. *Int J Mol Sci.* (2017) 18:656. doi: 10.3390/ijms18030656
19. Ma Y, Gao H, Liu J, Chen L, Zhang Q, Wang Z. Identification and determination of the chemical constituents in a herbal preparation, Compound Kushen injection, by HPLC and LC-DAD-MS/MS. *J Liquid Chromatogr. Related Tech.* (2014) 37:207–20. doi: 10.1080/10826076.2012.738623
20. Wang W, You R-L, Qin W-J, Hai L-N, Fang M-J, Huang G-H, et al. Antitumor activities of active ingredients in compound kushen injection. *Acta Pharmacol Sinica.* (2015). 36:676–79. doi: 10.1038/aps.2015.24
21. Gao L, Wang K-X, Zhou Y-Z, Fang J-S, Qin X-M, Du G-H. Uncovering the anticancer mechanism of Compound Kushen Injection against HCC by integrating quantitative analysis, network analysis and experimental validation. *Sci Rep.* (2018) 8:624. doi: 10.1038/s41598-017-18325-7
22. Li X, Wu L, Liu W, Jin Y, Chen Q, Wang L, et al. A network pharmacology study of Chinese medicine QiShenYiQi to reveal its underlying multi-compound, multi-target, multi-pathway mode of action. *PLoS ONE.* (2014) 9:e95004. doi: 10.1371/journal.pone.0095004
23. Aung TN, Nourmohammadi S, Qu Z, Harata-Lee Y, Cui J, Shen H, et al. Fractional deletion of Compound Kushen Injection, a natural compound mixture, indicates cytokine signaling pathways are critical for its perturbation of the cell cycle. *bioRxiv.* (2018) 462135. doi: 10.1101/462135
24. De Ieso ML, Pei JV. An accurate and cost-effective alternative method for measuring cell migration with the circular wound closure assay. *Biosci Rep.* 38:BSR20180698. doi: 10.1042/BSR20180698
25. O'Brien J, Wilson I, Orton T, Pognan F. Investigation of the Alamar Blue (resazurin) fluorescent dye for the assessment of mammalian cell cytotoxicity. *Eur J Biochem.* (2000) 267:5421–6. doi: 10.1046/j.1432-1327.2000.01606.x
26. Schindelin J, Arganda-Carreras I, Frise E, Kaynig V, Longair M, Pietzsch T, et al. Fiji: an open-source platform for biological-image analysis. *Nat Methods.* (2012) 9:676. doi: 10.1038/nmeth.2019
27. Tarca AL, Draghici S, Khatri P, Hassan SS, Mittal P, Kim J-S, et al. A novel signaling pathway impact analysis. *Bioinformatics.* (2008) 25:75–82. doi: 10.1093/bioinformatics/btn577
28. Luo W, Brouwer C. Pathview: an R/Bioconductor package for pathway-based data integration and visualization. *Bioinformatics.* (2013) 29:1830–1. doi: 10.1093/bioinformatics/btt285
29. Hu Y, Yan C, Hsu, CH, Chen, QR, Niu K, Komatsoulis GA, et al. OmicCircos: a simple-to-use R package for the circular visualization of multidimensional omics data. *Cancer Inform.* (2014) 13:S13495. doi: 10.4137/CIN.S13495
30. De Ieso ML, Yool AJ. Mechanisms of aquaporin-facilitated cancer invasion and metastasis. *Front. Chem.* (2018) 6:135. doi: 10.3389/fchem.2018.00135
31. Zhu H, Hao J, Niu Y, Liu D, Chen D, Wu X. Molecular targets of Chinese herbs: a clinical study of metastatic colorectal cancer based on network pharmacology. *Sci Rep.* (2018) 8:7238. doi: 10.1038/s41598-018-25500-x
32. Crawford S. Is it time for a new paradigm for systematic cancer treatment? Lessons from a century of cancer chemotherapy. *Front Pharmacol.* (2013) 4:68. doi: 10.3389/fphar.2013.00068
33. Brydøy M, Foss, SD, Dahl O, and Bjørø T. Gonadal dysfunction and fertility problems in cancer survivors. *Acta Oncologica.* (2007) 46:480–489. doi: 10.1080/02841860601166958
34. Chen H, Zhang J, Luo J, Lai F, Wang Z, Tong H, et al. Antiangiogenic effects of oxymatrine on pancreatic cancer by inhibition of the NF-κB-mediated VEGF signaling pathway. *Oncol Rep.* (2013) 30:589–95. doi: 10.3892/or.2013.2529
35. Guan L, Song Y, Gao J, Gao J, Wang K. Inhibition of calcium-activated chloride channel ANO1 suppresses proliferation and induces apoptosis of epithelium originated cancer cells. *Oncotarget.* (2016) 7:78619. doi: 10.18632/oncotarget.12524
36. Guo S, Chen Y, Pang C, Wang X, Shi S, Zhang H, et al. Matrine is a novel inhibitor of the TMEM16A chloride channel with antitumor adenocarcinoma effects. *J Cell Physiol.* (2018) 234:8698–708. doi: 10.1002/jcp.27529
37. Liu R, Peng J, Wang H, Li L, Wen X, Tan Y, et al. Oxysphocarpine retards the growth and metastasis of oral squamous cell carcinoma by targeting the Nrf2/HO-1 Axis. *Cell Physiol Biochem.* (2018) 49:1717–33. doi: 10.1159/000493615
38. Li S, Butler P, Wang Y, Hu Y, Han DC, Usami S, et al. The role of the dynamics of focal adhesion kinase in the mechanotaxis of endothelial cells. *Proc Natl Acad Sci.* (2002) 99:3546–51. doi: 10.1073/pnas.052018099
39. Yamaguchi H, Condeelis J. Regulation of the actin cytoskeleton in cancer cell migration and invasion. *Biochim Biophys Acta Mol Cell Res.* (2007) 1773:642–52. doi: 10.1016/j.bbamcr.2006.07.001
40. Janet MT, Cheng G, Tyrrell JA, Wilcox-Adelman SA, Boucher Y, Jain RK, et al. Mechanical compression drives cancer cells toward invasive phenotype. *Proc Natl Acad Sci USA.* (2012) 109:911–6. doi: 10.1073/pnas.1118910109
41. Chorev DS, Moscovitz O, Geiger B, Sharon M. Regulation of focal adhesion formation by a vinculin-Arp2/3 hybrid complex. *Nat Commun.* (2014) 5:3758. doi: 10.1038/ncomms4758
42. Zhang B, Wang X, Li Y, Wu M, Wang S-Y, Li S. Matrine is identified as a novel macropinosytosis inducer by a network target approach. *Front Pharmacol.* (2018) 9:10. doi: 10.3389/fphar.2018.00010
43. Heldin CH, Vanlandewijck M, Moustakas A. Regulation of EMT by TGFβ in cancer. *FEBS Lett.* (2012) 586:1959–70. doi: 10.1016/j.febslet.2012.02.037
44. Tan E-J, Olsson A-K, Moustakas A. Reprogramming during epithelial to mesenchymal transition under the control of TGFβ. *Cell Adhesion Migr.* (2015) 9:233–46. doi: 10.4161/19336918.2014.983794
45. Enomoto M, Utsumi M, Park MK. Gonadotropin-releasing hormone induces actin cytoskeleton remodeling and affects cell migration in a cell-type-specific manner in TSU-Pr1 and DU145 cells. *Endocrinology.* (2006) 147:530–42. doi: 10.1210/en.2005-0460
46. Nourmohammadi S, Aung TN, Cui J, Pei JV, De Ieso ML, Harata-Lee Y, et al. Effect of Compound Kushen Injection, a natural compound mixture, and its identified chemical components on migration and invasion of colon, brain and breast cancer cell lines. *bioRxiv.* (2018) doi: 10.1101/500124

**Conflict of Interest Statement:** The authors declare that the research was conducted in the absence of any commercial or financial relationships that could be construed as a potential conflict of interest.

Copyright © 2019 Nourmohammadi, Aung, Cui, Pei, De Ieso, Harata-Lee, Qu, Adelson and Yool. This is an open-access article distributed under the terms of the Creative Commons Attribution License (CC BY). The use, distribution or reproduction in other forums is permitted, provided the original author(s) and the copyright owner(s) are credited and that the original publication in this journal is cited, in accordance with accepted academic practice. No use, distribution or reproduction is permitted which does not comply with these terms.

# Chapter 4

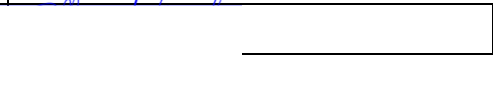
## The Secret Code Behind the Aquaporin Families; Discovery of New Subset of Ion Channels

Aquaporins (AQPs) are a subfamily of the Major Intrinsic Protein (MIP) that were initially considered to be water channels. However, followed by the first discovery of AQP, more of these proteins were identified and shown to act as multifunctional channels with a permeability to water and glycerol, as well as a broad range of solutes, including ions. The overall goal of this project was to investigate human AQPs for novel ion functionality and uncover the underlying molecular mechanism by which they facilitate cancer metastasis. As part of aim 1, I developed a yeast heterologous expression system and screened the potential for all 13 human AQPs to function as cation channels. The surprising outcome of aim 1, led me to utilize multiple lines of approaches, including site-directed mutagenesis, drug screening, fluorescent-based lithium probe imaging, confocal microscopy and alternative model such as *E.coli* organism model. This was followed by an electrophysiology study using two-electrode voltage clamp and *Xenopus laevis* oocyte to validate and evaluate the outcome from the prior results. This chapter is in the format of the manuscript to be submitted to a journal.

# Statement of Authorship

Title of Paper	The Secret Code Behind the Aquaporin families; Discovery of New Subset of Ion Channels
Publication Status	<input type="checkbox"/> Published <input type="checkbox"/> Accepted for Publication <input type="checkbox"/> Submitted for Publication <input checked="" type="checkbox"/> Unpublished and Unsubmitted work, written in manuscript style
Publication Details	Nourmohammadi S, Henderson SW, Ramesh SA, Yool AJ  *This work is in the final version of manuscript and will be submitted in about four weeks for publication.


## Principal Author


Name of Principal Author (Candidate)	Mr. Saeed Nourmohammadi		
Contribution to the Paper	First author and main contributor. Formulation of research question. Concept and methodological design. Designed and carried out the experiments, analysed data, figures and wrote the manuscript.		
Overall percentage (%)	80%		
Certification:	This paper reports on original research I conducted during the period of my Higher Degree by Research candidature and is not subject to any obligations or contractual agreements with a third party that would constrain its inclusion in this thesis. I am the primary author of this paper.		
Signature		Date	07/07/2022

## Co-Author Contributions

By signing the Statement of Authorship, each author certifies that:

- the candidate's stated contribution to the publication is accurate (as detailed above);
- permission is granted for the candidate to include the publication in the thesis; and
- the sum of all co-author contributions is equal to 100% less the candidate's stated contribution.

Name of Co-Author	Dr. Sam W Henderson		
Contribution to the Paper	Assisted with experiments and manuscript writing.		
Signature		Date	10/7/22

Name of Co-Author	Dr. Sunita A Ramesh		
Contribution to the Paper	Assisted with experiments and manuscript writing.		
Signature		Date	10/07/2022

Please cut and paste additional co-author panels here as required.

Name of Co-Author	Professor Andrea J Yool		
Contribution to the Paper	Concept and methodological design, supervised the research, assisted the research with funding, and manuscript writing.		
Signature		Date	8 Jul 2022

~

# Mass-throughput Yeast Screening to Study Aquaporin Ion channel Function and Drug Discovery.

Nourmohammadi S<sup>1</sup>, Henderson SW<sup>1</sup>, Ramesh SA<sup>2</sup>, Yool AJ<sup>1</sup>.

1- School of Biomedicine, University of Adelaide, Adelaide, SA 5005, Australia

2- College of Science and Engineering, Flinders University, Bedford Park, SA 5042, Australia

## Abstract

Aquaporins (AQPs) are multifunctional transmembrane channels that mediate passive transport of water, glycerol, signaling molecules, gases, and charged solutes including monovalent ions. The discovery and study of AQP ion channels has occurred at a considerably slower pace than other AQP substrates, possibly due to electrophysiology methods which are often time-consuming, labour intensive and require specialised equipment. Here, to overcome these barriers, yeast-based mass-throughput screening assays were developed to investigate the potassium (K<sup>+</sup>) and sodium (Na<sup>+</sup>) permeability of human AQP-1 (hAQP1). When heterologously expressed in *Saccharomyces cerevisiae*, hAQP1 was permeable to K<sup>+</sup> and Na<sup>+</sup> (at pH between 5.0-7.3), and was inhibited by known hAQP1 ion conductance inhibitors. The yeast-based AQP assays were optimised as a multifunctional mass-throughput tool to enable the simultaneous investigation of AQP1 ion activity for drug discovery, mutagenesis studies and signalling molecule screening, a combinatorial feat nearly impossible in other individual expression models, to study ion channel functionality. A previously developed lithium-sensitive photoswitchable probe was used to confirm hAQP1 ion permeability in the yeast strains used in this study. *Xenopus laevis* oocyte and *Escherichia coli* expression systems were used to further validate the results from yeast-based screening. The outcomes from this study are likely to provide insights into which additional AQPs may function as ion channels, and form an initial rapid system for screening AQP antagonists. The new candidate AQP ion channels remain to be discovered using the novel method we introduced in this study.

## 1. Introduction

Similar to many other channels and transporters, the channel activity of AQPs can be governed via factors including pH (1-13), phosphorylation (14-16), osmotic pressure (17-19), divalent cations (20-23) and voltage in some cases (24, 25). However, due to the limitation of current methods to study AQP ion activity, the discovery and study of the mechanisms of possible regulation of AQP ion conductance remain considerably at a slower pace compared to studying their other functional activities.

Although heterologous expression systems, such as yeast and bacteria, have been powerful approaches for the biological investigation of ion channels involved in fluid homeostasis and imbalance (26, 27), the models are poorly considered for discovering AQP ion channels. The need for designing a phenotypic-based condition assay in which ion permeability of AQPs is intimately tied with phenotypic changes has been a challenge mainly due to: *i*) the possibility that water and glycerol permeability of AQPs might indirectly interfere with yeast cellular homeostasis and result in an unspecific phenotypic changes; *ii*) non-selective permeability of these channels to ions would make analyses more challenging; *iii*) limited sources of information available on the structural basis of ion permeability studies and the mechanism of gating in different classes of AQPs (28),

Different approaches have been used to generate a diverse library of yeast mutant strains with specific transport deficits to study the effects of specific introduced ion channels in restoring yeast cell homeostasis (29). Following the first discovery of an AQP ion channel (24) at least eleven additional subtypes of AQPs have been discovered to be cation or anion channels (six in planta, four in mammals and one in insects) (28, 30). Growing evidence supports the physiological relevance of AQP ion permeability in regulation of cell volume, motility and response to environmental stress. The steadily increasing number of AQP ion channels being discovered from different phyla led to the design of a new high-throughput yeast-based screening approach as a potential unbiased tool overcoming some of the limitations to identify and study AQPs ion channel functionality.

There have been a few attempts to use yeast (*Saccharomyces cerevisiae*) heterologous expression systems to study the potential ion permeability of AQPs (3, 31, 32). Using a potassium (K<sup>+</sup>) deficient yeast strain, Wu et al, showed point mutations in rat AQP1 NPAs (the asparagine-proline-alanine sequences) and aromatic/arginine regions (N76, H180, R195) or (N192, H180, R195) were sufficient to complement the yeast growth defect in low K<sup>+</sup> concentration media. Byrt and colleagues (3) showed higher cytosolic sodium (Na<sup>+</sup>)



accumulation in yeast cells that expressed *Arabidopsis thaliana* PIP2;1. Recent studies from the same group illustrated the possibility that C-terminal phosphorylation of AtPIP2;1 controls ion permeability in a Na<sup>+</sup> efflux deficient yeast strain (32).

The primary goal of the work here was to define and optimise the conditions for yeast-based screening for hAQP1 ion channel function that could consequently expand to screen other AQPs for ion channel activity. Therefore, we aimed to develop a mass-throughput heterologous expression system based on the quantification of phenotypic changes in yeast. This enabled us to confirm the ion permeability of hAQP1 and optimise a high-throughput approach for exploring novel AQP ion channels, drug and signalling molecules screening, and mutagenesis study for the gating mechanism of AQPs ion permeability. The advantage of our optimised assay is that unlike traditional electrophysiology methods which are often expensive, time-consuming and labour intensive, this approach utilises conditions that provide an unbiased and effective screen of a broad range of AQPs from different phyla for the discovery of new ion channels, and the intracellular signals that might govern their activity and function. Moreover, high-throughput screening for drug discovery could help the development of aqua-*iono*-porin-targeted therapies for cancer, sickle cell anaemia, edema and other complex diseases (33-36). Using mutagenesis approach to study the consequences of inherited mutations on features of channel function in AQP-related disorders, as suggested by correlations with naturally occurring SNPs (Single Nucleotide Polymorphism) is another potential value of this assay. In the current work, we cloned hAQP1 into three different yeast mutant strains lacking either K<sup>+</sup> influx, Na<sup>+</sup> export capabilities or endogenous native aquaporins. A combination of different approaches was used to optimise the assays and define the most sensitive screening method for detecting effects of pH, altered substrate concentrations, inhibitors, signalling pathway stimulators, and mutagenesis on hAQP1 ion channel activity, as a foundation for new ion channel discovery and characterisation. AQPs are an intriguing class of membrane proteins that could be valuable targets for improved treatments of diverse conditions ranging from crop drought tolerance to human cancers.

## **2. Materials and methods**

### ***2.1. Cloning and transformation into yeast***

Open reading frames (ORF) of hAQP1 in the mammalian expression vector pCDNA3.1 were obtained from GenScript (Supplementary table S1). The full-length AQP gene, with and without stop codons, were amplified from pCDNA3.1 by PCR using Platinum™ PCR SuperMix High Fidelity (Thermo Fisher Scientific) and gene-specific primers. The amplified

PCR products were subcloned into the Gateway entry vector pENTR/D-TOPO (Thermo Fisher Scientific). To ensure high copy number in yeast, the yeast expression vector pYES-DEST52 was used for cloning by recombination using LR Clonase II Enzyme Mix (Thermo Fisher Scientific). The plasmids were transformed into chemically competent *E. coli* strain DH5- $\alpha$ , with appropriate antibiotic selection markers. Plasmid DNA from the transformants was isolated using GenElute Plasmid DNA Miniprep Kit (Sigma) and confirmed via Sanger sequencing prior to transformation into yeast.

For yeast screening assays, hAQP1 or control genes (AtKAT1, *Arabidopsis thaliana* potassium channel, or AtHKT1, *Arabidopsis thaliana* sodium transporter) cloned into the pYES-DEST52 vector (Invitrogen) downstream of the galactose-inducible GAL1 promoter were used. Plasmids were transformed into yeast using the LiAc method (37). The yeast strains were either a K<sup>+</sup> uptake-deficient yeast mutant strain CY162 ( $\Delta trk1$ ,  $\Delta trk2$ ) (38), a Na<sup>+</sup> efflux deficient strain B31 ( $\Delta ena1-4$ ,  $\Delta nha1$ ) (39) or aquaporin deficient strain, *aqy-null*, ( $\Delta aqy1$   $\Delta aqy2$ ) (19) (see Table 1 for more details). AtHKT1 was used as positive control for B31 cells, while AtKAT1 was the positive control for the CY162 strain.

Site-directed mutagenesis hAQP1 was performed using the QuickChange II Site-Directed Mutagenesis Kit (Agilent). For detection of cell surface expression in CY162 cells, hAQP1 was tagged with either GFP- (at the N-terminus) or -DsRed (at the C-terminus) by using the destination vectors pAG426GAL-EGFP-ccdB and pAG423GAL-ccdB-DsRed respectively (Addgene, Susan Lindquist collection).

## **2.2. Cloning, transformation, and growth experiments in *E. coli***

For expression in *E. coli*, hAQP1 was inserted into a modified pET-DEST42 expression plasmid by LR recombination. In the modified pET-DEST42 plasmid, the T7 promoter was replaced with the isopropyl $\beta$ -D-1-thiogalactopyranoside (IPTG) inducible TAC promoter. Plasmids, confirmed by sequencing, were then transfected in chemically competent *E. coli* strain ( $F^-$  thi lacZ amx82 rha  $\Delta[trkA]$   $trkD1$   $\Delta[Kdp-FAB]5$   $endA$ ) (40) by heat shock as described (41, 42).

In this screening, growth media, LB, was supplemented with additional 2 mM KCl (4 mM KCl in total including the nominal KCl concentration in the media). Overnight *E. coli* culture cell density (OD<sub>600</sub>) was measured and cells were washed 2-3 times and resuspended in the same washing culture media (low salt LB ~2 mM KCl) for the screening step. In each well of the microplate (Corning<sup>®</sup> 96 well plates), 200  $\mu$ L of media with or without CPT-cGMP (20

$\mu\text{M}/\text{mL}$ ) were inoculated with cells to a starting  $\text{OD}_{600}$  of 0.1. All test media were supplemented with carbenicillin (100  $\mu\text{g}/\text{mL}$ ), with or without 0.5 mM IPTG. The 96-well plates were inserted into FLUOstar Omega Fluorescence microplate reader (BMG LABTECH) set to 37 °C and  $\text{OD}_{600}$  was measured every 30 minutes for 40 hours with continuous double orbital shaking at 200 rpm.

### **2.3 Yeast growth conditions**

The *S. cerevisiae* strain CY162 (MAT $\alpha$  ura3-52 his4-15 trk1 $\Delta$  trk2 $\Delta$ 1::pCK64) was obtained from the National BioResource Project, Japan (NBRP) (<https://yeast.nig.ac.jp/yeast/>).

For growth experiments, cells were grown aerobically at 29 °C in Yeast Nitrogen Base, YNB, (~7.5 mM KCl, 6.7 g/L yeast nitrogen base without amino acids, 2% glucose, 2 g/L uracil-dropout amino acid mixture, supplemented with 100 mM KCl), and for screening conditions (inducing medium) K<sup>+</sup> free YNB (6.7 g/L yeast nitrogen base without amino acids, 2% glucose+2% raffinose, 1.98 g/L uracil-dropout amino acid mixture, supplemented with indicated KCl, and 2% agar for solid media) was used.

The *S. cerevisiae* strain B31 is a derivative of W303-1A (39), and was obtained from the Australian Centre for Plant Functional Genomics. For preparation, cells were grown aerobically at 29 °C on normal YNB (~7.5 mM KCl, 6.7 g/L yeast nitrogen base without amino acids, 2% glucose, 2 g/L uracil-dropout amino acid mixture), and for screening conditions normal YNB (~7.5 mM KCl, 6.7 g/L yeast nitrogen base without amino acids, 2% glucose+2% raffinose, 1.98 g/L uracil-dropout amino acid mixture and 2% agar for solid media) was used. The YNB media was supplemented with the indicated amount of NaCl in B31 assays. The *S. cerevisiae* strain *aqy-null* (MAT $\alpha$  leu2::hisG trp1::hisG his3::hisG ura3-52 aqy1::KanMX4 aqy2::HIS3) is a derivative of *S. cerevisiae* 10560-6B (19) and was kindly provided by Dr Grozman (ANU, Australia). Cells were cultivated similar to the B31 growth conditions except for the screening conditions in which additional indicated NaCl or KCl was added for the osmotic stress assays.

To avoid deactivating/overheating temperature sensitive ingredients, agar media preparation was done by preparing YNB ingredients for 1L volume and resuspended in 200 mL MQ water, filtered, stored at room temperature, and mixed with 800 mL autoclaved MQ water containing 2% agar/L.

For liquid screening, media was initially prepared in 2X concentration, half a volume was used to adjust pH and appropriate KCl concentrations, and then media was made up to the desired volume for 1X concentration, filtered and stored at 4 °C. To avoid having additional K<sup>+</sup> or Na<sup>+</sup>

interfering with non-selective permeability of AQPs, pH was adjusted using MES and Tris base. For pH 5.0, 5.7 and 6.4, 10 mM MES was added and Tris base was used to adjust the pH to the desired pH. pH 7.3 was adjusted using Tris base only.

Yeast cells grown to early logarithmic phase in Yeast Extract–Peptone–Dextrose (YPD) media for B31 and *aqy1aqy2* or YPD+100 mM KCl for CY162, and were transformed by a lithium acetate method (37). Cells were plated on normal YNB plates with no additional KCl for B31 and *aqy1aqy2*, or YNB+100 mM KCl for CY162.

#### ***2.4. Growth assay on agar plates of CY162 cells***

For yeast growth assays to infer the K<sup>+</sup> permeability of heterologously expressed genes, the transformants were grown on YNB+2% glucose+100 mM KCl agar plates for 3-4 days from glycerol stocks. Selected colonies were grown overnight in YNB+100 mM KCl and OD<sub>600</sub> was measured using a NanoDrop 2000 spectrophotometer in cuvette mode (Thermo Fisher Scientific) and adjusted to 0.5 with autoclaved MQ water. This was followed by five serial dilutions (10-fold) and 5 µl aliquots of each dilution were spotted on the YNB plates with indicated pH values and concentrations of KCl. Plates were incubated at 29 °C and the digital images of the cells were taken at the indicated times (usually days 3–5).

#### ***2.5. Liquid growth assay of yeast strains***

For testing the effect of pH on AQP-mediated growth rescue of CY162, the cells expressing hAQP1 were grown on solid YNB media (2% glucose+100 mM KCl) for 3-5 days. Single colonies were selected and grown overnight in the same media without agar. This was followed the next day by adjusting the cell density to desired OD<sub>600</sub> in the same media, which was followed by two washes with autoclaved MQ water and resuspension in unbuffered K<sup>+</sup> free YNB+2% galactose+2% raffinose+6 mM KCl medium. For screening of K<sup>+</sup>-uptake, cells were inoculated to a starting optical density (OD<sub>600</sub>) of 0.05-0.1.

The yeast cell wall in the stationary phase is stiffer and less permeable due to increased thickness of the wall as a result of mannoprotein layer formation (43). Thus, to screen for AQP modulators and drugs, the starting OD<sub>600</sub> was set to lower cell number (~0.005-0.01) for better comparison of growth differences between conditions. The pH of media was adjusted to 5.0, 5.7, 6.4, or 7.3 (± 0.1) using MES or Tris base as mentioned above. 200 µL cultures were grown in clear flat-bottom Corning® 96-well plates. The plate lid was removed, and wells were sealed by MicroAmp Optical Adhesive Film (Thermo Fisher Scientific). Double orbital shaking was

used for liquid cultures to avoid sedimentation and cell clumping during the repeated sampling assays.

To assess the potential effects of Na<sup>+</sup> permeability mediated by AQP expression on the growth of CY162, the initial cell numbers were set at OD<sub>600</sub> ~0.05-0.1. Adjusting the cell number can be slightly variable in different laboratory settings but can be optimised depending on the strain of yeast cell line used.

For testing the effect of Na<sup>+</sup> toxicity mediated by hAQP1 expressing B31, the same steps were taken as CY162 to grow and prepare the cells for liquid screening. Normal YNB (~7.5 mM KCl)-uracil+2% galactose+2% raffinose inducing media was used for B31) and media was supplemented with indicated additional Na<sup>+</sup> concentrations. For testing the effect of osmotic stress on aqy1aqy2 cells expressing hAQP1, the same media as B31 were used to grow and prepare cells, and the indicated K<sup>+</sup> and Na<sup>+</sup> concentrations were added to induce osmotic stress in the screening media.

## ***2.6. hAQP1 subcellular localization in yeast***

CY162 colonies carrying either GFP-hAQP1, hAQP1-DsRed or with pYES-DEST52-DsRed (control) were inoculated in 4 ml starter culture (YNB + glucose+100 mM KCl, without transcription inducer) and grown to stationary phase (overnight, 29 °C, 200 rpm). The overnight cultures were washed 2-3 times with autoclaved MQ-water and ~10 µl of cells were resuspended in 4 ml inducing medium and grown until cells reach stationary phase (~48 hours). About 5µl of yeast cells were spotted on polylysine coated slides (Thermofisher scientific) and mounted with cover slip and sealed with clear nail varnish. Sub-cellular GFP- or -DsRed signals were visualised on a Leica TCS SP5 laser-scanning confocal microscope (Leica, Wetzlar, Germany) with the x60 objective selected. eGFP was excited at 488 nm and emission was recorded at 495-570 nm. DsRed was excited at 558 nm and emission was recorded at 584-645 nm. Hoechst 33258 (cat # 861405; Sigma-Aldrich, St. Louis, MO) was used for nuclear staining (10 minutes at room temperature, in a 1:1000 dilution, at excitation 405 nm, and emission 461 nm). For membrane staining, MemBrite™ (green or red) were used and cells were stained as per manufacturer's instructions. The signal was recorded at Ex= 488 nm and Em = 513 nm for green signals and Ex= 561 nm and Em = 603 nm for red signals. Fiji (ImageJ) software (U.S. National Institutes of Health) was used to quantify signal as previously described (cite Victor's Lithium paper).

## ***2.7. Preparation and expression of human AQP1 in Xenopus laevis oocytes***

Frog surgery and oocyte preparation were done following the guide for the Care and Use of Laboratory Animals, (approval number M-2018-016) as described (20) using an approved protocol by the University of Adelaide Animal Ethics Committee. cRNA synthesis was carried out from NheI linearized pGEMHE plasmid with the mMessage mMachine T7 kit (Ambion) using published methods (3, 44). NCBI Protein Accession Numbers for hAQP1 cDNA construct used in the study is: NM\_198098.3 (HsAQP1, *Homo sapiens*). Collagenase A was used to defolliculate oocytes; stage V–VI oocytes were manually injected with 50 nL of 1 ng of hAQP1 cRNA using a microinjection pipette (Drummond Scientific, Broomall, PA, USA) and compared with control oocytes injected with 50 nL of RNase free water only or non-injected oocytes. Injected oocytes were incubated in standard Frog Ringers saline (mM: 96 NaCl, 2 KCl, 1.8 CaCl<sub>2</sub>, 1 MgCl<sub>2</sub>, 5 HEPES, 100 U/ml penicillin, and 100 µg/ml streptomycin, pH 7.4) for 2–3 days to allow protein expression. All oocytes were rinsed in Ca<sup>2+</sup> free Ringers saline prior to experiments and successful expression of hAQP1 was confirmed by osmotic swelling assays (20).

### **2.8. Two Electrode Voltage Clamp Recordings**

Using electrophysiological methods described previously (35), two-electrode voltage clamp recordings were used to record currents from control and hAQP1-expressing oocytes at room temperature in either isotonic K<sup>+</sup> saline (100 mM KCl, 1 mM NaCl, 1 mM MgCl<sub>2</sub>, 5 mM HEPES) or Na<sup>+</sup> saline (100 mM NaCl, 1 mM KCl, 1 mM MgCl<sub>2</sub>, 5 mM HEPES). The pH was adjusted by replacing 5 mM HEPES with MES for final pH values of 5 to 6 or adjusted by Tris/Base for pH 7.4 salines. Capillary glass electrodes (1–3 MΩ) were backfilled with 1 M KCl. Each oocyte was preincubated in the corresponding saline and indicated pH for ~10 minutes prior to the recording. Oocytes were clamped using a GeneClamp 500B amplifier (Molecular Devices, CA United States). A membrane permeable form of cyclic GMP, Cyclic nucleotide analogs [8-(4-chlorophenylthio)guanosine 3',5'-cyclic monophosphate (CPT-cGMP) (Sigma-Aldrich), was applied in the extracellular bath at a final concentration of 20 µM. Current responses were monitored over 30 minutes after cGMP addition using repeated steps to +40 mV (800-ms duration) every 6s from a holding potential of -40 mV, using Clampex 9.0 software (pClamp 9.0 Molecular Devices, Sunnyvale, CA, USA). CdCl<sub>2</sub> (600 µM) was applied at the to test for block hAQP1 ion conductance.

Conductance values were calculated from the slope of linear fits of current amplitudes as a function of step voltages from +60 to -120 mV, from a holding potential of -40 mV. Current responses to ramped voltages were captured with a protocol that stepped from the holding

potential of -40 to 0 mV, then ramped linearly up to +100 mV, followed by a step to 0 mV and ramp to -100 mV, over sweep durations of 20 sec each, repeated 4 times in succession. Data were analysed with Clampex 9.0 software (pClamp 9.0, Molecular Devices, CA United States) and GraphPad Prism 9 software.

### ***2.9. Photo switching experiments in Yeast***

The lithium sensitive photoswitchable probe (known as SHL) was prepared as described in our previous study (45). For cell preparation, empty vector and AQP1-expressing CY162 cells were initially grown overnight in liquid YNB, containing 2% glucose supplemented with 100 mM KCl. Cells were washed 2-3 times with autoclaved MQ water and aliquots were inoculated ( $OD_{600} \sim 0.2-0.5$ ) into induction culture medium ( $K^+$  free YNB, -uracil, 2% galactose+ 2% raffinose, 100 mM KCl). Cell cultures were incubated on a rotary shaker for  $\sim 48$  h (250 rpm, 29 °C) to allow time for protein expression. For confocal imaging, cells were spun down and washed 2-3 times with MQ water, resuspended in SHL buffer (1.8 M sorbitol, 50 mM SHL sensor, 5 mM  $CaCl_2$ , 10 mM Tris adjusted to pH 8 with HCl), and incubated on a rotary shaker for 60 min at 29 °C. Cells were then harvested by centrifugation (1000 G, 5 minutes), resuspended in imaging buffer (1.8 M sorbitol, 50 mM LiCl, 5 mM  $CaCl_2$ , 10 mM Tris adjusted to pH 8 with HCl) and transferred into eight-well uncoated Ibidi m-Slides (Ibidi, Munich, Germany). Slides were covered in aluminium foil and transported to the laser scanning confocal microscope, the University of Adelaide (Leica, Wetzlar, Germany). Initial images were taken after the cells were exposed to white light for 10 minutes (with the SHL probe in the OFF-state). Cells were exposed to UV radiation (632 nm) for 10 minutes, in order to convert the photoswitchable sensor back into a  $Li^+$ -sensitive activatable fluorescent state (ON-state), and a second image was taken (Imaging using Ex/Em=514 nm/550-650 nm). Confocal images and fluorescence intensities were quantified using Image J software (National Institutes of Health, MD USA).

## **3. RESULTS**

### ***Establishing a mass-throughput yeast assay to discover new AQP ion channel/s.***

Due to the limitations of electrophysiology methods (mentioned in the Introduction), we aimed to establish a high-throughput screening assay for AQP ion channel activity. To date, eleven AQPs from different kingdoms have been proposed to transport either cations or anions (46). We used yeast mutant strains with sensitivity to  $K^+$  and  $Na^+$  fluxes to investigate a novel

approach, addressing the gap in knowledge on how many of diverse classes of aquaporins serve as potential ion channels.

**Table 1: Yeast strains used in this study.**

Strain	Source/Reference	Phenotype	Amino Acid	Genotype
CY162	Ko and Gaber <i>et al.</i> (1991)	K <sup>+</sup> and Na <sup>+</sup> sensitive	Uracil	MAT $\alpha$ ura3-52 trk1 $\Delta$ his3 $\Delta$ 200 his4-15, and trk2 $\Delta$ :: pck64
B31	Bañuelos <i>et al.</i> (1998)	Na <sup>+</sup> sensitive	Uracil	MAT $\alpha$ ade2-1 can1-100 his3-11,15 leu2-3,112 trp1-1 ura3-1 mall0 ena1D::HIS3::ena4 $\Delta$ nha1D::LEU2
aqy1aqy2	Leitão <i>et al.</i> (2014)	Osmotic stress sensitive	Uracil	Mat $\alpha$ ; leu2::hisG; trp1::hisG, his3::hisG; ura352 aqy1D::KanMX aqy2D::KanMX

Both K<sup>+</sup>-uptake deficient (CY162) and Na<sup>+</sup>-efflux deficient (B31) yeast strains have been used previously for identifying novel cation channels and transporters (26). The CY162 line is defective in native K<sup>+</sup> uptake mechanisms, has a hyperpolarized resting membrane potential, is sensitive to low pH conditions (47), and shows strict discrimination for balancing net fluxes of alkali metals including sodium (48, 49). Rescue of cell survival in CY162 yeast is observed when the introduced genes complement the mutations and provide a pathway for K<sup>+</sup> entry into the yeast cells (50-53). Inhibition of growth by excessive Na<sup>+</sup> influx which causes cell toxicity also has been successfully used with CY162 (54, 55). Conversely, the B31 line lacks effective Na<sup>+</sup> efflux, and shows growth inhibition in high Na<sup>+</sup> media if the heterologous introduced genes act as inwardly directed (towards the cytoplasm) sodium-permeable channels (56-58).

We have used both approaches as tools to further investigate hAQP1 ion channel activity in the yeast model (28). The yeast system allows correlation of cloned channel function with cell viability, constituting an unbiased high-throughput phenotypic based assay. These assays not only showed potential for discovery of novel candidate AQP ion channels but also can be used to test a matrix of intracellular signaling stimuli, ion channel modulators, optical probes, and effects of site-directed mutagenesis to identify key residues involved in functional properties. Similarly, it is feasible to investigate the effects of environmental factors such as pH on channel function. The evaluation of a broad matrix of parameters that is feasible in the yeast high-throughput screening system would be a combinatorial feat nearly impossible to implement in the frog oocyte or other individual cell expression models.

### **3.1. Optimising and functional expression of hAQP1 in *S. cerevisiae* for AQP ion channels discovery.**



Potassium is the most abundant inorganic cation in cells and plays key role in the maintenance of cell functions. While yeast cells are capable of growing *in vitro* in a broad range of extracellular  $K^+$  concentrations (from mM to  $\mu$ M), intracellular levels are maintained by a set of transport mechanisms that allow adaption to the growth conditions (53). Studies using black lipid membrane (BLM) methods led to the discovery of first AQP ion channel, named as AQP0 (24). Subsequent discovery of hAQP1 as non-selective cation channel used the *Xenopus* oocytes as a heterologous expression model (59).

Here we used a high-copy number plasmid pYES-DEST52 to express hAQP1 in *S. cerevisiae* CY162, and analysed yeast cell survival and growth to explore the cation conducting properties of hAQP1 when cultured in a range of extracellular  $K^+$  concentrations (3, 6 or 9 mM KCl) (Figure 1A). AtKAT1 served as a positive control, and pYES-DEST52 (empty vector) was the negative control. After optimising ion concentrations and pH buffer conditions, the assays allowed reliable monitoring of the rates of growth of yeast cells with and without expression of classes of hAQP1. As shown in Figure 1A, the time course of growth in unbuffered growth media of hAQP1-expressing transformants (blue) in comparison with those carrying empty vector (red) in the inducing medium revealed nearly indistinguishable growth patterns for empty vector and a slight growth rescue in cells expressing hAQP1 at 6 and 9 mM extracellular  $K^+$ . Clones expressing AtKAT1 (green) showed robust growth that was also  $K^+$ -dependent. Growth rates were quantified as Area Under Curve (AUC). Graphs show average mean growth rates compiled from two independent experiments (n=3 each); error bars indicate standard deviation (mean  $\pm$  SD) (Figure 1C).

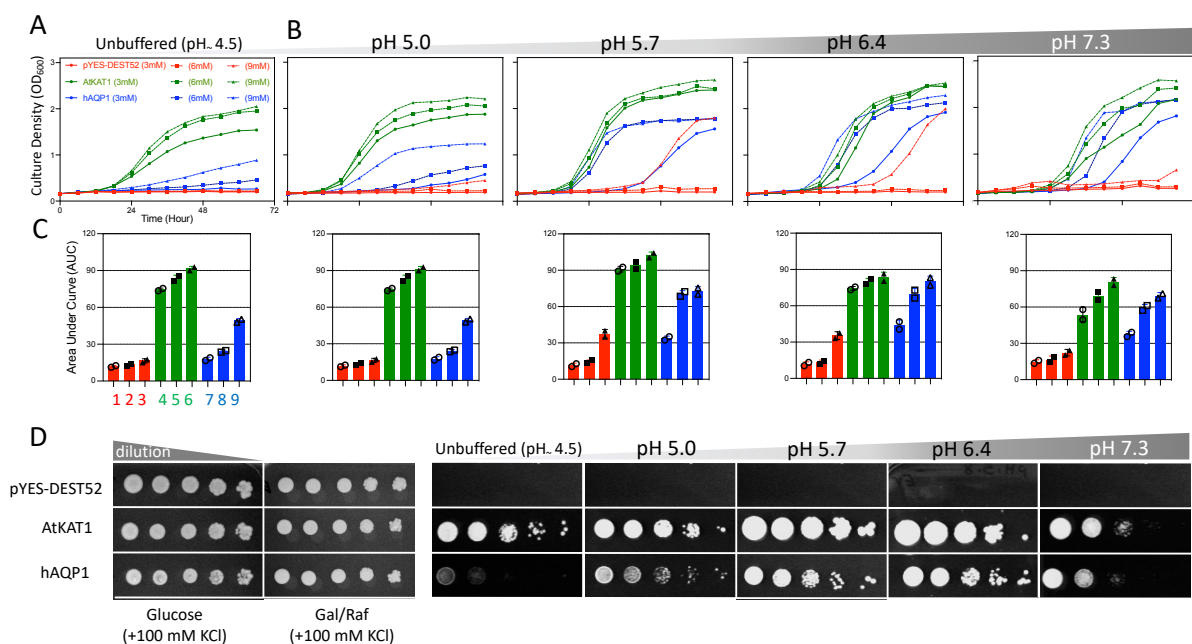


**Figure 1:** Complementation (evaluated as growth on both liquid and solid media and low  $K^+$  at different pH values) of  $K^+$ -uptake deficient CY162 yeast mutant line by transfection with hAQP1.

**A-B) hAQP1 mediates  $K^+$  uptake in a pH-dependence manner in yeast.** Yeast CY162 strain lacking both endogenous potassium channels *Trk1* and *Trk2* expressing hAQP1 were grown (200  $\mu$ l/well) in either A) unbuffered ( $\sim$ pH 4.5) inducing medium or B) adjusted pH 5.0, 5.7, 6.4 or 7.3. Medium was supplemented with either 3, 6 or 9 mM KCl. Mock transformed yeast (pYES-DEST52, red) or yeast transformed with an *Arabidopsis* potassium channel (AtKAT1, green) served as negative and positive controls respectively. OD<sub>600</sub> is plotted vs time (in hours). Growth curves represent the averages of two independent experiments. Growth was monitored at regular intervals spectrophotometrically by recording absorbance at 600 nm. The optical density was recorded every 15 min but only 6 hrs time point plotted for better visualisation of curves. Initial cell density (time 0) was  $\sim$  OD<sub>600</sub> 0.1. **C) Growth characteristics were determined by calculation of Area Under Curve (AUC).** **D) Phenotypic yeast assay on solid medium for  $K^+$  and pH-dependent of hAQP1.** Cells suspension expressing hAQP1 and controls (OD<sub>600</sub> = 1.0) were spotted in serial 1:10 dilutions on low-salt yeast nitrogen base medium at different pH, supplemented with 6 mM KCl and incubated for 5 days. Yeast expressing hAQP1 and controls grow equally well on standard mediums (controls: 2% glucose with addition of 100 mM KCl, or +2% galactose +2% raffinose with addition of 100 mM KCl). Panel C, number 1-3 = pYES-DEST52, represent 3, 6, and 9 mM KCl respectively, 4-6 = AtKAT1, 7-9 = hAQP1.

### 3.2. hAQP1 ion permeability is sensitive to extracellular pH in the yeast system.

Some ion channels expressed in yeast are only functional over a narrow pH range (60). Yeast has been used to investigate the effect of pH on AQP channel gating for water, glycerol and urea permeability (1, 2, 11, 31, 61, 62). We assessed the growth characteristics in liquid cultures of CY162 expressing empty, *AtKAT1* or *hAQP1* plasmids at extracellular pH values of 5.0, 5.7, 6.4 and 7.3 (Figure 1B). Both hAQP1-expressing and positive control cultures showed growth rates that were dependent on external  $K^+$  concentrations at all pH values. In acidic pH conditions (5.0 and 5.7), the final OD<sub>600</sub> levels that were reached at stationary phase for hAQP1 cells were lower than that seen for AtKAT1-expressing cells, indicating hAQP1 ion permeability is pH sensitive compared to the control in the yeast system. These results also indicated that hAQP1 ion conductance is functional at acidic and neutral pH values (pH 5.0-7.3), as reported previously (59).

While AtKAT1 growth was relatively pH-independent in the conditions tested, hAQP1-expressing cells showed enhanced growth in buffered media (pH 5.7, 6.4 and 7.3) as compared to unbuffered (pH  $\sim$ 4.2 $\pm$ 0.2) or pH 5.0. Near neutral pH (pH 6.4 and 7.3), growth rate differences between AtKAT1- and hAQP1-expressing cells were less evident (Figure 1B, last two panels). The greatest difference in growth rates between AtKAT1- and hAQP1-expressing cells was seen in acidic pH values ( $\sim$ 4.5-5.7) (Figure 1A and B), indicating the hAQP1 ion permeability appeared to be reduced at high extracellular proton concentrations ( $<$  pH 5.0). The highest growth rates for hAQP1-expressing cells occurred near neutral pH values (pH 6.4 and 7.3) indicating optimal channel permeability to  $K^+$  was favoured at physiological pH, which might reflect indirect effects of pH on the membrane environment or direct effects on

channel structure and function, or a combination. The Area Under Curve showed a negative correlation between proton concentration and cell-expressing hAQP1 growth (Figure 1C).

CY162 line expressing empty vector, *hAQP1* and *AtKAT1* were grown on solid minimal media containing 6 mM KCl, with either glucose or induction medium (Figure 1D). Growth rates were compared between unbuffered (pH  $\sim 4.5 \pm 0.2$ ) and buffered media (pH 5.0, 5.7, 6.4 and 7.3). In glucose medium lacking inducers of heterologous gene expression, all three clones grew at the same rates. However, in the induction medium, cells expressing hAQP1 and AtKAT1 showed enhanced growth rates relative to that of negative control cells.

The complementation of the growth defect in empty vector-expressing cells at the highest concentration of KCl (9 mM) in pH 5.7 and 6.4 (Figure 1A) could be due to a potential involvement of CY162 endogenous AQPs (AQY1 and AQY2) on ion permeability, an idea that remains to be explored in future work.

### **3.3. Analysis of water and ion channel activities of hAQP1 in the rescue of yeast cell growth.**

To test whether the rescue of growth by hAQP1 expression was mediated by increased water or cation transport, we analysed the effects of selected site-directed mutations, and the pharmacological effects of the previously described AQP1 inhibitors, CdCl<sub>2</sub> (a non-selective blocker of ion channels including AQP1) and mercury chloride (HgCl<sub>2</sub>, a blocker of AQP1 water pores) (Figure 2A-B). The C189F mutation is shown to impair hAQP1 water channel activity (63). A mutation that impairs both water and ion permeability, as shown in *AtPIP2;1* G103W (3), as well as its equivalent mutation in hAQP1 (G72W) were tested. Additionally, a mutation that is shown to switch cation to anion selectivity in rat AQP6 (K75E) (7) was included using equivalent mutations in *hAQP6* (K72E) to test whether there is a similar potential switch between selectivity in hAQP6 resulting a failure in growth rescue mediated by hAQP6 K<sup>+</sup> uptake.

Based on results of a dilution series (data not shown), 25  $\mu$ M HgCl<sub>2</sub> concentrations were selected in this study as doses that allowed AtKAT1 transformants and untreated cells to grow normally without evidence of toxicity in induction medium. Other mutations demonstrated to impair hAQP1 ion channels without altering water flux are addressed in Figure 5. There was no significant growth alteration observed between cells expressing wild type hAQP1 and C189F as well as when cells expressing were exposed to Hg<sup>2+</sup> (Figure 2A), suggesting the growth rescue of CY162 strain by hAQP1 is independent of its water transport. The mutation G103W in the yeast assay (Figure 2B) led to failure in rescuing growth of CY162 yeast cells expressing *AtPIP2;1*; the equivalent mutation in hAQP1 (G72W) also failed to rescue growth

though the comparable loss of hAQP1 channel function remains to be confirmed in an expression system such the oocyte. The predicted loss of growth in cells expressing hAQP6 K75E was not observed (Figure 2B); growth of yeast expressing the mutant construct was similar to wild type. It is possible that differences between human and rat channel conformations in the pore lining regions will show that the tested mutations G72W and G103W are not equivalent, and the key site remains to be identified in AQP6. Nonetheless, the results confirm that functional expression of hAQP1 can restore cell growth by complementing K<sup>+</sup> influx in the CY162 yeast type.

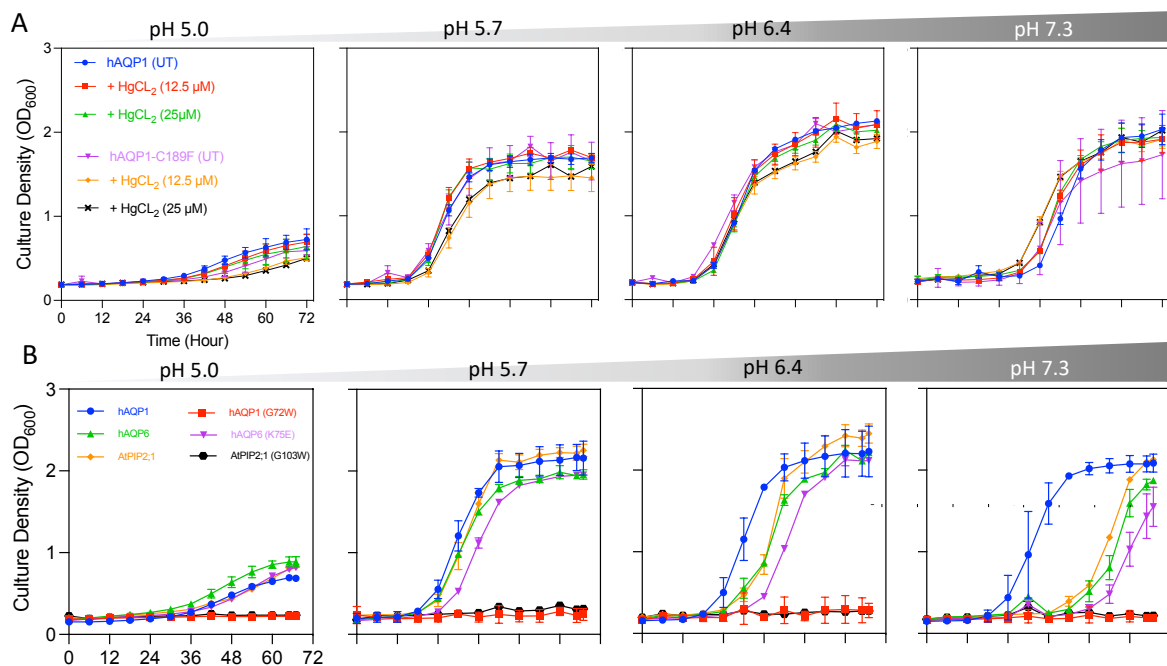


**Figure 2:** Effect of hAQP1 expression on mercury sensitivity of yeast. hAQP1-induced growth rescue in yeast is independent of their water transport functionality.

**A-B) Investigation the hAQP1 water permeability involvement in rescuing yeast growth defect.** A) CY162 yeast strain harbouring either hAQP1 or C189F mutants were grown with or without HgCl<sub>2</sub>. HgCl<sub>2</sub> treated cells show slight reduced growth in pH 5.0 as compared with pH 5.7-7.3. Impairing water permeability by substitution of hAQP1 mercury binding site (cysteine 189 to phenylalanine) showed no significant growth reduction. **B) hAQPs potassium permeability involvement in rescuing yeast growth defect.** CY162 growth rescue failed when expressing hAQP1 G72W (equivalent to AtPIP2;1 G103W), and AtPIP2;1 G103W but not hAQP6 K75E (equivalent to ratAQP6 K72E).

### 3.4. Fluorescence-tagging effects on subcellular localization of hAQP1 and ion conductance-dependent rescue of yeast growth.

Expression and localization of hAQP1 was visualised by fluorescence microscopy using N-terminal GFP- and C-terminal DsRed fusion constructs (Figure 3). Confocal images were taken with a 100X objective to evaluate the localization of markers for the nucleus and plasma membrane and the tagged protein and used to generate images merged with phase contrast

(Figure 3A panels 1-5). Nuclear staining indicated single cells (Figure 3A1). Relative fluorescence intensity measurements across the cell diameter were used to assess the level of colocalization of fluorescent-tagged protein and subcellular markers (Figure 3B). Colocalization of hAQP1 constructs was quantified by linear regression analyses. The correlation between signal intensities for hAQP1-tagged proteins and plasma membrane markers was plotted using ImageJ software (Figure 3C). Linear profiles of fluorescence intensities suggested a small proportion of the tagged fusion-protein channels showed plasma membrane localization for both GFP-hAQP1 and hAQP1-DsRed, though the predominant fractions remained intracellular. The percentages of green and red signals within the zone delineated by membrane marker were measured and standardised to total signal intensity from two separate images. This analysis estimated that  $8.5 \pm 3.1$  % of the GFP-AQP1 channel population and  $10.3 \pm 2.6$  % of the AQP1-DsRed population were in the plasma membrane.

The intracellular GFP fluorescence signals appeared to be mainly associated with endoplasmic reticulum and perinuclear structures for both constructs. Cells expressing DsRed plasmid only showed cytosolic signals (see Supplementary S1 for images of DsRed signals; and Supplementary S2 for a Z-stack 3D video for hAQP1-tagged fluorescence).

The C-terminal DsRed fusion protein did not rescue growth at any pH, suggesting a loss of ion channel function, an observation consistent with prior work showing the integrity of the C-terminal domain of AQP1 was necessary for ion channel activation but had no effect on water channel activity (64). A parallel attempt to tag the hAQP1 channel with C-terminal His-V5 epitope tag also showed limited success in rescuing yeast growth (data not shown). In contrast, the N-terminal tagged GFP construct was able to rescue growth at pH 5.7 and 6.4, though more slowly than wild type (Figure 3D). Neither fluorescent-fusion hAQP1 protein was able to rescue growth at acidic pH 5.0.

As an additional line of evidence to test whether the subpopulations of tagged hAQP1 channels that appeared to be in the plasma membrane (Figure 4B-C) were indeed present and functional, the water transport properties of the tagged proteins were assessed by osmotic stress assays using the *aqy1aqy2* yeast strain, which lacks native AQPs and shows sensitivity to osmotic stress (65). Both N- and C-terminal AQP1 fusion proteins showed water transport comparable to that wild-type, as seen by the failure of transformants to grow under hypertonic osmotic stress conditions. These results confirmed that the tagged AQPs that were expressed in the yeast plasma membrane were functional channels. In sum, the results support the interpretation

that the rescue of  $K^+$ -transport deficient yeast cells can be accomplished by a relatively small increase in cation conductance.

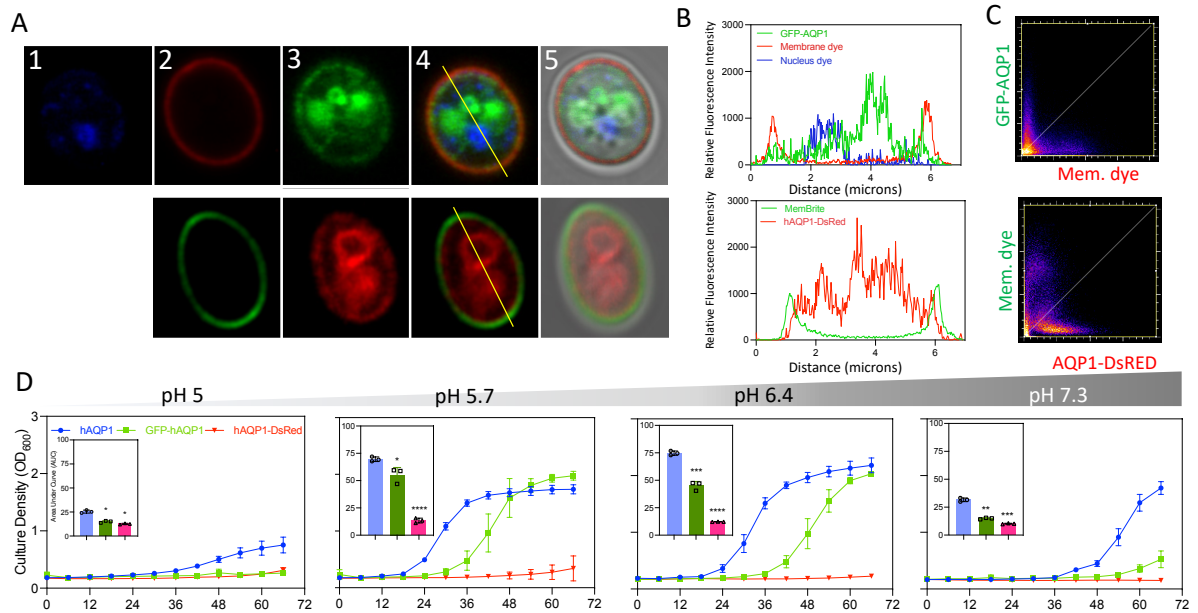


**Figure 3: Functionality and sub-cellular localization of GFP- and DsRed-tagged hAQP1 in yeast.**

**A) Tagging hAQP1 abolishes ion permeability dependent growth rescue in yeast.** Live cell bioimaging of *S. cerevisiae* expressing GFP- or -DsRED tagged hAQP1 at N-terminal or C-terminal respectively. DAPI fluorescence (1); red plasma membrane dye (2 upper row), and green plasma membrane dye (2, lower row); GFP-hAQP1 fluorescence (upper row) or hAQP1-DsRed (lower row) (3); merged (4); phase contrast (5). All images were generated at 100 times magnification. Scale bar, 1 $\mu$ m. Cells were grown in inducing medium containing (gal/raf + 6 mM KCl) for about 70 hours before imaging. **B)** One cross-section through cell centers were selected and signal intensities of hAQP1, membrane dye and nuclei dye (upper row) or hAQP1 and membrane dye (lower row) in the cross-sectional lines were plotted as a function of X-Y distance across the cells. DsRed only control showed diffuse cytosolic localized signal (supplementary 1). Z-stack video showing GFP- and hAQP1-DsRED expression (supplementary 1). **C)** Linear regression analyses quantified the correlation between hAQP1 signal intensities and membrane dye signal (upper plot for GFP- and lower plot for -DsRed). **D) Growth analysis of CY162-transformed hAQP1-fluorescent protein.** Cells transformed with plasmids encoding wild-type hAQP1 (blue), GFP- (green) or AQP-DsRed (red) were cultivated in YNB medium containing +2% (w/v) gal/raf+ 6 mM KCl at 29°C for 70 hours at different pH values. Area Under the Curve (AUC) for each construct-expressing cells are shown as bar plot (merged average of three independent experiments, n=6). See Figure 5C and D for further validation of membrane localization and water functionality of tagged-hAQP1.

### 3.5. Characterising hAQP1 ion permeability-dependent growth rescue by mutagenesis study in yeast

Our prior studies on structural mechanisms regulating the ion conductance properties of hAQP1 in the oocyte expression system identified a series of intracellular gating loop (loop D)

residues involved in channel activation by cGMP (66, 67). Seven mutations (the double mutant R159A+R160A, and single mutants D158P, R160P, G166P, G57N, E17N and G72W) were tested for capacity to rescue growth in CY162 K<sup>+</sup>-transport deficient yeast cells, as compared to hAQP1 wild type. The mutation equivalent to G103W in AtPIP2;1 was G72W in hAQP1. All of the hAQP1 mutations except R159A+R160A and D158P, failed to rescue yeast cell growth at pH 5.0, and significantly reduced the growth rate at pH 5.7. Closer to physiological pH (pH 6.4 and 7.3) R160P and G166P expressing cells showed growth rescue similar to wild type hAQP1. Cells bearing E17N and G72W mutants failed to rescue yeast growth at all pH values (Figure 4A). None of the mutant constructs introduced into yeast cells prevented growth in permissive control medium (gal/raf+100 mM KCl), indicating that yeast viability was not compromised by the exogenous expression of the hAQP1 mutants (Figure 4A, last panel).

The role of water permeation in osmotic stress tolerance in yeast has been examined previously for aquaporins, establishing feasibility of this heterologous expression system (65, 68). To determine the failure in growth rescue induced by tagged protein, and the mutants R159A+R160A (abbreviated RR/AA), E17N and G72W were not due to an impaired expression or localization, growth assays were performed under osmotic stress imposed by additional KCl or NaCl in the medium for *aqy-null* yeast strain. Figure 4B-C show growth tests for *aqy1aqy2* yeast with wild type and mutant hAQP1 constructs, and empty vector as a negative control in liquid YNB medium containing osmotically equivalent concentrations of 1.75 M KCl, 2.4 M sorbitol, or increased NaCl (0.25 M and 0.5 M). Normal YNB and YNB+sorbitol was used as a control for osmotic stress, showing all colonies grew equally, indicating correct protein function and membrane localization. High-throughput functional screening of AQP-expressing yeast using an osmotic stress approach allowed us to rule out the possibility that the loss of growth rescue by mutants and tagged-channels was due to failure to express the modified channels in the yeast plasma membrane. The observed changes in osmotic sensitivity confirmed that the channels were assembled and trafficked to plasma membrane and retained functionality as water pores. These results confirm that the gating domain mutations directly compromised growth rescue, indicating the key role of the introduced hAQP1 was in conferring ion conductivity.

Comparing the different clones, all cells bearing mutants showed growth reduction indicating the functional protein integrated to the membrane, with weaker growth inhibition for hAQP1-DsRed and G72W expressing cells.

Based on confocal microscopy data and osmotic stress assay for GFP- and DsRed-tagged hAQP1, we concluded that tagging the channel could potentially affect the membrane

localization expression levels and/or have some impact on the channel water and ion permeability. On the other hand, as was observed for AtPIP2;1 (G103W), hAQP1 G72W may cause a loss of function effect on water and ion permeability of the channel (Figure 4B, middle panel). Additionally, hAQP1 ion transport shown to be through the central pore and introducing tryptophan with less flexible side chain to the channel may have caused conformational changes or residues interaction which in turn may result in central pore deformation and loss of ion permeability. The idea remains to be explored for potential future work using electrophysiology in oocytes expressing hAQP1 G72W. On the other hand, only yeast expressing G72W in the 0.5 M NaCl medium, did not show a clear growth inhibition as compared to other constructs in which the growth rescue inhibition was  $p < 0.05$  (Figure 4C, right panel). The cells grew equally well in 0.25 M NaCl, although a slightly greater growth reduction was observed in hAQP1- and GFP-tagged expressing cells as compared to other constructs.

These results confirmed the membrane localization of the channels and showed water permeability of constructs (except for G72W and -DsRed constructs) are not affected and the other constructs grew relatively equal to wild-type hAQP1.

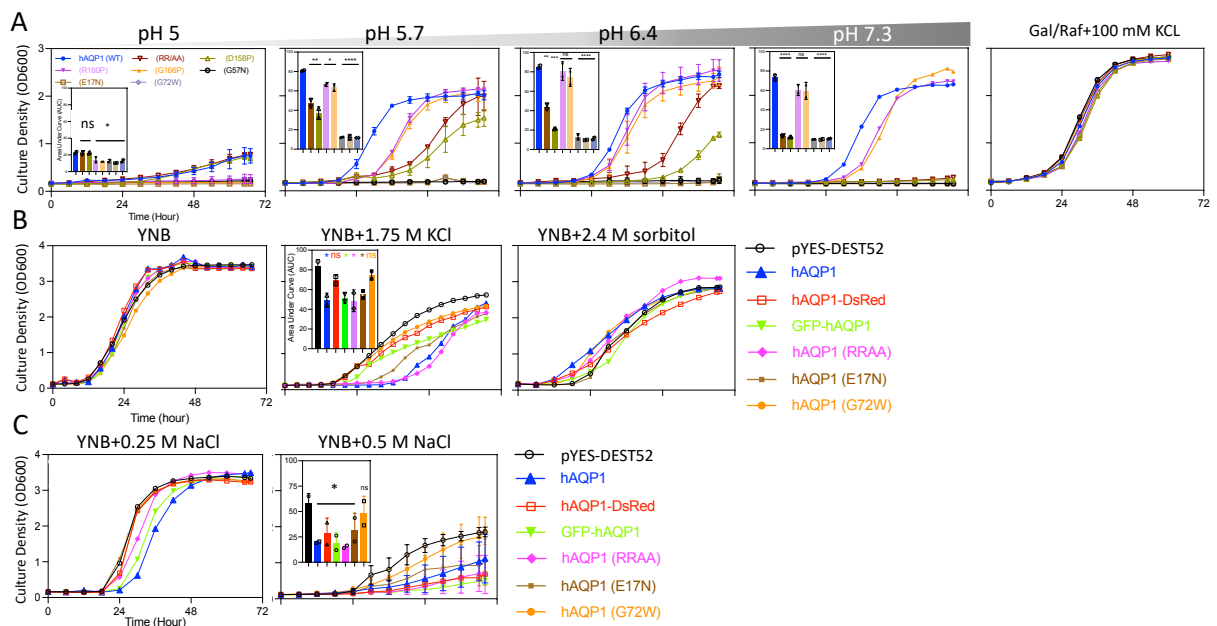


**Figure 4:** Investigation of pH-induced hAQP1-ion permeability dependent growth in yeast.

**A) Growth analysis of hAQP1 mutations affecting pH sensitivity or water and ion permeability of hAQP1.** CY162 transformed with hAQP1 (wild-type), ion-permeable related mutants (R159,R160/AA, D158P, R160P, G166P, G57N), water and ion-permeable mutant (G72W) or pH-dependent mutant (E17N) and  $K^+$  uptake-dependent growth rescue mediated by these constructs measured at different pH values. AUC plots showing the growth rate differences amongst the constructs. Growth curves of all constructs in control medium. **B-C) Yeast**



**membrane localization of hAQP1 constructs using *aqy*-null strain of *S. cerevisiae* under osmotic stress.** *S. cerevisiae* that does not express endogenous aquaporins (*aqy1* and *aqy2*) was transformed with mutants and fluorescent-tagged constructs that failed to rescue yeast growth defect and grow under osmotic stress at different pH values. pYES-DEST52 (control, black), hAQP1 (wild-type, blue), GFP- (green), -DsRed (red), RR/AA (pink), E17N (brown) and G72W (orange). Hyperosmotic stress was applied by osmo-equivalent concentration of either KCl, NaCl or sorbitol. Yeast containing the indicated plasmids were grown in 96-well plates in normal YNB medium supplemented with gal/raf and exposed to the indicated concentrations of KCl (B) and NaCl (C). YNB only or sorbitol conditions were used as control media in which all cells grow equally (B, first and last plot). The growth inhibition ratio mediated by efflux of water via functional channels under osmotic stress measure against control and plotted as AUC (merged average of two independent experiments). Empty vector and wild-type hAQP1 were served as controls.

### **3.6. hAQP1 exhibits sodium permeability in yeast cells.**

The yeast CY162 line deficient in Na<sup>+</sup> export has been used to characterise Na<sup>+</sup> permeability of exogenously expressed channels (54, 69-71), based on the demonstration that an accumulation of cytosolic Na<sup>+</sup> mediated by introduced Na<sup>+</sup> permeable channels results in growth inhibition of CY162 cells. *AtKAT1* and *hAQP1* were introduced into CY162 yeast and assessed for Na<sup>+</sup> permeability under different pH conditions and extracellular Na<sup>+</sup> concentrations. Initial assay optimisation determined the concentrations of Na<sup>+</sup> for liquid cultures that did not substantially impair growth of *AtKAT1* expressing cells (positive control, *AtKAT1* channels are K<sup>+</sup> but not Na<sup>+</sup> permeable) (54). The non-toxic concentrations of extracellular NaCl concentrations ranging from 25 to 100 mM were used for testing hAQP1, in media with 6 mM KCl at different pH values (Figure 5A-C).

When grown in 100 mM NaCl at different pH, cells harbouring hAQP1 did not reach stationary phase, whereas *AtKAT1*-expressing cells reached the maximal growth, although with a slight growth inhibition by NaCl as compared to untreated cells (Figure 5A-B). Growth of hAQP1-expressing cells was strongly inhibited by NaCl in a dose- and pH-dependent manner. All cells grew similar in different NaCl concentration in the control medium (2% gal+ 2% raf+100 mM KCl), ruling out the possibility of toxicity of tested concentration of NaCl on the cells. These results further validated the function of hAQP1 in yeast as a non-selective cation channel and demonstrated that yeast assay is a capable tool to be used for characterising ion permeabilities of diverse AQP subtypes and can potentially extended to identifying intracellular and environmental cues that govern mechanisms of novel AQP ion channel gating.

Data in Figure 5C showing the inhibition of growth seen in CY162 cells expressing hAQP1 but not in control was confirmed in an assay using solid medium with 6 mM KCl and 100 mM

NaCl, as in agreement with the results in [Figure 5A](#). This data shows the inhibition of CY162 cell growth requires a hAQP1 Na<sup>+</sup>-permeable channel functionality.

To gain further insight into the mechanism by which hAQPs are involved in inhibiting the mutant phenotype yeasts, we transformed B31 yeast strain with hAQP1. In this assay, we predict that Na<sup>+</sup> flows down its electrochemical gradient, when Na<sup>+</sup>-selective channels are present, and Na<sup>+</sup> efflux being thermodynamically unfavourable, requires energy for active transport. When a Na<sup>+</sup>-ATPase is expressed in B31, the yeast regain the ability to grow in high concentrations of extracellular Na<sup>+</sup> (72). As shown in [Figure 5D](#), B31 cells expressing empty vector (negative control), AtHKT1 (positive control) or hAQP1 screened in medium supplemented with 200-400 mM NaCl. The results indicated that hAQP1 did not complement the defect in B31, as expected since hAQP1 is an ion channel and not an ATPase pump. In contrast, the hAQP1 ion channel rescued growth in CY162 by allowing channel mediated K<sup>+</sup> influx, an effect that was boosted by addition of 20 μM cGMP as an activator of hAQP1 ion channels (see [Figure 6A](#)). These results suggest that the baseline levels of cGMP in yeast might be sufficient to activate a proportion of the hAQP1 ion channel population, or that additional regulatory factors such as tyrosine phosphorylation of the hAQP1 channel may be promoting an adequate baseline level of ion permeability. The results from the B31 yeast strain indicate the rescue observed in CY162 is unlikely to be an artifact of heterologous channel expression in upregulating endogenous yeast channels or transporters.

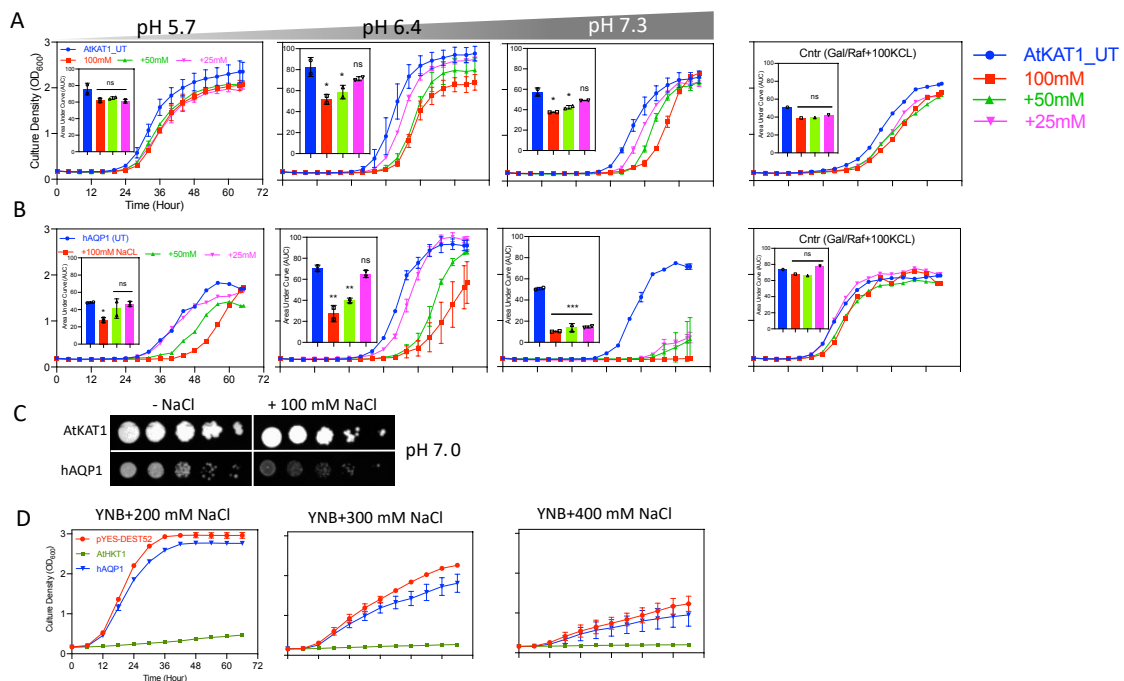


**Figure 5:** Na<sup>+</sup> permeability of hAQP1 is pH sensitive in yeast.

**Salt sensitivity of the hAQP1 growth inhibition assays in CY162 strains.** **A)** Na<sup>+</sup>-induced growth inhibition of CY162 expressing AtKAT1 or **B)** hAQP1 at pH 5.7, 6.4 or 7.3 (note that pH 5.0 condition was dropped out from our further screening as hAQP1-expressing cell growth rescue were negligible). **C)** Na<sup>+</sup>-mediated growth inhibition comparison in cells expressing hAQP1 or control on solid medium containing 6 mM KCl with or without indicated NaCl at pH 7.0. **D)** Growth inhibition comparison of B31 yeast strain cells (defective in Na<sup>+</sup> efflux, *Ena* and *Nha*) expressing AtHKT1 (positive control), pYES-DEST52 (negative control) or hAQP1. Cells were grown in YNB medium with the indicated concentrations of NaCl at 29 °C for 70 hours.

### ***3.7. Optimising the assay for mass-screening and drug discovery for aquaporin ion channel. hAQP1 ion channel, not water channel, blockers inhibit growth of *S. cerevisiae* in a dose-dependent manner.***

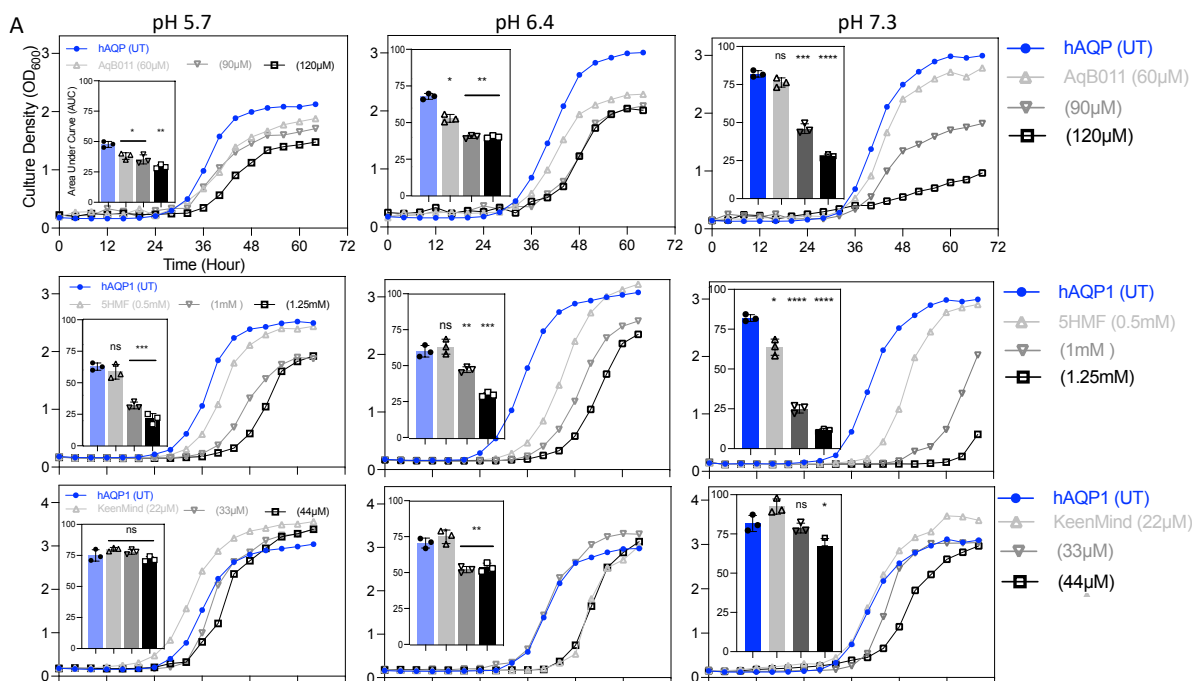
Knockout mice have been used to study the possible physiological significance of AQP channel functions and have supported the potential focus on these channels as therapeutic targets for drug discovery. Nevertheless, progress in the field of AQP drug discovery has been slow, in part due to complexities caused by diverse interactions with signaling pathways and proteins, and difficulties in defining screening methods to show efficacy and target specificity of the candidate drugs.

As an initial step towards addressing the unmet need for AQP ion channel drug discovery tools, we performed a pilot study using both a spot test and the liquid assay approaches, in which wild-type hAQP1-expressing cells were grown at different pH conditions in the presence of either water or ion channel inhibitors. Growth in liquid screening was more easily quantified than on solid medium, allowing the growth difference to distinguished between various conditions. A low starting cell density (~0.005-0.01 cells/200 µl as the initial condition) was more effective for detection of inhibitory drug actions.

To confirm the growth sensitivity of hAQP1-expressing cells in CY162 to known ion channel blockers, wild type hAQP1-expressing cells were treated with AqBO11 (60, 90, 120 µM), 5HMF (0.5, 1, 1.25 mM), KeenMind (22, 33, 44 µM), AqF026 (20, 30, 40 µM) or Acetazolamide (200, 300, 400 µM) in either pH 5.7, 6.4 or 7.3 ( $\pm$  0.1) for 70 hours. Growth was monitored by optical density (OD) at 600 nm by spectrophotometer every 30 minutes., but the plots show data only at 6 hours intervals for visual clarity. The hAQP1 ion channel inhibitors (AqBO11, 5HMF) caused dose-dependent inhibition of growth, in contrast to the lack of effect of hAQP1 water channel modulators (the blocker Bacopaside II as a major component of the herbal extract KeenMind, and the water channel agonist AqF026). A slight growth inhibition induced by KeenMind at pH 6.4 and 7.3 could be due to the presence of low levels of Bacopaside-I (which blocks hAQP1 ion permeability) (73). We also noted, a slight growth reduction by acetazolamide which was shown to inhibit hAQP1 water permeability. Based on the yeast result, however, it is worth testing acetazolamide on hAQP1 ion

permeability at different pH values in other expression models such as oocytes. The Area Under Curve quantification (bar plots) allows comparison of the inhibitory effect of each drug (Figure 6A). Possible pH sensitive effects of AqB011 and 5HMF for example might reflect proton competition for the binding site, or conformational changes resulting from pH sensitive amino acids in regions crucial for ion channel function.

Preservation of the viability of cells in the presence of the highest used concentrations drugs were confirmed by growth in control medium (gal/raf+100 mM KCl), in which cells grew equally well in the presence or absence of the drugs (Figure 6B). The inhibitory effect of ion channel but not water channel inhibitors on yeast growth showed that rescue depended on hAQP1 ion permeability. This modified yeast screening method thus shows promise as an effective screening system for detecting hAQPs channel modulators by quantifying small changes in growth rates and might be useful for high throughput discovery of novel agents for studying AQP ion channels across different phyla.



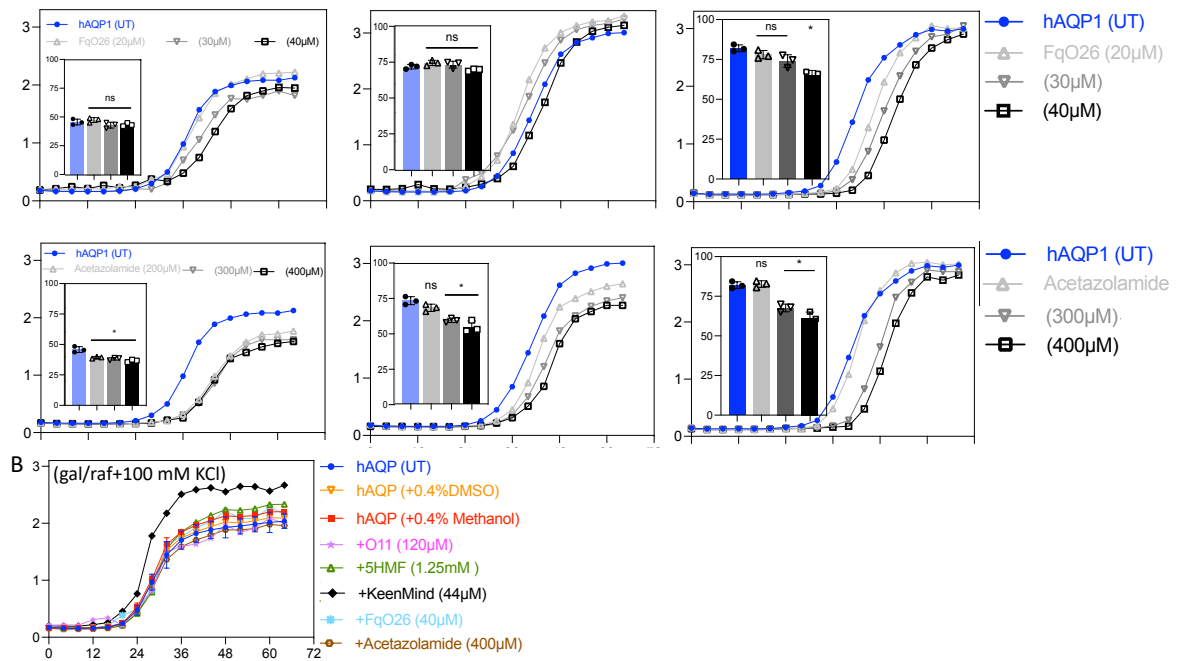


**Figure 6:** Effect of hAQP1 water or ion permeability inhibitors on the complementation of yeast strain CY162 growth defect.

**A)** Complementation of growth defect induced by hAQP1  $K^+$  uptake is inhibited by ion channel inhibitors not water transport inhibitors. CY162 yeast strain expressing hAQP1 were grown in inducing medium without (blue), with known hAQP1 ion permeability inhibitors (AqB011, 5HMF) or water transport inhibitors (KeenMind, AqF026 or Acetazolamide) for 68 hours in the presence of 6 mM KCl at pH 5.7, 6.4 or 7.3. (back=highest dose, bright grey=lowest dose). Growth rate differences were determined by calculation of a Area Under Curve (AUC). **B)** Yeast expressing hAQP1 and drug treatments (at their highest dose) grow equally well on standard medium, with the exception of an increased growth by KeenMind (control: 2% gal+2% raf with addition of 100 mM KCl). Relevant vehicle control was used as untreated (UT) for each drug as follow; DMSO for AqB011, 5HMF, methanol for KeenMind, water for AqF026 and acetazolamide. Merged average of three independent experiments with two technical replicates are shown.

### 3.8. The KCl-induced growth rescue by hAQP1 is attenuated by divalent cations.

As shown in Figure 7, CY162 cells exhibit  $K^+$ - and pH-dependent growth enhancement mediated by hAQP1 expression, in media supplemented with low KCl (6 mM). This growth was tested for inhibition by divalent cations and showed differential sensitivity with the rank order of  $CdCl_2 > CaCl_2 \gg BaCl_2 > CoCl_2, NiCl_2$  at pH 6.4 and 7.3. Except for  $CdCl_2$  less or no sensitivity to other divalent cations observed at pH 5.7.  $CdCl_2$  is known as a non-selective blocker of diverse classes of ion channels including AQPs (20). Cell viability at their highest used concentrations of divalent cations was not affected; all cells grew equally well in control medium (gal/raf+100mM KCL) (Figure 7B), showing no adverse effects of divalent cations on cell survival. These results confirm prior work showing ion permeability of hAQP1 can be inhibited by divalent cations (20).

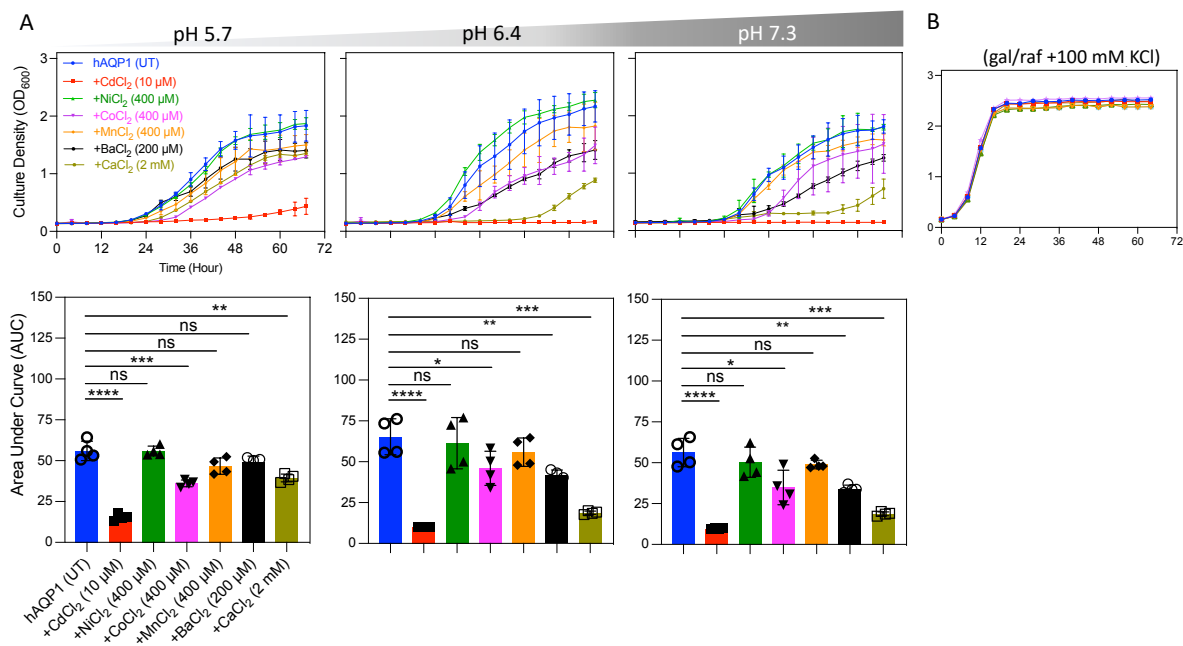


**Figure 7: The effect of divalent cation on hAQP1 ion permeability in yeast.**

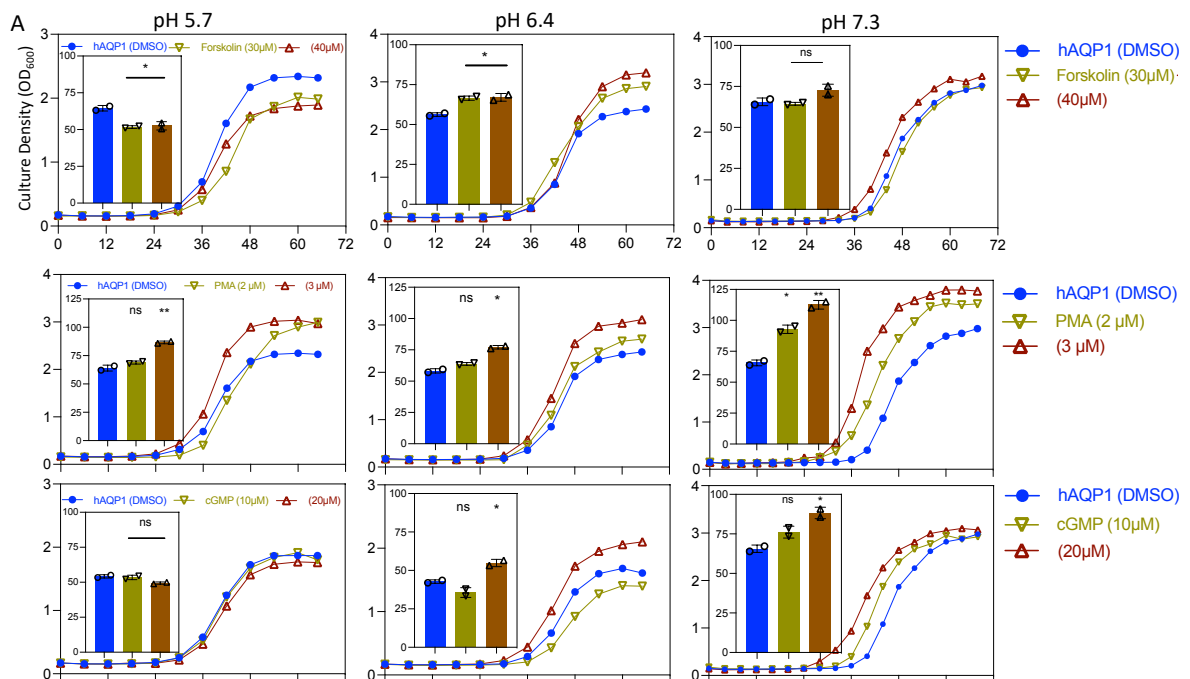
**A)** Effect of divalent cations on hAQP1 K<sup>+</sup> uptake-dependent growth rescue at different pH values. Growth of CY162 yeast strain expressing hAQP1 without (blue) or Cd<sup>2+</sup> (red), Ni<sup>2+</sup> (green), Co<sup>2+</sup> (pink), Mn<sup>2+</sup> (orange), Ba<sup>2+</sup> (black) and Ca<sup>2+</sup> (sage) in presence of 6 mM KCl and indicated pH values. Growth rate differences were determined by calculation of an Area Under Curve (AUC). **B)** Yeast expressing hAQP1 grow equally well on standard medium without (Blue) or with addition of divalent cations (control: 2% galactose+2% raffinose with addition of 100 mM KCl). Concentration of divalent cation decided based on previous studies on frog oocyte and our pilot screening in yeast in which indicated doses did not show any cell viability toxicity in control medium (data not shown). The average of at least two independent experiments with two technical replicates are shown with each point representing mean ± SD.

### 3.9. Optimising an assay for simultaneous testing of a matrix of intracellular signaling stimuli.

Yeast intracellular messenger systems have been shown to respond to protein kinase stimulators (74, 75). Despite the demonstrated value of yeast for discovery of proteins important for human biology including signaling proteins (76-78), using yeast to study mechanisms of channel gating has not been well explored. Post-translational modifications have key roles in controlling gating mechanisms of aquaporins (32) and other protein channels (79). Yeast as a heterologous system offers a unique method to define mechanisms of ion channel gating and modulation. This potential was tested here by investigating the effects of modified protein kinase (PK) signaling on aquaporin ion channel activity, assessed by the rescue of yeast cell growth.

In [Figure 8](#), the effects of PK stimulators on hAQP1 ion conductance activity, measured as the rescue of growth of CY162 in liquid medium with 6 mM KCl, was tested in the presence and

absence of pharmacological activators of PKs: Forskolin (Protein Kinase-A, PKA), PMA (Protein Kinase C, PKC), cGMP (Protein Kinase G, PKG), and the non-selective PK inhibitor H7, in pH 5.7, 6.4 or 7.3. PK modulators that resulted in increased hAQP1 ion channel permeability would be predicted to facilitate growth rescue, whereas PK modulators that decreased hAQP1 ion channel activity would be predicted to suppress yeast growth. Published work has demonstrated that the ion channel activity of hAQP1 was enhanced by tyrosine kinase mediated phosphorylation (80) and by threonine phosphorylation via PKA and PKC (81), or by activators of PKG (44). In agreement, we found that PKA, PKC and PKG activators, enhanced the growth rescue mediated by hAQP1 ion permeability in a pH-dependent manner as shown and quantified in Figure 8A. The rescue of growth by hAQP1 was inhibited by H7. These results independently confirm prior work showing that hAQP1 ion channel gating is modulated by post-translation modifications. Cells grown in the presence of highest concentration of PK agents were not affected and grew equally well in control medium (gal/raf+100 mM KCl) (Figure 8B) indicating the growth inhibition of yeast by H7 treatment was not an indirect effect of cell death.



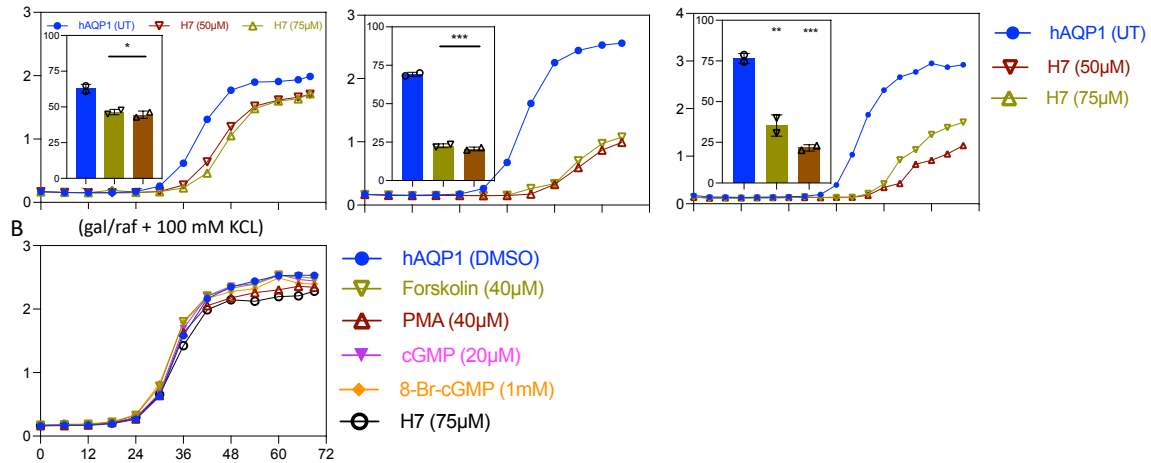


**Figure 8:** Stimulation of hAQP1-induced growth rescue by modulators of protein kinases.

**A)** The growth mediated by hAQP1 ion permeability in yeast is sensitive to PKA, C and G and reduced by PKs inhibitor in a pH-dependent manner. CY162 cells bearing hAQP1 were grown in YNB inducing medium+6 mM KCl at pH5.7, 6.4 or 7.3. Vehicle (0.4% (v/v) DMSO) or water (UT) was served as control condition and the growth rescue rate was compared with when cells were treated with protein kinase activator/inhibitor. Forskolin (PKA activator), PMA (PKC activator), cGMP (PKG activator) or H7 (PK inhibitor) were used at indicated doses based on studies on frog oocyte and our pilot screening (data not shown). **B)** Growth rate comparison between different treatment in control medium. The average of at least two independent experiments with two technical replicates are shown.

### 3.10. A lithium-sensitive probe confirms functional hAQP1 ion channels in yeast plasma membrane.

The role of hAQP1 ion channels in mediating fluxes of monovalent cations was assessed using a lithium-sensitive photo switchable probe (known as 'SHL') previously designed and characterised as an optical tool for detecting hAQP1 ion conductance (45). Extracellular  $\text{Li}^+$  is permeable through activated hAQP1 ion channels. The entry of  $\text{Li}^+$  into CY162 cells expressing hAQP1 or empty vector was tested in growth permissive YNB medium containing 2% gal+ 2% raf+100 mM KCl (Figure 9A, middle row), and compared to media in which hAQP1 expression was not induced (YNB + glucose+100 mM KCl, without transcription inducer) (Figure 9A, lower row).

Yeast cells were preincubated in the  $\text{Li}^+$  sensitive probe (SHL) for 2 hours, rinsed and transferred into  $\text{Li}^+$ -substituted saline, and imaged. An approximately 2.5-fold higher  $\text{Li}^+$  signal intensity was observed when cells expressing hAQP1 as compared to those with empty vector expressing cells (Figure 9B), independently demonstrating the presence of a non-selective cation channel specifically in the yeast strain expressing hAQP1 channels, and ruling endogenous yeast membrane permeability to  $\text{Li}^+$ , at least to a detectable level by microscopy. Since *Atrk1 Atrk2* yeast cells are sensitive to alkali metals (48) and hAQP1 is permeable to monovalent cations including  $\text{Li}^+$  (45), we tested the effect of  $\text{Li}^+$  on yeast viability for the



same duration of exposure used for the SHL experiment (6 hours), and confirmed the cells remained healthy. **Figure 9C** showing normal growth with  $\text{Li}^+$  ruled out the possibility that fluorescent signals were indirectly due to cell death. The low signal in control cells confirmed the background leak of  $\text{Li}^+$  through other channel pathways was minimal compared to that induced by hAQP1.

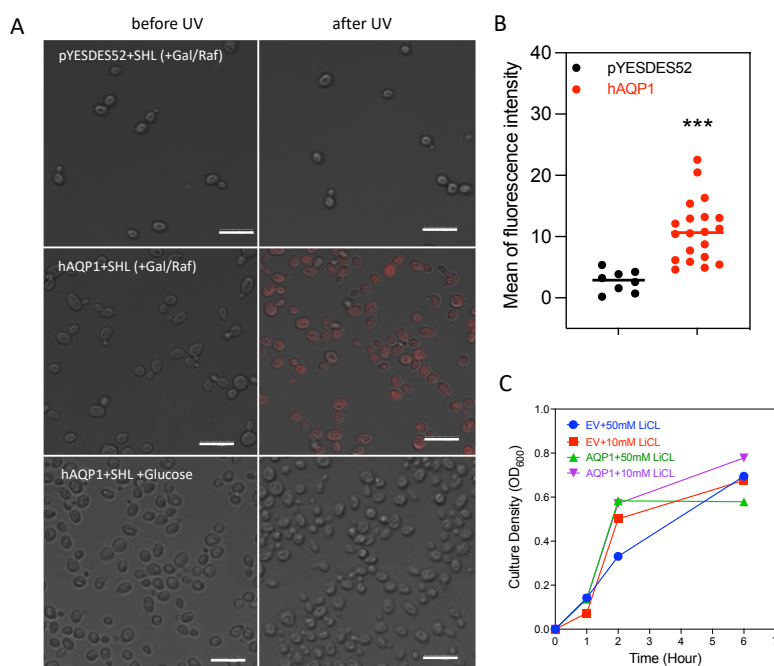


**Figure 9: Quantitative confocal analysis of functional hAQP1 ion permeability in yeast.**

**A)** Photo-switchable lithium probe confirms functional hAQP1 ion channel in yeast. CY162 cells bearing hAQP1 or empty vector (control) grown in inducing medium+100 mM KCl overnight and resuspended in sensor buffer and incubated on rotatory shaker at 29 °C for 90-120 minutes. Prior to imaging, cells were resuspended in imaging buffer and the sensor was turned on by UV radiation for 5 minutes. Imaging was done using Ex/Em=514 nm/550-650 nm. (see material and methods for more details). YNB+glucose+100 mM KCl used as control growth medium without inducing the protein expression (A, lower row). **B)** Total cellular fluorescence for 10-20 yeast cells, imaged as in A, was measured, and mean fluorescence intensities for all cells is presented as scatter plots. Student's t test was performed to assess significance ( $p < 0.0001$  \*\*\*). **C)** The effect of lithium on yeast cell viability bearing hAQP1 or empty vector in indicated concentration at pH 7.3. Scale bars are 10  $\mu\text{M}$ .

### 3.11. Using *E. coli* potassium deficient strain to investigate AQP1-dependent potassium permeability and growth rescue.

The bacterium *E. coli* was used as another heterologous system to test the growth rescue of hAQP1 mediated ion permeability (**Figure 10**). The *E. coli* strain TK2463 is defective in its native  $\text{K}^+$  uptake mechanisms (40) and has been used previously for characterising heterologously expressed ion channels (41). We transformed TK2463 bacteria with hAQP1 and control plasmids; protein expression was driven by the IPTG-inducible tac-promoter (41). In low  $\text{K}^+$  medium (4 mM KCl), expression of wild type hAQP1 improved growth substantially over the levels seen for the non-transfected control or transfected cells not treated with IPTG

(Figure 10), suggesting hAQP1 ion permeability can be characterised in the *E. coli* model. hAQP1-expressing cells treated with cGMP-CPT showed slight increased, though not statistically significant, *E. coli* growth. When hAQP1 expression was induced by IPTG, *E. coli* growth was restored compared to control ( $p < 0.05$  \*). *E. coli* thus shows promise as an alternative model for screening of AQPs ion channel activity as well as modulators and might be adapted to take advantage of differences in intracellular signaling pathways between bacteria and yeast to define the pathways controlling AQP ion channel activation.

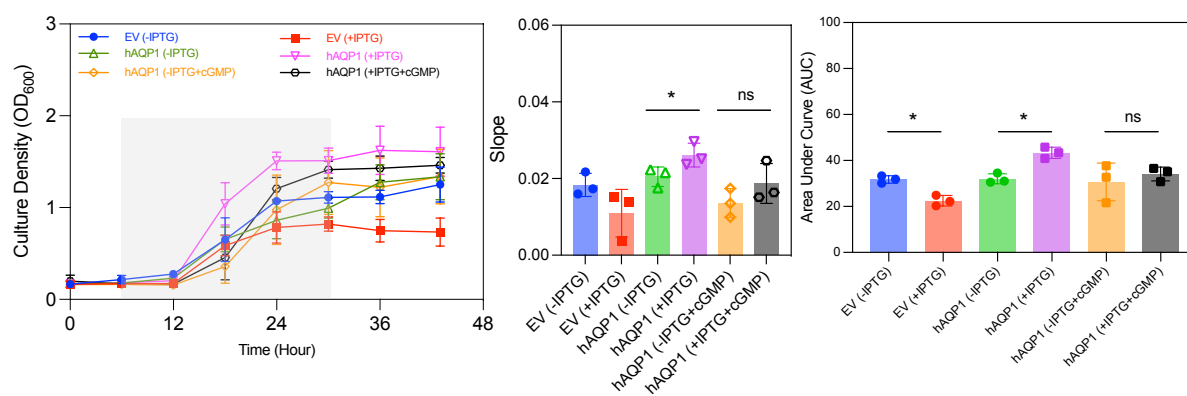


**Figure 10: Functional test of functional hAQP1 ion permeability in *E. coli*.**

Potassium deficient *E. coli* line TK2463 (defective in  $K^+$  uptake) bearing pET-DEST42 vector or with hAQP1 were grown in low  $K^+$  medium (4 mM KCl) with or without additional of gene expression inducer (0.6 mM isopropyl $\beta$ -D-1-thiogalactopyranoside, IPTG) in the present or absent of cGMP. 100  $\mu$ g/mL carbenicillin was used as selective marker (left panel). Growth rate of two independent experiments ( $n = 3$ ) was monitored in OD<sub>600</sub> every 6 hour in 96-well microplate reader. Growth rates were determined by calculation of a slope between 6-30 hours (highlighted) (middle panel). AUC plot indicating the growth rate different between conditions. Significant differences were analysed by unpaired *t* test and are reported as  $p < 0.05$ \*; ns, not significant (right panel). The average of at least two independent experiments with two technical replicates are shown.

### 3.12. hAQP1 does not elicit differential pH and voltage sensitive currents in *X. laevis* oocytes.

A correlation between pH and permeability of aquaporins to different substrates has been suggested (1-4, 23, 82). However, the possible pH-dependence of the ionic conductance associated with some of the classes of AQPs remains to be fully defined.

The CY162 yeast model has a strongly negative resting membrane potential and prompted further investigation of the possible effects of hyperpolarizing voltage steps on hAQP1 ion channel properties in the oocyte expression system using two-electrode voltage clamp. Voltage-clamped hAQP1-expressing oocytes were stepped from a resting membrane potential of -40 mV to -120 mV, and the voltage was ramped to +60 mV over 300 ms to evaluate the current-voltage responses (Figure 11).

hAQP1-expressing oocytes were activated by bath application of a membrane-permeable cyclic GMP analogue at 20  $\mu$ M (see Methods), as per established protocols (44) at pH 5.1, 6.1 or 7.4.

The current responses to the voltage ramp protocol showed slight stimulation toward more positive and negative voltage, however, the response did not seem to be significant or pH dependent (Figure 11C). The hAQP1 ion conductance was functional over a range of pH values (pH 5.1 to 7.3). At pH 7.4 the activated current amplitude was  $8.785 \pm 1.652 \mu\text{S}$  (n=5) and was blocked by  $\text{Cd}^{2+}$  ( $5.3 \pm 1.9 \mu\text{S}$ ). The mean current amplitude at pH 6.1 was  $5.1 \pm 1.1 \mu\text{S}$  (n=4), and blocked by  $\text{Cd}^{2+}$  ( $2.6 \pm 0.9 \mu\text{S}$ ). At pH 5.1 the activated current amplitude was  $7.7 \pm 1.4 \mu\text{S}$  (n=5), blocked by  $\text{Cd}^{2+}$  ( $2.5 \pm 1.9 \mu\text{S}$ ) (all means SEM) ( $600 \mu\text{M Cd}^{2+}$  was used in saline bath for each indicated pH values) (Figure 11A-B).

The initial ionic conductance seen in hAQP1 expressing oocyte in pH 7.4 or 6.1 immediately after the recording electrodes were inserted into the oocytes were slightly higher than those in pH 5.1, which might be due to low n values; or higher baseline activation of cGMP levels or channel conformation effects of the lower pH value (Figure 11B). No significant ion conductance after application of cGMP were observed in non-hAQP1 expressing control oocytes at different pH values during 30-minutes recording sessions ( $P > 0.05$ ) (Figure 11B).  $\text{Cd}^{2+}$  block of the ion conductance of the channel appeared to be greater at pH 7.3 than pH 5.1 or 6.1. The onset of  $\text{Cd}^{2+}$  block appeared to be slower at pH 5.1 (Figure 11C, blue arrows), in agreement with the observed pH-dependence of  $\text{Cd}^{2+}$  inhibition of yeast growth (Figure 7). A similar phenomena was proposed for regulation of plant AQPs by pH and  $\text{CdCl}_2$  (22). No activation was observed from water injected (Figure 11D) or uninjected control oocytes.

Significant differences were not detected for hAQP1 currents in the oocyte system in acidic and alkaline conditions (Figure 11E-F). Activating the channel in extracellular NaCl or KCl bath salines did alter the reversal potential, consistent with the non-selective cation permeability of the AQP1 ion channel. The oocyte results showed less evidence for pH-dependent ion conductance mediated by hAQP1 than was observed in the yeast system, which could be due to many reasons, including: a need for higher n values to distinguish more subtle effects in the oocyte, differences in membrane potential or membrane composition between these two models, or the comparatively short time intervals used for recording oocyte responses (<1h) as compared to 3 to 5 days for yeast screening (see discussion for a more detailed comparison). In agreement with our yeast screening, we found hAQP1 retains ion permeability over a range of pH values and might show pH sensitivity though this remains to be addressed in future work.

In summary, pH or membrane potential were not found to have a measurable impact on hAQP1  $\text{K}^+$  and  $\text{Na}^+$  conductance under the conditions tested.

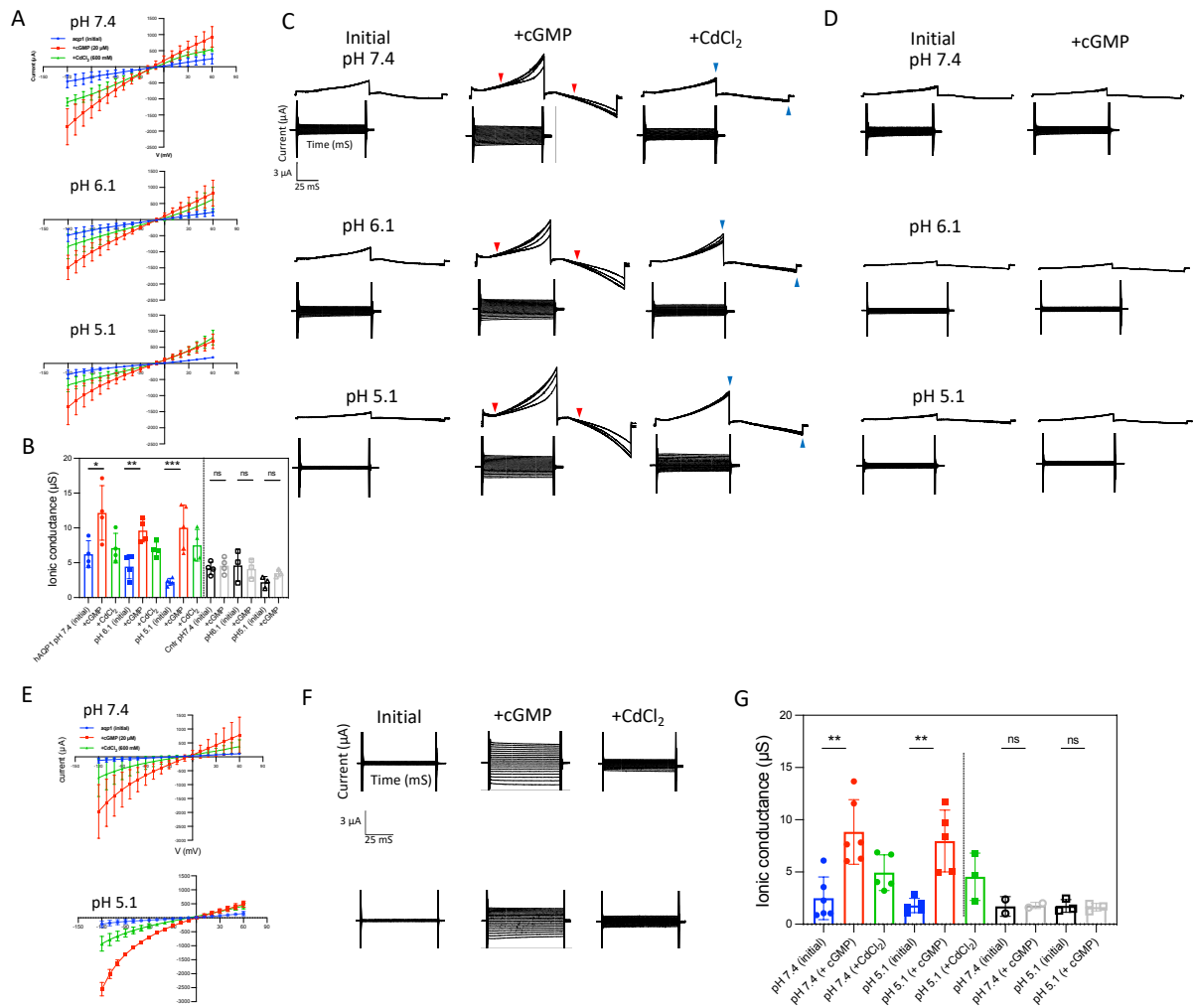


**Figure 11: Effects of pH on ionic current responses in oocytes expressing hAQP1.**

**A)** Current–voltage relationships were obtained by two-electrode voltage-clamp. Currents recorded from oocytes expressing hAQP1 channels in pH 5.1, 6.1 and 7.4 activated by 20  $\mu$ M cGMP (red) and blocked by 0.6 mM CdCl<sub>2</sub> (green). Voltage steps (from –120 to +60 mV, from a holding potential of –40 mV). **B)** Box plot summary of compiled data for control and hAQP1 expressing oocytes stimulated by cGMP before and after Cd<sup>2+</sup> application (n=4 from two independent batches of oocyte preparation, mean  $\pm$  SD). ( $p < 0.005^{***}$ ); ( $p < 0.05^{**}$ ); ( $p < 0.5^*$ ), ns (not significant); using ANOVA with post-hoc Bonferroni tests. **C-D)** A series of voltage steps were applied, and the resulting steady state currents recorded. The examples are from an oocyte expressing hAQP1 or water injected (control) bathed in 100 mM KCl at indicated pH, activated by cGMP, and blocked CdCl<sub>2</sub>. Control oocytes were not treated by CdCl<sub>2</sub> as no activation was observed by cGMP treatment. Current trace of an oocytes for both hAQP1 and control shown under voltage traces in panel C and D at indicated conditions. The initial early-point activation of hAQP1 ionic current under different series of voltages marked with red arrows. The inhibition comparison voltage traces by CdCl<sub>2</sub> at different pH marked with blue arrows.

**E)** The current amplitude of hAQP1 ion conductance in high Na<sup>+</sup> saline. Two-electrode voltage-clamp currents were recorded in high Na<sup>+</sup> saline from oocytes expressing hAQP1 channel at indicated pH values activated by cGMP and blocked by CdCl<sub>2</sub> and plotted as I-V plot. **G)** Box plot summary of compiled data for control and hAQP1 expressing oocytes activated by cGMP before and after Cd<sup>2+</sup> treatment (n=5 from two independent batches of oocyte, mean  $\pm$  SD). ( $p < 0.05^{**}$ ); ns (not significant). **F)** Current trace of an oocytes expressing hAQP1 at indicated pH are shown. IV plot and trace of currents from control oocyte not shown as they were similar to our previous studies. All solutions contained an additional (mM) 1 NaCl, 1 MgCl<sub>2</sub>, 5 HEPES Tris base for pH6.1 and 7.4, or 5 MES and Tris base for pH 5.1. Osmolality of different saline and indicated pH values was measure by osmo-meter.

## 4. Discussion

In the present study, we introduced a novel and an unbiased high-throughput system and confirmed that hAQP1 has the capacity to allow monovalent cation influx across membranes. This function appears to be modulated by intracellular signalling pathways such as phosphorylation by protein kinases or binding of signalling molecules (such as cGMP) as shown in the previous studies. It is exciting to consider the possibility that the approaches introduced here might be used to discover a vast array of ion-conducting AQP channels from all kingdoms of life.

### *Yeast versus conventional electrophysiologic models for ion channel studies*

The adaptable yeast expression system as a mass-throughput screening assay has proven useful for:

- i) exploring structure-function relationships of ion channels by mutagenesis (83, 84) and patch-clamp recording of heterologously expressed ion channels (85, 86);
- ii) defining fundamental eukaryote mechanisms for governing cellular ion homeostasis (26, 27);
- iii) validating unusual ion channels that lack signature sequence motifs such as the *Trypanosoma cruzi* cation channel (87);
- iv) studying channels that are not expressed in the plasma membrane of native host cells, but can be assessed in isolated yeast vacuoles (88, 89);
- v) testing the regulation of ion channels by protein-protein Interactions (90, 91).

This powerful system benefits from having a broad range of strain libraries including strains in which the growth phenotype changes and can be used to deduce the function of introduced ion channels. Furthermore, the yeast system can detect channels that are weakly or non-selectively permeable to ions. Gaber and colleagues showed a subset of KAT1 mutations that weakly restored growth in *S. cerevisiae*  $\Delta trk1\Delta trk2$  cells are impotent to show detectable ion currents when expressed in *Xenopus oocytes* (60). Yeast and oocyte expression systems both have been used to demonstrate the effects of pH on ion channel activity (92-94). The ability to identify weakly ion-permeable channels could be due to the time scale of the experiments, covering hours to days in yeast growth assays vs seconds to minutes timescales used in patch and voltage-clamp.

Yeast intracellular messenger systems including network activation and post-translational modifications sensitive to respond to a broad array of standard modulatory pharmacological agents (95-98), making it possible to study activation mechanisms of ion channels (e.g., classical cyclic nucleotide-gated ion channels, and cGMP-gated like hAQP1 ion channels) that

rely on concerted actions of stimuli and interactions and are governed at the converging point of several cell signaling mechanisms.

### *Limitations*

While there are many advantages of using a high-throughput expression system for ion channels and aquaporins, shortcomings must be noted for heterologous expression of genes in yeast or bacteria. For instance: i) not all ion channel genes are adequately expressed and localized in the membrane due to signal peptide variation between the host and heterologous expression system, ii) artifactual outcomes might arise by interference from yeast signalling pathways that are not necessarily involved in the native gating mechanism (99, 100) but induce false-positive phenotypes (101); iii) yeast cell walls represent a barrier that can limit access of agents to channels in the plasma membrane. Notwithstanding these limitations, the heterologous expression strategy has made numerous key contributions to our understanding of AQP water and solute homeostasis and will indubitably continue to provide invaluable insights for the field in the future.

### *Introducing a novel approach for mass-throughput yeast expression system for AQPs ion channel discovery*

All living organisms need a delicate balance of ions, including  $K^+$  and  $Na^+$ , to survive. When subjected to environmental stress, yeast employ unique transport systems that harvest  $K^+$  or exclude  $Na^+$  (56). Deletion or inactivation of  $K^+$  uptake genes, *S. cerevisiae* *Atrk1* $\Delta$ *Atrk2* (102), or  $Na^+$  efflux genes, *Aen1-4*, *Anhal* (39), have resulted in powerful systems for  $K^+$  and  $Na^+$  ion channel discovery. Some of the first plant (103) and mammalian (104) potassium channels were characterised using yeast mutant strains. This unicellular system also can be used for fluorescence-based detection of ion influx, allowing channel activity to be monitored optically (105). This yeast heterologous expression system can be extended to testing other classes of protein channels which have previously been thought to lack any ion permeability, such as the AQPs (3, 31).

Since the first cloning and characterisation of the AQP1 water channel about three decades ago (106), significant progress has advanced understanding of the structure and function of these channels. However, AQP drug discovery has progressed at a considerably slower pace, and the exploration of AQP substrates other than water and glycerol has been an increasing area of focus (36). One reason for the modest rate of progress might be limited adoption of high-

throughput heterologous expression systems as research tools. A facile reproducible system for identifying new AQP ion channels described here could be expanded to more effective screening of modulatory agents and permeation properties, with a long-term goal of uncovering novel therapeutic agents.

The intriguing possibility that emerges is maybe all AQPs, regardless of their origin, can be permeable to monovalent cation channels, although some would likely be at very low conductance levels. Additional lines of data indicate that classes of AQP ion channels show differential sensitivity to pH, intracellular messengers, and protein kinase-dependent signalling.

In agreement with previous studies (107, 108), we found hAQP1 integrate into the yeast plasma membrane, though the trafficking efficiency is reduced by fusion-protein tagging with a fluorescent marker (Figure 3 and 4). Intact N- and -C terminal domains are required for membrane targeting, ion channel activation, and regulation by phosphorylation (80). Cytosolic loops also serve as regulators of channel functions (22). hAQP1 with C-terminal tags failed to rescue yeast growth in low  $K^+$  medium, despite some level of membrane localization, suggesting physical interference or steric hindrance of the hAQP1 loop D domain required in ion channel gating (80) (Figure 3D). Conversely, tagging the channel at N-terminal reduced the level of membrane localization of the channel compared to wild type, and slowed but did not prevent the ion conductance needed for yeast growth rescue.

Plasma membrane localization and correct assembly of the AQP channel proteins in yeast were confirmed using an osmotic stress assay (Figure 4B-C), showing that constructs which failed to fully rescue yeast growth were not misfolded or mislocalized. In the osmotic stress assay, the presence of water-permeable pores (AQPs) caused inhibition of growth by water loss, showing the wild type and mutant AQPs were present in the membrane, and folded correctly into functional water channels. The loss of growth rescue in the CY162 strain can thus be attributed directly to the effect of the mutation on compromising ion channel functionality specifically.

### *Introducing a yeast-based screening for AQP ion channel modulators and drug discovery*

We tested for dose-dependent inhibition of hAQP1-mediated  $K^+$  uptake-dependent yeast growth by benchmarking responses to previously published modulators for AQP1 ion and water channel activity. The rescue of growth was inhibited by the hAQP1 ion channel blockers

AqB011, 5HMF, and partially by KeenMind. The hAQP1 water transport agonist, AqF026 (109, 110) showed no effect (ns) suggesting water permeation is not a rate-limiting factor for yeast growth. Acetazolamide a non-specific agent suggested to block AQP water channels showed a trend towards growth reduction though the effect was not dose-dependent (\* $p < 0.05$ =acetazolamide). Inhibiting hAQP1 water transport appears to have minimal effects on the yeast growth in the conditions tested. KeenMind exhibited some inhibition of the channel which was pH-dependent. This outcome might be attributed to the presence of the hAQP1 ion channel blocker *Bacopaside-I* in the plant extract mixture (73, 111), in addition to the major component *Bacopaside-II* which selectively blocks the hAQP1 water channel.

Success in screening divalent cations produced results (Figure 7) that agreed with our previous electrophysiological studies in oocytes (3, 20, 22); the rescue of yeast growth by hAQP1 was inhibited by divalent cations with the highest sensitivity to  $\text{Cd}^{2+} > \text{Ca}^{2+} > \text{Ba}^{2+} > \text{Co}^{2+}$ ,  $\text{Ni}^{2+}$  at pH 6.4 and 7.3. No block at pH 5.7 was seen for divalent ions except  $\text{Cd}^{2+}$ . This work suggests the possibility of the pH-sensitive sites of interaction with divalent cations or changes in conformation altering access to the divalent blocking site.

High-throughput screening of chemical libraries for modulators of AQP ion activities offers a promising method. We demonstrated feasibility of using the yeast system for one of the best studied AQP ion channels, AQP1, suggesting potential for future screening of large libraries and identification of more potent modulators. A long-term goal is building a definitive portfolio of AQP ion channel antagonist and agonist molecules as tools for basic research and clinical innovation in the ion channel field.

The yeast model described offers potential to validate many properties of AQP ion channels, including substrate specificity, sensitivity to kinases, and identification of pharmacological activators and inhibitors. In particular, we showed PKA (forskolin), PKC (PMA), PKG (cGMP) stimulators trigger the ion conductance of hAQP1 in the yeast system (Figure 8). In agreement with the oocyte studies, we found the rescue of yeast growth was increased by agents that activate hAQP1 ion channels, forskolin, and cGMP (close to physiological pH) or PMA (at all different pH values) in a dose-dependent manner. Using the protein kinase phosphorylation blocker agent (H7), we showed the enhanced growth rate mediated by hAQP1 ion uptake was reduced, consistent with the proposed role of phosphorylation in modifying AQP ion channel availability.

The yeast system can also be used for fluorescence-based detection in which the kinetics of ions transport linked to the target channel's ion activity can be monitored. Using a lithium prob sensor designed and developed in our lab, we further confirmed the permeability of hAQP1 in



CY162 in real-time (Figure 9). The potential use of unicellular models for AQP ion permeability discovery was also illustrated in the *E.coli* mutant strain defective in K<sup>+</sup> uptake (Figure 10). In agreement with our yeast screening for hAQP1, we showed K<sup>+</sup> and Na<sup>+</sup> conductance of hAQP1 in oocyte expression system between pH 5.1-7.4 (Figure 11).

### *Conclusion*

Attempts have been made using yeast as a heterologous expression to study the potential ion permeability of hAQP1 (31), and plant PIP aquaporins (3, 32, 112); however, contrasting findings might reflect differences between heterologous expression systems or a need for refined detection methods. The detection method introduced here might provide a tool to bypass some of the difficulties and limitations of current traditional electrophysiological methods and offer a combined platform for discovery of new classes of AQP ion channels, modes of action, mechanisms of gating, and potential target-specific drug discovery. A further benefit of the system is relatively ease and affordability. Since AQPs are expressed in all kingdoms of life, the expansion of roles into new functions as proposed here for all hAQPs might solve mysteries still surrounding ion homeostasis

### *Future directions*

Caveats must be considered regarding the future candidate AQPs ion channels proposed here, recognising that artefacts or confounding factors might contribute indirectly to the observed outcome. However, if the findings are validated by other groups, the impact on the field could be revolutionary. AQP ion permeability is likely to have both beneficial and detrimental consequences in physiology and remains as an open question. Outcomes of this study draw attention of emerging breadth of ion channel roles in the ancient story of AQPs.

## **5. References**

1. Mósca AF, De Almeida A, Wragg D, Martins AP, Sabir F, Leoni S, et al. Molecular basis of Aquaporin-7 permeability regulation by pH. *Cells*. 2018;7(11):207.
2. Rodrigues C, Mósca AF, Martins AP, Nobre T, Prista C, Antunes F, et al. Rat aquaporin-5 is pH-gated induced by phosphorylation and is implicated in oxidative stress. *International Journal of Molecular Sciences*. 2016;17(12):2090.
3. Byrt CS, Zhao M, Kourghi M, Bose J, Henderson SW, Qiu J, et al. Non-selective cation channel activity of aquaporin AtPIP2; 1 regulated by Ca<sup>2+</sup> and pH. *Plant, cell & environment*. 2017;40(6):802-15.

4. Leitão L, Prista C, Moura TF, Loureiro-Dias MC, Soveral G. Grapevine aquaporins: gating of a tonoplast intrinsic protein (TIP2; 1) by cytosolic pH. *PLoS One*. 2012;7(3):e33219.
5. Tournaire-Roux C, Sutka M, Javot H, Gout E, Gerbeau P, Luu D-T, et al. Cytosolic pH regulates root water transport during anoxic stress through gating of aquaporins. *Nature*. 2003;425(6956):393-7.
6. Yaneff A, Sigaut L, Gómez N, Fandiño CA, Alleva K, Pietrasanta LI, et al. Loop B serine of a plasma membrane aquaporin type PIP2 but not PIP1 plays a key role in pH sensing. *Biochimica et Biophysica Acta (BBA)-Biomembranes*. 2016;1858(11):2778-87.
7. Yasui M, Hazama A, Kwon T-H, Nielsen S, Guggino WB, Agre P. Rapid gating and anion permeability of an intracellular aquaporin. *Nature*. 1999;402(6758):184.
8. Zeuthen T, Klaerke DA. Transport of water and glycerol in aquaporin 3 is gated by H<sup>+</sup>. *Journal of Biological Chemistry*. 1999;274(31):21631-6.
9. De Almeida A, Martins A, Mósca A, Wijma H, Prista C, Soveral G, et al. Exploring the gating mechanisms of aquaporin-3: new clues for the design of inhibitors? *Molecular Biosystems*. 2016;12(5):1564-73.
10. Carbrey JM, Gorelick-Feldman DA, Kozono D, Praetorius J, Nielsen S, Agre P. Aquaglyceroporin AQP9: solute permeation and metabolic control of expression in liver. *Proceedings of the National Academy of Sciences*. 2003;100(5):2945-50.
11. Gotfryd K, Mósca AF, Missel JW, Truelsen SF, Wang K, Spulber M, et al. Human adipose glycerol flux is regulated by a pH gate in AQP10. *Nature communications*. 2018;9(1):1-11.
12. Choi H-J, Jung HJ, Kwon T-H. Extracellular pH affects phosphorylation and intracellular trafficking of AQP2 in inner medullary collecting duct cells. *American Journal of Physiology-Renal Physiology*. 2015;308(7):F737-F48.
13. Kaptan S, Assentoft M, Schneider HP, Fenton RA, Deitmer JW, MacAulay N, et al. H95 is a pH-dependent gate in aquaporin 4. *Structure*. 2015;23(12):2309-18.
14. Kalman K, Németh-Cahalan KL, Froger A, Hall JE. Phosphorylation determines the calmodulin-mediated Ca<sup>2+</sup> response and water permeability of AQP0. *Journal of Biological Chemistry*. 2008;283(30):21278-83.
15. Fischer G, Kosinska-Eriksson U, Aponte-Santamaría C, Palmgren M, Geijer C, Hedfalk K, et al. Crystal structure of a yeast aquaporin at 1.15 Å reveals a novel gating mechanism. *PLoS biology*. 2009;7(6):e1000130.
16. Törnroth-Horsefield S, Hedfalk K, Fischer G, Lindkvist-Petersson K, Neutze R. Structural insights into eukaryotic aquaporin regulation. *FEBS letters*. 2010;584(12):2580-8.
17. Soveral G, Madeira A, Loureiro-Dias MC, Moura TF. Membrane tension regulates water transport in yeast. *Biochimica et Biophysica Acta (BBA)-Biomembranes*. 2008;1778(11):2573-9.
18. Ozu M, Dorr RA, Gutiérrez F, Politi MT, Toriano R. Human AQP1 is a constitutively open channel that closes by a membrane-tension-mediated mechanism. *Biophysical journal*. 2013;104(1):85-95.
19. Leitão L, Prista C, Loureiro-Dias MC, Moura TF, Soveral G. The grapevine tonoplast aquaporin TIP2; 1 is a pressure gated water channel. *Biochemical and biophysical research communications*. 2014;450(1):289-94.
20. Kourghi M, Nourmohammadi S, Pei JV, Qiu J, McGaughey S, Tyerman SD, et al. Divalent cations regulate the ion conductance properties of diverse classes of aquaporins. *International journal of molecular sciences*. 2017;18(11):2323.
21. Németh-Cahalan KL, Hall JE. pH and calcium regulate the water permeability of aquaporin 0. *Journal of Biological Chemistry*. 2000;275(10):6777-82.

22. Verdoucq L, Grondin A, Maurel C. Structure–function analysis of plant aquaporin At PIP2; 1 gating by divalent cations and protons. *Biochemical Journal*. 2008;415(3):409-16.
23. Zelenina M, Bondar AA, Zelenin S, Aperia A. Nickel and extracellular acidification inhibit the water permeability of human aquaporin-3 in lung epithelial cells. *Journal of Biological Chemistry*. 2003;278(32):30037-43.
24. Zampighi GA, Hall JE, Kreman M. Purified lens junctional protein forms channels in planar lipid films. *Proceedings of the National Academy of Sciences*. 1985;82(24):8468-72.
25. Hub JS, Aponte-Santamaría C, Grubmüller H, de Groot BL. Voltage-regulated water flux through aquaporin channels in silico. *Biophysical journal*. 2010;99(12):L97-L9.
26. Mackie TD, Brodsky JL. Investigating potassium channels in budding yeast: A genetic sandbox. *Genetics*. 2018;209(3):637-50.
27. Locascio A, Andrés-Colás N, Mulet JM, Yenush L. *Saccharomyces cerevisiae* as a tool to investigate plant potassium and sodium transporters. *International Journal of Molecular Sciences*. 2019;20(9):2133.
28. Henderson SW, Nourmohammadi S, Ramesh SA, Yool AJ. Aquaporin ion conductance properties defined by membrane environment, protein structure, and cell physiology. *Biophysical Reviews*. 2022:1-18.
29. Minor Jr DL. Searching for interesting channels: pairing selection and molecular evolution methods to study ion channel structure and function. *Molecular BioSystems*. 2009;5(8):802-10.
30. Tyerman SD, McGaughey SA, Qiu J, Yool AJ, Byrt CS. Adaptable and multifunctional ion-conducting aquaporins. *Annual Review of Plant Biology*. 2021;72.
31. Wu B, Steinbronn C, Alsterfjord M, Zeuthen T, Beitz E. Concerted action of two cation filters in the aquaporin water channel. *The EMBO journal*. 2009;28(15):2188-94.
32. Qiu J, McGaughey SA, Groszmann M, Tyerman SD, Byrt CS. Phosphorylation influences water and ion channel function of AtPIP2; 1. *Plant, cell & environment*. 2020;43(10):2428-42.
33. Chow PH, Kourghi M, Pei JV, Nourmohammadi S, Yool AJ. 5-hydroxymethyl-furfural and structurally related compounds block the ion conductance in human aquaporin-1 channels and slow cancer cell migration and invasion. *Molecular Pharmacology*. 2020;98(1):38-48.
34. De Ieso ML, Pei JV, Nourmohammadi S, Smith E, Chow PH, Kourghi M, et al. Combined pharmacological administration of AQP1 ion channel blocker AqB011 and water channel blocker Bacopaside II amplifies inhibition of colon cancer cell migration. *Scientific reports*. 2019;9(1):1-17.
35. Chow P, Cox C, Pei J, Anabaraonye N, Nourmohammadi S, Henderson S, et al. Inhibition of the Aquaporin-1 Cation Conductance by Selected Furan Compounds Reduces Red Blood Cell Sickling. *Frontiers in pharmacology*. 2021;12.
36. Salman MM, Kitchen P, Yool AJ, Bill RM. Recent breakthroughs and future directions in drugging aquaporins. *Trends in Pharmacological Sciences*. 2022;43(1):30-42.
37. Gietz RD, Schiestl RH. High-efficiency yeast transformation using the LiAc/SS carrier DNA/PEG method. *Nature protocols*. 2007;2(1):31-4.
38. Anderson JA, Huprikar SS, Kochian LV, Lucas WJ, Gaber RF. Functional expression of a probable *Arabidopsis thaliana* potassium channel in *Saccharomyces cerevisiae*. *Proceedings of the National Academy of Sciences*. 1992;89(9):3736-40.
39. Kolacna L, Zimmermannova O, Hasenbrink G, Schwarzer S, Ludwig J, Lichtenberg-Fraté H, et al. New phenotypes of functional expression of the mKir2. 1 channel in potassium efflux-deficient *Saccharomyces cerevisiae* strains. *Yeast*. 2005;22(16):1315-23.

40. Epstein W, Buurman E, McLaggan D, Naprstek J. Multiple mechanisms, roles and controls of K<sup>+</sup> transport in *Escherichia coli*. *Biochemical Society Transactions*. 1993;21(4):1006-10.
41. Qu Y, Guan R, Bose J, Henderson SW, Wege S, Qiu L, et al. Soybean CHX-type ion transport protein GmSALT3 confers leaf Na<sup>+</sup> exclusion via a root derived mechanism, and Cl<sup>-</sup> exclusion via a shoot derived process. *Plant, Cell & Environment*. 2021;44(3):856-69.
42. Chanroj S, Lu Y, Padmanaban S, Nanatani K, Uozumi N, Rao R, et al. Plant-specific cation/H<sup>+</sup> exchanger 17 and its homologs are endomembrane K<sup>+</sup> transporters with roles in protein sorting. *Journal of Biological Chemistry*. 2011;286(39):33931-41.
43. Kilcher G, Delneri D, Duckham C, Tirelli N. Probing (macro) molecular transport through cell walls. *Faraday Discussions*. 2008;139:199-212.
44. Anthony TL, Brooks HL, Boassa D, Leonov S, Yanocho GM, Regan JW, et al. Cloned human aquaporin-1 is a cyclic GMP-gated ion channel. *Molecular pharmacology*. 2000;57(3):576-88.
45. Pei JV, Heng S, De Ieso ML, Sylvia G, Kourghi M, Nourmohammadi S, et al. Development of a photoswitchable lithium-sensitive probe to analyze nonselective cation channel activity in migrating cancer cells. *Molecular Pharmacology*. 2019;95(5):573-83.
46. Tyerman SD, McGaughey SA, Qiu J, Yool AJ, Byrt CS. Adaptable and multifunctional ion-conducting aquaporins. *Annual review of plant biology*. 2021;72:703-36.
47. Ko CH, Gaber RF. TRK1 and TRK2 encode structurally related K<sup>+</sup> transporters in *Saccharomyces cerevisiae*. *Molecular and Cellular Biology*. 1991;11(8):4266-73.
48. Bertl A, Ramos J, Ludwig J, Lichtenberg-Fraté H, Reid J, Bihler H, et al. Characterization of potassium transport in wild-type and isogenic yeast strains carrying all combinations of *trk1*, *trk2* and *tok1* null mutations. *Molecular microbiology*. 2003;47(3):767-80.
49. Sychrova H. Yeast as a model organism to study transport and homeostasis of alkali metal cations. *Physiological research*. 2004;53:S91-8.
50. Leng Q, Mercier RW, Yao W, Berkowitz GA. Cloning and first functional characterization of a plant cyclic nucleotide-gated cation channel. *Plant Physiology*. 1999;121(3):753-61.
51. Horie T, Brodsky DE, Costa A, Kaneko T, Lo Schiavo F, Katsuhara M, et al. K<sup>+</sup> transport by the OsHKT2; 4 transporter from rice with atypical Na<sup>+</sup> transport properties and competition in permeation of K<sup>+</sup> over Mg<sup>2+</sup> and Ca<sup>2+</sup> ions. *Plant Physiology*. 2011;156(3):1493-507.
52. Zimmermannova O, Felcmanova K, Sacka L, Colinet A-S, Morsomme P, Sychrova H. K<sup>+</sup>-specific importers *Trk1* and *Trk2* play different roles in Ca<sup>2+</sup> homeostasis and signalling in *Saccharomyces cerevisiae* cells. *FEMS Yeast Research*. 2021;21(3):foab015.
53. Ariño J, Ramos J, Sychrová H. Alkali metal cation transport and homeostasis in yeasts. *Microbiology and Molecular Biology Reviews*. 2010;74(1):95-120.
54. Ali Z, Park HC, Ali A, Oh D-H, Aman R, Kropornicka A, et al. TsHKT1; 2, a HKT1 homolog from the extremophile *Arabidopsis* relative *Thellungiella salsuginea*, shows K<sup>+</sup> specificity in the presence of NaCl. *Plant Physiology*. 2012;158(3):1463-74.
55. Nakamura RL, Anderson JA, Gaber RF. Determination of key structural requirements of a K<sup>+</sup> channel pore. *Journal of Biological Chemistry*. 1997;272(2):1011-8.
56. Yenush L. Potassium and sodium transport in yeast. *Yeast Membrane Transport*. 2016:187-228.

57. Yang Y, Tang RJ, Jiang CM, Li B, Kang T, Liu H, et al. Overexpression of the P t SOS 2 gene improves tolerance to salt stress in transgenic poplar plants. *Plant Biotechnology Journal*. 2015;13(7):962-73.
58. Benito B, Garcíadeblás B, Pérez-Martín J, Rodríguez-Navarro A. Growth at high pH and sodium and potassium tolerance in media above the cytoplasmic pH depend on ENA ATPases in *Ustilago maydis*. *Eukaryotic Cell*. 2009;8(6):821-9.
59. Yool AJ, Stamer WD, Regan JW. Forskolin stimulation of water and cation permeability in aquaporin1 water channels. *Science*. 1996;273(5279):1216-8.
60. Nakamura RL, Gaber RF. [6] Studying ion channels using yeast genetics. *Methods in enzymology*. 293: Elsevier; 1998. p. 89-104.
61. Beitz E, Becker D, Bülow Jv, Conrad C, Fricke N, Geadkaew A, et al. In vitro analysis and modification of aquaporin pore selectivity. *Aquaporins*. 2009:77-92.
62. Pettersson N, Hagström J, Bill RM, Hohmann S. Expression of heterologous aquaporins for functional analysis in *Saccharomyces cerevisiae*. *Current genetics*. 2006;50(4):247-55.
63. Zhang H, Verkman A. Aquaporin-1 water permeability as a novel determinant of axonal regeneration in dorsal root ganglion neurons. *Experimental neurology*. 2015;265:152-9.
64. Boassa D, Stamer WD, Yool AJ. Ion channel function of aquaporin-1 natively expressed in choroid plexus. *Journal of Neuroscience*. 2006;26(30):7811-9.
65. Sabir F, Leandro MJ, Martins AP, Loureiro-Dias MC, Moura TF, Soveral G, et al. Exploring three PIPs and three TIPs of grapevine for transport of water and atypical substrates through heterologous expression in aqy-null yeast. *PloS one*. 2014;9(8):e102087.
66. Kourghi M, De Ieso ML, Nourmohammadi S, Pei JV, Yool AJ. Identification of loop D domain amino acids in the human Aquaporin-1 channel involved in activation of the ionic conductance and inhibition by AqB011. *Frontiers in chemistry*. 2018;6:142.
67. Yu J, Yool AJ, Schulten K, Tajkhorshid E. Mechanism of gating and ion conductivity of a possible tetrameric pore in aquaporin-1. *Structure*. 2006;14(9):1411-23.
68. To J, Yeo CY, Soon CH, Torres J. A generic high-throughput assay to detect aquaporin functional mutants: potential application to discovery of aquaporin inhibitors. *Biochimica et Biophysica Acta (BBA)-General Subjects*. 2015;1850(9):1869-76.
69. Zhang H, Xiao W, Yu W, Yao L, Li L, Wei J, et al. Foxtail millet SiHAK1 excites extreme high-affinity K<sup>+</sup> uptake to maintain K<sup>+</sup> homeostasis under low K<sup>+</sup> or salt stress. *Plant cell reports*. 2018;37(11):1533-46.
70. Ding B, Zhang X, Xu Y, An L, Liu X, Su Q. The bacterial potassium transporter gene MbtrkH improves K<sup>+</sup> uptake in yeast and tobacco. *Plos one*. 2020;15(8):e0236246.
71. Shao Q, Han N, Ding T, Zhou F, Wang B. SsHKT1; 1 is a potassium transporter of the C3 halophyte *Suaeda salsa* that is involved in salt tolerance. *Functional Plant Biology*. 2014;41(8):790-802.
72. Drew DP, Hrmova M, Lunde C, Jacobs AK, Tester M, Fincher GB. Structural and functional analyses of PpENA1 provide insights into cation binding by type IID P-type ATPases in lower plants and fungi. *Biochimica et Biophysica Acta (BBA)-Biomembranes*. 2011;1808(6):1483-92.
73. Pei JV, Kourghi M, De Ieso ML, Campbell EM, Dorward HS, Hardingham JE, et al. Differential inhibition of water and ion channel activities of mammalian aquaporin-1 by two structurally related bacopaside compounds derived from the medicinal plant *bacopa monnieri*. *Molecular pharmacology*. 2016;90(4):496-507.

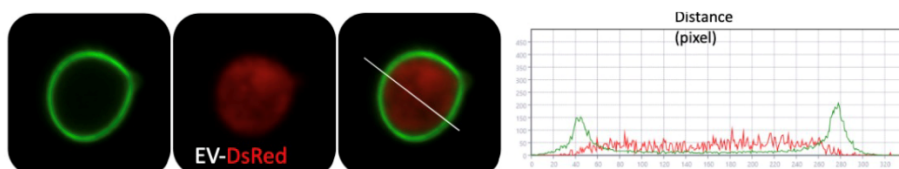
74. Casado C, González A, Platara M, Ruiz A, Ariño J. The role of the protein kinase A pathway in the response to alkaline pH stress in yeast. *Biochemical Journal*. 2011;438(3):523-33.
75. Rana S, Bisht D, Chakraborti PK. Synergistic activation of yeast-expressed rat androgen receptor by modulators of protein kinase-A. *Journal of molecular biology*. 1999;286(3):669-81.
76. Mishra R, van Drogen F, Dechant R, Oh S, Jeon NL, Lee SS, et al. Protein kinase C and calcineurin cooperatively mediate cell survival under compressive mechanical stress. *Proceedings of the National Academy of Sciences*. 2017;114(51):13471-6.
77. Tumolo JM, Hepowit NL, Joshi SS, MacGurn JA. A Snf1-related nutrient-responsive kinase antagonizes endocytosis in yeast. *PLoS genetics*. 2020;16(3):e1008677.
78. Sklodowski K, Riedelsberger J, Raddatz N, Riadi G, Caballero J, Chérel I, et al. The receptor-like pseudokinase MRH1 interacts with the voltage-gated potassium channel AKT2. *Scientific reports*. 2017;7(1):1-12.
79. Ismailov II, Benos DJ. Effects of phosphorylation on ion channel function. *Kidney international*. 1995;48(4):1167-79.
80. Campbell EM, Birdsell DN, Yool AJ. The activity of human aquaporin 1 as a cGMP-gated cation channel is regulated by tyrosine phosphorylation in the carboxyl-terminal domain. *Molecular pharmacology*. 2012;81(1):97-105.
81. Zhang W, Zitron E, Hoömme M, Kihm L, Morath C, Scherer D, et al. Aquaporin-1 channel function is positively regulated by protein kinase C. *Journal of Biological Chemistry*. 2007;282(29):20933-40.
82. Németh-Cahalan KL, Kalman K, Hall JE. Molecular basis of pH and Ca<sup>2+</sup> regulation of aquaporin water permeability. *The Journal of general physiology*. 2004;123(5):573-80.
83. Ros R, Lemaillet G, Fonrouge A, Daram P, Enjuto M, Salmon J-M, et al. Molecular determinants of the Arabidopsis AKT1 K<sup>+</sup> channel ionic selectivity investigated by expression in yeast of randomly mutated channels. *Physiologia Plantarum*. 1999;105(3):459-68.
84. Loukin S, Su Z, Zhou X, Kung C. Forward genetic analysis reveals multiple gating mechanisms of TRPV4. *Journal of Biological Chemistry*. 2010;285(26):19884-90.
85. Bertl A, Slayman CL, Gradmann D. Gating and conductance in an outward-rectifying K<sup>+</sup> channel from the plasma membrane of *Saccharomyces cerevisiae*. *The Journal of membrane biology*. 1993;132(3):183-99.
86. Palmer CP, Zhou X-L, Lin J, Loukin SH, Kung C, Saimi Y. A TRP homolog in *Saccharomyces cerevisiae* forms an intracellular Ca<sup>2+</sup>-permeable channel in the yeast vacuolar membrane. *Proceedings of the National Academy of Sciences*. 2001;98(14):7801-5.
87. Jimenez V, Docampo R. Molecular and electrophysiological characterization of a novel cation channel of *Trypanosoma cruzi*. *PLoS pathogens*. 2012;8(6):e1002750.
88. Bihler H, Eing C, Hebeisen S, Roller A, Czempinski K, Bertl A. TPK1 is a vacuolar ion channel different from the slow-vacuolar cation channel. *Plant Physiology*. 2005;139(1):417-24.
89. Hamamoto S, Marui J, Matsuoka K, Higashi K, Igarashi K, Nakagawa T, et al. Characterization of a tobacco TPK-type K<sup>+</sup> channel as a novel tonoplast K<sup>+</sup> channel using yeast tonoplasts. *Journal of Biological Chemistry*. 2008;283(4):1911-20.
90. Moosavi B, Mousavi B, Yang W-C, Yang G-F. Yeast-based assays for detecting protein-protein/drug interactions and their inhibitors. *European Journal of Cell Biology*. 2017;96(6):529-41.

91. Brückner A, Polge C, Lentze N, Auerbach D, Schlattner U. Yeast two-hybrid, a powerful tool for systems biology. *International journal of molecular sciences*. 2009;10(6):2763-88.
92. Bagriantsev SN, Minor DL. Using yeast to study potassium channel function and interactions with small molecules. *Chemical Neurobiology: Springer*; 2013. p. 31-42.
93. Barth D, Fronius M. Shear force modulates the activity of acid-sensing ion channels at low pH or in the presence of non-proton ligands. *Scientific Reports*. 2019;9(1):1-13.
94. Mould JA, Li H-C, Dudlak CS, Lear JD, Pekosz A, Lamb RA, et al. Mechanism for proton conduction of the M2 ion channel of influenza A virus. *Journal of Biological Chemistry*. 2000;275(12):8592-9.
95. Rana S, Bisht D, Chakraborti PK. Synergistic activation of yeast-expressed rat androgen receptor by modulators of protein kinase-A1. *Journal of molecular biology*. 1999;286(3):669-81.
96. Aquino-Piñero EE, Rodríguez-del Valle N. Different protein kinase C isoforms are present in the yeast and mycelium forms of *Sporothrix schenckii*. *Mycopathologia*. 1997;138(3):109-15.
97. Blumer KJ, Thorner J. Beta and gamma subunits of a yeast guanine nucleotide-binding protein are not essential for membrane association of the alpha subunit but are required for receptor coupling. *Proceedings of the National Academy of Sciences*. 1990;87(11):4363-7.
98. Castellanos R, Mazón MJ. Identification of phosphotyrosine in yeast proteins and of a protein tyrosine kinase associated with the plasma membrane. *Journal of Biological Chemistry*. 1985;260(14):8240-2.
99. Kanhonou R, Serrano R, Palau RR. A catalytic subunit of the sugar beet protein kinase CK2 is induced by salt stress and increases NaCl tolerance in *Saccharomyces cerevisiae*. *Plant molecular biology*. 2001;47(5):571-9.
100. Chen Y, Zong J, Tan Z, Li L, Hu B, Chen C, et al. Systematic mining of salt-tolerant genes in halophyte-*Zoysia matrella* through cDNA expression library screening. *Plant Physiology and Biochemistry*. 2015;89:44-52.
101. Veitia R, Caburet S, Birchler J. Mechanisms of Mendelian dominance. *Clinical Genetics*. 2018;93(3):419-28.
102. Sentenac H, Bonneaud N, Minet M, Lacroute F, Salmon J-M, Gaymard F, et al. Cloning and expression in yeast of a plant potassium ion transport system. *Science*. 1992;256(5057):663-5.
103. Rubio F, Gassmann W, Schroeder JI. Sodium-driven potassium uptake by the plant potassium transporter HKT1 and mutations conferring salt tolerance. *Science*. 1995;270(5242):1660-3.
104. Tang W, Ruknudin A, Yang WP, Shaw S-Y, Knickerbocker A, Kurtz S. Functional expression of a vertebrate inwardly rectifying K<sup>+</sup> channel in yeast. *Molecular biology of the cell*. 1995;6(9):1231-40.
105. Zhou X, Su Z, Anishkin A, Haynes WJ, Friske EM, Loukin SH, et al. Yeast screens show aromatic residues at the end of the sixth helix anchor transient receptor potential channel gate. *Proceedings of the National Academy of Sciences*. 2007;104(39):15555-9.
106. Preston GM, Carroll TP, Guggino WB, Agre P. Appearance of water channels in *Xenopus* oocytes expressing red cell CHIP28 protein. *Science*. 1992;256(5055):385-7.
107. Öberg F, Ekvall M, Nyblom M, Öberg F, Ekvall M, Nyblom M, et al. Insight into factors directing high production of eukaryotic membrane proteins; production of 13 human AQPs in *Pichia pastoris*. *Molecular membrane biology*. 2009;26(4):215-27.

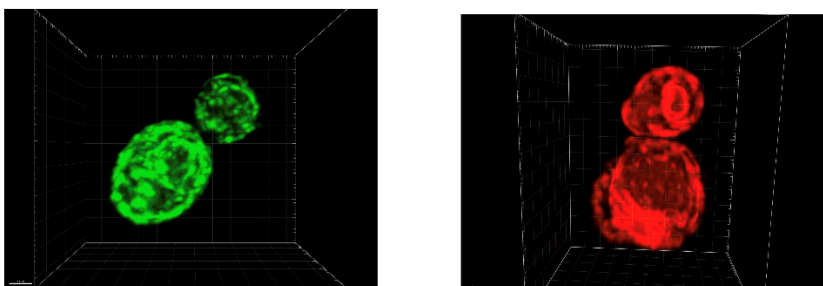
108. Bjørkskov FB, Krabbe SL, Nurup CN, Missel JW, Spulber M, Bomholt J, et al. Purification and functional comparison of nine human Aquaporins produced in *Saccharomyces cerevisiae* for the purpose of biophysical characterization. *Scientific reports*. 2017;7(1):16899.
109. Yool AJ, Morelle J, Cnops Y, Verbavatz J-M, Campbell EM, Beckett EA, et al. AqF026 is a pharmacologic agonist of the water channel aquaporin-1. *Journal of the American Society of Nephrology*. 2013;24(7):1045-52.
110. Ma B, Xiang Y, Mu S-M, Li T, Yu H-M, Li X-J. Effects of acetazolamide and anordiol on osmotic water permeability in AQP1-cRNA injected *Xenopus* oocyte. *Acta Pharmacol Sin*. 2004;25(1):90-7.
111. Montiel V, Bella R, Michel LY, Esfahani H, De Mulder D, Robinson EL, et al. Inhibition of aquaporin-1 prevents myocardial remodeling by blocking the transmembrane transport of hydrogen peroxide. *Science translational medicine*. 2020;12(564):eaay2176.
112. Groszmann M, De Rosa A, Chen W, Qiu J, McGaughey SA, Byrt CS, et al. Permeability profiling of all 13 *Arabidopsis* PIP aquaporins using a high throughput yeast approach. *bioRxiv*. 2021.

## 6. Supplementary

**Supplemental S1:** empty vector tagged fluorescent localization in the yeast membrane



**Supplemental S2:** Z-stack video of GFP-aqp1 and aqp1-DsRED





# Chapter 5

## Investigating the Role of Aquaporin Ion Channels in Cancer; is Beneficial or Detrimental, that is the Question.

As a result of chapter 4, that all hAQPs displayed potential ion permeability in a wide range of pH and given that most other ion channels are functional in a narrow pH spectrum, I hypothesized that AQP ion channel functionality could be the answer for the compensatory mechanism of ion homeostasis balance in cancer cells puzzle. The overall goal of this project was to investigate the correlation between AQPs and cancer severity and clinical outcome. In aim 1, I used bioinformatics tools and found a positive correlation between AQP expression and cancer stages. The transcriptomic data analysis suggested AQP9, 7, 5 and 3 as the most promising AQPs that their expression was significantly altered in almost all common cancer types. These results led me to study the potential regulatory mechanisms that govern the ion permeability of these four channels. This was achieved by means of the novel high-throughput yeast screening assay. This chapter is in the format of the manuscript to be submitted to a journal.

# Statement of Authorship

Title of Paper	Investigating the Role of Aquaporin Ion Channels in Cancer; is beneficial or detrimental, that is the question
Publication Status	<input type="checkbox"/> Published <input type="checkbox"/> Accepted for Publication <input type="checkbox"/> Submitted for Publication <input checked="" type="checkbox"/> Unpublished and Unsubmitted work, written in manuscript style
Publication Details	Nourmohammadi S, Aung TA, Henderson SW, Adelson DL, Yool AJ  *This work is in the final version of manuscript and will be submitted in about five weeks for publication.

## Principal Author

Name of Principal Author (Candidate)	Mr. Saeed Nourmohammadi		
Contribution to the Paper	First author and main contributor. Formulation of research question. Designed and carried out the experiments, analysed data, figures and wrote the manuscript.		
Overall percentage (%)	70%		
Certification:	This paper reports on original research I conducted during the period of my Higher Degree by Research candidature and is not subject to any obligations or contractual agreements with a third party that would constrain its inclusion in this thesis. I am the primary author of this paper.		
Signature		Date	07/07/2022

## Co-Author Contributions

By signing the Statement of Authorship, each author certifies that:

- i. the candidate's stated contribution to the publication is accurate (as detailed above);
- ii. permission is granted for the candidate to include the publication in the thesis; and
- iii. the sum of all co-author contributions is equal to 100% less the candidate's stated contribution.

Name of Co-Author	Dr. Thazin Nwe Aung		
Contribution to the Paper	Assisted with bioinformatic analysis, figures and manuscript writing.		
Signature		Date	10/07/2022

Name of Co-Author	Dr. Sam W Henderson		
Contribution to the Paper	Assisted with manuscript writing.		
Signature		Date	10/7/22

Name of Co-Author	Professor David L. Adelson		
Contribution to the Paper	Assisted with bioinformatics analysis and manuscript writing.		
Signature		Date	13/07/2022

Name of Co-Author	Professor Andrea J Yool		
Contribution to the Paper	Supervised the research, assisted the research with funding, experimental design and manuscript writing.		
Signature		Date	8 Jul 2022

## **Discovery of Novel Human Aquaporin Ion Channels and their Potential Role in Cancer; is beneficial or detrimental, that is the question!**

**Nourmohammadi S**<sup>1</sup>, Aung TN<sup>2</sup>, Henderson SW<sup>1</sup>, Adelson DL<sup>3</sup>, Yool AJ<sup>1</sup>.

1- School of Biomedicine, University of Adelaide, Adelaide, SA 5005, Australia

2- Department of Pathology, Yale School of Medicine, New Haven, CT, US

3- School of Biological Sciences, University of Adelaide, Adelaide, SA 5005, Australia

### **Abstract**

Human aquaporins (hAQPs) are multifunctional protein channels that are capable of transporting water, glycerol and expanding range of solutes. The permeability of a subset of AQPs to monovalent cations and anions is established. Moreover, our prior studies suggested the potential role of hAQP1 ion conductance in colon cancer cell migration, yet our understanding of the exact relationship between hAQP ion permeability and cancer is limited. Using the novel mass-throughput yeast-based assay we developed, herein we discovered a new set of hAQP ion channels and revealed their modulatory mechanism. Furthermore, we explored the prognostic values of all human aquaporins subclasses in 8 cancer types (10 cancer subtypes) using the publicly available mRNA expression data. We then performed both univariable and multivariable analyses using the tertile as the cutpoints to stratify the patients having high (33%) and low (67%) AQP expressions to correlate their associations with the survival outcome. In our analyses, four AQPs; AQP3, AQP5, AQP7 and AQP9 were significantly differently expressed in at least 5 of the 8 cancer types studied. In multivariable analysis using stage as a co-variate, higher AQP3, AQP5 and AQP7 expressions in later stages of cancer types are associated with worse outcomes and the hazard ratios increase as the tumor grades become higher. Using mass-throughput yeast-based assay we found all four AQPs we analysed were permeable to K<sup>+</sup> (to the same degree) and Na<sup>+</sup> (AQP9>7>>5>3) in a pH range between 5.0-7.3. AQP9 ion permeability was induced by protein kinase C and G activators, whereas AQP7 and -5 ion permeability were increased by PKC and PKG activator, respectively. All tested AQPs ion permeability mediated by PK activators were pH sensitive. Our results indicated that high expressions of four AQPs studied here predict worse outcomes with increasing tumor stages and appear to have stage dependent associations with survival outcomes highlighting their prognostic importance in human cancers. Work here also introduced a possible link between AQP ion functionality and cancer development, however, investigation of full range of properties of these AQPs partially shown here remain to be explored *in vivo* and in translational/clinical research.

## 1. Introduction

Despite the overall reduction in cancer deaths due to improved diagnosis and treatment advances, cancer remains one of the leading causes of death worldwide (1). Proliferation and metastasis, along with resistance and recurrence are known as cancer hallmarks. The development of cancer results from interactions of the tumor cells with their microenvironment leading to angiogenesis and metastasis (2, 3). Understanding the crosstalk between the tumor cells and the surrounding cellular and physical environment is crucial for identifying the unique features of tumor development that will ultimately lead to finding companion diagnostics tests for various treatment options.

Among them, pH-dependent signaling pathways and hypoxia are one of the key drivers of tumour development and have been recognized to be core processes for cancer persistence and progression as compared to normal tissue microenvironments (4-6). This acidotic process is mainly due to a metabolic shift of cancer cells towards glycolysis and lactate accumulation, resulting in increased levels of metabolic acids (pH<6.5) (7) and hypoxia (8, 9) in tumor microenvironments. Furthermore, compared to physiological pH conditions (~7.4), free proton concentration in tumor microenvironments can be up to 10-fold higher, creating acidosis which does not impair tumor development but dampens the immune system responses (10-13). Although these unique features offer a promising opportunity for developing target-specific therapies, understanding the physiology of Tumor Microenvironment (TME) is challenging and depends on distinguishing between many factors that often are shared between cancerous and non-cancerous tissues. One promising approach is to design pH-responsive drugs that can be activated at a specific pH value found in tumor microenvironment sites (14-16).

Many proteins including membrane proteins (17) function in a narrow spectrum of optimal pH, indicating the significance of pH to cell fate (6). Having pH-sensitive membrane sensors is vital for both normal and cancerous cells to adapt to pH alterations. This is accomplished in part by a set of transmembrane proteins known as ion channels (18). Although investigating the roles of ion channels in cancer has been a focus in the field, the pH landscape, and its effect on regulatory mechanisms of ion channels, as well as the potential pathophysiological consequences, remain less understood.

pH alteration is closely coupled to membrane potential changes (acidosis=depolarization and alkalinisation=hyperpolarization) and provides a fine-tuning for the cell process (6, 19, 20). Interestingly, having a depolarized resting membrane potential, ranging from -5 to -55 mV, is another unique feature of cancer cells as compared to normal cells (-35 to -95mV), which is a

critical factor for membrane protein functions and downstream signalling pathways (21, 22). Tumor microenvironment acidosis often shuts down the cation channel functions such as, potassium voltage-gated channel (23-26),  $\text{Ca}^{2+}$ -activated  $\text{K}^+$  channels (27, 28), potassium inwardly-rectifying channels (29, 30), sodium channels (31), transient receptor potential cation channels (32), calcium channels (26, 33), mechanosensitive ion channels (34, 35) and ligand-gated ion channels (36). Conversely, some ion channels are inhibited in alkali pH, including potassium channels (37-39) or activated at low pH (40, 41). Blocking potassium channels abolished pH-dependent resting membrane potential depolarization (19, 42). More specifically, some of  $\text{K}_{2p}$  family channels are only functional in a narrow physiological pH value, and their currents are inhibited by acidification (30) or alkalization of extracellular pH (37).  $\text{K}_{2p}$  known for their role for adjusting the membrane potential (43) and four members of their family functionally involved in tumor development (44). TRP channels have different sensitivity to extra- or intracellular proton concentration changes (45). The link between TRP family cancer proliferation (46, 47), cell migration (48, 49) has been suggested. Voltage-gated proton channel,  $\text{Hv1}$ , gating mechanism is governed by the pH gradient difference in intracellular and extracellular space (50). The association of  $\text{Hv1}$  pH-regulation and cancer cell migration demonstrated (51-53). Voltage-gated sodium channels (54) and Piezo1 channels (34) are inhibited by extracellular acidification and have shown to promote cancer cell migration, invasion and proliferation (35, 55-57). ATP-gated  $\text{Na}^+$ -,  $\text{K}^+$ - and  $\text{Ca}^{2+}$ -permeable channels,  $\text{P}_2\text{X}$ , are modulated by extracellular pH (58), and acidosis of the environment inhibits the channels' function. The association between  $\text{P}_2\text{X}$  family and cancer development has been studied (59). For instance, the association of colorectal and melanoma tumor progression with  $\text{P}_2\text{X}_7$  activity through tumor-infiltration immune cells has been suggested (60). On the other hand, low extracellular pH induced the acid-sensing ion channels resulting from a competition of multiple protons and  $\text{Ca}^{2+}$  at the channels activation site. However, these channel's functions are shown to be in a narrow acidification window ( $\sim 4.5$  for ASIC2a, pH  $\sim 6.5$  for ASIC1a and ASIC3;  $\sim 6.1$  for ASIC1b) with some depending on the presence of  $\text{Ca}^{2+}$  (61). Since activation of acid-sensing ion channels occurs in a narrow spectrum of pH (17, 62), cancer cells potentially use compensatory mechanisms, possibly through an alternative set of ion channels that have broader pH-insensitivity, to progress in unfavourable  $\text{Na}^+/\text{K}^+$  gradient created by inactivation of other ion channels as a consequence of pH alteration and hypoxia.

AQPs are a representative subfamily of the Major Intrinsic Protein (MIP) that are considered to be multifunctional channels with a permeability range from water and glycerol to a broader range of solutes (63, 64). Following the first discovery of AQP ion channels, (the bovine MIP,

now known as AQP0) (65, 66), more classes of AQPs have been identified as either cation or anion channels, from humans and plants to *Drosophila melanogaster*. Notably, these proteins are involved in many biological functions (63, 67, 68), and dysregulation (69-73), expression alteration (74-76) or inhibition of AQPs (77, 78) leads to disturbed cell water and ion homeostasis in both normal and cancerous organs making these channels an attractive therapeutic targets. The implications of several AQPs that have been identified in tumor angiogenesis, cellular dissociation, migration, invasion and expression patterns have been discussed and reviewed in (73, 79-82), yet their mechanisms of action, solute-dependent permeability and roles in regulating these processes still remain to be fully understood. Therefore, we hypothesised that investigating their functions and prognostic importance might reveal their potential for malignant transformation of different cancer types.

Although multifunctional AQPs solute permeability in human physiology and their regulatory by pH has been studied (83-90), but apart from their water, glycerol (91) and signalling molecules transport (92) in cancer progression, the exact mechanism of other solute, including ions and anions, permeability and the effect of pH on the channels gating remained poorly explored.

In the present study, we explored the correlation of AQPs and cancer severity and found them as potential prognostic marker for cancer. Moreover, we identified a new set of AQP ion channels, and explored the role of pH in regulating their function using *in vitro* yeast-based screening assays we previously developed. We further identified the roles of kinase signaling pathways in the regulation of ion permeability, assessed by phenotype complementation in the yeast model. To start, we retrieved data for 13 human AQPs that are prevalent across multiple types of cancers, for 8 cancer types from TCGA data base (<https://portal.gdc.cancer.gov/>), to access the possible correlations between transcript levels and cancer prognoses. The severity of cancer progression at different stages of tumors was associated with the patterns of AQP expression. The long-term goal of this work is to extend understanding of AQPs as independent prognostic factors for risk of cancer progression and explore functional contributions of the channels to cancer cell survival and invasiveness. The role of AQPs in human pathophysiologies such as cancer might lead to the development of novel therapeutics against cancer. Results in this study show cancer-linked classes of AQPs show cation permeability; however, the full range of channel properties including the pH-dependence and regulation by intracellular signaling pathways remain to be explored and defining the value of these channels as targets in cancer treatments awaits future *in vivo* and in clinical research.

## 2. Materials and methods

### 2.1. cDNA cloning and construction of yeast expression plasmids

Molecular biology, cloning and *In vitro* experiments preparation for yeast screening were done as described previously (see chapter 4). But briefly, coding sequence of all 13 human AQPs were designed and commercially synthesised by GenScript as Gateway-enabled entry vectors. Yeast harbouring AQPs plasmid were selected by colony PCR and glycerol stocks were made and kept at liquid nitrogen for long and -80 °C for short time storage to be used for weekly experiments. The yeast mutant strains CY162 and *aqy-null*, were used for further characterization of human AQPs.

### 2.2 Yeast growth conditions

For preparation, cells were grown aerobically at 29 °C on Yeast Nitrogen Base, YNB, (~7.5 mM KCl, 6.7 g/L yeast nitrogen base without amino acids, 2% glucose, 2 g/L uracil-dropout amino acid mixture, supplemented with 100 mM KCl for CY162 strain or without additional KCl for *aqy-null* strain), and for screening conditions (inducing medium) potassium free YNB (6.7 g/L yeast nitrogen base without amino acids, 2% glucose+2% raffinose, 1.98 g/L uracil-dropout amino acid mixture, supplemented with indicated KCl, and 2% agar for solid media) was used. The potassium free YNB media were supplemented with 6 mM KCl for liquid screening and indicated amount of sodium chloride was added where we examined these AQPs for Na<sup>+</sup> permeability in osmotic stress assay as described previously (see chapter 4).

### 2.3. Liquid growth assay of yeast strains

For testing the effect of pH on AQP-mediated growth rescue of CY162 under different conditions (i.e., Na<sup>+</sup> permeability or protein kinases stimuli molecules), the cells were grown on solid YNB media without uracil (2% glucose+ 100 mM KCl) for 3-5 days. Single colonies were selected and grown overnight in the same media without agar. This was followed the next day by washing the cells two times with autoclaved MQ water and resuspended in unbuffered potassium free YNB+6 mM KCl. For screening of potassium-uptake, cells were inoculated to a starting optical density (OD<sub>600</sub>) of 0.05-0.1 but increased 2-3 folds (initial OD<sub>600</sub>= ~0.2) for Na<sup>+</sup> permeability or osmotic stress assay. The yeast cell wall in late exponential toward stationary phase is stiffer, making it less accessible for molecules and drugs to reach the cell membrane. Therefore, when it comes to cell treatment or small molecules screening assays, we



found reducing the cell number to initial  $OD_{600} = \sim 0.005-0.01$  make it easier to distinguish the difference between the effect of treatments on cells expressing exogenous proteins. pH was adjusted to 5.0, 5.7, 6.4, or 7.4 using MES or Tris base as mentioned before. 200 $\mu$ L culture was used in Corning® 96-well clear flat-bottom. The plate lid was removed, and wells were sealed by MicroAmp Optical Adhesive Film (Thermo Fisher Scientific). Double orbital shaking option was used for liquid screening to avoid sedimentation and cell clumping during the kinetic assay.

#### ***2.4. Bioinformatics and omics analysis***

RNA-seq gene expression profiles of 3429 patients from 8 different cancer types (10 subtypes) were analysed in this study. The associated clinical information of the patients was obtained from the Cancer Genome Atlas (TCGA, <https://portal.gdc.cancer.gov/>) database. The FPKM (Fragments Per Kilobase of transcript per Million mapped reads) values were used as a measure of 13 different AQPs gene expression. Significantly differentially expressed AQP genes between primary and solid tissue normal samples were identified using edgeR in R studio with false discovery rate (FDR) < 0.05. Common genes that are significantly expressed were identified using ggvenn package in R studio. Four most commonly expressed AQP genes in most common cancer types (AQP9, AQP7, AQP5 and AQP3) were selected for further downstream analyses. Univariable analysis was performed for overall survival (OS) associated with AQP expression using Kaplan–Meier and log rank test analysis, comparing high and low gene expression groups for all cases and within each cancer type stages. RNA expression was dichotomized as high and low expression using the cut point as high-30% and low 70% for all genes in every cohort. To avoid using potentially biased cut-points splitting high and low AQPs expressing participant groups, a two-sample t-test using continuous AQP mRNA expression values (with no cut-point required) compared mRNA expression between alive and deceased participants. Statistical analyses were performed using GraphPad Prism 9 (GraphPad Software Inc., CA, USA) and RStudio 2022.02.0+443 (Inc., Boston, MA). Multivariable analysis for overall survival was also performed to determine whether mRNA expression was associated with OS in each tumor stage (I: IV). Finally, AQP mRNA expressions between normal tumor adjacent tissue and tumor samples from different stages were analysed with a one-way ANOVA (normal vs stage I, stage II, stage III and stage IV).

#### ***2.5. Statistics***

Statistical analyses were performed using GraphPad Prism 9.1.0 (GraphPad Software Inc., CA, USA) and R. studio 1.4.1106 (Inc., Boston, MA). All data shown are mean  $\pm$  SD. Different letters indicate significance ( $P < 0.05$ ) between values as determined by analysis of variance with post hoc tests as detailed in the figure legends or text. Kaplan–Meier plots for overall survival (OS) were computed and comparisons were made by the log-rank test using survival and survminer packages in R studio. Post hoc Benjamini-Hochberg (BH) multiple comparisons test was performed when the results for each variable in survival analyses were significant. To perform univariable analyses of AQP expressions associated with OS, a Cox proportional hazards model was fitted to predict survival. For the multivariable analysis, a Cox proportional hazards model was learned using high (30%) vs low (70%) and stage as predictors. For each test, we quote the hazards ratio associated with each level of a factor compared to the base reference level, and the associated p-values.

### 3. RESULTS

#### 3.1. Bioinformatics and omics analysis

The expression of hAQP1 facilitates cancer migration and metastasis in subtypes of cancer cells such as colorectal cancer and glioblastoma, and pharmacological inhibition of the channel water and ion permeability has been shown to slow cancer cell line cell migration and invasion (78). McCoy and colleagues showed the role of hAQP1 in glioma cell migration is not replaceable by hAQP4, suggesting a unique function of hAQP1 in cell migration (93). The full range of AQPs substrate permeabilities remains to be identified. The significance of AQPs in cancer progression has likely been underestimated to date, with more linkages yet to be discovered. Work here is focused on four classes of AQPs not previously shown to have ion channel activity; these classes were selected objectively based on an assessment of AQP transcript levels that correlated most strongly with the probabilities of overall survival for cancer patients across multiple cohorts of cancer types (Table 1). Transcriptional expression data for all 13 classes of AQPs from 3429 patients were compiled for cancer types representing 8 cancer cohorts, using FPKM with follow-up information from TCGA. The clinicopathological features of the patients in the cohorts are summarised in Table 1.

**Table 1: Clinicopathological features of the cohorts used for this study.**

Characteristic	Bladder (n=430)	Breast (n=1218)	Colon (n=512)	Liver (n=424)	Thyroid (n=568)	Rectal (n=177)	Lung- LUAD (n=585)	Lung-LUSC (n=550)	Kidney- KIRC (n=607)	Kidney- KIRP (n=321)
	N (%)	N (%)	N (%)	N (%)	N (%)	N (%)	N (%)	N (%)	N (%)	N (%)
Age										
Median (Range)	68(34-90)	58 (26-90)	67 (31-90)	60 (16-90)	41 (16-89)	64.5 (31-90)	65 (33-88)	67 (39-90)	61 (26-90)	62 (28-88)

Gender Demographic										
Male	313 (73)	13 (1)	266 (52)	281 (66)	156 (27)	94 (53)	269 (46)	406 (74)	401 (66)	234 (73)
Female	117 (27)	1203 (99)	244 (48)	143 (34)	412 (73)	83 (47)	316 (54)	144 (26)	206 (34)	87 (27)
Stage										
Not Reported/Not Determined	2 (0.5)	24 (2)	12 (2)			10 (6)	9 (2)			
I	3 (0.7)	202 (17)	82 (16)	191 (45)	321 (57)	34 (19)	316 (54)	270 (49)	294 (48)	187 (58)
II	134 (31)	693 (57)	205 (40)	98 (23)	59 (10)	53 (30)	135 (23)	179 (33)	69 (11)	23 (7)
III	148 (34)	275 (23)	139 (27)	97 (23)	124 (22)	53 (30)	97 (17)	89 (16)	139 (23)	63 (20)
IV	143 (33)	22 (2)	72 (14)	6 (1)	59 (10)	26 (15)	28 (5)	8 (8)	102 (17)	19 (6)
Vital Status										
Alive	236 (55)	1016 (84)	395 (77)	258 (61)	548 (96)	145 (82)	369 (63)	303 (55)	407 (67)	270 (84)
Dead	193 (45)	200 (16)	115 (23)	164 (39)	20 (4)	31 (18)	216 (37)	247 (45)	200 (33)	51 (16)
Not Reported	1 (0)	0 (0)	0 (0)	2 (0)	0 (0)	0 (0)	0 (0)	0 (0)	0 (0)	0 (0)
History of Neoadjuvant Treatment										
Yes	10 (2)	14 (1)	4 (1)	2 (0)	6 (1)	1 (1)	4 (1)	7 (1)	18 (3)	0 (0)
No	420 (98)	1200 (99)	506 (99)	422 (100)	562 (99)	175 (99)	580 (99)	543 (99)	589 (97)	321 (100)
Not Reported	0 (0)	3 (0)	0 (0)	0 (0)	0 (0)	0 (0)	0 (0)	0 (0)	0 (0)	0 (0)
Date of Data Extraction	April 17 2022	April 17 2022	April 17 2022	April 17 2022	April 17 2022	April 17 2022	April 17 2022	April 17 2022	April 17 2022	April 17 2022
Type of Data	RNA (FPKM)	RNA (FPKM)	RNA (FPKM)	RNA (FPKM)	RNA (FPKM)	RNA (FPKM)	RNA (FPKM)	RNA (FPKM)	RNA (FPKM)	RNA (FPKM)

### 3.2. The Correlation between AQPs Expression and Overall Survival and Cancer Severity

#### 3.2.1. Differences in AQP Expression in Several Cancer Types

The assessment human AQP transcript levels in eight different cancer types indicated that AQP3, AQP5, AQP7 and AQP9 showed the highest expression across multiple cancer types, as compared to levels of other hAQPs (Figure 1A). Significant expression of AQP9 was observed in five cancer types including Breast, Colon, Kidney, Liver and Lung cancers. AQP3, AQP5 and AQP7 showed significantly increased expression in four cancer types (Figure 1B). These four AQP classes were selected for further assessment of possible associations with clinical outcomes and deeper *in vitro* investigation on their functions, ion permeability and modulatory, in particular.

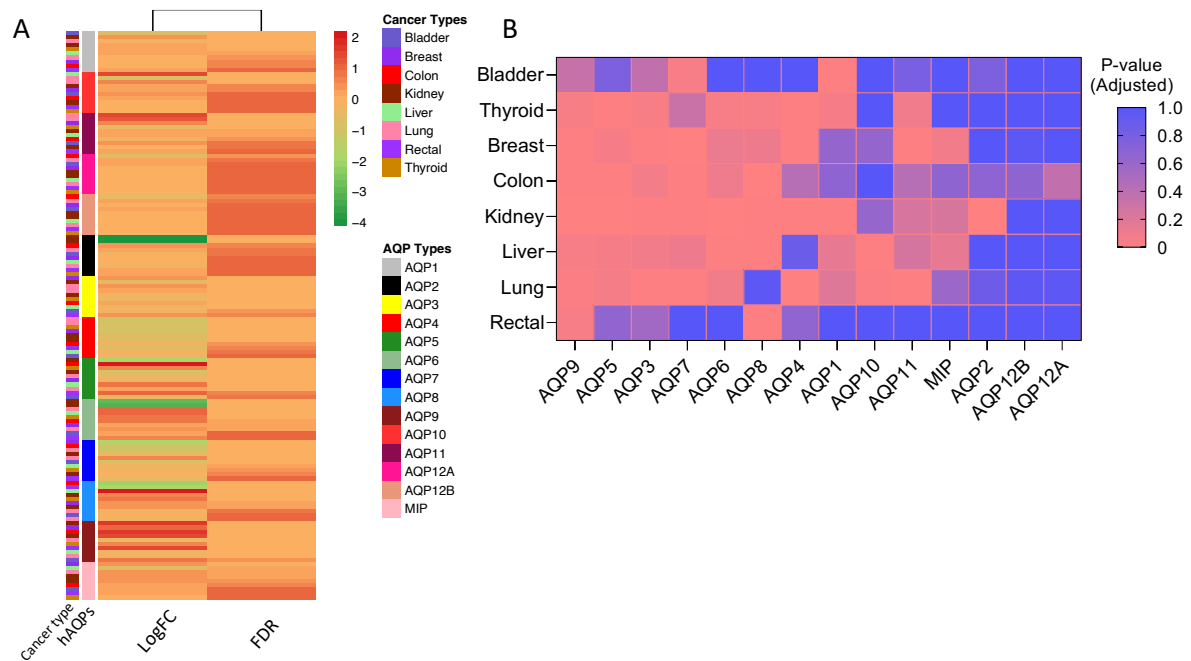


**Figure 1: Differential mRNA expression of AQPs in eight cancer types.**

**A)** A heatmap depicting the differential expression of 13 hAQPs from the publicly available TCGA database comparing the primary tumor regions against solid tissue normal. Expression difference in fold change (P values adjusted and shown as FDR; false discovery rate < 0.05). **(B)** Expression of common AQPs in eight cancer types. AQP3, AQP5, AQP7 and AQP9 were significantly expressed in most cancer types including breast, colon, kidney, liver and lung.

### 3.2.2. Association of AQP Expression with Survival.

Kaplan–Meier analyses of participants with Breast, Colon, Kidney, Liver and Lung cancers with respect to the expression of AQP3, 5, 7 and -9 (high-33% vs low-67%) were conducted. Results from a univariable cox regression model indicated that significantly better overall survival was associated with high expression of AQP7 in KIRC (Kidney Renal Clear Cell Carcinoma) (Hazard Ratio (HR) = 0.65, P = 0.003\*\*) and LUAD (Lung Adenocarcinoma) (HR = 0.73, P = 0.025\*) ([Supplementary S1](#)). AQP3 high expression was significantly associated with worse outcome in Breast and Liver (HR = 1.3), whereas significantly better overall survival was seen for Colon (HR=0.87), Kidney and Lung (HR=0.75). A trend towards association with worse outcome in Breast (HR=1) and Kidney (HR=1.1) was seen for AQP5, however, its high expression was positively associated with better survival in Colon (HR=0.89), Liver (HR=0.75) and Lung (HR=0.82). Although not significant, high AQP9 expression showed a trend towards association with worse outcome in Breast (HR = 1.3), Colon (HR = 1.1), Kidney (HR = 1.3) and Liver (HR = 0.83) ([Supplementary S1 and S2](#)). Investigation of whether AQP9 expression predicts OS (Overall Survival) with stage as a co-variate factor in multivariable survival analysis models showed that the hazard risk factor increased as a function of higher stages in all cancer types ([Figure 2](#)). Similarly, multivariable

analysis using stages as the predictor indicated that higher AQP3, AQP5 and AQP7 expressions in later stages of cancer types were associated with worse outcomes and the hazard ratio increased as the tumor grades became higher (Figure 3-5). For instance, in KIRC subtype of Kidney cancer, although high AQP3 expression predicted better outcomes (HR = 0.71, P = 0.021\*), increased HR was observed in stage II (HR = 1.33), stage III (HR = 2.79, p <0.001\*\*\*) and stage IV (HR = 7.04, p <0.001\*\*\*) as compared to stage I patients (Figure 5). Likewise, upon multivariable analysis, high AQP5 expression conferred worse prognosis in KIRC (HR = 1.2), with the strength of the effect increasing with tumor stage, for example in breast cancer, (stage I vs II (HR=1.4), stage I vs III (HR=2.7, p=0<0.001\*\*\*) and stage I vs IV (HR=7.1, p<0.001\*\*\*) (Figure 4).

Altogether, these results indicated all four classes of AQPs with increased expression levels were associated with worse outcomes, with severity increasing at advanced tumor stages. These results support to have stage dependent associations of high AQP3, 5, 7 and 9 expression levels with worse patient outcomes.

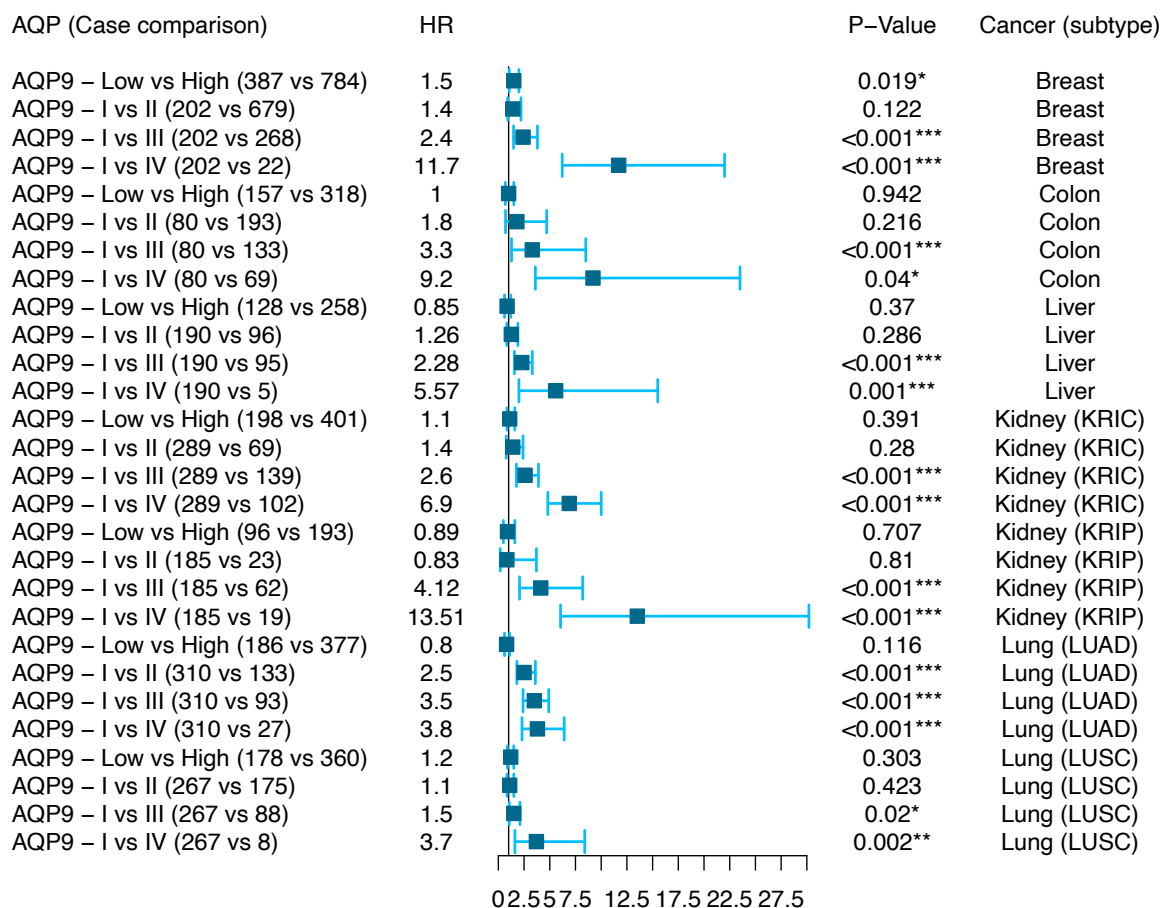


**Figure 2:** Multivariable analysis of AQP9 mRNA expression in breast, colon, liver, Kidney (KRIC and KRIP subtypes) and Lung (LUAD and LUSC subtypes). Hazard ratios with their 95% confident intervals as well as P-values resulting from the comparisons between low (67%) and high (33%), stage I vs stage II, III and IV are shown.

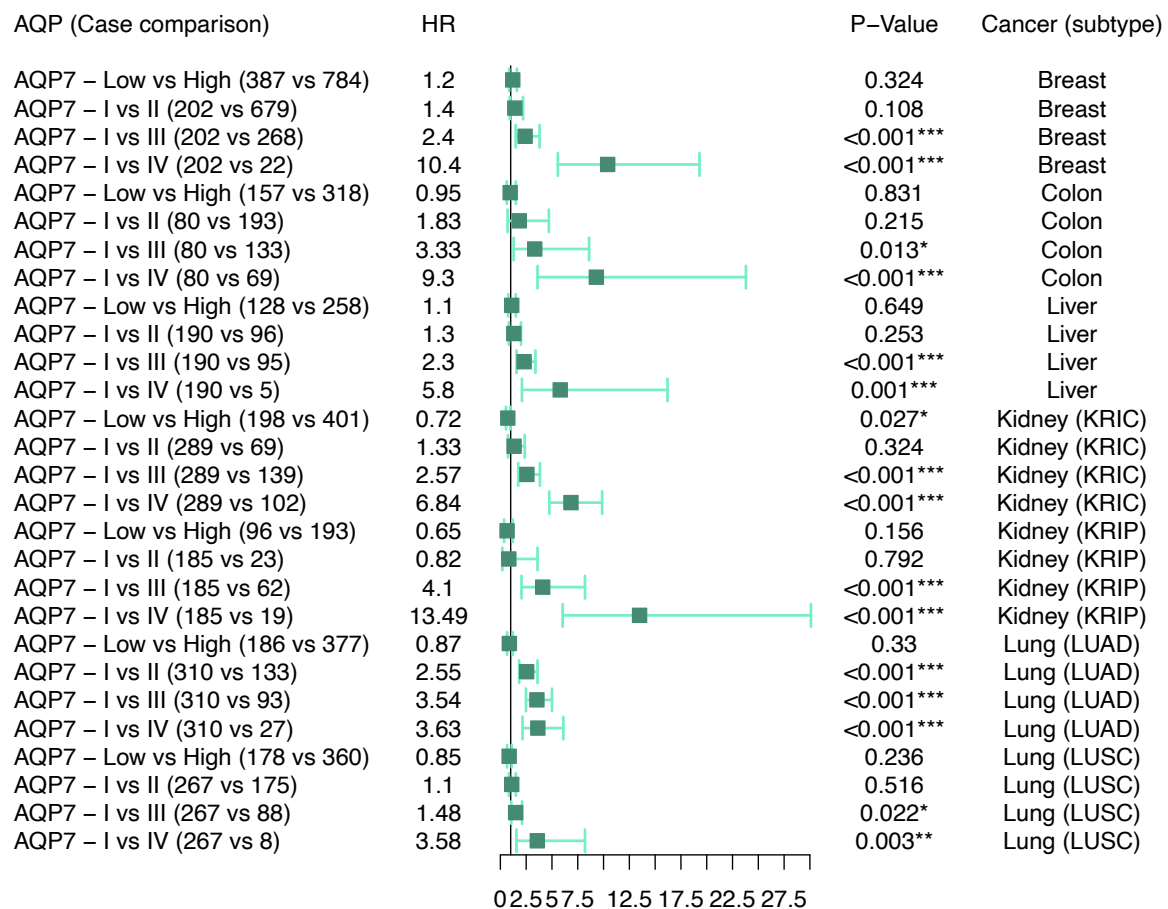


**Figure 3:** Multivariable analysis of AQP7 mRNA expression in breast, colon, liver, Kidney (KRIC and KRIP subtypes) and Lung (LUAD and LUSC subtypes). Hazard ratios with their 95% confident intervals as well as P-values resulting from the comparisons between low (67%) and high (33%), stage I vs stage II, III and IV are shown.

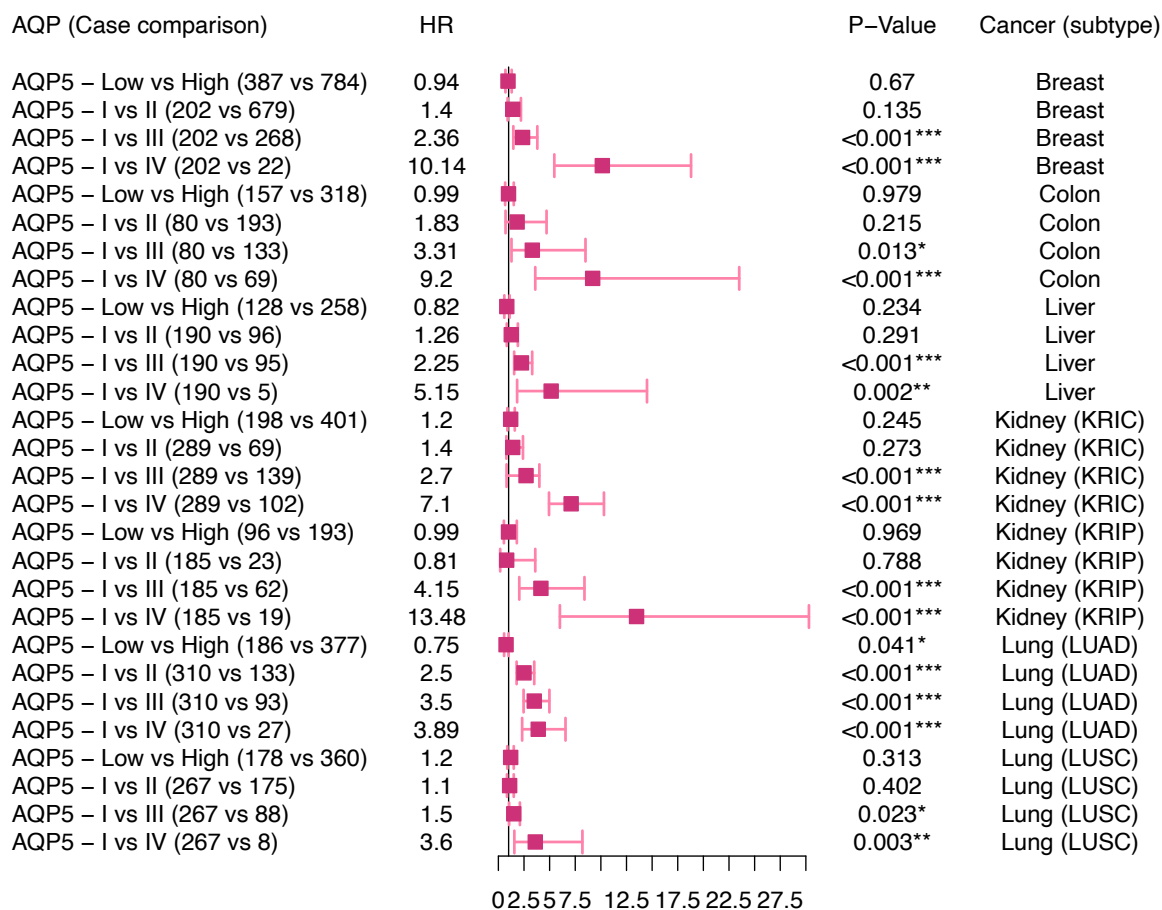


**Figure 4:** Multivariable analysis of AQP5 mRNA expression in breast, colon, liver, Kidney (KRIC and KRIP subtypes) and Lung (LUAD and LUSC subtypes). Hazard ratios with their 95% confidence intervals as well as P-values resulting from the comparisons between low (67%) and high (33%), stage I vs stage II, III and IV are shown.

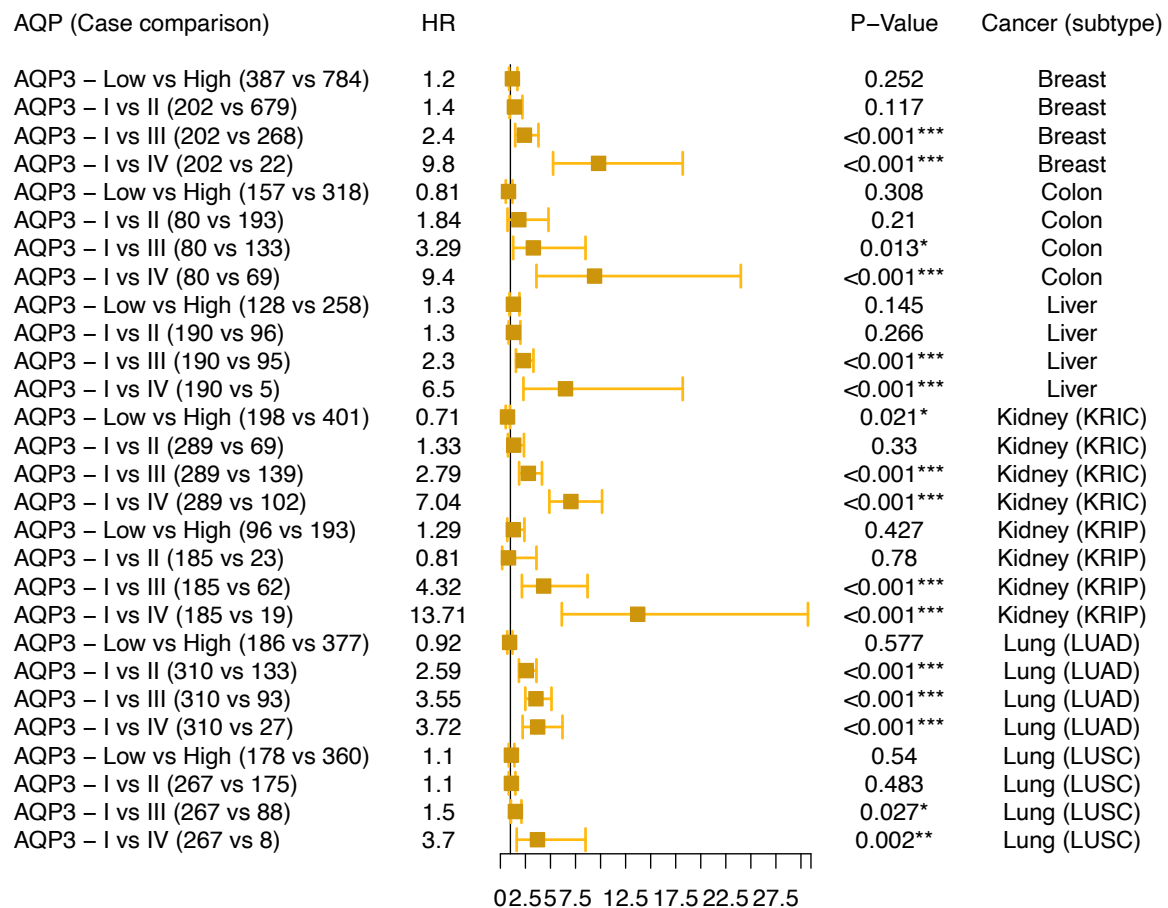


**Figure 5:** Multivariable analysis of AQP3 mRNA expression in breast, colon, liver, Kidney (KRIC and KRIP subtypes) and Lung (LUAD and LUSC subtypes). Hazard ratios with their 95% confident intervals as well as P-values resulting from the comparisons between low (67%) and high (33%), stage I vs stage II, III and IV are shown.

### 3.2.3. Differences of AQP Expressions between Cancer Stages

Levels of AQP expression were compared between tumor-adjacent healthy tissue and tumor samples from different stages and analysed via one-way ANOVA for each pair (Normal vs Stage I, Stage II, Stage III, and Stage IV). Results showed no significant difference in AQP5 and AQP7 expression levels between different stages across all cancer types. Although AQP9 expression was not statistically different between normal and cancer stages in Colon, Kidney, and Liver cancer types, significantly higher AQP9 transcript levels were observed in Breast and Lung cancers in normal tissues vs Stage I, Stage II, Stage III and Stage IV cancers (Supplementary S3). Similarly, significantly higher transcript levels for AQP3 were observed in normal tissues vs Stage I, Stage II, Stage III and Stage IV in Lung cancer (Supplementary S3-C), but not in Breast, Colon, Kidney and Liver cancers. These results while illustrating a recurring involvement for AQP3, 5, 7, and 9 in cancer progression, also highlight a large



variability in AQPs gene expression patterns for different cancer types, and variable associations with clinical outcomes and prognoses.

***3.2. Screening and Functional Expression of hAQPs in *S. cerevisiae* for AQP ion channels discovery. All hAQPs can potentially transport K<sup>+</sup> and Na<sup>+</sup> although to different degrees and conditions.***

After establishing a novel method carefully optimised to be suitable for investigating AQP ion channel permeability for K<sup>+</sup> and Na<sup>+</sup> (see chapter 4) we tested the hypothesis that whether other classes of hAQPs are ion channel, and thus capable of complementing the growth defect of CY162 yeast line in limited potassium conditions. Clones bearing the empty vector (pYES-DEST52), each of the 12 classes of *hAQPs* (AQP0-12, except hAQP1 that we previously investigated its ion permeability in yeast), and *AtKAT1* plasmid were grown on solid minimal medium (potassium-free YNB) supplemented with 6 mM KCl, and either glucose or galactose/raffinose +100 mM KCl at different pH values (Figure 6).

The growth rescue was measured in unbuffered (pH ~4.5+/-0.2) and buffered media (pH 5.0, 5.7, 6.4 or 7.3). In inducing medium supplemented with 100 mM KCl, all clones grew to the same extent, including controls as expected. At a lower extracellular K<sup>+</sup> concentration (6 mM), the cells expressing the hAQPs and *AtKAT1* proteins showed enhanced growth, in contrast to a lack of growth in negative control cells. The rescue of growth, similar to results with liquid media K<sup>+</sup> screening in Figure 7 was pH-dependent for hAQPs, but not for *AtKAT1*. The highest growth rates for K<sup>+</sup>-dependent growth rescue by AQPs expression were seen at 5.7-6.4 and minimum growth was observed in unbuffered or pH 5.0 media, suggesting the novel idea that ion conducting functionality is more ubiquitous property of AQPs than was previously considered. The slight differences in patterns of pH sensitivity observed across the classes of AQPs might suggest their ion channel conducting mechanisms are not identical, with cells expressing AQP 2, 6 or 12s for example showing less growth than those with other AQPs at pH 7.3 (Figure 6).

Since the cell number on solid media were lower (initial OD<sub>600</sub> ~ 0.5 followed by four 1:10 dilutions) than in liquid cultures (with initial OD<sub>600</sub> ~0.05 to 0.1), the detectable rescue of hAQP-expressing cell growth at pH 7.3 required more time for 3<sup>rd</sup> dilution and higher (photographed images shown are at 3 days incubation). All cells harbouring AQPs rescued the yeast growth defect at pH 7.3 when allowed to grow for 5 days (data not shown). These results indicated that all classes of hAQP proteins appear to be capable of mediating a level of

potassium uptake that is sufficient to confer rescue of growth when introduced into transport-defective yeast cells. The rescue of growth showed no pH sensitivity in yeast cells expressing AtKAT1, arguing against a non-specific effect of pH on yeast cell viability. Results here established that hAQPs are capable of rescuing yeast cell growth in limited potassium conditions by a process sensitive to extracellular pH.

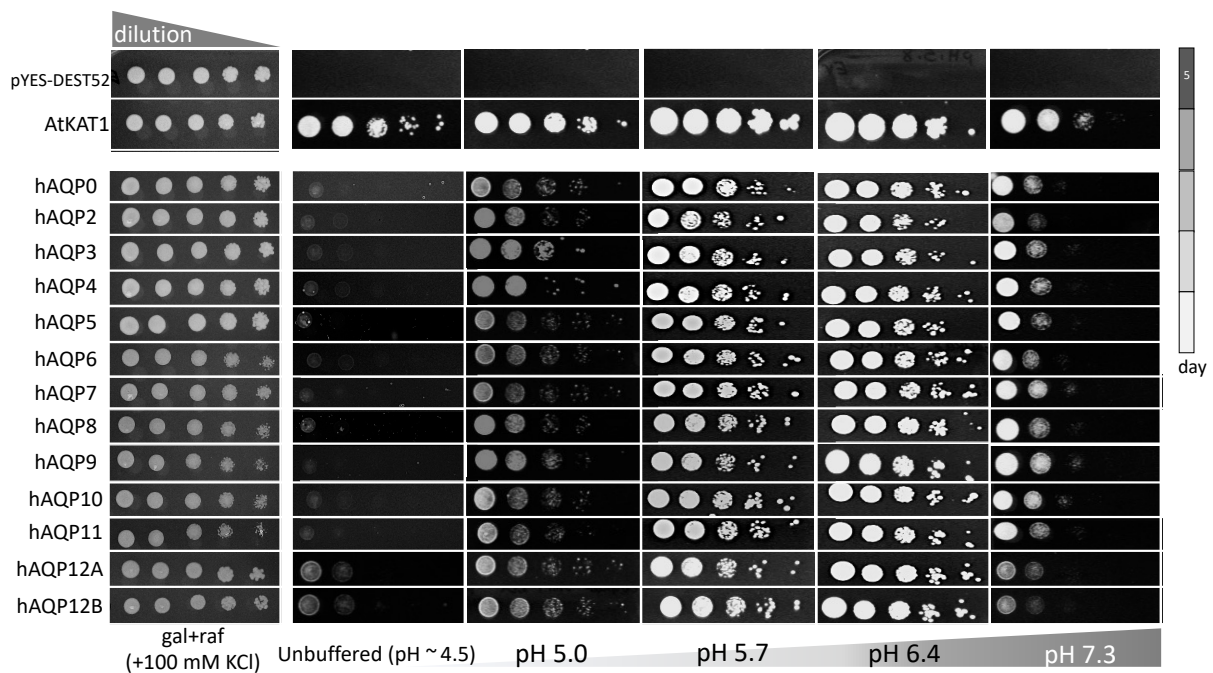


**Figure 6: Yeast-based phenotypic aquaporin assays in different pHs.**

**Phenotypic yeast assay on solid medium for potassium and pH-dependent of all hAQPs.** CY162 yeast mutant strain cells suspension expressing all human AQPs (0-12, except for AQP1 which was shown in figure 1) and controls ( $OD_{600} = 0.5$ ) were spotted in serial 1:10 dilutions on low-salt yeast nitrogen base medium at pH 5.0, 5.7, 6.4, 7.3 or unbuffered (pH ~ 4.5). Medium supplemented with 6 mM KCl. Growth shown is at 3 days. Yeast expressing hAQPs and controls grow equally well on standard medium (control: containing 2% galactose+2% raffinose (w/v) with addition of 100 mM KCl). Unlike yeast harbouring AtKAT1, cells that express the hAQPs show pH-dependent growth. Uptake of potassium is facilitated pH-independently by expression of a potassium channel (AtKAT1, positive control) or pH-dependently by hAQPs with highest rates at pH 5.7-7.3. Cells expressing empty vector grew on control but not low potassium medium. Longer lag phase noted at neutral pH (5-7 days to reach maximum growth, data not shown). This is possibly due to the yeast strain pH sensitivity at <pH7.0. All plates were incubated at 29 °C for 72 hours and photographed.

### **3.3. Analysis of water and ion channel activities of hAQPs in the rescue of yeast cell growth.**

We have previously showed the CY162 growth defect was rescued by  $K^+$  influx through hAQP1 (see chapter 4) which was independent of its water transport. To test whether the rescue of growth by other hAQPs expression was mediated by increased water or cation transport, we furthered analysed the pharmacological effects of  $CdCl_2$  (a non-selective blocker of ion channels) and  $HgCl_2$  (a blocker of AQPs water pores) (Figure 7). Based on results of a dilution series (data not shown), 5  $\mu M$   $Cd^{2+}$  and 25  $\mu M$   $Hg^{2+}$  concentrations were selected in this study

as doses that allowed AtKAT1 transformants and untreated cells to grow normally without evidence of toxicity in induction medium.

All hAQPs-expressing cultures showed slower growth rates in medium with 5  $\mu\text{M}$  cadmium chloride treatment (Figure 7A). Total growth quantified as Area Under Curve, as shown in the histogram plot, controls cells were less sensitive to  $\text{Cd}^{2+}$  than AQP-expressing cells, supporting the interpretation that the rescue of yeast growth was mediated by AQP ion conductance. The delay to onset of growth in hAQP-expressing cells was prolonged in the presence of  $\text{Cd}^{2+}$  but no significant growth alteration was observed when cells were exposed to  $\text{Hg}^{2+}$  (Figure 7B). The inhibitory effect of  $\text{Cd}^{2+}$  was stronger near neutral pH (7.3).  $\text{Hg}^{2+}$  showed a slight inhibition of growth at acidic pH (5.0), but no significant difference at higher pH values (Figure 7B). These data support the interpretation that the complementation of the yeast growth defect by hAQP-expression is independent of the channel water permeability.

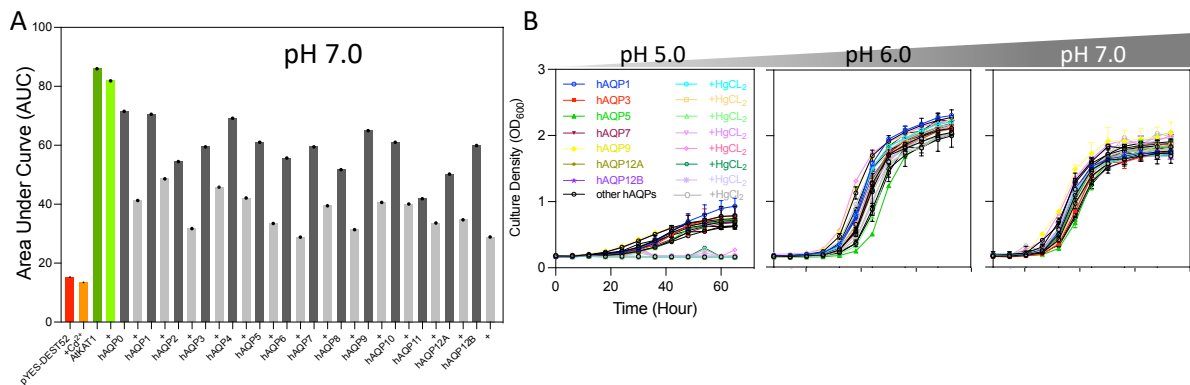


**Figure 7:** Effect of hAQPs expression on cadmium and mercury sensitivity of yeast.

AQPs-induced growth rescue in yeast is independent of their water transport functionality.

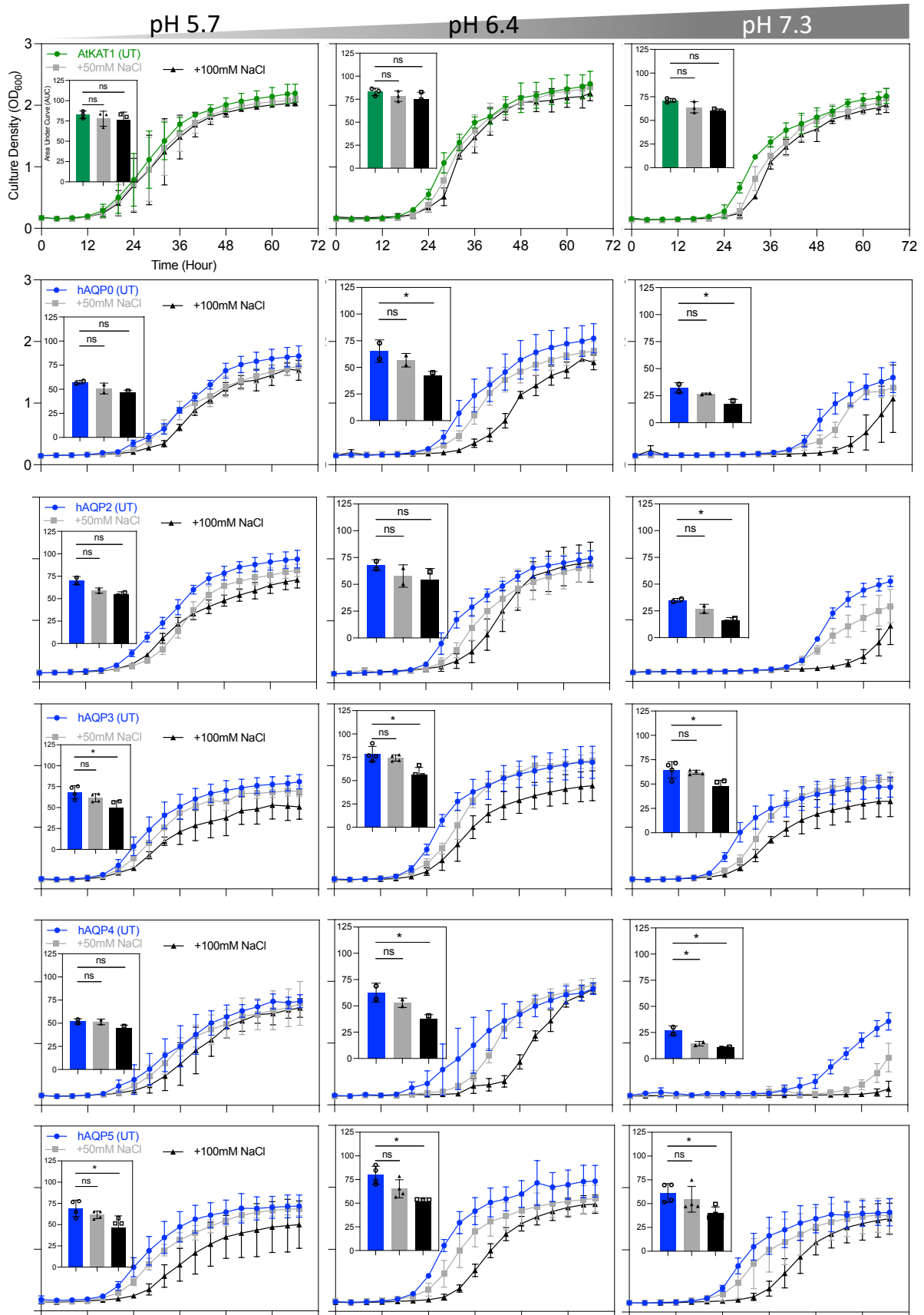
**A) Inhibition of potassium permeability by cadmium chloride ( $\text{CdCl}_2$ ) in yeast strains expressing hAQPs.** CY162 cells transformed with either pYES-DEST52, *AtKAT1* plasmid (controls) or *hAQPs* were grown on low potassium medium (6 mM) without or with 5  $\mu\text{M}$   $\text{CdCl}_2$  (*AtKAT1*: dark green bar for untreated and bright green bar represent  $\text{CdCl}_2$  treated, empty vector: red bar represents untreated and orange for  $\text{CdCl}_2$  treated, and hAQPs: dark gray bar represents untreated and bright gray bar for  $\text{CdCl}_2$  treated). Area Under the Curve (AUC) for each hAQPs and controls with or without  $\text{CdCl}_2$  are shown as bar plot (merged average of two experiments). hAQPs-expressing cells show different reduced growth treated with  $\text{CdCl}_2$  when compared to controls. **B) Investigation the hAQP water permeability involvement in rescuing yeast growth defect.** CY162 yeast strain harbouring AQP0-12 were grown with or without  $\text{HgCl}_2$  in pH 5.0, 6.0 or 7.0.  $\text{HgCl}_2$  treated cells show slight reduced growth in pH 5.0 as compared with pH 5.7-7.3. Some AQPs are highlighted for better visualisation between treated and untreated conditions.

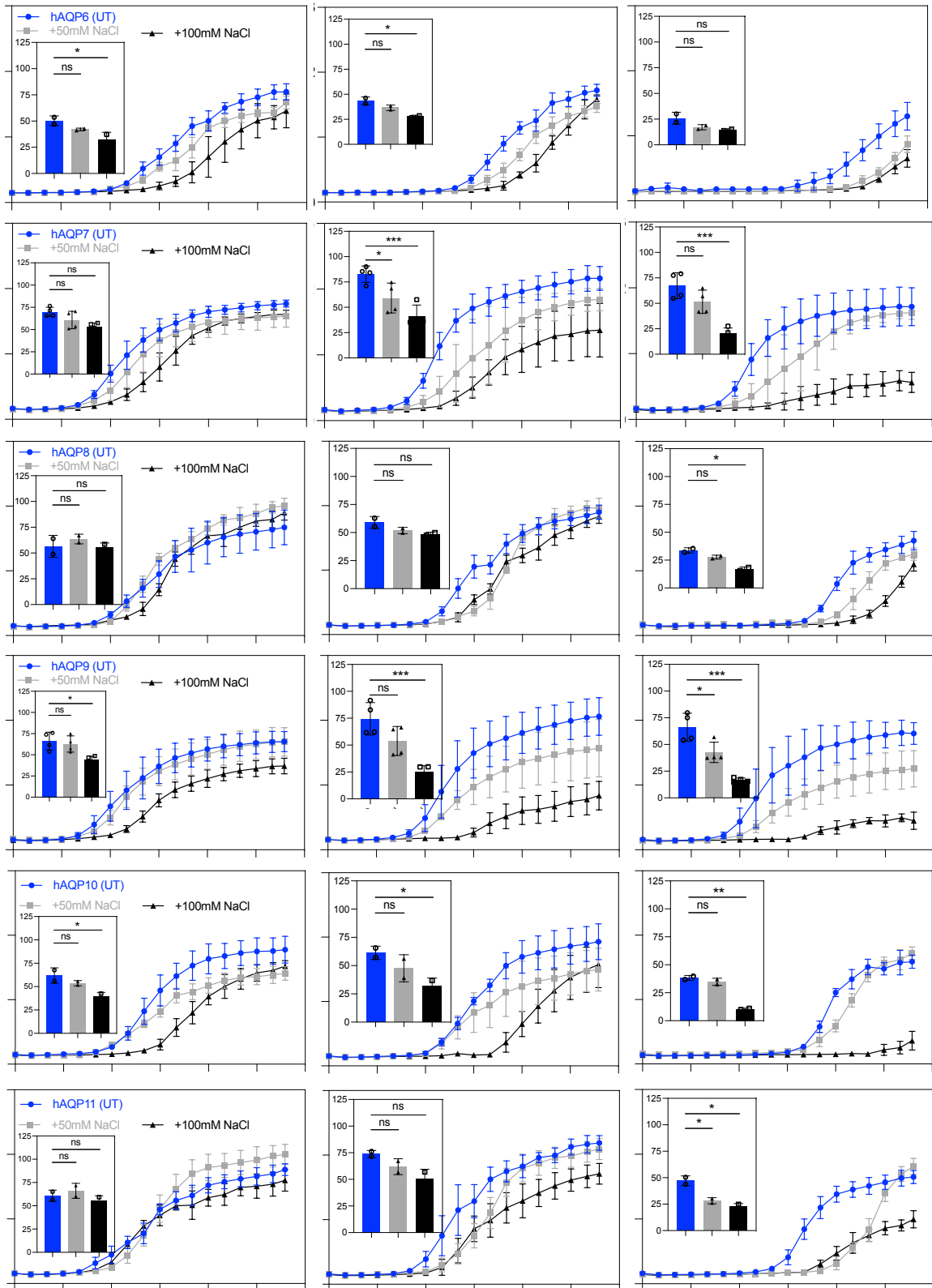
### 3.3. Using Phenotypic Yeast Assay for the Effect of AQP3, 5, 7, 9 on Yeast $\text{Na}^+$ Induced Growth Inhibition

Following on the idea that ion channel function of hAQP1 was demonstrated to be a factor in enhancing aggressive cancer cell migration, we used our novel high-throughput liquid screening approach to further confirm  $\text{K}^+$  permeability of hAQPs and test whether any of the AQP channels were permeable to  $\text{Na}^+$ . The CY162 yeast line was used to characterise AQPs

growth-induced or inhibiting effects of  $K^+$  or  $Na^+$  influx, respectively. 50 and 100 mM NaCl were added to the inducing medium containing 6 mM KCl, and growth of AQP-expressing and control cells was measured as function of time in liquid medium at pH 5.7, 6.4 and 7.3 (Figure 8).

In agreement with our solid medium screening, Figure 6, all of AQPs displayed a pattern of pH-sensitive of growth induced by extracellular  $K^+$ . Interestingly, growth inhibition induced by  $Na^+$  influx in cells expressing hAQPs in a dose-dependent manner. As expected, cells expressing our positive control (AtKAT1) did not show a significant growth reduction compared to untreated condition (only 6 mM KCl, no NaCl) as AtKAT1 is not permeable to  $Na^+$ . The reduction in growth was significantly higher for some AQPs close to physiological pH (Figure 8) whereas for some the growth inhibition was stronger toward acidic pH. The rescue of growth, similar to results shown in Figure 6 and 7, was pH-dependent for some hAQPs, but not for AtKAT1. However, we noted the highest growth rates and/or inhibition varies amongst hAQPs, suggesting their ion functionality could be associated with their native microenvironment pH conditions in their host organs. Furthermore, some AQPs showed less sensitivity to external sodium or pH (Figure 8). Growth induction or inhibition quantified as Area Under Curve and shown as bar plots.





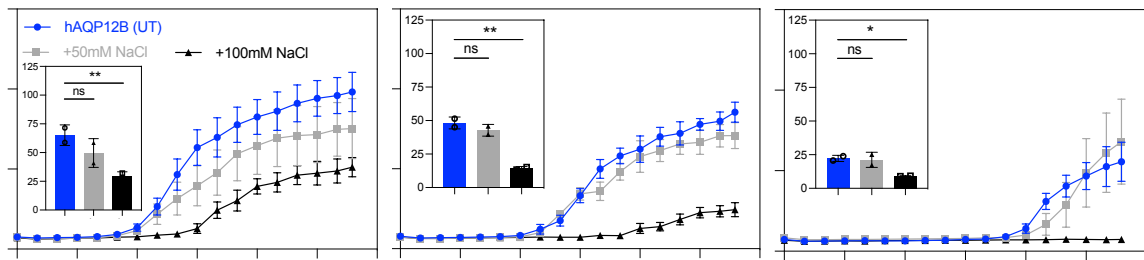


**Figure 8: Characterization of hAQPs  $K^+$  and  $Na^+$  permeability in yeast.**

$K^+$ -dependent growth rescue and  $Na^+$ -induced growth inhibition of CY162 expressing hAQPs at indicated pH and was investigated. ( $K^+$  concentration: 6 mM, and  $Na^+$  concentration: 50 or 100 mM). Cells expressing AtKAT1 (positive control) top left, first row (green curve). Cells were grown in inducing YNB medium with or without the indicated concentrations of NaCl at 29 °C for 70 hours. OD<sub>600</sub> is plotted vs time (in hours). Growth curves represent the averages of two independent experiments. Growth was monitored at regular intervals spectrophotometrically by recording absorbance at 600 nm. The optical density was recorded every 15 min but only 6 hours time-point plotted for better visualisation of curves. Initial cell density (time 0) was ~ OD<sub>600</sub> 0.05. Growth characteristics were determined by calculation of Area Under Curve (AUC). Statistical significance was shown as P < 0.05 (\*), P < 0.01 (\*\*), P < 0.001 (\*\*\*), and not significant (ns).

### 3.4. PKs-dependent Sodium Permeability in CY162 for AQP 3, 5, 7, 9.

To determine the regulatory mechanisms of new hAQPs ion channels, we next narrowed our screening to AQP3, 5, 7 and 9, as these four AQPs showed the highest expression across different common cancer types when compared to levels of other hAQPs.

We therefore extended our screening to determine the mechanism of these four AQPs  $Na^+$  permeability in the presence of different protein kinase activators. CY162 cells bearing AQP3, 5, 7 and 9 were grown on inducing medium+6 mM KCl. The medium was supplemented with 50 mM NaCl in the presence of either Forskolin (PKA), PMA (PKC), or cGMP (PKG) activator at pH 5.7, 6.4 or 7.3 (Figure 9). The expectation in this assay was if AQP  $Na^+$  permeability was triggered via phosphorylation (or prevention of phosphorylation), a concomitant growth inhibition would be observed.  $Cd^{2+}$  was used as a potential  $Na^+$  blocker in the assay in which by blocking the channel ion functionality, enhanced growth rate was expected. However, due to the non-specificity of cation channel inhibition by  $Cd^{2+}$ , there was a chance of blocking AQP channel  $K^+$  influx, required for the growth of CY162. As a result, we found  $Cd^{2+}$  treated cells grew less well when compared with their untreated controls and that the idea of blocking  $Na^+$  permeability and enhancing the growth rate did not work. However, we found the AQPs displayed a different patterns of pH-sensitivity to  $Cd^{2+}$  induced inhibition; with greater inhibition for AQP9>7>5 and 3 at pH 5.7, AQP9 and 5>7>3 at pH 6.4 and 7.3, suggesting the difference in response to  $Cd^{2+}$  was due to their ion permeability properties, e.g., ion transport via different pore domains as shown for some AQPs ion channels (94) However, further work would be required to validate this hypothesis.

In response to PK activators, inhibition of growth in AQP3-expressing cells was slightly reduced at pH 6.4 and 7.3 ( $p < 0.05^*$ ) as compared to untreated or vehicle control (quantified as Area Under Curve, shown in the bar plot) (Figure 9A). AQP5 and 9-expressing cells showed significant pH-sensitive inhibition of growth in response to cGMP at pH 6.4 and 7.3 ( $p < 0.01^{**}$ ). AQP9 Na<sup>+</sup> permeability was induced by PMA at pH 7.3 ( $p < 0.01^{**}$ ), cGMP and PMA at pH 6.4 although less than the pH 7.3 growth reduction ( $p < 0.05^*$ ) (Figure 9D). The fact that the growth inhibition induced by stimulators was pH-sensitive ruled out the possibility of any artifact or cell toxicity due to an indirect effect of stimulators on the growth rate. Inhibition of AQP7-expressing cell growth was induced by PMA in pH 7.3 ( $p < 0.05^*$ ), however, growth reduction induced by all stimuli was observed at pH 6.4 ( $p < 0.05^*$ ), and only PMA at pH 7.3 ( $p < 0.05^*$ ) (Figure 9C).

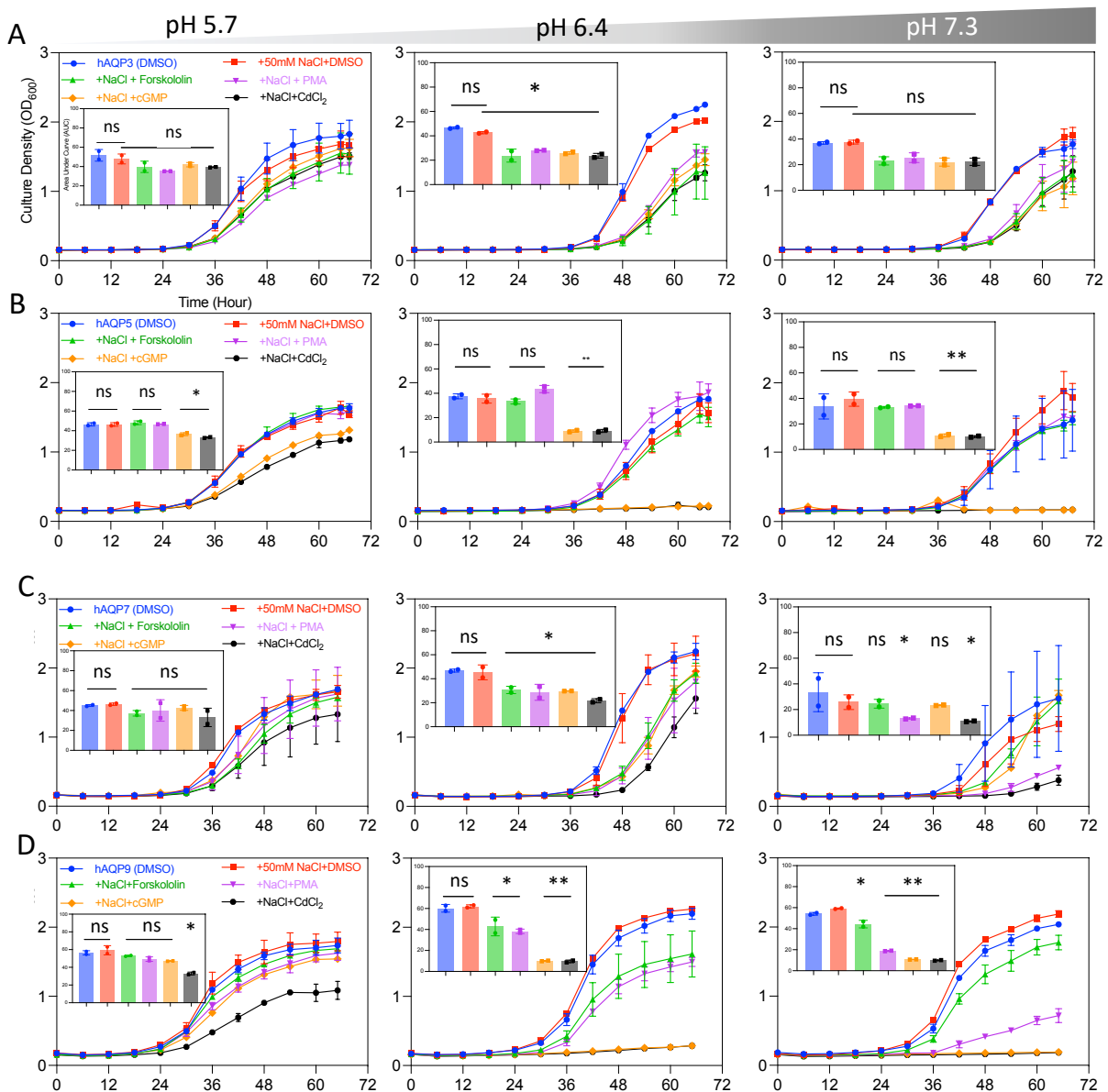


**Figure 9:** Characterization of AQP3, 5, 7 and 9 sodium uptake permeability gating mechanism.



**A-D) The growth inhibition mediated by hAQP3, 5, 7 and 9 sodium permeability in yeast is sensitive to activators and inhibitor of protein kinases in a pH-dependent manner.**

CY162 cells expressing the indicated AQPs were grown in a similar medium as panel A but supplemented with additional 50 mM NaCl (red), PK stimulators or inhibitor as indicated in different colours. Growth inhibition difference was plot as AUC at indicated pH values. Growth curves represent the averages of two independent experiments (n=3 replicates). Error bars indicating the standard deviation (mean  $\pm$  SD). (p < 0.05 \*\*); (p < 0.5\*), ns (not significant).

These results indicated the Na<sup>+</sup> transport by AQPs tested here are induced by PKs with AQP9 having Na<sup>+</sup> permeability mediated potentially by PKG>>PKC>PKA, followed by AQP7 with PKC>PKG, PKA, and AQP5 with PKG. The growth inhibition mediated by stimulators seemed to be pH-dependent with more potent induction at pH 6.4 and 7.3. Conversely, AQP3 showed growth reduction induced by all PK stimuli at pH 6.4 (p < 0.05\*).

Furthermore, the we tested the effect of the PK modulators on K<sup>+</sup> permeability of these four channels. H7 (PK inhibitor) were used for the direct validation of PK activators involment on K<sup>+</sup>-influx dependent growth rescue via AQPs (Figure 10). AQP3 and -5 expressing cells showed no obvious growth rescue alteration by PK stimuli and thus no reduction in response to H7 (Figure 10A-B). The rescue of AQP7 and -9 growth was enhanced in the presence of PMA at pH 6.4 and 7.3. Interestingly, complementation of the growth defect following PMA treatment was reduced by H7 as compared with untreated controls (Figure 10C-D). This observation suggested that growth rescue by AQP7 and -9 mediated K<sup>+</sup> uptake induced by PKC and can be inhibited by H7 (a non-specific PK signalling inhibitor). Additionally, the effect of PMA on K<sup>+</sup> uptake through AQP7 and 9 was similar to that with PMA, in showing pH-dependence (Figure 10C-D). In summary, the possible non-selective cation permeabilities of AQP5, 7 and 9 appear to be modulated by PK signaling pathways.

We herein established and illustrated a novel way of screening, characterising, and discovery of new candidate AQP ion channels for further research in heterologous expression systems.

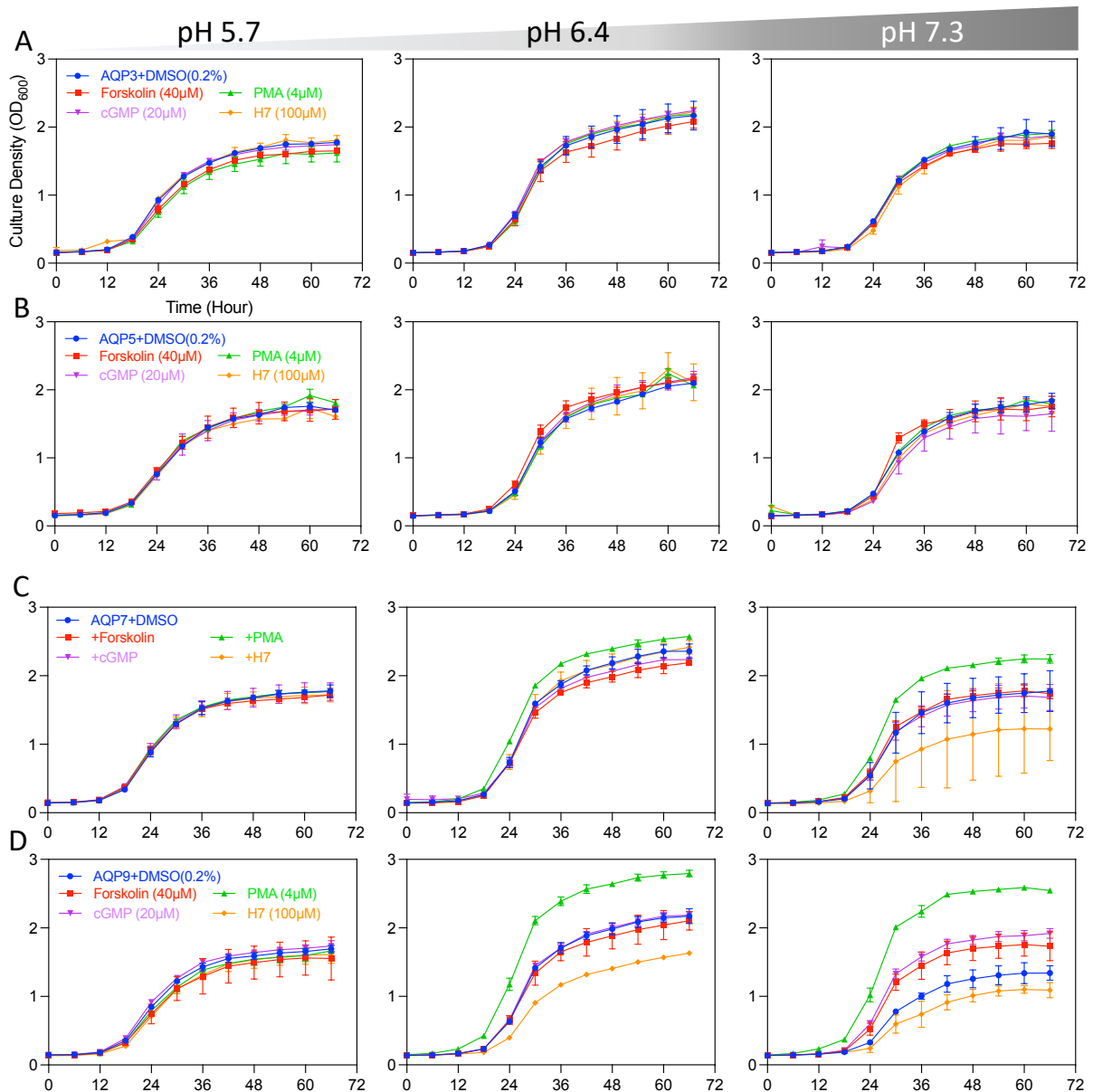


**Figure 10:** Characterisation of AQP3, 5, 7 and 9 potassium uptake permeability gating mechanism.

**A-D)** The growth mediated by AQP3, 5, 7 and 9 potassium permeability in yeast is sensitive to activators and inhibitor of protein kinases in a pH-dependent manner. CY162 cells expressing indicated AQPs were grown in YNB inducing medium+6 mM KCl at indicated pH values. Vehicle (0.2% (v/v) DMSO) or water (UT) served as control conditions and the growth rescue rate was compared between treated and untreated protein kinase activator/inhibitor. Forskolin, PMA, cGMP or H7 were used at indicated doses based on prior data for hAQP1 in yeast.

### 3.5. Proposed Significance of novel contribution of AQPs in cancer progression.

The excess proton ( $H^+$ ), created in the glycolytic pathway, is exported by NHE1 to the extracellular microenvironment to maintain intercellular pH ( $pH_i=7.1-7.7$ ). This results in acidic extracellular pH ( $pH_o=6.1-6.8$ ) (95) (Figure 11A). Voltage-gated potassium channels export positive charges from the intra- to the extracellular space initiating hyperpolarization (red line) required to facilitate the transition between G0/G1 to the S-phase. In contrast, opening of some  $Ca^{2+}$  and/or  $Na^+$  channels during the S-phase causes depolarization of

membrane potential. The transition of S- to G2/M phase is associated  $\text{Na}^+$  and/or  $\text{Ca}^{2+}$  channel activities causing depolarization (red line) of the cell until cell division and returning to hyperpolarization in the G0/G1 (96). Inhibition of  $\text{K}^+$  channels leads to prolonged depolarization and induces apoptosis (97) (Figure 11B). Following tumor microenvironmental acidosis, upper half of dash line, most of the ion channels, including  $\text{K}^+$ ,  $\text{Na}^+$  and  $\text{Ca}^{2+}$  function shut down (6). The effect of hypoxia, another tumor microenvironment stimuli, effecting ion channels causing an increase in some AQPs expression shown in lower half of dash line (48, 98). Briefly, the influx of  $\text{Ca}^{2+}$  via mechanosensitive families, TRPs, is shown to promote CaM-dependent protein kinases and facilitate AQPs phosphorylation and increase membrane localization, as shown in astrocytes (99) (Figure 11C). As shown in Figure 1-5, we found AQP9, 7, 5 and 3 have positive correlation with cancer severity and therefore, speculated hypoxia mediated upregulation AQPs could be one of the potential compensatory mechanisms that cancer cells use to cope with ion channel imbalance when in unfavourable microenvironmental conditions.

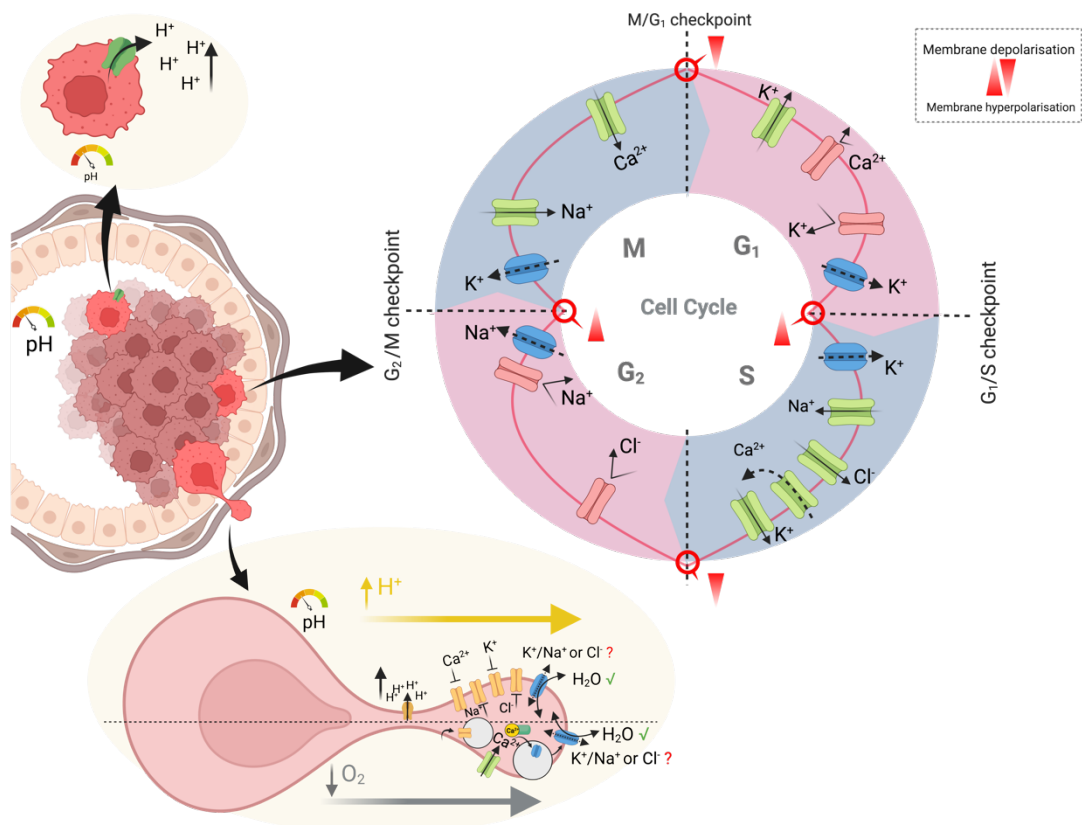


**Figure 11: Proposed mechanism of AQPs ion permeability in cancer progression.**

**A) Intra- and extracellular pH control by  $\text{Na}^+/\text{H}^+$  exchanger 1 (NHE1) in cancer cells.** The excess proton ( $\text{H}^+$ ), created in glycolytic pathway, is exported by NHE1 to the extracellular microenvironment to maintain intercellular pH ( $\text{pH}_i = 7.1-7.7$ ). This results in acidic extracellular pH ( $\text{pH}_o = 6.1-6.8$ ) (95). **B) Schematic representation of  $\text{Na}^+$ ,  $\text{K}^+$ ,  $\text{Cl}^-$  and  $\text{Ca}^{2+}$  channel activities during cancer cell cycle.** Voltage-gated potassium

channels export positive charges from the intra- to the extracellular space initiating hyperpolarization (red line) required to facilitate transition between G0/G1 to the S-phase. In contrast, opening of some  $\text{Ca}^{2+}$  and/or  $\text{Na}^{+}$  channels during the S-phase cause deperpolarization of membrane potential. The transition of S- to G2/M phase associated  $\text{Na}^{+}$  and/or  $\text{Ca}^{2+}$  channel activities causing depolarization (red line) of the cell until cell division and return to hyperpolarization in the G0/G1 (96). Inhibition of  $\text{K}^{+}$  channels lead to prolonged hyperpolarization and induce apoptosis (97). **C) Schematic representation of ion channel activity during cell migration under acidosis and hypoxia.** Following microenvironmental acidosis, upper half of the migrating cells, most of the ion channel function shuts down (6). On the other side, lower half of the migrating cells, hypoxia cause downregulation and/or inactivation of ion channels (48, 98) and initiates fluid imbalance. Influx of  $\text{Ca}^{2+}$  via mechanosensitive families, TRPs, shown to promotes CaM-dependent protein kinases and facilitate AQPs phosphorylation and increase membrane localization as shown in astrocytes (99). Proposed involvement of AQPs in cancer progression (proliferation and migration) is shown as a blue colour channel during microenvironmental stimuli (created with [https:// biorender.com](https://biorender.com)).

## 4. Discussion

Cancer therapeutics have revolutionised the treatment of various cancer types, but despite these improvements, cancer incidence is expected to increase in future decades at a rate of approximately 2% per year based on data from 2018-2020 (100, 101). Despite the large focus on personalised cancer medicine, a small number of patient population benefits from existing therapies, hence it is critical to identify new molecular targets and develop alternative target-specific therapies to enable proactive provision of more effective cancer treatment strategies. The role of ion channels in cancer progression has been an area of emerging interest as a process essential for cancer cell development and proliferation (6, 102). Notably, about 15% of currently used drugs in the market target ion channels (103), indicating the significance of this function in human physiology. A better understanding of tumor and normal tissue microenvironments and the molecular basis of cancer cells' responses to environmental stimuli is likely to advance the development of target-specific therapies. pH signaling is one of the critical drivers of malignant cancers (4, 104). Interestingly tumor microenvironment pH is shown to be distinct from that of normal tissue microenvironment (105, 106), and its alteration regulates ion channel function. Therefore, understanding the mechanism of pH changes and decoding the crosstalk between pH-regulated ion channels in cancerous cells, tumor immunity and TME is essential for developing novel pH-oriented therapeutic strategies. Remarkably, most ion channels are inhibited in acidic pH and hypoxic environments, causing lower level of available ATP, or have a narrow pH spectrum tolerance to maintain their physiological function. Whether ion channels inhibition mediated by acidosis results in ineffective innate tumor immunity remains to be answered. Nevertheless, cation transport is maintained in cancer cells, probably by upregulation of several channels, including TRPV4 required for  $\text{Ca}^{2+}$  influx and possibly AQPs that are shown to overexpressed after hypoxia insult (99) or with an acidic stimulus (i.e., upregulation of AQPs in tumor tissues). AQP regulation via  $\text{Ca}^{2+}$ -dependent

protein kinases was also reported in planta (107). Thus, in a phenomenon when ion channels are not functioning, we speculate the stage-dependent upregulation of AQPs in tumor tissues (compared to normal ones from the same origin shown in this study), could be a compensatory mechanism of alternative ion channel involvement to help facilitating cancer proliferation and metastasis.

In the present work, we found all classes of hAQPs as potential ion channels using yeast as a heterologous expression model. We further, aimed to investigate the potential significance of a subset of these novel ion channels that have been associated with cancer development based on transcriptomic analyses. The hypothesis was that there is a stage-dependent correlation between the level of hAQPs expression and the severity of common cancers when compared to adjacent normal tissue of the same patients, and that the predominant cancer-linked AQP classes have ion channel activity. The prognostic importance of all hAQPs in diverse cancer types was assessed from analyses of publicly available RNA-seq datasets for determination of their associations with patients' risk of death. We found AQP9, -5, -3 and -7 were the classes with the greatest differential expression in eight types of cancers (ten subtypes), as compared with the other 9 classes of hAQPs (Figure 1A-B). High transcript levels for AQP9 have been associated with poor prognoses and increased risk of distant metastases in the literature (108, 109), indicating its potential as an important prognostic factor in many cancer types. In the eight cancer types analysed, the most prominent differential expression of AQPs was noted in Breast, Colon, Liver, Kidney cancer subtypes KIRC and KIRP, and Lung cancer subtypes LUAC and LUSD. AQP9, -5, -3 and -7 roles in these five common cancer types were selected for further in-depth analyses.

In breast cancer, the upregulation of AQP9, -5, -3 and -7 expression, although not statistically significant, was associated with an increased risk of death (Supplementary S1 A-D). Previous findings (110, 111), reported moderately increased levels of AQP9, -5, -3 and -7 were found in breast cancer biopsies as compared to normal tissues. Similarly, we noted significant differential expression for AQP3, -4, -5, -6, -7, -9 and -11 in breast cancer (82, 110, 112-115). AQP1 expression is induced by estrogen (116) in breast cancer, and high levels of expression have been correlated with shorter overall survival (117). Interestingly, our analysis of AQP1 transcript levels in the TCGA data for the breast cancer cohort did not indicate higher AQP1 as compared to adjacent normal tissue from the same patients. AQP0 however emerged as a potential player in breast cancer (Figure 1A-B), although the protein expression levels and association with survival time remain to be determined.

In non-cancerous colon tissues, AQP1, -3, -4, -7 and -8 are the major isoforms (118), and have been shown to be expressed in colorectal cancer (119-124). A correlation between AQP1 expression and colorectal invasiveness and poor survival of patients has been suggested (125, 126), and supported by results showing that the knock down or inhibition of AQP1 by molecular and pharmacological means reduced colorectal cell migration (127-129). Prior work illustrated the importance of AQP1 dual water and ion channel function in enhancing colorectal cancer cell migration (78); however, upregulated AQP1 transcript levels were not observed in the TCGA colon cancer cohort, which showed no appreciable differences between primary cancer and normal tissues, indicating AQP1 is unlikely to be a robust prognostic marker for overall survival. AQP5 overexpression was shown to induce colorectal cell proliferation via the Ras-MAPK signalling pathway (130), Conversely, silencing of AQP5 expression lowered cell proliferation and induced apoptosis (44).

Investigating the correlations between AQP3, -5, -7, and -9 with overall survival indicated overexpression of AQP3 and -9 showed a trend towards association with worse prognoses in patients with colorectal cancer ([Supplementary S1](#)) although the difference was not statistically significant. Follow-on studies using different levels as cutpoints for categorising results might offer more insight into possible associations of AQP transcript levels with clinical outcomes. General categories grouped into set divisions (e.g., median, tertiles, quartiles, deciles), have not always been successful in reflecting the underlying importance of biological markers (131). Further work defining optimal cutpoints for stratifying patient samples into high and low AQP expression categories might reveal better predictive value for AQPs as prognostic factors, using a tool such as xTile for biomarker assessment and outcome-based cut-point optimization.

The association of immune cell infiltration and AQP9 expression in colorectal cancer development has been suggested (45). Colorectal cancer patients with higher expression of AQP9 showed more sensitivity to chemotherapy, highlighting the potential the significance of AQPs in regulating chemosensitivity (132). We observed AQP3 and -7 transcript levels were associated with better overall survival for patients with kidney cancer subtype KIRC ([Supplementary S1](#)). Similarly, high AQP7 levels showed a trend toward better outcomes for the KIRP kidney cancer patients, although not statistically significant. While the majority of AQP ion channels have been found to aid cancer progression, some AQPs such as AQP3 and -7 might facilitate the balancing of tumor microenvironment and have a protective role in some cancer types.

In lung cancer, significantly improved chances of survival were observed for patients with high expression of AQP3 (HR = 0.75, p = 0.05\*) and -7 (HR = 0.73, p = 0.025\*). Upregulation of AQP5 also appeared to favour better prognostic outcome although not statistically significant. Prior worked report that upregulation of both AQP3 and -5 was linked to poor survival (133), suggesting that combined assessment of two or more AQPs might strengthen the predictive value of these channels as prognostic markers (134), an idea that merits further study.

High transcript levels for AQP3 and -7 were associated with poor survival in liver cancer patients (Supplementary S1). Although AQP9 was negatively correlated with survival in breast, colon, kidney, and lung cancers, its high expression in liver cancer showed a trend towards better outcomes but this was not statistically significant.

Multivariable analyses were performed using stage as a co-variate to evaluate prognostic values of AQPs. All hazard ratios for all four AQPs showed incremental amplification as a function of higher tumor stage (Figure 2-5 and Supplementary S4-S10). Strikingly, all four AQPs in all five common cancer types (7 subtypes) showed stage-dependant associations with poor prognoses. Taken together, our analyses indicate that AQP expression is dynamically regulated in cancer development, and that the probabilities of overall survival decrease with increasing levels of expression of most classes of AQPs, as seen in higher tumor grades. The four classes of AQPs studied here were selected for the greatest changes in expression seen across a majority of cancer types (Figure 1B). Outcomes reinforce the idea that AQPs have value as prognostic markers in several common cancer types. As shown in Figure 1A and 1B, other AQPs (AQPs 0, 1, 2, 6, 8, 4, 10, and 11) show individual pattern of association with different cancers, and merit further investigation to highlight possible importance in particular types of cancers.

In summary, the patterns of AQPs expression inferred from transcript levels showed a strong association with worse prognoses in five common cancer types (7 subtypes) for most of the AQP classes, though a subset of AQPs appeared to correlate with protective effects and could serve as negative prognostic indicators. The mechanisms by which AQPs might facilitate cancer progression is an area of current interest. It is important to note that mRNA transcript and protein expression levels are not necessarily equivalent. Given that proteins play the functional roles in cells, further studies of AQP protein levels in different cancer types will be essential. The proposed association between AQPs mRNA expression levels and disease severity could inspire new therapeutic strategies exploring combinations of selected AQP modulating pharmacological agents as novel cancer therapeutics.

Using our yeast mass-throughput assay, we confirmed K<sup>+</sup> and Na<sup>+</sup> permeability with an apparent rank order of AQP9 > 7 >> 5 >3 (Figure 6-10), and showed that the regulation of AQP-mediated Na<sup>+</sup> and K<sup>+</sup> permeability was influenced by protein kinases by processes that appear to be sensitive to pH (Figure 9-10). The proposed link between hAQP ion channel functionality and cancer cell proliferation and metastasis is summarised in Figure 11, in which we illustrated the potential association between tumor microenvironmental stimuli and AQP ion permeability and the possibility of this function in cancer progression.

Work here sheds light on the link between ion channels in cancer development and paves the way for developing AQP-based therapies. The new candidate AQP ion channels reported here, if confirmed in future work could have a profound impact not only in cancer therapy but also in understanding the basic mechanisms for maintaining homeostasis in all types of organisms from plants to humans, with relevance to challenges spanning agriculture to medicine.

## 5. References

1. Jemal A, Ward EM, Johnson CJ, Cronin KA, Ma J, Ryerson AB, et al. Annual report to the nation on the status of cancer, 1975–2014, featuring survival. *JNCI: Journal of the National Cancer Institute*. 2017;109(9):dxx030.
2. Maman S, Witz IP. A history of exploring cancer in context. *Nature Reviews Cancer*. 2018;18(6):359-76.
3. Hanahan D, Coussens LM. Accessories to the crime: functions of cells recruited to the tumor microenvironment. *Cancer cell*. 2012;21(3):309-22.
4. Damaghi M, Wojtkowiak JW, Gillies RJ. pH sensing and regulation in cancer. *Frontiers in physiology*. 2013;4:370.
5. Czowski BJ, Romero-Moreno R, Trull KJ, White KA. Cancer and pH dynamics: Transcriptional regulation, proteostasis, and the need for new molecular tools. *Cancers*. 2020;12(10):2760.
6. Pethő Z, Najder K, Carvalho T, McMorro R, Todesca LM, Ruge M, et al. pH-channeling in cancer: How pH-dependence of cation channels shapes cancer pathophysiology. *Cancers*. 2020;12(9):2484.
7. Swietach P, Vaughan-Jones RD, Harris AL, Hulikova A. The chemistry, physiology and pathology of pH in cancer. *Philosophical Transactions of the Royal Society B: Biological Sciences*. 2014;369(1638):20130099.
8. Jing X, Yang F, Shao C, Wei K, Xie M, Shen H, et al. Role of hypoxia in cancer therapy by regulating the tumor microenvironment. *Molecular cancer*. 2019;18(1):1-15.
9. Peers C, Brahim-Horn MC, Pouyssegur J. Hypoxia in cancer cell metabolism and pH regulation. *Essays in biochemistry*. 2007;43:165-78.
10. Pedersen SF, Novak I, Alves F, Schwab A, Pardo LA. Alternating pH landscapes shape epithelial cancer initiation and progression: Focus on pancreatic cancer. *Bioessays*. 2017;39(6):1600253.



11. Gupta SC, Singh R, Asters M, Liu J, Zhang X, Pabbidi MR, et al. Regulation of breast tumorigenesis through acid sensors. *Oncogene*. 2016;35(31):4102-11.
12. Avagliano A, Fiume G, Pelagalli A, Sanità G, Ruocco MR, Montagnani S, et al. Metabolic plasticity of melanoma cells and their crosstalk with tumor microenvironment. *Frontiers in Oncology*. 2020;10:722.
13. Stopa KB, Kusiak AA, Szopa MD, Ferdek PE, Jakubowska MA. Pancreatic cancer and its microenvironment—recent advances and current controversies. *International Journal of Molecular Sciences*. 2020;21(9):3218.
14. Chu S, Shi X, Tian Y, Gao F. pH-Responsive Polymer Nanomaterials for Tumor Therapy. *Frontiers in Oncology*. 2022;12:855019-.
15. Choi H, Cao J, Qiao H, Chen I-W, Zhou R. Improving Cancer Detection and Treatment by pH-Sensitive Peptide Nanoparticle Drug Delivery Platform: Pharmacokinetics, Toxicity, and Immunogenicity Profile. *Advanced NanoBiomed Research*. 2022;2(3):2100081.
16. Choi H, Liu T, Nath K, Zhou R, Chen I-W. Peptide nanoparticle with pH-sensing cargo solubility enhances cancer drug efficiency. *Nano Today*. 2017;13:15-22.
17. Glitsch M. Protons and Ca<sup>2+</sup>: ionic allies in tumor progression? *Physiology*. 2011;26(4):252-65.
18. Prevarskaya N, Skryma R, Shuba Y. Ion channels and the hallmarks of cancer. *Trends in molecular medicine*. 2010;16(3):107-21.
19. Lyall V, Biber T. Potential-induced changes in intracellular pH. *American Journal of Physiology-Renal Physiology*. 1994;266(5):F685-F96.
20. Abdul Kadir L, Stacey M, Barrett-Jolley R. Emerging roles of the membrane potential: action beyond the action potential. *Frontiers in physiology*. 2018:1661.
21. Payne SL, Levin M, Oudin MJ. Bioelectric control of metastasis in solid tumors. *Bioelectricity*. 2019;1(3):114-30.
22. Chernet BT, Adams DS, Lobikin M, Levin M. Use of genetically encoded, light-gated ion translocators to control tumorigenesis. *Oncotarget*. 2016;7(15):19575.
23. Somodi S, Varga Z, Hajdu P, Starkus JG, Levy DI, Gáspár R, et al. pH-dependent modulation of Kv1. 3 inactivation: role of His399. *American Journal of Physiology-Cell Physiology*. 2004;287(4):C1067-C76.
24. Somodi S, Hajdu P, Gáspár R, Panyi G, Varga Z. Effects of changes in extracellular pH and potassium concentration on Kv1. 3 inactivation. *European Biophysics Journal*. 2008;37(7):1145-56.
25. Kazmierczak M, Zhang X, Chen B, Mulkey DK, Shi Y, Wagner PG, et al. External pH modulates EAG superfamily K<sup>+</sup> channels through EAG-specific acidic residues in the voltage sensor. *Journal of General Physiology*. 2013;141(6):721-35.
26. Tsujikawa H, Yu AS, Xie J, Yue Z, Yang W, He Y, et al. Identification of key amino acid residues responsible for internal and external pH sensitivity of Orai1/STIM1 channels. *Scientific reports*. 2015;5(1):1-16.
27. Strupp M, Staub F, Grafe P. A Ca<sup>2+</sup>-and pH-Dependent K<sup>+</sup> Channel of rat C6 glioma cells and its possible role in acidosis-induced cell swelling. *Glia*. 1993;9(2):136-45.
28. Doroszewicz J, Waldegger P, Jeck N, Seyberth H, Waldegger S. pH dependence of extracellular calcium sensing receptor activity determined by a novel technique. *Kidney international*. 2005;67(1):187-92.
29. Schulte U, Hahn H, Konrad M, Jeck N, Derst C, Wild K, et al. pH gating of ROMK (Kir1. 1) channels: control by an Arg-Lys-Arg triad disrupted in antenatal Bartter syndrome. *Proceedings of the National Academy of Sciences*. 1999;96(26):15298-303.

30. Sandoz G, Douguet D, Chatelain F, Lazdunski M, Lesage F. Extracellular acidification exerts opposite actions on TREK1 and TREK2 potassium channels via a single conserved histidine residue. *Proceedings of the National Academy of Sciences*. 2009;106(34):14628-33.
31. Vilin YY, Peters CH, Ruben PC. Acidosis differentially modulates inactivation in Nav1.2, Nav1.4, and Nav1.5 channels. *Frontiers in pharmacology*. 2012;3:109.
32. Starkus JG, Fleig A, Penner R. The calcium-permeable non-selective cation channel TRPM2 is modulated by cellular acidification. *The Journal of physiology*. 2010;588(8):1227-40.
33. Gavriliouk D, Scrimgeour N, Grigoryev S, Ma L, Zhou F, Barritt G, et al. Regulation of Orai1/STIM1 mediated ICRAC by intracellular pH. *Scientific reports*. 2017;7(1):1-12.
34. Bae C, Sachs F, Gottlieb PA. Protonation of the human PIEZO1 ion channel stabilizes inactivation. *Journal of Biological Chemistry*. 2015;290(8):5167-73.
35. Kuntze A, Goetsch O, Fels B, Najder K, Unger A, Wilhelmi M, et al. Protonation of Piezo1 impairs cell-matrix interactions of pancreatic stellate cells. *Frontiers in Physiology*. 2020:89.
36. Liu X, Ma W, Surprenant A, Jiang LH. Identification of the amino acid residues in the extracellular domain of rat P2X7 receptor involved in functional inhibition by acidic pH. *British journal of pharmacology*. 2009;156(1):135-42.
37. Sauter DR, Sørensen CE, Rapedius M, Brüggemann A, Novak I. pH-sensitive K<sup>+</sup> channel TREK-1 is a novel target in pancreatic cancer. *Biochimica et Biophysica Acta (BBA)-Molecular Basis of Disease*. 2016;1862(10):1994-2003.
38. Pei L, Wisner O, Slavin A, Mu D, Powers S, Jan LY, et al. Oncogenic potential of TASK3 (Kcnk9) depends on K<sup>+</sup> channel function. *Proceedings of the National Academy of Sciences*. 2003;100(13):7803-7.
39. Czirják Gb, Enyedi Pt. TASK-3 dominates the background potassium conductance in rat adrenal glomerulosa cells. *Molecular Endocrinology*. 2002;16(3):621-9.
40. Honoré E. The neuronal background K<sub>2</sub>P channels: focus on TREK1. *Nature reviews neuroscience*. 2007;8(4):251-61.
41. Suzuki M, Mizuno A, Kodaira K, Imai M. Impaired pressure sensation in mice lacking TRPV4. *Journal of Biological Chemistry*. 2003;278(25):22664-8.
42. Honasoge A, Shelton KA, Sontheimer H. Autocrine regulation of glioma cell proliferation via pH-sensitive K<sup>+</sup> channels. *American Journal of Physiology-Cell Physiology*. 2014;306(5):C493-C505.
43. Bustos D, Bedoya M, Ramírez D, Concha G, Zúñiga L, Decher N, et al. Elucidating the structural basis of the intracellular pH sensing mechanism of TASK-2 K<sub>2</sub>P channels. *International journal of molecular sciences*. 2020;21(2):532.
44. Williams S, Bateman A, O'Kelly I. Altered expression of two-pore domain potassium (K<sub>2</sub>P) channels in cancer. *PLoS One*. 2013;8(10):e74589.
45. Venkatachalam K, Montell C. TRP channels. *Annual review of biochemistry*. 2007;76:387.
46. Zeng X, Sikka S, Huang L, Sun C, Xu C, Jia D, et al. Novel role for the transient receptor potential channel TRPM2 in prostate cancer cell proliferation. *Prostate cancer and prostatic diseases*. 2010;13(2):195-201.
47. Chigurupati S, Venkataraman R, Barrera D, Naganathan A, Madan M, Paul L, et al. Receptor Channel TRPC6 Is a Key Mediator of Notch-Driven Glioblastoma Growth and Invasiveness Expression and Function of TRPC6 in Glioblastomas. *Cancer research*. 2010;70(1):418-27.

48. Nielsen N, Kondratska K, Ruck T, Hild B, Kovalenko I, Schimmelpfennig S, et al. TRPC6 channels modulate the response of pancreatic stellate cells to hypoxia. *Pflügers Archiv-European Journal of Physiology*. 2017;469(12):1567-77.
49. Gao H, Chen X, Du X, Guan B, Liu Y, Zhang H. EGF enhances the migration of cancer cells by up-regulation of TRPM7. *Cell calcium*. 2011;50(6):559-68.
50. DeCoursey TE. Voltage and pH sensing by the voltage-gated proton channel, Hv1. *Journal of The Royal Society Interface*. 2018;15(141):20180108.
51. Bare DJ, Cherny VV, DeCoursey TE, Abukhdeir AM, Morgan D. Expression and function of voltage gated proton channels (Hv1) in MDA-MB-231 cells. *Plos one*. 2020;15(5):e0227522.
52. Wang Y, Li SJ, Wu X, Che Y, Li Q. Clinicopathological and biological significance of human voltage-gated proton channel Hv1 protein overexpression in breast cancer. *Journal of Biological Chemistry*. 2012;287(17):13877-88.
53. Ribeiro-Silva L, Queiroz FO, da Silva AMB, Hirata AE, Arcisio-Miranda M. Voltage-gated proton channel in human glioblastoma multiforme cells. *ACS Chemical Neuroscience*. 2016;7(7):864-9.
54. Peters CH, Ghovanloo M-R, Gershon C, Ruben PC. pH modulation of voltage-gated sodium channels. *Voltage-gated Sodium Channels: Structure, Function and Channelopathies*. 2018:147-60.
55. Brackenbury WJ, Chioni A-M, Diss JK, Djamgoz M. The neonatal splice variant of Nav1.5 potentiates in vitro invasive behaviour of MDA-MB-231 human breast cancer cells. *Breast cancer research and treatment*. 2007;101(2):149-60.
56. Yang M, James AD, Suman R, Kasprovicz R, Nelson M, O'Toole PJ, et al. Voltage-dependent activation of Rac1 by Nav1.5 channels promotes cell migration. *Journal of cellular physiology*. 2020;235(4):3950-72.
57. Chen X, Wanggou S, Bodalia A, Zhu M, Dong W, Fan JJ, et al. A feedforward mechanism mediated by mechanosensitive ion channel PIEZO1 and tissue mechanics promotes glioma aggression. *Neuron*. 2018;100(4):799-815. e7.
58. Stoop R, Surprenant A, North RA. Different sensitivities to pH of ATP-induced currents at four cloned P2X receptors. *Journal of Neurophysiology*. 1997;78(4):1837-40.
59. Adinolfi E, Capece M, Amoroso F, De Marchi E, Franceschini A. Emerging roles of P2X receptors in cancer. *Current Medicinal Chemistry*. 2015;22(7):878-90.
60. Adinolfi E, Raffaghello L, Giuliani AL, Cavazzini L, Capece M, Chiozzi P, et al. Expression of P2X7 Receptor Increases In Vivo Tumor Growth P2X7 and Cancer. *Cancer research*. 2012;72(12):2957-69.
61. Vullo S, Kellenberger S. A molecular view of the function and pharmacology of acid-sensing ion channels. *Pharmacological research*. 2020;154:104166.
62. Sherwood TW, Frey EN, Askwith CC. Structure and activity of the acid-sensing ion channels. *American Journal of Physiology-Cell Physiology*. 2012;303(7):C699-C710.
63. Henderson SW, Nourmohammadi S, Ramesh SA, Yool AJ. Aquaporin ion conductance properties defined by membrane environment, protein structure, and cell physiology. *Biophysical Reviews*. 2022:1-18.
64. Tyerman SD, McGaughey SA, Qiu J, Yool AJ, Byrt CS. Adaptable and multifunctional ion-conducting aquaporins. *Annual review of plant biology*. 2021;72:703-36.
65. Zampighi GA, Hall JE, Kreman M. Purified lens junctional protein forms channels in planar lipid films. *Proceedings of the National Academy of Sciences*. 1985;82(24):8468-72.

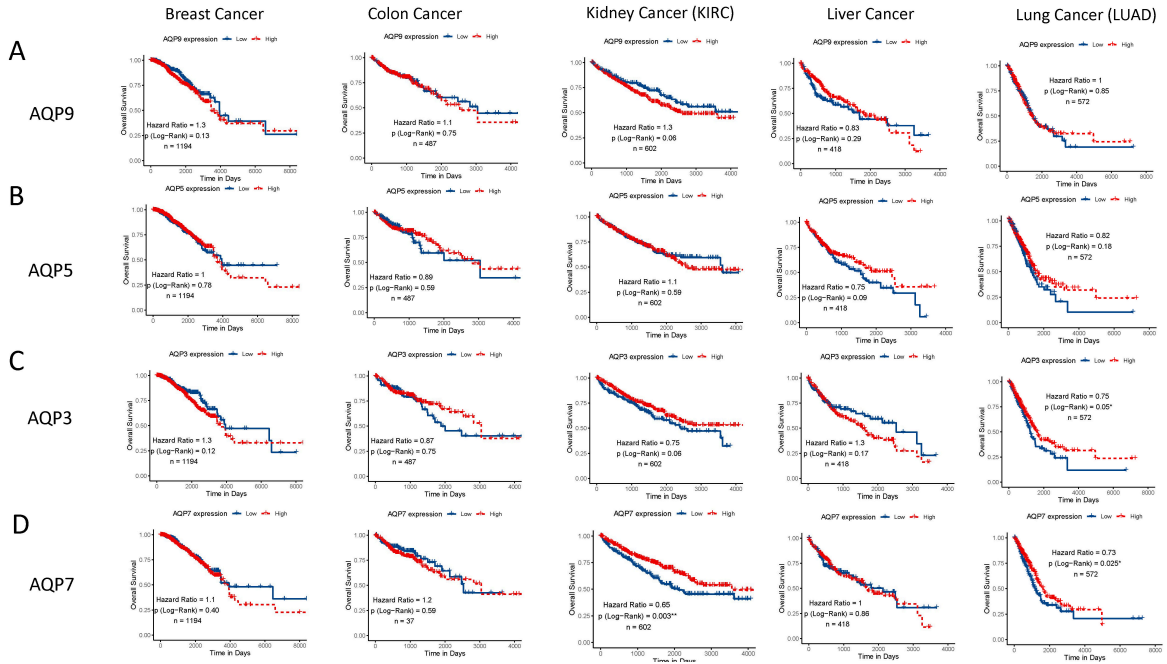
66. Ehring GR, Zampighi G, Horwitz J, Bok D, Hall JE. Properties of channels reconstituted from the major intrinsic protein of lens fiber membranes. *The Journal of General Physiology*. 1990;96(3):631-64.
67. Verkman A. Aquaporins in clinical medicine. *Annual review of medicine*. 2012;63:303.
68. Soveral G, Nielsen S, Casini A. *Aquaporins in health and disease: new molecular targets for drug discovery*: CRC Press; 2018.
69. Verkman A. More than just water channels: unexpected cellular roles of aquaporins. *Journal of cell science*. 2005;118(15):3225-32.
70. Nielsen S, Kwon TH, Frøkiaer J, Agre P. Regulation and dysregulation of aquaporins in water balance disorders. *Journal of internal medicine*. 2007;261(1):53-64.
71. Yool AJ, Campbell EM. Structure, function and translational relevance of aquaporin dual water and ion channels. *Molecular aspects of medicine*. 2012;33(5-6):553-61.
72. Verkman AS. Knock-out models reveal new aquaporin functions. *Aquaporins*. 2009:359-81.
73. Wang J, Feng L, Zhu Z, Zheng M, Wang D, Chen Z, et al. Aquaporins as diagnostic and therapeutic targets in cancer: how far we are? *Journal of translational medicine*. 2015;13(1):1-11.
74. Hoffert JD, Pisitkun T, Wang G, Shen R-F, Knepper MA. Quantitative phosphoproteomics of vasopressin-sensitive renal cells: regulation of aquaporin-2 phosphorylation at two sites. *Proceedings of the National Academy of Sciences*. 2006;103(18):7159-64.
75. Esteva-Font C, Jin BJ, Verkman A. Aquaporin-1 gene deletion reduces breast tumor growth and lung metastasis in tumor-producing MMTV-PyVT mice. *The FASEB Journal*. 2014;28(3):1446-53.
76. Abreu-Rodríguez I, Sánchez Silva R, Martins AP, Soveral G, Toledo-Aral JJ, López-Barneo J, et al. Functional and transcriptional induction of aquaporin-1 gene by hypoxia; analysis of promoter and role of Hif-1 $\alpha$ . *PloS one*. 2011;6(12):e28385.
77. De Ieso ML, Yool AJ. Mechanisms of Aquaporin-Facilitated Cancer Invasion and Metastasis. *Frontiers in Chemistry*. 2018;6.
78. De Ieso ML, Pei JV, Nourmohammadi S, Smith E, Chow PH, Kourghi M, et al. Combined pharmacological administration of AQP1 ion channel blocker AqB011 and water channel blocker Bacopaside II amplifies inhibition of colon cancer cell migration. *Scientific reports*. 2019;9(1):1-17.
79. De Ieso ML, Yool AJ. Mechanisms of aquaporin-facilitated cancer invasion and metastasis. *Frontiers in chemistry*. 2018;6:135.
80. Nico B, Ribatti D. Aquaporins in tumor growth and angiogenesis. *Cancer letters*. 2010;294(2):135-8.
81. Papadopoulos MC, Saadoun S. Key roles of aquaporins in tumor biology. *Biochimica et Biophysica Acta (BBA)-Biomembranes*. 2015;1848(10):2576-83.
82. Chow PH, Bowen J, Yool AJ. Combined systematic review and transcriptomic analyses of mammalian aquaporin classes 1 to 10 as biomarkers and prognostic indicators in diverse cancers. *Cancers*. 2020;12(7):1911.
83. Gotfryd K, Mósca AF, Missel JW, Truelsen SF, Wang K, Spulber M, et al. Human adipose glycerol flux is regulated by a pH gate in AQP10. *Nature communications*. 2018;9(1):1-11.
84. Mósca AF, De Almeida A, Wragg D, Martins AP, Sabir F, Leoni S, et al. Molecular basis of Aquaporin-7 permeability regulation by pH. *Cells*. 2018;7(11):207.

85. Németh-Cahalan KL, Hall JE. pH and calcium regulate the water permeability of aquaporin 0. *Journal of Biological Chemistry*. 2000;275(10):6777-82.
86. Németh-Cahalan KL, Kalman K, Hall JE. Molecular basis of pH and Ca<sup>2+</sup> regulation of aquaporin water permeability. *The Journal of general physiology*. 2004;123(5):573-80.
87. Zelenina M, Bondar AA, Zelenin S, Aperia A. Nickel and extracellular acidification inhibit the water permeability of human aquaporin-3 in lung epithelial cells. *Journal of Biological Chemistry*. 2003;278(32):30037-43.
88. Zeuthen T, Klaerke DA. Transport of water and glycerol in aquaporin 3 is gated by H<sup>+</sup>. *Journal of Biological Chemistry*. 1999;274(31):21631-6.
89. Kaptan S, Assentoft M, Schneider HP, Fenton RA, Deitmer JW, MacAulay N, et al. H95 is a pH-dependent gate in aquaporin 4. *Structure*. 2015;23(12):2309-18.
90. Yasui M, Hazama A, Kwon T-H, Nielsen S, Guggino WB, Agre P. Rapid gating and anion permeability of an intracellular aquaporin. *Nature*. 1999;402(6758):184-7.
91. Dajani S, Saripalli A, Sharma-Walia N. Water transport proteins–aquaporins (AQPs) in cancer biology. *Oncotarget*. 2018;9(91):36392.
92. Prata C, Hrelia S, Fiorentini D. Peroxiporins in cancer. *International Journal of Molecular Sciences*. 2019;20(6):1371.
93. McCoy E, Sontheimer H. Expression and function of water channels (aquaporins) in migrating malignant astrocytes. *Glia*. 2007;55(10):1034-43.
94. Kourghi M, Pei JV, De Ieso ML, Nourmohammadi S, Chow PH, Yool AJ. Fundamental structural and functional properties of Aquaporin ion channels found across the kingdoms of life. *Clinical and Experimental Pharmacology and Physiology*. 2018;45(4):401-9.
95. Spugnini EP, Sonveaux P, Stock C, Perez-Sayans M, De Milito A, Avnet S, et al. Proton channels and exchangers in cancer. *Biochimica et Biophysica Acta (BBA)-Biomembranes*. 2015;1848(10):2715-26.
96. Jonathan D, Josh H, Fukushima-Lopes DF, Laczynski D, Gentile S. Ion channels in breast cancer: From signaling to therapy. *Breast Cancer Biol Med*. 2017.
97. Rao VR, Perez-Neut M, Kaja S, Gentile S. Voltage-gated ion channels in cancer cell proliferation. *Cancers*. 2015;7(2):849-75.
98. Lai Q, Wang T, Guo Q, Zhang Y, Wang Y, Yuan L, et al. Positive correlation between the expression of hEag1 and HIF-1 $\alpha$  in breast cancers: an observational study. *BMJ open*. 2014;4(5):e005049.
99. Kitchen P, Salman MM, Halsey AM, Clarke-Bland C, MacDonald JA, Ishida H, et al. Targeting aquaporin-4 subcellular localization to treat central nervous system edema. *Cell*. 2020;181(4):784-99. e19.
100. Bray F, Ferlay J, Soerjomataram I, Siegel RL, Torre LA, Jemal A. Global cancer statistics 2018: GLOBOCAN estimates of incidence and mortality worldwide for 36 cancers in 185 countries. *CA: a cancer journal for clinicians*. 2018;68(6):394-424.
101. Sung H, Ferlay J, Siegel RL, Laversanne M, Soerjomataram I, Jemal A, et al. Global cancer statistics 2020: GLOBOCAN estimates of incidence and mortality worldwide for 36 cancers in 185 countries. *CA: a cancer journal for clinicians*. 2021;71(3):209-49.
102. Litan A, Langhans SA. Cancer as a channelopathy: ion channels and pumps in tumor development and progression. *Frontiers in cellular neuroscience*. 2015;9:86.
103. McManus OB. HTS assays for developing the molecular pharmacology of ion channels. *Current opinion in pharmacology*. 2014;15:91-6.
104. Ko M, Quiñones-Hinojosa A, Rao R. Emerging links between endosomal pH and cancer. *Cancer and Metastasis Reviews*. 2020;39(2):519-34.

105. Gerweck LE, Seetharaman K. Cellular pH gradient in tumor versus normal tissue: potential exploitation for the treatment of cancer. *Cancer research*. 1996;56(6):1194-8.
106. Kato Y, Ozawa S, Miyamoto C, Maehata Y, Suzuki A, Maeda T, et al. Acidic extracellular microenvironment and cancer. *Cancer cell international*. 2013;13(1):1-8.
107. Johansson I, Karlsson M, Shukla VK, Chrispeels MJ, Larsson C, Kjellbom P. Water transport activity of the plasma membrane aquaporin PM28A is regulated by phosphorylation. *The Plant Cell*. 1998;10(3):451-9.
108. Jing J, Sun J, Wu Y, Zhang N, Liu C, Chen S, et al. AQP9 Is a Prognostic Factor for Kidney Cancer and a Promising Indicator for M2 TAM Polarization and CD8+ T-Cell Recruitment. *Frontiers in Oncology*. 2021;11.
109. Xu W-H, Shi S-N, Xu Y, Wang J, Wang H-K, Cao D-L, et al. Prognostic implications of Aquaporin 9 expression in clear cell renal cell carcinoma. *Journal of Translational Medicine*. 2019;17(1):1-14.
110. Kang S, Chae YS, Lee SJ, Kang BW, Kim JG, Kim WW, et al. Aquaporin 3 expression predicts survival in patients with HER2-positive early breast cancer. *Anticancer Research*. 2015;35(5):2775-82.
111. Lee SJ, Chae YS, Kim JG, Kim WW, Jung JH, Park HY, et al. AQP5 expression predicts survival in patients with early breast cancer. *Annals of surgical oncology*. 2014;21(2):375-83.
112. Huang Y-T, Zhou J, Shi S, Xu H-Y, Qu F, Zhang D, et al. Identification of estrogen response element in aquaporin-3 gene that mediates estrogen-induced cell migration and invasion in estrogen receptor-positive breast cancer. *Scientific reports*. 2015;5(1):1-13.
113. Shi Z, Zhang T, Luo L, Zhao H, Cheng J, Xiang J, et al. Aquaporins in human breast cancer: identification and involvement in carcinogenesis of breast cancer. *Journal of surgical oncology*. 2012;106(3):267-72.
114. Moosavi M-S, Elham Y. Aquaporins 1, 3 and 5 in different tumors, their expression, prognosis value and role as new therapeutic targets. *Pathology & Oncology Research*. 2020;26(2):615-25.
115. Li X, Pei B, Wang H, Tang C, Zhu W, Jin F. Effect of AQP-5 silencing by siRNA interference on chemosensitivity of breast cancer cells. *OncoTargets and therapy*. 2018;11:3359.
116. Zou L-B, Shi S, Zhang R-J, Wang T-T, Tan Y-J, Zhang D, et al. Aquaporin-1 plays a crucial role in estrogen-induced tubulogenesis of vascular endothelial cells. *The Journal of Clinical Endocrinology & Metabolism*. 2013;98(4):E672-E82.
117. Yin T, Yu S, Xiao L, Zhang J, Liu C, Lu Y, et al. Correlation between the expression of aquaporin 1 and hypoxia-inducible factor 1 in breast cancer tissues. *Journal of Huazhong University of Science and Technology [Medical Sciences]*. 2008;28(3):346-8.
118. Zhu C, Chen Z, Jiang Z. Expression, distribution and role of aquaporin water channels in human and animal stomach and intestines. *International journal of molecular sciences*. 2016;17(9):1399.
119. Pei JV, Kourghi M, De Ieso ML, Campbell EM, Dorward HS, Hardingham JE, et al. Differential inhibition of water and ion channel activities of mammalian aquaporin-1 by two structurally related bacopaside compounds derived from the medicinal plant *bacopa monnieri*. *Molecular pharmacology*. 2016;90(4):496-507.
120. Kourghi M, Pei JV, De Ieso ML, Flynn G, Yool AJ. Bumetanide derivatives AqB007 and AqB011 selectively block the aquaporin-1 ion channel conductance and slow cancer cell migration. *Molecular pharmacology*. 2015:mol. 115.101618.

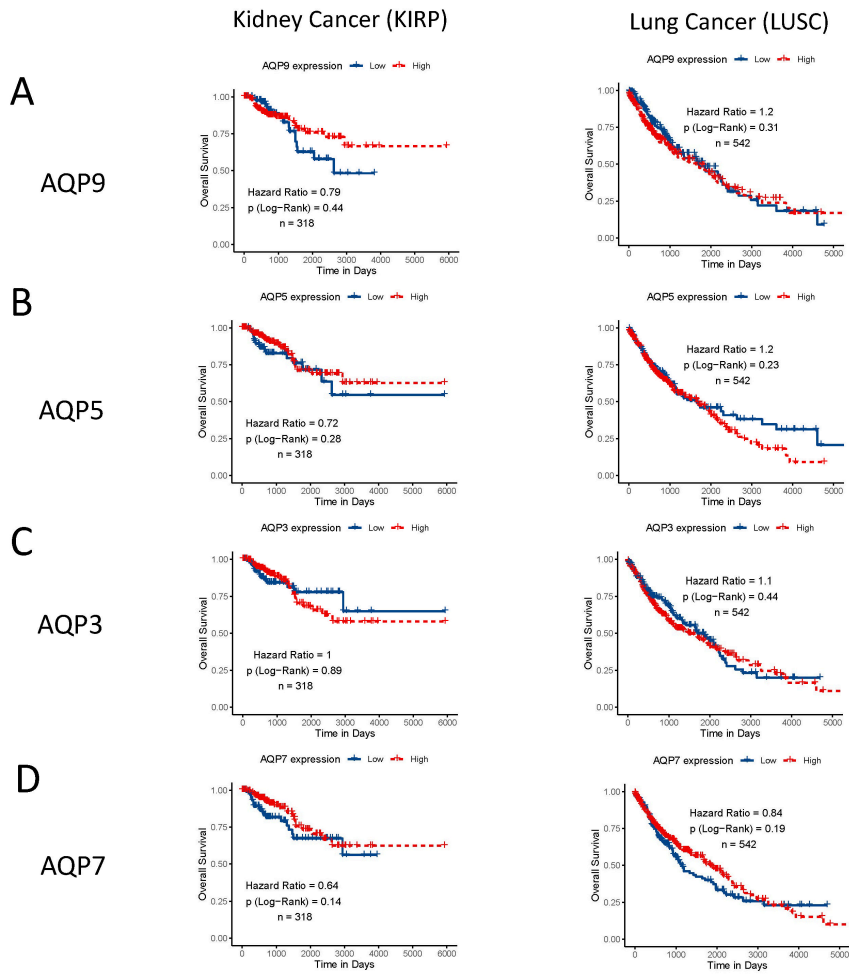
121. Kong B, Zhao S-P. Inhibitory effects of lentivirus mediated RNA interference targeting human AQP1 gene on the proliferation of human colon carcinoma SW480 cells and the expression of VEGF. *Int J Clin Exp Med*. 2016;9:8999-9006.
122. Li A, Lu D, Zhang Y, Li J, Fang Y, Li F, et al. Critical role of aquaporin-3 in epidermal growth factor-induced migration of colorectal carcinoma cells and its clinical significance. *Oncology Reports*. 2013;29(2):535-40.
123. Kang SK, Chae YK, Woo J, Kim MS, Park JC, Lee J, et al. Role of human aquaporin 5 in colorectal carcinogenesis. *The American journal of pathology*. 2008;173(2):518-25.
124. Chen C, Ma T, Zhang C, Zhang H, Bai L, Kong L, et al. Down-regulation of aquaporin 5-mediated epithelial-mesenchymal transition and anti-metastatic effect by natural product Cairicoside E in colorectal cancer. *Molecular Carcinogenesis*. 2017;56(12):2692-705.
125. Yoshida T, Hojo S, Sekine S, Sawada S, Okumura T, Nagata T, et al. Expression of aquaporin-1 is a poor prognostic factor for stage II and III colon cancer. *Molecular and clinical oncology*. 2013;1(6):953-8.
126. Mobasher A, Airley R, Hewitt SM, Marples D. Heterogeneous expression of the aquaporin 1 (AQP1) water channel in tumors of the prostate, breast, ovary, colon and lung: a study using high density multiple human tumor tissue microarrays. *International journal of oncology*. 2005;26(5):1149-58.
127. Kang BW, Kim JG, Chae YS, Lee SJ, Sohn SK, Moon JH, et al. AQP1 expression and survival in patients with colon cancer. *American Society of Clinical Oncology*; 2014.
128. Dorward HS, Du A, Bruhn MA, Wrin J, Pei JV, Evdokiou A, et al. Pharmacological blockade of aquaporin-1 water channel by AqB013 restricts migration and invasiveness of colon cancer cells and prevents endothelial tube formation in vitro. *Journal of Experimental & Clinical Cancer Research*. 2016;35(1):36.
129. Smith E, Palethorpe HM, Tomita Y, Pei JV, Townsend AR, Price TJ, et al. The purified extract from the medicinal plant *Bacopa monnieri*, bacopaside II, inhibits growth of colon cancer cells in vitro by inducing cell cycle arrest and apoptosis. *Cells*. 2018;7(7):81.
130. Shi X, Wu S, Yang Y, Tang L, Wang Y, Dong J, et al. AQP5 silencing suppresses p38 MAPK signaling and improves drug resistance in colon cancer cells. *Tumor Biology*. 2014;35(7):7035-45.
131. Camp RL, Dolled-Filhart M, Rimm DL. X-tile: a new bio-informatics tool for biomarker assessment and outcome-based cut-point optimization. *Clinical cancer research*. 2004;10(21):7252-9.
132. Huang D, Feng X, Liu Y, Deng Y, Chen H, Chen D, et al. AQP9-induced cell cycle arrest is associated with RAS activation and improves chemotherapy treatment efficacy in colorectal cancer. *Cell death & disease*. 2017;8(6):e2894-e.
133. Zhu Z, Jiao L, Li T, Wang H, Wei W, Qian H. Expression of AQP3 and AQP5 as a prognostic marker in triple-negative breast cancer. *Oncology letters*. 2018;16(2):2661-7.
134. Yool AJ, Ramesh S. Molecular targets for combined therapeutic strategies to limit glioblastoma cell migration and invasion. *Frontiers in pharmacology*. 2020;11:358.

## 7. Supplementary files

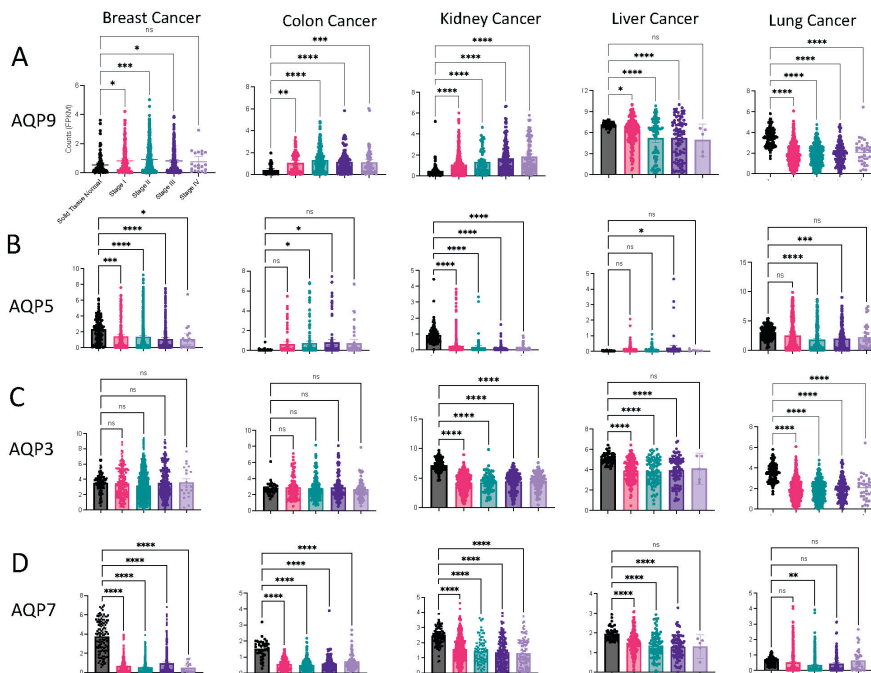


**Supplementary S1:** Univariable analysis of AQP9, -5, -3 and -7 in breast, colon, liver, Kidney (KRIP subtype) and Lung (LUAD subtype). Hazard ratios with their 95% confident intervals as well as P-values (log-rank) resulting from the comparisons between low (67%) and high (33%), are shown.

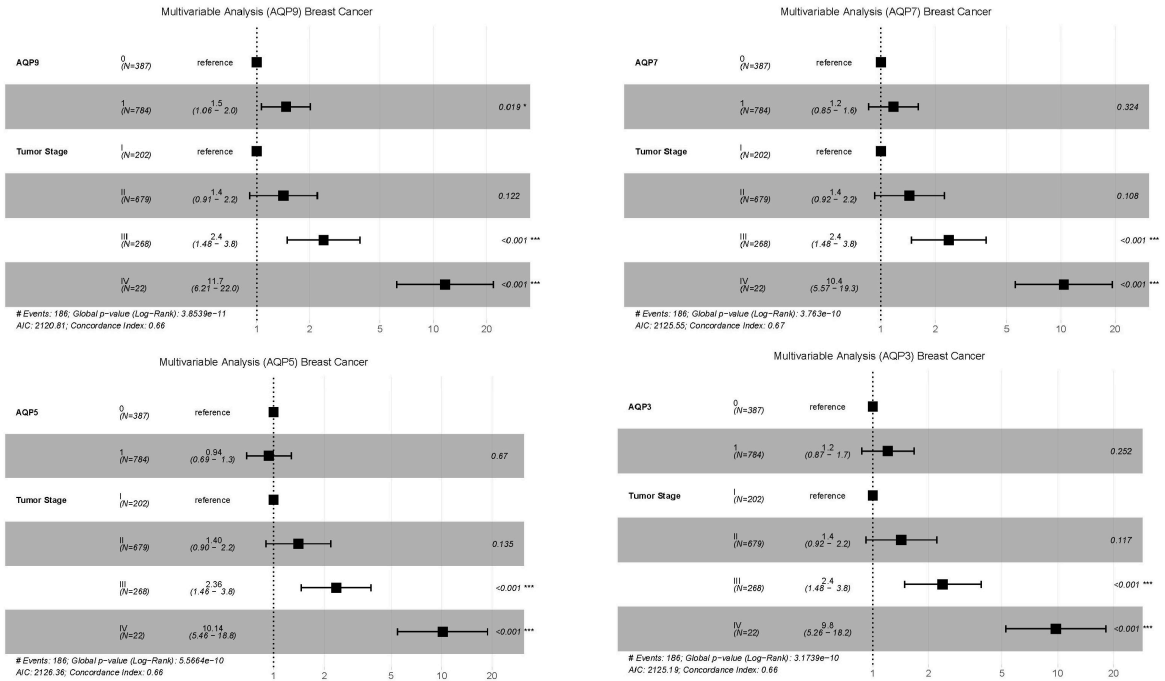




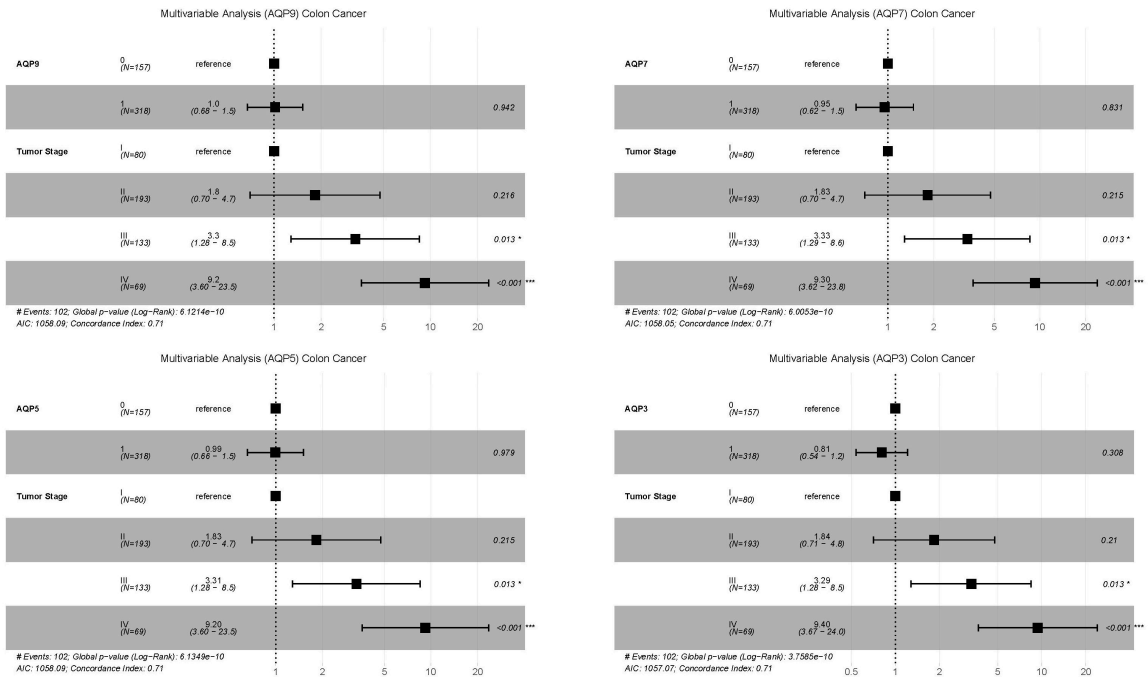
**Supplementary S2:** Univariable analysis of AQP9, -5, -3 and -7 in breast, colon, liver, Kidney (KRIP subtype) and Lung (LUAD subtype). Hazard ratios with their 95% confident intervals as well as P-values (log-rank) resulting from the comparisons between low (67%) and high (33%), are shown.



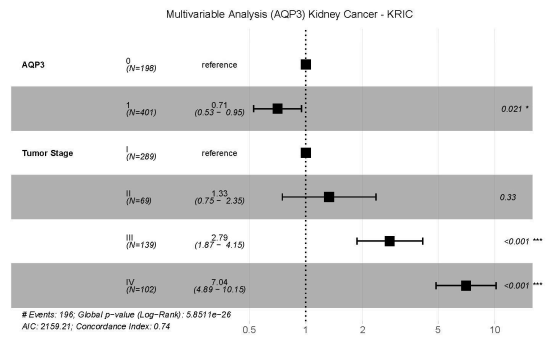
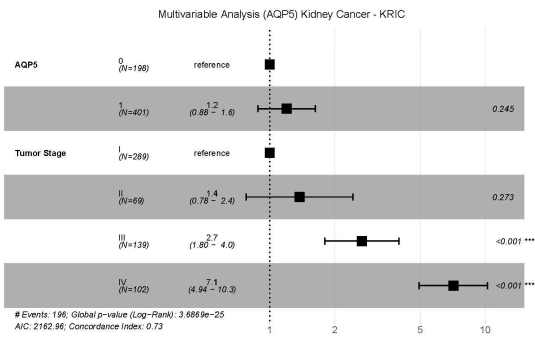
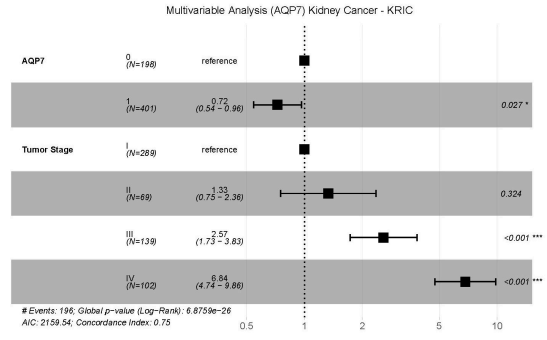
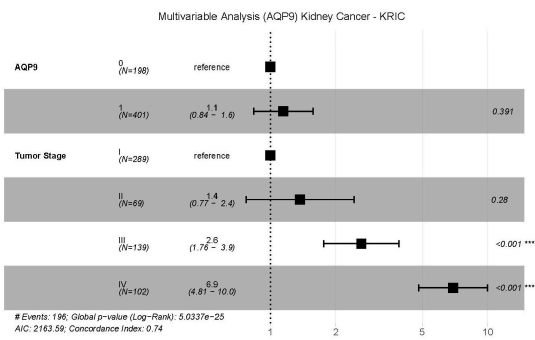
**Supplementary S3:** A two-sample t-test using continuous AQP mRNA expression values (with no cut-point required) to compare mRNA expression between normal tissues and stage I, stage II, stage III and stage IV patients. Statistical significance was shown as  $P < 0.05$  (\*),  $P < 0.01$  (\*\*),  $P < 0.001$  (\*\*\*),  $P < 0.0001$  (\*\*\*\*) and not significant (ns).



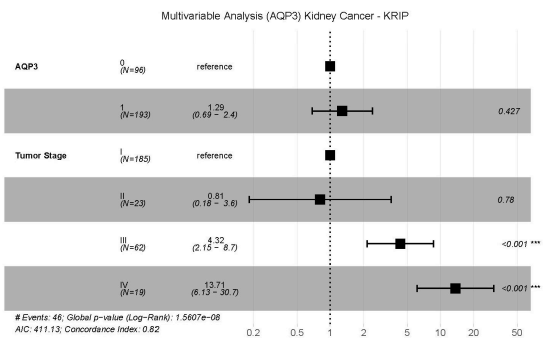
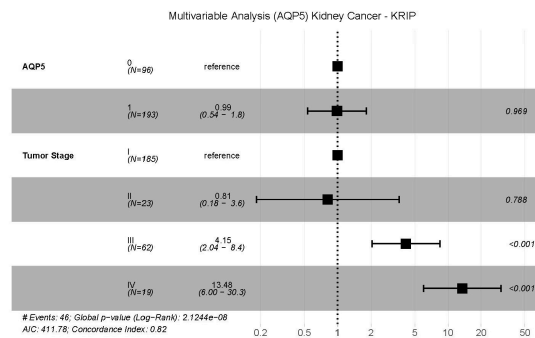
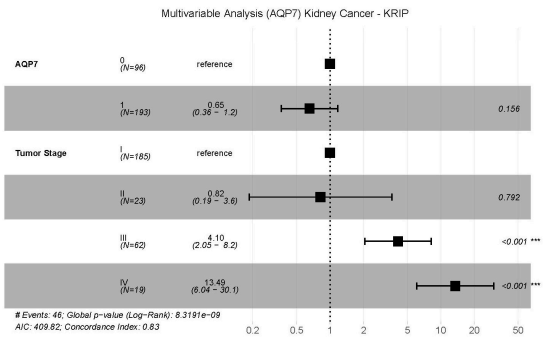
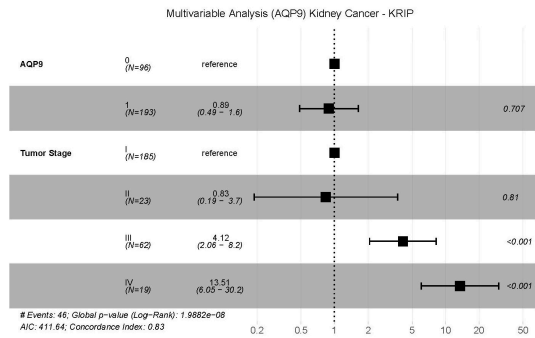
**Supplementary S4:** Multivariable analyses of AQP9, -7, -5 and -3 in breast cancer.



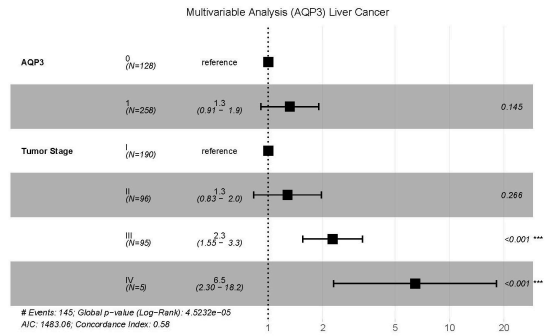
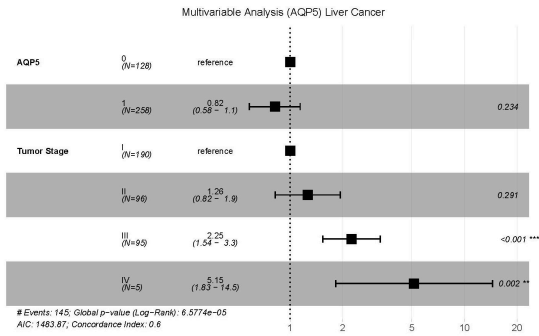
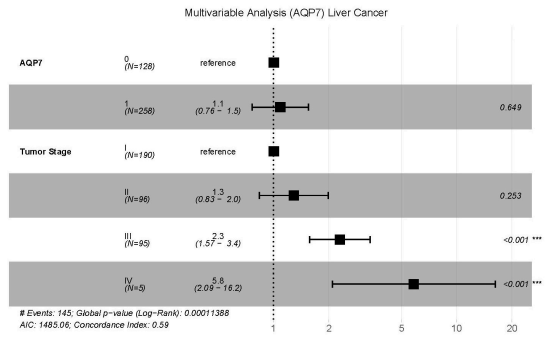
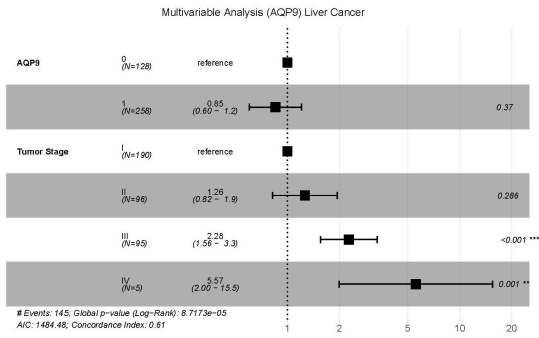
**Supplementary S5:** Multivariable analyses of AQP9, -7, -5 and -3 in colon cancer.



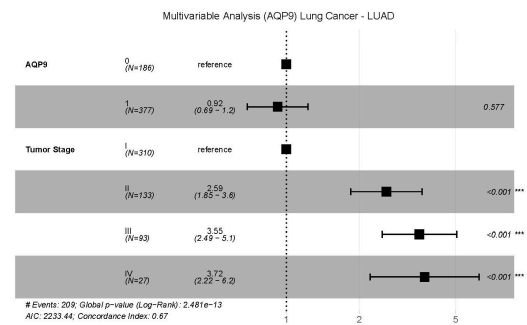
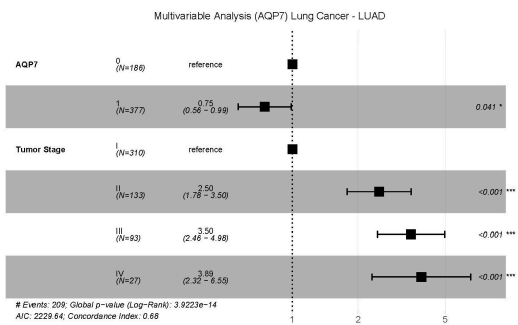
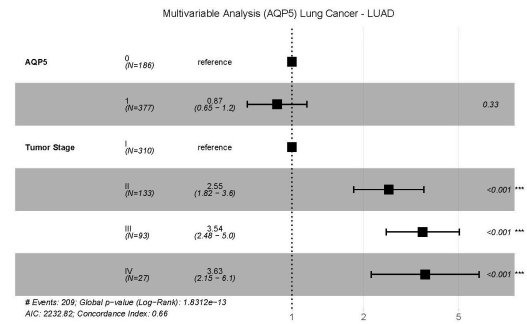
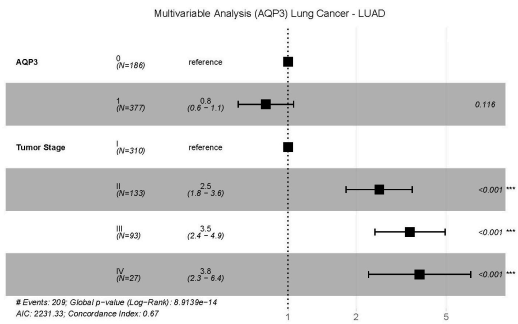
Supplementary S6: Multivariable analyses of AQP9, -7, -5 and -3 in kidney cancer (KRIC subtype).



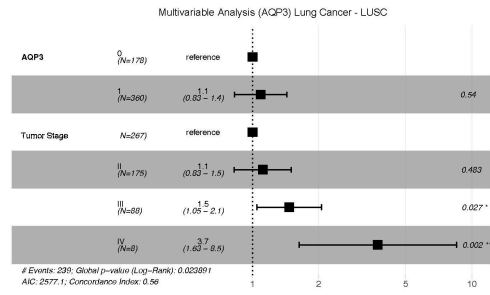
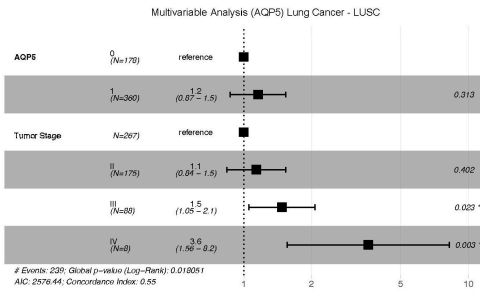
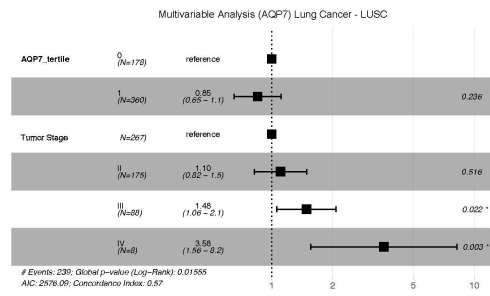
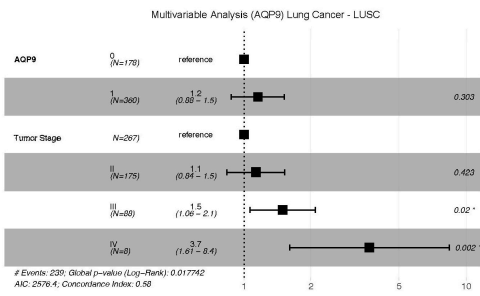
Supplementary S7: Multivariable analyses of AQP9, -7, -5 and -3 in kidney cancer (KRIP subtype).



Supplementary S8: Multivariable analyses of AQP9, -7, -5 and -3 in liver cancer.



Supplementary S9: Multivariable analyses of AQP9, -7, -5 and -3 in lung cancer (LUAD subtype).



Supplementary S10: Multivariable analyses of AQP9, -7, -5 and -3 in lung cancer (LUSC subtype).

# Chapter 6

## General discussion and future directions

### 6.1 Review of aims and hypotheses

Many approaches to cancer management with single anti-cancer agents are often ineffective due to adverse reactions, drug resistance or inadequate target specificity. In contrast, a combinatorial approach where the application of two or more anti-cancer agents at their respective effective dosages can achieve a synergistic effect that boosts the cytotoxicity of cancer cells. In cancer, aberrant apoptotic pathways allow the survival of cells that should be killed, leading to cancer progression. Mutations that arise during apoptosis can consequently result in chemoresistance during the treatment. Moreover, the development of cancer resulting from interactions with their microenvironment leads to angiogenesis and metastasis which make it challenging to deal mainly when the tumor cells have spread to several distant organs in the body. Despite advances in target-specific and personalized cancer therapies, we are yet to define and optimize pharmacological agents and approaches to better understand the unique mechanisms that the cancer cells utilize in conditions that favour their development. In this regard, naturally occurring mixtures of compounds that are believed to have multiple specific targets with minimal acceptable side-effects are now of interest to many researchers. However, understanding the molecular mechanisms underlying the combinatorial effect of complex drugs is a complicated task. The best possible natural compound combinations, including herbal mixtures and conventional drugs, are based on an understanding of the cancer-specific context of the target genes as well as their regulatory pathways. On the other hand, membrane protein channels, including AQPs and ion channels, have recently been of interest as therapeutic targets for treatment strategies in diverse classes of cancers. Although studying the role of these channels has been the main focus of channelopathy studies in cancer, the effect of tumor microenvironmental stimuli, such as pH or hypoxia and their regulatory actions upon the channels are poorly understood. Therefore, the aims of this dissertation were to address these gaps using two different distinct approaches.

## 6.2 The first phase of this thesis

In the first approach, we seek to reveal these complications by utilizing computational biology approaches to identify the potential mechanisms of Compound Kushen Injection (CKI), a traditional Chinese medicine, on the hallmarks of cancer (i.e., proliferation and invasion).

Compound Kushen Injection (CKI), a combination of alkaloid and flavonoid compounds extracted from two herbal medicines Kushen (*Radix Sophorae Flavescentis*) and Baituling (*Rhizoma Smilacis Glabrae*), has been shown to reduce toxicity as a combined chemotherapeutic drug. It modulates immunity, decreases inflammation, relieves cancer pain, and, most importantly, causes antineoplasticity. Twenty one chromatographic peaks which represent the compounds piscidic acid, macrozamin, 5 $\alpha$ ,9 $\alpha$ -hydroxymatine, oxysophoridine, 9 $\alpha$ -hydroxysophocarpine, sophornol, oxymatine, oxysophocarpine, sophoridine, matrine, sophocarpine, 9 $\alpha$ -hydroxymatine, lamprolobine, isomatrine, baptifoline, N-methylcytisine, and trifolirhizin were identified in CKI. Excluding macrozamin (which came from *Heterosmilacis japonicae rhizomae*), almost all identified compounds in CKI are derived from *Sophorae flavescentis radix* and trifolirhizin is the only flavonoid detected in the drug.

This was divided into two different projects (published and included as chapter 2 and 3).

In more detail, the first project was divided into three phases (chapter 2-3); 1- using a chemistry analytical approach, fractionated compounds were collected and grouped. A total of nine standard compounds 1) Adenine, 2) Macrozamin, 3) Sophoridine, 4) Oxymatine, 5) Matrine, 6) Sophocarpine, 7) Oxysophocarpine, 8) N-methylcytidine, and 9) Trifolirhizin, were standardized and fractionated from the original compound mixture. 2- *in vitro* cellular approach was used to investigate the effect of these fractionated mixtures on cancer cells phenotypes. Of all the fractionated and reconstituted standard compounds of CKI, the best possible combination that gave the highest cytotoxic activity were selected for further analysis by RNA-seq. In more detail, we tested CKI as a whole mixture as well as HPLC (high-performance liquid chromatography) fractionated components to systematically explore the interactions of the compounds within the drug mixture with respect to phenotypic changes after CKI treatment. We used MDA-MB-231 as an *in vitro* model and integrated HPLC, LC/MS (Mass Spectrometry), cell viability and apoptosis assays. 3- computational biology approach was conducted to unrevealed the underlying mode of action of these mixtures in breast cancer cells. As the result, we found depleting two specific

compounds (i.e., oxymatrine and oxysophocarpine) had the most potential effects of CKI. Removing N-OmtOspecparadoxically from the mixture displayed the most inhibitory effect on the cell cycle and caused apoptosis. In this phase, using LC-MS/MS we have successfully identified the nine major known compounds in both crud and fractionated mixtures, which in turn facilitated our analytical comparison of the fractionated mixtures when compared to the original mixture. Future experiments can benefit using this fractional deletion approach and the application of LC-MS/MS when studying natural medicine. RNA sequencing and transcriptomics analysis to reveal the underlying molecular mode of action of CKI. As a result, we have developed a novel research strategy for dissecting the molecular mode of action of components within CKI by associating phenotypic and global gene expression changes.

This was followed by linking our transcriptome data from various fractionated mixtures to map the alteration of gene expression associated with cancer hallmarks and phenotypic cell changes (second project). In that regard, the effect of different mixtures on six cancer cell lines cell migration and invasion were investigated. HPLC was used to separate minor compounds from majors and use them in different migration and invasion assays. We found the inhibitory effect of CKI, as a whole mixture more effective compared to either of major and minor mixtures, suggesting both fractions synergistically contribute to the activity of the original mixture. Moreover, we showed the underlying mechanism of the inhibition is associated with actin cytoskeleton formation and perturbation of lamellipodial extension through downregulation of gene products.

One advantage of using natural mixture is that, unlike a single drug treatment, several targets can be affected by multiple components. As a summary of the first phase of this dissertation, we unveiled the unpredictable interactions between components in CKI and support the concept that single compounds in natural mixture may not have obvious effects, but those combinations of such compounds can have significant effects on cancer cells with less side effect compare to common chemigraphy treatment.

Natural compounds have been shown to stimuli tumor microenvironment in several ways including inhibition of ECM degradation and angiogenesis and reversing immunosuppression. In our signaling pathway analyses from CKI treated cancer cells, significant perturbation of, protein channels (e.g., ion channels and aquaporins), cytokine-cytokine and ECM-receptor interaction, and chemokine signaling pathways were detected by CKI treatment suggesting its potential impact



on the tumor microenvironment. The *in vitro* experiments conducted here were initially intended to be used for drug development. However, the fundamental data provided may still have uncertainty on the fact that not always *in vitro* outcomes can be used for translational medicine. It is worthy to note that when using the herbal drug mixture, the impurities need to take into account which as a result as may provide false-positive results of the molecules during drug screening. Therefore, a suitable *in vivo* model is further required to examine CKI in follow-on experiments to ensure better outcomes in cancer treatment. The main contribution of phase one of this dissertation is that we introduced a novel way for compound-specific target gene identification that uses a systematic fractionation methodology.

Nevertheless, the exact protein targets affected by these compounds remained to be answered. As potential future work, characterisation of the specific proteins that compounds bind to, needs to be considered in order to address a clinically important of CKI.

One approach to answer this gap is the use of yeast as a model for high-throughput screening on target proteins. Budding yeast, *Saccharomyces cerevisiae*, has been used as a powerful model organism for genomic, *genetic*, and proteomic technologies as well as for studying cellular process and proteins of distant phyla, including humans. Moreover, potassium deficient yeast mutant strains have been used previously for identifying new cation transporters and channels; clones are selected by the observed rescue of yeast cell survival when introduced genes complement the mutations and provide a pathway for K<sup>+</sup> entry into the yeast cells. *S. cerevisiae* has two orthodox aquaporins and one aquaglyceroporin. AQY1 which is spore-specific water channel and AQY2 that only expressed in dividing cells and controlled by osmotic signalling pathways AQY2 is shown to be regulated by two regulatory pathways; protein kinase A reverse the repression of this channel expression whereas Kss1 mitogen-activated protein kinase pathway suppresses its expression. The advantage of a mass screening technique using yeast rescue is that it will enable simultaneous testing of a matrix of intracellular signalling stimuli on the candidate AQP channels, a combinatorial feat nearly impossible in the frog oocyte or other individual expression models. Yeast intracellular messenger systems have been shown to respond to agents, such as forskolin and 8B-cAMP to stimulate cAMP and protein kinase A, okadaic acid to block protein phosphatases, and H7 to block protein kinases, sodium nitroprusside to stimulate cGMP, phorbol esters to activate and block protein kinase C, and tyrosine kinase and G-protein activators and

inhibitors. Therefore, using this model, we aimed to investigate human AQPs for discovery of new ion channels and explore their potential as a target for cancer development and metastasis.

### **6.3 Role of AQPs in migration and invasion**

The Role of AQPs water permeability in migration and invasion has been suggested. Cell polarization is the first key feature in cancer cell migration and is established by the trafficking of lipids, small GTPases, and proteins, positioning of organelle, the activity of cytoskeletal dynamics, and maintenance of functional cytoplasmic and plasma membrane domains. The involvement of various aquaporins in the process of cell migration such as polarization and protrusion have been reported, and AQP1, 2, 3, 4, 8 and 9 have been recognized to play important role in this polarization process. For example, single particle imaging analysis showed that rapid polarization of the cell was facilitated by the movement of AQP1 in the plasma membrane and a functional polarization of astrocytes foot process in vivo was largely distributed by high expression of AQP4. Subsequently, decreased E-cadherin expression is an important characteristic of epithelia and mesenchymal transition (EMT) and correlation between AQP4 knockdown with the increased expression of E-cadherin as well as AQP1 overexpression with E-cadherin downregulation in lung adenocarcinoma cells has been reported. Besides, its association with EMT, AQP1 is over-expressed in multiple human cancer types, in which AQP1 expression at the leading edge of the migrating cells was shown to accelerate migration, for instance, in mouse melanoma B16F10 and breast cancer 4T1 cell lines in vitro. These observations suggested that AQPs play crucial roles in migration and invasion. Cell protrusion and the extension of cellular membranes caused by lamellipodia and filopodia protrusions is the second important feature of cell migration process. It was shown that high AQP9 expression induces filopodial protrusions in several cell types suggesting the involvement of AQP9 in the migration process. These experiments highlighted the importance of various AQPs in cell migration and invasion process.

#### **6.3.1 Prior work showing AQP genetic knockdown decreases migration and invasion**

Although, it is evident from various experiments that cell migration is highly dependent upon the expression of AQPs, the genetic analyses of changes in AQP expressions caused by environmental factors and drug treatments are still not complete. Therefore, genetic screenings of AQP expression

to identify the functionally cryptic AQPs, would enhance the search for therapeutics in treating various diseases. Functions of AQP channels can be explored in vitro using site directed mutagenesis. The deletion of AQP1 destabilizes the Lin-7/beta-catenin/F-actin complex resulting in the decreased migration and invasion of human endothelial and melanoma cell lines. Knockdown of AQP1 expression by genetic deletion or small-interfering-RNAs has been shown to substantially impair cell migration in vitro. It was also shown that migration of fibroblasts was impaired by knocking down AQP3 RNA expression. In addition, RNA interference of AQP4 expression massively reduced migration and invasion of glioblastoma cells in vitro and in vivo. Modification of amino acid sequence of AQPs will be a critical tool for uncovering the cryptic functions of AQPs and their integrated signalling networks. For example, AQP1 ionic current activation was impaired by mutation of aspartate (D237) and lysine (K243) in the carboxyl terminal domain, indicating the C-terminal domain influences the efficacy of cGMP-mediated activation. The blocking effect is improved by substituting amino acid AQP4 valine-189 to alanine in AQP1. Substitution of two amino acids in the water pore region of AQP1 creates new permeability to glycerol. Single amino acid substitution in AQP 11 causes renal failure. To explore more classes of AQP ionic permeabilities, a potassium-transport deficient yeast strain can be used to identify new cation transporters and AQP channels; by introducing AQP genes that complement the potassium deficient channels and therefore rescue the yeast survival in low potassium environment. Collectively, these results altogether pinpointed that impairment of AQPs function is highly responsible for the cell migration inhibition and that AQP channels merit exploration as therapeutics that target cancer cell migration and invasion.

### **6.3.2 The effect of Pharmacological blocking of AQPs on cell migration**

In addition to genetic interference, functions of AQPs can be studied using pharmacological interventions. Understanding the underlying molecular mechanisms under the treatment of AQP blockers is essential for developing the therapies relative to diseases caused by aquaporin dysfunction. Agents blocking water flux have been shown to slow cancer cell migration. Heavy-metal based compounds have been shown to effectively block AQP water permeability. For instance, silver compound based AQP blocker, AgNO<sub>3</sub>, strongly inhibits the AQP1 water channel in red blood cell. Mercury was shown to block AQP1 yet it was reported to have highly toxic profiles for treatment in clinics. In addition, synthetic and natural compounds derived AQP

blockers have been shown to inhibit the water and/or ion permeability of AQP channels. Invasive feature of astrocytomas has been associated with highly expressed AQP4 level involved in glial cells migration, and blockers including sumatriptan and thiazide have been claimed to inhibit AQP channel suggesting their efficacies as anti-migration agents. Unfortunately, confirmation of the effect of these compounds have been reported as failures in follow-on experiments. On the other hand, a derivative of bumetanide, AqB013, is an AQP blocker that was shown to inhibit AQP1 and AQP4 water channels leading to the migration reduction of HT29 and HCT-116 colon cancer cell lines. Other bumetanide derivatives such as AqB011 and AqB007 blocked AQP1 ionic conductance in oocyte expression system and strongly inhibited cancer cell migration in AQP1 expressing cell line HT29, suggesting that the cation channel activity can have a key physiological role in cancer cell migration. A conserved pair of arginine residues in loop D are required for inhibition of the AQP1 ion channel by AqB011, confirming that the compound interacts at the loop D gating region. Research also showed that blocking of EGF-induced AQP3 expression by curcumin was found to be associated with the reduction of human ovarian cancer cells migration, through the inhibition of AKT/ERK and PI3K pathways. These works suggested the pharmacological block of AQPs can impair cell migration and invasion.

### **6.3.3 AQP ion channel inhibitors reduce metastasis *in vivo***

Several AQP inhibitors that were shown to effectively block the migration and invasion of cancer cells have been applied to *in vivo* models of disease to develop new strategies for intervention. Although some agents consistently showed effective blockade both *in vitro* and *in vivo*, some failed to produce therapeutic efficacy. For example, AqB050 inhibits proliferation, motility, and metastasis of mesothelioma *in vitro* but showed no profound effect in an *in vivo* system. On the other hand, acetazolamide diminishes tumor metastasis in mice harbouring Lewis lung carcinoma. Moreover, suppressing of AQP1 water channel function by topiramate treatment leads to the significant reduction of lewis lung carcinoma metastasis in mice. Therefore, many types of AQP inhibitors such as aphen for AQP3, AqB011 for AQP1 ion channel and bacopaside II for AQP1 water channel, which have been shown to block migration and invasion of different cell types are needed to explore their effectiveness in an *in vivo* system. These compounds merits further investigation to investigate to what extent these suppress cancer invasion and metastasis.

### **6.3.4 Genetic knockdown of AQPs decreased metastasis**

Besides pharmacological intervention, impairment of cancer metastasis can be achieved by genetic interference of AQP function. It was demonstrated that AQP1 deletion decreases metastasis and tumor growth in mice. Knocking down AQP1 dramatically inhibited the angiogenesis in chick embryo chorioallantoic membrane, and deletion of AQP1 in mice showed reduced angiogenesis and tumor growth in B16F10 melanoma cells implanted transgenic mice. These results showed that blocking AQP1 dual ion and water function either by genetic deletion or by pharmacological blocker facilitates impairment of cancer metastasis and angiogenesis *in vivo*. Other classes of AQPs that might potentially possess both dual ion and water permeability virtue further investigation for the development of treatment interventions based on the findings from *in vitro* experiments.

### **6.3.5 Effect of pharmacological agents remain unknown**

The discovery of small molecule pharmacological AQP modulators have been developed for therapeutic interventions over the years. Despite of the advancement of many pharmacological agents with target specificity *in vitro* further works using *in vivo* models are required to translate into the therapeutic development. In addition, new AQP modulators that are being identified are required to define their differential contributions in various diseases related to fluid imbalance disorders.

## **6.4 Second phase of this thesis**

Therefore, the second approach of this dissertation was plan to study AQPs ion permeability in cancer. The second approach thus was divided into two phases (chapter 4-5); 1- to develop a mass-throughput heterologous model suitable for AQP ion channel discovery and pharmacological inhibitors screening, 2- to determine the physiological significance and regulation of this function in human related diseases.

To answer some longstanding mysteries surrounding cellular ion leaks in fluid transport and ion homeostasis disorders in humans such as cancer and to overcome some limitations of time-consuming, relatively costly to operate and labour-intensive electrophysiology methods, we first

successfully developed a novel high-throughput assay to enable simultaneous screening of all 13 AQPs from humans for discovering new AQP(s) that serve as dual water and ion channels. All 13 human AQPs were initially subcloned in potassium- and sodium-deficient yeast mutant strains for further analysis and discovery of new AQP ion channels. Aquaporin-deficient yeast strain was used for studying water permeability of the channels as well as high-throughput membrane localization of AQPs under osmotic pressure. As discussed in chapter 3, we ended up with a surprising outcome that all AQPs could potentially serve as ion channel in a wide range of pH values. To have more lines of evidence on this finding, we used hAQP1 as a known ion channel to optimize the assays for different approaches including drug discovery, signalling pathways analysis, mutagenesis for functional study and used a fluorescent-based probs designed and developed in our lab to monitor the kinetic of monovalent cation, lithium, in yeast expressing AQPs. We further, validated our assay, using other heterologous expression assay, *E.coli* potassium deficient strain.

Secondly, using a combination of electrophysiology and computational tools, we investigated mechanisms contributing toward signalling and ion channel gating, which could aid in the development of a definitive portfolio of AQP agonist and antagonist compounds as tools for clinical innovation and basic research. This was followed by using bioinformatics tools to analyse genomic datasets to determine the relationship between AQP expression, cancer severity and clinical outcomes in common cancers. As a result, we identified a positive association between different stages of tumor grades as one important predictor dependant on different AQP expressions. The goal of this effort was to extend our understanding of AQP in clinical importance and shed more light on the primary dogma that aquaporins (AQP) are *only* permeable to water and glycerol. The outcome of this phase highlighted the potential of AQP as independent prognostic factors for cancer progression.

## **6.5 Future directions**

To further investigate the role of CKI single compounds as a potential inhibitor for AQP ion and/or water permeability, and to characterise the pathophysiological significance of these novel functions and potential agonist or antagonist in vitro model under different microenvironmental stimuli including different pH is recemented is required.

Other classes of AQPs might be discovered as ion channels using the assay we developed here. This is the first systematic, objective, and comprehensive approach to begin to address a huge gap in research knowledge, the number of classes of aquaporins that can function as cation channels, opening new areas of research with translational impact in agriculture and health applications.

## **6.6 Implications for clinical management of cancer**

Uncovering the functional and regulatory role of aquaporin dual water and ion channels is important for understanding their value as therapeutic targets. Yet, knowledge on the direct role of specific AQPs in animal pathologies is still limited due to large number of different AQP isoforms and the lack of selective pharmacological modulators. Study of hAQP ion channels here is expected to increase the understanding of mechanistic changes and pathways associated with cancer progression. This proposal aimed to assist the development of new disease control and cancer therapy strategies. The outcome of this research could uncover the molecular mechanisms by which block of AQP ion channels impedes cancer migration and metastasis. A long-term goal of this research is to elucidate the regulatory pathways of AQP involved in imbalances of fluid homeostasis in mammals and other fields.

## **6.7 Concluding remarks**

In this thesis, the effect of a natural compound mixtures was investigated to determine their mechanism of action on breast, colon, and brain cancer cell lines. Results obtained introduced a novel approach on dissecting complex mixture and a systematic approach was used indicate that a unique combination of single compounds can be developed for specific cancer types. However, additional research is required for validation of this outcomes *in vivo*.

We also developed a high-throughput assay which led us to discover a new set of AQP ion channels. Our bioinformatics further revealed AQPs as a prognostic marker in common cancer types for future study. Further research is required to determine whether these AQPs and their

novel function enabling cancer in real time and whether impairing their function by means of pharmacological or genetic approach will inhibit cancer progression.

Future work is anticipated to utilize the effective drugs with minimal toxic side effects in terms of achieving optimal effectiveness to block the AQPs in human diseases and to study the mechanisms of action of AQPs inhibitors at a molecular level via different biophysical methods. In future, cancer therapeutic interventions such as surgical, chemo and radiotherapy, might be found to benefit from adjunct treatment with AQP blockers for slowing cancer metastasis.

I also extended our screening to other subtype of AQPs from malaria and drosophila (manuscripts under preparation) and found the results in agreement with our conclusion mentioned for all AQPs can potentially function as ion channel, but to different degree. However, that was beyond of the scope of this thesis and hence not included.



## 6.7 References

1. Drubin DG, Nelson WJ. Origins of cell polarity. *Cell*. 1996;84(3):335-44.
2. Rash JE, Yasumura T, Hudson CS, Agre P, Nielsen S. Direct immunogold labeling of aquaporin-4 in square arrays of astrocyte and ependymocyte plasma membranes in rat brain and spinal cord. *Proceedings of the National Academy of Sciences*. 1998;95(20):11981-6.
3. Papadopoulos M, Saadoun S, Verkman A. Aquaporins and cell migration. *Pflügers Archiv-European Journal of Physiology*. 2008;456(4):693-700.
4. Verkman A. More than just water channels: unexpected cellular roles of aquaporins. *Journal of cell science*. 2005;118(15):3225-32.
5. Loitto VM, Huang C, Sigal YJ, Jacobson K. Filopodia are induced by aquaporin-9 expression. *Experimental cell research*. 2007;313(7):1295-306.
6. Crane JM, Van Hoek AN, Skach WR, Verkman A. Aquaporin-4 dynamics in orthogonal arrays in live cells visualized by quantum dot single particle tracking. *Molecular biology of the cell*. 2008;19(8):3369-78.
7. Yun S, Sun P-L, Jin Y, Kim H, Park E, Park SY, et al. Aquaporin 1 is an independent marker of poor prognosis in lung adenocarcinoma. *Journal of pathology and translational medicine*. 2016;50(4):251.
8. Hu J, Verkman A, Hu J, Verkman A. Increased migration and metastatic potential of tumor cells expressing aquaporin water channels. *The FASEB Journal*. 2006;20(11):1892-4.
9. Kourghi M, De Ieso ML, Nourmohammadi S, Pei JV, Yool AJ. Identification of loop D domain amino acids in the human Aquaporin-1 channel involved in activation of the ionic conductance and inhibition by AqB011. *Frontiers in chemistry*. 2018;6:142.
10. Monzani E, Bazzotti R, Perego C, La Porta CA. AQP1 is not only a water channel: it contributes to cell migration through Lin7/beta-catenin. *PLoS One*. 2009;4(7):e6167.
11. Saadoun S, Papadopoulos MC, Hara-Chikuma M, Verkman A. Impairment of angiogenesis and cell migration by targeted aquaporin-1 gene disruption. *Nature*. 2005;434(7034):786.
12. Cao C, Sun Y, Healey S, Bi Z, Hu G, Wan S, et al. EGFR-mediated expression of aquaporin-3 is involved in human skin fibroblast migration. *Biochemical Journal*. 2006;400(2):225-34.
13. Boassa D, Yool AJ. Single amino acids in the carboxyl terminal domain of aquaporin-1 contribute to cGMP-dependent ion channel activation. *BMC physiology*. 2003;3(1):12.
14. Migliati E, Meurice N, DuBois P, Fang JS, Somasekharan S, Beckett E, et al. Inhibition of aquaporin-1 and aquaporin-4 water permeability by a derivative of the loop diuretic bumetanide acting at an internal pore-occluding binding site. *Molecular pharmacology*. 2009;76(1):105-12.

15. Lagree V, Froger A, Deschamps S, Hubert J-F, Delamarche C, Bonnec G, et al. Switch from an aquaporin to a glycerol channel by two amino acids substitution. *Journal of Biological Chemistry*. 1999;274(11):6817-9.
16. Tchekneva EE, Khuchua Z, Davis LS, Kadkina V, Dunn SR, Bachman S, et al. Single amino acid substitution in aquaporin 11 causes renal failure. *Journal of the American Society of Nephrology*. 2008;19(10):1955-64.
17. Klebe S, Griggs K, Cheng Y, Driml J, Henderson DW, Reid G. Blockade of aquaporin 1 inhibits proliferation, motility, and metastatic potential of mesothelioma in vitro but not in an in vivo model. *Disease markers*. 2015;2015.
18. Ma B, Xiang Y, Mu S-M, Li T, Yu H-M, Li X-J. Effects of acetazolamide and anordiol on osmotic water permeability in AQP1-cRNA injected *Xenopus* oocyte. *Acta Pharmacol Sin*. 2004;25(1):90-7.
19. Ma B, Xiang Y, Li T, Yu H-M, Li X-J. Inhibitory effect of topiramate on Lewis lung carcinoma metastasis and its relation with AQP1 water channel. *Acta Pharmacol Sin*. 2004;25(1):54-60.
20. De Ieso ML, Yool AJ. Mechanisms of Aquaporin-Facilitated Cancer Invasion and Metastasis. *Frontiers in Chemistry*. 2018;6.

# **Appendix A**

**Co-author Publications as PDFs Arising from This Thesis**



# Objective assessment of tumor infiltrating lymphocytes as a prognostic marker in melanoma using machine learning algorithms

Thazin Nwe Aung,<sup>a</sup> Saba Shafi,<sup>a</sup> James S. Wilmott,<sup>b,j,l</sup> Saeed Nourmohammadi,<sup>c</sup> Ioannis Vathiotis,<sup>a</sup> Niki Gavrielatou,<sup>a</sup> Aileen Fernandez,<sup>a</sup> Vesal Yaghoobi,<sup>a</sup> Tobias Sinnberg,<sup>f,m</sup> Teresa Amaral,<sup>f,m</sup> Kristian Ikenberg,<sup>n</sup> Kiarash Khosrotehrani,<sup>g,o</sup> Iman Osman,<sup>h</sup> Balazs Acs,<sup>a,d,e</sup> Yalai Bai,<sup>a</sup> Sandra Martinez-Morilla,<sup>a</sup> Myrto Moutafi,<sup>a</sup> John F. Thompson,<sup>b,j</sup> Richard A. Scolyer,<sup>b,j,k,l</sup> and David L. Rimm<sup>a,i,\*</sup>

<sup>a</sup>Department of Pathology, Yale School of Medicine, New Haven, CT, USA

<sup>b</sup>Melanoma Institute Australia, The University of Sydney, Sydney, NSW, Australia

<sup>c</sup>Adelaide Medical School, The University of Adelaide, Adelaide, SA, Australia

<sup>d</sup>Department of Oncology and Pathology, Karolinska Institutet, Stockholm, Sweden

<sup>e</sup>Department of Clinical Pathology and Cytology, Karolinska University Laboratory, Stockholm, Sweden

<sup>f</sup>University Tübingen, Tübingen, Germany

<sup>g</sup>University of Queensland, UQ Diamantina Institute, Brisbane, QLD, Australia

<sup>h</sup>Department of Medicine, Grossman School of Medicine, New York University, USA

<sup>i</sup>Department of Internal Medicine (Medical Oncology), Yale University School of Medicine, New Haven, CT, USA

<sup>j</sup>Faculty of Medicine and Health, The University of Sydney, Sydney, NSW, Australia

<sup>k</sup>Tissue Pathology and Diagnostic Oncology, Royal Prince Alfred Hospital and NSW Health Pathology, Sydney, NSW, Australia

<sup>l</sup>Charles Perkins Centre, The University of Sydney, Sydney, NSW, Australia

<sup>m</sup>Cluster of Excellence iFIT (EXC 2180) "Image-Guided and Functionally Instructed Tumor Therapies", 72076 Tübingen, Germany

<sup>n</sup>Institute of Pathology and Molecular Pathology, University Hospital Zurich, Zurich, Switzerland

<sup>o</sup>Department of Dermatology, Princess Alexandra Hospital, Brisbane, QLD, Australia

## Summary

**Background** The prognostic value of tumor-infiltrating lymphocytes (TILs) assessed by machine learning algorithms in melanoma patients has been previously demonstrated but has not been widely adopted in the clinic. We evaluated the prognostic value of objective automated electronic TILs (eTILs) quantification to define a subset of melanoma patients with a low risk of relapse after surgical treatment.

**Methods** We analyzed data for 785 patients from 5 independent cohorts from multiple institutions to validate our previous finding that automated TIL score is prognostic in clinically-localized primary melanoma patients. Using serial tissue sections of the Yale TMA-76 melanoma cohort, both immunofluorescence and Hematoxylin-and-Eosin (H&E) staining were performed to understand the molecular characteristics of each TIL phenotype and their associations with survival outcomes.

**Findings** Five previously-described TIL variables were each significantly associated with overall survival ( $p < 0.0001$ ). Assessing the receiver operating characteristic (ROC) curves by comparing the clinical impact of two models suggests that eTILs (electronic total TILs) (AUC: 0.793, specificity: 0.627, sensitivity: 0.938) outperformed eTILs (AUC: 0.77, specificity: 0.51, sensitivity: 0.938). We also found that the specific molecular subtype of cells representing TILs includes predominantly cells that are CD3+ and CD8+ or CD4+ T cells.

**Interpretation** eTIL% and eTILs scores are robust prognostic markers in patients with primary melanoma and may identify a subgroup of stage II patients at high risk of recurrence who may benefit from adjuvant therapy. We also show the molecular correlates behind these scores. Our data support the need for prospective testing of this algorithm in a clinical trial.

**Funding** This work was also supported by a sponsored research agreements from Navigate Biopharma and Next-Cure and by grants from the NIH including the Yale SPORE in Skin Cancer, P50 CA121974, the Yale SPORE in

\*Corresponding author at: Professor of Pathology, Director, Yale Pathology Tissue Services, Department of Pathology, BML 116, Yale University School of Medicine, 310 Cedar Street P.O. Box 208023, New Haven, CT 06520-8023, USA.

E-mail address: david.rimm@yale.edu (D.L. Rimm).

Lung Cancer, P50 CA196530, NYU SPORE in Skin Cancer P50CA225450 and the Yale Cancer Center Support Grant, P30CA016359.

**Copyright** © 2022 The Author(s). Published by Elsevier B.V. This is an open access article under the CC BY license (<http://creativecommons.org/licenses/by/4.0/>)

**Key words:** Tumor-infiltrating lymphocytes (TILs); Digital image analysis; Machine learning cell segmentation algorithm; Early-stage melanoma; Prognostic marker

### Research in context

#### *Evidence before this study*

TIL scores visually assessed by the pathologists have not been broadly clinically implemented due to the lack of reproducibility caused by subjective assessment between pathologists and institutions. Automated TIL% (eTILs%) score, defined by the machine learning algorithm NN192, developed using open-source software, QuPath, has been shown to be prognostic in melanoma<sup>1</sup> but its clinical utility has not yet been broadly proven.

#### *Added value of this study*

This study pools patients with melanoma from a series of international cohorts and supports the previous finding that automated TIL score (eTIL%) is an independent prognostic marker in primary melanoma patients.

#### *Implications of all the available evidence*

we additionally show that the prognostic performance of eTIL% is stage specific. The use of NN192 machine learning algorithm could be a valuable and easy-to-implement tool for prospective testing of patients with early-stage melanoma and could be validated as a selector for patients that can safely omit immunotherapy in the adjuvant setting.

## Introduction

Melanoma is considered a highly immunogenic tumor and is responsive to immunotherapy.<sup>2</sup> Checkpoint inhibitor immunotherapies targeting programmed cell death protein 1 (PD-1) or cytotoxic T-lymphocyte-associated protein 4 (CTLA-4) have been shown to significantly improve the overall survival of patients with advanced stage metastatic disease.<sup>3,4</sup> Furthermore, adjuvant treatment with immune checkpoint blockade (or BRAF pathway targeted therapy in BRAF mutant melanoma patients) improved relapse-free survival (RFS) compared to placebo in phase 3 clinical trials<sup>5,6</sup> and is now regarded as standard of care in high-risk stage III melanoma patients. Furthermore, it was recently

reported that adjuvant anti-PD1 immunotherapy improved relapse-free survival in high-risk stage II melanoma patients. However, up to 30% of stage III patients treated with adjuvant immunotherapy developed disease recurrence. Furthermore, treatment-related adverse events occur in at least one in five patients, and treatment related fatalities have been reported in up to one in one hundred patients.<sup>5,7</sup> There is therefore an urgent need to identify patients at high risk of disease relapse who may benefit from adjuvant therapies and those patients at low risk of relapse who can be safely spared further treatment and the concomitant risks of treatment related adverse events.

Tumor-infiltrating lymphocytes (TILs) reflect the host's immune response against cancer cells.<sup>2,8</sup> Correlation between different TILs infiltrates and improved survival in melanoma patients has been reported in multiple studies.<sup>9-12</sup> Traditionally, TIL scores have been visually assessed by the pathologists, but due to the lack of reproducibility caused by subjective assessment between pathologists and institutions, TIL scoring techniques have not been broadly clinically implemented.<sup>13</sup> To increase objectivity, a machine learning algorithm developed using open source software, QuPath, has been shown to facilitate the investigation of complex spatial patterns by firstly classifying four cell types, including tumor cells, TILs, stromal cells, and "other" cells, for the assessment of the proportion TILs within different cell populations.<sup>1,14</sup> Acs et al. highlighted the robustness of the NN192 machine learning algorithm by comparing the performance between eTIL scores and pathologist TIL scores.<sup>1</sup> The latter study also showed that TILs score assessed by the NN192 algorithm was an independent prognostic marker in melanoma.

Here, we used the same cell classifier to validate the association of percent electronic TILs (eTIL%) with disease-specific survival in patients with melanoma in a broad set of cohorts from melanoma centers around the world. For this effort, we used the previously established cut-point of eTIL%<sup>1</sup> to test The Cancer Genome Atlas (TCGA) melanoma cohort and four other melanoma cohorts from Yale School of Medicine, Melanoma Institute Australia, Tübingen University, and New York University. Furthermore, we also tested both cell types and area, variables that pathologists cannot easily calculate, for their prognostic significance. The goal of this effort is not to help pathologists more accurately assess TIL,

but to validate this prognostic assay for potential pathologist-independent use in future prospective trials to determine which melanoma patients might be spared immunotherapy in the adjuvant setting. We aimed to specify the most reliable operator-independent identification of eTIL%, which can be prospectively validated in future studies. Finally, we assessed the prognostic role of the immunophenotypic subtypes of TILs, as defined by CD45+, CD3+, CD4+, CD8+, CD56+, CD20+, and FOXP3+ cells, using the Yale cohort to better understand the TIL subsets/phenotypes and their associations with patients' survival. Our ultimate goal was to determine the best approach for utilizing TIL infiltrates to predict disease outcome in melanoma patients that can be validated prospectively with the goal of proving clinical utility to select the high-risk subset of melanoma patients that are likely to not require immunotherapy in the adjuvant setting.

## Methods

### Study population

We assessed retrospectively collected samples from 5 independent cohorts from: (1) the Department of Pathology, Yale University, (2) the Melanoma Institute Australia (MIA), (3) Tubingen University, (4) TCGA and (5) Langone Medical Center, New York University (NYU). Two cohorts were in tissue micro-array (TMA) format and 3 in Whole Tissue Sections (WTS) format. The Yale University cohort comprised tissues from 187 stage I and II patients diagnosed between 1998 and 2011 with a median follow-up of 64 months. The Tubingen University TMA cohort consisted of 231 stage I and II and 20 stage III and IV melanoma patients diagnosed between 1992 and 2000 with 97 months median follow-up. The MIA WTS cohort consisted of 55 stage I and II patients and 41 stage III and IV patients diagnosed between 1998 and 2019 with 70.3 months median follow-up. The NYU WTS cohort consists of 88 high-staged patients diagnosed between 2009 and 2019 with 2.3 months median follow-up. The publicly available WTS-TCGA melanoma cohort comprised 139 stage I and II patients diagnosed between 1994 and 2013 with 38.6 months median follow-up (<https://portal.gdc.cancer.gov/repository>). Patients in the TCGA cohort were classified according to the 4<sup>th</sup>, 5<sup>th</sup>, 6<sup>th</sup>, and 7<sup>th</sup> Editions of the American Joint Committee on Cancer (AJCC) tumor, node, metastasis (TNM) staging system. All other cohorts were classified according to the 8<sup>th</sup> edition of the AJCC tumor,<sup>15,16</sup> node, metastasis (TNM) staging system (Table 1).

### Ethics

All tissue samples from Yale cohorts were collected with approval from the Yale Human Investigation Committee protocol #9505008219. Written informed consent,

or waiver of consent in some cases, was obtained from Yale cohort patients with the approval of the Yale Human Investigation Committee. Tissue samples from MIA cohort were collected with approval from the Sydney Local Health District (RPAH Zone) protocols #X17-0312 & 2019/ETH07604 and #X15-0311 & 2019/ETH06854. Tissue samples from Tuebingen cohort were collected with approval protocol #883/2019BO2. Tissue samples from NYU cohort were collected from the NYU Interdisciplinary Melanoma Cooperative Group: A Clinicopathological Database protocol # C10362. To ensure scientific integrity, the investigator was blinded to the clinical information during image processing.

### Digital image analysis using NN192 algorithm

H & E images for the Yale cohort TMA, and the WTS H & E slides from the Sydney and NYU cohorts were digitised using the Aperio ScanScope XT platform (Leica Biosystems, Wetzlar, Germany) slide scanner at 20x with a pixel size of 0.4986  $\mu\text{m}$  x 0.4986  $\mu\text{m}$ . The WTS digital TCGA images were downloaded from the NIH CDC porta specimen repository (<https://portal.gdc.cancer.gov/repository>). The H & E-stained TMA slide of the Tubingen cohort was digitised using Hamamatsu Nanozoomer HT slide scanner at 20x with a pixel size of 0.4986  $\mu\text{m}$  x 0.4986  $\mu\text{m}$ . QuPath open-source software (version 0.1.2)<sup>7</sup> based NN192 melanoma machine learning algorithm with neural network method<sup>1</sup> was applied for cell classification in this study. For WTS, the tumor and a 1–2-millimeter (mm) diameter surrounding tumor microenvironment to be analysed were carefully selected for accurate prediction of TILs. The area selection was reviewed by a pathologist. Due to the varying intensity both between and within cohorts, the “estimate stain vectors”, ESV, function in QuPath was used to refine the H&E stain for each digitised slide. The workflow for stain normalisation using ESV function was shown in Supplementary Figure 2. The number of cells identified as tumor and immune cells (in %) across multiple centers were shown in Supplementary Figure 3. Cell segmentation and classification were performed using the parameters previously described.<sup>1</sup>

### Assessment of eTILs using five variables

The machine-defined TILs variables were constructed using five different methods, as previously described.<sup>17</sup> The first and established method was to calculate eTIL% representing the proportion of TILs over tumor cells, calculated as (TILs/TILs + tumor cells) x 100.<sup>1</sup> Four additional methods were used to measure TILs as follows:

- 1) Measurement of the proportion of TILs over total cells: eTIL % = (TILs/total cells) x 100

Characteristic	Sydney Cohort (n=97) N (%)	Tubingen Cohort (n=253) N (%)	Yale Cohort (n=202) N (%)	NYU Cohort (n=88) N (%)	TCGA Cohort (n=139) N (%)
Age	NA	NA			
Median (Range)			63 (6-98)	69.7 (24.5-89.5)	63 (15-90)
Gender	NA	NA			
Male			116 (60.7)	54 (61.4)	53 (38.1)
Female			76 (39.3)	34 (38.6)	86 (61.9)
Morphology			NA	NA	NA
Superficial spreading	21 (21.6)	200 (79.1)			
Lentigo maligna	3 (3.2)	20 (7.9)			
Nodular	40 (41.2)	17 (6.7)			
Other	33 (34.0)	14 (5.5)			
Breslow depth					
Median (Range)	3.30 (1.05-50.00)	0.70 (0.13-20.00)	1.40 (0.50-16.00)		
Ulceration					
Yes	42 (43.3)	23 (9.1)	37 (19.4)		
No	46 (47.4)	228 (90.1)	154 (80.6)		
Stage (8 <sup>th</sup> Edition)					Stage (4 <sup>th</sup> , 5 <sup>th</sup> , 6 <sup>th</sup> , 7 <sup>th</sup> Edition)
I	0 (0)	202 (79.8)	124 (66.3)	0 (0)	41 (29.5)
II	56 (57.7)	25 (9.9)	63 (33.7)	0 (0)	98 (70.5)
III	41 (42.3)	17 (6.7)	0 (0)	27 (30.7)	0 (0)
IV	0 (0)	7 (2.8)	0 (0)	61 (69.3)	0 (0)
Clark's level		NA		NA	NA
I	0 (0)		1 (0.6)		
II	0 (0)		2 (1.1)		
III	11 (11.3)		30 (16.6)		
IV	62 (63.9)		144 (79.6)		
V	22 (22.7)		4 (2.2)		
BRAF status		NA	NA		NA
Wild type	0 (0)			61 (69.3)	
Mutant	0 (0)			22 (25)	
Not Assessed	72 (74.2)			5 (5.7)	
BRAF positive	8 (8.2)			0 (0)	
NRAS positive	3 (3.1)			0 (0)	
Both Negative	14 (14.4)			0 (0)	
Treatment	NA	NA	NA		NA
Ipilimumab (Ipi)				8 (9.1)	
Nivolumab (Nivo)				6 (6.8)	
Ipi+Nivo				16 (18.2)	
Ipi/(Ipi/Nivo)				20 (22.7)	
Pembrolizumab				30 (34.1)	
Other treatment				8 (9.1)	
Dead of disease					NA
Yes	38 (39.2)	28 (11.1)	54 (26.3)	28 (31.8)	
No	59 (60.8)	225 (88.9)	148 (73.7)	60 (68.2)	
Dead of any cause			NA	NA	
Yes	46 (47.4)	49 (19.4)			26 (18.7)
No	51 (52.6)	204 (80.6)			113 (81.3)

Table 1: Clinicopathological features of five cohorts from multiple institutions.

- 2) Measurement of the proportion of TILs over stromal cells:  $\text{esTIL \%} = (\text{TILs}/\text{total cells} - \text{tumor cells}) \times 100$
- 3) Measurement of the density of TILs over tumor region:  $\text{eaTILs (mm}^2\text{)} = \text{TILs}/\text{sum of tumor region areas analysed (mm}^2\text{)}$
- 4) Measurement of the density of TILs over stromal area:  $\text{easTIL \%} = [\text{sum of TIL area (mm}^2\text{)} / \text{stroma area (sum of tumor region areas analysed (mm}^2\text{)} - \text{sum of tumor cell area (mm}^2\text{)}] \times 100$

The last method mimics the manual pathologist scoring of stromal TILs according to the International Immuno-Oncology Biomarker Working Group on Breast Cancer.<sup>18</sup> The variables are shown schematically in Figure 3a.

#### Immunofluorescence staining for immunophenotypic subtyping of TILs

Eleven commercially available antibodies including CD34 (1:4500; clone: QBE10, Dako), CD56 (1:200; clone: 123C3, Cell Signaling Technology), CD66b (1:500; clone: 80H3, LifeSpan Biosciences), FOXP3 (1:100; clone: D2W8E, CST), CD8 (1:250; clone: 144B, Dako), CD14 (1:500; clone: D7A2T, Cell Signaling Technology), CD3 (1:100; clone: SP7, Novus Biologicals), CD45 (1:200; clone: 2B11 + PD7/26, Dako), CD68 (1:200; clone: C8/144B, Dako), CD20 (1:150; clone: L26, Dako) and CD4 (1:100; clone: SP35, SpringBio) were tested in four multiplex panels including: (1) CD14/CD66b/CD68/S100/DAPI, (2) CD14/CD45, CD34/S100/DAPI, (3) CD3/CD56/CD20/S100/DAPI and (4) CD4/CD8/FOXP3/S100/DAPI. Multiplexed immunofluorescent (IF) staining on four serial sections of Yale TMA 76 (YTMA-76) was performed as described previously for simultaneous detection of multiple markers.<sup>19</sup> Briefly, formalin-fixed paraffin-embedded (FFPE) TMA sections were deparaffinised and incubated using xylene and ethanol. The pretreatment heating device PT Module (Lab Vision, Thermo Fisher Scientific) was used for antigen retrieval in EDTA buffer pH 8 at 97°C for 20 minutes. To block endogenous peroxidase activity, 2.5% hydroxyl peroxide in methanol was used, and incubated the TMA slides for 30 minutes at room temperature. Non-specific antigens were then blocked with 0.3% Bovine Serum Albumin in 0.1 mol/L of Tris-buffered saline with 0.05% Tween 20 for 30 minutes. TMA sections were then incubated with the primary antibodies of interest. Primary monoclonal antibodies for cell profiling were co-incubated or sequentially incubated one after the other at room temperature for 1 hour, followed by the incubation of three horseradish peroxidase (HRP)-conjugated secondary antibodies at room temperature for 1 hour before tyramide-based labeling for 10 min. To quench HRP activity, the sections were

incubated with 1 mM benzoic hydrazide solution with 0.15% hydrogen peroxide for 10 minutes. The secondary antibodies used in this study were anti-rabbit EnVision (Dako), anti-mouse EnVision (Dako), anti-mouse IgG3 (1:700; Abcam), and anti-mouse IgG2a (1:200; Abcam). The substrates were biotin tyramide (1:50; PerkinElmer), TSA Plus Cy3 tyramide (1:100; PerkinElmer), and Cy5 tyramide (1:50; PerkinElmer), respectively. Sections were then treated with streptavidin–Alexa Fluor 750 conjugate (1:100; Invitrogen) for 1 hour. Finally, to identify melanoma cells, sections were incubated with mouse anti-S100 (1:100; 15E2E2; BioGenex) and goat anti-mouse Alexa 488 (1:100; Invitrogen) for 1 hour. The slides were then counterstained with 4',6-diamidino-2-phenylindole (DAPI) and mounted with ProLong Gold Mounting Medium (Invitrogen) to visualise nuclei.

#### Multispectral image acquisition and cell counting on serial sections YTMA-76

Image acquisition of the stained slides was performed using Vectra/Polaris (Akoya Biosciences, Marlborough, MA) microscope to obtain MSIs (multispectral images). Briefly, a low magnification scan of the whole TMA slide was performed at 4×. The regions of interest (ROI) scan were then selected from a low-resolution using the Phenochart viewer (Akoya Biosciences), and the ROIs were subsequently acquired at the higher resolution MSIs at 20×. To analyse the MSIs, the spectra were extracted from acquired images to build the spectral library consisting of all fluorophores using inForm image analysis software version 2.4.9 (Akoya Biosciences), and the absence of spectral overlap between channels was checked by evaluating the unmixed images. The acquired multispectral images were then decomposed using a spectral library. Tumor, stroma, and background were identified using the trainable tissue segmentation option in InForm. Cell segmentation within tumor and stroma regions was performed using the parameters including minimum nuclear size and splitting sensitivity and the signals of the nuclei, cytoplasm, and membrane components as individual cells. Once the machine learning cell segmentation algorithm was optimised, cells were then phenotyped. CD34+, CD68+, CD56+, CD66b+, FOXP3+, CD8+, CD14+, CD3+, CD45+, CD20+ and CD4+ cells from MSIs were counted. Finally, the phenotype counts, density, and mean expression data were analysed using phenoptrReports (Akoya Biosciences) in R to generate the data for cell densities/area (mm<sup>2</sup>).

#### Hematoxylin & Eosin (H & E) staining for serial sections of YTMA-76

To count total TILs in the same TMA sections where molecular subtypes of cells were determined, coverslips



were removed, and H & E staining was performed. The fluorescently stained YTMA-76 serial sections were incubated overnight with gentle shaking in 10X TBST to remove the coverslips. The YTMA-76 sections were stained with Hematoxylin (Dako) for 5 minutes, followed by Eosin Y for 60 seconds. The brightfield H & E images were digitised at 20X using the ScanScope AT2 platform (Leica Biosystems, Wetzlar, Germany).

### Statistical analysis

Statistical analyses were performed using GraphPad Prism 9.1.0 (GraphPad Software Inc., CA, USA) and R studio 1.4.1106 (Inc., Boston, MA). The cut-points for cell types and area variables were determined using X-tile cut-point finder.<sup>20</sup> Kaplan–Meier plots for disease-specific survival (DSS) and overall survival (OS) were computed and comparisons were made by the log-rank test using survival and survminer packages in R studio. *Post hoc* Benjamini-Hochberg (BH) multiple comparisons test was performed when the results for each variable in survival analyses were significant. ROC curves were constructed from logistic regression models for the prediction of DSS. All statistical tests were two-sided, and significance was represented as (\*)  $p < 0.05$ , (\*\*)  $p < 0.01$ , (\*\*\*)  $p < 0.001$ , (\*\*\*\*)  $p < 0.0001$ , or not significant (ns). To perform univariable analyses of each factor, a Cox proportional hazards model was fitted to predict survival from each factor in turn. For the multivariable analysis, a Cox proportional hazards model was learned using eTIL%, age, gender and stage as predictors. These variables were chosen, since they were all present in a common group of 3 cohorts. For each test, we quote the hazards ratio associated with each level of a factor compared to the base reference level, and the associated p-values.

### Role of funding source

None of the funders were directly involved in the study design, data collection, analyses, interpretation, or writing of the manuscript. The corresponding author (David L Rimm) has full access to all the data and the final responsibility for the decision to submit for publication.

## Results

### Measurement of eTIL% as a prognostic variable in cohorts from multiple-institutions

Assessment of eTIL% using the NN192 machine learning cell classifier and the established cut-point of 16.6% in the five cohorts from multiple institutions showed that high eTIL% was associated with longer overall survival in TCGA cohort (hazard ratio (HR) = 0.1,  $p < 0.0001$ ), better disease-specific survival in Tubingen cohort (HR = 0.31,  $p = 0.013$ ), and Yale cohort (HR = 0.37,  $p = 0.005$ ) (Figure 1c, 1e, 1f), but not in the

NYU or Sydney cohorts (Figure 1a, 1b). However, the assessment of visual pathologist-read TILs in Yale Cohort showed no significant association with disease specific survival (Log-Rank  $p = 0.39$ , Figure 1g). Evaluation of the stage distribution of these cohorts showed that approximately 98% of patients in the NYU cohort and 43% of patients in the Sydney cohort were stage III and IV patients, whereas stage III and IV patients in the Tubingen, Yale and TCGA cohorts were 6%, 0% and 0% respectively (Figure 1d). The results indicated that assessing eTIL% scores as a prognostic factor for patients with melanoma may be stage dependent as high eTIL% were associated with better prognosis mainly in patients with stage I and II disease. We generated a combined cohort containing 764 patients from Yale, Tubingen, Sydney, TCGA, and NYU cohorts. Univariable and multivariable analyses were performed to assess the association of eTIL% and the clinical pathological features with survival (Table 2). eTIL% (with a predefined 16.6% cut-point), Stage, Breslow, ulceration and histogenesis were all significantly associated with survival in univariable analyses. The multivariable analysis showed that eTIL% was a significant predictor, even when combined with the other pathological features in a single model. Further, in an analysis of stage 2 only patients of the combined cohort with the 16.6% cut-point, the results showed that higher eTIL% is associated with better prognosis (HR = 0.45,  $p = 0.00068$ ) (Figure 2a), but not stage III and IV (HR = 1.48,  $p = 0.14$ ) (Figure 2b). Our results could support the previous finding that patients with eTIL%  $\geq 16.6$  have a significantly better prognosis.

### Assessment of five TIL variables in multi-institutional stage I and II combined cohort

To identify the best approach to measure eTILs for potential future clinical adoption, we tested five different methods to assess the densities and proportions of eTILs based on the cell types and the area analyzed. We used the TCGA cohort as a training set to find every possible cut-point and the association of each TIL variable with patient outcome. The optimal cut-points defined in the TCGA cohort for each variable, the p-values, and HRs derived for measurement of the cohorts from assessing the optimal cut-points are shown. Since the purpose of this assessment was to compare the performance of five variables, it is statistically unsound to compare the p-values of each variable but ok to compare the HRs to determine relative prognostic strength. We compared the estimated difference between the HRs, with confidence intervals (CIs), between variables, and reported the p-value evaluating the null hypothesis of no association between the prognostic variable and outcome. Our results show a significant association of all variables with OS (Figure 3b). The HRs between all five TIL variables are similar, but eTILs (HR=0.31, 95% CI

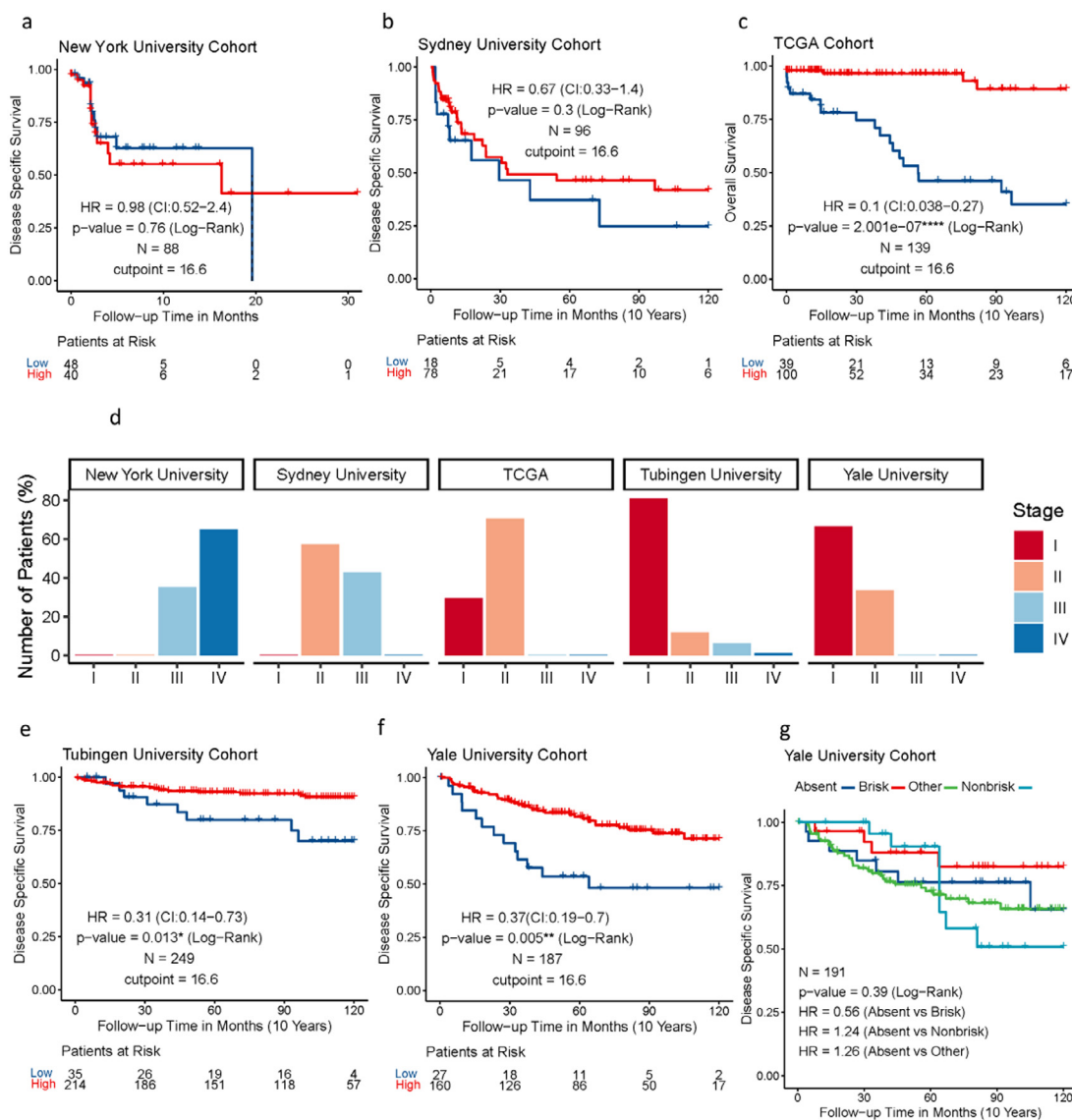


**Figure 1.** Assessment of eTIL% using the NN192 machine learning cell classifier and the established cut-point of 16.6% in the five cohorts from multiple institutions. (a) Kaplan-Meier curves of DSS in WTS NYU validation cohort (b) DSS in WTS Sydney University cohort, (c) OS in WTS TCGA cohort, (e) DSS in TMA Tubingen University Cohort, (f) DSS in TMA Yale University Cohort by eTIL% dichotomised at 16.6 % (g) pathologist's TIL scores. (d) Bar plot depicting the stage distribution of each cohort.

(confidence interval) = 0.19-0.5,  $p < 0.0001$ ) and eTILs (HR=0.29, 95% CI=0.18-0.44,  $p < 0.0001$ ) appeared to be more robust methods in the combined cohort (although not statistically significantly better). This indicates that eTILs and eTILs might be better performing methods than the remaining three methods in large future cohorts. This is concordant with the prognostic results with eTIL% previously reported in melanoma.<sup>1</sup>

### Identification of molecular subtypes of TILs

Lymphocytic subtypes of TILs were identified by multiplexed IF on the serial sections of a Yale melanoma

cohort (YTMA-76). Representative multispectral IF (MIF) images of the first panel (CD14/CD45/CD34) were shown in Figure 4a and of the panel (CD4/CD8/FOXP3/S100B) were shown in Supplementary Figure 4. The representative image of H & E staining on the same tissue section and cell classification using NN192 is shown in Figure 4b. In addition to the lymphoid lineage markers including CD3, CD4, CD8, CD20, CD45, CD56, and FOXP3, we also examined myeloid lineage markers such as CD14, CD68, CD34 to accurately identify the specific cell types within the tumor microenvironment of YTMA-76. The relationship between each molecular subtype of cell and TILs% was assessed by

Variables	Univariable Analysis		Multivariable Analysis	
	HR (95% CI)	P value	HR (95% CI)	P value
eTILs%	0.4 (0.29-0.55)	<0.001	0.5 (0.30-0.75)	0.001
Age	1.0 (0.99-1)	0.63	1.0 (0.98-1.01)	0.751
Gender (M vs F)	0.7 (0.46-1.1)	0.11	0.7 (0.46-1.09)	0.116
Stage (vs I)				
II	3.0 (2.1-4.3)	0.001	1.5 (0.87-2.41)	0.153
III	5.3 (3.4-8.1)	0.001	3.1 (0.98-9.91)	0.055
IV	19.9 (10.2-38.8)	<0.001	6.0 (2.56-14.12)	<0.001
Breslow (vs <0.8)				
1>4.0	8.1 (4.5-14.6)	<0.001		
10.8-1.0	3.2 (1.5-6.7)	0.002		
11.0-2.0	2.4 (1.4-4.4)	0.003		
12.0-4.0	4.3 (2.4-7.7)	<0.001		
Ulceration (Yes vs No)	2.0 (1.2-3.2)	0.01		
Histogenesis (11 Categories)				
	Max: 2.90E+07 (NA)	<0.001		
	Min: 9.97E-01 (NA)			

**Table 2: Univariable and multivariable Cox-proportional Hazards Regression analyses to assess the association of eTIL% and the clinical pathological features regarding disease-specific overall survival in all stage multi-institutional combined cohort.**

Pearson linear regression which showed a high positive correlation of TILs with cell types including CD45 (R = 0.83, p < 2.2e-16), CD3 (R = 0.78, p = 8.6e-15), CD8 (R = 0.76, p = 8e-14), CD20 (R = 0.62, p = 1.4e-08), CD4 (R = 0.52, p = 6.8e-06) and a weak correlation with cell types such as FOXP3 (R = 0.3), CD56 (R = 0.12) and CD66b (R = 0.02) (Figure 4c). These results indicate that the lymphocytic phenotypic marker most highly

correlated to TILs is CD45 (leukocyte common antigen), and the specific phenotypic subtype of cells representing TILs may be CD3+ or CD8+ or CD4+ T cells. This was similarly reported previously in melanoma.<sup>1,21</sup> These findings were corroborated by the cell type-specific survival analyses, which showed similar profiles (Supplementary Figure 1). The Kaplan–Meier estimates of survival test using the median as a cut-point showed

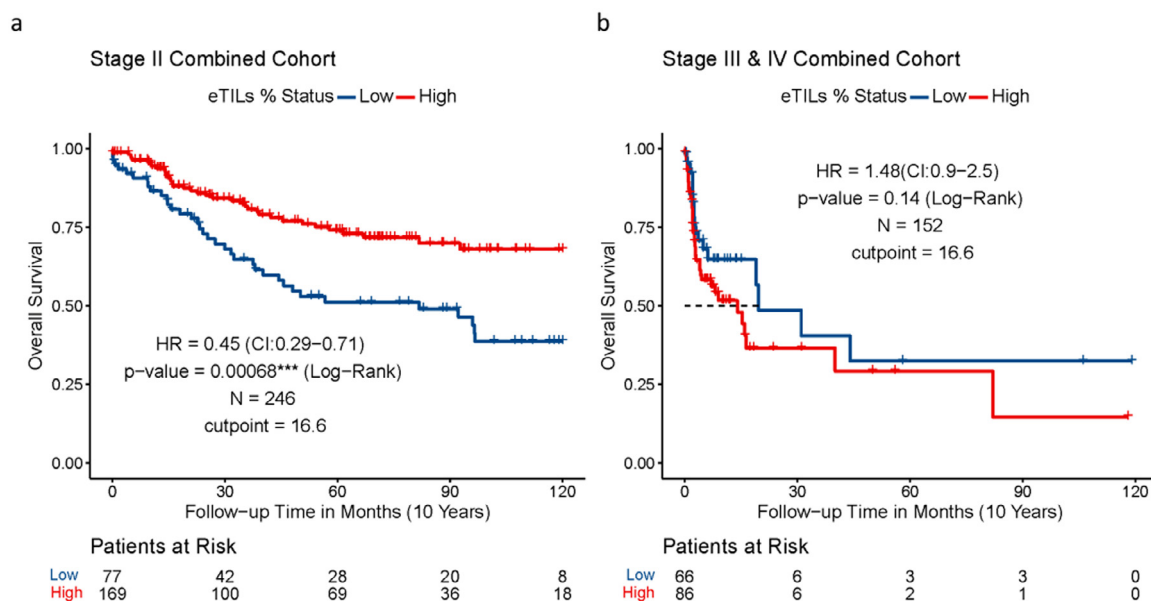


**Figure 2.** Assessment of eTIL% in stage specific combined cohorts. (a) Kaplan-Meier curve of OS in stage II only combined cohort and (b) Kaplan–Meier curve of OS in stage III and IV combined cohorts by eTIL% dichotomised at 16.6 %.

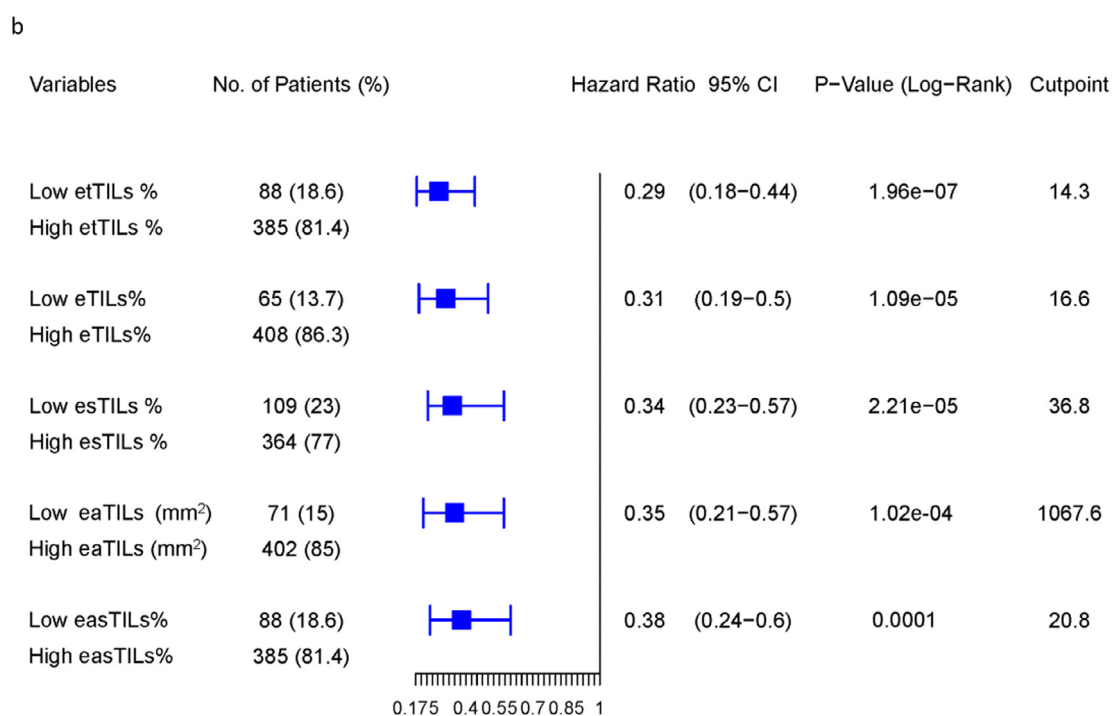
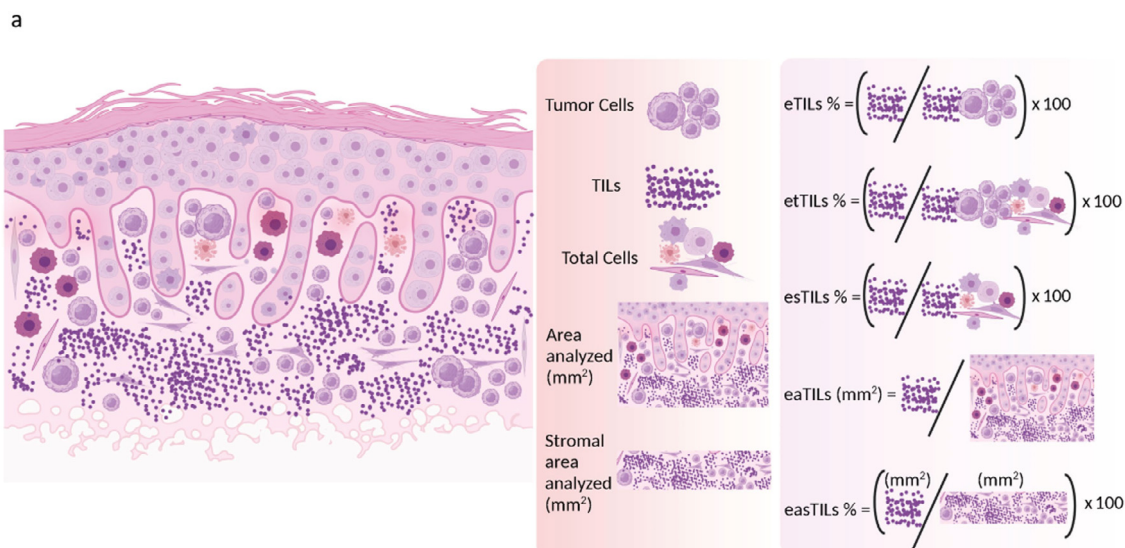


**Figure 3.** Assessment of five TILs variables including eTILs, etTILs, esTILs, eaTILs and easTILs. **(a)** Schematic diagram illustrating the variables (created with BioRender.com). **(b)** Forest plot of DSS in stage I and II combined discovery set. The optimal cut-points defined in the TCGA cohort as a training set for each variable, the p-values (log-rank) and HRs with 95% CI derived for measurement of the cohorts from assessing the optimal cut-points were shown.

that patients with high cell counts of CD3 (HR = 0.21,  $p = 0.015$ ) and CD8 (HR = 0.2,  $p = 0.015$ ), as well as myelocytic macrophage marker CD68 (HR = 0.33,  $p = 0.015$ ) have significantly improved DSS (Figure 4d). As accumulated evidence showed that CD3+ and CD8+ lymphocytic cell infiltration is the primary determinant of immunotherapy outcome, evaluating the combination of both TILs and a group of specific molecular

subtypes of TILs in association with the clinical outcome might assist in defining a subset of patients that might respond to immunotherapy.

Next, we assessed the utility of TILs and specific molecular subtypes of cells to predict event risk. We generated the area under the receiver operating characteristic (ROC) curves (C-statistic) for TILs variables such as eTILs and etTILs, and all lymphocytic markers

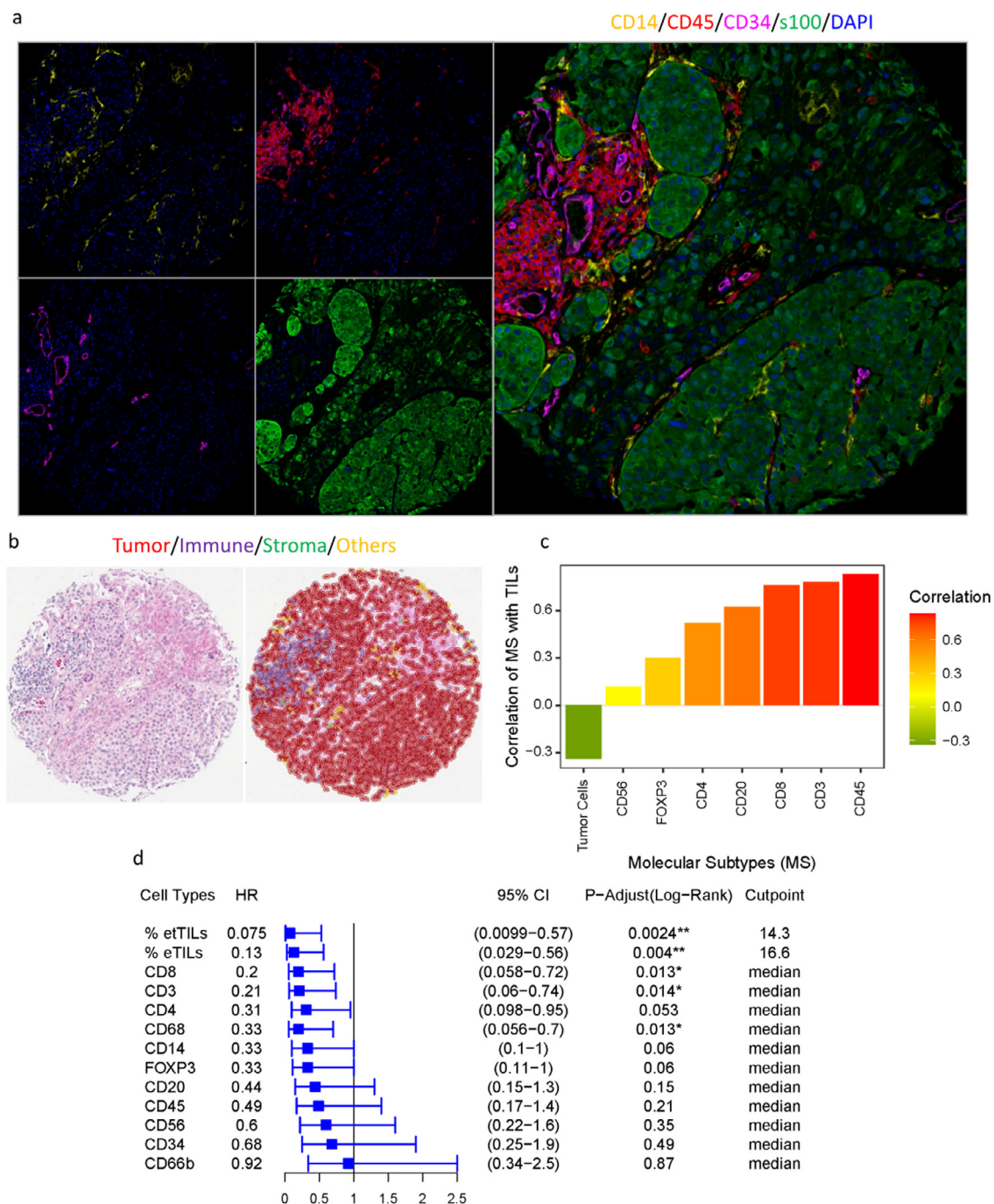


**Figure 4.** Identification of molecular subtypes of TILs. **(a)** Representative multispectral IF images of the panel (CD14/CD45/CD34) profiling in YTMA-76, tissue block 2, cut-64. **(b)** The representative H & E image and cell classification on the same tissue section using NN192. **(c)** Pearson linear regression between each molecular subtype of cells and TILs. **(d)** Forest plot of DSS in stage YTMA-76. The predefined cut-point 16.6% for eTILs, the optimal cut-point 14.3 defined in the TCGA cohort for eTILs and the median cut-points for all other cell types were used to stratify the patients. The adjusted p-values (log-rank, adjusted by Benjamini and Hochberg, BH) and HRs with 95% CI derived for measurement of the cohorts from assessing the optimal cut-points were shown.

including CD4, CD3, CD8, CD45, CD20, FOXP3 and CD56 (Figure 5) to measure the risk prediction associated with these markers. eTILs achieved a favorable

prognostic performance where the area under the curve (AUC) value for DSS was 0.77 (CI: 0.642-0.894). Of seven markers tested for AUC, CD4 (AUC: 0.723, CI:

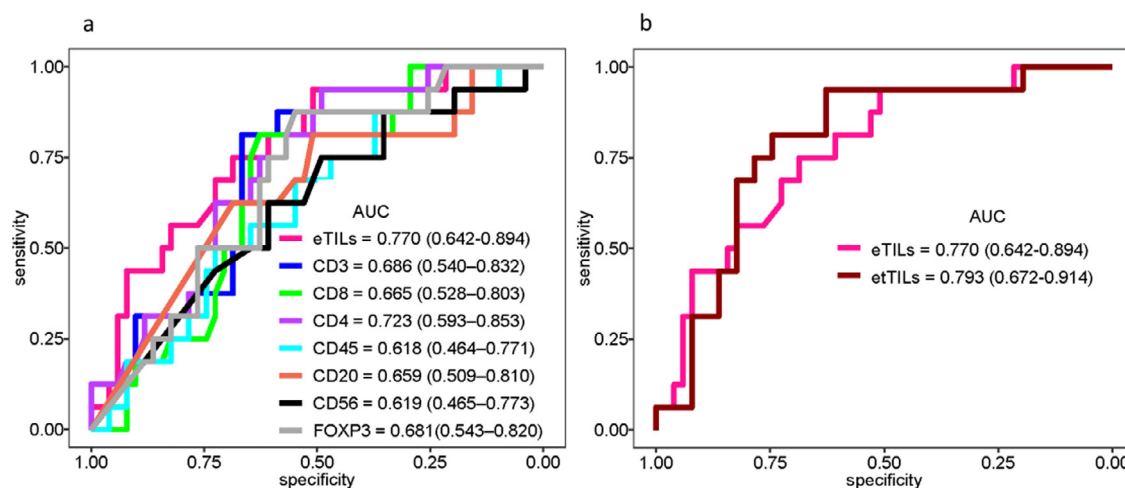


**Figure 5.** Identification of TIL variables for use as clinical utilities. **(a)** ROC curves indicating predictive accuracy of the markers: eTILs, CD3, CD8, CD4, CD45, CD20, CD56 and FOXP3. **(b)** ROC curves showing predictive accuracy, sensitivity, and specificity of eTILs and etTILs variables.

0.593–0.853) showed the highest prognostic performance (Figure 5a). In agreement with the prior work,<sup>21</sup> our results suggested that the prognostic value of TILs appeared to be driven by CD4+ T cells. The AUC of myelocytic macrophage marker CD68 was 0.678 (CI: 0.535–0.823), exhibiting a higher prognostic value. Our AUC analysis of eTILs variable predicting event risk in YTMA-76 showed that eTILs (AUC: 0.793, CI: 0.672–0.914, specificity: 0.627 and sensitivity: 0.938) outperformed eTILs (AUC: 0.77, CI: 0.642–0.897, specificity: 0.51 and sensitivity: 0.938) which validated our finding in a low-stage combined cohort from multiple institutions (Figure 5b). Taken together, assessment of ROC curves by comparing the clinical impact of two variable models (i.e., eTILs and etTILs) suggests that etTIL% might be a more robust variable to use clinically.

## Discussion

The use of immunotherapies, including Pembrolizumab and Ipilimumab in the adjuvant setting, has been shown to successfully manage stage III melanoma.<sup>5,7</sup> However, since more patients with stage I or II melanoma are diagnosed than stage III,<sup>22</sup> it is important to evaluate the role of these agents as adjuvant therapies in patients with early-stage melanoma. This is especially important because only one in five of stage III melanoma patients benefit from immunotherapy, and 50% are cured by surgery alone as seen in the placebo arm.<sup>5</sup> These data suggest that we could identify the subset of patients that could potentially be spared immunotherapy toxicity since they are unlikely to benefit.<sup>1</sup> Our study pools patients with melanoma from international cohorts and supports the previous finding that eTIL% score is an independent prognostic marker in

melanoma and shows that the effect is seen only in low stage patients, the population containing the stage 2 patients that receive adjuvant therapy.

A highly reproducible estimate of the TIL calculation is needed to use the machine learning TIL score in the clinic. Unlike the NN192 algorithm, which relies on cell detection and classification, there are many machine learning models that train with patches rather than with cell detection to generate a TIL map that characterises lymphocytic infiltrates in intra-tumoral, peri-tumoral, and adjacent stromal regions.<sup>23</sup> To identify the best approach for calculating TILs, we considered using multiple variables based on both the cell types (tumor cells, immune cells, fibroblasts, or other cells) and the area of interest (tumor and adjacent 1,2 mm diameter stroma). The test of five TIL variables in the low stage multi-institutional combined cohort showed that all TIL variables had comparable prognostic value; but eTIL% and etTILs % had the best performance. We note that TILs can also be predictive for immunotherapy, but evaluation of these variables in the context of immunotherapy is beyond the scope of this work.

A key limitation of our work is that we have used a machine learning algorithm that is susceptible to cell assignment error during cell classification. Another limitation is that melanoma cells have uneven membrane patterns and highly irregular cell shapes. Since melanoma cells change their shape and can adopt the appearance of other cells to invade any tissue in the body,<sup>24</sup> it is often difficult to accurately classify tumor cells resulting in misclassification of malignant melanoma cells as the fibroblasts or other cells. As etTIL% was calculated using total cells as the denominator, the likelihood of incorrect percentage automated TIL calculation due to assignment error might be reduced as

opposed to eTIL% method, which used the sum of only immune and tumor cells as its denominator. As a result, etTIL% may have higher reproducibility than eTIL% in patients with melanoma. However, we found no statistically significant difference between our two-best model variables. Finally, the use of 0.6-mm diameter tissue cores TMAs is an additional limitation of this study. The advantage of large numbers of cases accessible by TMA is the trade-off between assessing the fraction of the tumor and maximizing the number of samples. As such, the evaluation of TILs in both TMA and WTA formats show significant association with survival. Further we note the the TILs quantification done here is to illustrate the heterogeneity of the immune infiltrate that is recognized as eTIL. We do not attempt to validation the prognostic value of molecularly defined TIL in this work.

TILs comprise a heterogeneous cell population including natural killer (NK) cells, B cells and various subsets of T cells with complex functional states (e.g., naive, effector, memory, and dysfunctional) and thus, the prognostic value of the automated TIL may arise from the unbiased combination of distinct molecular subtypes.<sup>25</sup> Here, we evaluated various molecular subtypes of lymphocytes within the TILs population and their prognostic values assessed by DSS. Concordant with the study by Piras, *et al.*,<sup>26</sup> our results show that high CD8+ and CD3+ cells were associated with favorable DSS though the hazard ratio was higher than that of eTIL% and etTIL% variables (0.2 versus 0.13 and 0.075). In the study of Acs, *et al.*, only a weak-fair correlation was reported between eTILs and CD4 and CD8 expression.<sup>1</sup> The inherently subjective nature of the user-supervised training process for cell segmentation of IF images using cell segmentation algorithm might be a major contributor to this variation. The cell count analyses using IF cell segmentation platforms can lead to inconsistent outcomes, especially if the assessed cohort is not statistically powered. The provisional solution might be to use a combined application of both IF and H & E that are sufficiently generic to be easily trainable while consistently achieving high sensitivity and specificity with validation.

In summary, we validated that eTIL% score is a robust prognostic marker in patients with early-stage melanoma and identified distinct TIL subpopulations that carry the prognostic value. Pending prospective validation, the use of the NN192 machine learning algorithm might evolve into a useful and easy-to-implement tool that will aid in risk stratification of patients with early-stage melanoma. In the future, the use of eTILs might be complemented with molecular subtyping of cells for more discriminating analyses. The use of a combined marker signature may be proven to be the best approach to define a subset of patients that will not benefit from immunotherapy or might develop significant toxicities.

### Contributors

Conception and design: T.N. Aung, D.L. Rimm, Development of methodology: T.N. Aung, Y. Bai, B. Acs, D.L. Rimm, Acquisition of data (provided animals, acquired, and managed patients, provided facilities, etc.): T.N. Aung, J. Wilmott, S. Nourmohammadi, V. Yaghoobi, T. Sinnberg, K. Khosrotehrani, I. Osman, J.F. Thompson, R.A. Scolyer, D.L. Rimm, Analysis and interpretation of data (e.g., statistical analysis, biostatistics, computational analysis): T.N. Aung, V. Yaghoobi, S. Nourmohammadi, I. Vathiotis, A. Fernandez, M. Moutafi, N. Gavrielatou, S. Martinez-Morilla, Writing, review, and/or revision of the manuscript: T.N. Aung, S. Shafi, J. Wilmott, S. Nourmohammadi, I. Vathiotis, N. Gavrielatou, T. Sinnberg, K. Khosrotehrani, I. Osman, V. Yaghoobi, Y. Bai, B. Acs, A. Fernandez, S. Martinez-Morilla, M. Moutafi, T. Amara, K. Ikenberg, J.F. Thompson, R.A. Scolyer, D.L. Rimm, Administrative, technical, or material support (i.e., reporting or organizing data, constructing databases): T.N. Aung, J. Wilmott, V. Yaghoobi, T. Sinnberg, T. Amara, K. Ikenberg, K. Khosrotehrani, I. Osman, J.F. Thompson, R.A. Scolyer, D.L. Rimm, Study supervision: T.N. Aung, D.L. Rimm. Data verification: All data generated in this study will be accessible from the date this work is published by contacting D.L. Rimm (david.rimm@yale.edu) or T. N. Aung (thazin.aung@yale.edu). All authors read and approved the final version of the manuscript.

### Data sharing statement

Raw images were submitted to <https://www.ebi.ac.uk/bioimage-archive> with the accession number (S-BIAD470).

### Declaration of interests

David L. Rimm has served as an advisor for Astra Zeneca, Agendia, Amgen, BMS, Cell Signaling Technology, Cepheid, Daiichi Sankyo, Genoptix/Novartis, GSK, Konica Minolta, Merck, NanoString, PAIGE.AI, Perkin Elmer, Roche, Sanofi, Ventana and Ultivue. Astra Zeneca, Cepheid, NavigateBP, NextCure, Nanostring, Lilly, and Ultivue fund research in David L. Rimm's lab. Ana Bosch has participated in Advisory Board meetings for Pfizer and Novartis and received a travel grant from Roche. Dr. Rimm is supported for efforts in melanoma by Navigate Biopharma and the Yale SPORC in Skin Cancer: P50 CA121974 (M. Bosenberg and H. Kluger, PIs).

Richard A Scolyer has received fees for professional services from Evaxion, Provectus Biopharmaceuticals Australia, Qbiotics, Novartis, Merck Sharp & Dohme, NeraCare, AMGEN Inc., Bristol-Myers Squibb, Myriad Genetics and GlaxoSmithKline. Richard A Scolyer is supported by an Australian National Health and Medical Research Council Practitioner Fellowship. Richard A

Scolyer and John F Thompson are the recipients of an Australian National Health and Medical Research Council Program Grant (APP1093017). John F Thompson has received honoraria for advisory board participation from BMS Australia, MSD Australia, GSK and Provectus Inc, and travel and conference support from GSK, Provectus Inc and Novartis.

Tobias Sinnberg reports grants from Neracare GmbH, Novartis, SkylineDx Pierre Fabre, and Pascoe GmbH and personal fees or travel support from BMS, Novartis, CeCaVa outside the submitted work.

CTSA Grant Number TL1 TR001864 supporting Dr. Aileen Fernandez from the National Center for Advancing Translational Science (NCATS), a component of the National Institutes of Health (NIH).

Iman Osman was supported by NCI R01 and NCI Melanoma SPORE.

Kiarash Khosroshirani was supported by Cancer Council QLD grant 1125237 and Cancer Council QLD grant ACCR-000095.

Teresa Amaral was supported by Novartis, Neracare, Sanofi, SkylineDx and receives consulting fees from Pierre Fabre and BMS as an invited speaker. She acts as an advisor for CeCaVa.

Balazs Acs was supported for a postdoctoral grant supporting by The Swedish Society for Medical Research (Svenska Sällskapet för Medicinsk Forsknings - SSMF).

Saeed Nourmohammadi is supported for doctoral degree program by the University of Adelaide Research Scholarship.

All other authors report no conflicts of interest.

## Acknowledgments

We would like to thank Lori Charette, and the team at the Yale Pathology Tissue Service and Developmental Histology Facility for its valuable contributions. The authors thank Dr. Jonathan H Warrell for his statistical advice. We thank The Swedish Society for Medical Research (Svenska Sällskapet för Medicinsk Forsknings - SSMF) for a postdoctoral grant supporting Balazs Acs. We thank the Melanoma Research Alliance for support of Iman Osman. The authors also gratefully acknowledge assistance from colleagues at their respective institutions. This work was also supported by a sponsored research agreements from Navigate Biopharma and NextCure and by grants from the NIH including the Yale SPORE in Skin Cancer, P50 CA121974, the Yale SPORE in Lung Cancer, P50 CA196530, NYU SPORE in Skin Cancer P50CA225450 and the Yale Cancer Center Support Grant, P30CA016359.

## Supplementary materials

Supplementary material associated with this article can be found in the online version at doi:10.1016/j.ebiom.2022.104143.

## References

- 1 Acs B, Ahmed FS, Gupta S, et al. An open source automated tumor infiltrating lymphocyte algorithm for prognosis in melanoma. *Nat Commun.* 2019;10(1):1–7.
- 2 Kluger HM, Zito CR, Barr ML, et al. Characterization of PD-L1 expression and associated T-cell infiltrates in metastatic melanoma samples from variable anatomic sites. *Clin Cancer Res.* 2015;21(13):3052–3060.
- 3 Wolchok JD, Chiarion-Sileni V, Gonzalez R, et al. Overall survival with combined nivolumab and ipilimumab in advanced melanoma. *N Engl J Med.* 2017;377(14):1345–1356.
- 4 Robert C, Schachter J, Long GV, et al. Pembrolizumab versus ipilimumab in advanced melanoma. *N Engl J Med.* 2015;372(26):2521–2532.
- 5 Eggermont AM, Blank CU, Mandala M, et al. Adjuvant pembrolizumab versus placebo in resected stage III melanoma. *N Engl J Med.* 2018;378(19):1789–1801.
- 6 Eggermont AM, Chiarion-Sileni V, Grob J-J, et al. Adjuvant ipilimumab versus placebo after complete resection of high-risk stage III melanoma (EORTC 18071): a randomised, double-blind, phase 3 trial. *Lancet Oncol.* 2015;16(5):522–530.
- 7 Bankhead P, Loughrey MB, Fernández JA, et al. QuPath: Open source software for digital pathology image analysis. *Sci Rep.* 2017;7(1):1–7.
- 8 Schatton T, Scolyer RA, Thompson JF, et al. Tumor-infiltrating lymphocytes and their significance in melanoma prognosis. *Mol Diagnostics Melanoma.* 2014;287–324.
- 9 Mihm MC, Mulé JJ. Reflections on the histopathology of tumor-infiltrating lymphocytes in melanoma and the host immune response. *Cancer Immunol Res.* 2015;3(8):827–835.
- 10 Azimi F, Scolyer RA, Rumcheva P, et al. Tumor-infiltrating lymphocyte grade is an independent predictor of sentinel lymph node status and survival in patients with cutaneous melanoma. *J Clin Oncol.* 2012;30(21):2678–2683.
- 11 Clark Jr WH, Elder DE, Guerry IV D, et al. Model predicting survival in stage I melanoma based on tumor progression. *J Natl Cancer Inst.* 1989;81(24):1893–1904.
- 12 Aivazian K, Ahmed T, El Sharouni M-A, et al. Histological regression in melanoma: impact on sentinel lymph node status and survival. *Mod Pathol.* 2021;1–10.
- 13 Kos Z, Roblin E, Kim RS, et al. Pitfalls in assessing stromal tumor infiltrating lymphocytes (sTILs) in breast cancer. *NPJ Breast Cancer.* 2020;6(1):1–16.
- 14 Klauschen F, Müller K, Binder A, et al., editors. Scoring of tumor-infiltrating lymphocytes: from visual estimation to machine learning. *Seminars in Cancer Biology.* 2018: Elsevier.
- 15 Gershenwald JE, Scolyer R, Hess K, et al. Melanoma of the skin. *AJCC Cancer Staging Manual.* 2017;8:563–585.
- 16 Gershenwald JE, Scolyer RA, Hess KR, et al. Melanoma staging: evidence-based changes in the American joint committee on cancer eighth edition cancer staging manual. *CA Cancer J Clin.* 2017;67(6):472–492.
- 17 Bai Y, Cole K, Martinez-Morilla S, et al. An open-source, automated tumor-infiltrating lymphocyte algorithm for prognosis in triple-negative breast cancer. *Clin Cancer Res.* 2021;27(20):5557–5565.
- 18 Salgado R, Denkert C, Demaria S, et al. The evaluation of tumor-infiltrating lymphocytes (TILs) in breast cancer: recommendations by an International TILs Working Group 2014. *Ann Oncol.* 2015;26(2):259–271.
- 19 Brown JR, Wimberly H, Lannin DR, et al. Multiplexed quantitative analysis of CD3, CD8, and CD20 predicts response to neoadjuvant chemotherapy in breast cancer. *Clin Cancer Res.* 2014;20(23):5995–6005.



- 20 Camp RL, Dolled-Filhart M, Rimm DL. X-tile: a new bioinformatics tool for biomarker assessment and outcome-based cut-point optimization. *Clin Cancer Res.* 2004;10(21):7252-7259.
- 21 Wong PF, Wei W, Smithy JW, et al. Multiplex quantitative analysis of tumor-infiltrating lymphocytes and immunotherapy outcome in metastatic melanoma. *Clin Cancer Res.* 2019;25(8):2442-2449.
- 22 Poklepovic AS, Luke JJ. Considering adjuvant therapy for stage II melanoma. *Cancer.* 2020;126(6):1166-1174.
- 23 Saltz J, Gupta R, Hou L, et al. Spatial organization and molecular correlation of tumor-infiltrating lymphocytes using deep learning on pathology images. *Cell Rep.* 2018;23(1):181-193.e7.
- 24 Cooper S, Sadok A, Bousgouni V, et al. Apolar and polar transitions drive the conversion between amoeboid and mesenchymal shapes in melanoma cells. *Mol Biol Cell.* 2015;26(22):4163-4170.
- 25 Fridman WH, Pages F, Sautes-Fridman C, et al. The immune contexture in human tumours: impact on clinical outcome. *Nat Rev Cancer.* 2012;12(4):298-306.
- 26 Piras F, Colombari R, Minerba L, et al. The predictive value of CD8, CD4, CD68, and human leukocyte antigen-D-related cells in the prognosis of cutaneous malignant melanoma with vertical growth phase. *Cancer.* 2005;104(6):1246-1254.

## **Contribution of TLR4 to Colorectal Tumor Microenvironment, Etiology and Prognosis**

Elise E Crame<sup>a</sup>, Saeed Nourmohammadi<sup>a</sup>, Hannah R Wardill<sup>a, c</sup>, Janet K Coller<sup>b</sup>, Joanne M Bowen<sup>a</sup>

<sup>a</sup>Discipline of Physiology, School of Biomedicine, The University of Adelaide, Adelaide, SA, Australia; <sup>b</sup>Discipline of Pharmacology, School of Biomedicine, The University of Adelaide, Adelaide, SA, Australia; <sup>c</sup> Precision Medicine (Cancer), The South Australian Health and Medical Research Institute, Adelaide, SA, Australia

**Corresponding Author:** Mrs. Elise E Crame; Address: Level 2 Helen Mayo South, the University of Adelaide, North Terrace, Adelaide SA 5000; Phone number: +614 20495642; Email: [elise.crame@adelaide.edu.au](mailto:elise.crame@adelaide.edu.au)

### **Abstract**

#### **Purpose**

Toll-like receptor 4 (TLR4) is increasingly recognized for its ability to govern the etiology and prognostic outcomes of colorectal cancer (CRC) due to its profound immunomodulatory capacity. Despite widespread interest in TLR4 and CRC, no clear analysis of current literature and data exists. Therefore, translational advances have failed to move beyond conceptual ideas and suggestions.

#### **Methods**

We aimed to determine the relationship between TLR4 and CRC through a systematic review and analysis of published literature and datasets. Data was extracted from nine studies that reported survival, CRC staging and tumor progression data in relation to TLR4 expression. Primary and metastatic tumor samples with associated clinical data were identified through the Cancer Genome Atlas (TCGA) database.

## **Results**

Systematic review identified heterogeneous relationships between TLR4 and CRC traits, with no clear theme evident across studies. A total of 448 datasets were identified through the TCGA database. Analysis of TCGA datasets revealed TLR4 mRNA expression is decreased in advanced CRC stages ( $P < 0.05$  for normal vs Stage II, Stage III and Stage IV). Stage-dependent impact of TLR4 expression on survival outcomes were also found, with high TLR4 expression associated with poorer prognosis (stage I vs III (HR = 4.2,  $P = 0.008$ ) and stage I vs IV (HR = 11.3,  $P < 0.001$ )).

## **Conclusion**

While TLR4 mRNA expression aligned with CRC staging, it appeared to heterogeneously regulate survival outcomes depending on the stage of disease. This underscores the complex relationship between TLR4 and CRC, with unique impacts dependent on disease stage.

**Keywords:** Toll-Like Receptor 4, Colorectal Neoplasms, Systematic Review, Humans

## **Introduction**

Colorectal cancer (CRC) remains one of the most prevalent cancer diagnoses worldwide, with incidence rates in the United States of America of 37.8 per 100,000 (National Cancer Institute: Surveillance 2021). This places CRC as the fourth most common cancer in western populations (Australian Institute of Health and Welfare 2020; National Cancer Institute: Surveillance 2021) which when coupled with its high mortality rates, cements this disease as a major healthcare burden. While significant advances have been made in identifying high level risk factors for CRC, heterogeneity in tumor progression and treatment response continues to challenge the understanding of its etiology (Buikhuisen, Torang & Medema 2020). Few factors remain significant when traditional, largely unmodifiable risk factors (e.g. age, sex) are adjusted for, pointing to complex mechanisms governing tumor microenvironment which dictate growth trajectory and vulnerability to anti-cancer therapy (Buikhuisen, Torang & Medema 2020).

The tumor microenvironment is a complex system of molecular and cellular components, produced by both host and tumor (Wang J. J, Lei K F & Han F 2018). The microenvironment's contribution to prognosis and clinical outcome has proven controversial, although evidence supports both beneficial and inhibitory roles. For example, the microenvironment facilitates immune invasion and destruction of tumor tissue (Fang et al. 2014). In contrast, it also contributes to tumor development, cancer cell survival and treatment resistance (Zhao et al. 2019). Irrespective of this complexity, it is clear that infiltration of peripheral immune cells into the tumor microenvironment is related to CRC progression and prognosis. A 2019 study using the cancer genome atlas (TCGA) and gene expression omnibus (GEO) databases reported that M<sub>0</sub> macrophages, M<sub>1</sub> macrophages and CD4<sup>+</sup> memory T cells were more abundant in CRC tissue compared to healthy tissues ( $P < 0.02$ ) (Ge et al. 2019). Furthermore, higher infiltration of M<sub>1</sub> macrophage populations in CRC tissue correlated with lower participant survival ( $P = 0.04$ ) (Ge et al. 2019). This underscores the involvement of the host immune system in CRC.

In light of the strong immune-mediated mechanisms that appear to be linked with CRC etiology and treatment response, there has been substantial interest in the potential role of the innate immune surveillance protein, toll-like receptor 4 (TLR4). TLR4 is a pattern recognition receptor, which upon activation, initiates a strong inflammatory response (Takeda & Akira 2004). TLR4 requires the accessory proteins myeloid differentiation factor 2 (MD-2) and cluster of differentiation 14 (CD14) to efficiently bind to ligands including, LPS, heat shock proteins (Hsp70 and Hsp90) and high-mobility group protein I (HMGBI) (Cheng Z et al. 2015). TLR4 signaling is vital to intestinal homeostatic maintenance, as previously reviewed (Bruning et al. 2021). TLR4 is notably upregulated in the intestine under inflammatory states including in people with ulcerative colitis, and this is further linked to ulcerative colitis-associated CRC risk and development (Fukata M et al. 2007). Furthermore, genetic variants of *TLR4* (rs10116253, rs192791 1, rs7873784) have been linked to CRC (Huang, BZ et al. 2018).

TLR4 is expressed on a range of different cell types within the tumor microenvironment, including dendritic, stromal, macrophage and epithelial cells (Li J et al. 2017). The importance of site-specificity of TLR4 expression in healthy and diseased states, including CRC, is well documented (Bruning et al. 2021). Pre-clinical CRC models indicate that TLR4 has both pro- and anti- tumor roles, with expression sites being a possible differentiating factor between whether TLR4 aids in cancer destruction or survival (Li J et al. 2017). To add further complexity, TLR4 has also been identified to modulate toxicity following cancer therapy, including diarrhea and pain (Wardill et al. 2016). As such, it is currently unclear whether TLR4 is beneficial, or, potentially harmful in the CRC microenvironment, and whether it is a rationale target for intervention. We therefore aimed to systematically review current published evidence and datasets to crystalize the relationship between TLR4 and CRC staging, treatment toxicity and survival.

## **Methods**

### ***Search strategy, study selection and data retrieval***

PubMed, Cochrane Library and Embase were searched between January and February 2022 for peer-reviewed journal publications using keywords listed in Supporting Information Table 1 and were screened for inclusion based on specific criteria; original research, clinical trials and studies conducted between 2010-2021; archival human tissue; CRC; participant survival; tumor recurrence; prognosis; toxicity; and TLR4 expression. Exclusion criteria included: animal models; cell lines; and cancer types other than CRC. Eligible publications were reviewed with the following data being extracted manually by two independent authors (EEC, JKC) using a computer-based template: sample size; CRC stage; chemotherapy treatments; participant demographics; type of TLR4 analysis; TLR4 specific outcomes (including expression rates and site-specificity); survival data (overall survival (OS), progression-free survival (PFS) or disease-free survival (DFS)); and tumor progression data. Summary outcomes are presented in Table 1.

### ***TCGA clinical CRC cases database extraction and statistical analysis***

RNA sequencing data and associated clinical metadata with a total of 512 samples in read counts (HTSeq-Counts) of CRC were obtained from the TCGA data portal (<https://portal.gdc.cancer.gov/>, accessed in December 2020). Data related to TLR4 mRNA expression, CRC staging and OS were extracted. TLR4 mRNA expression was dichotomized into high and low expression using the tertile cut point. The OS curve was constructed using Kaplan–Meier and log-rank test analysis, comparing high and low TLR4 expression groups for all cases and within each CRC stage. Statistical analyses were performed using GraphPad Prism 8.3.1 (GraphPad Software Inc., CA, USA) and R. studio 1.2.5033 (Inc., Boston, MA).

Multivariate analysis was also performed to determine whether mRNA expression was associated with OS in each tumor stage where variables included tumor stage (I: IV), sex and age. To avoid using potentially biased cut-points splitting low and high TLR mRNA expressing participant groups, a two sample t-test using continuous TLR4 mRNA expression values (with no cut-point required) compared mRNA expression between alive and deceased participants. Finally, TLR4 mRNA expression between normal tumor adjacent tissue and tumor samples from different stages were analyzed with a one-way ANOVA (normal vs stage I, stage II, stage III and stage IV).

### **Results**

180 publications were initially identified, with 9 meeting inclusion criteria for final analysis (Figure 1). 6 publications were clinical trials with a combined participant total of 1081. The remaining 3 publications used archival tissue from previous clinical research. Only 2 publications analyzed advanced stage CRC (non-resectable tumor stage II – IV), whereas 7 publications included mixed analysis of varying CRC stage. Participant survival data was extracted from 8 publications, inclusive of DFS, PFS and OS dependant on individual study outcomes. Only 1 publication included data regarding toxicity in relation to TLR4 expression. Finally, CRC recurrence was analyzed in 3 publications. TLR4 expression in the publications was assessed using immunohistochemistry (5/9, all of which used different primary antibodies), polymerase chain reaction (PCR) (3/9) and flow cytometry (1/9). Only 4 publications included site-specific analysis of TLR4 expression in CRC (Table 1) (Cammarota et al. 2010; Eiro N 2013; Formica et al. 2013; Sussman et al. 2014). Of the 9 publications, 4 analyzed formalin fixed and paraffin embedded tissue blocks, 4 analyzed peripheral blood samples and 1 (Sussman et. al. 2014) analyzed tumour tissue microarray slides provided by the NCI Cancer Diagnosis Program (CDP).

***Impact of TLR4 genotype and expression on CRC survival***

Of the 8 publications to report on CRC survival, one reported that wild-type (WT) *TLR4* genotype was beneficial to CRC participant survival rates (Tesniere et al. 2010). Metastatic CRC participants with the WT *TLR4* allele had higher PFS (hazard ratio (HR): 0.73; 95% confidence interval (CI) = 0.53 – 1.00;  $P < 0.05$ ) and OS (HR = 0.72; 95% CI = 0.52 – 1.01;  $P = 0.05$ ) compared with participants bearing the *TLR4* loss-of-function (Asp299Gly) variant post-oxaliplatin chemotherapy treatment (Tesniere et al. 2010). No differences in DFS among participants bearing the WT versus the variant *TLR4* alleles were observed.

In contrast, 2 publications suggested that increased TLR4 expression is detrimental to participant survival (Cammarota et al. 2010; Wang et al. 2010). Cammarota et al. found that in mixed stage CRC tissue, participants with lower TLR4 expression in the tumor stroma compartment had improved DFS compared to participants with higher TLR4 expression (risk ratio (RR) 2.36; log-rank chi-square 4.25,  $P < 0.05$ ) (Cammarota et al. 2010). Furthermore, participants with pT<sub>3</sub> adenocarcinoma with high TLR4 expression (over 50% positive cells) relapsed sooner (14 months) compared to participants with low TLR4 expression (40 months, RR 3.15; log-rank chi-square 4.03,  $P < 0.05$ ) (Cammarota et al. 2010). This is supported by Wang and colleagues, who confirmed that CRC tissue displayed expression of TLR4 in 78 of 108 samples (72%), of which 22 displayed high TLR4 expression (Wang et al. 2010). In addition, increased TLR4 expression was associated with liver metastasis ( $P = 0.0015$ ) and advanced tumor stage (stage IV) ( $P = 0.0197$ ). Upon univariate analysis there was no difference in 5-year DFS rate for low versus high TLR4 expression, but OS was reduced with high TLR4 expression (HR (95% CI) 2.17 (1.15 – 4.07),  $P = 0.015$ ) (Wang et al. 2010). However, this was not retained in multivariate analysis. In contrast, when samples exhibited high expression of both TLR4 and the adapter protein MyD88, DFS and OS were poorer (HR (95% CI) 2.11 (1.05 – 4.23)  $P = 0.0352$ ) (Wang et al. 2010).



The conflicting nature of outcomes may be reflective of the lack of site-specific TLR4 investigations throughout human CRC research. Eiro and colleagues reported TLR4 expression by fibroblasts, not tumor cells themselves, was associated with a shortened OS of CRC participants ( $P = 0.022$ ). Furthermore, TLR4 expression in fibroblasts was a significant and independent factor associated with DFS ( $P = 0.0001$ ), and OS ( $P = 0.013$ ) (Eiro N 2013).

Four publications reported that TLR4 expression does not impact upon CRC survival. Formica and colleagues found that in 31 metastatic CRC participants, neutrophil TLR4 expression at baseline, or 1-month post-chemotherapy, had no association with PFS ( $P > 0.05$ ) (Formica et al. 2013). This is supported by Sussman and colleagues who, in  $N = 279$ , found no association between TLR4 expression in stromal tissue and OS after correcting for both CRC stage and grade. Furthermore, epithelial TLR4 expression was also not associated with OS (Sussman et al. 2014).

More recently, Zhang and colleagues found that in an advanced CRC cohort ( $N = 94$ ) post-standard Fluorouracil-based adjuvant chemotherapy and radical surgery, the measured level of TLR4 expression was independent of DFS; hence no impact of TLR4 on overall DFS (Zhang et al. 2019). In addition, TLR4 was not a significant factor in survival outcomes following univariate or multivariate analyses (Zhang et al. 2019). However, high amounts of *Fusobacterium (Fn)*, an anaerobic bacterium known to activate the TLR4 pathway in CRC cells, correlated with poor DFS ( $P = 0.028$ ) (Zhang et al. 2019). Finally, Gray and colleagues analyzed previously collected tissues from two large-scale clinical trials, the SCOT (ISRCTN59757862) trial and COIN (ISRCTN27286448) trial (Gray et al. 2019). Data generated from SCOT showed no association of any *TLR4* single nucleotide polymorphism (SNP) with survival (Gray et al. 2019). There was also no association of the *TLR4* SNP, rs867228, with DFS in cases with functional polymorphisms (Gray et al. 2019). Data from

COIN showed no association of any tested *TLR4* SNP with OS by either log-rank test or univariate or multivariable Cox regression (Gray et al. 2019).

### ***CRC Recurrence***

Three publications reported on TLR4s contribution to CRC recurrence, with 2 publications identifying a detrimental role of TLR4 in CRC recurrence (Wang et al. 2010; Zhang et al. 2019). Wang and colleagues (2010) report upon 5 year follow-up of 108 mixed stage CRC participants, 53 participants had tumor recurrence (DFS rate: 49%), with participants exhibiting high expression of TLR4 and its accessory protein MyD88 displaying increased recurrence rates compared to those with low expression (TLR4+MyD88 (low vs high) 5-year DFS HR (95% CI) = 2.25 (1.27 – 3.99) P = 0.0053) (Wang et al. 2010). Furthermore, participants with CRC and liver metastasis showed higher TLR4 and MyD88 expression versus CRC without liver metastasis (Wang et al. 2010). Among the 14 liver metastases obtained by hepatectomy, 12 were TLR4 positive and 6 showed a high expression (Wang et al. 2010). These findings are supported by Zhang and colleagues who showed high expression of TLR4 (P = 0.036) were more likely detected in participants with CRC recurrence, compared with participants without recurrence (Zhang et al. 2019).

In contrast, Eiro and colleagues observed that recurrence was dependent on the site of TLR4 expression, not its overall quantitative expression such that TLR4 expression by tumor cells was associated with a lower rate of recurrence in tumors from left colon/rectum compared to those from right colon/rectum (P = 0.028) (Eiro N 2013). Further, TLR4 expression by fibroblasts was associated with a high rate of recurrence (P = 0.0001) in left colon/rectum tumors (Eiro N 2013).

### ***Toxicity post-chemotherapy in participants with CRC***

Only 1 publication investigated the role of TLR4 in relation to post-chemotherapy toxicity outcomes, including diarrhea and nausea. Wong and colleagues investigated a cohort of 46 advanced stage CRC (stage III – IV), treated with first cycle of irinotecan-based chemotherapy (irinotecan monotherapy or in combination with fluorouracil and leucovorin - IFL regimen) (Wong et al. 2021). Participants the variant *TLR4* SNPs rs4986790 and rs4986791 had more severe diarrhoea (50%) compared to those without the variants (15%) (Wong et al. 2021). When looking at diarrhea of all severities, all participants (100%) with the variant *TLR4* SNPs developed diarrhea, compared to only 50% of those without the variants (20 participants each, rs4986790, P = 0.012 vs. rs4986791, P = 0.012).(Wong et al. 2021) There was no association with nausea (Wong et al. 2021).

### **TCGA Database Results**

#### ***TLR4 expression differs due to cancer stage***

Summary of participant clinical data is presented in supporting information Table 2. Although TLR4 expression was not statistically different between normal and stage I, significantly higher TLR4 expression was observed in normal tissues vs Stage II, Stage III and Stage IV (Figure 2A).

#### ***TLR4 expression is associated with survival in respect to tumor stage***

Number of participants per tumor stage is presented in Figure 2C. OS of participants with CRC with respect to TLR4 expression (low vs high) was conducted. TLR4 expression was not a significant prognostic factor (HR = 1.1, P = 0.64) when all stages were combined (Figure 2B) or compared between stages (Figure 3). In contrast, multivariate analysis revealed high TLR4 expression prior to treatment conferred worse prognosis, with the strength of the effect increasing with tumor stage (stage I vs II (HR = 2.2, P = 0.138), stage I vs III (HR = 4.2, P =

0.008) and stage I vs IV (HR = 11.3,  $P < 0.001$ ); Figure 4). Sex and age had no impact on OS (Figure 4). In stage I disease, those that were alive had lower TLR4 expression at diagnosis ( $P = 0.034$ ). For all other stages TLR4 expression at diagnosis was higher in those still alive ( $P = 0.035$ ) (Figure 5).

## **Discussion**

TLR4 is an attractive target for controlling cancer development and optimizing treatment response due to its potent regulation of systemic immune responses. Our analysis exposes the significant heterogeneity in CRC outcomes linked with TLR4 expression. We have shown that TLR4 expression decreases with increasing CRC tumor stage at prognosis, and appears to have stage-dependent associations with participant outcomes. We highlight two novel findings related to high TLR4 expression in early- and late-stage CRC being; (1) in stage I CRC results in worse participant outcomes, and (2) in stage IV CRC results in improved participant outcomes. With TLR4 expression decreasing in higher grade CRC, this potential reduction of innate immune signaling may prove to be the causative mechanism behind unfavourable treatment responses and reduced survival.

TLR4 expression relative to tumor stage is well documented in the literature (Li et al. 2019; Omrane et al. 2014). These patterns of TLR4 expression reflect its core physiological mechanism of inducing inflammation, a process known to be carcinogenic. Our data showed a significant decrease in TLR4 expression in later stage CRC (stages II – IV) compared to normal tissue. This decrease in TLR4 expression was not found in stage I tumors, suggesting that the slightly higher TLR4 expression in early CRC may align with the well-defined concept that inflammatory processes are involved in the early development of CRC (Karin & Greten 2005). However, our analysis did show that non-tumour comparative tissue had the highest TLR4 expression. As this tissue was primarily collected from adjacent tissue in the same participants,

systemic inflammatory responses may have impacted on interpretation. The finding that TLR4 expression decreases with tumor growth is also consistent with the current understanding of tumor development, with tumors often adapting to evade immune detection and control. Activation of the receptor, programmed death 1 (PD-1), has been found to inhibit immune control of tumor growth, with the PD-1 ligand, PD-L1, being significantly upregulated in solid tumors like CRC (Hino et al. 2010). Therefore, this upregulation of PD-L1 is suggested to play a crucial role in the tumors ability to evade host immune system (Dong et al. 2002). This is of particular interest in the context of TLR4 research, as PD-L1 has also been shown to block the cytolytic activity of PD-1+ tumor infiltrating CD4<sup>+</sup> and CD8<sup>+</sup> T cells, which are reliant on dendritic cell -TLR4 interaction (Brahmer et al. 2012; Fife et al. 2009). In addition, Xiao et. al. (2016) reported that inhibition of TLR4 signaling via a blocking antibody significantly reduced the number of PD-1+ B cells in human hepatoma tissues, where PD-1+ B cell populations promoted cancer growth (Xiao et al. 2016). Furthermore, Huang (2018) found that improvement in clinical outcome is resultant of cytosolic HMGB1 triggering dendritic cell maturation through TLR4 activation, whereby consequently recruiting PD-1+ tumor-infiltrating lymphocytes to the tumor site (Huang, CY et al. 2018). These findings highlight the importance of TLR4 to this particular tumor kill pathway and outlines the importance for TLR4 expression for improved clinical outcomes of people living with CRC.

While our findings suggest a likely relationship between TLR4 expression and tumor stage, the relationship between TLR4 and long-term outcome was less clear cut in both our systematic review and genetic analyses. When looking at all tumor stages, there was no significant impact on OS in low vs high TLR4 expressing tumors. This contradicts existing data, as a metaanalysis of 212 people living with CRC found that high TLR4 expression associated with a significantly reduced OS and poorer prognosis (HR (95% CI) 2.30 (1.41,3.75), P = 0.001) (Hao B et al. 2018). However, this analysis did not classify the cohort based on CRC stage which may have

masked some findings and increased bias towards advanced stage disease. While our initial analyses showed no effect of TLR4 expression on OS, analysis of this relationship within specific tumor stages revealed that TLR4 may in fact have an impact but, in a stage-specific manner. Specifically, we showed that TLR4 expression in Stage IV disease was higher in tumors from people still alive compared to those that were not. While we weren't able to show this in our longitudinal OS analyses, this may reflect the lack of power when breaking down our cohort of 488 into specific stages.

This heterogeneity in how TLR4 may act to regulate overall survival for Stage I vs Stage IV disease is likely to reflect the differences in how these disease stages are treated. Stage I disease is almost always treated with surgery, but no cytotoxic therapy, whereas stage IV disease will certainly contain cytotoxic therapy. TLR4 is considered to exert its impact on treatment outcomes via its ability to modulate immunogenic cell death (Fang et al. 2014; Kroemer et al. 2013). Immunogenic cell death acts in concert with direct cytotoxicity, and collectively results in more thorough tumor clearance, and thus long-term survival. As such, higher TLR4 expression would theoretically confer a larger immune response and thus better response in late-stage CRC. This is supported by the Isambert et al. study (2013) which found that increased activation of TLR4 via a lipid A analogue (OM-174) enhanced inflammatory anti-tumor response in metastatic CRC and improved clinical outcomes (Isambert N et al. 2013). Furthermore, data from Huang and colleagues (2018) showed improved DFS in people living with late-stage rectal cancer with increased activation of TLR4 via HGMB1 binding (Huang, CY et al. 2018).

Despite new interpretation of stage-specific roles of TLR4, we must acknowledge some limitations of our approach. Firstly, the studies included within the literature review were varied, often with low sample sizes and differing approaches to measuring TLR4 expression. Furthermore, our genetic analysis relied on previously collected data and exhibited low power

when analysing within the specific CRC stages. It is also important to acknowledge that we relied solely on TLR4 tumor-expression data; whereas evidence from pre-clinical work suggests expression of TLR4 in host tissues (typically non-cancerous) may be critical in setting immune tone of host and thus response (Li J et al. 2017). Nonetheless, our findings indicate a general trend towards higher TLR4 expression being associated with favourable OS outcomes in stage IV CRC suggesting its ability to induce immunogenic cell death is critical in CRC prognosis.

## References

Australian Institute of Health and Welfare 2020, 'National Bowel Cancer Screening Program Monitoring report 2020', *Cancer series no.128. Cat. no. CAN 133*.

Brahmer, JR, Tykodi, SS, Chow, LQ, Hwu, WJ, Topalian, SL, Hwu, P, Drake, CG, Camacho, LH, Kauh, J, Odunsi, K, Pitot, HC, Hamid, O, Bhatia, S, Martins, R, Eaton, K, Chen, S, Salay, TM, Alaparthi, S, Grosso, JF, Korman, AJ, Parker, SM, Agrawal, S, Goldberg, SM, Pardoll, DM, Gupta, A & Wigginton, JM 2012, 'Safety and activity of anti-PD-L1 antibody in patients with advanced cancer', *N Engl J Med*, vol. 366, no. 26, Jun 28, pp. 2455-2465.

Bruning, EE, Collier, JK, Wardill, HR & Bowen, JM 2021, 'Site-specific contribution of Toll-like receptor 4 to intestinal homeostasis and inflammatory disease', *J Cell Physiol*, vol. 236, no. 2, Feb, pp. 877-888.

Buikhuisen, JY, Torang, A & Medema, JP 2020, 'Exploring and modelling colon cancer inter-tumour heterogeneity: opportunities and challenges', *Oncogenesis*, vol. 9, no. 7, Jul 9, p. 66.

Cammarota, R, Bertolini, V, Pennesi, G, Bucci, EO, Gottardi, O, Garlanda, C, Laghi, L, Barberis, MC, Sessa, F, Noonan, DM & Albini, A 2010, 'The tumor microenvironment of colorectal cancer: stromal TLR-4 expression as a potential prognostic marker', *J Transl Med*, vol. 8, Nov 8, p. 112.

Cheng Z, Taylor B, Ourthiague D & A, H 2015, 'Distinct single-cell signaling characteristics are conferred by the MyD88 and TRIF pathways during TLR4 activation', *Sci Signal*, vol. 8, p. ra69.

Dong, H, Strome, SE, Salomao, DR, Tamura, H, Hirano, F, Flies, DB, Roche, PC, Lu, J, Zhu, G, Tamada, K, Lennon, VA, Celis, E & Chen, L 2002, 'Tumor-associated B7-H1 promotes T-cell apoptosis: a potential mechanism of immune evasion', *Nat Med*, vol. 8, no. 8, Aug, pp. 793-800.

Eiro N, GL, Gonzalez L, Fernandez-Garcia B, Andicoechea A, Barbon E, Garcia-Muniz J, Vizoso F, 2013, 'Toll-like Receptor-4 Expression by Stromal Fibroblasts Is Associated With Poor Prognosis in Colorectal Cancer', *J Immunother*, vol. 36, no. 6, pp. 342-349.

Fang, H, Ang, B, Xu, X, Huang, X, Wu, Y, Sun, Y, Wang, W, Li, N, Cao, X & Wan, T 2014, 'TLR4 is essential for dendritic cell activation and anti-tumor T-cell response enhancement by DAMPs released from chemically stressed cancer cells', *Cell Mol Immunol*, vol. 11, no. 2, Mar, pp. 150-159.

Fife, BT, Pauken, KE, Eagar, TN, Obu, T, Wu, J, Tang, Q, Azuma, M, Krummel, MF & Bluestone, JA 2009, 'Interactions between PD-1 and PD-L1 promote tolerance by blocking the TCR-induced stop signal', *Nat Immunol*, vol. 10, no. 11, Nov, pp. 1185-1192.

Formica, V, Cereda, V, di Bari, MG, Grenga, I, Tesauro, M, Raffaele, P, Ferroni, P, Guadagni, F & Roselli, M 2013, 'Peripheral CD45RO, PD-1, and TLR4 expression in metastatic colorectal cancer patients treated with bevacizumab, fluorouracil, and irinotecan (FOLFIRI-B)', *Med Oncol*, vol. 30, no. 4, Dec, p. 743.

Fukata M, Chen A, Vamadevan A, Cohen J, Breglio K, Krishnareddy S, Xu R, Harpaz N, Dannenberg A, Subbaramaiah K, Cooper H, Itzkowitz S & Abreu M 2007, 'Toll-like receptor-4 promotes the development of colitis-associated colorectal tumors', *Gastroenterology*, vol. 133, pp. 1869-1881.

Ge, P, Wang, W, Li, L, Zhang, G, Gao, Z, Tang, Z, Dang, X & Wu, Y 2019, 'Profiles of immune cell infiltration and immune-related genes in the tumor microenvironment of colorectal cancer', *Biomed Pharmacother*, vol. 118, Oct, p. 109228.

Gray, V, Briggs, S, Palles, C, Jaeger, E, Iveson, T, Kerr, R, Saunders, MP, Paul, J, Harkin, A, McQueen, J, Summers, MG, Johnstone, E, Wang, H, Gatcombe, L, Maughan, TS, Kaplan, R, Escott-Price, V, Al-Tassan, NA, Meyer, BF, Wakil, SM, Houlston, RS, Cheadle, JP, Tomlinson, I & Church, DN 2019, 'Pattern Recognition Receptor Polymorphisms as Predictors of Oxaliplatin Benefit in Colorectal Cancer', *J Natl Cancer Inst*, vol. 111, no. 8, Aug 1, pp. 828-836.

Hao B, Chen Z, Baochen B, Miaomei Y, Yao S, Feng Y, Yu Y, Pan L, Di D, Luo G & Zhang X 2018, 'Role of TLR4 as a prognostic factor for survival in various cancers: a meta-analysis', *Oncotarget*, vol. 9, pp. 13088-13099.

Hino, R, Kabashima, K, Kato, Y, Yagi, H, Nakamura, M, Honjo, T, Okazaki, T & Tokura, Y 2010, 'Tumor cell expression of programmed cell death-1 ligand 1 is a prognostic factor for malignant melanoma', *Cancer*, vol. 116, no. 7, Apr 1, pp. 1757-1766.

Huang, BZ, Tsilidis, KK, Smith, MW, Hoffman-Bolton, J, Visvanathan, K, Platz, EA & Joshi, CE 2018, 'Polymorphisms in genes related to inflammation and obesity and colorectal adenoma risk', *Mol Carcinog*, vol. 57, no. 10, Oct, pp. 1278-1288.

Huang, CY, Chiang, SF, Ke, TW, Chen, TW, Lan, YC, You, YS, Shiau, AC, Chen, WT & Chao, KSC 2018, 'Cytosolic high-mobility group box protein 1 (HMGB1) and/or PD-1+ TILs in the tumor microenvironment may be contributing prognostic biomarkers for patients with locally advanced rectal cancer who have undergone neoadjuvant chemoradiotherapy', *Cancer Immunol Immunother*, vol. 67, no. 4, Apr, pp. 551-562.



Isambert N, Fumoleau P, Paul C, Ferrand C, Zanetta S, Bauer J, Ragot K, Lizard G, Jeannin JF & Bardou M 2013, 'Phase I study of OM-174, a lipid A analogue, with assessment of immunological response, in patients with refractory solid tumors', *BMC Cancer*, vol. 13, no. 172, p. 172.

Karin, M & Greten, FR 2005, 'NF-kappaB: linking inflammation and immunity to cancer development and progression', *Nat Rev Immunol*, vol. 5, no. 10, Oct, pp. 749-759.

Kroemer, G, Galluzzi, L, Kepp, O & Zitvogel, L 2013, 'Immunogenic cell death in cancer therapy', *Annu Rev Immunol*, vol. 31, pp. 51-72.

Li J, Yang F, Wei F & Ren X 2017, 'The role of toll-like receptor 4 in tumor microenvironment.', *Oncotarget*, vol. 8, pp. 66656-66667.

Li, N, Xu, H, Ou, Y, Feng, Z, Zhang, Q, Zhu, Q & Cai, Z 2019, 'LPS-induced CXCR7 expression promotes gastric Cancer proliferation and migration via the TLR4/MD-2 pathway', *Diagn Pathol*, vol. 14, no. 1, Jan 12, p. 3.

National Cancer Institute: Surveillance, E, and End Results Program (SEER) 2021, *SEER Cancer Stat Facts: Colorectal Cancer*, Bethesda, MD2022.

Omrane, I, Baroudi, O, Kourda, N, Bignon, YJ, Uhrhammer, N, Desrichard, A, Medimegh, I, Ayari, H, Stambouli, N, Mezlini, A, Bouzayenne, H, Marrakchi, R, Benammar-Elgaaid, A & Bougatef, K 2014, 'Positive link between variant Toll-like receptor 4 (Asp299Gly and Thr399Ile) and colorectal cancer patients with advanced stage and lymph node metastasis', *Tumour Biol*, vol. 35, no. 1, Jan, pp. 545-551.

Sussman, DA, Santaolalla, R, Bejarano P. A., Garcia-Buitrago M. T., Perez M. T., Abreu M & Clarke J 2014, 'In silico and Ex vivo approaches identify a role for toll-like receptor 4 in colorectal cancer', *J Exp Clin Cancer Res*, vol. 33, p. 45.

Takeda, K & Akira, S 2004, 'TLR signaling pathways', *Semin Immunol.*, vol. 16, no. 1, pp. 3-9.

Tesniere, A, Schlemmer, F, Boige, V, Kepp, O, Martins, I, Ghiringhelli, F, Aymeric, L, Michaud, M, Apetoh, L, Barault, L, Mendiboure, J, Pignon, JP, Jooste, V, van Endert, P, Ducreux, M, Zitvogel, L, Piard, F & Kroemer, G 2010, 'Immunogenic death of colon cancer cells treated with oxaliplatin', *Oncogene*, vol. 29, no. 4, Jan 28, pp. 482-491.

Wang, EL, Qian, ZR, Nakasono, M, Tanahashi, T, Yoshimoto, K, Bando, Y, Kudo, E, Shimada, M & Sano, T 2010, 'High expression of Toll-like receptor 4/myeloid differentiation factor 88 signals correlates with poor prognosis in colorectal cancer', *Br J Cancer*, vol. 102, no. 5, Mar 2, pp. 908-915.

Wang J. J, Lei K F & Han F 2018, 'Tumor microenvironment: recent advances in various cancer treatments ', *Eur Rev Med Pharmacol Sci*, vol. 22, pp. 3855-3864.

Wardill, HR, Gibson, RJ, Van Seville, YZ, Secombe, KR, Coller, JK, White, IA, Manavis, J, Hutchinson, MR, Staikopoulos, V, Logan, RM & Bowen, JM 2016, 'Irinotecan-Induced Gastrointestinal Dysfunction and Pain Are Mediated by Common TLR4-Dependent Mechanisms', *Mol Cancer Ther*, vol. 15, no. 6, Jun, pp. 1376-1386.

Wong, DVT, Holanda, RBF, Cajado, AG, Bandeira, AM, Pereira, JFB, Amorim, JO, Torres, CS, Ferreira, LMM, Lopes, MHS, Oliveira, RTG, Pereira, AF, Sant'Ana, RO, Arruda, LM, Ribeiro-Junior, HL, Pinheiro, RF, Almeida, PRC, Carvalho, RF, Chaves, FF, Rocha-Filho, DR, Cunha, FQ & Lima-Junior, RCP 2021, 'TLR4 deficiency upregulates TLR9 expression and enhances irinotecan-related intestinal mucositis and late-onset diarrhoea', *Br J Pharmacol*, vol. 178, no. 20, Oct, pp. 4193-4209.

Xiao, X, Lao, XM, Chen, MM, Liu, RX, Wei, Y, Ouyang, FZ, Chen, DP, Zhao, XY, Zhao, Q, Li, XF, Liu, CL, Zheng, L & Kuang, DM 2016, 'PD-1hi Identifies a Novel Regulatory B-cell Population in Human Hepatoma That Promotes Disease Progression', *Cancer Discov*, vol. 6, no. 5, May, pp. 546-559.

Zhang, S, Yang, Y, Weng, W, Guo, B, Cai, G, Ma, Y & Cai, S 2019, 'Fusobacterium nucleatum promotes chemoresistance to 5-fluorouracil by upregulation of BIRC3 expression in colorectal cancer', *J Exp Clin Cancer Res*, vol. 38, no. 1, Jan 10, p. 14.

Zhao, J, Meng, Z, Xie, C, Yang, C, Liu, Z, Wu, S, Wang, B, Fan, P, Jin, X & Wu, H 2019, 'B7-H3 is regulated by BRD4 and promotes TLR4 expression in pancreatic ductal adenocarcinoma', *Int J Biochem Cell Biol*, vol. 108, Mar, pp. 84-91.

## Statements and Declarations

**Funding Statement:** Elise E Crame is funded by an Australian Government RTP Scholarship, (2019–2022), Hannah R Wardill the recipient of a National Health and Medical Research Council CJ Martin Biomedical Research Fellowship, (2018– 2022).

**Competing Interest:** The authors have no relevant financial or non-financial interests to disclose.

**Author Contribution Statement:** All authors contributed to the study conception and design. Literature review material preparation, data collection and analysis were performed by Elise E Crame and TCGA data collection and analysis were performed by Saeed Nourmohammadi. The first draft of the manuscript was written by Elise E Crame and all authors commented on previous versions of the manuscript. All authors read and approved the final manuscript.

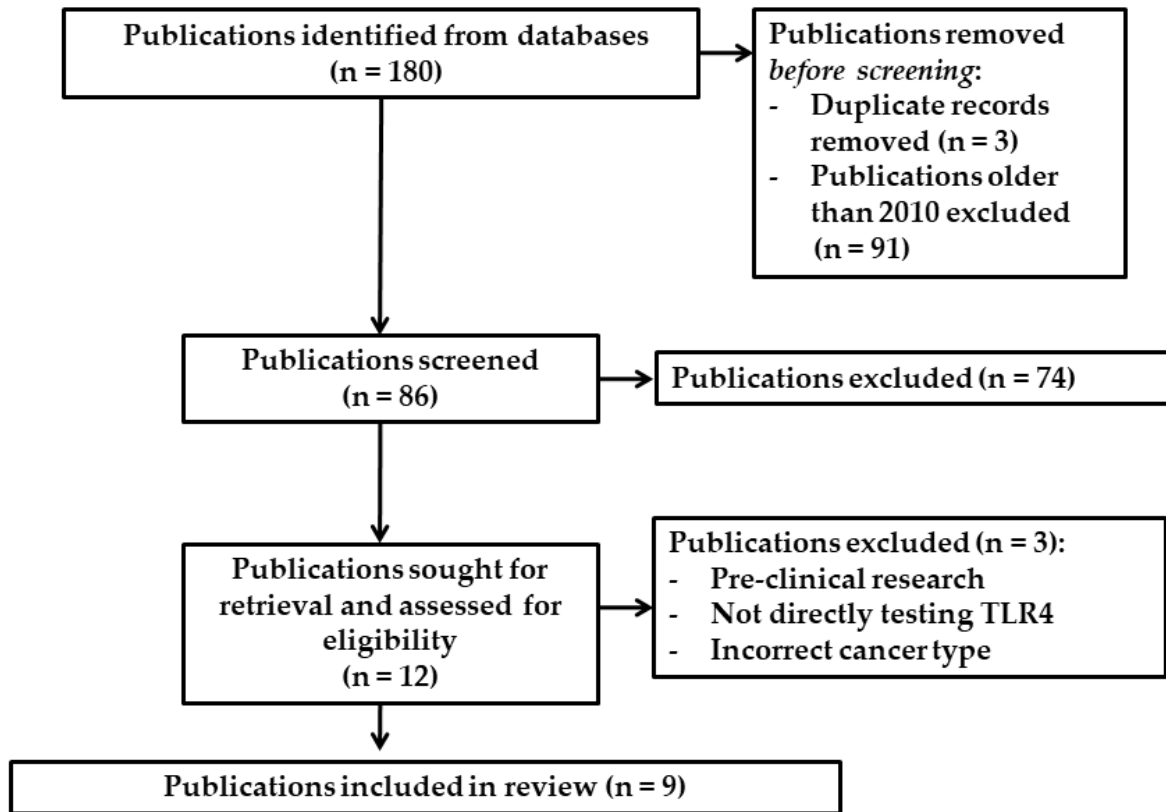


**Figure 1:** Flow diagram of literature search results for systematic review.

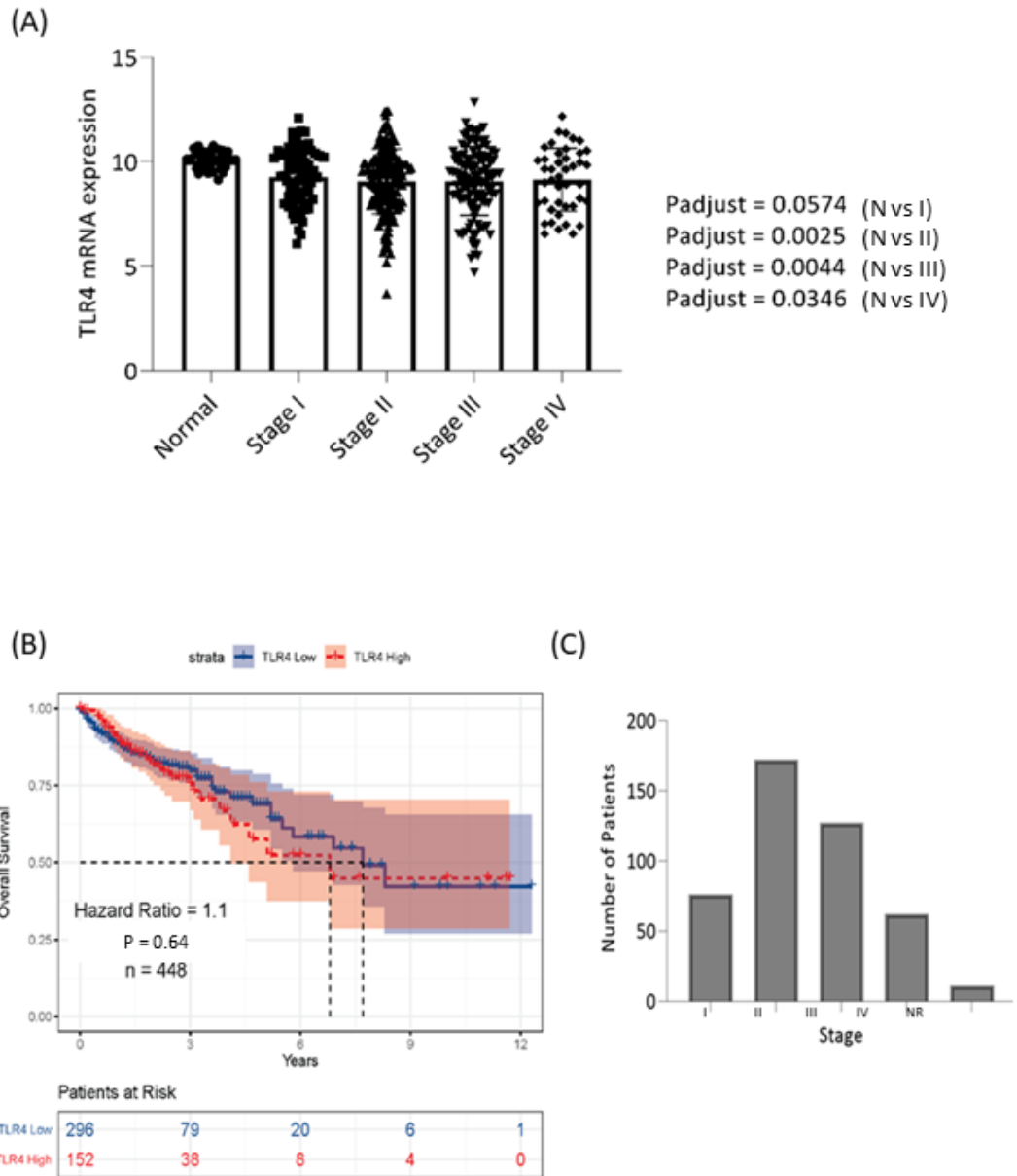


**Figure 2:** (A) Comparison of TLR4 expression between stage specific tumor and adjacent normal tissues from TCGA cohort. One-way ANOVA was performed by comparing solid tissue normal vs stage I, stage II, stage III, and stage IV participants. Statistical significance was represented as  $P < 0.05$ . (B, C) Assessment of TLR4 mRNA expression using the tertile cut-point. (B) Kaplan-Meier curves of overall survival (OS) in TCGA cohort. (C) Bar plot depicting the stage distribution of the cohort.

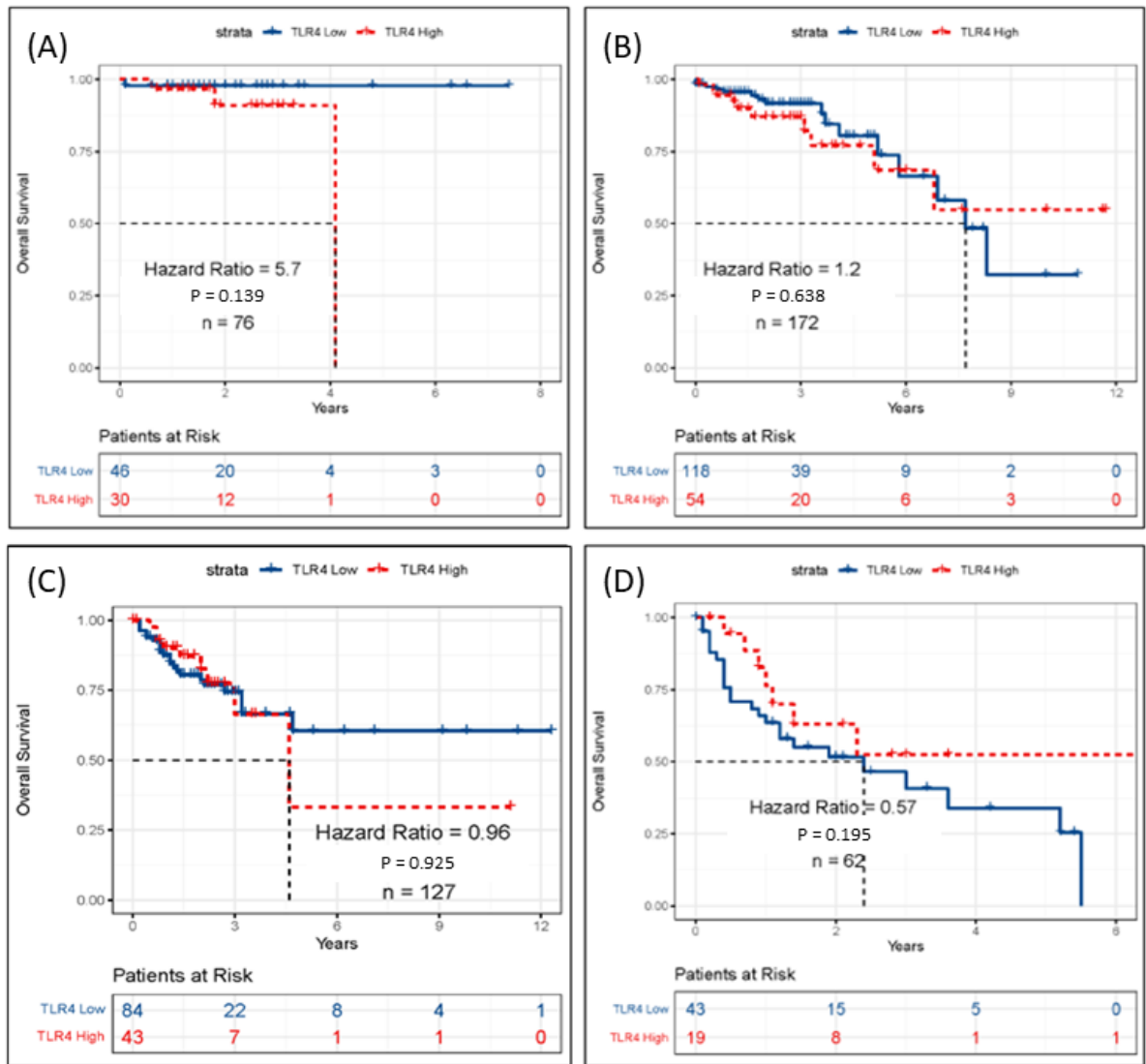


**Figure 3:** Assessment of TLR4 mRNA expression in stage specific CRC participants from TCGA cohort. (A) Kaplan-Meier curves depicting the OS in stage I participants (B) stage II participants, (C) stage III participants and (D) stage IV participants using the tertile cut point. No significant difference between groups.

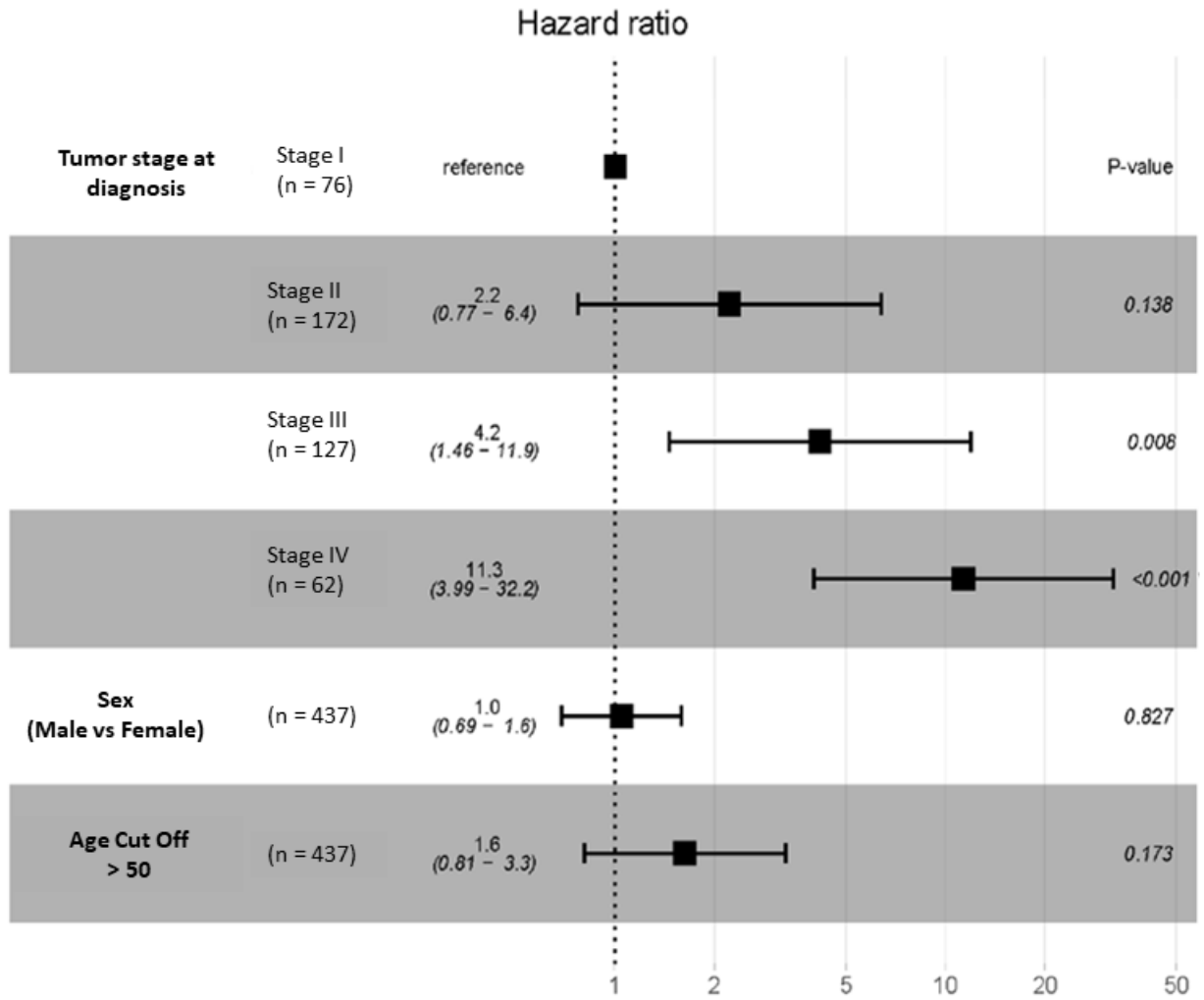


**Figure 4:** Forest plot of OS in stage specific participants. The tertile cut-point, the p-values and HRs with 95% CI derived for measurement of the cohorts from assessing the cut-point were shown. Statistical significance was represented as  $P < 0.05$ .

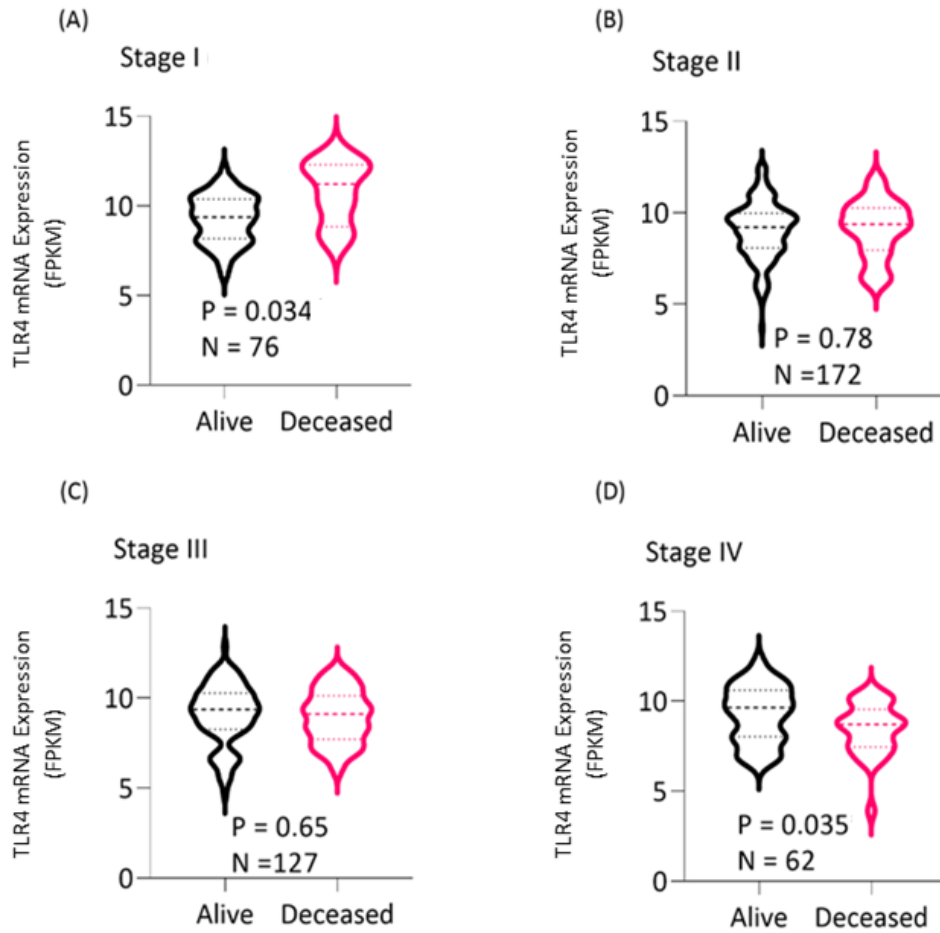


**Figure 5:** Comparison of TLR4 expression in Fragments per Kilobase of transcript, per Million mapped reads (FPKM) with respect to OS. Analysis of TLR4 expression using two sample t-test based on participants' survival in (A) stage I, (B) stage II, (C) stage III, and (D) stage IV participants. Statistical significance was represented as  $P < 0.05$ .

TLR4 in Clinical Colorectal Cancer

Table 1: Summary of studies investigating impacts of TLR4 expression on human CRC clinical outcome

Author (Date)	Archival / Clinical Study	Sample Size (n)	CRC Stage	Anti-Cancer Treatments	TLR4 Analysis	Site-Specific TLR4 (Y/N)	Survival Outcomes (Y/N)	Type of Survival	Cancer Recurrence (Y/N)	Key Findings
Cammarota et. al. (2010)	Archival	132	Mixed stage, stages I - IV	NR	IHC	Y	Y	DFS	Y	- ↑ TLR4 cells = ↑ grade of dysplasia. - ↓ % of TLR4+ cells in the tumor stromal compartment = ↑ DFS and later relapse compared to ↑ % of TLR4+ cells in the stromal compartment (RR 2.36; log rank chi-square 4.25, p < 0.05).
Tesniere et. al. (2010)	Clinical trial	668	Non-resectable metastases of colorectal adenocarcinoma and Stage II non-metastatic CRC	LV5FU2 followed by FOLFOX6 to FOLFOX6 and by FOLFIRI, or, surgical removal of the tumor	PCR <i>TLR4</i>	N	Y	PFS, or, progression 5 years after diagnosis	Y	- WT <i>TLR4</i> allele = ↑ PFS (HR: 0.73; CI=0.53–1.00; P<0.05) and OS (HR=0.72; CI =0.52–1.01); P=0.05), compared to loss-of-function <i>TLR4</i> allele following treatment.
Wang et. al. (2010)	Clinical trial	138	Mixed stage, stages I - IV	Surgery, chemotherapy and/or radiation treatment details NR.	IHC	N	Y	DFS and OS	N	- ↑ TLR4 = ↓ 5-year DFS (HR (95% CI) 1.62 (0.87 – 2.99), P = 0.1213) and ↓ 5-year OS (HR (95% CI) 2.17 (1.15 – 4.07), P = 0.015). - ↑ TLR4+MyD88 = ↓ 5-year DFS (HR (95% CI) 2.25 (1.27 – 3.99) P = 0.0053) and ↓ 5-year OS (HR (95% CI) 2.97 (1.64 – 5.38) P = 0.0003).



TLR4 in Clinical Colorectal Cancer

										<ul style="list-style-type: none"> <li>- ↑ TLR4 expression was significantly associated with liver metastasis (P=0.0001)</li> <li>- ↑ co-expression of TLR4/MyD88 was significantly associated with vascular invasion (P=0.0186), liver metastasis (P=0.0002), and TNM stage (P=0.0036).</li> </ul>
Eiro et. al. (2013)	Clinical trial	104	Resectable, mixed stage, tumor stages I - IV	Surgery, varying chemotherapy and radiation treatments throughout sample population	IHC	Y	Y	OS	Y	<ul style="list-style-type: none"> <li>- ↑ TLR4 expression by tumor cells = ↓ rate of tumor recurrence (P=0.01)</li> <li>- ↑ TLR4 expression by fibroblasts = ↑ tumor recurrence (P=0.019)</li> <li>- TLR4 expression by fibroblasts = ↓ OS (P=0.022).</li> <li>- TLR4 expression by fibroblasts was an independent factor associated with relapse-free survival (P=0.0001), and OS (P=0.013).</li> </ul>
Formica et. al. (2013)	Clinical trial	31	Mixed stage, stages I to III	FOLFIRI with bevacizumab	FC of TLR4 on neutrophils	Y	Y	PFS and OS	N	<ul style="list-style-type: none"> <li>- No association between baseline or one-month post-treatment neutrophilic TLR4 expression and PFS or OS (P = 0.30 and P = 0.34 respectively).</li> </ul>
Sussman et. al. (2014)	Archival	279	Mixed stage, stages I - IV	NR	IHC	Y	Y	OS	N	<ul style="list-style-type: none"> <li>- No difference in TLR4 stromal staining and OS (P = 0.16), no difference in epithelial TLR4 staining and OS (P = 0.11).</li> </ul>

TLR4 in Clinical Colorectal Cancer

										<ul style="list-style-type: none"> <li>- ↑ TLR4 tumor stroma intensity score in stages 3 and 4 compared to stage 1 (Stage 1 = 2.80, Stage 2 = 3.24, Stage 3 = 4.36, Stage 4 = 3.75; p = NS, 0.0004, and 0.04, respectively).</li> <li>- ↑ TLR4 tumor epithelium intensity score for stages 2 and 3 compared to stage 1 (Stage 1 = 0.17, Stage 2 = 0.64, Stage 3 = 0.64, Stage 4 = 0.92; p = 0.01, 0.002, and NS, respectively).</li> </ul>
Gray et. al. (2019)	Clinical trial	4877	Mixed stages inclusive of stage II, stage III and stable or responding metastatic CRC	SCOT trial (ISRCTN59757862): oxaliplatin-based adjuvant chemotherapy COIN trial (ISRCTN27286448): cetuximab added to oxaliplatin-based chemotherapy	PCR <i>TLR4</i>	N	Y	DFS and OS	N	<ul style="list-style-type: none"> <li>- SCOT trial: no statistically significant association of any <i>TLR4</i> SNP and OS or DFS.</li> <li>- COIN trial: no statistically significant association of either <i>TLR4</i> SNP with OS or DFS.</li> </ul>
Zhang et. al. (2019)	Clinical trial	94	Advanced stage, stages II and III	Standard 5-Fu-based adjuvant chemotherapy after radical surgery	WB, IHC	N	Y	DFS	Y	<ul style="list-style-type: none"> <li>- ↑ Fn (P = 0.028) and ↑ BIRC3 expression (P = 0.046) correlated with ↓ DFS.</li> <li>- TLR4 expression was independent of DFS; TLR4 was not a factor in univariate or multivariate cox regression analyses for DFS.</li> </ul>

TLR4 in Clinical Colorectal Cancer

										- ↑ TLR4 (p = 0.036) and ↑ BIRC3 (p = 0.008) resulted in ↑ recurrence.
Wong et. al. (2021)	Clinical trial	46	Mixed stage, stages III-IV	Irinotecan monotherapy or in combination with 5-Fu and IFL regimen	PCR <i>TLR4</i>	N	N	NR	N	- Participants with <i>TLR4</i> SNPs rs4986790, rs4986791 ↑ severe diarrhoea (50%) than wild-type homozygous (15%). - Participants with <i>TLR4</i> SNPs presented any grade of diarrhoea, contrasting with one half of the AA and CC WT groups (20 patients each, AG + GG, P = 0.012 vs. AA; and CT + TT, P = 0.012 vs. CC) that showed no signs of gastrointestinal toxicity - No impact of <i>TLR4</i> polymorphisms on occurrence / severity of nausea

\* Calcium leucovorin, citrovorum factor, folinic acid (LV5FU2), folinic acid, fluorouracil, and oxaliplatin (FOLFOX6), fluorouracil, leucovorin and irinotecan (FOLFIRI), Fluorouracil (5-Fu), irinotecan, folinic acid, and fluorouracil (IFL). Immunohistochemistry (IHC), polymerase-chain reaction (PCR), flow cytometry (FC), western blot (WB). Overall survival (OS), disease-free survival (DFS), progression-free survival (PFS). No record (NR)

Supporting information Table 1: literature database search strategies and publication results.

TLR4 in Clinical Colorectal Cancer

Database	Date Accessed	Search Strategy	Identified Literature
PubMed	January 2022 – February 2022	“Toll-Like Receptor 4”[mh] OR TLR4[tiab] OR Toll 4 Receptor[tiab] OR Toll Like Receptor 4[tiab] AND “Antineoplastic Protocols”[mh] OR chemotherap*[tiab] NOT (“Animals”[Mesh] NOT (“Animals”[Mesh] AND “Humans”[Mesh])) and (((“Toll-Like Receptor 4”[mh] OR TLR4[tiab] OR Toll 4 Receptor[tiab] OR Toll Like Receptor 4[tiab]) AND (“Antineoplastic Protocols”[mh] OR chemotherap*[tiab])) AND (colon OR colo* OR bowel)) AND (cancer OR cancer* OR tumour* OR tumor) NOT (“Animals”[Mesh] NOT (“Animals”[Mesh] AND “Humans”[Mesh])) AND (((“Toll-Like Receptor 4”[mh] OR TLR4[tiab] OR Toll 4 Receptor[tiab] OR Toll Like Receptor 4[tiab]) AND (“Antineoplastic Protocols”[mh] OR chemotherap*[tiab])) AND (colon OR colo* OR bowel)) AND (cancer OR cancer* OR tumour* OR tumor) NOT (“Animals”[Mesh] NOT (“Animals”[Mesh] AND “Humans”[Mesh]))).	36 individual publications <ul style="list-style-type: none"> <li>- 34 when within 2010 – 2021 timeframe</li> <li>- only 2 conformed with eligibility criteria</li> </ul>
Cochrane Library	January 2022 – February 2022	“Trials AND TLR4 AND cancer and colorectal”	5 individual publications <ul style="list-style-type: none"> <li>- No publications conformed with eligibility criteria</li> </ul>
Embase	January 2022 – February 2022	“Toll Like Receptor 4”/de OR TLR4:ti,ab OR “Toll 4 Receptor*”:ti,ab OR “Toll Like Receptor 4”:ti,ab AND “Antineoplastic Protocols”:ti,ab OR chemotherap*:ti,ab OR chemotherapy/exp NOT ([animals]/lim NOT [humans]/lim) and ('toll like receptor 4'/de OR tlr4:ti,ab OR 'toll 4 receptor*':ti,ab OR 'toll like receptor 4':ti,ab) AND ('antineoplastic protocols':ti,ab OR chemotherap*:ti,ab OR 'chemotherapy'/exp) AND (colon OR colorectal OR bowel OR intestine) NOT ([animals]/lim NOT [humans]/lim) AND (cancer OR tumour OR tumor OR 'malignant neoplasm').  and  ((Toll Like Receptor 4 or TLR4 or Toll 4 Receptor* or Toll Like Receptor 4) and (Antineoplastic Protocols or chemotherap* or chemotherapy) and (toll like receptor 4 or tlr4 or toll 4 receptor* or toll like receptor 4) and (antineoplastic protocols or chemotherap* or 'chemotherapy) and (colon or colorectal or bowel or intestine) and (cancer or tumour or tumor or malignant neoplasm)).af	139 individual publications <ul style="list-style-type: none"> <li>- 52 when within 2010 – 2021 timeframe</li> <li>- 3 duplicates removed</li> <li>- 4 articles removed due to ineligibility with inclusion and exclusion criteria</li> <li>- Only 7 conformed with eligibility criteria</li> </ul>

**Supporting Information Table 2:** Summary of clinical participant data (n = 448) from TCGA analyses. Data are n (%) unless otherwise stated. Data extracted on 6/6/2020.

<b>Characteristic</b>	<b>N (%)</b>
<b>Age</b>	
Median (Range)	68.00 (31-90)
<b>Sex</b>	
Male	239 (53)
Female	209 (47)
<b>CRC stage at prognosis</b>	
I	76 (17)
II	172 (38)
III	127 (28)
IV	62 (14)
not reported	11 (2)
<b>TLR4 (CPM)</b>	
Median (Range)	9.23 (3.7-2.8)
<b>Site of resection or biopsy</b>	
Ascending colon	87 (19)
Cecum	90 (20)
Colon, NOS	98 (22)
Descending colon	16 (4)
Hepatic flexure of colon	15 (3)
Recto sigmoid junction	8 (2)
Sigmoid colon	110 (25)
Splenic flexure of colon	5 (1)
Transverse colon	19 (4)
<b>Vital Status</b>	
Alive	352 (79)
Deceased	96 (21)
<b>History of neo-adjuvant treatment</b>	
Yes	0 (0)
No	448 (100)



# Aquaporin ion conductance properties defined by membrane environment, protein structure, and cell physiology

Sam W. Henderson<sup>1</sup> · Saeed Nourmohammadi<sup>1</sup> · Sunita A. Ramesh<sup>2</sup> · Andrea J. Yool<sup>1</sup>

Received: 22 October 2021 / Accepted: 9 December 2021 / Published online: 11 January 2022  
© International Union for Pure and Applied Biophysics (IUPAB) and Springer-Verlag GmbH Germany, part of Springer Nature 2021

## Abstract

Aquaporins (AQPs) are multifunctional transmembrane channel proteins permeable to water and an expanding array of solutes. AQP-mediated ion channel activity was first observed when purified AQP0 from bovine lens was incorporated into lipid bilayers. Electrophysiological properties of ion-conducting AQPs since discovered in plants, invertebrates, and mammals have been assessed using native, reconstituted, and heterologously expressed channels. Accumulating evidence is defining amino acid residues that govern differential solute permeability through intrasubunit and central pores of AQP tetramers. Rings of charged and hydrophobic residues around pores influence AQP selectivity, and are candidates for further work to define motifs that distinguish ion conduction capability, versus strict water and glycerol permeability. Similarities between AQP ion channels thus far include large single channel conductances and long open times, but differences in ionic selectivity, permeability to divalent cations, and mechanisms of gating (e.g., by voltage, pH, and cyclic nucleotides) are unique to subtypes. Effects of lipid environments in modulating parameters such as single channel amplitude could explain in part the variations in AQP ion channel properties observed across preparations. Physiological roles of the ion-conducting AQP classes span diverse processes including regulation of cell motility, organellar pH, neural development, signaling, and nutrient acquisition. Advances in computational methods can generate testable predictions of AQP structure–function relationships, which combined with innovative high-throughput assays could revolutionize the field in defining essential properties of ion-conducting AQPs, discovering new AQP ion channels, and understanding the effects of AQP interactions with proteins, signaling cascades, and membrane lipids.

**Keywords** Aquaporin · Patch clamp · Ion channel · Phospholipid bilayer · Membrane · Protein structure

## Introduction

Aquaporins (AQPs) are multifunctional proteins known for their capacity to facilitate water flux across cell membranes. They are governed by a diverse array of physiologically relevant control mechanisms, including phosphorylation, pH,  $\text{Ca}^{2+}$  and osmotic gradients (Tyerman et al. 2021). In addition to facilitating water flux, AQPs across phyla have an unexpected breadth of roles in transporting gases such as carbon dioxide ( $\text{CO}_2$ ) and oxygen ( $\text{O}_2$ ); ions such as sodium ( $\text{Na}^+$ ), potassium ( $\text{K}^+$ ) and chloride ( $\text{Cl}^-$ ); signaling agents

such as hydrogen peroxide ( $\text{H}_2\text{O}_2$ ), purines and pyrimidines; metabolites and nutrients including glycine, lactic acid, urea, ammonia ( $\text{NH}_3$ ), glycerol, polyols and more, contributing much more than simple water permeation to cells and tissues (Conde et al. 2010; Hachez and Chaumont 2010; Wagner et al. 2021; Ishibashi et al. 1994; Hara-Chikuma et al. 2015; Bienert et al. 2008; Jahn et al. 2004; Uehlein et al. 2003). Preceding the first discovery that AQPs mediated transmembrane water permeability (Preston et al. 1992), the bovine (*Bos taurus*) Major Intrinsic Protein of lens fiber 26 (MIP26, now classified as AQP0), was shown to conduct ions using black lipid membrane (BLM) bilayer electrophysiological techniques (Ehring et al. 1990; Shen et al. 1991; Zampighi et al. 1985). Since then, more subtypes of AQPs have been identified as either anion or cation permeable channels, including two classes from human, one from *Drosophila melanogaster* and four from plants. Emerging evidence supports the physiological relevance of AQP ion

✉ Andrea J. Yool  
andrea.yool@adelaide.edu.au

<sup>1</sup> School of Biomedicine, University of Adelaide, Adelaide, SA 5005, Australia

<sup>2</sup> College of Science and Engineering, Flinders University, Bedford Park, SA 5042, Australia

channel functions in motility, volume regulation, and adaptive responses to environmental stimuli. In silico and micro-organism-based approaches are promising tools that could be used for characterizing AQP ion channel activity that, with electrophysiological approaches, could help address remaining knowledge gaps of AQP-mediated ion channel function.

## AQP ion channel activity in native, heterologous and recombinant expression systems

Ion conduction properties are evident from published studies of AQP channels across different phyla, with continuing work beginning to identify the structural components that regulate ion conduction through AQP monomeric and tetrameric pores. Three of the classes of ion-conducting AQPs have been tested in bilayers as well as expression systems; these are described below, summarizing ion selectivity, mechanisms of activation, and regulation of function.

### 1. Major intrinsic protein of lens tissue (MIP)

Bovine MIP (MIP26, referred to here as BtAQP0) was the first cloned mammalian AQP (Gorin et al. 1984), later redesignated AQP0 (Agre et al. 1993). AQP0 is highly expressed in ocular lens fibre cells, and was initially considered to be a gap junction protein, not a water channel. Cloned BtAQP0 cDNA was predicted to encode a 26 kDa protein comprising six transmembrane segments that formed a channel-like pore (Gorin et al. 1984), features later confirmed as ubiquitous across the AQP family. Ion channel activity was evident within 5 to 10 min after purified BtAQP0-enriched lens membrane proteins were added to a preformed planar lipid bilayer (Zampighi et al. 1985). Channels were voltage dependent with a single channel amplitude of 200 pS in 100 mM KCl (Zampighi et al. 1985). HPLC-purified BtAQP0 was relatively anion selective in planar bilayers ( $P_{Cl^-}/P_{K^+}$  approximately 1.8) and showed two main conductance states (160 and 380 pS) plus multiple sub-conductance states in 100 mM KCl (Ehring et al. 1990). Further experiments using spectrometry in liposomes and electrophysiology in planar bilayers showed that BtAQP0 was permeable to  $K^+$ , sucrose, and  $Na^+$  (Shen et al. 1991). The open probability of the channel was inversely proportional to voltage, and  $Cs^+$  reduced the mean channel opening time (0.13 s) but did not decrease the single-channel conductance in 100 mM KCl (Shen et al. 1991), implying that BtAQP0 gating but not pore permeation is modulated by cations. Phosphorylation of BtAQP0 at serine-243 located near the C-terminus is required for voltage-dependent closure of the channels, reconstituted into planar lipid bilayers (Ehring et al. 1992). Sucrose permeability of BtAQP0

reconstituted into liposomes, measured by osmotic swelling, was blocked in the presence of  $Ca^{2+}$  and calmodulin (CaM);  $Mg^{2+}$  had no effect (Girsch and Peracchia 1985). Membranes from chicken lens enriched in a MIP homolog (originally named MIP28, referred to here as GdAQP0) also formed channels with functional properties similar to those of BtAQP0 (Modesto et al. 1990); two prominent unitary conductances (60 and 290 pS in symmetric 150 mM KCl) were voltage-dependent, closing at  $\pm 80$  mV. Channels were relatively anion preferring, with a permeability ratio ( $P_{Cl^-}/P_{K^+}$ ) of 1.87; open probability was reduced in the presence of 5 mM  $Ca^{2+}$  (Modesto et al. 1996). However unlike BtAQP0, GdAQP0 channels were not phosphorylated at the C-terminus. A C-terminal truncated variant generated by partial hydrolysis, lacking the equivalent serine-243 of BtAQP0, retained conductance and voltage sensitivity properties similar to those of the full-length GdAQP0 channel (Modesto et al. 1996). These studies showed in liposomes and planar bilayers that AQP0 proteins are non-selective ion channels with long open and closed times, and multiple conductance states that are modulated by phosphorylation (in BtAQP0) and  $Ca^{2+}$ .

Although the original studies showed robust and reproducible ion channel activity in artificial bilayers, no currents associated with BtAQP0 expression were detected in *Xenopus laevis* oocytes using the two-electrode voltage clamp (TEVC) technique (Mulders et al. 1995). This work did confirm that BtAQP0-expressing oocytes showed a 4- to fivefold increase in water permeability as compared to water-injected control oocytes (Mulders et al. 1995). The water channel activity of BtAQP0 expressed in oocytes showed positive correlations with the concentrations of  $Ca^{2+}$  and protons ( $H^+$ ) (Németh-Cahalan et al. 2013). Each BtAQP0 monomer was suggested to act cooperatively in the tetrameric AQP0 channel (Németh-Cahalan et al. 2013). A comparison of the single channel properties of AQP0 in oocytes with those previously determined in BLMs would be interesting to assess details of  $Ca^{2+}$  and pH modulation, and possible effects of membrane lipid environments.

### 2. Nodulin-26

Nodulin-26 (NOD26) is the major protein present in peribacteroid membranes of the nitrogen-fixing root nodules in soybean *Glycine max* (Fortin et al. 1987). Cloned GmNOD26 was noted to show amino acid sequence similarities to AQP0 and AQP1, and proposed to facilitate nutrient fluxes between the plant and the symbiotic bacteria living within the root nodules (Miao and Verma 1993). The first functional characterisation involved the incorporation of purified native GmNOD26 from soybean root membranes into BLMs, revealing GmNOD26 was an ion channel with a large unitary conductance (3.1 nS) in 1 M KCl (Weaver

et al. 1994). Weakly selective for anions, as indicated by a permeability ratio ( $P_{\text{Cl}^-}/P_{\text{K}^+}$ ) of 1.21, GmNOD26 displayed channel open times ranging from 1 to 50 ms, and subconductance states ranging from 0.5 to 2.5 nS. Recombinant poly-histidine tagged GmNOD26 protein produced in *E. coli* showed almost identical biophysical properties to native GmNOD26 in BLMs (Lee et al. 1995). A Ser-262-Asp phosphomimetic mutant of GmNOD26 showed more frequent closure and preferential occupancy of lower subconductance states than wild type, which indicated phosphorylation modulates NOD26 ion conductivity (Lee et al. 1995). The physical properties of GmNOD26 in planar lipid bilayers are strikingly similar to those of MIP channels measured in the same system.

Using *Xenopus* oocytes and proteoliposomes, GmNOD26 was later shown to be a water channel with a relatively low transport rate, as well as a glycerol facilitator (Dean et al. 1999; Rivers et al. 1997). Treatment of GmNOD26-expressing oocytes with the phosphatase type 1 and 2A inhibitor okadaic acid, led to a fourfold increase in water permeability (Guenther et al. 2003). This suggested that  $\text{Ca}^{2+}$ -dependent protein kinase phosphorylation at Ser-262, which occurs *in planta*, stimulates GmNOD26 water channel activity (Guenther et al. 2003). It is interesting that phosphorylation at Ser-262 stimulated NOD26 water channel activity in oocytes, but inhibited its ion channel activity in BLMs. Supporting the originally proposed role of GmNOD26 in nutrient flux, the recombinant channel reconstituted into proteoliposomes was shown to be  $\text{NH}_3$  permeable.  $\text{NH}_3$  uptake, protonation, and subsequent alkalisation of the liposome interior were measured by monitoring decreased fluorescence of preloaded carboxyfluorescein using stopped-flow spectrophotometry (Hwang et al. 2010). Hence GmNOD26 is now considered to be multifunctional.

### 3. Aquaporin 1 (AQP1)

The Channel-forming Integral Protein of 28 kDa (CHIP28) isolated from erythrocytes showed an amino acid similarity with BtAQP0 that prompted the idea it might have channel-like activity (Smith and Agre 1991). Expressed in *Xenopus* oocytes, CHIP28 showed constitutive water channel activity (Preston et al. 1992) and was renamed AQP1 (referred to here as HsAQP1). A non-selective monovalent cationic conductance with a permeability sequence  $\text{K}^+ \approx \text{Cs}^+ > \text{Na}^+ > \text{tetraethylammonium (TEA}^+)$  was shown using TEVC in HsAQP1-expressing oocytes, after indirect activation by forskolin or intracellular injection of protein kinase A catalytic subunit (Yool et al. 1996) via an H7-sensitive kinase signaling pathway proposed to enhance cGMP (Yool and Stamer 2004). Single HsAQP1 channels from inside-out patches of oocyte membranes were directly activated by cGMP, and showed a unitary conductance of 150 pS in

symmetrical 0.1 M  $\text{K}^+$  with flickery subconductance states (Anthony et al. 2000). To assess native AQP1 ion channels, the rat (*Rattus norvegicus*) homolog (RnAQP1) was examined in primary cultured choroid plexus cells, patch-clamped in whole cell and excised patch configurations. A cGMP-activated,  $\text{Cd}^{2+}$ -sensitive, monovalent cation conductance of 166 pS was characterized, with properties comparable to those of HsAQP1 channels expressed in oocytes (Boassa et al. 2006; Anthony et al. 2000). The cGMP-dependent AQP1-like channel activity was abrogated in cells transfected with siRNA constructs to knock down RnAQP1 expression (Boassa et al. 2006). However when purified native or recombinant HsAQP1 was reconstituted into planar lipid bilayers, cGMP activation gave rise to channel events with small unitary conductances of 2, 6, and 10 pS in 0.1 M  $\text{Na}^+$  or  $\text{K}^+$  (Saparov et al. 2001). The small unitary conductances might reflect differences in the physical properties of the bilayers in reconstituted versus eukaryotic cell membranes. The recombinant HsAQP1 channels studied by Saparov et al. (2001) were assessed in bilayers formed with *E. coli* total lipids, consisting predominantly of phosphatidylethanolamine (PE). Preliminary data in our lab (Henderson et al., unpublished) suggest that recombinant HsAQP1 produces high conductance single channels ( $\sim 75$  pS) with long open times when reconstituted into proteoliposomes made with soybean azolectin (Fig. 1) which consists predominantly of phosphatidylcholine (PC), as used successfully for studies of mechanosensitive and other ion channels (Martinaic et al. 2010). The difference in headgroups (ethanolamine or choline) between PE and PC can influence transmembrane protein structure, as shown for  $\mu$  opioid receptors with conformational states controlled by lipid interactions (Angladon et al. 2019). Lipids affect properties of many channel types (see below), and might be expected to influence the structure and function of AQP channels as well. Patch-clamping proteoliposomes with various defined lipid compositions should enable comparisons of environmental effects on ion channel activity of AQP1 and other AQPs to test the hypothesis that membrane lipids modulate AQP channel activity.

### Differences in aquaporin channel properties could depend on membrane composition

Membrane protein activity (e.g., of mechanosensitive channels, KcsA  $\text{K}^+$  channels, and nicotinic acetylcholine receptors) is affected by the physical properties of the surrounding lipid environment, including thickness, elasticity, viscosity, and tension (Lee 2004). As summarized above, properties of ion conducting AQPs differ between membrane preparations. The sensitivity of AQPs to the lipid environment is supported by results of studies of water channel activity, which also show variability when



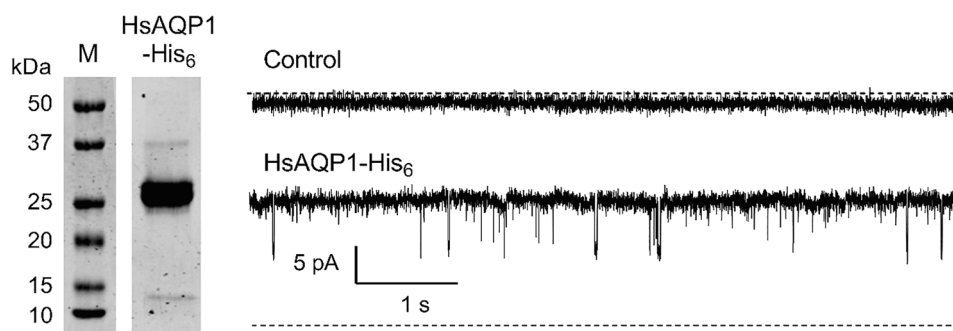


**Fig. 1** Single channel activity of recombinant histidine-tagged human AQP1 reconstituted into proteoliposomes measured using the patch-clamp technique. (Left) Coomassie stained SDS-PAGE of purified recombinant HsAQP-His<sub>6</sub>. (Right) Upper trace is a patch from a control (empty) liposome showing no channel activity. Lower trace is a

patch from an HsAQP1-His<sub>6</sub> reconstituted liposome showing closing events (downward deflections, estimated unitary conductance 75 pS). Both patches were recorded in the presence of 10  $\mu$ M CPT-cGMP at a holding potential of +100 mV in symmetrical K<sup>+</sup>. Dashed lines indicate the zero current levels

channels are reconstituted into proteoliposomes comprising different lipid types and proportions. Single channel water fluxes in two reconstituted human AQP4 isoforms decreased with increasing membrane bilayer compressibility and thickness, induced by addition of cholesterol and sphingomyelin (Tong et al. 2012). Similarly, the unitary water permeability of purified BtAQP0 was lower in proteoliposomes containing high cholesterol or sphingomyelin (Tong et al. 2013). Liposomes made from 1,2-dioleoyl-sn-glycero-3-phosphocholine (DOPC) showed high water permeability when reconstituted with AQPZ from *E. coli*; however, AQPZ did not enhance water permeability in liposomes made with 1,2-Dioleoyl-sn-glycero-3-phosphoglycerol (DOPG) (Zhao et al. 2013). The absence of cardiolipin, which is naturally prevalent in bacterial and mitochondrial membranes, was shown to reduce AQPZ water permeability in proteoliposomes (Laganowsky et al. 2014). Another factor setting the optimal water permeability of AQPZ was the lipid-to-protein ratio, which was maximal at 200:1 in proteoliposomes (Zhao et al. 2013).

The functional properties of several ion channels, for example K<sup>+</sup> ion channels and ligand-gated nicotinic acid receptors, are modified by the surrounding lipids or by direct lipid-protein interactions (Poveda et al. 2014; Tillman and Cascio 2003). It is reasonable to postulate that AQP ion channel activity is also modulated by changes in the lipid environment surrounding the protein, and could explain the variability in single channel conductance values reported for the same AQP in different cell or lipid bilayer preparations (Table 1). Experiments to determine AQP ion channel modulation by lipid composition should be feasible with proteoliposomes and BLMs. Some ion channel AQPs thus far have been tested only in eukaryotic cells such as *Xenopus* oocytes or human embryonic kidney (HEK) cells, so the potential influence of bilayer composition on channel properties remains to be determined.

## Other classes of ion channel AQPs

In addition to ion channel AQP classes presented in the “Introduction,” “AQP ion channel activity in native, heterologous and recombinant expression systems,” and “Differences in aquaporin channel properties could depend on membrane composition” sections above, several other subtypes have been shown to mediate macroscopic ion currents in expression systems, primarily *Xenopus* oocytes, but have not yet been characterized in purified reconstituted preparations. These classes are summarized below.

### 4. Aquaporin (AQP6)

Conflicting lines of evidence have been reported for the properties and gating of aquaporin 6 (AQP6). The human AQP6 coding sequence was first isolated from a kidney cDNA library, and denoted hKID (Ma et al. 1996). hKID mapped to the 12q13 locus, which also contained AQP0 and AQP2. When expressed in *Xenopus* oocytes, hKID (referred to here as HsAQP6) elicited a 2.6-fold increase in osmotic water permeability, which was inhibited 72% by mercury (Hg<sup>2+</sup>), in agreement with the precedent set for Hg<sup>2+</sup>-inhibition of AQP1-mediated osmotic water permeability (Preston et al. 1992). HsAQP6 expression in oocytes conferred no measurable glycerol or urea flux, suggesting that water was the only permeable substrate (Ma et al. 1996).

The homolog from rat (RnAQP6) initially could not be characterized (Ma et al. 1993) though subsequently was successfully expressed in oocytes. Unexpectedly, it was not blocked but was activated by Hg<sup>2+</sup>, which enhanced both water and ion fluxes (Yasui et al. 1999a). The ion conductance but not water permeability of RnAQP6 also was activated by acidic pH, which unlike Hg<sup>2+</sup> has relevance as a physiological stimulus. A positive shift in  $E_{rev}$  measured for acid-activated RnAQP6 when external Cl<sup>-</sup> was replaced with

**Table 1** Comparison of aquaporin ion channel properties measured using different techniques and preparations (N.D., not determined; N/A, not applicable)

AQP	Species of origin	Single channel cond	Sub-cond. states	Solutions	Gating	Selectivity	Method used	Reference
MIP26	Bovine purified from lens	380 pS and 160 pS	Yes	Symmetrical 0.1 M KCl	Voltage sensitive closure	$P_{Cl^-}/P_{K^+} < 1.8$	BLM	Ehring et al. (1990)
MIP26	Bovine HPLC-purified from lens	120 pS	No	Symmetrical 0.1 M KCl	Voltage sensitive closure	permeable to $K^+$ , sucrose, and $Na^+$	BLM and proteo-liposomes	Shen et al. (1991)
MIP26	Bovine Detergent solubilized lens	200 pS	Yes	Symmetrical 0.1 M KCl or NaCl	Voltage sensitive closure	$Na^+ = K^+$	BLM	Zampighi et al. (1985)
MIP28	Chicken (purified lens tissue)	290 pS and 60 pS	Yes	Symmetrical 0.15 M KCl	Voltage sensitive closure	$P_{Cl^-}/P_{K^+} = 1.87$	BLM	Modesto et al. (1996)
MIP <sub>tryp</sub>	Chicken purified lens tissue, trypsinated	1.5 nS	N.D	Symmetrical 0.3 M $K_2SO_4$	Voltage sensitive closure	N.D	BLM	Modesto et al. (1996)
NOD26	Soybean	3.1 nS	0.5, 1.1, 1.6, 1.9, and 2.5 nS	Symmetrical 1 M KCl	High voltage increased the occupancy of subconductance states	$P_{K^+}/P_{Cl^-} = 1.21$	BLM	Weaver et al. (1994)
NOD26-His	Soybean Recombin	3.1 nS and 2.2 nS	Infrequent occupancy of lower subconductance levels	cis 0.2 M/trans 1 M KCl	Kinase-dependent voltage gating	Slightly anionic	BLM	Lee et al. (1995)
NOD26-His S262A	Soybean Recombin	3.1 nS and 2.2 nS	N.D	cis 0.2 M/trans 1 M KCl	Infrequent transitions to lower subconductance states	Slightly anionic	BLM	Lee et al. (1995)
NOD26-His S262D	Soybean Recombin	3.1 nS	1.8 and 0.6 nS	cis 0.2 M/trans 1 M KCl	High voltage increased the occupancy of subconductance states	Slightly anionic	BLM	Lee et al. (1995)
AQP6	Rat	N/A	N/A	NaCl, Na-Glu, NMDG-Cl	Hg, acidic pH	$Cl^-$	Xenopus TEVC	Yasui et al. (1999a)
AQP6	Rat	49 pS	No	Symmetrical 0.1 M NaCl	Hg, acidic pH	$Na^+ = Cl^-$	Xenopus patch-clamp	Hazama et al. (2002)
AQP6	Rat	N/A	N/A	NaCl, $NaNO_3$	N/A	$NO_3^- > Cl^-$	Xenopus TEVC	Liu et al. (2005)
GFP-AQP6	Rat	N/A	N/A	Various	Acidic pH	$NO_3^- > \Gamma > Br^- > Cl^- > SO_4^{2-}$ ( $P_{NO_3^-}/P_{Cl^-} > 9.8$ )	HEK293 whole cell patch-clamp	Ikeda et al. (2002)
AQP1	Human	N/A	N/A	0.1 M Saline	Forskolin, cAMP	$Na^+ = K^+$	Xenopus TEVC	Yool et al. (1996)
AQP1	Human	150 pS	Yes	Symmetrical 0.1 M $K^+$	cGMP	$K^+ = Cs^+ > Na^+ > TEA^+$	Xenopus, patch-clamp	Anthony et al. (2000)

Table 1 (continued)

AQP	Species of origin	Single channel cond	Sub-cond. states	Solutions	Gating	Selectivity	Method used	Reference
AQP1	Human (red cells)	2, 6, and 10 pS	N.D	Symmetrical 0.1 M KCl or NaCl	cGMP	$P_{Cl^-}/P_{K^+} = 12$	BLM	Saparov et al. (2001)
His <sub>10</sub> -AQP1	Human (recombinant, <i>E. coli</i> )	2, 6, and 10 pS	N.D	Symmetrical 0.1 M KCl or NaCl	cGMP	$P_{Cl^-}/P_{K^+} = 12$	BLM	Saparov et al. (2001)
AQP1-His <sub>6</sub>	Human (recombinant, Yeast)	2, 6, and 10 pS	N.D	Symmetrical 0.1 M KCl or NaCl	cGMP	$P_{Cl^-}/P_{K^+} = 12$	BLM	Saparov et al. (2001)
AQP1	Rat	166 pS	N.D	Symmetrical monovalent cations	cGMP	Na <sup>+</sup> , K <sup>+</sup> , TEA <sup>+</sup> , and Cs <sup>+</sup>	Patch-clamp of choroid plexus cells	Boassa et al. (2006)
PIP2;1	Arabidopsis	N/A	N/A	96 mM NaCl, 2 mM KCl	Not gated. Blocked by Ca <sup>2+</sup> and Cd <sup>2+</sup>	Na <sup>+</sup>	Xenopus TEVC	Byrt et al. (2017)
PIP2;2	Arabidopsis	N/A	N/A	100 mM NaCl, 2 mM KCl	Not gated. Blocked by Ca <sup>2+</sup> , Cd <sup>2+</sup> , and Ba <sup>2+</sup>	Na <sup>+</sup>	Xenopus TEVC	Kourghi et al. (2017a)
PIP2;8	Barley	N/A	N/A	100 mM NaCl or 100 mM KCl	Not gated. Blocked by Ca <sup>2+</sup> , Cd <sup>2+</sup> , and Ba <sup>2+</sup>	Na <sup>+</sup> and K <sup>+</sup> (not Cs <sup>+</sup> , Rb <sup>+</sup> , or Li <sup>+</sup> )	Xenopus TEVC	Tran et al. (2020)
BIB	Drosophila	N/A	N/A	100 NaCl, 2 KCl, 4.5 MgCl <sub>2</sub>	Not gated. Blocked by Ca <sup>2+</sup> and Ba <sup>2+</sup>	K <sup>+</sup> > Na <sup>+</sup> >> TEA <sup>+</sup>	Xenopus TEVC	Yanochko and Yool (2002); Yanochko and Yool (2004)

gluconate, but not when  $\text{Na}^+$  was replaced with *N*-Methyl-D-glucamine (NMDG) (Yasui et al. 1999a), suggested currents were carried by  $\text{Cl}^-$  not  $\text{Na}^+$ . However,  $\text{Hg}^{2+}$ -activated single channels measured in inside-out patches of RnAQP6-expressing oocytes showed, in contrast, no change in  $E_{\text{rev}}$  when either  $\text{Na}^+$  or  $\text{Cl}^-$  were reduced, suggesting equal permeability to  $\text{Na}^+$  and  $\text{Cl}^-$  (Hazama et al. 2002). The  $\text{Na}^+$  permeability of  $\text{Hg}^{2+}$ -activated RnAQP6-expressing oocytes was validated with a  $^{22}\text{Na}$  radiotracer influx assay (Hazama et al. 2002). Similar tests showed fluxes of  $^{14}\text{C}$ -glycerol and  $^{14}\text{C}$ -urea in  $\text{Hg}^{2+}$ -activated RnAQP6-expressing oocytes (Holm et al. 2004), highlighting a potentially remarkable substrate diversity, but also illustrating the diversity of conclusions that have been drawn from different studies. Experimental parameters that influence channel function and baseline membrane permeability apparently remain to be fully defined.

In mammalian cells, the intracellular vesicular localization of RnAQP6 made electrophysiological analyses of ion channel activity difficult until a N-terminal GFP fusion construct was found to localize to plasma membrane in transfected HEK293 cells (Ikeda et al. 2002), enabling whole-cell patch-clamp measurement of acid-activated RnAQP6 currents. The GFP-RnAQP6 fusion protein showed permeability to halide anions with a permeability sequence:  $\text{NO}_3^- \geq \text{I}^- \geq \text{Br}^- \geq \text{Cl}^-$  (Ikeda et al. 2002). When Asn-60 was mutated to Gly, the anion permeability of RnAQP6 was abolished and the protein became highly water permeable in a  $\text{Hg}^{2+}$ -independent manner (Liu et al. 2005).

Differences in ionic selectivity of RnAQP6 when gated by  $\text{Hg}^{2+}$  (selective to water, anions, cations, glycerol and urea) or pH (selective to anions) suggest that  $\text{Hg}^{2+}$  and protons induce different structural changes that impact the AQP6 monomeric pore (Yasui et al. 1999a). The relevance of acid activation of RnAQP6 anion fluxes aligns with the subcellular localization of this channel in intracellular vesicles of acid-secreting cells of the kidney (Beitz et al. 2006a). Intriguingly, AQP6 anion channel activity has only been demonstrated for RnAQP6, and not for HsAQP6 despite high (77%) sequence identity. Opposing effects of  $\text{Hg}^{2+}$  on the water permeability of HsAQP6 and RnAQP6 warrant further clarification, since the cysteine residues that define the  $\text{Hg}^{2+}$  sensitivity of RnAQP6 have been identified (Cys-158 and Cys-193) (Yasui et al. 1999a), and are conserved in HsAQP6. Residues that determine pH-gating of RnAQP6 remain an area of interest for future investigation.

## 5. *Drosophila* big brain

*Drosophila* BIB amino acid sequence similarities to the AQPs MIP26, NOD26, and the *E. coli* glycerol facilitator GlpF led to speculation that BIB also was a channel-like protein (Rao et al. 1990). Unlike orthologous AQPs,

BIB showed no appreciable water channel activity when expressed in oocytes (Yanochko and Yool 2002). Conversely, BIB mediated a voltage-insensitive, nonselective cation conductance in oocytes with a permeability sequence of  $\text{K}^+ > \text{Na}^+ \gg \text{TEA}^+$  (Yanochko and Yool 2002). The BIB ion conductance was blocked by divalent cations  $\text{Ba}^{2+}$  and  $\text{Ca}^{2+}$  but not  $\text{Mg}^{2+}$  (Yanochko and Yool 2004). BIB currents were inactivated by tyrosine phosphorylation and activated by a tyrosine kinase inhibitor, consistent with regulated signaling roles for BIB in early nervous system development in the fly (Yanochko and Yool 2004; Rao et al. 1990).

## 6. Plasma membrane intrinsic protein 2;1 (PIP2;1) and homologs

A renaissance of AQP ion channel research in plants was catalyzed by the characterization of Plasma membrane Intrinsic Protein 2;1 (PIP2;1) from the model plant *Arabidopsis thaliana* as a non-selective cation channel when expressed in *Xenopus* oocytes, measured using TEVC (Byrt et al. 2017). Currents in AtPIP2;1-expressing oocytes resembled a  $\text{Ca}^{2+}$ -sensitive cation conductance previously measured in isolated *Arabidopsis* root cell protoplasts but not identified at the protein level (Demidchik and Tester 2002). AtPIP2;1 is now thought to be the molecular mechanism for the leak current (Byrt et al. 2017). An ortholog, AtPIP2;2 also elicited an ionic conductance when expressed in oocytes (Byrt et al. 2017). A homolog from barley, HvPIP2;8 in oocytes showed  $\text{Na}^+$  and  $\text{K}^+$  (but not  $\text{Cl}^-$ ) conductances that were inhibited by divalent cations (Tran et al. 2020). Other plant ion-channel AQPs likely await discovery. Phosphorylation status regulates the ionic conductance of AtPIP2;1 in oocytes (Qiu et al. 2020), fitting the broad theme seen across diverse AQP ion channel types reviewed here. To date, heterologous expression in *Xenopus* oocytes has been the primary experimental system used for measuring ion channel activity of PIP-type AQPs. Further research on plant AQP ion channel properties using proteoliposome reconstitution is in progress.

In summary, AQP ion channels show a panel of similar features. They are generally permeable to monovalent anions and/or cations, blocked by divalent cations (except  $\text{Mg}^{2+}$ ), can display large unitary conductances in permissive environments, with multiple conductance states and long open and closed times that are gated by subtype-specific signaling mechanisms (including for example pH, voltage, cyclic nucleotides, and phosphorylation). The activation of ion-conducting RnAQP6 intrasubunit pores by  $\text{Hg}^{2+}$  and the block of intrasubunit water pores in other AQPs relies on covalent modification of cysteine residues likely inducing protein conformational changes, rather than electrostatic interactions that reversibly block the pores (seen for example with  $\text{Ba}^{2+}$  and  $\text{Ca}^{2+}$ ). The cell type or membrane used

to measure AQP ion conductance can profoundly influence the observed ion channel activity. These properties are summarized in Table 1. Application of classical biophysical approaches, such as reconstitution into artificial membranes, may help further elucidate the functional properties of AQP ion channels, and guide future structure–function studies.

## The structural basis of AQP-mediated transport activity

In addition to the signature asparagine-proline-alanine (NPA) motifs in loops B and E, AQPs also show high conservation of a Glu residue in M1, and a His residue proximal to the first NPA domain in loop B, found with few exceptions across the broad MIP family (Reizer et al. 1993), as illustrated in the subset of ion channel AQPs shown in Fig. 2. An in-depth analysis of the conserved Glu/His pair in the aquaglyceroporin HsAQP10 (Gotfryd et al. 2018) showed glycerol permeability of the intrasubunit pore was regulated by a pH-dependent interaction of the M1 Glu residue with the conserved loop B His residue. Expressed in adipocytes, AQP10 mediates an increased rate of glycerol flux in response to an acidic change in intracellular pH during lipolysis in response to beta-adrenergic stimulation, enabling the physiological release of glycerol. Molecular modeling by Gotfryd and colleagues indicated that protonation of H80 in HsAQP10 at low pH facilitated reorientation and interaction with E27, widening the diameter of the intrasubunit pore to allow glycerol flux, without changing the basal level of water flux. The presence of the Glu/His gate alone is not sufficient to endow glycerol permeability; a comparison with other AQPs which have identical amino acids in equivalent positions showed no glycerol permeability at any pH (for example in the orthodox channel AQP2), or glycerol permeability at neutral not acidic pH in aquaglyceroporins AQPs 3, 7 and 9 (Gotfryd et al. 2018). It is interesting to speculate that this Glu/His pair of residues could be a ubiquitous subcomponent of complex AQP gating mechanisms that would appear to need involvement of other subtype-specific domains to achieve specialized mechanisms of action. A possible role in regulating ion channel AQPs, particularly subtypes such as RnAQP6 and DmBIB thought to allow ion permeation via the intrasubunit rather than the central pore (Yool and Campbell 2012; Yool 2007), remains to be determined.

Differential block of water and ion fluxes by pharmacological agents in mammalian AQP1 supports the presence of independent parallel permeation pathways that use the central pore for ion conduction and intrasubunit pores for water (Pei et al. 2016; Kourghi et al. 2017b). In a subset of AQPs, sites have been identified for reversible block of water flux by extracellular TEA<sup>+</sup> at Tyr (Y), and covalent block by mercuric compounds at Cys (C), as noted in Fig. 2a and covered

in prior reviews. Mutation of loop D residues changes ion channel activation and sensitivity to blockers of the ionic conductance (Kourghi et al. 2017b). A comparison of the level of sequence homology for the ion-conducting classes of AQPs is depicted as a phylogenetic tree (Fig. 2b), interestingly showing that the anion-preferring subtypes AQPs 0 and 6 are clustered together, as are the cation-preferring subtypes human AQP1 and plant PIP2;1 along with insect BIB. More distantly related are human AQP8 and plant NOD26, which are both permeable to NH<sub>3</sub> (Hwang et al. 2010; Saparov et al. 2007) and perhaps ammonium (NH<sub>4</sub><sup>+</sup>) based on AQP8-induced rescue of NH<sub>4</sub><sup>+</sup>-transporter-deficient yeast (Beitz et al. 2006b). The motifs that define the ion-conducting AQP subtypes are yet to be identified, but the process will be complicated for now by the likelihood that not all AQPs capable of conducting ions have been identified, and their potential activating stimuli remain unknown.

The substrate selectivity of the intrasubunit water pore is influenced by an electrostatic barrier formed by Asn side chains from the two NPA motifs, and by residues on the extracellular side of the NPA hourglass known as the aromatic/arginine selectivity filter that forms the narrowest section of the pore (Wang and Tajkhorshid 2007; Beitz et al. 2006b). The intrasubunit pore diameter is narrower in orthodox AQPs as compared with glycerol-permeable classes, accommodating single file water movement. The limiting diameter of the intrasubunit pore creates a selectivity filter, which in the water channel *E. coli* AQPZ, is framed by Phe and His as aromatic residues on one side, faced by a charged Arg on the opposite side. The aromatic residues at equivalent positions in the aquaglyceroporin *E. coli* GlpF are Trp and Phe, comparatively less polar than in the water-selective channels. Combined mutations of residues H-180, R-195, and F-56 in HsAQP1 enhanced permeability to NH<sub>3</sub>, urea or glycerol without altering water permeability, whereas mutations neutralizing the Arg charge appeared to allow the passage of protons, reinforcing the role of these residues in AQP substrate selectivity in the intrasubunit pore (Beitz et al. 2006b).

The central pore, located at the four-fold axis of symmetry in the tetramer, mediates cyclic GMP-dependent activation of a nonselective cation conductance in mammalian AQP1, gated by the loop D domain (Yu et al. 2006). In crystal structures presumed to reflect the ion channel closed state, the central pore is lined by inner and outer rings of hydrophobic Leu and Val residues contributed by the M2 and M5 domains of the four subunits. As well, at the intracellular face of the central pore, the distal half (Leu, Gly, Gly) of the four loop D domains covers the cytoplasmic vestibule, flanked by charged Arg-rich proximal half of the loop D domains which serve as the site of interaction with cyclic GMP (Fig. 2c). Binding of cGMP is proposed to facilitate a conformational change in loop D, opening the loops outward



away from the center of symmetry. In silico modeling suggests the loop D reorientation triggers the opening of the inner hydrophobic barrier, followed by pore hydration, opening of the outer hydrophobic barrier, and  $\text{Na}^+$  permeation. Site-directed double mutation of the first two Arg residues in the gating loop to Ala disrupted ion current activation by cGMP without altering osmotic water permeability, confirming the mutant channels were functional and targeted to the plasma membrane but lacked the Arg sites necessary for ion channel activation (Yu et al. 2006). The role of the central hydrophobic rings as barriers to ion permeation was tested by quadruple mutation of Val-50, Leu-54, Leu-170, Leu-174 all to Ala, which induced inward rectification and increased permeability to the bulky cation  $\text{TEA}^+$  compared to wild type AQP1. In the same study, mutation of Lys-51 to Cys at the external side of the central pore (in a cysteineless background) created de novo sensitivity of the ion conductance to block by mercury (Campbell et al. 2012). The C-terminus was found to have a modulatory role for AQP1 ion channel function (Boassa and Yool 2002). Phosphorylation of Tyr-253 in the carboxyl terminal domain, confirmed by Western blot, modulated the availability of the AQP1 channels to be activated by cGMP, suggesting that tyrosine phosphorylation state acts as a master switch (Campbell et al. 2012), perhaps one of many layers of control that sets the proportion of the AQP channel population that are dual water-and-ion channels, versus electrically silent pathways for principally just osmotic water flux. Even if only a tiny proportion ( $<0.002\%$ ) of AQP1 proteins were functional as ion channels in an epithelium, the outcome was predicted to have a meaningful physiological effect on net fluid and  $\text{Na}^+$  transport, based on quantitative modeling of renal proximal tubule function (Yool and Weinstein 2002).

Other AQPs such as AQP6 have been proposed to use the intrasubunit pores as the ion conducting pathways, based on the effects of specific mutations near the intrasubunit NPA domain and correlated effects on water permeation. Asn 60 in the AQP6 M2 domain (Fig. 2a) when mutated to Gly (characteristic of other AQP sequences at this position) was reported to eliminate the  $\text{Hg}^{2+}$ -induced anion permeation and enhance an otherwise low osmotic water flux as compared with wild type AQP6 (Liu et al. 2005). Lys-72 on the proximal side of the loop B NPA motif (Fig. 2a) when mutated to Glu changed AQP6 ion selectivity from anionic to cationic (Yasui et al. 1999a). A similar possibility has been proposed for the insect DmBIB aquaporin, which does not mediate osmotic water flux, but carries a nonselective cation current with properties that are strongly influenced by mutations of the conserved M1 Glu residue involved in intrasubunit pore gating (Yanochko and Yool 2004; Yool and Campbell 2012; Yool 2007).

In addition to gating the central pore in channels such as mammalian AQP1, loop D domains found in plant AQPs

such as spinach SoPIP2;1 are regulated by phosphorylation to control activity of the intrasubunit water pores, in response to changes in pH and salinity (Törnroth-Horsefield et al. 2006). The extended length of the SoPIP2;1 loop D domain allows it to interact in the unphosphorylated state, via H-bonds with the N-terminus, to occlude the intrasubunit pore and impose a closed state. Supported by molecular modeling, phosphorylation was shown to disrupt tethering, unblocking the pore by releasing loop D from the cytoplasmic vestibule site, and also retracting a hydrophobic barrier in the pore-lining domain to promote water flux, as an open state (Törnroth-Horsefield et al. 2006).

In sum, aquaporin channels in the MIP family serve as key mechanisms for transport and homeostatic regulation of diverse processes in prokaryotes and eukaryotes, facilitating transmembrane fluxes of water, glycerol, urea,  $\text{CO}_2$ , nitric oxide, and other small solutes. Emerging evidence across mammalian, insect and plant classes of AQPs shows that subsets of these channels also can conduct ions, as has been shown thus far for AQPs 0, 1, and 6, *Drosophila* BIB, soybean NOD26, and *Arabidopsis* AtPIP2;1. More classes are likely to be discovered.

## Physiological relevance of AQP ion conductivity

The biological roles of the subset of aquaporins that can transport both water and ions is a fascinating area of work that has only begun to be explored. AQP0, expressed in lens fibers, functions as an adhesive protein forming thin membrane junctions with low water permeability when expressed in *Xenopus* oocytes (Bloemendal and Hockwin 1982; Zampighi et al. 1985), and has been linked to regulation of gap junction channels, cell–cell adhesion and maintenance of ocular lens transparency (Chandy et al. 1997; Chepelinsky 2009). Reduced membrane expression of AQP0 channels due to missense mutations leads to impaired water flux and congenital cataracts in humans and mice (Berry et al. 2000; Varadaraj et al. 1999). Expression of AQP1 in the lens of AQP<sup>-/-</sup> knockout mice only partially restored lens transparency, which could reflect the additional role of AQP0 in cell–cell adhesion (Varadaraj et al. 2010). AQP0 but not AQP5 null mice showed a reduced compressive load-bearing capacity in lens, suggesting the cell–cell adhesion function of AQP0 contributes to biomechanical properties (Sindhu Kumari et al. 2015). AQP0 permeability to ions has been demonstrated in bilayers, but the physiological function of the ion conductance remains to be defined. The role of AQP0 ion channels in maintaining optimal lens transparency could involve the generation of osmotic gradients or regulation of transmembrane signals.

In addition to normal physiological roles in fluid transport and homeostasis, some classes of AQPs have been implicated in augmenting cancer cell invasion and metastasis, by mechanisms suggested to involve local volume regulation supporting membrane process extension and cytoskeletal assembly (De Ieso and Yool 2018; McLennan et al. 2020). Expression of HsAQP1 is upregulated in gliomas, mammary, lung and colorectal carcinomas, hemangioblastoma, glioblastoma, ovarian, and gastric cancers and multiple myeloma (Saadoun et al. 2002; El Hindy et al. 2013; Endo et al. 1999; Hoque et al. 2006; Moon et al. 2003; Vacca et al. 2001; Chen et al. 2006; Longatti et al. 2006; Nagashima et al. 2006; Verkman et al. 2008; Wang et al. 2020; Wei and Dong 2015; Zhang et al. 2012). AQP1 plays a significant role in tumor cell metastasis and invasion, which are critical in cancer progression (De Ieso and Yool 2018). Water flux mediated by AQPs has an important role in facilitating formation of lamellipodia involved in cell motility and migration (Oster and Perelson 1987). AQP1-mediated osmotic water flux could occur in response to solute influx and actin depolymerisation at the leading edges of migrating cells (Papadopoulos and Verkman 2013). AQP1 facilitated water fluxes may also enable changes in cell shape and volume of migrating tumor cells, particularly relevant during movement through tight extracellular spaces (Papadopoulos et al. 2008). An ‘osmotic engine model’ proposed by Stroka and colleagues linked the water flux and ion transport mediated by aquaporins and  $\text{Na}^+/\text{H}^+$  pumps as keys for rapid cell migration (Stroka et al. 2014). Polarized distributions of ion channels and transporters such as AQP1,  $\text{K}^+$  and  $\text{Cl}^-$  channels in the leading edges of migrating cells are consistent with a direct role in osmotic fluid flow for membrane extension and motility (Schwab and Stock 2014; Stock and Schwab 2015). Inhibiting the AQP1 ion conductance with pharmacological blockers AqB011 and 5-hydroxymethyl furfural impaired invasiveness of colorectal (HT29) and breast cancer (MDA) tumor cells (De Ieso et al. 2019; Chow et al. 2020; Kourghi et al. 2016). Combined block of both ion and water fluxes mediated by AQP1 more potently inhibited cell migration in colon cancer cells than either alone (De Ieso et al. 2019). Both water flux and ion currents mediated by AQP1 contribute to the acceleration of cell migration and invasion in subtypes of cancers that upregulate this class of channel during pathological cancer progression.

AQP6, in intracellular acid-secreting vesicles intercalated in the renal collecting duct, is co-localized with  $\text{H}^+$ -ATPase (Kwon et al. 2001; Yasui et al. 1999b). The V-type  $\text{H}^+$ -ATPase causes acidification of intracellular organelles in the kidney renal collecting duct; the  $\text{Cl}^-$  channel CIC-5 co-localized with  $\text{H}^+$ -ATPase is thought to provide electroneutral balance (Günther et al. 1998). Interestingly, CIC-5 deactivates at pH values below 6.5 while the anion conductance of AQP6 is turned on at pH values below 6.5,

suggesting AQP6 and CLC-5 functions could be complementary (Rambow et al. 2014). AQP6 mediated  $\text{NO}_3^-$  permeation across the vesicle membrane could be linked to the regulation of  $\text{H}^+$ -ATPase activity in acid-secreting intercalated cells (Arai et al. 1989; Ikeda et al. 2002). AQP6 is expressed in some ovarian cancers and appears to have a protective role in certain viral pathologies but mechanisms and roles in these processes remain unknown (Ma et al. 2016; Molinas et al. 2016).

Big Brain in *Drosophila*, in parallel with the other neurogenic genes Notch (transmembrane receptor) and Delta (ligand for Notch), regulates early development of the nervous system (Artavanis-Tsakonas et al. 1999), contributing to interactions that govern the neuroblast versus epidermal cell fate by a process of lateral inhibition (Doherty et al. 1997; Rao et al. 1990). Loss of function mutations in this gene cause defects in cell fate determination during neurogenesis, and deleterious overgrowth of the nervous system (Lehmann et al. 1983; Brand and Campos-Ortega 1988; Artavanis-Tsakonas et al. 1999). BIB functions as a voltage insensitive non-selective monovalent cation channel when expressed in *Xenopus* oocytes, but unlike most AQPs shows no water permeability (Yanochko and Yool 2002; Yool and Stamer 2004). Ion conductance is decreased when oocytes expressing BIB are treated with insulin, and enhanced by the tyrosine kinase inhibitor lavendustin A. The level of BIB activity depends on the pattern of phosphorylation at multiple tyrosine kinase consensus sites in the long C-terminal domain. Tyrosine kinases downstream of growth factor receptors mediate multiple aspects of neural development; the cation conductance mediated by BIB has been proposed to lead to membrane depolarisation in turn influencing epidermal cell fate determination (Yanochko and Yool 2002). Mutation of a glutamate residue in the first transmembrane domain to asparagine (E71N) in BIB abolishes ion channel activity, and when E71N is co-expressed with wild type BIB, it appears to impose a dominant-negative effect (Yool 2007).

Nitrogen is an essential plant macronutrient required for growth and reproduction. The ion-conducting AQP GmNOD26 in soybean could contribute to the essential role of the nodule in nitrogen fixation. The symbiosome compartment is acidic due to  $\text{H}^+$ -ATPase activity, which would compromise neutral  $\text{NH}_3$  export out of the symbiosome (Masalkar et al. 2010). As  $\text{NH}_3$  is protonated to ammonium  $\text{NH}_4^+$ , the movement of charged  $\text{NH}_4^+$  across the symbiosome membrane is facilitated by the transmembrane potential generated by  $\text{H}^+$ -ATPase activity (Udvardi and Day 1997). A non-selective cation channel (NSCC) conductance permeable to  $\text{NH}_4^+$  was identified in symbiosome membranes in soybean and *Lotus japonicus* but the molecular identity remained unknown (Obermeyer and Tyerman 2005; Roberts and Tyerman 2002; Tyerman et al. 1995). NOD26 has a binding site in the C-terminus for glutamine



synthetase (GS) which carries out the first enzymatic step in the  $\text{NH}_3$  assimilation pathway, and uses  $\text{NH}_4^+$  as a substrate. It is interesting to consider the idea that NOD26, if shown to be permeable to  $\text{NH}_4^+$ , could contribute to a protein complex which exports fixed nitrogen (such as  $\text{NH}_4^+$ ) from the nodule into the host plant, supporting the symbiotic relationship (Eisenberg et al. 2000; Masalkar et al. 2010). The proposed role of NOD26 as the NSCC permeable to  $\text{NH}_4^+$  remains to be explored.

Arabidopsis PIP2;1 in plant cell plasma membranes is highly permeable to water, and regulated by divalent cations,  $\text{Ca}^{2+}$  and low pH (Alexandersson et al. 2005; Verdoucq et al. 2008). Expression of AtPIP2;1 in *Xenopus* oocytes confers cation conductance ( $\text{Na}^+$ ) also sensitive to  $\text{Ca}^{2+}$  and low pH (Byrt et al. 2017). Two related PIPs AtPIP2;1 and AtPIP2;2 from Arabidopsis and one from barley HvPIP2;8 also serve as ion-permeable channels (Qiu et al. 2020; McGaughey et al. 2018; Tran et al. 2020). The NSCC identified in roots (Demidchik and Tester 2002) appears to be mediated by the AtPIP classes of non-selective cation channels (Byrt et al. 2017).

The adaptive benefits of dual ion and water transport by plant aquaporins are likely to include improved tolerance of salinity stress. Increased salinity leads to reduced phosphorylation, internalization of AtPIP2;1 into intracellular vesicles, and recycling in vacuoles (Boursiac et al. 2005; Ueda et al. 2016; Luu et al. 2012).  $\text{Na}^+$  taken in during the endocytosis is sequestered in vacuoles as a mechanism to reduce  $\text{Na}^+$  toxicity (McGaughey et al. 2018). Regulation of AQP ion and water conducting states via phosphorylation is likely to be a key mechanism for modulating relative ion fluxes ( $\text{Na}^+$  and  $\text{K}^+$ ) and water across cell membranes in response to salinity, limiting water loss as a mechanism for survival in saline soils. Among the kingdoms of life, plants have the greatest diversity of classes of aquaporins, leaving open the possibility that there are many aquaporins with yet unidentified functions that might provide a portfolio of highly specialized ion and water conducting states, which can be tuned for optimal growth promoting responses to diverse environmental conditions.

## Future directions

### Functional insights from heterologous hosts

Heterologous expression systems, such as yeast or bacteria, are useful approaches for studying ion channel function (Tomita et al. 2017; Locascio et al. 2019; Fairbairn et al. 2000). Examples include screening of known ion channels for channel modulators (Zaks-Makhina et al. 2004; Kawada et al. 2016), mutagenesis to identify key residues (Ros et al. 1999), and evaluation of intracellular trafficking mechanisms

(Bernstein et al. 2013; Bagriantsev et al. 2014). Heterologous expression systems also can be adapted as through-pot screening tools to enable discovery of new classes of ion channels. The main challenges are in establishing a robust phenotype that shows ion selective effects, and in developing tools for correlating the ion channel function with measurable parameters such as cell growth or optical probe signal intensity.

Yeast and bacteria have evolved selective transport systems for acquiring  $\text{K}^+$  and excluding  $\text{Na}^+$  (Yenush 2016; Stautz et al. 2021). Inactivation of  $\text{K}^+$  uptake genes in the *S. cerevisiae* yeast strain  $\Delta trk1 \Delta trk2$  (Sentenac et al. 1992) and in *E. coli* (Epstein et al. 1993) has yielded cell lines that survive only when supplemented with high concentrations of external  $\text{K}^+$ . Expression of plant (Rubio et al. 1995) and mammalian (Tang et al. 1995)  $\text{K}^+$  channel genes rescues cell growth in standard low extracellular  $\text{K}^+$ , enabling the mass-throughput characterization of channel activity and  $\text{K}^+$  conduction. Fluorescence-based monitoring of ion flux kinetics also is possible using heterologous expression systems (Zhou et al. 2007). A few studies have used heterologous expression in yeast to study the potential ion permeability of AQP1 (Wu et al. 2009) and plant PIP aquaporins (Byrt et al. 2017; Qiu et al. 2020). Yeast mass-throughput assays could provide a rapid tool for the future evaluation of novel classes of AQPs as possible cation channels, and identify candidate pharmacological and regulatory compounds as tools for further research.

### In silico predictions

Molecular dynamics (MD) simulations have been used to provide insight into channel functions that are difficult to dissect with conventional methods. The number of MD studies focused on investigating AQPs is increasing steadily in parallel with those on other channels (Fig. 3). Solving the structural architectures of AQP1 (Murata et al. 2000; Sui et al. 2001), bacterial aquaglyceroporin (GlpF) (Fu et al. 2000), and others has allowed in depth analyses of substrate permeation through AQP pores at the atomic level (Tajkhorshid et al. 2002). The first AQP shown by MD simulation to be permeable to ions was HsAQP1 (Yu et al. 2006). Sodium and  $\text{Cl}^-$  transport via monomeric and central pores of HsAQP4 has also been predicted (Bernardi et al. 2019). MD simulations of AQPs have provided views into the molecular basis of features such as substrate selectivity (Hub and De Groot 2008), proton exclusion (Chakrabarti et al. 2004), gating mechanisms (Törnroth-Horsefield et al. 2006; Fischer et al. 2009), and the conduction of gases and signaling molecules (Wang et al. 2007; Yusupov et al. 2018). MD simulations have provided insights into the critical residues (Hadidi and Kamali 2021), post-translational modifications (Sachdeva and Singh 2014), drug interactions (De Almeida

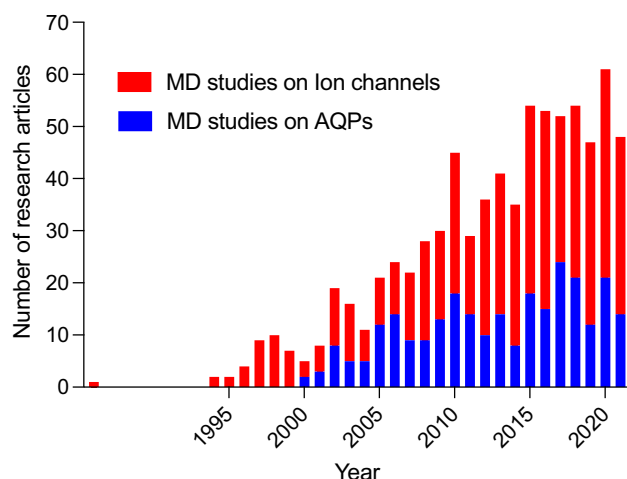


**Fig. 3** Comparison of Molecular Dynamics Simulation studies in ion channel and aquaporin fields. The number of publications per year from Web of Science that includes the term “molecular dynamic” and “ion channels” or “aquaporins” in either the title, abstract or keywords. (<https://www.webofscience.com/>) in August 2021

et al. 2017), and voltage-dependence properties (Hub et al. 2010; Mom et al. 2021) that impact the channel function. Given the large number of structures (~50) determined for aquaporins by X-ray diffraction and cryo-electron microscopy, computational techniques to simulate permeation of ions or coupling of water and ion transport via these channels are within reach as exciting new areas of research. Further applications might include simulating protein channel activity in different lipid mixtures relevant to a variety of cell membranes (Aponte-Santamaría et al. 2012; Gu et al. 2017), modeling multiple aquaporins isoforms simultaneously (Pei et al. 2019; Kapilan et al. 2018), and evaluating mechanisms of block and potentiation of ion conductance and other substrate fluxes by pharmacological AQP modulators that have been derived from synthetic (Chow et al. 2020; Huber et al. 2007; De Ieso et al. 2019) and natural (Aung et al. 2019) sources.

## Conclusions

The first AQP ion channels were discovered almost 40 years ago. Their biophysical properties are likely to be defined not only by their tetrameric architecture, but also by the lipid environments in which the AQP tetramers reside, as well as interacting proteins and signaling mechanisms. Residues involved in the selectivity, gating, and permeation pathways of the central and intrasubunit pores of ion-conducting AQP tetramers are being uncovered. These candidate motifs can be investigated with the classical array of electrophysiological methods, but continuing work will benefit from

incorporating novel approaches using microorganisms (e.g., yeast, bacteria) and computational methods such as MD simulation, to further define the functional roles of ion conductivity in classes of AQPs across all the biological kingdoms of life.

**Acknowledgements** We thank Boris Martinac and Yoshitaka Nakayama for assistance with patch-clamp electrophysiology data and methods.

**Funding** This work was supported by the Australian Research Council (19ARC\_DP190101745), and the Medical Advances Without Animals (MAWA) Trust.

## Declarations

**Ethics approval and consent to participate** This study did not use animals or human subjects and did not require ethics approval. This study did not involve human participants. Informed consent is not applicable.

**Consent for publication** This manuscript does not contain any individual person’s data in any form. Informed consent is not applicable.

**Conflict of interest** The authors declare no competing interests.

## References

- Agre P, Sasaki S, Chrispeels MJ (1993) Aquaporins: a family of water channel proteins. *Am J Physiol* 265(3 Pt 2):F461. <https://doi.org/10.1152/ajprenal.1993.265.3.F461>
- Alexandersson E, Fraysse L, Sjövall-Larsen S, Gustavsson S, Fellert M, Karlsson M, Johanson U, Kjellbom P (2005) Whole gene family expression and drought stress regulation of aquaporins. *Plant Mol Biol* 59(3):469–484. <https://doi.org/10.1007/s11103-005-0352-1>
- Angladon M-A, Fossépré M, Leherte L, Vercauteren DP (2019) Interaction of POPC, DPPC, and POPE with the  $\mu$  opioid receptor: a coarse-grained molecular dynamics study. *PLoS One* 14(3):e0213646. <https://doi.org/10.1371/journal.pone.0213646>
- Anthony TL, Brooks HL, Boassa D, Leonov S, Yanochko GM, Regan JW, Yool AJ (2000) Cloned human aquaporin-1 is a cyclic GMP-gated ion channel. *Mol Pharmacol* 57(3):576–588. <https://doi.org/10.1124/mol.57.3.576>
- Aponte-Santamaría C, Briones R, Schenk AD, Walz T, de Groot BL (2012) Molecular driving forces defining lipid positions around aquaporin-0. *Proc Natl Acad Sci* 109(25):9887–9892. <https://doi.org/10.1073/pnas.1121054109>
- Arai H, Pink S, Forgac M (1989) Interaction of anions and ATP with the coated vesicle proton pump. *Biochemistry* 28(7):3075–3082. <https://doi.org/10.1021/bi00433a051>
- Artavanis-Tsakonas S, Rand MD, Lake RJ (1999) Notch signaling: cell fate control and signal integration in development. *Science* 284(5415):770–776. <https://doi.org/10.1126/science.284.5415.770>
- Aung T, Nourmohammadi S, Qu Z, Harata-Lee Y, Cui J, Shen H, Yool A, Pukala T, Du H, Kortschak R (2019) Fractional Deletion of compound Kushen injection indicates cytokine signaling pathways are critical for its perturbation of the cell cycle. *Sci Rep* 9(1):1–16. <https://doi.org/10.1038/s41598-019-50271-4>
- Bagriantsev SN, Chatelain FC, Clark KA, Alagem N, Reuveny E, Minor DL Jr (2014) Tethered protein display identifies a novel Kir3. 2 (GIRK2) regulator from protein scaffold libraries. *ACS*

- Chem Neurosci 5(9):812–822. <https://doi.org/10.1021/cn5000698>
- Beitz E, Liu K, Ikeda M, Guggino WB, Agre P, Yasui M (2006a) Determinants of AQP6 trafficking to intracellular sites versus the plasma membrane in transfected mammalian cells. *Biol Cell* 98(2):101–109. <https://doi.org/10.1042/BC20050025>
- Beitz E, Wu B, Holm LM, Schultz JE, Zeuthen T (2006b) Point mutations in the aromatic/arginine region in aquaporin 1 allow passage of urea, glycerol, ammonia, and protons. *Proc Natl Acad Sci U S A* 103(2):269–274. <https://doi.org/10.1073/pnas.0507225103>
- Bernardi M, Marracino P, Liberti M, Gárate J-A, Burnham CJ, Apollonio F, English NJ (2019) Controlling ionic conductivity through transprotein electropores in human aquaporin 4: a non-equilibrium molecular-dynamics study. *Phys Chem Chem Phys* 21(6):3339–3346. <https://doi.org/10.1039/C8CP06643D>
- Bernstein JD, Okamoto Y, Kim M, Shikano S (2013) Potential use of potassium efflux-deficient yeast for studying trafficking signals and potassium channel functions. *FEBS Open Biol* 3:196–203. <https://doi.org/10.1016/j.fob.2013.04.002>
- Berry V, Francis P, Kaushal S, Moore A, Bhattacharya S (2000) Missense mutations in MIP underlie autosomal dominant ‘polymorphic’ and lamellar cataracts linked to 12q. *Nat Genet* 25(1):15–17. <https://doi.org/10.1038/75538>
- Bienert GP, Thorsen M, Schüssler MD, Nilsson HR, Wagner A, Tamás MJ, Jahn TP (2008) A subgroup of plant aquaporins facilitate the bi-directional diffusion of As(OH)<sub>3</sub> and Sb(OH)<sub>3</sub> across membranes. *BMC Biol* 6(1):26. <https://doi.org/10.1186/1741-7007-6-26>
- Bloemendal H, Hockwin O (1982) Lens protein. *Crit Rev Biochem* 12(1):1–38. <https://doi.org/10.3109/10409238209105849>
- Boassa D, Yool AJ (2002) A fascinating tail: cGMP activation of aquaporin-1 ion channels. *Trends Pharmacol Sci* 23(12):558–562. [https://doi.org/10.1016/S0165-6147\(02\)02112-0](https://doi.org/10.1016/S0165-6147(02)02112-0)
- Boassa D, Stamer WD, Yool AJ (2006) Ion Channel Function of Aquaporin-1 Natively Expressed in Choroid Plexus. *J Neurosci* 26(30):7811–7819. <https://doi.org/10.1523/jneurosci.0525-06.2006>
- Boursiac Y, Chen S, Luu D-T, Sorieul M, van den Dries N, Maurel C (2005) Early effects of salinity on water transport in Arabidopsis roots. Molecular and cellular features of aquaporin expression. *Plant Physiol* 139(2):790–805. <https://doi.org/10.1104/pp.105.065029>
- Brand M, Campos-Ortega JA (1988) Two groups of interrelated genes regulate early neurogenesis in *Drosophila melanogaster*. *Roux Arch Dev Biol* 197(8):457–470. <https://doi.org/10.1007/BF00385679>
- Byrt CS, Zhao M, Kourghi M, Bose J, Henderson SW, Qiu J, Gilliam M, Schultz C, Schwarz M, Ramesh SA, Yool A, Tyerman S (2017) Non-selective cation channel activity of aquaporin AtPIP2;1 regulated by Ca<sup>2+</sup> and pH. *Plant Cell Environ* 40(6):802–815. <https://doi.org/10.1111/pce.12832>
- Campbell EM, Birdsell DN, Yool AJ (2012) The Activity of Human Aquaporin 1 as a cGMP-Gated Cation Channel Is Regulated by Tyrosine Phosphorylation in the Carboxyl-Terminal Domain. *Mol Pharmacol* 81(1):97–105. <https://doi.org/10.1124/mol.111.073692>
- Chakrabarti N, Tajkhorshid E, Bt Roux, Pomès R (2004) Molecular basis of proton blockage in aquaporins. *Structure* 12(1):65–74. <https://doi.org/10.1016/j.str.2003.11.017>
- Chandy G, Zampighi G, Kremar M, Hall J (1997) Comparison of the water transporting properties of MIP and AQP1. *J Membr Biol* 159(1):29–39. <https://doi.org/10.1007/s002329900266>
- Chen Y, Tachibana O, Oda M, Xu R, Hamada J-i, Yamashita J, Hashimoto N, Takahashi JA (2006) Increased expression of aquaporin 1 in human hemangioblastomas and its correlation with cyst formation. *J Neurooncol* 80(3):219–225. <https://doi.org/10.1007/s11060-005-9057-1>
- Chepelinsky AB (2009) Structural function of MIP/aquaporin 0 in the eye lens; genetic defects lead to congenital inherited cataracts. *Handb Exp Pharmacol* 190:265–297. [https://doi.org/10.1007/978-3-540-79885-9\\_14](https://doi.org/10.1007/978-3-540-79885-9_14)
- Chow PH, Kourghi M, Pei JV, Nourmohammadi S, Yool AJ (2020) 5-hydroxymethyl-furfural and structurally related compounds block the ion conductance in human aquaporin-1 channels and slow cancer cell migration and invasion. *Mol Pharmacol* 98(1):38–48. <https://doi.org/10.1124/mol.119.119172>
- Conde A, Diallinas G, Chaumont F, Chaves M, Geros H (2010) Transporters, channels, or simple diffusion? Dogmas, atypical roles and complexity in transport systems. *Int J Biochem Cell Biol* 42(6):857–868. <https://doi.org/10.1016/j.biocel.2009.12.012>
- De Almeida A, Mósca AF, Wragg D, Wenzel M, Kavanagh P, Barone G, Leoni S, Soveral G, Casini A (2017) The mechanism of aquaporin inhibition by gold compounds elucidated by biophysical and computational methods. *Chem Commun* 53(27):3830–3833. <https://doi.org/10.1039/C7CC00318H>
- De Ieso ML, Pei JV, Nourmohammadi S, Smith E, Chow PH, Kourghi M, Hardingham JE, Yool AJ (2019) Combined pharmacological administration of AQP1 ion channel blocker AqB011 and water channel blocker Bacopaside II amplifies inhibition of colon cancer cell migration. *Sci Rep* 9(1):12635. <https://doi.org/10.1038/s41598-019-49045-9>
- De Ieso ML, Yool AJ (2018) Mechanisms of aquaporin-facilitated cancer invasion and metastasis. *Front Chem* 6(135). <https://doi.org/10.3389/fchem.2018.00135>
- Dean RM, Rivers RL, Zeidel ML, Roberts DM (1999) Purification and functional reconstitution of soybean nodulin 26. An aquaporin with water and glycerol transport properties. *Biochemistry* 38(1):347–353. <https://doi.org/10.1021/bi982110c>
- Demidchik V, Tester M (2002) Sodium fluxes through nonselective cation channels in the plasma membrane of protoplasts from Arabidopsis roots. *Plant Physiol* 128(2):379–387. <https://doi.org/10.1104/pp.010524>
- Doherty D, Jan LY, Jan YN (1997) The *Drosophila* neurogenic gene big brain, which encodes a membrane-associated protein, acts cell autonomously and can act synergistically with Notch and Delta. *Development* 124(19):3881–3893. <https://doi.org/10.1242/dev.124.19.3881>
- Ehring GR, Zampighi G, Horwitz J, Bok D, Hall JE (1990) Properties of channels reconstituted from the major intrinsic protein of lens fiber membranes. *J Gen Physiol* 96(3):631–664. <https://doi.org/10.1085/jgp.96.3.631>
- Ehring GR, Lagos N, Zampighi GA, Hall JE (1992) Phosphorylation modulates the voltage dependence of channels reconstituted from the major intrinsic protein of lens fiber membranes. *J Membr Biol* 126(1):75–88. <https://doi.org/10.1007/bf00233462>
- Eisenberg D, Gill HS, Pfluegl GM, Rotstein SH (2000) Structure–function relationships of glutamine synthetases. *Biochim Biophys Acta* 1477(1–2):122–145. [https://doi.org/10.1016/S0167-4838\(99\)00270-8](https://doi.org/10.1016/S0167-4838(99)00270-8)
- El Hindy N, Bankfalvi A, Herring A, Adamzik M, Lambertz N, Zhu Y, Siffert W, Sure U, Sandalcioglu IE (2013) Correlation of aquaporin-1 water channel protein expression with tumor angiogenesis in human astrocytoma. *Anticancer Res* 33(2):609–613
- Endo M, Jain RK, Witwer B, Brown D (1999) Water channel (aquaporin 1) expression and distribution in mammary carcinomas and glioblastomas. *Microvasc Res* 58(2):89–98. <https://doi.org/10.1006/mvres.1999.2158>
- Epstein W, Buurman E, McLaggan D, Naprstek J (1993) Multiple mechanisms, roles and controls of K<sup>+</sup> transport in *Escherichia coli*. *Biochem Soc Trans* 21(4):1006–1010. <https://doi.org/10.1042/bst0211006>

- Fairbairn DJ, Liu W, Schachtman DP, Gomez-Gallego S, Day SR, Teasdale RD (2000) Characterisation of two distinct HKT1-like potassium transporters from *Eucalyptus camaldulensis*. *Plant Mol Biol* 43(4):515–525. <https://doi.org/10.1023/A:1006496402463>
- Fischer G, Kosinska-Eriksson U, Aponte-Santamaría C, Palmgren M, Geijer C, Hedfalk K, Hohmann S, De Groot BL, Neutze R, Lindkvist-Petersson K (2009) Crystal structure of a yeast aquaporin at 1.15 Å reveals a novel gating mechanism. *PLoS Biol* 7(6):e1000130. <https://doi.org/10.1371/journal.pbio.1000130>
- Fortin MG, Morrison NA, Verma DP (1987) Nodulin-26, a peribacteroid membrane nodulin is expressed independently of the development of the peribacteroid compartment. *Nucleic Acids Res* 15(2):813–824. <https://doi.org/10.1093/nar/15.2.813>
- Fu D, Libson A, Miercke LJ, Weitzman C, Nollert P, Krucinski J, Stroud RM (2000) Structure of a glycerol-conducting channel and the basis for its selectivity. *Science* 290(5491):481–486. <https://doi.org/10.1126/science.290.5491.481>
- Girsch SJ, Peracchia C (1985) Lens cell-to-cell channel protein: I. Self-assembly into liposomes and permeability regulation by calmodulin. *J Membr Biol* 83(3):217–225. <https://doi.org/10.1007/BF01868696>
- Gorin MB, Yancey SB, Cline J, Revel J-P, Horwitz J (1984) The major intrinsic protein (MIP) of the bovine lens fiber membrane: Characterization and structure based on cDNA cloning. *Cell* 39(1):49–59. [https://doi.org/10.1016/0092-8674\(84\)90190-9](https://doi.org/10.1016/0092-8674(84)90190-9)
- Gotfryd K, Mósca AF, Missel JW, Truelsen SF, Wang K, Spulber M, Krabbe S, Hélix-Nielsen C, Laforenza U, Soveral G, Pedersen PA, Gourdon P (2018) Human adipose glycerol flux is regulated by a pH gate in AQP10. *Nat Commun* 9(1):4749. <https://doi.org/10.1038/s41467-018-07176-z>
- Gu R-X, Ingólfsson HI, De Vries AH, Marrink SJ, Tieleman DP (2017) Ganglioside-lipid and ganglioside-protein interactions revealed by coarse-grained and atomistic molecular dynamics simulations. *J Phys Chem B* 121(15):3262–3275. <https://doi.org/10.1021/acs.jpcc.6b07142>
- Guenther JF, Chanmanivone N, Galetovic MP, Wallace IS, Cobb JA, Roberts DM (2003) Phosphorylation of soybean nodulin 26 on serine 262 enhances water permeability and is regulated developmentally and by osmotic signals. *Plant Cell* 15(4):981–991. <https://doi.org/10.1105/tpc.009787>
- Günther W, Lüchow A, Cluzeaud F, Vandewalle A, Jentsch TJ (1998) CIC-5, the chloride channel mutated in Dent's disease, colocalizes with the proton pump in endocytotically active kidney cells. *Proc Natl Acad Sci* 95(14):8075–8080. <https://doi.org/10.1073/pnas.95.14.8075>
- Hachez C, Chaumont F (2010) Aquaporins: a family of highly regulated multifunctional channels. *Adv Exp Med Biol* 679:1–17. [https://doi.org/10.1007/978-1-4419-6315-4\\_1](https://doi.org/10.1007/978-1-4419-6315-4_1)
- Hadidi H, Kamali R (2021) Molecular dynamics study of water transport through AQP5-R188C mutant causing palmoplantar keratoderma (PPK) using the gating mechanism concept. *Biophys Chem* 277:106655. <https://doi.org/10.1016/j.bpc.2021.106655>
- Hara-Chikuma M, Satooka H, Watanabe S, Honda T, Miyachi Y, Watanabe T, Verkman AS (2015) Aquaporin-3-mediated hydrogen peroxide transport is required for NF- $\kappa$ B signalling in keratinocytes and development of psoriasis. *Nat Commun* 6(1):7454. <https://doi.org/10.1038/ncomms8454>
- Hazama A, Kozono D, Guggino WB, Agre P, Yasui M (2002) Ion permeation of AQP6 water channel protein: single-channel recordings after Hg<sup>2+</sup> activation. *J Biol Chem* 277(32):29224–29230. <https://doi.org/10.1074/jbc.M204258200>
- Holm LM, Klaerke DA, Zeuthen T (2004) Aquaporin 6 is permeable to glycerol and urea. *Pflugers Arch* 448(2):181–186. <https://doi.org/10.1007/s00424-004-1245-x>
- Hoque MO, Soria J-C, Woo J, Lee T, Lee J, Jang SJ, Upadhyay S, Trink B, Monitto C, Desmaze C (2006) Aquaporin 1 is overexpressed in lung cancer and stimulates NIH-3T3 cell proliferation and anchorage-independent growth. *Am J Pathol* 168(4):1345–1353. <https://doi.org/10.2353/ajpath.2006.050596>
- Hub JS, De Groot BL (2008) Mechanism of selectivity in aquaporins and aquaglyceroporins. *Proc Natl Acad Sci* 105(4):1198–1203. <https://doi.org/10.1073/pnas.0707662104>
- Hub JS, Aponte-Santamaría C, Grubmüller H, de Groot BL (2010) Voltage-regulated water flux through aquaporin channels in silico. *Biophys J* 99(12):L97–L99. <https://doi.org/10.1016/j.bpj.2010.11.003>
- Huber VJ, Tsujita M, Yamazaki M, Sakimura K, Nakada T (2007) Identification of arylsulfonamides as aquaporin 4 inhibitors. *Bioorg Med Chem Lett* 17(5):1270–1273. <https://doi.org/10.1016/j.bmcl.2006.12.010>
- Hwang JH, Ellingson SR, Roberts DM (2010) Ammonia permeability of the soybean nodulin 26 channel. *FEBS Lett* 584(20):4339–4343. <https://doi.org/10.1016/j.febslet.2010.09.033>
- Ikeda M, Beitz E, Kozono D, Guggino WB, Agre P, Yasui M (2002) Characterization of aquaporin-6 as a nitrate channel in mammalian cells: requirement of pore-lining residue threonine 63. *J Biol Chem* 277(42):39873–39879. <https://doi.org/10.1074/jbc.M207008200>
- Ishibashi K, Sasaki S, Fushimi K, Uchida S, Kuwahara M, Saito H, Furukawa T, Nakajima K, Yamaguchi Y, Gojobori T et al (1994) Molecular cloning and expression of a member of the aquaporin family with permeability to glycerol and urea in addition to water expressed at the basolateral membrane of kidney collecting duct cells. *Proc Natl Acad Sci U S A* 91(14):6269–6273. <https://doi.org/10.1073/pnas.91.14.6269>
- Jahn TP, Møller ALB, Zeuthen T, Holm LM, Klærke DA, Mohsin B, Kühlbrandt W, Schjøerring JK (2004) Aquaporin homologues in plants and mammals transport ammonia. *FEBS Lett* 574(1):31–36. <https://doi.org/10.1016/j.febslet.2004.08.004>
- Kapilan R, Vaziri M, Zwiazek JJ (2018) Regulation of aquaporins in plants under stress. *Biol Res* 51(1):1–11. <https://doi.org/10.1186/s40659-018-0152-0>
- Kawada H, Inanobe A, Kurachi Y (2016) Isolation of proflavine as a blocker of G protein-gated inward rectifier potassium channels by a cell growth-based screening system. *Neuropharmacology* 109:18–28. <https://doi.org/10.1016/j.neuropharm.2016.05.016>
- Kourghi M, Pei JV, De Ieso ML, Flynn G, Yool AJ (2016) Bumetanide derivatives AqB007 and AqB011 selectively block the aquaporin-1 ion channel conductance and slow cancer cell migration. *Mol Pharmacol* 89(1):133–140. <https://doi.org/10.1124/mol.115.101618>
- Kourghi M, Nourmohammadi S, Pei JV, Qiu J, McGaughey S, Tyerman SD, Byrt CS, Yool AJ (2017) Divalent cations regulate the ion conductance properties of diverse classes of aquaporins. *Int J Mol Sci* 18(11):2323. <https://doi.org/10.3390/ijms18112323>
- Kourghi M, Pei JV, De Ieso ML, Nourmohammadi S, Chow PH, Yool AJ (2017b) Fundamental structural and functional properties of aquaporin ion channels found across the kingdoms of life. *Clin Exp Pharmacol Physiol*. <https://doi.org/10.1111/1440-1681.12900>
- Kwon T-H, Hager H, Nejsum LN, Andersen M-LE, Føkiær J, Nielsen S (2001) Physiology and pathophysiology of renal aquaporins. *Semin Nephrol* 21(3):231–238. <https://doi.org/10.1053/snep.2001.21647>
- Laganowsky A, Reading E, Allison TM, Ulmschneider MB, Degiacomi MT, Baldwin AJ, Robinson CV (2014) Membrane proteins bind lipids selectively to modulate their structure and function. *Nature* 510(7503):172–175. <https://doi.org/10.1038/nature13419>

- Lee AG (2004) How lipids affect the activities of integral membrane proteins. *Biochim Biophys Acta Biomembr* 1666(1):62–87. <https://doi.org/10.1016/j.bbamem.2004.05.012>
- Lee JW, Zhang Y, Weaver CD, Shomer NH, Louis CF, Roberts DM (1995) Phosphorylation of nodulin 26 on serine 262 affects its voltage-sensitive channel activity in planar lipid bilayers. *J Biol Chem* 270(45):27051–27057. <https://doi.org/10.1074/jbc.270.45.27051>
- Lehmann R, Jiménez F, Dietrich U, Campos-Ortega JA (1983) On the phenotype and development of mutants of early neurogenesis in *Drosophila melanogaster*. *Wilhelm Roux Arch Dev Biol* 192(2):62–74. <https://doi.org/10.1007/BF00848482>
- Liu K, Kozono D, Kato Y, Agre P, Hazama A, Yasui M (2005) Conversion of aquaporin 6 from an anion channel to a water-selective channel by a single amino acid substitution. *Proc Natl Acad Sci U S A* 102(6):2192–2197. <https://doi.org/10.1073/pnas.0409232102>
- Locascio A, Andrés-Colás N, Mulet JM, Yenush L (2019) *Saccharomyces cerevisiae* as a tool to investigate plant potassium and sodium transporters. *Int J Mol Sci* 20(9):2133. <https://doi.org/10.3390/ijms20092133>
- Longatti P, Basaldella L, Orvieto E, Dei Tos A, Martinuzzi A (2006) Aquaporin (s) expression in choroid plexus tumours. *Pediatr Neurosurg* 42(4):228–233. <https://doi.org/10.1159/000092359>
- Luu DT, Martiniere A, Sorieul M, Runions J, Maurel C (2012) Fluorescence recovery after photobleaching reveals high cycling dynamics of plasma membrane aquaporins in Arabidopsis roots under salt stress. *Plant J* 69(5):894–905. <https://doi.org/10.1111/j.1365-3113.2011.04841.x>
- Ma TH, Frigeri A, Skach W, Verkman AS (1993) Cloning of a novel rat kidney cDNA homologous to CHIP28 and WCH-CD water channels. *Biochem Biophys Res Commun* 197(2):654–659. <https://doi.org/10.1006/bbrc.1993.2529>
- Ma T, Yang B, Kuo W-L, Verkman AS (1996) cDNA cloning and gene structure of a novel water channel expressed exclusively in human kidney: evidence for a gene cluster of aquaporins at chromosome locus 12q13. *Genomics* 35(3):543–550. <https://doi.org/10.1006/geno.1996.0396>
- Ma J, Zhou C, Yang J, Ding X, Zhu Y, Chen X (2016) Expression of AQP6 and AQP8 in epithelial ovarian tumor. *J Mol Histol* 47(2):129–134. <https://doi.org/10.1007/s10735-016-9657-4>
- Martinac B, Rohde PR, Battle AR, Petrov E, Pal P, Foo AFW, Vásquez V, Huynh T, Kloda A (2010) Studying mechanosensitive ion channels using liposomes. In: Weissig V (ed) *Liposomes: Methods and Protocols*, Volume 2: Biological Membrane Models. Humana Press, Totowa, pp 31–53. [https://doi.org/10.1007/978-1-60761-447-0\\_4](https://doi.org/10.1007/978-1-60761-447-0_4)
- Masalkar P, Wallace IS, Hwang JH, Roberts DM (2010) Interaction of cytosolic glutamine synthetase of soybean root nodules with the C-terminal domain of the symbiosome membrane nodulin 26 aquaglyceroporin. *J Biol Chem* 285(31):23880–23888. <https://doi.org/10.1074/jbc.M110.135657>
- McGaughey SA, Qiu J, Tyerman SD, Byrt CS (2018) Regulating root aquaporin function in response to changes in salinity. *Ann Plant Rev Online* 1:381–416. <https://doi.org/10.1002/9781119312994.apr0626>
- McLennan R, McKinney MC, Teddy JM, Morrison JA, Kasemeier-Kulesa JC, Ridenour DA, Manthe CA, Giniunaite R, Robinson M, Baker RE, Maini PK, Kulesa PM (2020) Neural crest cells bulldoze through the microenvironment using Aquaporin 1 to stabilize filopodia. *Development* 147(1). <https://doi.org/10.1242/dev.185231>
- Miao GH, Verma DP (1993) Soybean nodulin-26 gene encoding a channel protein is expressed only in the infected cells of nodules and is regulated differently in roots of homologous and heterologous plants. *Plant Cell* 5(7):781–794. <https://doi.org/10.1105/tpc.5.7.781>
- Modesto E, Barcellos L, Campos-de-Carvalho AC (1990) MIP 28 forms channels in planar lipid bilayers. *Braz J Med Biol Res* 23(10):1029–1032
- Modesto E, Lampe PD, Ribeiro MC, Spray DC, Campos de Carvalho AC (1996) Properties of chicken lens MIP channels reconstituted into planar lipid bilayers. *J Membr Biol* 154(3):239–249. <https://doi.org/10.1007/s002329900148>
- Molinas A, Mirazimi A, Holm A, Loitto VM, Magnusson K-E, Vikström E (2016) Protective role of host aquaporin 6 against Hazara virus, a model for Crimean–Congo hemorrhagic fever virus infection. *FEMS Microbiol Lett* 363(8):fnw058. <https://doi.org/10.1093/femsle/fnw058>
- Mom R, Muries B, Benoit P, Robert-Paganin J, Réty S, Js V, Pádua A, Label P, Auguin D (2021) Voltage-gating of aquaporins, a putative conserved safety mechanism during ionic stresses. *FEBS Lett* 595(1):41–57. <https://doi.org/10.1002/1873-3468.13944>
- Moon C, Soria J-C, Jang SJ, Lee J, Hoque MO, Sibony M, Trink B, Chang YS, Sidransky D, Mao L (2003) Involvement of aquaporins in colorectal carcinogenesis. *Oncogene* 22(43):6699–6703. <https://doi.org/10.1038/sj.onc.1206762>
- Mulders SM, Preston GM, Deen PMT, Guggino WB, van Os CH, Agre P (1995) Water channel properties of major intrinsic protein of lens \*. *J Biol Chem* 270(15):9010–9016. <https://doi.org/10.1074/jbc.270.15.9010>
- Murata K, Mitsuoka K, Hirai T, Walz T, Agre P, Heymann JB, Engel A, Fujiyoshi Y (2000) Structural determinants of water permeation through aquaporin-1. *Nature* 407(6804):599–605. <https://doi.org/10.1038/35036519>
- Nagashima G, Fujimoto T, Suzuki R, Asai J-i, Itokawa H, Noda M (2006) Dural invasion of meningioma: a histological and immunohistochemical study. *Brain Tumor Pathol* 23(1):13–17. <https://doi.org/10.1007/s10014-006-0193-x>
- Németh-Cahalan KL, Clemens DM, Hall JE (2013) Regulation of AQP0 water permeability is enhanced by cooperativity. *J Gen Physiol* 141(3):287–295. <https://doi.org/10.1085/jgp.201210884>
- Obermeyer G, Tyerman SD (2005) NH<sup>4+</sup> currents across the peribacteroid membrane of soybean. Macroscopic and microscopic properties, inhibition by Mg<sup>2+</sup>, and temperature dependence indicate a subpicoSiemens channel finely regulated by divalent cations. *Plant Physiol* 139(2):1015–1029. <https://doi.org/10.1104/pp.105.066670>
- Oster GF, Perelson AS (1987) The physics of cell motility. *J Cell Sci* 1987(Supplement\_8):35–54. [https://doi.org/10.1242/jcs.1987.Supplement\\_8.3](https://doi.org/10.1242/jcs.1987.Supplement_8.3)
- Papadopoulos MC, Verkman AS (2013) Aquaporin water channels in the nervous system. *Nat Rev Neurosci* 14(4):265–277. <https://doi.org/10.1038/nrn3468>
- Papadopoulos M, Saadoun S, Verkman A (2008) Aquaporins and cell migration. *Pflügers Arch Eur J Physiol* 456(4):693–700. <https://doi.org/10.1007/s00424-007-0357-5>
- Pei JV, Burton JL, Kourghi M, De Ieso ML, Yool AJ (2016) Drug discovery and therapeutic targets for pharmacological modulators of aquaporin channels. In: Several G, Casinin A, Nielsen S (eds) *Aquaporins in Health and Disease: New Molecular Targets For Drug Discovery*. CRC Press, Oxfordshire, pp 275–297
- Pei JV, Heng S, De Ieso ML, Sylvia G, Kourghi M, Nourmohammadi S, Abell AD, Yool AJ (2019) Development of a photoswitchable lithium-sensitive probe to analyze nonselective cation channel activity in migrating cancer cells. *Mol Pharmacol* 95(5):573–583. <https://doi.org/10.1124/mol.118.115428>
- Poveda JA, Giudici AM, Renart ML, Molina ML, Montoya E, Fernández-Carvajal A, Fernández-Ballester G, Encinar JA (1838) González-Ros JM (2014) Lipid modulation of ion channels through specific binding sites. *Biochim Biophys Acta*

- Biomembr 6:1560–1567. <https://doi.org/10.1016/j.bbmem.2013.10.023>
- Preston GM, Carroll TP, Guggino WB, Agre P (1992) Appearance of water channels in *Xenopus* oocytes expressing red cell CHIP28 protein. *Science* 256(5055):385–387. <https://doi.org/10.1126/science.256.5055.385>
- Qiu J, McGaughey SA, Groszmann M, Tyerman SD, Byrt CS (2020) Phosphorylation influences water and ion channel function of AtPIP2;1. *Plant Cell Environ* 43(10):2428–2442. <https://doi.org/10.1111/pce.13851>
- Rambow J, Wu B, Rönfeldt D, Beitz E (2014) Aquaporins with anion/monocarboxylate permeability: mechanisms, relevance for pathogen–host interactions. *Front Pharmacol* 5(199). <https://doi.org/10.3389/fphar.2014.00199>
- Rao Y, Jan LY, Jan YN (1990) Similarity of the product of the *Drosophila* neurogenic gene big brain to transmembrane channel proteins. *Nature* 345(6271):163–167. <https://doi.org/10.1038/345163a0>
- Reizer J, Reizer A, Saier MH Jr (1993) The MIP family of integral membrane channel proteins: sequence comparisons, evolutionary relationships, reconstructed pathway of evolution, and proposed functional differentiation of the two repeated halves of the proteins. *Crit Rev Biochem Mol Biol* 28(3):235–257. <https://doi.org/10.3109/10409239309086796>
- Rivers RL, Dean RM, Chandy G, Hall JE, Roberts DM, Zeidel ML (1997) Functional analysis of nodulin 26, an aquaporin in soybean root nodule symbiosomes. *J Biol Chem* 272(26):16256–16261. <https://doi.org/10.1074/jbc.272.26.16256>
- Roberts DM, Tyerman SD (2002) Voltage-dependent cation channels permeable to  $\text{NH}_4^+$ ,  $\text{K}^+$ , and  $\text{Ca}^{2+}$  in the symbiosome membrane of the model legume *Lotus japonicus*. *Plant Physiol* 128(2):370–378. <https://doi.org/10.1104/pp.010568>
- Ros R, Lemaillet G, Fonrouge A, Daram P, Enjuto M, Salmon J-M, Thibaud J-B, Sentenac H (1999) Molecular determinants of the Arabidopsis AKT1  $\text{K}^+$  channel ionic selectivity investigated by expression in yeast of randomly mutated channels. *Physiol Plant* 105(3):459–468. <https://doi.org/10.1034/j.1399-3054.1999.105310.x>
- Rubio F, Gassmann W, Schroeder JI (1995) Sodium-driven potassium uptake by the plant potassium transporter HKT1 and mutations conferring salt tolerance. *Science* 270(5242):1660–1663. <https://doi.org/10.1126/science.270.5242.1660>
- Saadoun S, Papadopoulos M, Davies D, Bell B, Krishna S (2002) Increased aquaporin 1 water channel expression in human brain tumours. *Br J Cancer* 87(6):621–623. <https://doi.org/10.1038/sj.bjc.6600512>
- Sachdeva R, Singh B (2014) Phosphorylation of Ser-180 of rat aquaporin-4 shows marginal affect on regulation of water permeability: molecular dynamics study. *J Biomol Struct Dyn* 32(4):555–566. <https://doi.org/10.1080/07391102.2013.780981>
- Saparov SM, Kozono D, Rothe U, Agre P, Pohl P (2001) Water and ion permeation of aquaporin-1 in planar lipid bilayers: major differences in structural determinants and stoichiometry. *J Biol Chem* 276(34):31515–31520. <https://doi.org/10.1074/jbc.M104267200>
- Saparov SM, Liu K, Agre P, Pohl P (2007) Fast and selective ammonia transport by aquaporin-8. *J Biol Chem* 282(8):5296–5301. <https://doi.org/10.1074/jbc.M609343200>
- Schwab A, Stock C (2014) Ion channels and transporters in tumour cell migration and invasion. *Philos Trans R Soc B Biol Sci* 369(1638):20130102. <https://doi.org/10.1098/rstb.2013.0102>
- Sentenac H, Bonneaud N, Minet M, Lacroute F, Salmon J-M, Gaynard F, Grignon C (1992) Cloning and expression in yeast of a plant potassium ion transport system. *Science* 256(5057):663–665. <https://doi.org/10.1126/science.1585180>
- Shen L, Shrager P, Girsch SJ, Donaldson PJ, Peracchia C (1991) Channel reconstitution in liposomes and planar bilayers with HPLC-purified MIP26 of bovine lens. *J Membr Biol* 124(1):21–32. <https://doi.org/10.1007/BF01871361>
- Sindhu Kumari S, Gupta N, Shiels A, FitzGerald PG, Menon AG, Mathias RT, Varadaraj K (2015) Role of Aquaporin 0 in lens biomechanics. *Biochem Biophys Res Commun* 462(4):339–345. <https://doi.org/10.1016/j.bbrc.2015.04.138>
- Smith BL, Agre P (1991) Erythrocyte Mr 28,000 transmembrane protein exists as a multisubunit oligomer similar to channel proteins. *J Biol Chem* 266(10):6407–6415. [https://doi.org/10.1016/S0021-9258\(18\)38133-X](https://doi.org/10.1016/S0021-9258(18)38133-X)
- Stautz J, Hellmich Y, Fuss MF, Silberberg JM, Devlin JR, Stockbridge RB, Hänel I (2021) Molecular mechanisms for bacterial potassium homeostasis. *J Mol Biol* 433(16):166968. <https://doi.org/10.1016/j.jmb.2021.166968>
- Stock C, Schwab A (2015) Ion channels and transporters in metastasis. *Biochim Biophys Acta Biomembr* 10:2638–2646. <https://doi.org/10.1016/j.bbmem.2014.11.012>
- Stroka KM, Jiang H, Chen S-H, Tong Z, Wirtz D, Sun SX, Konstantopoulos K (2014) Water permeation drives tumor cell migration in confined microenvironments. *Cell* 157(3):611–623. <https://doi.org/10.1016/j.cell.2014.02.052>
- Sui H, Han B-G, Lee JK, Walian P, Jap BK (2001) Structural basis of water-specific transport through the AQP1 water channel. *Nature* 414(6866):872–878. <https://doi.org/10.1038/414872a>
- Tajkhorshid E, Nollert P, Jensen MØ, Miercke LJ, O’Connell J, Stroud RM, Schulten K (2002) Control of the selectivity of the aquaporin water channel family by global orientational tuning. *Science* 296(5567):525–530. <https://doi.org/10.1126/science.1067778>
- Tang W, Ruknudin A, Yang WP, Shaw S-Y, Knickerbocker A, Kurtz S (1995) Functional expression of a vertebrate inwardly rectifying  $\text{K}^+$  channel in yeast. *Mol Biol Cell* 6(9):1231–1240. <https://doi.org/10.1091/mbc.6.9.1231>
- Tillman TS, Cascio M (2003) Effects of membrane lipids on ion channel structure and function. *Cell Biochem Biophys* 38(2):161–190. <https://doi.org/10.1385/CBB:38:2:161>
- Tomita Y, Dorward H, Yool AJ, Smith E, Townsend AR, Price TJ, Hardingham JE (2017) Role of Aquaporin 1 signalling in cancer development and progression. *Int J Mol Sci* 18(2):299. <https://doi.org/10.3390/ijms18020299>
- Tong J, Briggs MM, McIntosh TJ (2012) Water permeability of aquaporin-4 channel depends on bilayer composition, thickness, and elasticity. *Biophys J* 103(9):1899–1908. <https://doi.org/10.1016/j.bpj.2012.09.025>
- Tong J, Canty JT, Briggs MM, McIntosh TJ (2013) The water permeability of lens aquaporin-0 depends on its lipid bilayer environment. *Exp Eye Res* 113:32–40. <https://doi.org/10.1016/j.exer.2013.04.022>
- Törnroth-Horsefield S, Wang Y, Hedfalk K, Johanson U, Karlsson M, Tajkhorshid E, Neutze R, Kjellbom P (2006) Structural mechanism of plant aquaporin gating. *Nature* 439(7077):688–694. <https://doi.org/10.1038/nature04316>
- Tran STH, Horie T, Imran S, Qiu J, McGaughey S, Byrt CS, Tyerman SD, Katsuhara M (2020) A survey of barley PIP aquaporin ionic conductance reveals  $\text{Ca}^{2+}$ -sensitive HvPIP2;8  $\text{Na}^+$  and  $\text{K}^+$  conductance. *Int J Mol Sci* 21(19):7135. <https://doi.org/10.3390/ijms21197135>
- Tyerman SD, Whitehead LF, Day DA (1995) A channel-like transporter for  $\text{NH}_4^+$  on the symbiotic interface of  $\text{N}_2$ -fixing plants. *Nature* 378(6557):629–632. <https://doi.org/10.1038/378629a0>
- Tyerman SD, McGaughey SA, Qiu J, Yool AJ, Byrt CS (2021) Adaptable and multifunctional ion-conducting aquaporins. *Annu Rev Plant Biol* 72(1):703–736. <https://doi.org/10.1146/annurev-arplant-081720-013608>
- Udvardi MK, Day DA (1997) Metabolite transport across symbiotic membranes of legume nodules. *Annu Rev Plant Biol*

- 48(1):493–523. <https://doi.org/10.1146/annurev.arplant.48.1.493>
- Ueda M, Tsutsumi N, Fujimoto M (2016) Salt stress induces internalization of plasma membrane aquaporin into the vacuole in *Arabidopsis thaliana*. *Biochem Biophys Res Commun* 474(4):742–746. <https://doi.org/10.1016/j.bbrc.2016.05.028>
- Uehlein N, Lovisolio C, Siefritz F, Kaldenhoff R (2003) The tobacco aquaporin NtAQP1 is a membrane CO<sub>2</sub> pore with physiological functions. *Nature* 425(6959):734–737. <https://doi.org/10.1038/nature02027>
- Vacca A, Frigeri A, Ribatti D, Nicchia GP, Nico B, Ria R, Svelto M, Dammacco F (2001) Microvessel overexpression of aquaporin 1 parallels bone marrow angiogenesis in patients with active multiple myeloma. *Br J Haematol* 113(2):415–421. <https://doi.org/10.1046/j.1365-2141.2001.02738.x>
- Varadaraj K, Kushmerick C, Baldo G, Bassnett S, Shiels A, Mathias R (1999) The role of MIP in lens fiber cell membrane transport. *J Membr Biol* 170(3):191–203. <https://doi.org/10.1007/s002329900549>
- Varadaraj K, Kumari SS, Mathias RT (2010) Transgenic expression of AQP1 in the fiber cells of AQP0 knockout mouse: effects on lens transparency. *Exp Eye Res* 91(3):393–404. <https://doi.org/10.1016/j.exer.2010.06.013>
- Verdoucq L, Grondin A, Maurel C (2008) Structure–function analysis of plant aquaporin At PIP2;1 gating by divalent cations and protons. *Biochem J* 415(3):409–416. <https://doi.org/10.1042/BJ20080275>
- Verkman A, Hara-Chikuma M, Papadopoulos MC (2008) Aquaporins—new players in cancer biology. *J Mol Med* 86(5):523–529. <https://doi.org/10.1007/s00109-008-0303-9>
- Wagner K, Unger L, Salman MM, Kitchen P, Bill RM, Yool AJ (2021) Signaling mechanisms and pharmacological modulators governing diverse aquaporin functions in human health and disease. *Biochim Biophys Acta Biomembr* in press
- Wang Y, Tajkhorshid E (2007) Molecular mechanisms of conduction and selectivity in aquaporin water channels. *J Nutr* 137(6):1509S–1515S. <https://doi.org/10.1093/jn/137.6.1509S>
- Wang Y, Cohen J, Boron WF, Schulten K, Tajkhorshid E (2007) Exploring gas permeability of cellular membranes and membrane channels with molecular dynamics. *J Struct Biol* 157(3):534–544. <https://doi.org/10.1016/j.jsb.2006.11.008>
- Wang Z, Wang Y, He Y, Zhang N, Chang W, Niu Y (2020) Aquaporin-1 facilitates proliferation and invasion of gastric cancer cells via GRB7-mediated ERK and Ras activation. *Anim Cells Syst* 24(5):253–259. <https://doi.org/10.1080/19768354.2020.1833985>
- Weaver CD, Shomer NH, Louis CF, Roberts DM (1994) Nodulin 26, a nodule-specific symbiosome membrane protein from soybean, is an ion channel. *J Biol Chem* 269(27):17858–17862. [https://doi.org/10.1016/S0021-9258\(17\)32388-8](https://doi.org/10.1016/S0021-9258(17)32388-8)
- Wei X, Dong J (2015) Aquaporin 1 promotes the proliferation and migration of lung cancer cell in vitro. *Oncol Rep* 34(3):1440–1448. <https://doi.org/10.3892/or.2015.4107>
- Wu B, Steinbronn C, Alsterford M, Zeuthen T, Beitz E (2009) Concerted action of two cation filters in the aquaporin water channel. *EMBO J* 28(15):2188–2194. <https://doi.org/10.1038/emboj.2009.182>
- Yanochko GM, Yool AJ (2002) Regulated cationic channel function in *Xenopus* oocytes expressing *Drosophila* big brain. *J Neurosci* 22(7):2530–2540. <https://doi.org/10.1523/jneurosci.22-07-02530.2002>
- Yanochko GM, Yool AJ (2004) Block by extracellular divalent cations of *Drosophila* big brain channels expressed in *Xenopus* oocytes. *Biophys J* 86(3):1470–1478. [https://doi.org/10.1016/S0006-3495\(04\)74215-0](https://doi.org/10.1016/S0006-3495(04)74215-0)
- Yasui M, Hazama A, Kwon T-H, Nielsen S, Guggino WB, Agre P (1999a) Rapid gating and anion permeability of an intracellular aquaporin. *Nature* 402(6758):184–187. <https://doi.org/10.1038/46045>
- Yasui M, Kwon T-H, Knepper MA, Nielsen S, Agre P (1999) Aquaporin-6: an intracellular vesicle water channel protein in renal epithelia. *Proc Natl Acad Sci* 96(10):5808–5813. <https://doi.org/10.1073/pnas.96.10.5808>
- Yenush L (2016) Potassium and sodium transport in yeast. In: Ramos J, Sychrová H, Kschischo M (eds) *Yeast Membrane Transport*. Springer International Publishing, Cham, pp 187–228. ([https://doi.org/10.1007/978-3-319-25304-6\\_8](https://doi.org/10.1007/978-3-319-25304-6_8))
- Yool AJ (2007) Dominant-negative suppression of big brain ion channel activity by mutation of a conserved glutamate in the first transmembrane domain. *Gene Expr* 13(6):329–337. <https://doi.org/10.3727/00000006781510688>
- Yool AJ, Campbell EM (2012) Structure, function and translational relevance of aquaporin dual water and ion channels. *Mol Aspects Med* 33(5):553–561. <https://doi.org/10.1016/j.mam.2012.02.001>
- Yool AJ, Weinstein AM (2002) New roles for old holes: ion channel function in aquaporin-1. *News Physiol Sci* 17:68–72
- Yool AJ, Stamer WD, Regan JW (1996) Forskolin stimulation of water and cation permeability in aquaporin1 water channels. *Science* 273(5279):1216–1218. <https://doi.org/10.1126/science.273.5279.1216>
- Yool AJ, Stamer WD (2004) Novel roles for aquaporins as gated ion channels. In: Maui RA (eds) *Molecular and cellular insights to ion channel biology*. Elsevier, Amsterdam, pp 351–379. [https://doi.org/10.1016/S1569-2558\(03\)32015-6](https://doi.org/10.1016/S1569-2558(03)32015-6)
- Yu J, Yool AJ, Schulten K, Tajkhorshid E (2006) Mechanism of gating and ion conductivity of a possible tetrameric pore in aquaporin-1. *Structure* 14(9):1411–1423. <https://doi.org/10.1016/j.str.2006.07.006>
- Yusupov M, Yan D, Cordeiro RM, Bogaerts A (2018) Atomic scale simulation of H<sub>2</sub>O<sub>2</sub> permeation through aquaporin: toward the understanding of plasma cancer treatment. *J Phys D Appl Phys* 51(12):125401. <https://doi.org/10.1088/1361-6463/aaae7a>
- Zaks-Makhina E, Kim Y, Aizenman E, Levitan ES (2004) Novel neuroprotective K<sup>+</sup> channel inhibitor identified by high-throughput screening in yeast. *Mol Pharmacol* 65(1):214–219. <https://doi.org/10.1124/mol.65.1.214>
- Zampighi GA, Hall JE, Kreman M (1985) Purified lens junctional protein forms channels in planar lipid films. *Proc Natl Acad Sci* 82(24):8468–8472. <https://doi.org/10.1073/pnas.82.24.8468>
- Zhang JX, Xie C, Zhu Z, Huang H, Zeng Z (2012) Potential role of AQP1 and VEGF in the development of malignant pleural effusion in mice. *Med Oncol* 29(2):656–662. <https://doi.org/10.1007/s12032-011-9960-6>
- Zhao Y, Vararattanavech A, Li X, Hélixnielsen C, Vissing T, Torres J, Wang R, Fane AG, Tang CY (2013) Effects of proteoliposome composition and draw solution types on separation performance of aquaporin-based proteoliposomes: implications for seawater desalination using aquaporin-based biomimetic membranes. *Environ Sci Technol* 47(3):1496–1503. <https://doi.org/10.1021/es304306t>
- Zhou X, Su Z, Anishkin A, Haynes WJ, Friske EM, Loukin SH, Kung C, Saimi Y (2007) Yeast screens show aromatic residues at the end of the sixth helix anchor transient receptor potential channel gate. *Proc Natl Acad Sci* 104(39):15555–15559. <https://doi.org/10.1073/pnas.0704039104>

**Publisher's note** Springer Nature remains neutral with regard to jurisdictional claims in published maps and institutional affiliations.



# Inhibition of the Aquaporin-1 Cation Conductance by Selected Furan Compounds Reduces Red Blood Cell Sickling

Pak Hin Chow<sup>1</sup>, Charles D. Cox<sup>2,3</sup>, Jinxin V. Pei<sup>4</sup>, Nancy Anabaraonye<sup>5</sup>, Saeed Nourmohammadi<sup>1</sup>, Sam W. Henderson<sup>1</sup>, Boris Martinac<sup>2,3</sup>, Osheiza Abdulmalik<sup>5</sup> and Andrea J. Yool<sup>1\*</sup>

<sup>1</sup>Aquaporin Physiology and Drug Discovery Program, School of Biomedicine, University of Adelaide, Adelaide, SA, Australia, <sup>2</sup>Victor Chang Cardiac Research Institute, Darlinghurst, NSW, Australia, <sup>3</sup>St Vincent's Clinical School, University of New South Wales, Darlinghurst, NSW, Australia, <sup>4</sup>Research School of Biology, College of Science, Australian National University, Canberra, ACT, Australia, <sup>5</sup>Division of Hematology, Children's Hospital of Philadelphia, Philadelphia, PA, United States

## OPEN ACCESS

### Edited by:

Maurizio Tagliatela,  
University of Naples Federico II, Italy

### Reviewed by:

Alcira Nesse,  
Universidad de Buenos Aires,  
Argentina  
Stephan Kellenberger,  
University of Lausanne, Switzerland

### \*Correspondence:

Andrea J. Yool  
andrea.yool@adelaide.edu.au

### Specialty section:

This article was submitted to  
Pharmacology of Ion Channels and  
Channelopathies,  
a section of the journal  
Frontiers in Pharmacology

**Received:** 14 October 2021

**Accepted:** 06 December 2021

**Published:** 17 January 2022

### Citation:

Chow PH, Cox CD, Pei JV, Anabaraonye N, Nourmohammadi S, Henderson SW, Martinac B, Abdulmalik O and Yool AJ (2022) Inhibition of the Aquaporin-1 Cation Conductance by Selected Furan Compounds Reduces Red Blood Cell Sickling. *Front. Pharmacol.* 12:794791. doi: 10.3389/fphar.2021.794791

In sickle cell disease (SCD), the pathological shift of red blood cells (RBCs) into distorted morphologies under hypoxic conditions follows activation of a cationic leak current (Psickle) and cell dehydration. Prior work showed sickling was reduced by 5-hydroxymethyl-2-furfural (5-HMF), which stabilized mutant hemoglobin and also blocked the Psickle current in RBCs, though the molecular basis of this 5-HMF-sensitive cation current remained a mystery. Work here is the first to test the hypothesis that Aquaporin-1 (AQP1) cation channels contribute to the monovalent component of Psickle. Human AQP1 channels expressed in *Xenopus* oocytes were evaluated for sensitivity to 5-HMF and four derivatives known to have differential efficacies in preventing RBC sickling. Ion conductances were measured by two-electrode voltage clamp, and osmotic water permeability by optical swelling assays. Compounds tested were: 5-HMF; 5-PMFC (5-(phenoxymethyl)furan-2-carbaldehyde); 5-CMFC (5-(4-chlorophenoxymethyl)furan-2-carbaldehyde); 5-NMFC (5-(2-nitrophenoxymethyl)-furan-2-carbaldehyde); and VZHE006 (tert-butyl (5-formylfuran-2-yl)methyl carbonate). The most effective anti-sickling agent, 5-PMFC, was the most potent inhibitor of the AQP1 ion conductance (98% block at 100  $\mu$ M). The order of sensitivity of the AQP1 conductance to inhibition was 5-PMFC > VZHE006 > 5-CMFC  $\geq$  5-NMFC, which corresponded with effectiveness in protecting RBCs from sickling. None of the compounds altered AQP1 water channel activity. Combined application of a selective AQP1 ion channel blocker AqB011 (80  $\mu$ M) with a selective hemoglobin modifying agent 5-NMFC (2.5 mM) increased anti-sickling effectiveness in red blood cells from human SCD patients. Another non-selective cation channel known to be expressed in RBCs, Piezo1, was unaffected by 2 mM 5-HMF. Results suggest that inhibition of AQP1 ion channels and capacity to modify hemoglobin are combined features of the most effective anti-sickling agents. Future therapeutics aimed at both targets could hold promise for improved treatments for SCD.

**Keywords:** AQP1, cyclic GMP, Piezo1 channel, psickle, erythrocyte, RBC, sickle cell anemia



## 1 INTRODUCTION

Sickle cell disease (SCD) results from an inherited mutation in the oxygen-carrying molecule hemoglobin in red blood cells. Unlike wild type hemoglobin (Hb), hemoglobin carrying the SCD mutation (HbS) polymerizes more readily in low oxygen conditions into stiff strands which distort red blood cell morphology into diagnostic dysfunctional shapes. The SCD single point mutation in HbS converts a key glutamate residue to valine (Pauling et al., 1949; Eaton 2020). When deoxygenated, HbS molecules aggregate into rigid polymers, changing red blood cell shape, and increasing fragility, solute loss and stickiness (Pauling et al., 1949; Joiner 1993). Clinical concerns include chronic anemia, acute ischemia, severe pain episodes, and organ damage (Steinberg 1999; Rees et al., 2010). Current interventions include blood transfusions to alleviate symptoms, and hydroxyurea treatment to reduce pain crises and anemia, but chronic side effects and variability in individual responsiveness to hydroxyurea limit its usefulness (Perutz and Mitchison 1950; Charache et al., 1987; Segal et al., 2008). Transplanting stem cells from donor bone marrow is the only cure for SCD (Saraf and Rondelli 2019), an option not available to most patients around the world.

Pharmacological treatment strategies have focused on identifying chemical modifiers to stabilize HbS. Promising compounds such as aromatic aldehydes and benzaldehydes have been tested in sickle cells (Zaugg et al., 1977; Beddell et al., 1984; Abraham et al., 1991). 5-Hydroxymethyl-2-furfural (5-HMF) forms a Schiff base with HbS, increasing oxygen affinity, reducing polymerization risk, and protecting red blood cells from sickling (Abdulmalik et al., 2005). Building on this discovery, Abdulmalik, Safo and others (Xu et al., 2017) engineered a group of ester and ether derivatives of 5-HMF which they tested for effectiveness in modifying Hb, improving oxygen affinity, and preventing hypoxia-induced sickling of human SCD red blood cells. Of interest, four of the 12 synthesized compounds conferred better protection from sickling than 5-HMF (at 2 mM) and were effective in modifying hemoglobin, pointing to a new generation of candidate therapeutics. Curiously, some derivatives in the group such as 5-NMFC and 5-CMFC (despite yielding significant modification of Hb), were similar or worse than 5-HMF in preventing sickling (Zaugg et al., 1977; Xu et al., 2017). We considered this a clue that effective anti-sickling agents might serendipitously be affecting secondary targets, in addition to hemoglobin.

Volume regulation in RBCs involves a network of ion and water transport mechanisms which enable careful control of hemoglobin concentration within a narrow window (Gallagher 2017). In the resting state, normal RBC membrane cation permeability is low, but increases in cation fluxes are evident during SCD cell sickling, mediated by the  $K^+$ - $Cl^-$  cotransporter (KCC), the  $Ca^{2+}$ -activated  $K^+$  (Gardos) channel, and a less well understood leak pathway known as “Psickle” (Joiner 1993; Lew and Bookchin 2005). The involvement of a cation leak current in the sickling process has been appreciated for decades based on imbalances in  $K^+$  and  $Na^+$  levels in SCD cells (Tosteson et al.,

1952). However, a mystery concerning the molecular basis of Psickle has persisted, despite widespread interest in finding a Psickle inhibitor for expanding therapeutic strategies (Lew et al., 1997; Hannemann et al., 2014; Al Balushi et al., 2019; Kaestner et al., 2020). Cation leak currents are activated in sickle cell RBCs during deoxygenation (Joiner 1993; Joiner et al., 1988; Ma et al., 2012) and can be potentiated by membrane shear stress (Johnson and Gannon 1990), such as that experienced in the microcirculation (McMahon 2019).

AQP1 is expressed in red blood cells (Ma et al., 1998; Maeda et al., 2009), and tissues including kidney, vascular system, heart, brain and others (Venero et al., 2001; Badaut et al., 2002; Papadopoulos et al., 2002; Speake et al., 2003; Montiel et al., 2020). AQP1 serves dual roles as a water channel and a non-selective cation channel regulated by cGMP acting at the loop D domain (Yu et al., 2006; Kourghi et al., 2018). Although initially controversial, converging lines of evidence have shown AQP1 conducts non-selective monovalent cations via the central pore of the tetramer, which is functionally and pharmacologically distinct from the water-selective pores in the monomeric subunits (Anthony et al., 2000; Saparov et al., 2001; Boassa and Yool, 2003; Yu et al., 2006; Zhang et al., 2007). As reviewed elsewhere, other classes of AQPs also function as ion channels including AQP0, AQP6, *Drosophila* Big Brain, soybean Nodulin and *Arabidopsis* PIP2; 1 (Yool and Campbell 2012; Tyerman et al., 2021).

A possible role for AQP1 ion channels as the monovalent component of the Psickle conductance has not previously been considered. Recent work demonstrated that 5-HMF caused dose-dependent block of the AQP1 ion conductance, inducing 90% block of the cGMP activated ion current at 10 mM, 74% at 1 mM and 43% at 0.5 mM, with no effect on AQP1-mediated water fluxes (Chow et al., 2020), supporting the hypothesis tested here that the furan derivatives which are effective in reducing red blood cell sickling also act as pharmacological inhibitors of the AQP1 cation conductance.

In summary, results here showed two furan derivatives that are effective in preventing SCD cell sickling, 5-PMFC and VZHE006, significantly inhibited the AQP1 cation conductance, as did the parent compound 5-HMF. No inhibition of the AQP1 ion conductance was observed with 5-NMFC or 5-CMFC, which modified hemoglobin but were less effective in reducing sickling. Piezo1, a mechanosensitive cation channel proposed to mediate Psickle in RBCs, is unlikely to account in full for the Psickle current, since it was not affected by 5-HMF. However, a further role for Piezo1 in  $Ca^{2+}$  entry associated with the Psickle current and RBC dehydration seems likely. AQP1 ion channels are selective for monovalent cations, not  $Ca^{2+}$  (Yool et al., 1996), whereas Piezo1 enables  $Ca^{2+}$  permeation (Gnanasambandam et al., 2015). To test the idea that effective anti-sickling furan agents acted on both HbS and AQP1, red blood cells from human SCD patients were tested with 5-NMFC which modifies Hb, in combination with the bumetanide derivative AqB011 which blocks AQP1 ion channels (Kourghi et al., 2016). Results showed that combined agents increased the duration of protection from sickling in human SCD cells in hypoxic conditions as compared to either agent alone, and approached

the protective effect of 5-PMFC which affects both targets simultaneously.

This work is the first to identify AQP1 as a molecular component of the monovalent Psickle current, and to establish AQP1 as a therapeutic target for consideration in the development of anti-sickling treatments. In practice, useful therapeutic agents would not need to prevent sickling completely, but simply would need to slow the process of HbS polymerization sufficiently that a larger proportion of RBCs could successfully pass through the microcirculation (Eaton 2020). Novel therapeutic agents with combined actions on AQP1 ion channel inhibition and HbS stabilization could offer the desired slowing of dehydration and HbS polymerization, a goal of international interest for expanding the range of affordable clinical options for treating sickle cell disease.

## 2 MATERIALS AND METHODS

### 2.1 Furan Compounds

5-HMF (5-hydroxymethyl-2-furfural); 5-PMFC (5-(phenoxyethyl)furan-2-carbaldehyde); 5-CMFC (5-(4-chlorophenoxyethyl)furan-2-carbaldehyde); and 5-NMFC (5-(2-nitrophenoxy methyl)-furan-2-carbaldehyde) were purchased from Sigma Aldrich Chemicals (MO, United States). VZHE006 (tert-butyl (5-formylfuran-2-yl)methyl carbonate), synthesized at Virginia Commonwealth University (United States) as described previously (Xu et al., 2017) was kindly provided by Dr Martin Safo. 5-HMF was dissolved in water, and other compounds were dissolved in dimethylsulfoxide (DMSO) to create 1,000x stock solutions, which were diluted 1  $\mu$ l/ml into experimental salines to final concentrations. The AQP1 ion channel antagonist AqB011 (Kourghi et al., 2016) also was made as a 1,000x stock solution in DMSO for dilution in experimental salines. Pharmacological agents as powders were stored dry at  $-20^{\circ}\text{C}$ , resuspended as stock solutions in DMSO and kept at  $4^{\circ}\text{C}$  for up to 8 months, and diluted in fresh saline prior to experimental use. Equivalent amounts of DMSO alone in saline served as the vehicle control.

### 2.2 Oocyte Preparation and Injection

Unfertilized oocytes were harvested from *Xenopus laevis* frogs in accord with national guidelines (Australian Code of Practice for the Care and Use of Animals for Scientific Purposes), using a protocol approved by the University of Adelaide Animal Ethics Committee (#M2018-016). Oocytes were defolliculated with collagenase type 1A (2 mg/ml) in isotonic saline (100 mM NaCl, 2 mM KCl, 5 mM  $\text{MgCl}_2$ , and 5 mM HEPES; pH 7.6) at approximately  $16\text{--}18^{\circ}\text{C}$  for 1.5 h. Oocytes were washed 3–4 times at  $\sim 10$  min intervals with isotonic saline and kept at  $18^{\circ}\text{C}$  in frog Ringers saline (isotonic saline supplemented with 0.6 mM  $\text{CaCl}_2$ , 5% horse serum (v/v), 100 units/ml penicillin, 0.1 mg/ml streptomycin, and 0.5 mg/ml tetracycline). Human AQP1 (Genbank # NM..198098) and human AQP4 (Genbank #NM..001650, OriGene) genes were subcloned into a *Xenopus*  $\beta$ -globin expression vector (Anthony et al., 2000). AQP1 cDNA was linearized with BamHI and cRNA was synthesized *in vitro* with the T3 mMessage mMachine kit (Invitrogen,

United States). Human AQP4 cDNA was linearized with NheI-HF (BioLabs) and synthesized *in vitro* with the T7 mMessage mMachine Kit. RNAs were resuspended in sterile water and stored at  $-80^{\circ}\text{C}$ . Oocytes were injected with 50 nl of sterile water (sham injection) or 50 nl of water containing 1 ng of AQP1 or AQP4 wild type cRNA. Injected oocytes were incubated in frog Ringer's saline at  $18^{\circ}\text{C}$  for 48 h or more to allow time for protein expression. All chemicals were from Sigma-Aldrich (St. Louis, MO United States), unless otherwise indicated.

### 2.3 Quantitative Swelling Assays

Prior to swelling assays, sham-injected (non-AQP1 controls) and AQP1-expressing oocytes were rinsed in isotonic saline (without serum, antibiotic-free) for at least 1 h at room temperature. Swelling rates were measured in 50% hypotonic saline (isotonic  $\text{Na}^+$  saline diluted with an equal volume of water, without test compounds present) and quantified by changes in the oocyte cross-sectional area imaged by videomicroscopy (Cohu, CA United States) at 1 frame per second for 30–60 s, using NIH ImageJ software (National Institutes of Health, MD United States). In double-swelling assays, swelling was first measured without drug treatment (first swelling “S1”). Oocytes were then incubated for 2 h in isotonic saline with vehicle or one of the test compounds, and reassessed in a second swelling assay (“S2”) in hypotonic saline without pharmacological agents, as described previously (Migliati et al., 2009). Swelling rates were measured from slopes of linear regression fits of relative volume as a function of time using Prism software (GraphPad Inc., CA United States).

### 2.4 Electrophysiology

Two-electrode voltage clamp recordings of non-AQP1 control and AQP1-expressing oocytes in isotonic  $\text{Na}^+$  saline were done with capillary glass electrodes (1–3 M $\Omega$ ) filled with 1 M KCl, using a GeneClamp 500B (Molecular Devices, CA United States) amplifier. Bath application of membrane permeable 8CPT-cGMP (8-(4-chlorophenylthio)-guanosine 3',5'-cyclic monophosphate) at 10  $\mu$ M final or SNP (sodium nitroprusside) at 1–3 mM final was used to activate the ionic conductance in AQP1-expressing oocytes, as described previously (Campbell et al., 2012; Kourghi et al., 2018). Changes in current as a function of time were monitored by repeated +40 mV voltage steps from a holding potential of  $-40$  every 6 s. Conductance values were measured as the slope of linear fits (from  $-40$  to +60 mV) using a current-voltage protocol with steps from +60 to  $-110$  or  $-120$  mV. Recordings were filtered at 2 kHz, and stored to hard disk for offline analysis. Data were analyzed with Clampex 9.0 software (pClamp 9.0, Molecular Devices, CA United States) and Prism software.

Piezo1 $^{-/-}$  HEK293T cells (a kind gift from Ardem Patapoutian) stably transfected with human Piezo1 were plated on 35 mm dishes for patch-clamp analysis. The extracellular solution for cell-attached patches consisted of 90 mM potassium aspartate, 50 mM KCl, 1 mM  $\text{MgCl}_2$  and 10 mM HEPES (pH 7.2; adjusted using KOH). The pipette solution contained 140 mM NaCl, 3 mM KCl, 1 mM  $\text{CaCl}_2$ , 1 mM  $\text{MgCl}_2$  with 10 mM HEPES (pH 7.2; adjusted using NaOH).

Negative pressure was applied to patch pipettes using a High-Speed Pressure Clamp-1 (ALA Scientific Instruments) and recorded in millimeters of mercury (mmHg) using a piezoelectric pressure transducer (WPI, Sarasota, FL, United States). Borosilicate glass pipettes (Sigma, St Louis, MO, United States) were pulled using a vertical pipette puller (PP-83, Narashige, Japan) to produce electrodes with resistances of 2.0–2.3 M $\Omega$ . Single-channel Piezo1 currents were amplified using an AxoPatch 200B amplifier (Axon Instruments), and data were acquired at a sampling rate of 10 kHz with 1 kHz filtration and analyzed using pCLAMP10 software (Axon Instruments). Boltzmann distribution functions were used to analyze dependence of mesoscopic Piezo1 channel currents and open probability on the negative pressure applied via patch pipettes. The Boltzmann plots were obtained by fitting open probability  $P_o \sim I/I_{max}$  versus negative pressure using the expression  $P_o/(1-P_o) = \exp[\alpha(P-P_{1/2})]$ , where  $P$  is the negative pressure (suction) [mmHg],  $P_{1/2}$  is the negative pressure at which  $P_o = 0.5$ , and  $\alpha$  [mmHg $^{-1}$ ] is the slope of the plot  $\ln[P_o/(1-P_o)] = [\alpha(P-P_{1/2})]$  reflecting the channel mechanosensitivity.

## 2.5 Analyses of Sickling in Human SDC Red Blood Cells

Blood samples from homozygous SCD patients were used with informed consent in accord with an Institutional Review Board approved protocol for research involving human subjects at the Children's Hospital of Philadelphia. Blood suspensions (hematocrit values of 20%) were incubated under air with and without 80  $\mu$ M AqB011 and furan compounds 5-NMFC and 5-PMFC at 2.5 mM concentrations at 37°C for 1 h, then subjected to hypoxia (100% nitrogen) at 37°C for 1 h. Samples were fixed without exposure to air in buffered 2% glutaraldehyde solution, and imaged by microscope for quantitative assessment of the percentages of cells showing sickling morphologies in the treatment conditions. The percentages of sickled cells were determined using validated NIH ImageJ machine-learning software analyses of microscopic images, a method enabling reliable and reproducible detection of sickled shapes based on a combination of circular and elliptical shape factors, as previously reported (Abdulmalik et al., 2005; Xu et al., 2017).

## 2.6 In Silico Docking Modeling

*In silico* modeling was carried out using methods successfully employed previously to identify candidate sites for pharmacological modulators of AQP1 channels (Kourghi et al., 2016). The human AQP1 protein crystal structure (PDB ID: 1FQY) was obtained from the NIH National Center for Biotechnology Information Structure database (available at [www.ncbi.nlm.nih.gov/Structure/pdb/1FQY](http://www.ncbi.nlm.nih.gov/Structure/pdb/1FQY)). Structures for 5-HMF and the derivatives were downloaded from NIH PubChem ([pubchem.ncbi.nlm.nih.gov](http://pubchem.ncbi.nlm.nih.gov)) and converted into software-compatible 3D structures in .pdb format using the online SMILES Translator and Structure File Generator (National Cancer Institute, U.S. Department Health and Human Services, Washington DC). MGLtools was used for

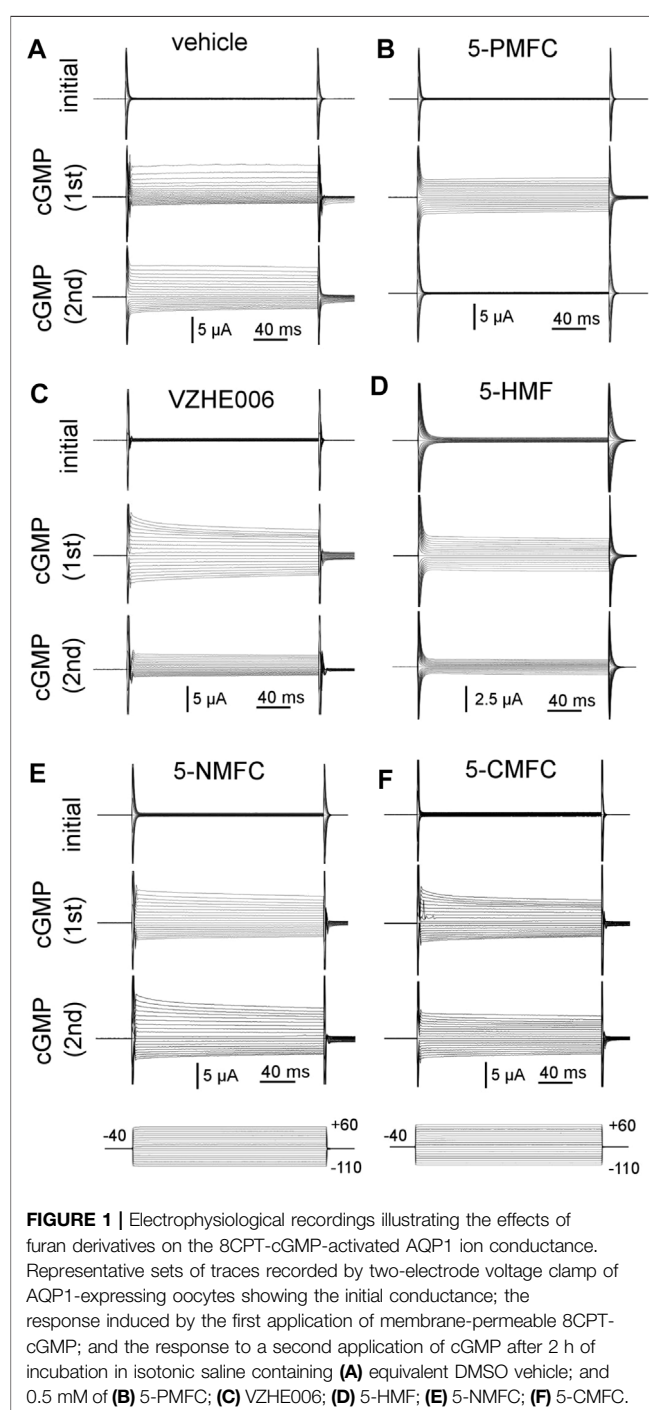


**FIGURE 1** | Electrophysiological recordings illustrating the effects of furan derivatives on the 8CPT-cGMP-activated AQP1 ion conductance. Representative sets of traces recorded by two-electrode voltage clamp of AQP1-expressing oocytes showing the initial conductance; the response induced by the first application of membrane-permeable 8CPT-cGMP; and the response to a second application of cGMP after 2 h of incubation in isotonic saline containing (A) equivalent DMSO vehicle; and 0.5 mM of (B) 5-PMFC; (C) VZHE006; (D) 5-HMF; (E) 5-NMFC; (F) 5-CMFC.

preparing both AQP1 and ligand docking coordinates. The docking was performed using Autodock Vina (Trott and Olson 2010), setting the docking grid to cover the intracellular face of the tetrameric pore.

## 2.7 Data Analysis and Statistics

Results compiled from replicate experiments are presented as box plots to show the full range of data points. Boxes represent 50% of the data points; the error bars indicate the full ranges; horizontal

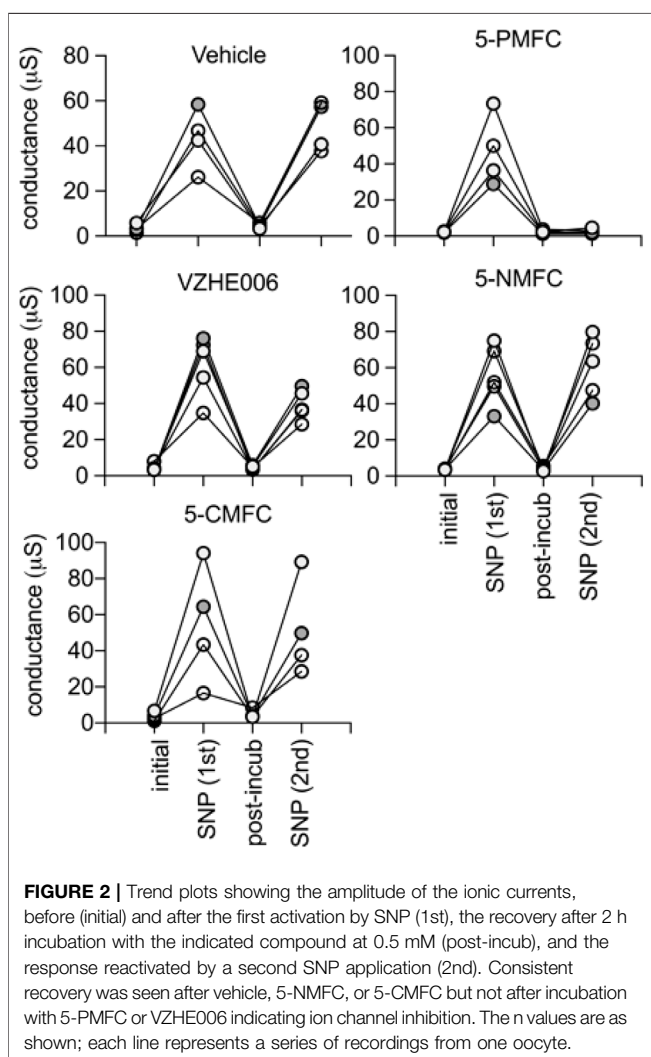


**FIGURE 2 |** Trend plots showing the amplitude of the ionic currents, before (initial) and after the first activation by SNP (1st), the recovery after 2 h incubation with the indicated compound at 0.5 mM (post-incub), and the response reactivated by a second SNP application (2nd). Consistent recovery was seen after vehicle, 5-NMFC, or 5-CMFC but not after incubation with 5-PMFC or VZHE006 indicating ion channel inhibition. The *n* values are as shown; each line represents a series of recordings from one oocyte.

bars are median values. Statistically significant differences were evaluated as indicated in the Figure legends.

### 3 RESULTS

Electrophysiological analyses tested the effects of four furan derivatives, 5-PMFC, VZHE006, 5-NMFC, and 5-CMFC at 0.5 mM each, on the 8CTP-cGMP-activated ionic conductance in human AQP1-expressing oocytes (Figure 1), and confirmed block by the original scaffold compound 5-HMF at 0.5 mM. Currents were measured before (“initial”) and after activation by the cyclic GMP agonist (“cGMP 1st”), at approximately 30 min for 8CPT-cGMP (Campbell et al., 2012) or 10–15 min for SNP (Kourghi et al., 2018). After the initial recording, oocytes were removed from the bath chamber, then incubated for 2 h in isotonic saline with vehicle or the indicated agents, and then returned to the bath chamber for another set of voltage clamp recordings of responses to the second application of cGMP agonist (“cGMP 2nd”) without furans present in the bath saline. Prior work demonstrated that the establishment of

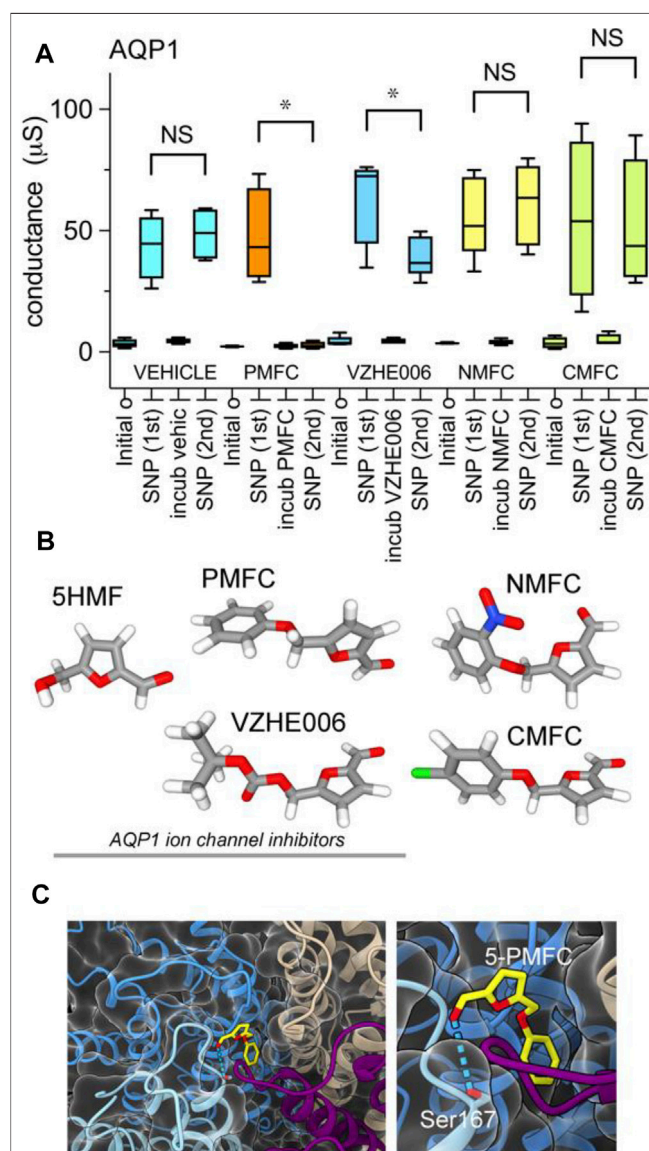


**FIGURE 3 |** Compiled data showing the effects of furan derivatives on the amplitude of the cGMP-dependent AQP1 ion conductance activated by SNP. **(A)** Compiled box plot data showing statistically significant inhibition of the AQP1 ion conductance by 5-PMFC or VZHE006, but not vehicle, 5-NMFC or 5-CMFC. *n* values were four each for all but 5-NMFC which was 5. Statistical significance was determined by paired Student's *t* test; \**p* < 0.05; NS not significant. **(B)** Space filling structures of the compounds tested; the three on the left act as AQP1 inhibitors. **(C)** In silico docking model illustrating the predicted site for the most favorable interaction of 5-PMFC with AQP1, located near the central pore vestibule of the tetrameric channel in the loop D gating domain, which is seen as a curved purple strand connecting transmembrane helices (left panel). Higher magnification view of the predicted hydrogen bond interaction between 5-PMFC and Ser167 (right panel).

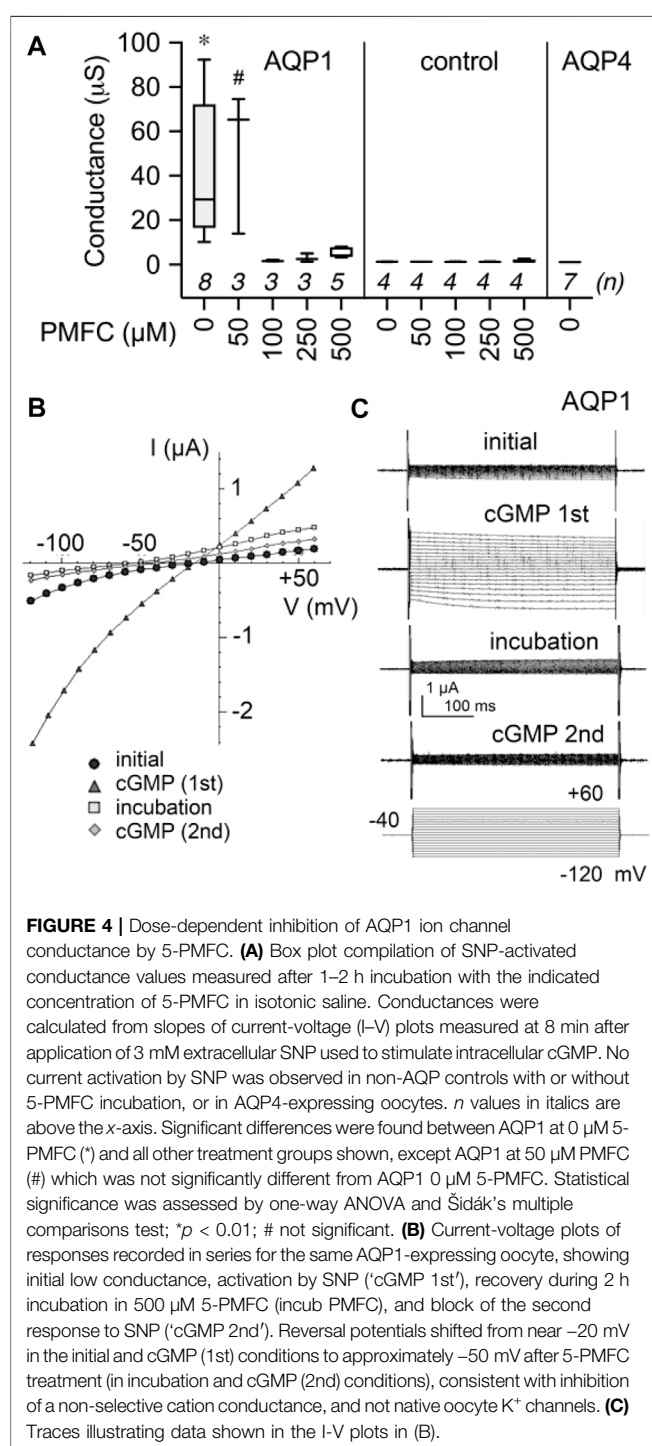
AQP1 block by 5HMF was time-dependent, and required 1 h pre-incubation for full inhibition (Chow et al., 2020). Consistent with an intracellular site of action, the block was slowly reversible, showing recovery over hours after washout. Incubation with vehicle did not impair subsequent conductance responses of

AQP1-expressing oocytes to cGMP agonists, which remained comparable in amplitude in repeated trials. Conductance responses were differentially inhibited following incubation in 0.5 mM 5-HMF, 5-PMFC, or VZHE006. No appreciable changes in responsiveness to cGMP were observed after incubation with 0.5 mM 5-NMFC or 5-CMFC.

During the 2 h incubation period (without the cGMP agonist SNP present), the ionic conductance recovered completely, as confirmed in trend plots tracking the conductance values for vehicle saline-incubated individual oocytes through the treatment series (Figure 2). Amplitudes of ion conductances after the incubation period (“post incub”) in all treatment groups were comparable to those in the initial condition, showing responses were uniformly reversible, and ruling out toxicity or cell damage. Second applications of cGMP agonist in normal saline were used to assess the level of block established during the incubation period. The AQP1 conductance was fully reactivated in oocytes incubated in vehicle treatment, showing that repeated recordings were well tolerated. The profound lack of AQP1 reactivation by cGMP after 2 h incubation in 0.5 mM 5-PMFC demonstrated effective block of the ion conductance. VZHE006 caused moderate inhibition, whereas 5-NMFC and 5-CMFC showed no appreciable blocking effect. No current activation by cGMP or effects of furan compounds were seen in non-AQP-expressing controls (see Figure 4 below).

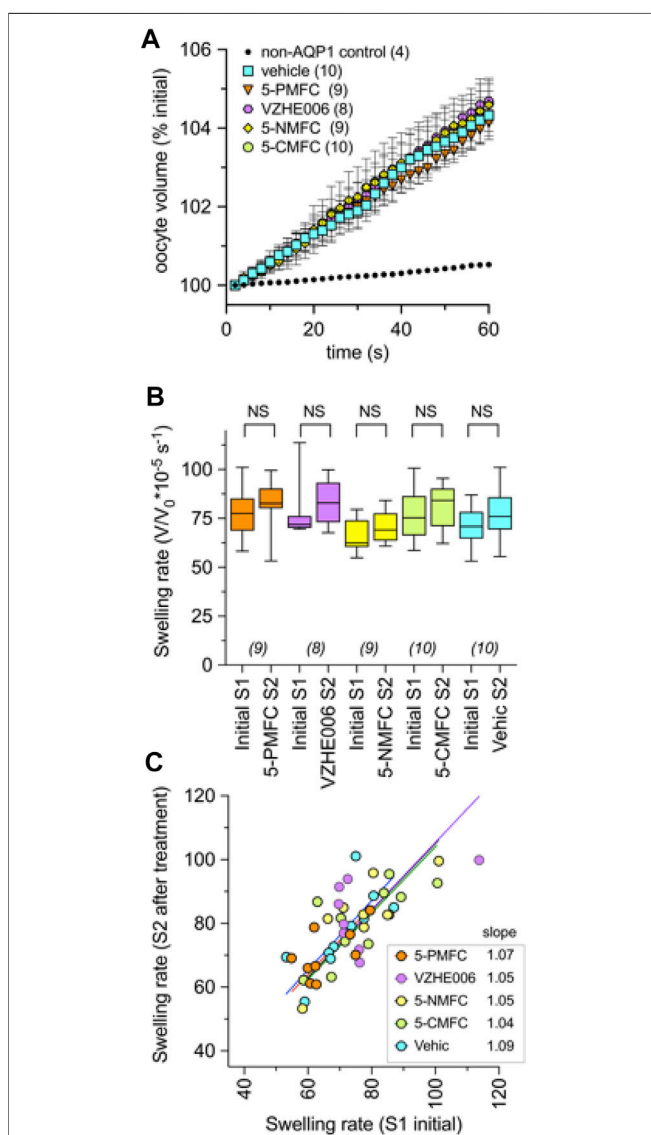
Ion conductance values were calculated from linear slope values from of current-voltage recordings, and compiled in a box plot (Figure 3) and dot plots (Supplementary Figure S1) to evaluate cGMP-activated conductance levels in AQP1-expressing oocytes, and effects of incubation with vehicle or furan compounds. Responses measured from the same oocytes after incubation with 5-PMFC or VZHE006 were significantly reduced as compared to initial responses to SNP used to induce intracellular cGMP signaling (Figure 3A). Structures of the furan derivatives are illustrated in (Figure 3B). Figure 3C shows the results of in silico modeling of the predicted binding site for 5-PMFC on the AQP1 channel, suggesting that the most energetically favourable site for interaction is located at the intracellular side of the central pore of the tetramer, in the gating domain (loop D) at a highly conserved serine residue (serine 167 in human AQP1). The predicted interaction energy of 5-PMFC at this site is  $-5.1$  kcal/mol, which is more favorable than the predicted energy of interaction of 5HMF ( $-4.9$  kcal/mol), consistent with the greater effectiveness of 5-PMFC in blocking the AQP1 ion conductance (Figure 3A). This region in the loop D domain appears to be important for channel activation; mutation of an adjacent highly conserved residue, glycine 166 to proline, was found previously to significantly augment cGMP activation of the AQP1 ion conductance (Kourghi et al., 2018). Additional poses identified by in silico docking for AQP1 and predicted energies of interaction with 5-PMFC are illustrated in Supplementary Figure S2.

Figure 4 shows the dose-dependent block of nonselective cation current by 5-PMFC in AQP1-expressing oocytes, with no effect in non-AQP-expressing control oocytes. The boxplot (Figure 4A) shows compiled data for conductance levels activated by 3 mM



**FIGURE 4 |** Dose-dependent inhibition of AQP1 ion channel conductance by 5-PMFC. **(A)** Box plot compilation of SNP-activated conductance values measured after 1–2 h incubation with the indicated concentration of 5-PMFC in isotonic saline. Conductances were calculated from slopes of current-voltage (*I*-*V*) plots measured at 8 min after application of 3 mM extracellular SNP used to stimulate intracellular cGMP. No current activation by SNP was observed in non-AQP controls with or without 5-PMFC incubation, or in AQP4-expressing oocytes. *n* values in italics are above the *x*-axis. Significant differences were found between AQP1 at 0 µM 5-PMFC (\*) and all other treatment groups shown, except AQP1 at 50 µM 5-PMFC (#) which was not significantly different from AQP1 0 µM 5-PMFC. Statistical significance was assessed by one-way ANOVA and Šidák’s multiple comparisons test; \**p* < 0.01; # not significant. **(B)** Current-voltage plots of responses recorded in series for the same AQP1-expressing oocyte, showing initial low conductance, activation by SNP (“cGMP 1st”), recovery during 2 h incubation in 500 µM 5-PMFC (incubation), and block of the second response to SNP (“cGMP 2nd”). Reversal potentials shifted from near  $-20$  mV in the initial and cGMP (1st) conditions to approximately  $-50$  mV after 5-PMFC treatment (in incubation and cGMP (2nd) conditions), consistent with inhibition of a non-selective cation conductance, and not native oocyte  $K^+$  channels. **(C)** Traces illustrating data shown in the *I*-*V* plots in (B).

SNP, measured from slopes of current-voltage plots. AQP1-expressing oocytes showed plateau activation of ion conductances by 8 min after 3 mM SNP application, which was blocked by 1–2 h incubation in isotonic saline with 5-PMFC at doses of 100–500 µM. No significant inhibition was observed at 50 µM. Control oocytes and AQP4-expressing oocytes showed no current activation in response to SNP. AQP4-expressing oocytes had high osmotic water permeability but showed no current



**FIGURE 5 |** Osmotic water permeability of AQP1-expressing oocytes is not altered by treatment with the furan derivatives. **(A)** Mean swelling responses of AQP1 expressing oocytes in 50% hypotonic saline were not affected after 2 h of preincubation in the furan derivatives (2 mM). Data are mean  $\pm$  SEM; *n* values are as shown in the key. **(B)** Compiled box plot data showing comparable swelling rates measured in the same oocytes for the first (S1) assay before and second (S2) assay after 2-h incubation in saline with indicated treatments. Statistical significance was assessed by ANOVA and post hoc paired Student *T* tests; NS not significant. **(C)** The plot of S1 vs. S2 swelling rates for individual oocytes shows a linear relationship (slope values near 1.0) in all treatment conditions, indicating no effect on water channel activity, and no change in oocyte membrane integrity or levels of AQP1 channel expression during pharmacological incubation or repeated assays. "Vehic" is vehicle control (equivalent DMSO).

activation by SNP, confirming that the capacity for aquaporins to show cGMP-induced ion currents depends on the type of AQP expressed and is not an indirect effect of increased osmotic water permeability in the oocyte expression system. A set of current-voltage plots for a single AQP1-expressing oocyte taken through a

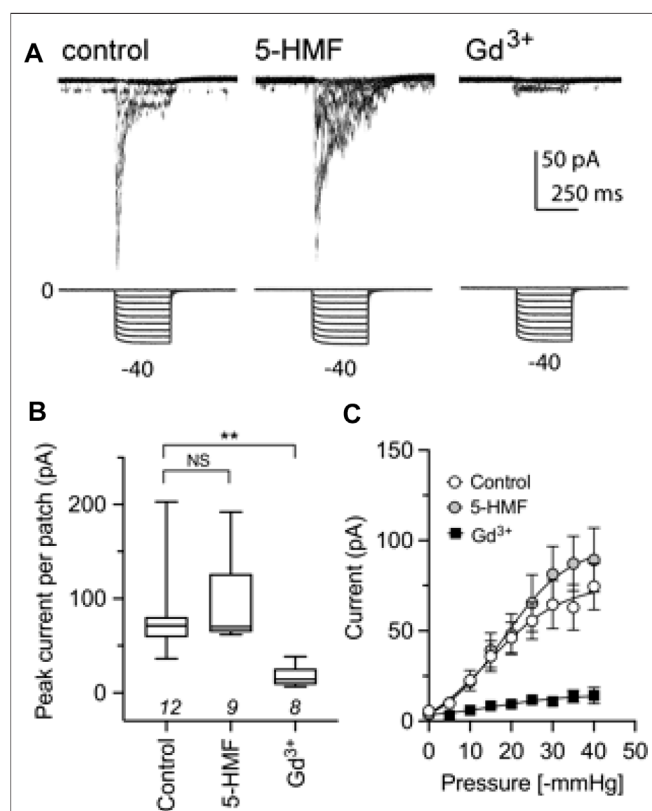
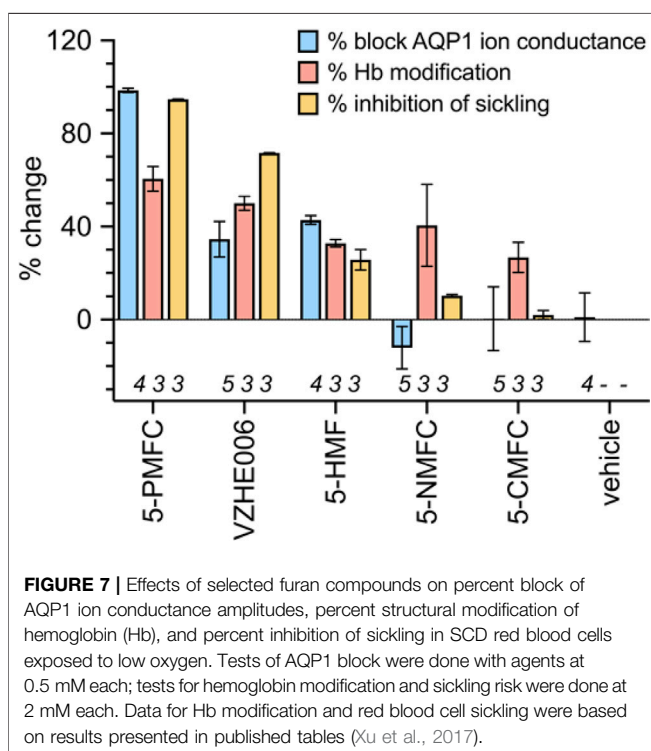


**FIGURE 6 |** The Piezo1 ion channel conductance is not sensitive to block by 5-HMF. **(A)** Representative traces from cell-attached recordings of human Piezo1 currents (upper row) measured in HEK293T cells stably transfected with Piezo1, shown for cells in the control treatment (left), after 2 mM 5-HMF for 60 min (center), or after 100  $\mu\text{M}$   $\text{GdCl}_3$  applied in the bath for  $\geq 5$  min before patching (right). Square wave pressure pulses (lower row) were applied to the patch pipette using a high-speed pressure clamp. **(B)** Amplitudes of peak currents recorded from cell attached patches from HEK293T cells in control, 5-HMF and  $\text{Gd}^{3+}$  treatment groups as specified in panel A. \*\* is  $p < 0.01$ ; NS is not significant; *n* values are above the x-axis. **(C)** Pressure-sensitive activation of Piezo1 currents in control, 5-HMF and  $\text{Gd}^{3+}$  treatment groups. Statistical significance was assessed by Kruskal-Wallis ANOVA and post hoc Dunn's multiple comparisons tests; \*\* $p < 0.01$ ; NS not significant.

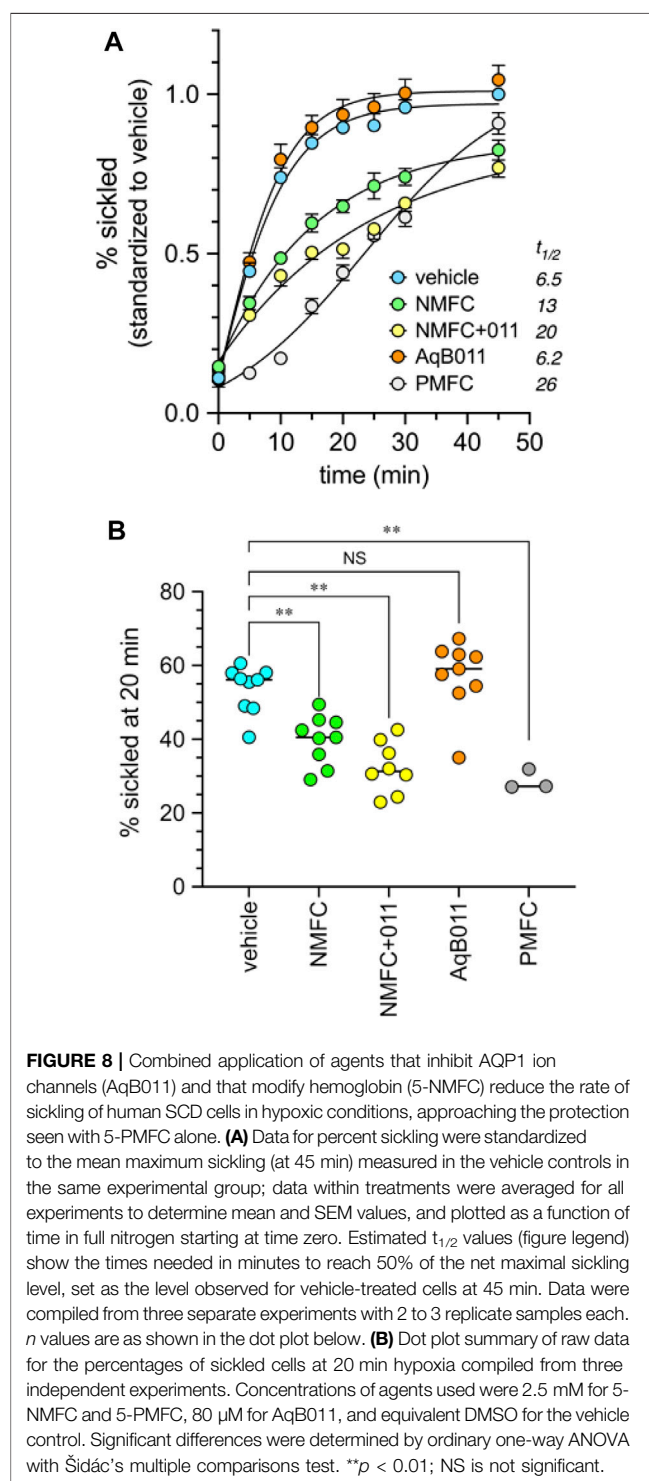
series of treatments (Figure 4B) shows low initial current, subsequent activation of the ion current by SNP, recovery to baseline after incubation in saline with 500  $\mu\text{M}$  5-PMFC, and inhibition of the subsequent current activation by SNP, illustrating channel inhibition. The negative shift in the reversal potential between recordings done before and after 5-PMFC treatment was consistent with block of a non-selective cation channel and not endogenous  $\text{K}^+$  channels. Figure 4C shows traces corresponding to the data shown in the current-voltage plots in Figure 4B.

None of the furan derivatives had any effect on AQP1-mediated osmotic water permeability (Figure 5). AQP1 water channel activity depends on intrasubunit water pores rather than the central pore, and has been shown previously to differ from the central pore in pharmacological sensitivities to inhibitors (Yool and Campbell 2012). Non-AQP-expressing control oocytes as



expected showed very little osmotic swelling. Oocytes expressing AQP1 after 2 h incubation in saline with the indicated compounds (2 mM) or an equivalent vehicle, were assessed for osmotic water permeability using an optical swelling assay without blocker (Figure 5A). All AQP1-expressing oocytes showed strong swelling in hypotonic extracellular saline. AQP1-mediated swelling showed no effects of vehicle or furan treatments, as summarized in the box plot (Figure 5B). AQP1-expressing oocytes were tested in double swelling assays, in which each oocyte was tested before and after 2 h incubation in isotonic saline containing vehicle or the furan compounds at 2 mM. There were no significant differences between the first (S1) and second (S2) swelling rates for individual oocytes in any of the treatment groups (Figure 5C), as indicated by the slope values near 1.0 in plots of S1 versus S2 swelling rates. These results showed that none of the furan compounds affected AQP1 osmotic water permeability, and also confirmed that the AQP1 channels remained functionally intact and localized in oocyte plasma membrane through the experimental treatments.

Piezo1, a cation channel present in human RBCs and previously proposed to contribute to the Psickle current (Cahalan et al., 2015), showed no effect of treatment with 2 mM 5-HMF in bath saline after 1 h incubation (Figure 6). As expected, Piezo1 current was inhibited within 5 min by the known blocker  $Gd^{3+}$  at 100  $\mu$ M, shown previously to block mechanosensitive ion channels (Yang and Sachs 1989) including Piezo1 (Coste et al., 2010). The  $Gd^{3+}$  blocker was added to the bath for Piezo1-expressing HEK cells in advance of cell-attached electrophysiological recording. This protocol achieved full channel block, serving as a positive control. Human Piezo1 channel currents were recorded in cell-attached



patches from stably transfected HEK293T cells, and activated by square-wave pressure pulses (Figure 6A). Currents were significantly reduced in amplitude after treatment with  $Gd^{3+}$ , but not 5-HMF (Figure 6B). 5-HMF did not alter the pressure dependence of Piezo1 for ion channel activation (Figure 6C).

A comparison of the effects of 5HMF and structural derivatives on the amplitude of the AQP1 ion conductance

(results here), and the level of hemoglobin modification, and the percentage of SCD cell sickling in hypoxic conditions (summarised from prior work for comparison) is illustrated in **Figure 7**. The magnitude of sickle cell inhibition at 2 mM was 5-PMFC > VZHE006 > 5-HMF > 5-NMFC > 5-CMFC (Xu et al., 2017). The agents 5-PMFC, VZHE006 and 5-HMF significantly inhibited the AQP1 ion channel at 0.5 mM, whereas 5-NMFC and 5-CMFC were not effective at concentrations up to 2 mM. Interestingly, though 5-PMFC and VZHE006 yielded levels of Hb modification similar to those of 5-HMF and 5-NMFC, these agents did not protect SCD RBCs from sickling, indicating that Hb modification alone does not account for a full beneficial effect. Instead the furan agents showed efficacies consistent with a dependence on both the ability to modify Hb and the ability to block the AQP1 ion channel conductance, supporting a novel dual targeting mechanism.

The prediction that a combination of AQP1 block and HbS modification should improve protection from sickling over either treatment alone was tested by co-application of AqB011 (a pharmacological inhibitor of the AQP1 ion conductance (Kourghi et al., 2016)), and the furan derivative 5-NMFC which causes Hb modification (Xu et al., 2017) without blocking AQP1. Data in **Figure 8** show that the presence of 80  $\mu$ M AqB011 in combination with 2.5 mM 5-NMFC conferred a significant increase in protection of human SCD red blood cells from sickling during hypoxia. The combination was more effective than either alone. The time ( $t_{1/2}$ ) needed for the proportion of sickled cells to reach 50% of maximum (referenced to the % sickled cells in vehicle treatment at 45 min) differed across the treatment groups (**Figure 8A**). Rapid onset of sickling was seen in vehicle-treated and AqB011-treated groups (estimated  $t_{1/2}$  6–7 min). The window of protection was doubled with 5-NMFC alone ( $t_{1/2}$  13 min), but was substantially increased in treatment with combined 5-NMFC + AqB011, and treatment with 5-PMFC, for which  $t_{1/2}$  values were prolonged 3 to 4 fold over vehicle control ( $t_{1/2}$  20 min or more). The percentages of sickled cells after 20 min hypoxia (**Figure 8B**) were reduced significantly by coapplication of AqB011 with 5-NMFC, as compared with 5-NMFC alone. 5-PMFC was the most effective of the agents tested in reducing sickling in human SCD cells.

## 4 DISCUSSION

Cellular loss of  $K^+$ ,  $Cl^-$  and water drives dehydration and increases the concentration of HbS in red blood cells of patients with SCD, leading to cell sickling (Joiner 1993; Gibson and Ellory 2002; Lew and Bookchin 2005). Compounds structurally related to 5-HMF were shown previously by Abdulmalik and others to protect SCD cells from sickling, with differences in efficacies thought to be due to levels of modification of HbS and oxygen affinity (Xu et al., 2017). Prior observations that 5-HMF inhibited the Psickle cation leak (Hannemann et al., 2014), and blocked the AQP1 ion conductance (Chow et al., 2020) suggested a novel link with cation conductance pathways. Results here demonstrate that the

most effective of the anti-sickling 5-HMF derivatives, 5-PMFC, is the most potent inhibitor of the cationic conductance of AQP1. AQP1 has not previously been considered as a component of Psickle, but results here support it as a strong candidate for the monovalent cation leak component that is pharmacologically distinct from the Piezo1, KCC and Gardos channels, and important as an early step in the dehydration cascade leading to the sickling phenomenon.

Multiple lines of evidence now support the initially controversial concept that AQP1 is an ion channel (Yool et al., 1996; Agre et al., 1997; Yool and Campbell 2012), permeable to  $Na^+$ ,  $K^+$ ,  $Cs^+$  and  $Li^+$  but not divalent cations, as demonstrated by electrophysiology experiments, structure-function analyses, molecular dynamic modeling, and real-time visualization with a photoswitchable optical probe (Anthony et al., 2000; Yool and Weinstein 2002; Yu et al., 2006; Campbell et al., 2012; Kourghi et al., 2016; Kourghi et al., 2017; Pei et al., 2019). Unlike classic cyclic nucleotide-gated channels in sensory cells (Broillet and Firestein 1999), the AQP1 ion channel shows very slow activation and deactivation kinetics in response to cGMP on a time scale of minutes, with slow modal behavior marked by a low probability of initial opening, and long bursts of large conductance openings once channels are activated (Anthony et al., 2000). In heterologous expression systems, only a small percentage of the AQP1 water channels are active as ion channels (Saparov et al., 2001; Yool and Campbell 2012); nonetheless this low proportion has been modeled as being sufficient to impose meaningful changes in net ion transport across membranes (Yool and Weinstein 2002). The proportion of AQP1 available for ion channel gating in the total water channel population is modulated by tyrosine phosphorylation in the carboxyl terminal domain (Campbell et al., 2012) and potentially by other factors such as membrane and cytoskeletal protein interactions (Cowan et al., 2000).

5-HMF is known to decrease sickling of RBCs from disease-affected patients, with effects originally attributed to decreased hemoglobin crosslinking (Safó et al., 2004). Of interest to us was the observation that 5-HMF blocked the Psickle current at doses comparable to those used to reduce RBC sickling (Hannemann et al., 2014). At millimolar concentrations, 5-HMF reduced the Psickle component as measured by  $Rb^+$  uptake in SCD cells; the magnitude of the monovalent ion flux compared for treated and untreated cells correlated strongly with the percentage of cell sickling. In contrast, Gardos activity showed a small reduction by 5-HMF, and no evidence of direct block (Hannemann et al., 2014). SCD cell membranes show increased permeability to  $K^+$ ,  $Na^+$ ,  $Cs^+$ ,  $Rb^+$  and  $Li^+$  (Joiner et al., 1993), and an accumulation of intracellular radiolabelled  $Ca^{2+}$  that was attributed to increased membrane  $Ca^{2+}$  permeability (Etzion et al., 1993). The concept that Psickle was caused by one class of leak channel was adopted, with the logical caution that a single pathway for both mono- and divalent ions remained unproven (Lew et al., 1997), and thus cation leaks might rely on more than one mechanism (Kaestner et al., 2020). Consistent with the idea of more than one pathway for monovalent and divalent leak currents, deoxygenation-induced fluxes of  $K^+$  and  $Na^+$  in sickle cells were found to be



blocked by extracellular divalent cations; 2 mM  $\text{Ca}^{2+}$  reduced  $\text{Na}^+$  influx by approximately 30% as compared to  $\text{Ca}^{2+}$ -free solution, and reduced  $\text{K}^+$  efflux by 10% (Joiner et al., 1995), suggesting  $\text{Ca}^{2+}$  blocked part of the monovalent cation component directly, with an asymmetry possibly reflecting outward rectification.

RBCs deformed by shear stress showed an increase in  $\text{Na}^+$  influx and  $\text{K}^+$  efflux, not dependent on  $\text{Ca}^{2+}$  or  $\text{Cl}^-$ , without an overall change in cation content (Ney et al., 1990). A typical RBC resting potential around  $-10$  mV (Hoffman and Laris 1984) near the  $\text{Cl}^-$  and  $\text{HCO}_3^-$  equilibrium potentials would be expected to impose similar driving forces for  $\text{Na}^+$  entry and  $\text{K}^+$  exit through a non-selective cation channel pathway, consistent with the lack of effect of Psickle activity on overall transmembrane osmotic gradients. Dehydration results from progressive intracellular ion loss, which could be driven in part by a  $\text{Na}^+$ -leak induced activation of the  $\text{Na}^+$ - $\text{K}^+$ -ATPase pump which asymmetrically moves 3 cations out ( $\text{Na}^+$ ) for 2 cations in ( $\text{K}^+$ ), in a background of high anion and water permeability (Joiner et al., 1986). The molecular identity of the Psickle current has been elusive. Since human RBCs lack DNA, proteins mediating Psickle could reasonably be assumed to be expressed in all RBCs, where their contribution to normal homeostatic control would be expected to provide some selective advantage, perhaps subtle enough to go undetected in normal conditions, but rising dysfunctionally in SCD cells under hypoxic conditions. A random low-probability channel activation during successive hypoxic events is needed to explain the observed stochastic behavior of Psickle, and the broad distribution of sickle cell phenotypes within RBC populations (Lew and Bookchin 2005).

The mechanosensitive Piezo1 channel was suggested previously as a molecular candidate for the Psickle current, based on observations that Piezo1 is expressed in RBCs, activated by membrane deformation (Cox et al., 2016), permeable to mono- and divalent cations, affected by inherited mutations linked to erythrocyte hydration disorders (Gallagher 2017; Lew and Tiffert 2017), and sensitive to block by a tarantula spider toxin which appeared to partially inhibit Psickle monovalent cation fluxes in deoxygenated conditions, as measured by whole cell patch clamp in SCD cells (Ma et al., 2012). Psickle activation has been associated with  $\text{Ca}^{2+}$  entry and  $\text{Mg}^{2+}$  exit (Ortiz et al., 1990; Willcocks et al., 2002). Piezo1 channels are permeable to  $\text{K}^+$ ,  $\text{Na}^+$ ,  $\text{Cs}^+$ ,  $\text{Ba}^{2+}$ ,  $\text{Ca}^{2+}$  and  $\text{Mg}^{2+}$  (Gnanasambandam et al., 2015). Shear stress increases monovalent cation flux in RBCs (Johnson and Gannon 1990). Piezo1 is gated directly by membrane tension with rapid response times on the order of milliseconds, and is expressed across diverse phyla for feedback control of adaptive responses to environmental physical stressors (Cox et al., 2019). Based on data shown here, the insensitivity of Piezo1 channels to 5-HMF suggests that they do not account for all Psickle properties. We propose the Psickle current is mediated by more than one ion conduction pathway, with Piezo1 positioned as a strong candidate for the divalent cation leak, and AQP1 a logical mechanism accounting for the 5HMF-sensitive monovalent cation leak.

A number of properties of AQP1 ion channels are consistent with a direct contribution to the Psickle conductance. These are:

- 1) Psickle currents are found in red blood cells, in which AQP1 is expressed (Agre et al., 1995).
- 2) The Psickle current is blocked by 5-HMF (Hannemann et al., 2014), which also blocks the AQP1 ion conductance (Chow et al., 2020). As shown here, anti-sickling efficacies of 5-HMF-related derivatives correlate with their effectiveness in blocking the AQP1 ion current.
- 3) SCD cells show elevated levels of cGMP as compared with controls, consistent with an increased activity of the cGMP-dependent AQP1 ion conductance. As measured by enzyme-linked immunosorbent assay (ELISA), cGMP was 6-fold higher in sickle RBCs as compared to control (Conran et al., 2004). In the homozygous Townes mouse model of SCD, cGMP levels in RBCs were elevated 9- to 13-fold as compared to control animals (Almeida et al., 2020).
- 4) Psickle monovalent currents are reduced by extracellular  $\text{Ca}^{2+}$  (Joiner et al., 1995). Multiple classes of AQPs that act as ion channels (including AQP1) show outwardly rectifying block by extracellular divalent cations (1 mM  $\text{Ca}^{2+}$ ,  $\text{Cd}^{2+}$  or  $\text{Ba}^{2+}$ , but not  $\text{Mg}^{2+}$ ), suggesting a conserved mechanism across phyla (Kourghi et al., 2017). AQP1 binding sites for divalent cations also have independently been proposed from effects on the AQP1 central pore structure seen in electron cryo-crystallography analyses (Ren et al., 2000) and the presence of a putative candidate  $\text{Ca}^{2+}$ -binding motif in the carboxyl terminal domain (Fotiadis et al., 2002).
- 5) The stochastic behavior of Psickle suggests a dependence on low-probability channel activation events (Lew and Bookchin 2005). The probability of AQP1 channel opening is low, modulated by tyrosine phosphorylation state, and the kinetics of channel gating are slow (Anthony et al., 2000; Campbell et al., 2012), consistent with a low amplitude background current that might escape detection in normal cells and account for the stochastic nature of Psickle in hypoxic SCD cells.

Considering current drug discovery work for SCD, it is interesting to note that the compound GBT1118 is structurally related to Voxelotor, an approved drug recently shown in the HOPE Phase III clinical trial to be effective in increasing SCD patient hemoglobin concentrations, which in turn correlated with reduced incidence of vaso-occlusive crises (Howard et al., 2021). GBT1118 reduces RBC sickling, increases oxygen affinity, stabilizes HbS structure, and decreases cation fluxes mediated by Psickle, Gardos and KCC pathways (Al Balushi et al., 2019). Psickle (defined as the clotrimazole-insensitive component measured by radiolabelled  $\text{Rb}^+$  entry in low oxygen) was the component most sensitive to block by GBT1118 (with an estimated  $\text{IC}_{50}$  near 0.6 mM). In the presence of GBT1118, an expected correlation between Psickle activity and Gardos activity was lost (Al Balushi et al., 2019), perhaps suggesting the GBT1118-sensitive Psickle  $\text{K}^+$  current is separate from the  $\text{Ca}^{2+}$  permeation pathway. The possibility that AQP1 is an unrecognized secondary target of action for Voxelotor is currently being explored.

Results here are the first to identify AQP1 as a molecular candidate for the monovalent Psickle current. In the SCD red blood cell, optimal anti-sickling agents might act in parallel to reduce HbS polymerization (countering morphological deformation), and to block the AQP1 ion channel (countering the Psickle leak). Further optimization of the agents and

treatment conditions will be needed, and further analyses of roles for other candidates such as Piezo1 channels are of interest for future work. It is interesting to note the proposal by Eaton and others that beneficial agents do not need to block sickling completely, but should slow the process of sickling to facilitate the successful passage of more RBCs through the microcirculation (Eaton 2020). Our data suggest that combined targeting of AQP1 and HbS might achieve this essential aim, prolonging the window of protection.

In addition to RBCs, AQP1 channels are expressed in endothelial and epithelial membranes of many cells (Ma et al., 1998; Agre 2004; Maeda et al., 2009) including vascular endothelium, which is a key player in SCD vaso-occlusion events. The endothelial cell could be an important additional site of action of AQP1 pharmacological inhibitors. AQP1 merits consideration as a co-target in the development of anti-sickling treatments. Candidate drugs, perhaps similar to 5-PMFC with combined actions on both HbS stabilization and AQP1 ion channel inhibition, could be valuable starting points for generating affordable clinical options for treating sickle cell disease around the world.

## DATA AVAILABILITY STATEMENT

The raw data supporting the conclusion of this article will be made available by the authors, without undue reservation.

## ETHICS STATEMENT

The studies involving human participants were reviewed and approved by Institutional Review Board for Research involving Human Subjects at the Children's Hospital of Philadelphia. The patients/participants provided their written informed consent to participate in this study. The animal study was reviewed and

## REFERENCES

- Abdulmalik, O., Safo, M. K., Chen, Q., Yang, J., Brugnara, C., Ohene-Frempong, K., et al. (2005). 5-Hydroxymethyl-2-Furfural Modifies Intracellular Sickle Haemoglobin and Inhibits Sickling of Red Blood Cells. *Br. J. Haematol.* 128 (4), 552–561. doi:10.1111/j.1365-2141.2004.05332.x
- Abraham, D. J., Mehanna, A. S., Wireko, F. C., Whitney, J., Thomas, R. P., and Orringer, E. P. (1991). Vanillin, a Potential Agent for the Treatment of Sickle Cell Anemia. *Blood* 77 (6), 1334–1341. doi:10.1182/blood.v77.6.1334.bloodjournal7761334
- Agre, P., Smith, B. L., and Preston, G. M. (1995). ABH and Colton Blood Group Antigens on Aquaporin-1, the Human Red Cell Water Channel Protein. *Transfus. Clin. Biol.* 2 (4), 303–308. doi:10.1016/s1246-7820(05)80096-5
- Agre, P., Lee, M. D., Devidas, S., and Guggino, W. B. (1997). Aquaporins and Ion Conductance. *Science* 275 (5305), 1490–1492. doi:10.1126/science.275.5305.1490
- Agre, P. (2004). Nobel Lecture. Aquaporin Water Channels. *Biosci. Rep.* 24 (3), 127–163. doi:10.1007/s10540-005-2577-2
- Al Balushi, H., Dufu, K., Rees, D. C., Brewin, J. N., Hannemann, A., Oksenberg, D., et al. (2019). The Effect of the Antisickling Compound GBT1118 on the Permeability of Red Blood Cells from Patients with Sickle Cell Anemia. *Physiol. Rep.* 7 (6), e14027. doi:10.14814/phy2.14027

approved by University of Adelaide Animal Ethics Committee (#M2018-016).

## AUTHOR CONTRIBUTIONS

Conception and design of the work: AJY and OA. Data collection: PHC, AJY, CDC, NA, SN, SWH, and OA. Data analysis and interpretation: PHC, CDC, JVP, NA, BM, OA, and AJY. Drafting the article: PHC and AJY. Writing and editing the article: AJY and OA. Final approval of the version to be published: PHC, CDC, JVP, NA, SN, SWH, BM, OA, and AJY.

## FUNDING

Funding was provided by an Australian Research Council grant (19ARC\_DPI190101745) to AY; the National Health and Medical Research Council (NHMRC) of Australia to BM for a Principal Research Fellowship (APP1135974); and National Institutes of Health grant R01MD009124 to OA. CC is supported by an NSW Health EMCR Fellowship. PC, JP, and SN were supported by University of Adelaide International Scholarships.

## ACKNOWLEDGMENTS

We thank Dr Martin K Safo for providing the compound VZHE006.

## SUPPLEMENTARY MATERIAL

The Supplementary Material for this article can be found online at: <https://www.frontiersin.org/articles/10.3389/fphar.2021.794791/full#supplementary-material>

- Almeida, L. E. F., Kamimura, S., de Souza Batista, C. M., Spornick, N., Nettleton, M. Y., Walek, E., et al. (2020). Sickle Cell Disease Subjects and Mouse Models Have Elevated Nitrite and cGMP Levels in Blood Compartments. *Nitric Oxide* 94, 79–91. doi:10.1016/j.niox.2019.10.011
- Anthony, T. L., Brooks, H. L., Boassa, D., Leonov, S., Yanochko, G. M., Regan, J. W., et al. (2000). Cloned Human Aquaporin-1 Is a Cyclic GMP-Gated Ion Channel. *Mol. Pharmacol.* 57 (3), 576–588. doi:10.1124/mol.57.3.576
- Badaut, J., Lasbennes, F., Magistretti, P. J., and Regli, L. (2002). Aquaporins in Brain: Distribution, Physiology, and Pathophysiology. *J. Cereb. Blood Flow Metab.* 22 (4), 367–378. doi:10.1097/00004647-200204000-00001
- Beddell, C. R., Goodford, P. J., Kneen, G., White, R. D., Wilkinson, S., and Wootton, R. (1984). Substituted Benzaldehydes Designed to Increase the Oxygen Affinity of Human Haemoglobin and Inhibit the Sickling of Sickle Erythrocytes. *Br. J. Pharmacol.* 82 (2), 397–407. doi:10.1111/j.1476-5381.1984.tb10775.x
- Boassa, D., and Yool, A. J. (2003). Single Amino Acids in the Carboxyl Terminal Domain of Aquaporin-1 Contribute to cGMP-dependent Ion Channel Activation. *BMC Physiol.* 3, 12. doi:10.1186/1472-6793-3-12
- Broillet, M. C., and Firestein, S. (1999). Cyclic Nucleotide-Gated Channels. Molecular Mechanisms of Activation. *Ann. N. Y. Acad. Sci.* 868, 730–740. doi:10.1111/j.1749-6632.1999.tb11352.x
- Cahalan, S. M., Lukacs, V., Ranade, S. S., Chien, S., Bandell, M., and Patapoutian, A. (2015). Piezo1 Links Mechanical Forces to Red Blood Cell Volume. *Elife* 4, e07370. doi:10.7554/eLife.07370

- Campbell, E. M., Birdsell, D. N., and Yool, A. J. (2012). The Activity of Human Aquaporin 1 as a cGMP-Gated Cation Channel Is Regulated by Tyrosine Phosphorylation in the Carboxyl-Terminal Domain. *Mol. Pharmacol.* 81 (1), 97–105. doi:10.1124/mol.111.073692
- Charache, S., Dover, G. J., Moyer, M. A., and Moore, J. W. (1987). Hydroxyurea-Induced Augmentation of Fetal Hemoglobin Production in Patients with Sickle Cell Anemia. *Blood* 69 (1), 109–116. doi:10.1182/blood.v69.1.109.109
- Chow, P. H., Kourghi, M., Pei, J. V., Nourmohammadi, S., and Yool, A. J. (2020). 5-Hydroxymethyl-Furfural and Structurally Related Compounds Block the Ion Conductance in Human Aquaporin-1 Channels and Slow Cancer Cell Migration and Invasion. *Mol. Pharmacol.* 98 (1), 38–48. doi:10.1124/mol.119.119172
- Conran, N., Oresco-Santos, C., Acosta, H. C., Fattori, A., Saad, S. T., and Costa, F. F. (2004). Increased Soluble Guanylate Cyclase Activity in the Red Blood Cells of Sickle Cell Patients. *Br. J. Haematol.* 124 (4), 547–554. doi:10.1111/j.1365-2141.2004.04810.x
- Coste, B., Mathur, J., Schmidt, M., Earley, T. J., Ranade, S., Petrus, M. J., et al. (2010). Piezo1 and Piezo2 Are Essential Components of Distinct Mechanically Activated Cation Channels. *Science* 330 (6000), 55–60. doi:10.1126/science.1193270
- Cowan, C. A., Yokoyama, N., Bianchi, L. M., Henkemeyer, M., and Fritsch, B. (2000). EphB2 Guides Axons at the Midline and Is Necessary for normal Vestibular Function. *Neuron* 26 (2), 417–430. doi:10.1016/s0896-6273(00)81174-5
- Cox, C. D., Bae, C., Ziegler, L., Hartley, S., Nikolova-Krstevski, V., Rohde, P. R., et al. (2016). Removal of the Mechanoprotective Influence of the Cytoskeleton Reveals Piezo1 Is Gated by Bilayer Tension. *Nat. Commun.* 7, 10366. doi:10.1038/ncomms10366
- Cox, C. D., Bavi, N., and Martinac, B. (2019). Biophysical Principles of Ion-Channel-Mediated Mechanosensory Transduction. *Cell Rep* 29 (1), 1–12. doi:10.1016/j.celrep.2019.08.075
- Eaton, W. A. (2020). Hemoglobin S Polymerization and Sickle Cell Disease: A Retrospective on the Occasion of the 70th Anniversary of Pauling's Science Paper. *Am. J. Hematol.* 95 (2), 205–211. doi:10.1002/ajh.25687
- Etzion, Z., Tiffert, T., Bookchin, R. M., and Lew, V. L. (1993). Effects of Deoxygenation on Active and Passive Ca<sup>2+</sup> Transport and on the Cytoplasmic Ca<sup>2+</sup> Levels of Sickle Cell Anemia Red Cells. *J. Clin. Invest.* 92 (5), 2489–2498. doi:10.1172/JCI116857
- Fotiadis, D., Suda, K., Tittmann, P., Jenö, P., Philippsen, A., Müller, D. J., et al. (2002). Identification and Structure of a Putative Ca<sup>2+</sup>-Binding Domain at the C Terminus of AQP1. *J. Mol. Biol.* 318 (5), 1381–1394. doi:10.1016/s0022-2836(02)00143-2
- Gallagher, P. G. (2017). Disorders of Erythrocyte Hydration. *Blood* 130 (25), 2699–2708. doi:10.1182/blood-2017-04-590810
- Gibson, J. S., and Ellory, J. C. (2002). Membrane Transport in Sickle Cell Disease. *Blood Cell Mol Dis* 28 (3), 303–314. doi:10.1006/bcmd.2002.0515
- Gnanasambandam, R., Bae, C., Gottlieb, P. A., and Sachs, F. (2015). Ionic Selectivity and Permeation Properties of Human Piezo1 Channels. *PLoS One* 10 (5), e0125503. doi:10.1371/journal.pone.0125503
- Hannemann, A., Cytlak, U. M., Rees, D. C., Tewari, S., and Gibson, J. S. (2014). Effects of 5-Hydroxymethyl-2-Furfural on the Volume and Membrane Permeability of Red Blood Cells from Patients with Sickle Cell Disease. *J. Physiol.* 592 (18), 4039–4049. doi:10.1113/jphysiol.2014.277681
- Hoffman, J. F., and Laris, P. C. (1984). Membrane Electrical Parameters of normal Human Red Blood Cells. *Soc. Gen. Physiol. Ser.* 38, 287–293.
- Howard, J., Ataga, K. I., Brown, R. C., Achebe, M., Nduba, V., El-Beshlawy, A., et al. (2021). Voxelotor in Adolescents and Adults with Sickle Cell Disease (HOPE): Long-Term Follow-Up Results of an International, Randomised, Double-Blind, Placebo-Controlled, Phase 3 Trial. *Lancet Haematol.* 8 (5), e323–e33. doi:10.1016/S2352-3026(21)00059-4
- Johnson, R. M., and Gannon, S. A. (1990). Erythrocyte Cation Permeability Induced by Mechanical Stress: A Model for Sickle Cell Cation Loss. *Am. J. Physiol.* 259 (5 Pt 1), C746–C751. doi:10.1152/ajpcell.1990.259.5.C746
- Joiner, C. H., Platt, O. S., and Lux, S. E. (1986). Cation Depletion by the Sodium Pump in Red Cells with Pathologic Cation Leaks. *Sickle Cells and Xerocytes. J. Clin. Invest.* 78 (6), 1487–1496. doi:10.1172/JCI112740
- Joiner, C. H., Dew, A., and Ge, D. L. (1988). Deoxygenation-Induced Cation Fluxes in Sickle Cells: Relationship between Net Potassium Efflux and Net Sodium Influx. *Blood Cells* 13 (3), 339–358.
- Joiner, C. H., Morris, C. L., and Cooper, E. S. (1993). Deoxygenation-Induced Cation Fluxes in Sickle Cells. III. Cation Selectivity and Response to pH and Membrane Potential. *Am. J. Physiol.* 264 (3 Pt 1), C734–C744. doi:10.1152/ajpcell.1993.264.3.C734
- Joiner, C. H., Jiang, M., and Franco, R. S. (1995). Deoxygenation-Induced Cation Fluxes in Sickle Cells. IV. Modulation by External Calcium. *Am. J. Physiol.* 269 (2 Pt 1), C403–C409. doi:10.1152/ajpcell.1995.269.2.C403
- Joiner, C. H. (1993). Cation Transport and Volume Regulation in Sickle Red Blood Cells. *Am. J. Physiol.* 264 (2 Pt 1), C251–C270. doi:10.1152/ajpcell.1993.264.2.C251
- Kaestner, L., Bogdanova, A., and Egee, S. (2020). Calcium Channels and Calcium-Regulated Channels in Human Red Blood Cells. *Adv. Exp. Med. Biol.* 1131, 625–648. doi:10.1007/978-3-030-12457-1\_25
- Kourghi, M., Pei, J. V., De Ieso, M. L., Flynn, G., and Yool, A. J. (2016). Bumetanide Derivatives AqB007 and AqB011 Selectively Block the Aquaporin-1 Ion Channel Conductance and Slow Cancer Cell Migration. *Mol. Pharmacol.* 89 (1), 133–140. doi:10.1124/mol.115.101618
- Kourghi, M., Nourmohammadi, S., Pei, J. V., Qiu, J., McGaughey, S., Tyerman, S. D., et al. (2017). Divalent Cations Regulate the Ion Conductance Properties of Diverse Classes of Aquaporins. *Int. J. Mol. Sci.* 18 (11), 2323. doi:10.3390/ijms18112323
- Kourghi, M., De Ieso, M. L., Nourmohammadi, S., Pei, J. V., and Yool, A. J. (2018). Identification of Loop D Domain Amino Acids in the Human Aquaporin-1 Channel Involved in Activation of the Ionic Conductance and Inhibition by AqB011. *Front. Chem.* 6, 142. doi:10.3389/fchem.2018.00142
- Lew, V. L., and Bookchin, R. M. (2005). Ion Transport Pathology in the Mechanism of Sickle Cell Dehydration. *Physiol. Rev.* 85 (1), 179–200. doi:10.1152/physrev.00052.2003
- Lew, V. L., and Tiffert, T. (2017). On the Mechanism of Human Red Blood Cell Longevity: Roles of Calcium, the Sodium Pump, Piezo1, and Gardos Channels. *Front. Physiol.* 8, 977. doi:10.3389/fphys.2017.00977
- Lew, V. L., Ortiz, O. E., and Bookchin, R. M. (1997). Stochastic Nature and Red Cell Population Distribution of the Sickling-Induced Ca<sup>2+</sup> Permeability. *J. Clin. Invest.* 99 (11), 2727–2735. doi:10.1172/JCI119462
- Ma, T., Yang, B., Gillespie, A., Carlson, E. J., Epstein, C. J., and Verkman, A. S. (1998). Severely Impaired Urinary Concentrating Ability in Transgenic Mice Lacking Aquaporin-1 Water Channels. *J. Biol. Chem.* 273 (8), 4296–4299. doi:10.1074/jbc.273.8.4296
- Ma, Y. L., Rees, D. C., Gibson, J. S., and Ellory, J. C. (2012). The Conductance of Red Blood Cells from Sickle Cell Patients: Ion Selectivity and Inhibitors. *J. Physiol.* 590 (9), 2095–2105. doi:10.1113/jphysiol.2012.229609
- Maeda, N., Hibuse, T., and Funahashi, T. (2009). Role of Aquaporin-7 and Aquaporin-9 in Glycerol Metabolism; Involvement in Obesity. *Handb Exp. Pharmacol.* 190, 233–249. doi:10.1007/978-3-540-79885-9\_12
- McMahon, T. J. (2019). Red Blood Cell Deformability, Vasoactive Mediators, and Adhesion. *Front. Physiol.* 10, 1417. doi:10.3389/fphys.2019.01417
- Migliati, E., Meurice, N., DuBois, P., Fang, J. S., Somasekharan, S., Beckett, E., et al. (2009). Inhibition of Aquaporin-1 and Aquaporin-4 Water Permeability by a Derivative of the Loop Diuretic Bumetanide Acting at an Internal Pore-occluding Binding Site. *Mol. Pharmacol.* 76 (1), 105–112. doi:10.1124/mol.108.053744
- Montiel, V., Bella, R., Michel, L. Y. M., Esfahani, H., De Mulder, D., Robinson, E. L., et al. (2020). Inhibition of Aquaporin-1 Prevents Myocardial Remodeling by Blocking the Transmembrane Transport of Hydrogen Peroxide. *Sci. Transl. Med.* 12 (564), eaay2176. doi:10.1126/scitranslmed.aay2176
- Ney, P. A., Christopher, M. M., and Heibel, R. P. (1990). Synergistic Effects of Oxidation and Deformation on Erythrocyte Monovalent Cation Leak. *Blood* 75 (5), 1192–1198. doi:10.1182/blood.v75.5.1192.bloodjournal7551192
- Ortiz, O. E., Lew, V. L., and Bookchin, R. M. (1990). Deoxygenation Permeabilizes Sickle Cell Anaemia Red Cells to Magnesium and Reverses its Gradient in the Dense Cells. *J. Physiol.* 427, 211–226. doi:10.1113/jphysiol.1990.sp018168
- Papadopoulos, M. C., Krishna, S., and Verkman, A. S. (2002). Aquaporin Water Channels and Brain Edema. *Mt Sinai J. Med.* 69 (4), 242–248.
- Pauling, L., Itano, H. A., Singerand, S. J., and Wells, I. C. (1949). Sickle Cell Anemia, a Molecular Disease. *Science* 110 (2865), 443–448. doi:10.1126/science.110.2865.443
- Pei, J. V., Heng, S., De Ieso, M. L., Sylvia, G., Kourghi, M., Nourmohammadi, S., et al. (2019). Development of a Photoswitchable Lithium-Sensitive Probe to

- Analyze Nonspecific Cation Channel Activity in Migrating Cancer Cells. *Mol. Pharmacol.* 95 (5), 573–583. doi:10.1124/mol.118.115428
- Perutz, M. F., and Mitchison, J. M. (1950). State of Haemoglobin in Sickle-Cell Anaemia. *Nature* 166 (4225), 677–679. doi:10.1038/166677a0
- Rees, D. C., Williams, T. N., and Gladwin, M. T. (2010). Sickle-Cell Disease. *Lancet* 376 (9757), 2018–2031. doi:10.1016/S0140-6736(10)61029-X
- Ren, G., Cheng, A., Melnyk, P., and Mitra, A. K. (2000). Polymorphism in the Packing of Aquaporin-1 Tetramers in 2-D Crystals. *J. Struct. Biol.* 130 (1), 45–53. doi:10.1006/jbsi.2000.4211
- Safo, M. K., Abdulmalik, O., Danso-Danquah, R., Burnett, J. C., Nokuri, S., Joshi, G. S., et al. (2004). Structural Basis for the Potent Antisickling Effect of a Novel Class of Five-Membered Heterocyclic Aldehydic Compounds. *J. Med. Chem.* 47 (19), 4665–4676. doi:10.1021/jm0498001
- Saparov, S. M., Kozono, D., Rothe, U., Agre, P., and Pohl, P. (2001). Water and Ion Permeation of Aquaporin-1 in Planar Lipid Bilayers. Major Differences in Structural Determinants and Stoichiometry. *J. Biol. Chem.* 276 (34), 31515–31520. doi:10.1074/jbc.M104267200
- Saraf, S. L., and Rondelli, D. (2019). Allogeneic Hematopoietic Stem Cell Transplantation for Adults with Sickle Cell Disease. *J. Clin. Med.* 8 (10), 1565. doi:10.3390/jcm8101565
- Segal, J. B., Strouse, J. J., Beach, M. C., Haywood, C., Witkop, C., Park, H., et al. (2008). Evidence Reports/Technology Assessments No.165. Report No. 08: E007. Rockville, MD: Agency for Healthcare Research and Quality (US).
- Speake, T., Freeman, L. J., and Brown, P. D. (2003). Expression of Aquaporin 1 and Aquaporin 4 Water Channels in Rat Choroid Plexus. *Biochim. Biophys. Acta* 1609 (1), 80–86. doi:10.1016/s0005-2736(02)00658-2
- Steinberg, M. H. (1999). Management of Sickle Cell Disease. *N. Engl. J. Med.* 340 (13), 1021–1030. doi:10.1056/NEJM199904013401307
- Tosteson, D. C., Shea, E., and Darling, R. C. (1952). Potassium and Sodium of Red Blood Cells in Sickle Cell Anemia. *J. Clin. Invest.* 31 (4), 406–411. doi:10.1172/JCI102623
- Trott, O., and Olson, A. J. (2010). AutoDock Vina: Improving the Speed and Accuracy of Docking with a New Scoring Function, Efficient Optimization, and Multithreading. *J. Comput. Chem.* 31 (2), 455–461. doi:10.1002/jcc.21334
- Tyerman, S. D., McGaughey, S. A., Qiu, J., Yool, A. J., and Byrt, C. S. (2021). Adaptable and Multifunctional Ion-Conducting Aquaporins. *Annu. Rev. Plant Biol.* 72, 703–736. doi:10.1146/annurev-arplant-081720-013608
- Venero, J. L., Vizuet, M. L., Machado, A., and Cano, J. (2001). Aquaporins in the central Nervous System. *Prog. Neurobiol.* 63 (3), 321–336. doi:10.1016/s0301-0082(00)00035-6
- Willcocks, J. P., Mulquaney, P. J., Ellory, J. C., Veech, R. L., Radda, G. K., and Clarke, K. (2002). Simultaneous Determination of Low Free Mg<sup>2+</sup> and pH in Human Sickle Cells Using <sup>31</sup>P NMR Spectroscopy. *J. Biol. Chem.* 277 (51), 49911–49920. doi:10.1074/jbc.M207551200
- Xu, G. G., Pagare, P. P., Ghatge, M. S., Safo, R. P., Gazi, A., Chen, Q., et al. (2017). Design, Synthesis, and Biological Evaluation of Ester and Ether Derivatives of Antisickling Agent 5-HMF for the Treatment of Sickle Cell Disease. *Mol. Pharm.* 14 (10), 3499–3511. doi:10.1021/acs.molpharmaceut.7b00553
- Yang, X. C., and Sachs, F. (1989). Block of Stretch-Activated Ion Channels in *Xenopus* Oocytes by Gadolinium and Calcium Ions. *Science* 243 (4894 Pt 1), 1068–1071. doi:10.1126/science.2466333
- Yool, A. J., and Campbell, E. M. (2012). Structure, Function and Translational Relevance of Aquaporin Dual Water and Ion Channels. *Mol. Aspects Med.* 33 (5), 553–561. doi:10.1016/j.mam.2012.02.001
- Yool, A. J., and Weinstein, A. M. (2002). New Roles for Old Holes: Ion Channel Function in Aquaporin-1. *News Physiol. Sci.* 17, 68–72. doi:10.1152/nips.01372.2001
- Yool, A. J., Stamer, W. D., and Regan, J. W. (1996). Forskolin Stimulation of Water and Cation Permeability in Aquaporin 1 Water Channels. *Science* 273 (5279), 1216–1218. doi:10.1126/science.273.5279.1216
- Yu, J., Yool, A. J., Schulten, K., and Tajkhorshid, E. (2006). Mechanism of Gating and Ion Conductivity of a Possible Tetrameric Pore in Aquaporin-1. *Structure* 14 (9), 1411–1423. doi:10.1016/j.str.2006.07.006
- Zaugg, R. H., Walder, J. A., and Klotz, I. M. (1977). Schiff Base Adducts of Hemoglobin. Modifications that Inhibit Erythrocyte Sickling. *J. Biol. Chem.* 252 (23), 8542–8548. doi:10.1016/s0021-9258(19)75254-5
- Zhang, W., Zitron, E., Hömme, M., Kihm, L., Morath, C., Scherer, D., et al. (2007). Aquaporin-1 Channel Function Is Positively Regulated by Protein Kinase C. *J. Biol. Chem.* 282 (29), 20933–20940. doi:10.1074/jbc.M703858200

**Conflict of Interest:** OA is a co-inventor on a patent application for prodrugs and derivatives of 5HMF.

The authors declare that the research was conducted in the absence of any commercial or financial relationships that could be construed as a potential conflict of interest.

**Publisher's Note:** All claims expressed in this article are solely those of the authors and do not necessarily represent those of their affiliated organizations, or those of the publisher, the editors and the reviewers. Any product that may be evaluated in this article, or claim that may be made by its manufacturer, is not guaranteed or endorsed by the publisher.

Copyright © 2022 Chow, Cox, Pei, Anabaraonye, Nourmohammadi, Henderson, Martinac, Abdulmalik and Yool. This is an open-access article distributed under the terms of the Creative Commons Attribution License (CC BY). The use, distribution or reproduction in other forums is permitted, provided the original author(s) and the copyright owner(s) are credited and that the original publication in this journal is cited, in accordance with accepted academic practice. No use, distribution or reproduction is permitted which does not comply with these terms.

# 5-Hydroxymethyl-Furfural and Structurally Related Compounds Block the Ion Conductance in Human Aquaporin-1 Channels and Slow Cancer Cell Migration and Invasion

Pak Hin Chow, Mohamad Kourghi, Jinxin V. Pei, Saeed Nourmohammadi, and Andrea J. Yool

Adelaide Medical School, University of Adelaide, Adelaide, Australia (P.H.C., M.K., J.V.P., S.N., A.J.Y.) and College of Science, The Australian National University, Canberra, Australia (J.V.P.)

Received December 18, 2019; accepted April 20, 2020

## ABSTRACT

Aquaporin-1 (AQP1) dual water and ion channels enhance migration and invasion when upregulated in leading edges of certain classes of cancer cells. Work here identifies structurally related furan compounds as novel inhibitors of AQP1 ion channels. 5-Hydroxymethyl-2-furfural (5HMF), a component of natural medicinal honeys, and three structurally related compounds, 5-nitro-2-furoic acid (5NFA), 5-acetoxymethyl-2-furaldehyde (5AMF), and methyl-5-nitro-2-furoate (M5NF), were analyzed for effects on water and ion channel activities of human AQP1 channels expressed in *Xenopus* oocytes. Two-electrode voltage clamp showed dose-dependent block of the AQP1 ion current by 5HMF (IC<sub>50</sub> 0.43 mM), 5NFA (IC<sub>50</sub> 1.2 mM), and 5AMF (IC<sub>50</sub> ~3 mM) but no inhibition by M5NF. In silico docking predicted the active ligands interacted with glycine 165, located in loop D gating domains surrounding the intracellular vestibule of the tetrameric central pore. Water fluxes through separate intrasubunit pores were unaltered by the furan compounds (at concentrations up to 5 mM). Effects on cell migration, invasion, and cytoskeletal organization in vitro were tested in high-AQP1-expressing cancer lines, colon cancer (HT29) and AQP1-expressing breast cancer (MDA),

and low-AQP1-expressing SW480. 5HMF, 5NFA, and 5AMF selectively impaired cell motility in the AQP1-enriched cell lines. In contrast, M5NF immobilized all the cancer lines by disrupting actin cytoskeleton. No reduction in cell viability was observed at doses that were effective in blocking motility. These results define furans as a new class of AQP1 ion channel inhibitors for basic research and potential lead compounds for development of therapeutic agents targeting aquaporin channel activity.

## SIGNIFICANCE STATEMENT

5-Hydroxymethyl-2-furfural (5HMF), a component of natural medicinal honeys, blocks the ion conductance but not the water flux through human Aquaporin-1 (AQP1) channels and impairs AQP1-dependent cell migration and invasiveness in cancer cell lines. Analyses of 5HMF and structural analogs demonstrate a structure-activity relationship for furan compounds, supported by in silico docking modeling. This work identifies new low-cost pharmacological antagonists for AQP1 available to researchers internationally. Furans merit consideration as a new class of therapeutic agents for controlling cancer metastasis.

## Introduction

Aquaporin (AQP) channels, found in all kingdoms of life, serve essential roles in transmembrane fluid and solute fluxes, enabling regulation of volume and osmotic gradients across cell membranes (Agre et al., 1993; Reizer et al., 1993; Hohmann et al., 2000; Gomes et al., 2009). AQP channels are tetramers of subunits with monomeric pores that facilitate osmotic water flux (Jung et al., 1994; Sui et al., 2001). In AQP1, the central pore is a cGMP-gated nonselective cation channel, permeable to monovalent cations such as Na<sup>+</sup>, K<sup>+</sup>,

Cs<sup>+</sup>, and Li<sup>+</sup>, and pharmacologically distinct from the intrasubunit water pores (Yool et al., 1996; Saparov et al., 2001; Boassa and Yool, 2003; Yu et al., 2006; Campbell et al., 2012; Kourghi et al., 2018; Pei et al., 2019). Ion channel activity has been reported for other AQPs expressed in mammals (AQP0, AQP6), as well as in insects (*Drosophila* Big Brain) and plants (soybean nodulin 26 and rockcress AtPIP2; 1) (Weaver et al., 1994; Anthony et al., 2000; Hazama et al., 2002; Yanochko and Yool, 2002; Boassa et al., 2006; Byrt et al., 2017).

Chemical modulators of AQP water and glycerol channel activities have been characterized by research teams around the world (Yool et al., 2010; Huber et al., 2012; Martins et al., 2013; Seeliger et al., 2013; Pei et al., 2016a). Inhibitors of the human AQP1 ion conductance identified thus far include bacopaside I from the Ayurvedic medicinal plant *Bacopa monnieri* and derivatives of bumetanide, AqB007 and AqB011,

**Primary laboratory of origin:** (AJ Yool; Aquaporin Physiology and Drug Discovery Program, Adelaide Medical School, University of Adelaide, Adelaide, Australia).

This work was supported by the Australian Research Council [Grants 16ARC\_DP16010464 and 19ARC\_DP190101745].  
<https://doi.org/10.1124/mol.119.119172>

**ABBREVIATIONS:** 5AMF, 5-acetoxymethyl-2-furaldehyde; AQP, aquaporin; 8CPT-cGMP, 8-(4-chlorophenylthio)-guanosine 3',5'-cyclic monophosphate; DMEM, Dulbecco's modified Eagle's medium; 5HMF, 5-hydroxymethyl-2-furfural; MDA, MDA-MB-231; M5NF, methyl-5-nitro-2-furoate; 5NFA, 5-nitro-2-furoic acid; PCR, polymerase chain reaction; RPS13, ribosomal protein S13.

which also act to slow cell migration and decrease invasiveness in classes of cancer cell lines that express high levels of AQP1 (Kourghi et al., 2016; Pei et al., 2016b). Divalent cations, such as  $\text{Cd}^{2+}$  and  $\text{Ca}^{2+}$ , also inhibit AQP1 ion conductance (Boassa et al., 2006; Kourghi et al., 2017). The ongoing search for modulators is important for developing a pharmacological armamentarium for AQP research, for identifying drug candidates aimed at potential future clinical translations, and for building understanding of ligand structure-activity relationships for diverse classes of AQPs.

Traditional medicines have been used by humans for more than 4000 years as valuable mixtures of agents with likely therapeutic effects, including anticancer activities (Khan, 2014; He et al., 2019). Natural remedies based on manuka and tualang honeys are reported to have antioxidant (Khalil et al., 2012), anti-inflammatory (Gasparrini et al., 2018), antibacterial (Girma et al., 2019), and antidiabetic (Lori et al., 2019) effects, with benefits in gastrointestinal disorders (Ghosh and Playford, 2003), wound infections (Shan, 2019), and cancers (Attia et al., 2008; Aryappalli et al., 2017; Abel et al., 2018; Afrin et al., 2018). Medicinal extracts have been useful as sources of new pharmacological agents to modulate proteins involved in diverse physiologic functions, including for example ion channels, receptors, and transporters (Sucher and Carles, 2015).

One of the compounds naturally occurring in both manuka and tualang honeys is 5-hydroxymethyl-2-furfural (5HMF), which shows differences in concentration levels that have been suggested to correlate with therapeutic effectiveness (Ahmed and Othman, 2013). 5HMF confers protective effects in brain and cardiac ischemic injury models. Intraperitoneally injected 5HMF (12 mg/kg) reduced neurologic deficits and brain edema in mice after transient global cerebral ischemia (Ya et al., 2017). In perfused isolated rat hearts, 5 mM 5HMF reduced damage during 20-minute no-flow ischemia, enhanced coronary artery relaxation, and accelerated recovery to normal sinus rhythm during reperfusion (Wölkart et al., 2017).

Work here tested for effects of 5HMF and related compounds on the ion conductance and the water channel activity of human AQP1 channels expressed in *Xenopus* oocytes and evaluated the effects of the same agents on the rates of migration and invasiveness of AQP1-expressing breast cancer (MDA) and colon cancer (HT29) cell lines and a colon cancer line with low levels of AQP1 (SW480). Results showed that 5HMF blocked the ion conductance but not the osmotic water flux mediated by AQP1, and provided evidence for a structure-activity relationship for furan compounds, which was supported by results from in silico docking modeling. Block of cell migration in AQP1-positive lines correlated with effectiveness in inhibiting AQP1 for three (5HMF, 5ANF, 5NFA) of the four agents tested. The fourth compound, M5NF, blocked motility in all cell lines by an AQP1-independent mechanism. These results expand the panel of known AQP1 modulatory agents and identify new low-cost pharmacological antagonists that are available from commercial suppliers internationally. Possible therapeutic activities of improved furan derivatives in animal models of cancer metastasis could be of interest in future research.

## Materials and Methods

**Oocyte Preparation and cRNA Injection.** Unfertilized oocytes were harvested from anesthetized female *Xenopus laevis* frogs in

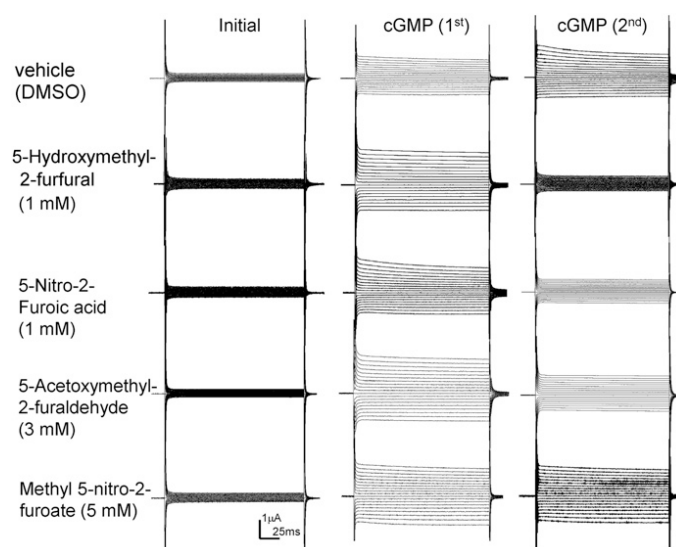


**Fig. 1.** Electrophysiological recordings illustrating the effects of 5HMF and related compounds on the cGMP-activated AQP1 ion conductance. 5-Hydroxymethyl-2-furfural, 5-nitro-2-furoic acid, 5-acetoxyethyl-2-furaldehyde, and methyl 5-nitro-2-furoate were tested for effects on the ionic conductance of AQP1-expressing oocytes. Each row shows responses recorded during the sequential treatment of a single oocyte: first, prior to application of 8CPT-cGMP (initial; left); second, at 30 minutes after the first application of 8CPT-cGMP (cGMP first; middle); and third, after 2 hours incubation in the indicated treatment followed by 30 minutes reapplication of 8CPT-cGMP (cGMP second; right).

accordance with national guidelines (Australian Code of Practice for the Care and Use of Animals for Scientific Purposes), using protocols approved by the University of Adelaide Animal Ethics Committee (M2018-016). Harvested oocytes were defolliculated in collagenase type 1A (2 mg/ml) in isotonic saline (100 mM NaCl, 2 mM KCl, 5 mM  $\text{MgCl}_2$ , and 5 mM HEPES; pH 7.6) for 1.5 hours at approximately 18°C. Oocytes were washed three times with isotonic saline and transferred into frog Ringer's saline [isotonic saline supplemented with 0.6 mM  $\text{CaCl}_2$ , 5% horse serum (v/v), 100 U/ml penicillin, 0.1 mg/ml streptomycin, and 0.5 mg/ml tetracycline]. Healthy oocytes were injected with 50 nl of sterile water (non-AQP1 control oocytes) or 50 nl wild-type human AQP1 cRNA (approximately 1 ng in sterile water). Injected oocytes were incubated in frog Ringer's saline at 18°C for 48 hours or more to allow time for protein expression. Prior to experimental assays, control and AQP1-expressing oocytes were rinsed in isotonic saline (without serum, antibiotic free) for at least 1 hour.

Human AQP1 cDNA (National Center for Biotechnology Information GenBank NM\_198098) (Preston et al., 1992) subcloned in a *Xenopus*  $\beta$ -globin expression plasmid was linearized with BamHI and transcribed using T3 polymerase (T3 mMessage mMach; Ambion, Austin, TX). The cRNA was resuspended in sterile water and stored at  $-80^\circ\text{C}$ . All chemicals are from Sigma-Aldrich Chemicals (St. Louis, MO) unless otherwise indicated.

**Furan Compounds.** 5HMF and three structurally related compounds: 5-nitro-2-furoic acid (5NFA); 5-acetoxyethyl-2-furaldehyde 9 (5AMF), and methyl 5-nitro-2-furoate (M5NF), were purchased from Sigma-Aldrich Chemicals. 5HMF was dissolved in water, whereas other compounds were dissolved in DMSO to create 1000 $\times$  stock solutions, diluted 1  $\mu\text{l}/\text{ml}$  into experimental salines to final concentrations. The equivalent amount of DMSO alone (0.1%) in saline or cell culture medium was used as the vehicle control.

**Quantitative Swelling Assay.** For the swelling assays, each oocyte served as its own control, as described previously (Migliati et al., 2009). Each oocyte was tested first without drug treatment, incubated for 2 hours in isotonic saline with vehicle or with one of the furfural-related compounds, and then reassessed in a second swelling

assay. Swelling rates were measured in 50% hypotonic saline (isotonic saline diluted with an equal volume of water, without test compounds present). Oocytes were imaged with a grayscale camera (Cohu, San Diego, CA) on a dissecting microscope (Olympus SZ-PT; Olympus, Macquarie Park, Australia) at one frame per second for 30 seconds using NIH ImageJ software. Oocytes were then incubated in isotonic saline alone, with vehicle, or with the indicated compound and were reassessed in a second swelling assay. The swelling rates were calculated from slope values of linear regression fits of cross-sectional areas as a function of time using GraphPad Prism.

**Electrophysiology.** Two-electrode voltage-clamp recordings of control and AQP1-expressing oocytes in isotonic Na<sup>+</sup> saline were done with capillary glass electrodes (1–3 M $\Omega$ ) filled with 1 M KCl using a GeneClamp amplifier. Bath application of membrane-permeable 8-(4-chlorophenylthio)-guanosine 3',5'-cyclic monophosphate (8CPT-cGMP) activated the ionic conductance in AQP1-expressing oocytes, as described previously (Campbell et al., 2012). The ionic conductance in AQP1-expressing oocytes was activated by application of a bolus of 8CPT-cGMP to achieve a final bath concentration of 10  $\mu$ M. Changes in current over time were monitored by brief repeated voltage step protocols to +40 mV from a holding potential of –40 every 6 seconds. Conductance values were measured using voltage steps from +60 to –110 mV. Recordings were filtered at 2 kHz and stored to hard disk for offline analysis. Data were analyzed with Clampex 9.0 software (pClamp 9.0; Molecular Devices, Sunnyvale, CA) and Prism software (GraphPad, San Diego, CA).

**Molecular Modeling.** In silico modeling was conducted as reported previously (Pei et al., 2016b). The protein crystal structures of human AQP1 were obtained from the Protein Data Bank (Protein Data Bank ID:1FQY). Structures for 5HMF and related compounds were downloaded from PubChem and converted into software-compatible three-dimensional structures in .pdb format using the online SMILES Translator and Structure File Generator (National Cancer Institute, U.S. Department Health and Human Services, Washington, DC). Both AQP1 and ligand coordinates were prepared for docking using MGLtools (version 1.5.4; Scripps Institute, San Diego, CA). The docking was carried using Autodock Vina (Trott and Olson, 2010), with a docking grid covering the intracellular face of the tetrameric pore.

**Cancer Cell Culture and Migration Assays.** HT29 and SW480 colon cancer cell lines and MDA-MB-231 (referred to here as “MDA”) breast cancer cell lines (from American Type Culture Collection, Manassas, VA) were grown in Dulbecco's modified Eagle's medium (DMEM) supplemented with 1 $\times$  glutaMAX (Life Technologies, Mulgrave, Australia), penicillin and streptomycin (100 U/ml each), and 10% FBS (v/v) at 37°C in a 5% CO<sub>2</sub> humidified environment. For wound healing assays of two-dimensional migration over flat surfaces, confluent cultures of cancer cell lines were tested using the circular wound closure method (De Ieso and Pei, 2018) to measure the effect of 5HMF and related compounds on the rates of cell migration. Cells were plated in flat-bottomed 96 well plates at 1.25  $\times$  10<sup>5</sup> cells per well for HT29, or 1  $\times$  10<sup>5</sup> cells per well for MDA and SW480 lines, in DMEM supplemented with 1 $\times$  glutaMAX (Life Technologies), penicillin and streptomycin (100 U/ml each), and 10% FBS. Cultures were incubated at 37°C in 5% CO<sub>2</sub> for 18–24 hours. Once cells achieved 80%–90% confluence, the culture medium was replaced with reduced serum (2% FBS) DMEM medium with 400 nM of the mitotic inhibitor 5-fluoro-2'-deoxyuridine, and cells were incubated overnight to achieve a confluent monolayer. Circular wounds were created with a sterile p10 pipette tip; wells were washed two times with PBS to remove cell debris. Reduced serum DMEM culture medium (containing either vehicle or furan derivatives) was applied into the wells. Images of wounds were taken at 0 and 24 hours with a Canon 6D camera on an Olympus CK2 microscope (10 $\times$  objective). Wound areas were quantified using NIH ImageJ software (US National Institutes of Health) as described previously (De Ieso and Pei, 2018).

Transwell invasion assays were used to measure three-dimensional migration through an extracellular matrix. Cells were grown to

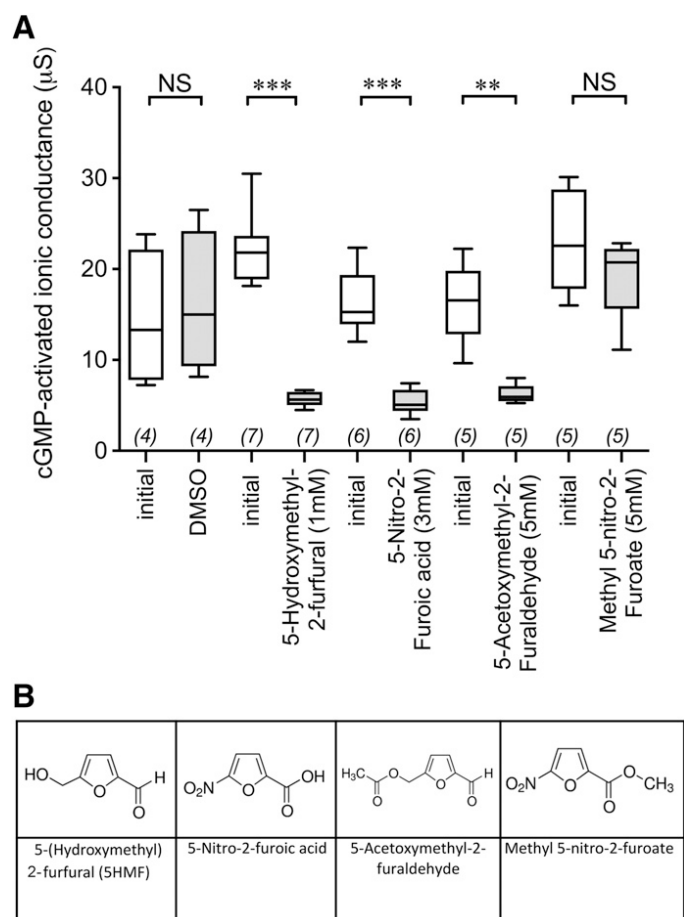


**Fig. 2.** Differential inhibition of the cGMP-activated AQP1 conductance by 5HMF and related compounds. (A) Box plot showing inhibition of the cGMP-activated AQP1 ionic conductance with 5-hydroxymethyl-2-furfural, 5-nitro-2-furoic acid, and 5-acetoxyethyl-2-furaldehyde but not with vehicle (DMSO) or methyl 5-nitro-2-furoate. Boxes contain 50% of the data points; bars show the full range of data values; horizontal bars show the median value. *n* values are above the *x*-axis. Statistical comparisons used two-tailed paired *t* tests within treatment groups. (B) Structures of the compounds tested. Statistical comparisons are indicated as *P* < 0.0001 (\*\*\*); *P* < 0.001 (\*\*); or N.S. (*P*  $\geq$  0.05); see Methods for details.

approximately 40% confluence under normal culture conditions and transferred into reduced serum (2% FBS) DMEM medium for 32–34 hours before seeding. Corning Transwell polycarbonate membrane cell culture inserts (8- $\mu$ m pore size; product #3422; Sigma-Aldrich) were prepared by coating the upper surface of the filter with 40  $\mu$ l of extracellular matrix-like gel from Engelbreth-Holm-Swarm murine sarcoma (diluted to 25  $\mu$ g/ml in sterile water; Sigma-Aldrich), allowed to dry overnight in a sterile hood, and then rehydrated with 50  $\mu$ l of serum-free DMEM 2 hours before cell seeding. In the lower chamber, 600  $\mu$ l of DMEM with 10% serum (chemoattractant) was added with or without the vehicle or furan agents. Cells were seeded into the upper chamber at 2.5  $\times$  10<sup>5</sup> cells per well for HT29, 1.5  $\times$  10<sup>5</sup> cells per well for SW480, and 1  $\times$  10<sup>5</sup> cells per well for MDA in serum-free DMEM, with DMSO or furan agents matching in the lower chamber. Durations of incubations for Transwell assays were optimized empirically in previous work (Nourmohammadi et al., 2019); durations used were 6 hours for MDA and 24 hours for HT29 and SW480, at 37°C in 5% CO<sub>2</sub>. For quantitation of invasion, nonmigrated cells were wiped from the upper surface of the membrane with a cotton swab; migrated cells on the trans (lower) surface were counted after staining with crystal violet (Sigma-Aldrich). Numbers of migrated cells were determined for three fields per replicate, with two replicates per

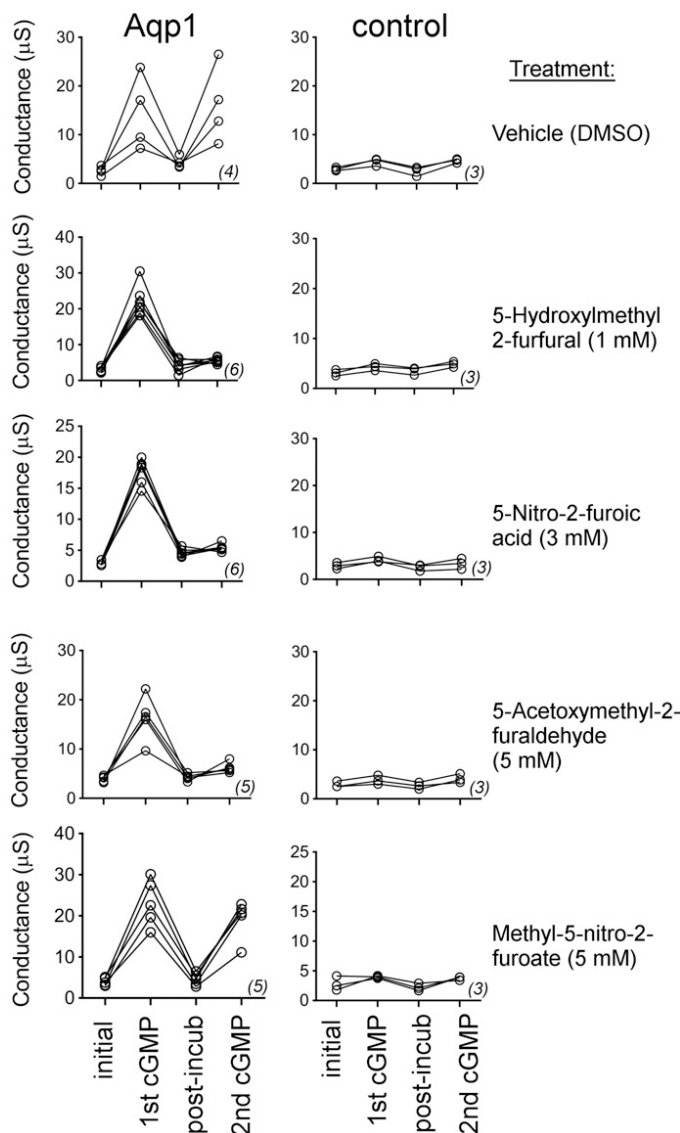


**Fig. 3.** Trend plots showing the effects of 5HMF and related compounds on ion conductances. Conductance values were measured for AQP1-expressing (left) and non-AQP-expressing (right) oocytes. Lines link the values for single oocytes recorded before 8CPT-cGMP (initial), 30 minutes after 8CPT-cGMP (“1st cGMP”), after 2-hour incubation in saline with vehicle or furan compounds without cGMP (“post-incub”), and after reapplication of 8CPT-cGMP (“2nd cGMP”). Treatments (listed right) were applied during the 2-hour recovery interlude between “1st cGMP” and “post-incub” steps. *n* values are shown in italics above the x-axis.

experiment, and normalized to the mean number of migrated cells in the vehicle control treatment of the same cell line.

**Cell Viability Assay.** HT29, MDA, and SW480 cell viabilities were assessed using the alamarBlue assay (Molecular Probes, Eugene, OR). Cells were plated at  $10^4$  cells per well in 96-well plates, and fluorescence signals were measured with a FLUOstar Optima microplate reader (BMG Labtech, Ortenberg, Germany) after 24 hours of incubation with vehicle, 5HMF, or related furan compounds.

**Actin Staining.** HT29, SW480, and MDA cells were cultured in  $\mu$ -plate eight-well dishes (Ibidi, Munich, Germany) in 2% FBS with 5-fluoro-2'-deoxyuridine (400 nM) and incubated at 37°C in 5% CO<sub>2</sub>. After 12–18 hours of incubation, cells were treated with DMSO (vehicle) or furan derivatives and incubated for another 24 hours. Cells were then washed with PBS and fixed with 4% paraformaldehyde at room temperature for 10–30 minutes. Fixed cells were rinsed two to three times with PBS and permeabilized with 200  $\mu$ l of

0.1% Triton X-100 in PBS for 3–5 minutes at room temperature. Phalloidin-iFluor 488 Reagent CytoPainter (ab176753; Abcam, MA) at 1:1000 dilution was used to stain F-actin cytoskeleton at room temperature in the dark for 1–2 hours. Hoechst stain (diluted 1:1000; catalog # 861405; Sigma-Aldrich) was used to label cell nuclei. Cells were visualized using an SP5 laser scanning confocal microscope (Leica, Germany) at Adelaide Microscopy core facilities.

**Quantitative Polymerase Chain Reaction Analysis of AQP1 Expression.** HT29, SW480, and MDA cells were seeded in triplicate at  $4 \times 10^5$  cells per well in six well plates and incubated at 37°C in humidified 5% CO<sub>2</sub> environment overnight. The PureLink RNA Mini Kit (Invitrogen, Carlsbad, CA) was used for total RNA extraction for all cancer cell lines. cDNA was synthesized from 1  $\mu$ g of extracted RNA using QuantiTect Reverse Transcription Kit (Qiagen, Hilden, Germany). Synthesized cDNA was quantified using a NanoDrop (Life Technologies, Carlsbad, CA). A final concentration of 50 ng cDNA was used to perform real-time quantitative Reverse Transcription-PCR analyses using SYBR Green PCR Master Mix (Applied Biosystems,

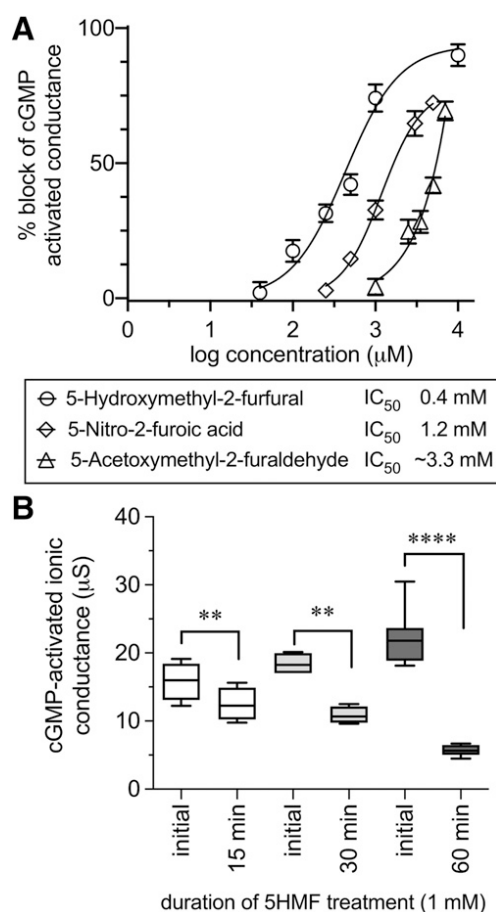


**Fig. 4.** Dose dependence and rate of onset of block of the cGMP-activated AQP1 ionic conductance. (A) Dose-response curves showing mean percent block ( $\pm$ S.E.M.) as a function of concentration of the furan compounds. Estimated IC<sub>50</sub> values are listed in the legend. *n* values were three per dose for 5-hydroxymethyl-2-furfural (except 1 mM which was *n* = 7), three per dose for 5-nitro-2-furoic acid, and three per dose for 5-acetoxy-methyl-2-furaldehyde (except 5 mM, which was *n* = 4). *n* values indicate individual oocytes; data were combined from four batches of oocytes. (B) Time of onset of block of AQP1 ionic conductance during incubation in 1 mM 5HMF. The mean level of inhibition of the AQP1 ionic conductance ( $\pm$ S.D.) was 21%  $\pm$  3% at 15 minutes (*n* = 4), 41%  $\pm$  6% at 30 minutes (*n* = 4), and 75%  $\pm$  5% at 60 minutes (*n* = 8) of incubation time. *n* values indicate individual oocytes; data were combined from two batches of oocytes. Statistical analyses used two-tailed paired *t* tests to compare initial and second timepoints for the same oocytes. Statistical comparisons are indicated as *P* < 0.00001 (\*\*\*\*); or *P* < 0.001 (\*\*); see Methods for details.



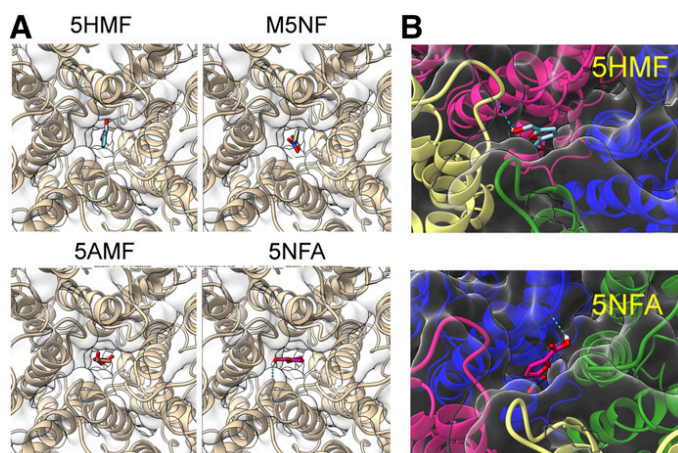


**Fig. 5.** In silico modeling of predicted binding sites for 5HMF and related compounds. (A) Docking modeling results suggested the most favorable energy of interaction for the ligands was in the loop D domains, which surround the tetrameric central pore. Glycine 165 in human AQP1 is predicted to interact by hydrogen bonding (blue dotted line) with polar aldehyde or acid moieties of 5HMF and 5NFA, respectively. 5AMF and M5NF appeared to fit into the central pore domain, but specific amino acid interactions were not identified by the model. (B) Magnified views of hydrogen bonding interactions for 5HMF and 5NFA with Gly165 as predicted by in silico modeling.

Foster City, CA). StepOne Plus real-time PCR software was used for data analysis. The primer sequences used for AQP1 were forward 5'-CGCAGAGTGTGGGCCACATCA- 3' and reverse 5' -CCCGAGTTCACACCATCAGCC - 3', amplifying a product of 217 bp. Ribosomal protein S13 (RPS13) was used as a standard, and target mRNA levels relative to RPS13 were calculated from the differences in cycle thresholds quantified using the individual-efficiency-corrected method.

**Data Analysis and Statistics.** Results compiled from replicate experiments are presented as box plots to show the full range of data points. Boxes represent 50% of the data, the error bars indicate the full range, and the horizontal bar is the median value. Statistical differences were evaluated using one-way ANOVA, paired or unpaired Student's *t* tests, or Dunnett's Multiple Comparisons as indicated. Symbols used in figures show  $P < 0.00001$  (\*\*\*\*);  $P < 0.0001$  (\*\*\*);  $P < 0.001$  (\*\*);  $P < 0.05$  (\*); or N.S. ( $P \geq 0.05$ ).

## Results

**Effects of Furan Compounds on the AQP1 Ion Channel Conductance.** Effects of 5HMF and three structurally related compounds (5NFA, 5AMF, and M5NF) were assessed using two-electrode voltage clamp to record ion conductance amplitudes in AQP1-expressing oocytes (Fig. 1). Currents were measured before ("initial") and 30 minutes after activation by 8CPT-cGMP ("cGMP first"). Oocytes were then incubated 2 hours in isotonic saline with vehicle or the indicated agents. During the incubation period (without 8CPT-cGMP present), the ionic conductance recovered to initial levels as described previously (Kourghi et al., 2016). Incubation with the vehicle (DMSO) did not impair the second conductance response to 8CPT-cGMP ("cGMP second"). Responses were inhibited after incubation in 5HMF or 5NFA at 1 mM, and partially in 5AMF at 3 mM. No appreciable block was observed after incubation with M5NF (5 mM).

Compiled data for conductance responses (Fig. 2) show amplitudes of cGMP-activated conductances in AQP1-expressing

oocytes, with each oocyte measured before and after incubation with vehicle or a furan derivative, as indicated. Paired *t* tests were used for statistical comparisons with treatment groups. Conductance responses to cGMP were reduced after treatment with 5HMF, 5NFA, or 5AMF as compared with the initial cGMP-activated responses in the same oocytes (Fig. 2A). M5NF was not effective. Structures of the furan derivatives are illustrated in Fig. 2B. The active agents have a carboxylic acid (5NFA) or aldehyde (5HMF, 5AMF) group on the furan ring; methylation of the carboxylic acid group in M5NF correlated with absence of any apparent inhibition of AQP1 ion channels.

Trend plots (Fig. 3) summarize conductance responses measured by two-electrode voltage clamp for AQP1-expressing and non-AQP-expressing (control) oocytes. Initial conductances in AQP1-expressing and control oocytes were similarly low before addition of 8CPT-cGMP. After application of the agonist

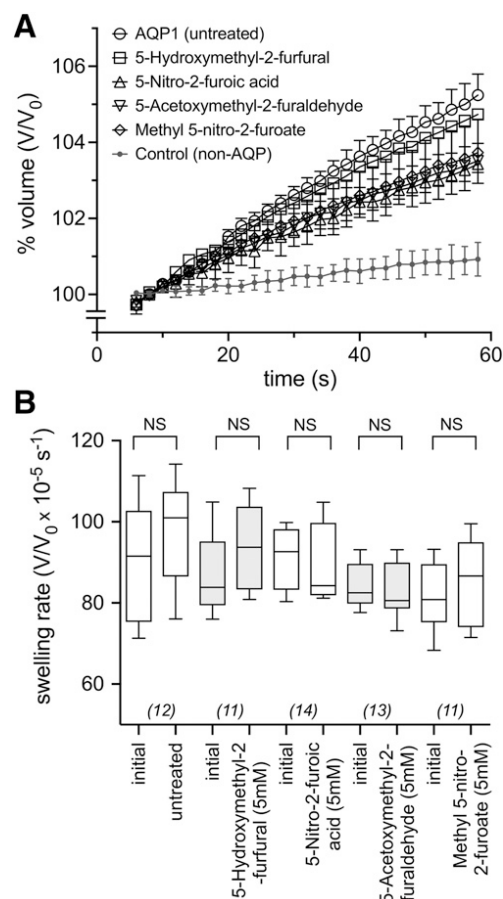


**Fig. 6.** Osmotic water permeability of AQP1-expressing oocytes is not altered by treatment with 5HMF or related compounds. (A) Osmotic swelling was monitored as the increase in oocyte volume, standardized to initial volume, as a function of time after introduction of each oocyte into 50% hypotonic saline at time zero. Data are means  $\pm$  S.E.M. The control *n* value was 10; other *n* values were as shown in B. (B) Linear regression fits of responses (illustrated in A) were used to calculate slope values indicating swelling rates, which were compiled into a box plot. Swelling rates of AQP1-expressing oocytes were measured before (initial) and after 2 hours of incubation in saline with vehicle or 5 mM furan compounds as indicated. Boxes show 50% of the data; whiskers show the full range; horizontal bars are median values; *n* values are in italics above the *x*-axis. None of the treatment groups showed responses that were different from untreated, based on ANOVA  $P = 0.1799$  and two-tailed paired *t* tests within treatment groups. Statistical comparisons indicating no significant difference are shown as NS ( $P \geq 0.05$ ); see Methods for details.

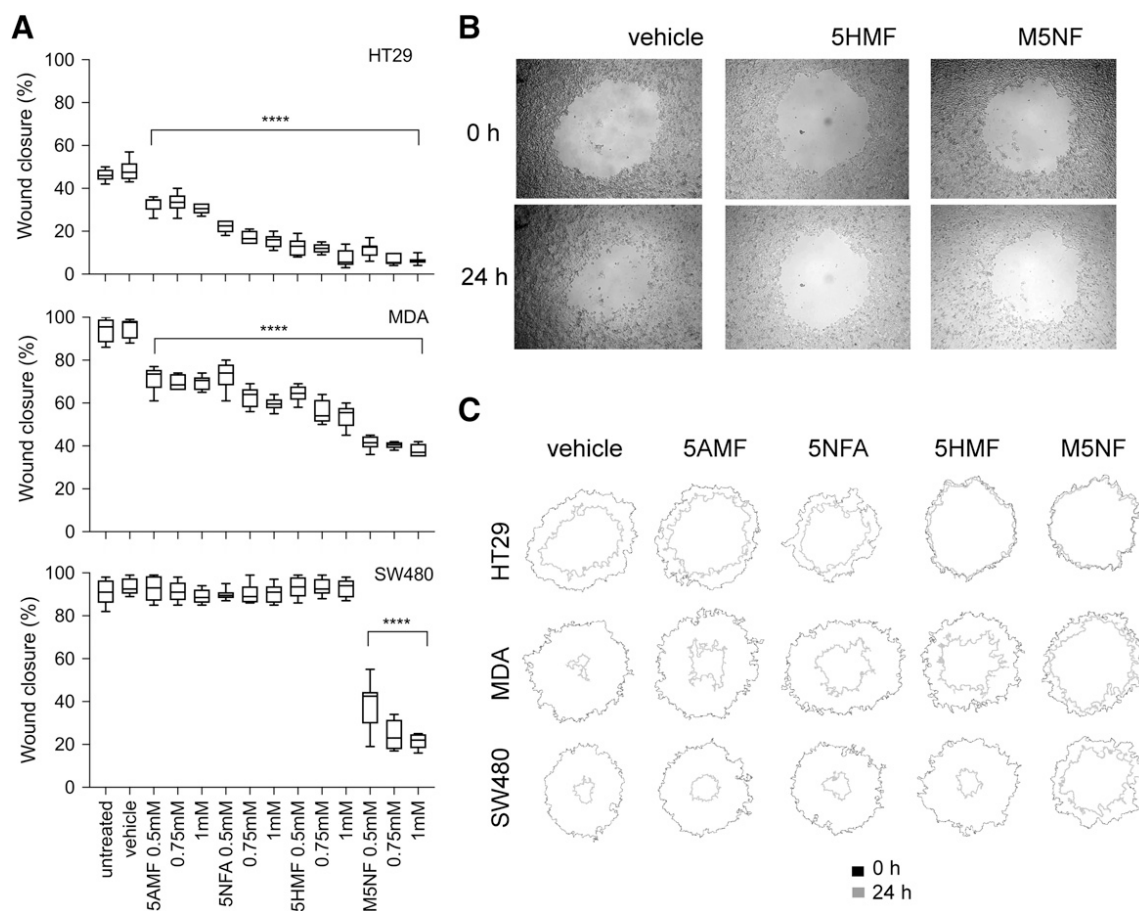


**Fig. 7.** Circular wound closure in HT29, MDA, and SW480 cells is differentially impaired by 5HMF and related compounds. (A) Box plots depicting results for percent wound closure of HT29, MDA, and SW480 cells after treatment with or without vehicle or furan derivatives. HT29 and MDA showed block by all compounds; SW480 was sensitive only to M5NF.  $n = 8$  for all groups except HT29 5NFA (0.75 mM) and HT29 M5NF (0.75 mM), which were  $n = 7$  each. Statistical analyses were done with one-way ANOVA and Dunnett's Multiple Comparisons tests for each column as compared with vehicle control. (B) Representative images showing circular wounds at 0 (upper row) and 24 hours (bottom row) in cultured HT29 cells treated with vehicle, 5HMF, or M5NF. (C) Superimposed outlines of circular wound perimeters at 0 (black) and 24 (gray) hours for representative examples from each treatment group were generated by ImageJ software. Statistical comparisons are indicated as  $P < 0.00001$  (\*\*\*\*); see Methods for details.

("first cGMP"), currents in AQP1-expressing oocytes increased to a maximum amplitude by approximately 30 minutes, whereas control oocytes showed no substantial effect of cGMP in the same timeframe. Oocytes were then transferred into incubation salines containing vehicle or the indicated furan derivatives for 2 hours. Initial ionic conductances recorded after the incubation period ("post-incub") were comparable to those in the starting initial condition, confirming that ion channel activation was reversible. Second applications of 8CPT-cGMP in normal saline were used to assess levels of inhibition established during the incubation period. The AQP1 conductance was fully reactivated by 8CPT-cGMP ("second cGMP") after incubation in saline with vehicle, showing that repeated recordings were well tolerated. The impairment of AQP1 reactivation by cGMP after incubation in 1 mM 5HMF, 3 mM 5NFA, or 5 mM 5AMF indicated inhibition of the ionic conductance. M5NF showed no appreciable blocking effect. Non-AQP1-expressing control oocytes showed little or no effects of cGMP, vehicle, or furan derivatives.

The effects of the active furan derivatives on the AQP1 ionic conductance were dose-dependent and required time to establish (Fig. 4). Dose-response relationships (Fig. 4A) for percent block (mean  $\pm$  S.E.M.) provided estimated  $IC_{50}$  values for 5HMF (0.43 mM), 5NFA (1.2 mM), and 5AMF (3 mM or higher). The onset of block of the AQP1 conductance by 5HMF

was not immediate, requiring time for establishment (Fig. 4B). 8CPT-cGMP-activated ion conductance responses were measured for the same AQP1-expressing oocytes at time zero and at a second time point thereafter. During the interlude, oocytes were incubated in 1 mM 5HMF for 15, 30, or 60 minutes before being rinsed in standard saline and tested for reactivation with the second application of 8CPT-cGMP. Statistical comparisons were done with paired  $t$  tests. The magnitude of block increased with longer times of incubation in 1 mM 5HMF, reaching near maximal block after 1 hour of incubation (Fig. 4B). The time needed to establish block was consistent with a predicted intracellular site of action of 5HMF at the AQP1 channel. Similar latencies for onset of block (1 to 2 hours) have been described for agents such as AqB013, AqB011, and bacopasides that act at the intracellular side of the AQP1 channel (Migliati et al., 2009; Kourghi et al., 2016; Pei et al., 2016b) and require time to cross the plasma membrane.

In silico docking analyses were used to investigate candidate sites for interaction of the ligand 5HMF with the human AQP1 channel (Fig. 5). Views from the intracellular side of the channel show the site that emerged as having the most favorable energy of interaction was in the loop D regions, which surround the intracellular face of the central pore

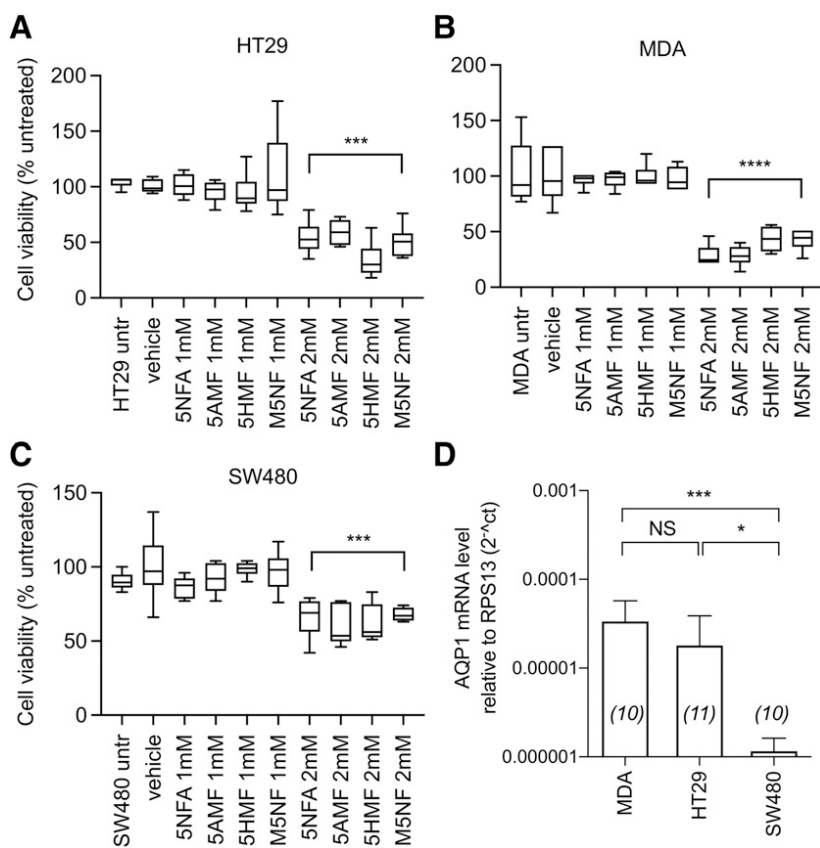


**Fig. 8.** Analysis of dose-dependent cytotoxic effects of treatments and confirmation of AQP1 mRNA expression levels in the cancer cell lines. Cell viability shown in box plot summaries was measured by alamarBlue assay for (A) HT29, (B) MDA, and (C) SW480 cells. Data were standardized to results for untreated cells. Statistical analyses were done with one-way ANOVA and Dunnett's Multiple Comparisons tests for each column as compared with vehicle control.  $n = 6$  in all treatment groups. (D) AQP1 transcript levels, standardized to transcript levels of RPS13, were higher in HT29 and MDA than in SW480, as determined by quantitative reverse-transcription PCR. Histogram bars show means  $\pm$  S.D.;  $n$  values are indicated in italics. Statistical comparisons are indicated as  $P < 0.00001$  (\*\*\*\*);  $P < 0.0001$  (\*\*\*);  $P < 0.05$  (\*); or N.S. ( $P \geq 0.05$ ); see Methods for details.

(Fig. 5A). These cytoplasmic loops, connecting the fourth and fifth transmembrane domains of each subunit, modulate AQP channel gating (Yu et al., 2006; Nyblom et al., 2009; Kourghi et al., 2018). In silico models of predicted binding sites for 5HMF and 5NFA suggest formation of hydrogen bond interactions between the ligand and glycine 165 (Fig. 5B), a residue conserved in AQP1 amino acid loop D sequences across species (Kourghi et al., 2018). Predicted energies of interaction (kcal/mol) estimated from the in silico docking model were 5HMF ( $-4.9$ ), 5NFA, ( $-4.3$ ), 5AMF ( $-4.0$ ), and M5NF ( $-3.9$ ).

**Effects of Furan Compounds on AQP1 Osmotic Water Fluxes.** The furan derivatives did not inhibit AQP1 osmotic water permeability (Fig. 6). Oocytes expressing AQP1 and non-AQP1 control oocytes were assessed for osmotic water permeability as quantified by swelling rates in 50% hypotonic saline (Fig. 6A) as per published methods (Migliati et al., 2009). Swelling rates were measured for the same oocytes before and after treatment with furan compounds (Fig. 6B). AQP1-expressing and non-AQP control oocytes were tested in initial swelling assays and then transferred into isotonic saline with DMSO vehicle ("untreated") or with furan derivatives (5 mM) for 1 hour. After incubation, oocytes were rinsed briefly in saline and tested again for swelling in hypotonic saline. Based on paired  $t$  test evaluations within treatment groups, there were no differences between the first and second swelling rates (Fig. 6B), indicating that none of the furan compounds appreciably affected AQP1 water permeability.

**Effects of Furan Derivatives on Cancer Cell Migration Rates.** Effects of the furan derivatives on the migration of breast and colon cancer cell lines were tested using a circular wound closure assay. Results in Fig. 7 show that HT29 cell

migration was reduced by furan derivatives as compared with vehicle control. Cell migration was reduced 85% by 5HMF ( $P < 0.0001$ ), 68% by 5NFA ( $P < 0.0001$ ), and 37% by 5AMF ( $P < 0.0001$ ) (each at 1 mM), indicating that the agents that were found to block the AQP1 ion conductance were also effective in reducing motility. A similar pattern was observed for MDA cell migration, which was reduced 43% by 5HMF ( $P < 0.0001$ ), 37% by 5NFA ( $P < 0.0001$ ), and 27% by 5AMF ( $P < 0.0001$ ). In contrast, SW480 cells showed no sensitivity to 5HMF ( $P = 0.9997$ ), 5NFA ( $P = 0.929$ ), or 5AMF ( $P = 0.4849$ ), with migration rates comparable to that of vehicle control and consistent with the low level of membrane AQP1 protein in the SW480 cell line. However, M5NF (which did not affect AQP1 water or ion channel activities), unexpectedly inhibited migration in all three cell lines, reducing HT29 cell migration by 87% ( $P < 0.0001$ ), SW480 by 77% ( $P < 0.0001$ ), and MDA by 60% ( $P < 0.0001$ ). These results suggest that M5NF targets a widespread process that is required for cell motility but is not mediated by AQP1.

Cell metabolic activity as an estimator of viability was measured with the alamarBlue assay, with results normalized to metabolic activity levels of vehicle-treated groups in the same cell lines (Fig. 8). Metabolic activity was not impaired by 5HMF or related compounds at 1 mM in any of the cell lines (Fig. 8, A–C), suggesting the reduced cancer cell motility seen at this concentration could not be attributed primarily to reduced cell viability. Furan derivatives did impair metabolic activity at higher concentration (2 mM) in all cell lines, suggesting an upper limit for a potential therapeutic window, depending on cell type. Oocytes showed no evidence of toxicity from any of the agents at any of the doses tested (up to 5 mM),

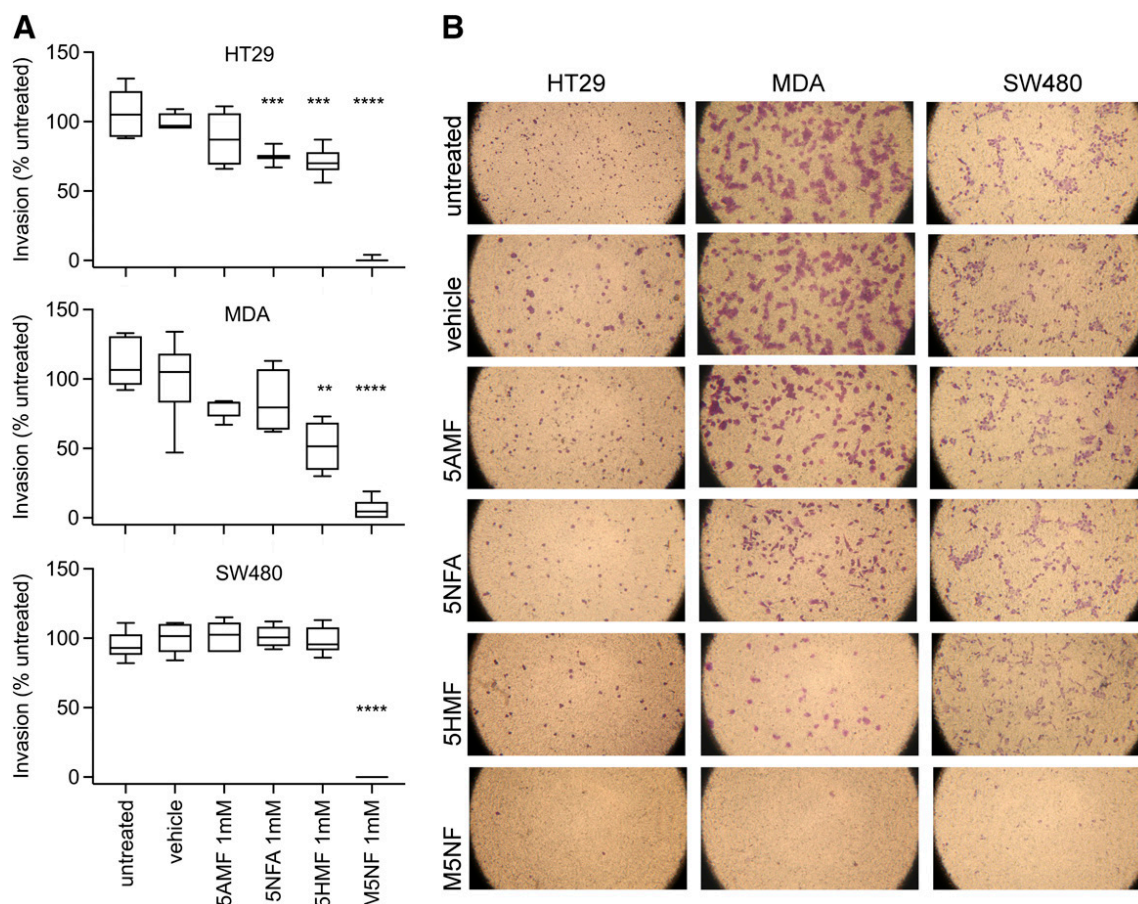


**Fig. 9.** Effects of 5HMF and related compounds on Transwell cell invasiveness of HT29, MDA, and SW480 cells. (A) Box plots depicting HT29, MDA, and SW480 cell migration across Transwell filters with extracellular matrix with or without treatment with vehicle or furan derivatives at 1 mM as indicated. Statistical comparisons were done with ANOVA and unpaired *t* tests compared with vehicle controls. *n* values are seven each per treatment group for HT29 and six each per treatment group for SW480 and MDA. (B) Images illustrating differences in the abundance of successfully migrated cells (stained purple) on the trans sides of filters for the three cell lines untreated and in the different treatment conditions (at 1 mM, or equivalent DMSO for vehicle). Statistical comparisons are indicated as  $P < 0.00001$  (\*\*\*\*);  $P < 0.0001$  (\*\*\*); or  $P < 0.001$  (\*\*); see Methods for details.

based on the observed maintenance of normal low ionic conductances in non-AQP1 control oocytes throughout the treatment protocols (Fig. 3), normal appearance, and typical resting membrane potentials (data not shown).

Levels of AQP1 transcript measured using quantitative PCR were confirmed to be high in MDA and HT29 cell lines and low in SW480 cells (Fig. 8D), consistent with results reported previously (Pei et al., 2016b, 2019; Nakhjavani et al., 2019). The low level of AQP1 protein that is expressed in SW480 cells has been shown to be mainly intracellular, consistent with the insensitivity of these cells to effects of AQP1 channel blockers (De Ieso et al., 2019).

**Effects of Furan Derivatives on Cancer Cell Invasiveness.** The effect of furan derivatives on cancer cell invasiveness was tested using a Transwell invasion assay, in which cells migrated through an extracellular matrix-like material layered on a semipermeable membrane toward a chemoattractant (FBS) and then were stained with crystal violet and counted on the trans-side of the filter (Fig. 9). HT29 cell invasiveness was impaired 30% by 5HMF ( $P < 0.001$ ) and 25% by 5NFA ( $P < 0.001$ ), as compared with vehicle control; 5AMF ( $P = 0.1175$ ) was not effective. In MDA cells, invasion was blocked 49% by 5HMF ( $P < 0.001$ ); NFA ( $P = 0.6415$ ) and 5AMF ( $P = 0.9858$ ) were not effective. SW480 cells showed no block of invasion by 5HMF ( $P = 0.9958$ ), 5NFA ( $P = 0.9996$ ), or

5AMF ( $P = 0.9971$ ). However, M5NF intriguingly caused almost complete block of invasion in all three cell lines, suggesting effects on a ubiquitous motility mechanism.

**Effect of Furan Derivatives on Actin Polymerization.** Pathways involved in cancer cell motility and metastasis are frequently found to include kinase and GTPase signaling cascades that converge on the regulation of actin cytoskeletal organization (Foxall et al., 2016). To examine the effects of M5NF on F-actin polymerization as an endpoint (Hinz and Jucker, 2019), HT29, MDA, and SW480 cells were treated with furan derivatives and then labeled with fluorescent phalloidin, which binds F-actin polymers with high affinity and reveals actin parallel fiber and network structures (Wulf et al., 1979).

Confocal imaging showed that fluorescence signal intensities were reduced in all three cell lines after treatment with M5NF, which disrupted the transverse parallel fiber tracts of actin, leaving trace residual staining against cell boundaries (Fig. 10). In contrast, treatments of HT29, MDA, and SW480 cells with the other furan derivatives had no discernable effects on actin signal intensity or structural organization as compared with vehicle control or untreated. M5NF effects on cell motility were distinct from those of the other furan derivatives and appeared to involve pathways controlling actin organization or assembly.

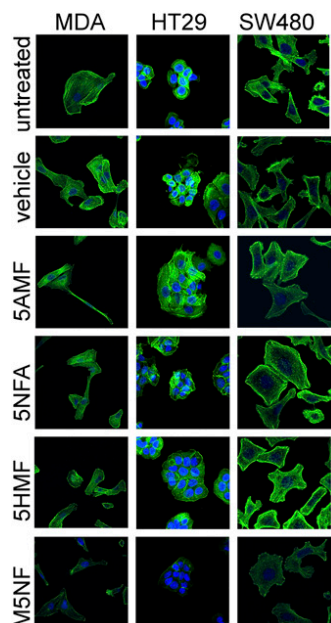


**Fig. 10.** Abundance and patterns of distribution of polymerized F-actin seen in MDA, HT29, and SW480 cells after treatment with or without vehicle or furan derivatives. F-actin was labeled with fluorescently tagged phalloidin (green). Nuclei were visualized by Hoechst stain (blue). Fluorescence signal intensities and the apparent organization of filaments into parallel strands were visibly reduced in cells treated with M5NF but not those treated with other furan compounds or vehicle. Scale bar, 25  $\mu\text{m}$  (lower right).

## Discussion

AQP1 is upregulated in classes of breast, glioblastoma, colorectal, and other cancers and has been suggested to correlate with poor prognoses (El Hindy et al., 2013; Yoshida et al., 2013; Wang et al., 2017; Luo et al., 2018; Shimasaki et al., 2018). The dual water and ion channel function of AQP1 facilitates cancer cell migration and invasiveness in vitro (Kourghi et al., 2016; Pei et al., 2016b; De Ieso et al., 2019; Tomita et al., 2019), suggesting this channel might be of interest when considering new approaches to control cell motility (De Ieso and Yool, 2018). Fifteen classes of AQP (AQP0–14) have been identified to date in mammals (Denker et al., 1988; Preston and Agre, 1991; Ishibashi et al., 2009; Finn et al., 2014). Furans remain to be tested on other classes of AQPs. AQP1 expression has been linked to migration in certain aggressive cancer subtypes and has been proposed as a potential target for treatments to restrain cancer metastasis (Hu and Verkman, 2006; McCoy and Sontheimer, 2007; Jiang et al., 2009; Dorward et al., 2016; Pei et al., 2016a; De Ieso and Yool, 2018). In these cancer subtypes, AQP1 is localized at the leading edges of the migrating cells (McCoy and Sontheimer, 2007; Pei et al., 2019), where it is thought to facilitate rapid volume changes during process extension and retraction (Verkman et al., 2008; Yool and Campbell, 2012).

5HMF is a naturally occurring compound in alternative medicinal treatments, with diverse reported effects, including benefits in some edema-associated conditions. This study tested the hypothesis that 5HMF might act as an inhibitor of AQP1 water or ion channel activities. Results showed that 5HMF blocked the cationic conductance of AQP1 with an  $\text{IC}_{50}$  value of approximately 400  $\mu\text{M}$ , but it did not alter water channel activity. The AQP1 ion current was also inhibited by

5NFA and 5AMF; however, no AQP1 inhibition was observed with M5NF. Excluding M5NF, the AQP1-inhibitory efficacy appeared to be inversely related to the size of the moiety at position 5 on the furan ring; the most potent agent, 5HMF, has the smallest group (hydroxy-methyl), and the least effective agent, 5AMF, has the largest group (acetoxy-methyl), although other differences could also be important. The methyl ester group on M5NF would be expected to increase relative hydrophobicity, and if anything, enhance membrane permeability and thus access to a proposed intracellular binding site; however, this feature did not rescue any AQP1 channel blocking effect. An amino acid predicted by in silico docking to be involved in ligand interaction is glycine 165, located in the loop D domain, a region which has been suggested to gate AQP channel activities (Tornroth-Horsefield et al., 2006; Yu et al., 2006; Kourghi et al., 2018). Predicted interactions of other ligands with loop D similarly have been correlated with inhibition of AQP1 ion channel activity (Kourghi et al., 2016; Pei et al., 2016b). Results here are consistent with the idea that furan ligands do not interact with intrasubunit pores to alter osmotic water fluxes but could alter loop D gating to inhibit ion conductance through the central pore.

Several lines of evidence support the conclusion that 5HMF and certain structural analogs pharmacologically target the AQP1 ion channel directly to slow migration and invasion in AQP1-expressing cancer cell lines. The high-AQP1-expressing cell lines HT29 and MDA were sensitive to furan-based AQP1 ion channel blockers, whereas the low-AQP1-expressing cell line SW480 was not. The absence of effects of 5HMF, 5NFA, and 5AMF on SW480 cells showed that the agents did not impair motility indirectly via general cytotoxicity. Histologic analyses ruled out the idea that AQP1-blocking furans impaired migration indirectly by disrupting cytoskeleton. Furan compounds at 5 mM did not alter osmotic water fluxes in oocytes, confirming that the pharmacological treatments did not reduce AQP1 protein levels in oocyte plasma membranes, nor did they disrupt AQP1 tetrameric subunit organization which is a prerequisite for water channel activity (Jung et al., 1994). In contrast, M5FA impaired migration through a general mechanism that did appear to involve actin disorganization.

In summary, results here showed that 5HMF and related furan compounds 5NFA and 5AMF are AQP1 ion channel blockers. The level of pharmacological inhibition is dose-dependent and differs between compounds, suggesting a chemical structure-activity relationship. Cancer wound closure and invasion are inhibited by AQP1-blocking furan derivatives in AQP1-enriched cancer cell lines. These outcomes add support for the proposal that the ion channel function of AQP1 is an important component of mechanisms of migration in some classes of cells. Development of furan agents using 5HMF as a lead compound might have promise for the development of new AQP1-based therapeutics for selected cancers and other disorders.

## Acknowledgments

We thank the South Australian core facility Adelaide Microscopy for access to confocal microscopy facilities and Jane Sibbons for microscopy training and assistance.

## Authorship Contributions

Participated in research design: Chow, Kourghi, Yool.

*Conducted experiments:* Chow, Kourghi, Pei, Nourmohammadi.

*Performed data analysis:* Chow, Kourghi, Pei, Nourmohammadi, Yool.

*Wrote or contributed to the writing of the manuscript:* Chow, Kourghi, Yool.

*Reviewed and approved the final manuscript:* Chow, Kourghi, Pei, Nourmohammadi, Yool.

## References

- Abel SDA, Dadhwal S, Gamble AB, and Baird SK (2018) Honey reduces the metastatic characteristics of prostate cancer cell lines by promoting a loss of adhesion. *PeerJ* **6**:e5115.
- Afrin S, Giampieri F, Gasparrini M, Forbes-Hernández TY, Cianciosi D, Reboledo-Rodríguez P, Manna PP, Zhang J, Quiles JL, and Battino M (2018) The inhibitory effect of Manuka honey on human colon cancer HCT-116 and LoVo cell growth. Part 2: induction of oxidative stress, alteration of mitochondrial respiration and glycolysis, and suppression of metastatic ability. *Food Funct* **9**:2158–2170.
- Agre P, Preston GM, Smith BL, Jung JS, Raina S, Moon C, Guggino WB, and Nielsen S (1993) Aquaporin CHIP: the archetypal molecular water channel. *Am J Physiol* **265**:F463–F476.
- Ahmed S and Othman NH (2013) Review of the medicinal effects of tualang honey and a comparison with manuka honey. *Malays J Med Sci* **20**:6–13.
- Anthony TL, Brooks HL, Boassa D, Leonov S, Yanochko GM, Regan JW, and Yool AJ (2000) Cloned human aquaporin-1 is a cyclic GMP-gated ion channel. *Mol Pharmacol* **57**:576–588.
- Aryappalli P, Al-Qubaisi SS, Attoub S, George JA, Arafat K, Ramadi KB, Mohamed YA, Al-Dhaheri MM, Al-Sbiei A, Fernandez-Cabezudo MJ, et al. (2017) The IL-6/STAT3 signaling pathway is an early target of manuka honey-induced suppression of human breast cancer cells. *Front Oncol* **7**:167.
- Attia WY, Gabry MS, El-Shaikh KA, and Othman GA (2008) The anti-tumor effect of bee honey in Ehrlich ascite tumor model of mice is coincided with stimulation of the immune cells. *Egypt J Immunol* **15**:169–183.
- Boassa D, Stamer WD, and Yool AJ (2006) Ion channel function of aquaporin-1 natively expressed in choroid plexus. *J Neurosci* **26**:7811–7819.
- Boassa D and Yool AJ (2003) Single amino acids in the carboxyl terminal domain of aquaporin-1 contribute to cGMP-dependent ion channel activation. *BMC Physiol* **3**:12.
- Byrt CS, Zhao M, Kourghi M, Bose J, Henderson SW, Qiu J, Gilliam M, Schultz C, Schwarz M, Ramesh SA, et al. (2017) Non-selective cation channel activity of aquaporin AQP2:1 regulated by Ca<sup>2+</sup> and pH. *Plant Cell Environ* **40**:802–815.
- Campbell EM, Birdsall DN, and Yool AJ (2012) The activity of human aquaporin 1 as a cGMP-gated cation channel is regulated by tyrosine phosphorylation in the carboxyl-terminal domain. *Mol Pharmacol* **81**:97–105.
- De Ieso ML and Pei JV (2018) An accurate and cost-effective alternative method for measuring cell migration with the circular wound closure assay. *Biosci Rep* **38**.
- De Ieso ML, Pei JV, Nourmohammadi S, Smith E, Chow PH, Kourghi M, Hardingham JE, and Yool AJ (2019) Combined pharmacological administration of AQP1 ion channel blocker AqB011 and water channel blocker Bacopaside II amplifies inhibition of colon cancer cell migration. *Sci Rep* **9**:12635.
- De Ieso ML and Yool AJ (2018) Mechanisms of aquaporin-facilitated cancer invasion and metastasis. *Front Chem* **6**:135.
- Denker BM, Smith BL, Kuhajda FP, and Agre P (1988) Identification, purification, and partial characterization of a novel Mr 28,000 integral membrane protein from erythrocytes and renal tubules. *J Biol Chem* **263**:15634–15642.
- Dorward HS, Du A, Bruhn MA, Wrin J, Pei JV, Evdokiou A, Price TJ, Yool AJ, and Hardingham JE (2016) Pharmacological blockade of aquaporin-1 water channel by AqB013 restricts migration and invasiveness of colon cancer cells and prevents endothelial tube formation in vitro. *J Exp Clin Cancer Res* **35**:36.
- El Hindy N, Rump K, Lambertz N, Zhu Y, Frey UH, Bankfalvi A, Siffert W, Sure U, Peters J, Adamzik M, et al. (2013) The functional Aquaporin 1 -783G/C-polymorphism is associated with survival in patients with glioblastoma multiforme. *J Surg Oncol* **108**:492–498.
- Finn RN, Chauvigné F, Hlidberg JB, Cutler CP, and Cerdà J (2014) The lineage-specific evolution of aquaporin gene clusters facilitated tetrapod terrestrial adaptation. *PLoS One* **9**:e113686.
- Foxall E, Pipili A, Jones GE, and Wells CM (2016) Significance of kinase activity in the dynamic invadosome. *Eur J Cell Biol* **95**:483–492.
- Gasparrini M, Afrin S, Forbes-Hernández TY, Cianciosi D, Reboledo-Rodríguez P, Amici A, Battino M, and Giampieri F (2018) Protective effects of Manuka honey on LPS-treated RAW 264.7 macrophages. Part 2: control of oxidative stress induced damage, increase of antioxidant enzyme activities and attenuation of inflammation. *Food Chem Toxicol* **120**:578–587.
- Ghosh S and Playford RJ (2003) Bioactive natural compounds for the treatment of gastrointestinal disorders. *Clin Sci (Lond)* **104** (6):547–556.
- Girma A, Seo W, and She RC (2019) Antibacterial activity of varying UMF-graded Manuka honeys. *PLoS One* **14**:e0224495.
- Gomes D, Agasse A, Thiébaud P, Delrot S, Gerós H, and Chaumont F (2009) Aquaporins are multifunctional water and solute transporters highly divergent in living organisms. *Biochim Biophys Acta* **1788**:1213–1228.
- Hazama A, Kozono D, Guggino WB, Agre P, and Yasui M (2002) Ion permeation of AQP6 water channel protein. Single channel recordings after Hg<sup>2+</sup> activation. *J Biol Chem* **277**:29224–29230.
- He M, Grkovic T, Evans JR, Thornburg CC, Akee RK, Thompson JR, Whitt JA, Harris MJ, Loyal JA, Britt JR, et al. (2019) The NCI library of traditional Chinese medicinal plant extracts - preliminary assessment of the NCI-60 activity and chemical profiling of selected species. *Fitoterapia* **137**:104285.
- Hinz N and Jücker M (2019) Distinct functions of AKT isoforms in breast cancer: a comprehensive review. *Cell Commun Signal* **17**:154.
- Hohmann I, Bill RM, Kayingo I, and Prior BA (2000) Microbial MIP channels. *Trends Microbiol* **8**:33–38.
- Hu J and Verkman AS (2006) Increased migration and metastatic potential of tumor cells expressing aquaporin water channels. *FASEB J* **20**:1892–1894.
- Huber VJ, Tsujita M, and Nakada T (2012) Aquaporins in drug discovery and pharmacotherapy. *Mol Aspects Med* **33**:691–703.
- Ishibashi K, Hara S, and Kondo S (2009) Aquaporin water channels in mammals. *Clin Exp Nephrol* **13**:107–117.
- Jiang Q, Cao C, Lu S, Kivlin R, Wallin B, Chu W, Bi Z, Wang X, and Wan Y (2009) MEK/ERK pathway mediates UVB-induced AQP1 downregulation and water permeability impairment in human retinal pigment epithelial cells. *Int J Mol Med* **23**:771–777.
- Jung JS, Preston GM, Smith BL, Guggino WB, and Agre P (1994) Molecular structure of the water channel through aquaporin CHIP. The hourglass model. *J Biol Chem* **269**:14648–14654.
- Khalil I, Moniruzzaman M, Boukraâ L, Benhanifa M, Islam A, Islam N, Sulaiman SA, and Gan SH (2012) Physicochemical and antioxidant properties of Algerian honey. *Molecules* **17**:11199–11215.
- Khan H (2014) Medicinal plants in light of history: recognized therapeutic modality. *J Evid Based Complementary Altern Med* **19**:216–219.
- Kourghi M, De Ieso ML, Nourmohammadi S, Pei JV, and Yool AJ (2018) Identification of loop D domain amino acids in the human aquaporin-1 channel involved in activation of the ionic conductance and inhibition by AqB011. *Front Chem* **6**:142.
- Kourghi M, Pei JV, De Ieso ML, Flynn G, and Yool AJ (2016) Bumetanide derivatives AqB007 and AqB011 selectively block the aquaporin-1 ion channel conductance and slow cancer cell migration. *Mol Pharmacol* **89**:133–140.
- Kourghi M, Nourmohammadi S, Pei JV, Qiu J, McGaughy S, Tyerman SD, Byrt CS, and Yool AJ (2017) Divalent cations regulate the ion conductance properties of diverse classes of aquaporins. *Int J Mol Sci* **18**:11.
- Lori G, Cecchi L, Mulinacci N, Melani F, Caselli A, Cirri P, Pazzagli L, Luti S, Mazzoli L, and Paoli P (2019) Honey extracts inhibit PTP1B, upregulate insulin receptor expression, and enhance glucose uptake in human HepG2 cells. *Biomed Pharmacother* **113**:108752.
- Luo L, Yang R, Zhao S, Chen Y, Hong S, Wang K, Wang T, Cheng J, Zhang T, and Chen D (2018) Decreased miR-320 expression is associated with breast cancer progression, cell migration, and invasiveness via targeting Aquaporin 1. *Acta Biochim Biophys Sin (Shanghai)* **50**:473–480.
- Martins AP, Ciancetta A, de Almeida A, Marrone A, Re N, Soveral G, and Casini A (2013) Aquaporin inhibition by gold(III) compounds: new insights. *ChemMedChem* **8**:1086–1092.
- McCoy E and Sontheimer H (2007) Expression and function of water channels (aquaporins) in migrating malignant astrocytes. *Glia* **55**:1034–1043.
- Migliati E, Meurice N, DuBois P, Fang JS, Somasekharan S, Beckett E, Flynn G, and Yool AJ (2009) Inhibition of aquaporin-1 and aquaporin-4 water permeability by a derivative of the loop diuretic bumetanide acting at an internal pore-occluding binding site. *Mol Pharmacol* **76**:105–112.
- Nakhjavani M, Palethorpe HM, Tomita Y, Smith E, Price TJ, Yool AJ, Pei JV, Townsend AR, and Hardingham JE (2019) Stereoselective anti-cancer activities of ginsenoside Rg3 on triple negative breast cancer cell models. *Pharmacocell (Basel)* **12**.
- Nourmohammadi S, Aung TN, Cui J, Pei JV, De Ieso ML, Harata-Lee Y, Qu Z, Adelson DL, and Yool AJ (2019) Effect of compound kushen injection, a natural compound mixture, and its identified chemical components on migration and invasion of colon, brain, and breast cancer cell lines. *Front Oncol* **9**:314.
- Nyblom M, Frick A, Wang Y, Ekval M, Hallgren K, Hedfalk K, Neutze R, Tajkhorshid E, and Törnroth-Horsefield S (2009) Structural and functional analysis of SoPIP2:1 mutants adds insight into plant aquaporin gating. *J Mol Biol* **387**:653–668.
- Pei JV, Burton JL, Kourghi M, De Ieso ML, and Yool AJ (2016a) Drug discovery and therapeutic targets for pharmacological modulators of aquaporin channels, in *Aquaporins in Health and Disease: New Molecular Targets for Drug Discovery* (Soveral G, Casini A, and Nielsen S 275–297, CRC Press, Oxfordshire, UK).
- Pei JV, Heng S, De Ieso ML, Sylvia G, Kourghi M, Nourmohammadi S, Abell AD, and Yool AJ (2019) Development of a photoswitchable lithium-sensitive probe to analyze nonselective cation channel activity in migrating cancer cells. *Mol Pharmacol* **95**:573–583.
- Pei JV, Kourghi M, De Ieso ML, Campbell EM, Dorward HS, Hardingham JE, and Yool AJ (2016b) Differential inhibition of water and ion channel activities of mammalian aquaporin-1 by two structurally related bacopaside compounds derived from the medicinal plant *Bacopa monnieri*. *Mol Pharmacol* **90**:496–507.
- Preston GM and Agre P (1991) Isolation of the cDNA for erythrocyte integral membrane protein of 28 kilodaltons: member of an ancient channel family. *Proc Natl Acad Sci USA* **88**:11110–11114.
- Preston GM, Carroll TP, Guggino WB, and Agre P (1992) Appearance of water channels in *Xenopus* oocytes expressing red cell CHIP28 protein. *Science* **256**:385–387.
- Reizer J, Reizer A, and Saier MH Jr. (1993) The MIP family of integral membrane channel proteins: sequence comparisons, evolutionary relationships, reconstructed pathway of evolution, and proposed functional differentiation of the two repeated halves of the proteins. *Crit Rev Biochem Mol Biol* **28**:235–257.
- Saparov SM, Kozono D, Rothe U, Agre P, and Pohl P (2001) Water and ion permeation of aquaporin-1 in planar lipid bilayers. Major differences in structural determinants and stoichiometry. *J Biol Chem* **276**:31515–31520.
- Seeliger D, Zapater C, Krenc D, Haddoub R, Flitsch S, Beitz E, Cerdà J, and de Groot BL (2013) Discovery of novel human aquaporin-1 blockers. *ACS Chem Biol* **8**:249–256.
- Shan Y (2019) Medicinal honey in clinical practice: viable alternative or useful adjunct in wound care management? *Br J Nurs* **28**:S23–S30.

- Shimasaki M, Kanazawa Y, Sato K, Tsuchiya H, and Ueda Y (2018) Aquaporin-1 and -5 are involved in the invasion and proliferation of soft tissue sarcomas. *Pathol Res Pract* **214**:80–88.
- Sucher NJ and Carles MC (2015) A pharmacological basis of herbal medicines for epilepsy. *Epilepsy Behav* **52** (Pt B):308–318.
- Sui H, Han BG, Lee JK, Walian P, and Jap BK (2001) Structural basis of water-specific transport through the AQP1 water channel. *Nature* **414**:872–878.
- Tomita Y, Palethorpe HM, Smith E, Nakhjavani M, Townsend AR, Price TJ, Yool AJ, and Hardingham JE (2019) Bumetanide-derived aquaporin 1 inhibitors, AqB013 and AqB050 inhibit tube formation of endothelial cells through induction of apoptosis and impaired migration in vitro. *Int J Mol Sci* **20**.
- Törnroth-Horsefield S, Wang Y, Hedfalk K, Johanson U, Karlsson M, Tajkhorshid E, Neutze R, and Kjellbom P (2006) Structural mechanism of plant aquaporin gating. *Nature* **439**:688–694.
- Trott O and Olson AJ (2010) AutoDock Vina: improving the speed and accuracy of docking with a new scoring function, efficient optimization, and multithreading. *J Comput Chem* **31**:455–461.
- Verkman AS, Hara-Chikuma M, and Papadopoulos MC (2008) Aquaporins—new players in cancer biology. *J Mol Med (Berl)* **86**:523–529.
- Wang Y, Fan Y, Zheng C, and Zhang X (2017) Knockdown of AQP1 inhibits growth and invasion of human ovarian cancer cells. *Mol Med Rep* **16**:5499–5504.
- Weaver CD, Shomer NH, Louis CF, and Roberts DM (1994) Nodulin 26, a nodule-specific symbiosome membrane protein from soybean, is an ion channel. *J Biol Chem* **269**:17858–17862.
- Wölkart G, Schrammel A, Koyani CN, Scherübel S, Zorn-Pauly K, Malle E, Pelzmann B, Andrá M, Ortner A, and Mayer B (2017) Cardioprotective effects of 5-hydroxymethylfurfural mediated by inhibition of L-type  $Ca^{2+}$  currents. *Br J Pharmacol* **174**:3640–3653.
- Wulf E, Deboen A, Bautz FA, Faulstich H, and Wieland T (1979) Fluorescent phallotoxin, a tool for the visualization of cellular actin. *Proc Natl Acad Sci USA* **76**:4498–4502.
- Ya BL, Li HF, Wang HY, Wu F, Xin Q, Cheng HJ, Li WJ, Lin N, Ba ZH, Zhang RJ, et al. (2017) 5-HMF attenuates striatum oxidative damage via Nrf2/ARE signaling pathway following transient global cerebral ischemia. *Cell Stress Chaperones* **22**: 55–65.
- Yanochko GM and Yool AJ (2002) Regulated cationic channel function in *Xenopus* oocytes expressing *Drosophila* big brain. *J Neurosci* **22**:2530–2540.
- Yool AJ, Brown EA, and Flynn GA (2010) Roles for novel pharmacological blockers of aquaporins in the treatment of brain oedema and cancer. *Clin Exp Pharmacol Physiol* **37**:403–409.
- Yool AJ and Campbell EM (2012) Structure, function and translational relevance of aquaporin dual water and ion channels. *Mol Aspects Med* **33**:553–561.
- Yool AJ, Stamer WD, and Regan JW (1996) Forskolin stimulation of water and cation permeability in aquaporin 1 water channels. *Science* **273**:1216–1218.
- Yoshida T, Hojo S, Sekine S, Sawada S, Okumura T, Nagata T, Shimada Y, and Tsukada K (2013) Expression of aquaporin-1 is a poor prognostic factor for stage II and III colon cancer. *Mol Clin Oncol* **1**:953–958.
- Yu J, Yool AJ, Schulten K, and Tajkhorshid E (2006) Mechanism of gating and ion conductivity of a possible tetrameric pore in aquaporin-1. *Structure* **14**:1411–1423.

---

**Address correspondence to:** Andrea Yool, Professor of Physiology, Helen Mayo South, Level G, Frome Rd., University of Adelaide, Adelaide SA 5005 Australia. E-mail: andrea.yool@adelaide.edu.au

---

OPEN

# Combined pharmacological administration of AQP1 ion channel blocker AqB011 and water channel blocker Bacopaside II amplifies inhibition of colon cancer cell migration

Michael L. De Ieso<sup>1</sup>, Jinxin V. Pei<sup>1</sup>, Saeed Nourmohammadi<sup>1</sup>, Eric Smith<sup>1,2</sup>, Pak Hin Chow<sup>1</sup>, Mohamad Kourghi<sup>1</sup>, Jennifer E. Hardingham<sup>1,2</sup> & Andrea J. Yool<sup>1</sup>

Aquaporin-1 (AQP1) has been proposed as a dual water and cation channel that when upregulated in cancers enhances cell migration rates; however, the mechanism remains unknown. Previous work identified AqB011 as an inhibitor of the gated human AQP1 cation conductance, and bacopaside II as a blocker of AQP1 water pores. In two colorectal adenocarcinoma cell lines, high levels of AQP1 transcript were confirmed in HT29, and low levels in SW480 cells, by quantitative PCR (polymerase chain reaction). Comparable differences in membrane AQP1 protein levels were demonstrated by immunofluorescence imaging. Migration rates were quantified using circular wound closure assays and live-cell tracking. AqB011 and bacopaside II, applied in combination, produced greater inhibitory effects on cell migration than did either agent alone. The high efficacy of AqB011 alone and in combination with bacopaside II in slowing HT29 cell motility correlated with abundant membrane localization of AQP1 protein. In SW480, neither agent alone was effective in blocking cell motility; however, combined application did cause inhibition of motility, consistent with low levels of membrane AQP1 expression. Bacopaside alone or combined with AqB011 also significantly impaired lamellipodial formation in both cell lines. Knockdown of AQP1 with siRNA (confirmed by quantitative PCR) reduced the effectiveness of the combined inhibitors, confirming AQP1 as a target of action. Invasiveness measured using transwell filters layered with extracellular matrix in both cell lines was inhibited by AqB011, with a greater potency in HT29 than SW480. A side effect of bacopaside II at high doses was a potentiation of invasiveness, that was reversed by AqB011. Results here are the first to demonstrate that combined block of the AQP1 ion channel and water pores is more potent in impairing motility across diverse classes of colon cancer cells than single agents alone.

Cancer is a leading cause of death worldwide, and accounted for 8.2 million deaths in 2012 according to the World Health Organization<sup>1</sup>, primarily due to metastasis<sup>2,3</sup>. Colorectal cancer is the second most common cancer in women and third in men<sup>1</sup>. A link between disease severity and upregulation of aquaporin-1 (AQP1) expression in certain cancer types has been documented previously<sup>4,5</sup>. AQP1 normally serves essential roles in fluid absorption and secretion in tissues including kidney, brain, eye and vascular system<sup>6</sup>. In aggressive cancers including subtypes of colorectal cancers, gliomas, lung adenocarcinoma, laryngeal cancer and cholangiocarcinomas, AQP1 channels are upregulated<sup>7–11</sup>. Levels of AQP1 expression show a positive correlation with angiogenesis, tumour

<sup>1</sup>Adelaide Medical School, University of Adelaide, Adelaide, SA, 5005, Australia. <sup>2</sup>Oncology Department, The Basal Hetzel Institute, The Queen Elizabeth Hospital, Woodville, SA, 5011, Australia. Michael L. De Ieso and Jinxin V. Pei contributed equally. Correspondence and requests for materials should be addressed to A.J.Y. (email: [andrea.yool@adelaide.edu.au](mailto:andrea.yool@adelaide.edu.au))



progression, growth, migration and metastasis<sup>12</sup>. Knockdown of AQP1 with small-interfering RNAs substantially impaired cancer cell migration *in vitro*<sup>13</sup>. Conversely, transfection of AQP1 into deficient lines (B16F10 melanoma, and 4T1 mammary gland tumour) accelerated cell migration *in vitro* and increased the likelihood of lung metastases in mice *in vivo*<sup>14</sup>. Colon cancer cells (HT20) transfected with AQP1 similarly exhibited increased cell migration rates and enhanced extravasation after injection via the tail vein in mice<sup>15</sup>. AQP1 channels have been proposed to facilitate extension of the leading edges (lamellipodia) of migrating cells to speed the rate of movement<sup>16</sup>.

Inhibition of AQP1 channel activity is a strategy of interest for potential therapeutic control of metastasis in AQP1-expressing cancers. In AQP1-dependent cancer lines, other mammalian water channels such as AQP4 do not substitute for AQP1 in facilitating movement<sup>17</sup>, suggesting the migration-enhancing property relies on more than water permeability. Converging lines of evidence support the idea that AQP1 is dual water and ion channel, mediating osmotic water flow through individual subunit pores, and cation conductance through the central pore of the tetramer<sup>18–20</sup>. The non-selective monovalent cation conductance is gated by cGMP and depends on loop D structural integrity for channel activation<sup>19,21–24</sup>. In some expression systems, AQP1 ion channels have a low opening probability<sup>25</sup> or are not detectable<sup>26</sup>, suggesting gating of AQP1 is subject to additional regulation such as tyrosine phosphorylation<sup>27</sup>. The idea that the AQP1 cation pore at the four-fold axis of symmetry is separate from the individual water pores in each monomer<sup>19,27,28</sup> is supported by differences in pharmacological sensitivities and differential effects of site-directed mutations<sup>25,29,30</sup>. There is a gap in knowledge regarding the properties of AQP1 that permit its migration-enhancing effect, but the inability of other water-selective channels to substitute suggests the dual ion and water channel activities of AQP1 might be involved<sup>31</sup>. The discovery of pharmacological modulators of AQP1 has allowed dissection of the mechanisms of action of AQP1 in cell migration at a level not possible previously.

Pharmacological modulators of the AQP1 ion conductance include the agonist cyclic GMP<sup>21</sup>, and antagonists cadmium<sup>32</sup>, calcium<sup>33</sup> and pharmacological derivatives of bumetanide such as AqB007 and AqB011<sup>34</sup>. Blocking native AQP1 ion channels in choroid plexus with Cd<sup>2+</sup> was shown to alter net cerebrospinal fluid production *in vitro*<sup>32</sup>. AqB011 is a bumetanide derivative that selectively blocks the ion pore of AQP1, binding at the intracellular loop D gating domain<sup>24</sup> without affecting water fluxes, and slows the migration of AQP1-expressing cancer cells<sup>34</sup>. Pharmacological modulators of the AQP1 water pore include the antagonists mercury<sup>35</sup>, tetraethylammonium<sup>29,36,37</sup>, metals<sup>38</sup>, AqB013<sup>39</sup> and bacopasides<sup>40</sup>, and the agonist AqF026<sup>30</sup>. The inhibitor AqB013 and a related compound, AqB050, have been shown to reduce cancer cell migration rates *in vitro*<sup>41,42</sup>. The natural medicinal plant product, Bacopaside II, isolated from *Bacopa monnieri* appears to dock in the cytoplasmic vestibule of the AQP1 water pore, occluding water flux without affecting the AQP1 ion conductance, and slows cell migration in an AQP1-expressing colon cancer line<sup>40</sup>.

Prior reports have focused on measuring effects of single AQP1 modulators using two-dimensional wound closure assays of cancer lines. This study is the first to assess synergistic actions of AQP1 ion and water channel inhibitors applied together, and to evaluate effects on three-dimensional invasion through extracellular matrix. The two human colorectal adenocarcinomas cell lines with epithelial morphologies selected for comparison were: HT29 with high levels of AQP1 expression, and SW480 with low levels of AQP1 expression<sup>40,43</sup>. Results here showed that combined administration of AQP1 water and ion channel blockers produced an amplified block of colon cancer cell migration in both colon cancer lines. Inhibition of the AQP1 ion channel reduced cancer cell invasiveness. The relative efficacy of the AQP1 inhibitors was dependent on the abundance and localization of AQP1 protein in the plasma membranes, which was greater in HT29 than in SW480 cells. In summary, AQP1 water and ion fluxes appear to have a coordinated role in facilitating AQP1-dependent cancer cell migration. Simultaneous targeting of both the water and ion channel functions of AQP1 appears to offer opportunities to control cancer metastasis at lower doses and across more diverse classes of cancers than would be possible with single agents alone.

## Results

**AQP1 expression and localization in HT29 and SW480 cell lines.** Levels of AQP1 expression were quantified previously in HT29 and SW480 cell lines by western blot and quantitative real-time reverse-transcription polymerase chain reaction (qRT-PCR), and showed that AQP1 transcript and protein levels were significantly higher in HT29 than in SW480 cells<sup>40,43</sup>. Quantitative PCR on the same passages of cells used in the present study demonstrated a fifteen-fold higher level of AQP1 transcript in HT29 as compared to SW480 cells (Fig. 1A), confirming prior results. Confocal imaging demonstrated that HT29 further exceeded SW480 in AQP1 levels when the subcellular distribution in the plasma membrane was considered. Membrane-associated AQP1 protein was almost three-fold higher in HT29 cells than in SW480 cells (Fig. 1B). Amplitudes of colocalized plasma membrane and AQP1 fluorescence signals were significantly lower in SW480 ( $0.38 \pm 0.04$ ;  $n = 6$ ) than in HT29 ( $1.05 \pm 0.15$ ) cells.

AQP1 signal localization in HT29 and SW480 cells was assessed in greater detail by immunofluorescent labelling of AQP1 in combination with a fluorogenic membrane dye (MemBrite™), and Hoechst nuclear stain (Fig. 2A). Using Fiji software (ImageJ, National Institutes of Health), intensities were quantified for anti-AQP1 and membrane dye signals, and plotted as a function of cross-sectional distance for six transects in each cell line (Fig. 2B,C). Anti-AQP1 signals showed a robust correlation with the membrane signal in HT29 cells, whereas in SW480 cells the AQP1 signals were predominantly in the submembrane and cytoplasmic domains.

**Combined treatment with bacopaside II and AqB011 produced enhanced block of wound closure in colon cancer cells.** The effects of AqB011 and bacopaside II alone and combined on two-dimensional migration of HT29 and SW480 cells were tested using circular wound closure assays (Fig. 3A,B). In HT29 cells at 24 h, significant impairment of migration was observed with AqB011 alone (at 20 to 100 μM), or

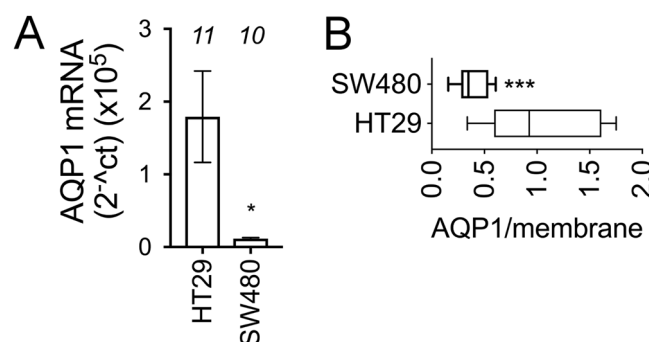


**Figure 1.** AQP1 transcript and membrane expression levels were higher in HT29 cells than SW480 cells. (A) AQP1 mRNA levels in HT29 cells (n = 11) and SW480 cells (n = 10), as determined by qRT-PCR. (B) Ratios of signal intensity (anti-AQP1 to membrane dye), in HT29 and SW480 cells showing relative levels of membrane AQP1 expression. See methods for statistical analysis details.

bacopaside II alone (at 7.5 and 15  $\mu\text{M}$ ), as compared to vehicle control (Fig. 3C), confirming previous findings<sup>34,40</sup>. With agents applied singly, migration was reduced 38% by AqB011 (20  $\mu\text{M}$ ), and 44% by bacopaside II (15  $\mu\text{M}$ ). However, the combined treatment produced a block of 81%, significantly greater than with either agent alone. Conversely, SW480 cells showed no appreciable sensitivity of migration to individual AqB011 or bacopaside II treatments (Fig. 3D), again confirming previous findings<sup>34,40</sup>. However, the combined treatment of SW480 cells with AqB011 (20  $\mu\text{M}$ ) and bacopaside II (15  $\mu\text{M}$ ) resulted in a 50% block of migration, showing that the combination of inhibitors was more potent than either agent alone. These data indicate AqB011 and bacopaside II applied in combination can slow migration in a line that would otherwise escape control by single agents alone at non-cytotoxic doses.

Timelapse video files show the migration processes in vehicle control and treatment groups in more detail (Supplementary Videos ‘HT29’ and ‘SW480’).

**Cell viability was not affected by AqB011 and bacopaside II.** Cell viability data measured with the alamarBlue assay were standardized to results for untreated groups in each cell line (Fig. 4). HT29 cell viability was  $99.6 \pm 1.4\%$  in AqB011 (100  $\mu\text{M}$ ), and  $94.5 \pm 0.7\%$  in combined treatment. In contrast, cytotoxic mercuric chloride (5  $\mu\text{M}$ ) resulted in  $3.1 \pm 0.04\%$  viability. SW480 cell viability was  $97.6 \pm 0.2\%$  in AqB011 (100  $\mu\text{M}$ ),  $96.2 \pm 0.6\%$  in combined treatment, and  $2.4 \pm 0.04\%$  in mercuric chloride (5  $\mu\text{M}$ ). The lack of effects of bacopaside II and AqB011 on cell viability demonstrated that cytotoxicity did not account indirectly for the reduced cell migration.

**Knockdown of AQP1 reduced the sensitivity of HT29 cells to block by bacopaside II and AqB011.** The role of AQP1 as a primary target of action for the combined inhibitors was tested using siRNA transfection with two different AQP1-siRNA sequences (siRNA1 and siRNA2), as compared with scrambled controls. Figure 5A shows that siRNA2 significantly reduced AQP1 transcripts levels (~44 fold decrease), as compared to scrambled control siRNA. In contrast, siRNA1 was not effective in knocking down AQP1. Matched scrambled controls also had no effect on AQP1 transcript levels.

AQP1 knockdown via siRNA has been shown previously to reduce cell migration<sup>44–46</sup>. In Fig. 5B, in order to highlight differences in pharmacological sensitivity that were due specifically to siRNA effects, all results for percent block were standardized to the mean percent block measured in the scrambled siRNA control group (Scr Dual, set by definition as 100%). Only siRNA2 significantly impaired the effect of the combined inhibitors in slowing migration. The other groups (untreated, siRNA1) showed no change in pharmacological sensitivity as compared with scrambled siRNA. At 24 hours, vehicle-treated cells transfected with scrambled siRNA achieved  $20 \pm 1\%$  wound closure. Vehicle-treated cells transfected with AQP1 siRNA1 achieved  $17 \pm 1\%$  wound closure. When cells transfected with scrambled siRNA were treated with combined inhibitors, wound closure was almost completely blocked ( $0.5 \pm 0.4\%$ ). The cells transfected with AQP1 siRNA2 retained a greater capacity for wound closure in the presence of the combined inhibitors ( $6 \pm 0.6\%$ ), demonstrating a reduced pharmacological sensitivity to the AQP1 inhibitors. These results suggested that the effectiveness of the inhibitors on cell migration correlated with the level of AQP1 expression.

**Live cell imaging of bacopaside II and AqB011 effects on individual cell migration trajectories.** The effects of the AQP1 modulators on individual cell trajectories were tracked over 24 hours for HT29 (Fig. 6), and SW480 (Fig. 7) cells using live cell imaging. In HT29 cells, slowed wound closure with AQP inhibitors was evident in time lapse images of the wound edge (Fig. 6A). Impaired velocity and direction of migration were evident in the short convoluted trajectories in the treatment groups as compared with untreated and vehicle controls (Fig. 6B). In contrast, SW480 cells showed normal wound edge closure (Fig. 7A) and migration trajectories (Fig. 7B) in the treatment groups with single agents; however the combined agents appeared to reduce the total distance travelled, yielding shorter trajectories.

Total distance travelled (the cumulative length of the trajectory) and net displacement (the difference in position between the starting and ending point) per cell were quantified from analyses of live cell imaging results (Fig. 8). HT29 cells showed a dose-dependent effect of AqB011 in decreasing total distance travelled as compared

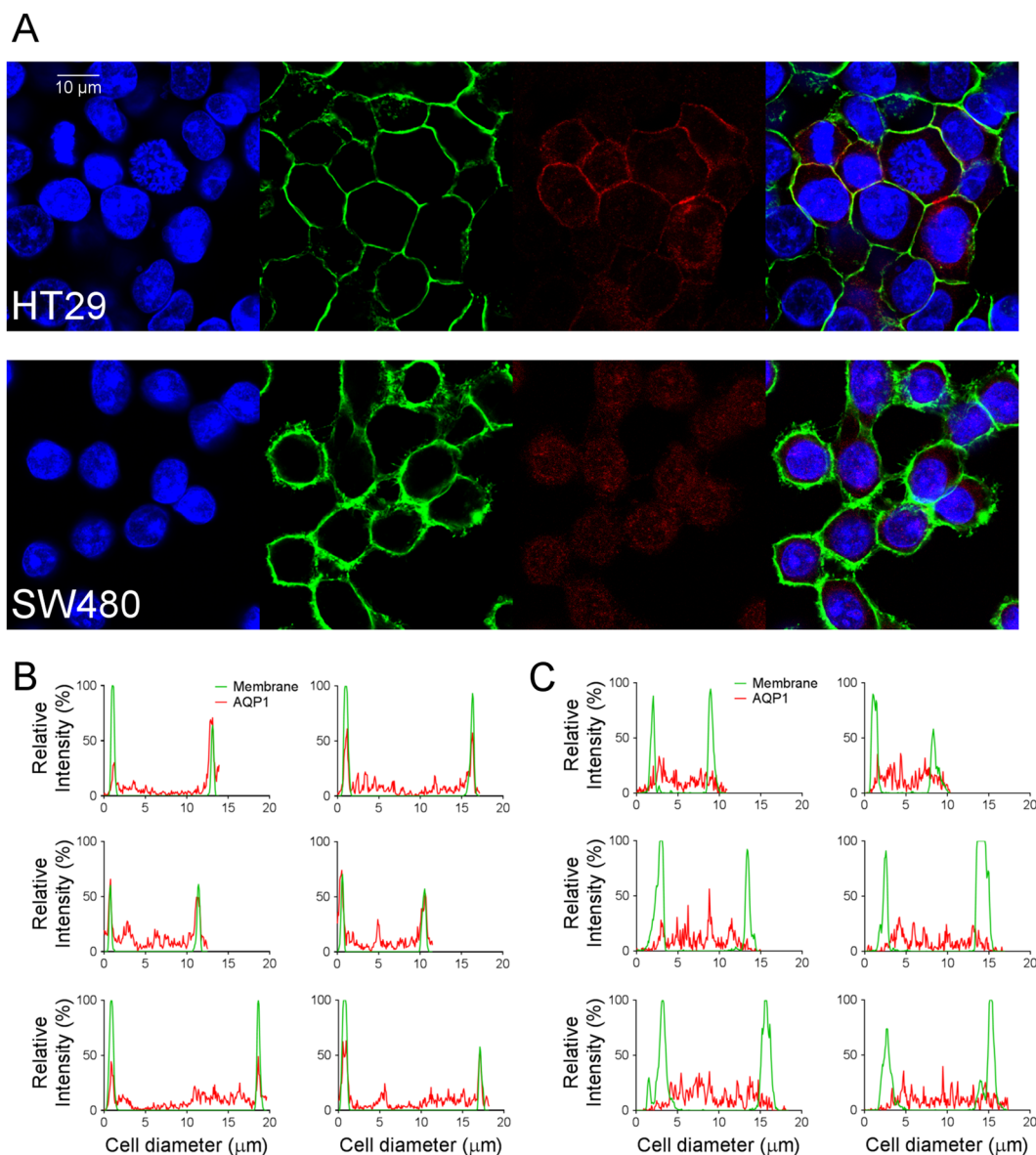


**Figure 2.** Confocal images and quantitative analyses of AQP1 subcellular localization measured by immunolabelling. **(A)** Confocal images of a single field of view for HT29 (top row) and SW480 (bottom row) cells. The panels in each row (from left to right) depict nuclear staining (blue); membrane staining (green); AQP1 signal (red); and an overlay of the three images (right). **(B,C)** Each graph shows the intensities (y-axis) of the membrane stain (green) and the AQP1 signal (red), as a function of distance across the diameters of individual HT29 (**B**) or SW480 (**C**) cells, for two cross-sections per cell.

with vehicle-treated cells (Fig. 8A). Bacopaside II at 15  $\mu\text{M}$  also significantly reduced total distance. Combined AqB011 (20  $\mu\text{M}$ ) and bacopaside II (15  $\mu\text{M}$ ) was more effective than either agent alone in HT29 cells. In contrast, SW480 showed no effect of AqB011 alone (Fig. 8B); the total distance after treatment with 100  $\mu\text{M}$  AqB011; was not significantly different from vehicle-treated cells. Similarly, bacopaside II (15  $\mu\text{M}$ ) alone had no appreciable effect on SW480 cell total distance travelled. Combined AqB011 (20  $\mu\text{M}$ ) and bacopaside II (15  $\mu\text{M}$ ) treatment appeared to reduce total distance travelled, but the difference was not statistically significant.

Net displacement over 24 h was significantly reduced in all treatment groups as compared with vehicle in HT29 cells (Fig. 8C). In SW480 cells, a significant decrease of net displacement (Fig. 8D) was seen only with the combined pharmacological treatment. Bacopaside II alone or AqB011 alone yielded net displacement values in SW480 cells comparable to vehicle-treated cells. The overall distances travelled were greater in SW480 than HT29 cells, illustrating an inherently higher two-dimensional migration velocity (Fig. 8E) with a low sensitivity to AQP1 modulators, indicating mechanisms other than AQP1 can enable motility in some cancer lines. However, the significant impairment of net displacement suggested that the directionality of movement (i.e., the ability to maintain a consistent vector over successive intervals) was compromised by the combined treatment in both cell lines.

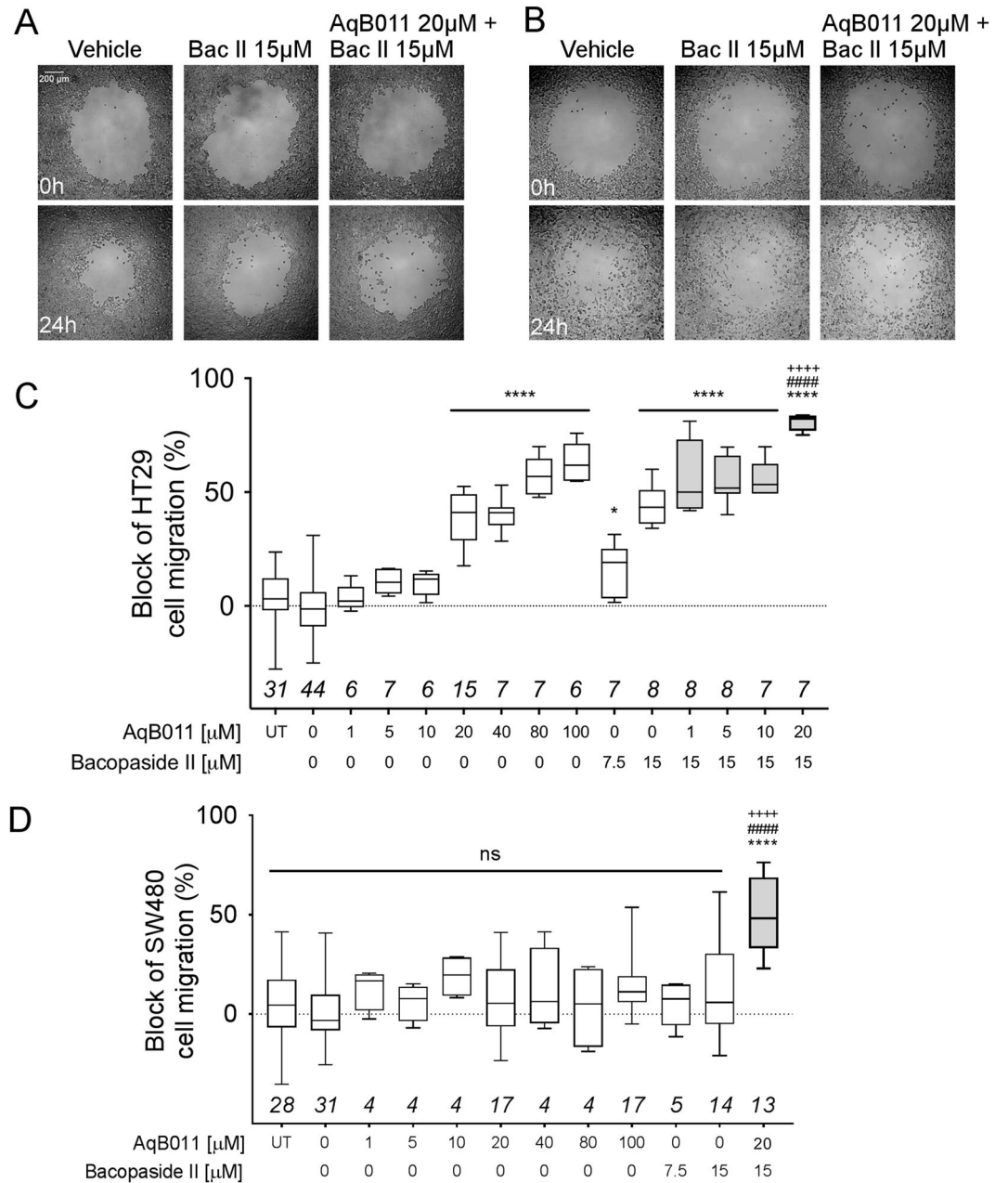


**Figure 3.** Wound closure assay showing the block of cell migration in HT29 cells by bacopaside II, AqB011 and combined treatments. **(A)** Representative images showing HT29 cells treated with vehicle, bacopaside II (15 µM), and combined treatment at 0 hours (upper row) and 24 hours (bottom row). Scale bar applies for both **(A,B)**. **(B)** Representative images showing SW480 cells treated with vehicle, bacopaside II (15 µM), and combined treatment at 0 hours (upper row) and 24 hours (bottom row). **(C)** Box plot depicting percent block (%) of HT29 wound closure after 24 hours. White bars represent single treatments; grey bars represent combined treatment with AqB011 and bacopaside II. AqB011 (20 µM) and bacopaside II (15 µM) treatment yielded block that was significantly greater than vehicle (\*\*\*\*), AqB011 (20 µM) alone (####), and bacopaside II (15 µM) alone (++++), suggesting an additive interaction; n-values are in italics above the x-axis for **(C,D)**. **(D)** Box plot depicting wound closure block (%) for SW480 after 24 hours. White bars represent single treatments; grey bars represent combined treatment with AqB011 and bacopaside II. SW480 cells were insensitive to block by AqB011 or bacopaside II alone. AqB011 (20 µM) and bacopaside II (15 µM) combined treatment yielded block that was significantly greater than vehicle (\*\*\*\*), AqB011 (20 µM) alone (####), or bacopaside II (15 µM) alone (++++).

**Effects of bacopaside II and AqB011 on lamellipodial formation.** Cell migration typically involves the formation of membrane protrusions such as actin-rich lamellipodia, which extend in the direction of locomotion and provide a base on which cells move forward<sup>12,47</sup>. A loss of lamellipodial structures has been associated

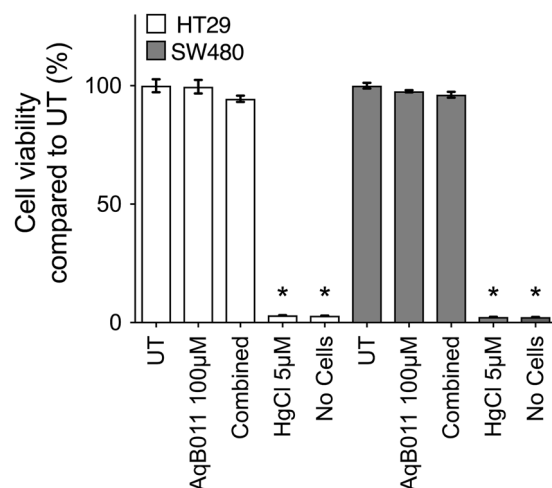


**Figure 4.** Summary histogram of the effects of pharmacological treatments on viability measured by alamarBlue assay for HT29 and SW480 cells. ‘Combined’ indicated cotreatment with AqB011 (20 µM) and bacopaside II (15 µM). Mercuric chloride served as a positive control for cell death; ‘no-cell’ controls confirmed minimal background fluorescence. All treatments were  $n = 4$ . Data were standardized to results for untreated (UT) cells.

with reduced rates of migration<sup>48</sup>. Images of representative cells illustrate the differential effects seen with single and combined inhibitor treatments in HT29 (Fig. 9A) and SW480 (Fig. 9B) cells. Vehicle-treated control groups in both cell were characterized by a high proportion of cells with membrane protrusions. Most HT29 control cells had flat sheet-like protrusions or bipolar wing-like processes. Most SW480 control cells had a primary lamellipodium that was slender, long, and ramified into a flattened lobed protrusion at the distal end.

In all treatments (bacopaside II and AqB011, alone and combined), HT29 lamellipodia were reduced in length as compared to vehicle-treated cells (Fig. 9A), and in frequency, seen as a smaller proportion of the cell population that showed processes. In contrast, SW480 lamellipodial extensions appeared to be unaffected by AqB011. However SW480 extensions were reduced in size and number in treatments with bacopaside II alone, or combined agents (Fig. 9B).

To quantify morphological data objectively, a score for ‘cell complexity’ was developed. Computer-based analyses were used to transform single cell images into skeletonized segments connected in branchworks to represent the morphological structures including cellular processes. Scores for cell complexity were calculated as the summed lengths of segments per cell (Fig. 9C,D). Simple circular cells were captured by a single line across the diameter, giving a low score. Complex cells with multiple or branched processes required a branchwork of skeletonized segments, giving a higher score. Scores in Arbitrary Units (AU) are based on the number of pixels. In HT29, cell complexity scores were significantly lower in all treatment groups, with AqB011 (mean  $58 \pm 3$  AU), bacopaside II ( $51 \pm 4$ ), or combined ( $43 \pm 6$ ), as compared to vehicle control ( $98 \pm 10$ ). In SW480, cell complexity scores in AqB011 ( $129 \pm 15$ ) were not significantly different from vehicle control, but were reduced in bacopaside II ( $86 \pm 7$ ) and combined groups ( $79 \pm 6$ ), as compared to vehicle ( $150 \pm 18$ ). In summary, AqB011 reduced cell complexity scores in HT29 but not SW480 cells; bacopaside II reduced cell complexity scores for both cell lines; and combined treatment reduced complexity scores for both cell lines. The treatments which compromised lamellipodial structures were consistent with the loss of directional movement measured by net displacement (Fig. 8).

**AqB011, but not bacopaside II, inhibits colon cancer cell invasiveness.** In cancer metastasis, cells move in three dimensional space across tissue boundaries and through extracellular matrix (ECM), involving attributes that are not fully captured in two-dimensional wound closure models. The effects of AQP1 inhibitors were tested on transwell invasion through an ECM layer on a semi-permeable filter towards a chemoattractant (FBS), quantified by staining and counting migrated cells at set times (Fig. 10).

Treatment with AqB011 alone resulted in approximately 40% reduction of HT29 cell invasiveness at concentrations  $\geq 10$  µM (Fig. 10A; row 1). The highest dose of AqB011 (80 µM) also impaired SW480 cell invasiveness; lower doses had no significant effect (Fig. 10B; row 1). Unexpectedly, higher doses of bacopaside II alone potentiated invasiveness in both cell lines (row 2), increasing transwell movement by 2.7 fold in HT29 cells, and 4.5 fold in SW480 cells. Bacopaside II potentiation in HT29 cells was reversed in full by co-application of AqB011 (Fig. 10A, row 3), and partially reversed in SW480 (Fig. 10B, row 3). Transwell invasion required the presence of a chemotactic gradient (FBS), and an ECM gel layer (Fig. 10D). Even though the average surface migration velocity was slower for HT29 cells (Fig. 8E), their capacity for invasion ( $269 \pm 16$  cells per field of view;  $n = 15$ ) was significantly greater than SW480 ( $90 \pm 8$  cells per field of view;  $n = 15$ ) (Fig. 10E).

This work is the first to show the anti-invasive effects of AQP1 ion channel blocker AqB011 in colon cancer cells, suggesting a novel role for AQP1 ion conductance in facilitating cancer invasion. HT29 was more sensitive to the inhibitory effect of AqB011 than SW480, consistent with observations from 2D assays. In contrast, bacopaside II surprisingly enhanced cancer cell invasion in both cell lines, suggesting this agent is likely

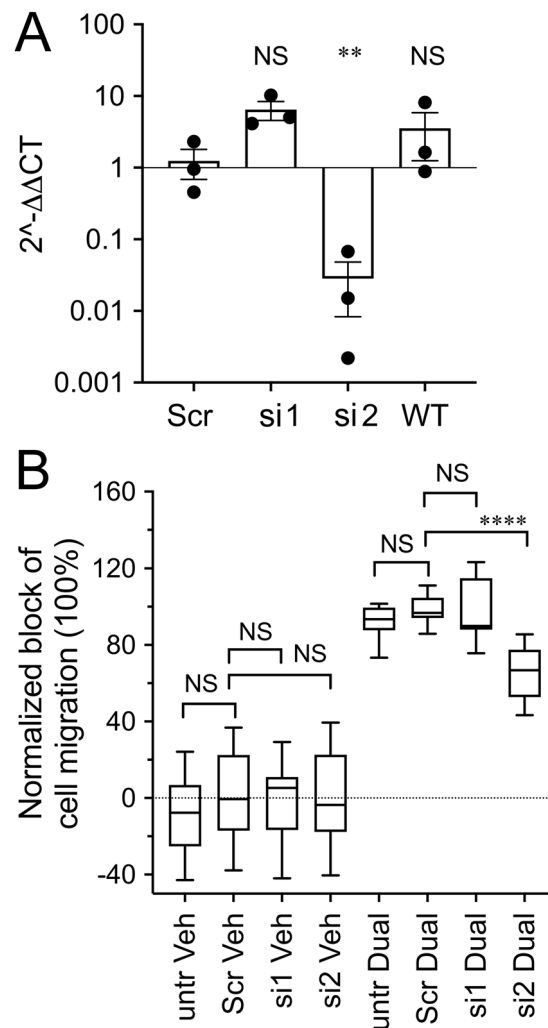


**Figure 5.** Effects of siRNA knockdown of AQP1 on the pharmacological sensitivity of HT29 cell migration to block by the combined inhibitors AqB011 and bacopaside II. **(A)** AQP1 siRNA2 (si2) but not siRNA1 (si1) significantly decreased AQP1 mRNA levels, as compared with scrambled control siRNA (Scr) and untreated (WT) in HT29 cells ( $n = 3$  per group). **(B)** Box plot showing the decreased sensitivity of HT29 cell migration to pharmacological block after siRNA knockdown of AQP1. Values for HT29 wound closure at 24 h were standardized as a percentage of the scrambled control treated with combined inhibitors (Scr Dual; 100%), specifically to illustrate the differences in pharmacological effectiveness of the combined agents in siRNA1, siRNA2, and untreated. The effectiveness of the combined inhibitors was significantly impaired only in the siRNA2-transfected group (si2 Dual). siRNA1 (si1 Dual), scrambled (Scr Dual) and non-transfected (untr Dual) groups showed no loss of sensitivity to the combined inhibitors ( $n = 14$  per group).

to have multiple targets of action, and that its side effects are mediated at least in part at a level upstream of AQP1-dependent signalling.

## Discussion

Cell migration and invasion are key pathological processes in cancer metastasis. Upregulation of AQP1 expression has been shown to enhance cell migration and metastasis in certain subtypes of cancers<sup>13–15</sup>. In other types of cancers, AQP3, AQP4, or AQP5 are increased in expression and influence viability, proliferation and migration<sup>12,49–52</sup>. Process formation during migration is thought to be driven by reversible assembly of actin filaments<sup>53–55</sup>, and local cell volume increases facilitated by water and ion fluxes<sup>31,56,57</sup>. To achieve a paired water and ion flux at the membrane leading edges, classes of AQPs that are upregulated in cancers would in theory be dual water and ion channels themselves, or water channels that can be co-localized with ion transporters or channels. AQP1-mediated water influx at leading edges, leading to local volume changes associated with process extension and cell movement<sup>31</sup>, enhances cancer cell motility and invasion. In glioma cells AQP4 colocalizes with the chloride channel (ClC2) and the potassium-chloride co-transporter 1 (KCC1), which could provide a driving force for water efflux leading to cell shrinkage, augmenting invasiveness<sup>58,59</sup>. AQP5 is not known to have an ion channel function<sup>21</sup>, but can colocalize with ion channels or transporters such as the Na<sup>+</sup>/H<sup>+</sup> exchanger in breast cancer cells<sup>56</sup>.

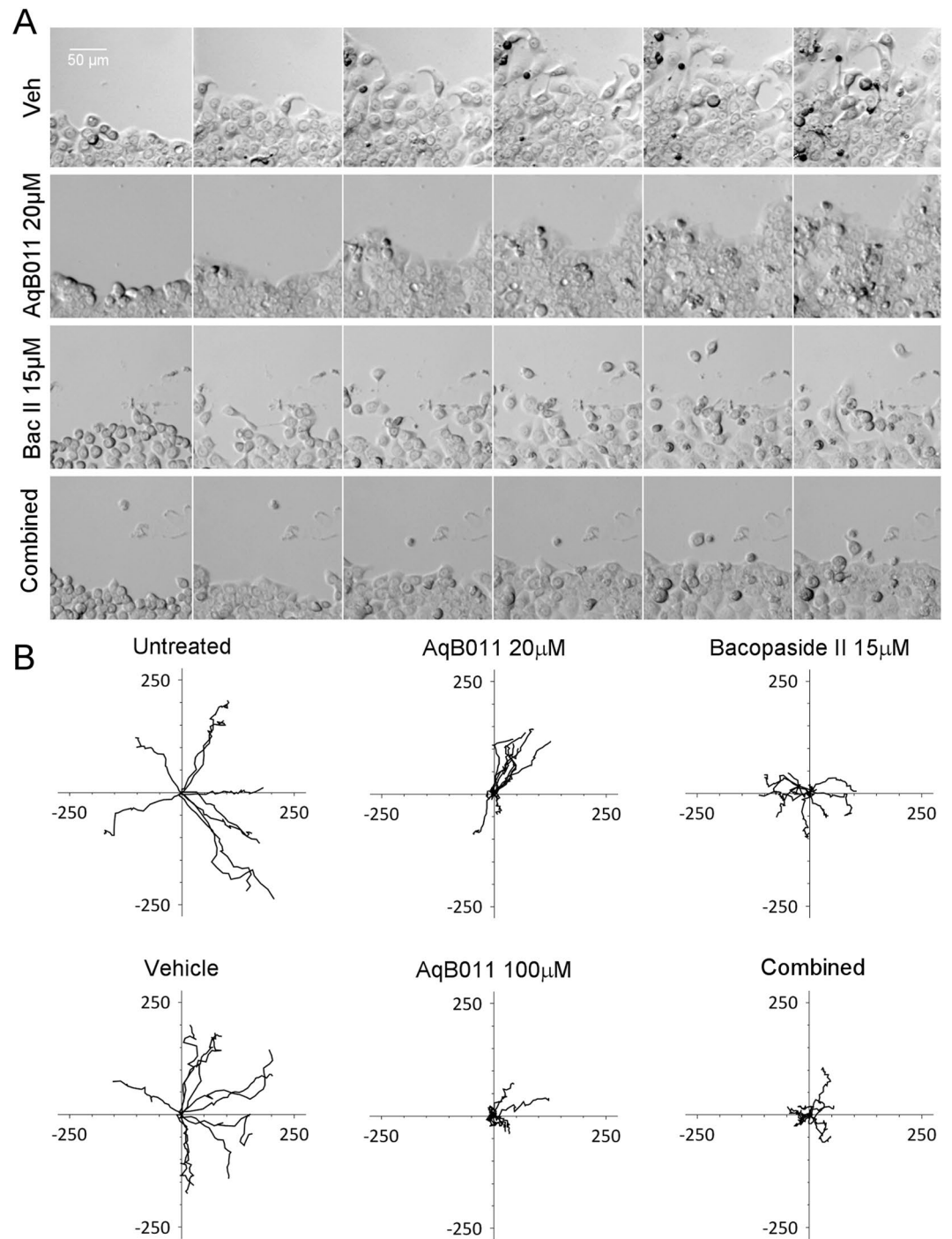


**Figure 6.** Live cell imaging of HT29 cells and plots of migration trajectories in treatments with bacopaside II and AqB011 alone, and in combination. Single cells at the boundaries of circular wounds were tracked with time-lapse images taken at 30 minute intervals for 24 hours at 37°C. **(A)** Panels of six images each from time-lapse series are shown at 4-hour intervals, for treatments with vehicle, AqB011 (20 µM), bacopaside II (15 µM), and combined AqB011 and bacopaside II. **(B)** Trajectory plots of individual cells (n = 9–11 per treatment group), monitored by the position of the cell nucleus at 60 minute intervals over 24 hours. Movement was referenced to the starting position set as 0,0 on graph axes; X and Y units are µm.

Results here showed that efficacy of AqB011 in impairing motility required the plasma membrane localization of AQP1 in the cancer cells. The block of migration by combined treatment with AqB011 and bacopaside II was significantly reduced following knockdown of AQP1 via siRNA transfection in HT29 cells. These data showed that the effectiveness of the blockers AqB011 and bacopaside II correlated with the levels of AQP1 expression in the membrane. AqB011 was not effective in blocking cell migration and invasion in SW480 as compared to HT29, an effect consistent with the low membrane levels of AQP1 measured in SW480. The fast rate of two dimensional

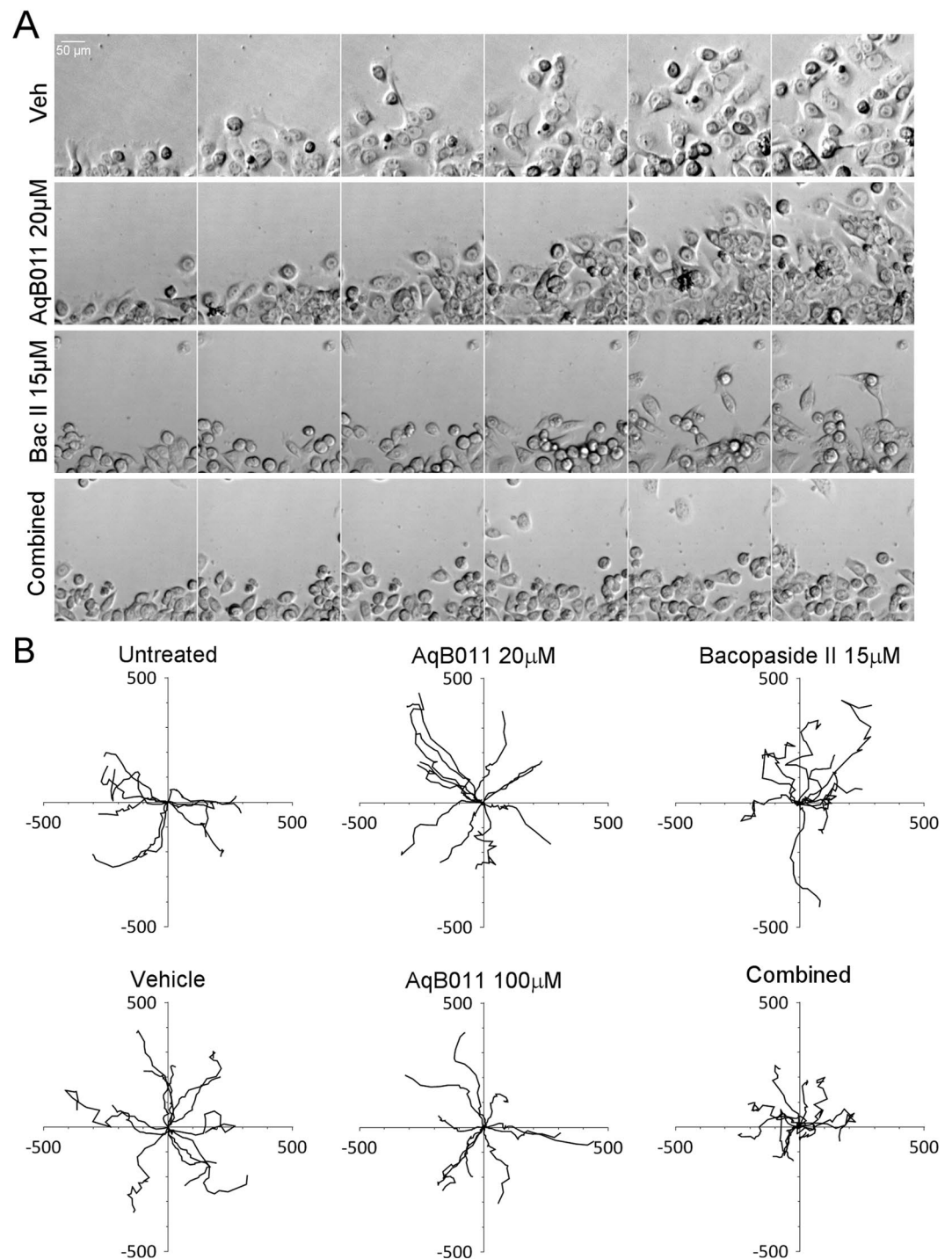


**Figure 7.** Live cell imaging of SW480 cells and plots of migration trajectories in treatments with bacopaside II and AqB011 alone, and in combination. Single cells at the boundaries of circular wounds were tracked with time-lapse images taken at 30-minute intervals for 24 hours at 37 °C. **(A)** Panels of six images each from time-lapse series are shown at 4-hour intervals, for vehicle, AqB011 (20 µM), bacopaside II (15 µM), and combined (Combined) treatment groups. **(B)** Trajectory plots of individual cells ( $n = 10-12$ ) per treatment group, monitored by the position of the cell nucleus at 60 minute intervals over 24 hours; X and Y values are in µm.

migration in the low-AQP1-expressing SW480 cells suggested alternative mechanisms can drive fast movement, but interestingly the high surface velocity did not translate into an increased invasive potential across extracellular matrix. The higher invasive potential correlated with the high-AQP1-expressing HT29 cells. In both cell lines, combined block of the AQP1 ion channel and water pores was more potent in impairing motility across colon cancer types than single agents alone. The combined agents were able to restrain migration in the SW480 line, which escaped control by either single agent alone. The ability of SW480 cells to show normal wound closure with



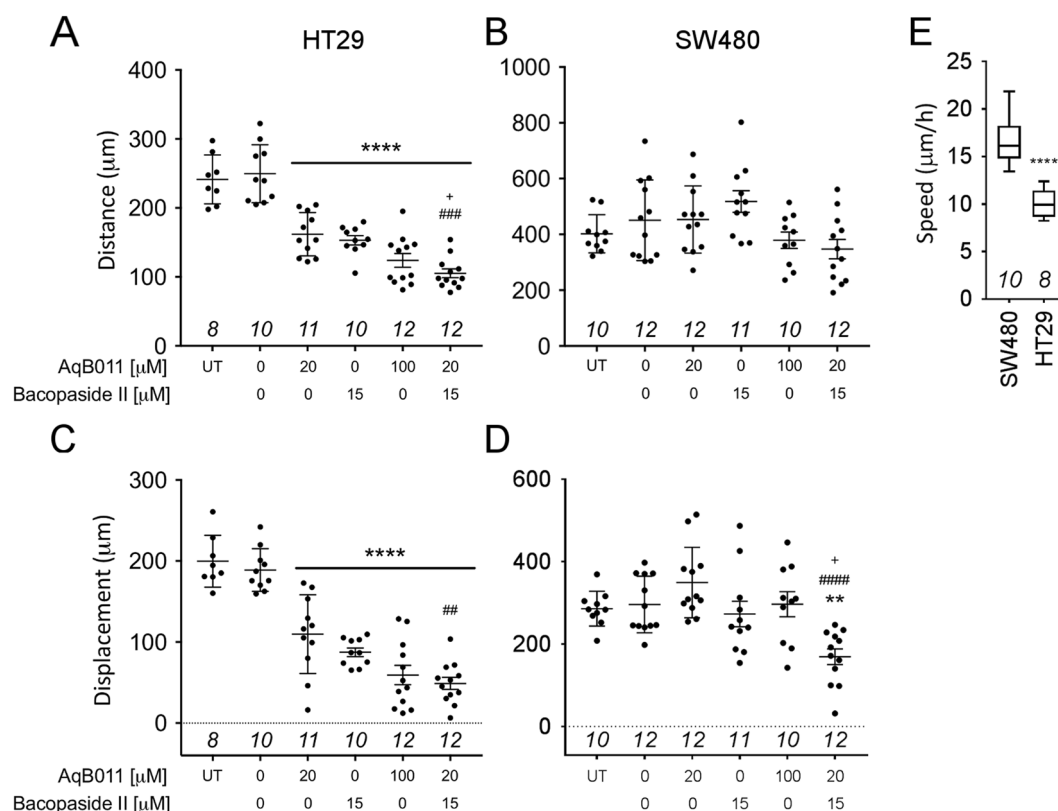


**Figure 8.** Summary plots of total distances travelled and net displacement of HT29 and SW480 cells in each treatment group, measured by live cell imaging. **(A)** 20 µM AqB011 or 15 µM bacopaside II treatments alone significantly reduced the total distance migrated by HT29 cells as compared to vehicle-treated (0 AqB011, 0 Bacopaside II). The level of inhibition was significantly enhanced in the combined treatment as compared with either agent alone (###). **(B)** No significant block of SW480 total distance was seen in any treatment as compared with vehicle. **(C)** Net displacement in HT29 cells was reduced by all treatments as compared to vehicle. Combined treatment showed a significantly greater block of HT29 net displacement than either treatment alone (##). **(D)** Only the combined treatment reduced SW480 net displacement as compared to vehicle, or as compared to either treatment alone (####). **(E)** SW480 mean migration velocity was significantly greater than that of HT29. Distance and displacement measures for untreated (UT) showed no significant differences from vehicle-treated in all panels (A–D; symbols not shown). *n*-values in italics are above the x-axis.

AqB011 or bacopaside II suggested these blockers did not act by causing non-specific disruption of cell membrane transport, metabolism, cytoskeletal structure, or other essential processes.

SW480 cells showed uniformly fast two-dimensional migration rates minimally affected by AqB011, suggesting that this class of cells achieves rapid migration via mechanisms largely independent of AQP1. The small amount of AQP1 that was seen in the SW480 plasma membrane might contribute to parallel roles such as steering, as needed to maintain a consistent direction of movement, or other functions. Low levels of AQP1 in the SW480 plasma membrane might contribute in small part to the enhanced cell motility. Contributions of other classes of AQPs remain to be explored; for example, SW480 cells express high levels of AQP5<sup>60–62</sup>. The role of the intracellular pool of AQP1 in SW480 cells remains to be defined. For example, in rat cholangiocytes, secretin stimulates translocation of AQP1 from vesicles to the plasma membrane and increases osmotic water permeability, an effect blocked by mercuric chloride<sup>63</sup>. Future work might identify signals that induce trafficking of intracellular AQP1 to the membrane, and alter motility in cancer lines.

Two-dimensional migration and three-dimensional invasiveness rely on different mechanisms. Surprisingly, bacopaside II alone strongly increased the invasiveness of both HT29 and SW480 cell lines, contradicting expectations based on wound closure assays. AqB011 fully reversed the pro-invasive effects of bacopaside II in HT29 cells, and partially reversed the enhanced invasion in SW480, in a pattern that was consistent with the levels of AQP1 membrane localization. Bacopaside II is a chemically complex molecule with a triterpene backbone<sup>64</sup>, unlikely to be selective for AQPs alone. Based on docking modelling<sup>40</sup>, the terpene is not involved in the AQP1 water pore block, which is mediated by the bacopaside sugar groups. Improved compounds in the future might use a trimmed version of the compound carrying the specific AQP1 channel blocking moiety. Terpenes increase the overall fluidity in phospholipid bilayers such as in parasites and mammalian cells<sup>65–67</sup>. Increased membrane fluidity correlates with augmented cancer invasiveness<sup>68</sup>, and invasive capacity of cancer cells can be suppressed by pharmacological reduction of membrane fluidity<sup>69</sup>. Unexpected effects of bacopaside on invasiveness reported here might be due to the membrane-fluidizing effects of the terpene component; this mechanism remains to be

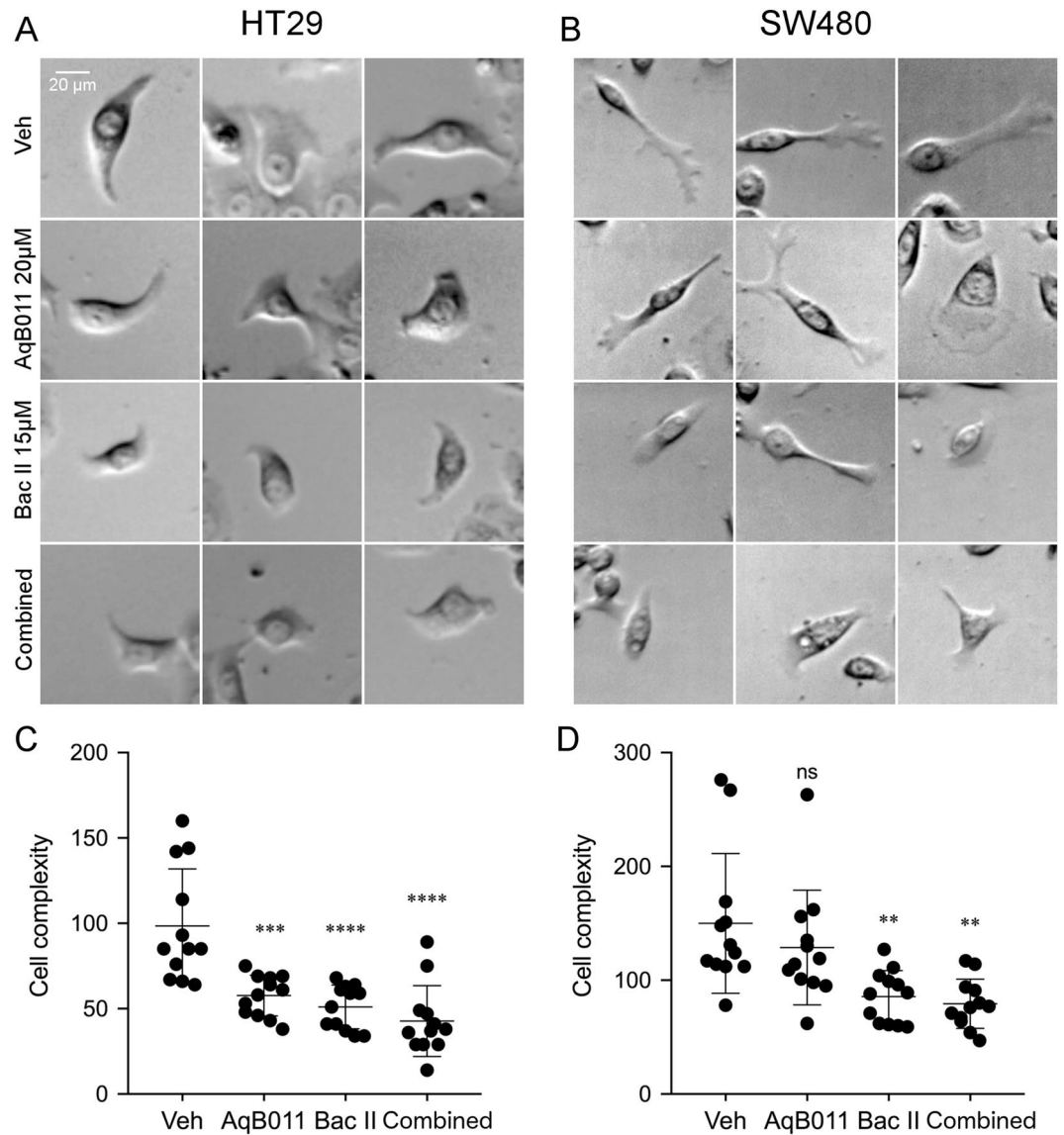


**Figure 9.** Images of actively migrating HT29 and SW480 cells in different treatment groups, showing three representative examples each. Vehicle-treated HT29 (A) and SW480 (B) cells (top row) showed distinct membrane protrusions. AqB011 and bacopaside II reduced protrusion sizes of HT29 cells as compared to vehicle in all treatment groups (A; rows 2–4). For SW480 cells, cellular protrusions appeared smaller in bacopaside II (B; rows 3 and 4) but not changed by AqB011 (B; row 2). “Cell complexity” values were quantified as the summed lengths of skeletonized morphological structures for individual cells (see Methods for details) located at wound frontier positions for HT29 (C) and SW480 (D) cells (n = 12 per group). (C) HT29 cells treated with 10 µM AqB011 (AqB011), 15 µM bacopaside II (Bac II) or combined treatment (Combined) showed significant decrease in cell complexity compared with vehicle control (Veh). (D) In SW480 cells, bacopaside II and combined treatment decreased cell complexity as compared with vehicle control (Veh), but AqB011 had no appreciable effect.

tested. However, bacopaside II appeared to reduce cell size and promote separation of individual cells from adjacent cells, suggesting a boost in invasiveness also might come from reduced cell-to-cell adhesion and decreased cell volumes, which could facilitate movement through narrow passages. The chemotactic gradient imposed by serum might restore the capacity for directional movement which appeared to be lost following bacopaside II treatment. At high doses bacopaside II is cytotoxic; at non-toxic doses it inhibits colon cancer growth by inducing cell cycle arrest, apoptosis<sup>45</sup>, and reducing angiogenesis<sup>70</sup>. Thus, bacopaside II and its metabolites *in vivo* are likely to affect a diverse array of processes, which could account for some of the observed effects on cell migration and invasion, as well as its beneficial effects as a traditional medicinal herb in a variety of applications<sup>71,72</sup>.

Results here are the first to show that AQP1 ion channel blocker AqB011 reduces colon cancer cell invasiveness *in vitro*, and to show that sensitivity to this agent depends on AQP1 localization in the plasma membrane. In summary, AQP1 water fluxes and ion conductance appear to exhibit a coordinated role in facilitating cell migration in AQP1-dependent cancer cell lines. Combined pharmacological block of both the AQP1 water and

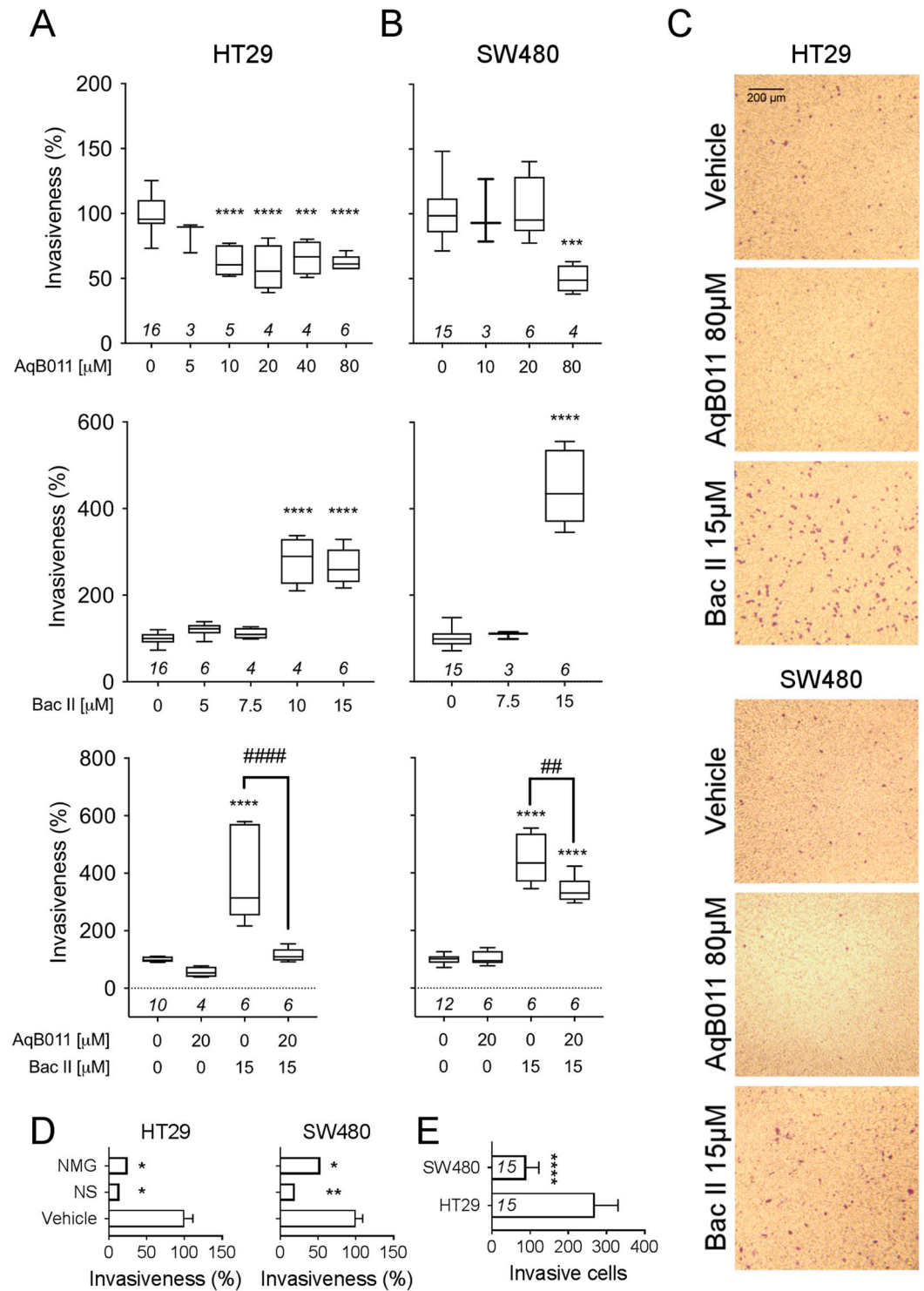


**Figure 10.** Transwell invasiveness of HT29 and SW480 cells in treatments with bacopaside II, AqB011, and combined agents. Box plots depicting cell invasiveness at 24 hours for HT29 (A) and SW480 (B) cells treated with AqB011 (row 1), bacopaside II (row 2), or both (row 3). (A) HT29 cell invasiveness was inhibited by AqB011 (10 to 80 µM). In contrast, bacopaside II (10 and 15 µM) potentiated HT29 invasiveness. Combined treatment blocked invasiveness, overriding the potentiation effect. (B) SW480 cell invasiveness was inhibited by AqB011 only at the highest dose tested (80 µM), and potentiated by bacopaside II (15 µM). Combined treatment partially counteracted the potentiation effect. (C) Images of HT29 and SW480 show cells that successfully crossed the ECM-like layer to reach the trans-side of the chamber in treatments with vehicle, AqB011 80 µM, or bacopaside II 15 µM. (D) Histograms showing the reduced invasiveness of HT29 and SW480 cells in the absence of ECM (no matrix gel; NMG), or in the absence of a serum gradient (no serum; NS), as compared with vehicle controls (vehicle) having both a serum gradient and ECM. (E) Untreated HT29 cells were significantly more invasive than SW480 cells. *n*-values are shown in italics above the y-axis (or in panel E, within the histogram bars).

ion channels in HT29 and SW480 colon cancer cells amplified the inhibition of 2D cell migration, as compared with effects of either inhibitor alone. The prospect of a cooperative role between the AQP1 water flux and ion conductance is promising, in that lower doses of two compounds when combined could produce a beneficial level of cell migration impairment. Combined AQP1 inhibitors could act on target cells (such as migrating cancers) that require both the AQP1 water and ion channel activities, while minimizing side effects on other cells and tissues by being applied at lower concentrations. Future work is needed to explore effects of AQP1 inhibitors on other cancer cell types, to optimize bacopaside-related compounds for modulating AQP1 water flow, and to test the effectiveness of AQP1 agents in restraining metastasis *in vivo*.

## Methods

**Cell lines.** Human colorectal adenocarcinoma cell lines HT29 (ATCC HTB-38TM) and SW480 (ATCC CCL-228TM) were cultured in T-75 plates in Dulbecco's Modified Eagle Medium (DMEM; Life Technologies, Grand Island, NY, USA) supplemented with 10% fetal bovine serum (FBS; Life Technologies), 1% Gibco GlutaMAX (Life Technologies) and 100 units/ml each of penicillin and streptomycin (Life Technologies). Cell cultures were grown at 37 °C in a humidified 5% CO<sub>2</sub> incubator.

**Quantitative PCR analysis of AQP1 expression.** Cells plated in triplicate wells at  $4 \times 10^5$  cells/well were incubated at 37 °C in a humidified 5% CO<sub>2</sub> incubator overnight. Total RNA was extracted using PureLink™ RNA Mini Kit (Invitrogen™); 1 µg total RNA was used for cDNA synthesis. cDNA was synthesized using QuantiTect® Reverse Transcription Kit (Qiagen®). cDNA was quantified using NanoDrop™ (Life Technologies); 50 ng cDNA was used in the polymerase chain reaction. Real-time qRT-PCR analyses were performed using SYBR™ Green PCR Master Mix (Applied Biosystems™) in a final volume of 10 µl with StepOne Plus™ Real-Time PCR system (Applied Biosystems™). Data were analysed by StepOne Plus™ Real-Time PCR software v2.3. The primer sequences for AQP1 were forward: 5'-CGCAGAGTGTGGGCCACATCA-3', and reverse: 5'-CCCGAGTTCACACCATCAGCC-3', amplifying a product of 217 bp. *RPS13* was used as a standard and target mRNA levels relative to *RPS13* were calculated using the formula  $2^{-\Delta\text{CT}^{73}}$ .

**Immunofluorescence.** Cells were seeded 2–3 days prior to cell fixation on 8-well uncoated Ibidi® µ-Slides (Ibidi, Munich, Germany) at a density of  $5 \times 10^4$  cells/well. Once 80% confluent, cells were stained with MemBrite™ Fix Cell Surface Staining Kit (Biotium, Fremont, CA, USA; cat # 30093), and purchased from Gene Target Solutions (Dural, NSW, Australia). Membrane staining was performed prior to cell fixation, as per manufacturer's instructions. Cells were fixed with 1:1 (v/v) acetone and methanol at –20 °C and incubated for 15 min at room temperature. Immunofluorescence staining was conducted as previously described by Wardill *et al.*<sup>74</sup>. The AQP1 primary antibody used for immunofluorescence was H-55 rabbit polyclonal (Santa Cruz Biotechnology, Dallas, TX, USA). The secondary antibody was Goat anti-Rabbit IgG (H + L) Cross-Adsorbed Secondary Antibody, Alexa Fluor 568 (Life Technologies; cat# A-11011). For nuclear staining, cells were incubated for 10 minutes at room temperature in a 1:1000 dilution of Hoechst 33258 (cat # 861405; Sigma-Aldrich, St. Louis, MO). The µ-Slide was imaged using an Olympus FV3000 Confocal Microscope. For the signal emitted by Hoechst 33258, excitation (Ex = 405 nm) and emission (Em = 461 nm) settings were used. For Alexa Fluor 568, settings were Ex = 561 nm and Em = 603 nm. For MemBrite™, settings were Ex = 488 nm and Em = 513 nm. Fiji (ImageJ) software (U.S. National Institutes of Health) was used to measure relative intensities of AQP1 signal standardized to membrane marker signal as a function of cross-sectional distance per cell as previously described<sup>75</sup>.

**AQP1 Inhibitors.** The bumetanide derivative AqB011 (*A*quaporin ligand; *B*umetanide derivative; number *11* in a series) was synthesized by Dr Gary A. Flynn (SpaceFill Discovery LLC, West Yellowstone, MT, USA)<sup>34</sup>. Powdered AqB011 was dissolved in dimethyl sulfoxide (DMSO) to create 1000x stock solutions and diluted in culture medium to final concentrations for testing in the circular wound closure<sup>76</sup>, transwell invasion, live cell imaging, and alamarBlue assays. Bacopaside II was purchased from Sigma-Aldrich (St. Louis, MO), solubilized in methanol to yield 100x stock solutions, and stored at –20 °C in an airtight vial to minimize evaporation. For experimental use, bacopaside II stocks were diluted at 1/100 in culture medium. A combination of DMSO (1 µL/ml) and methanol (10 µL/ml) in culture medium was used as the vehicle control.

**Circular wound closure assay.** Circular wound closure assays were performed using methods described by De Ieso and Pei<sup>76,77</sup>. In brief, cells were plated at  $1 \times 10^5$  cells/mL in DMEM culture medium with GlutaMAX and antibiotics (as above), reduced serum (2% FBS), and 400 nM of the mitotic inhibitor 5-fluoro-2'-deoxyuridine (FUDR). A confluent monolayer was achieved at 2–3 days following plating; circular wounds were created with a sterile p10 pipette tip. After washing two to three times with phosphate-buffered saline to remove cell debris, media were applied with and without AQP inhibitors or vehicle in low serum (2% FBS) DMEM with FUDR for the wound closure assay. Complete wounds were imaged at 10x magnification with a Canon 6D camera on a Nikon inverted microscope. Images were standardized using XnConvert software, and wound areas were quantified using Fiji software (ImageJ; version 1.51 h; U.S. National Institutes of Health). Closure was calculated as a percentage of the initial wound area for the same well as a function of time. All experiments were repeated in duplicate wells.

**Cytotoxicity assay.** Cell viability was quantified using an alamarBlue assay<sup>78</sup>, following manufacturer's guidelines (Life Technologies). Cells were plated at  $10^5$  cells/mL in 96-well plates, in the same FUDR-containing low serum culture media as used in the migration assays. At 12–18 hours after plating, treatments were applied, and cells were incubated 24 hours. At 24 hours, cells were treated with 10% alamarBlue solution for 1–2 hours. Fluorescence signal levels were measured with a FLUOstar Optima microplate reader for control and treatment

groups. Mercuric chloride (HgCl<sub>2</sub>) served as a positive control for inducing cytotoxic cell death, and a no-cell control was included to confirm low background fluorescence.

**Small interfering RNA transfection.** The experiment was performed using a similar method as previously published<sup>79</sup>. Prior to transfection, HT29 cells were grown to 30% confluence in DMEM medium with 10% FBS. DharmaFECT 1 transfection reagent (T-2001-01; Dharmacon) was used to transfect Ambion Silencer Select AQP1 siRNA (siRNA1; 4390824; Life Technologies), Dharmacon ON-TARGETplus AQP1 siRNA (siRNA2; J-021494-05-0002; Dharmacon), and scrambled siRNA (4390843; Life Technologies). Each siRNA was administered at a concentration of 50 nM. Cells were incubated in 5% CO<sub>2</sub> at 37°C for 48 hours prior to wound closure assay and quantitative reverse-transcription polymerase chain reaction (RT-PCR) analyses.

**Live cell imaging.** Cells were seeded on eight-well uncoated Ibidi  $\mu$ -Slides (Ibidi) at a density of  $1 \times 10^5$  cells/mL. A confluent monolayer was achieved 2–3 days after plating. Cells were conditioned in low serum culture medium (2% FBS) in the presence of FUDR (400 nM) for 12–18 hours before wounding. Three circular wounds were created in each well using techniques described above for the wound closure assays. Slides were mounted on a Nikon Ti E Live Cell Microscope (Nikon, Tokyo, Japan) in an enclosed humidified chamber kept at 37°C with 5% CO<sub>2</sub>. Images were taken at 30-minute intervals for 24 hours, using Nikon NIS-Elements software. AVI files were exported from NIS-Elements and converted into TIFF files using Fiji (ImageJ). Converted files were analyzed using Fiji software<sup>80</sup> with the Manual Tracking plug-in. Total distance per cell was calculated as the cumulative distance travelled over the full duration of the experiment. Displacement was calculated as the net distance travelled between the first and last time points.

**Quantification of cell morphology.** Images generated from the circular wound closure assay at the 24 hour time point were processed using FIJI. Images were first converted into binary file (Process > Binary > Make Binary) and then skeletonized (Process > Binary > Skeletonize). Individual cells were randomly chosen for analysis from the leading edge of the wound. The total skeleton length of an individual cell was measured (Analyze > Measure) and classified as cell “complexity”.

**Transwell invasion assay.** Assays were performed using 6.5 mm Corning® Transwell® polycarbonate membrane cell culture inserts with 8  $\mu$ m pore size (cat #3422; Sigma-Aldrich, St. Louis, MO), as previously described<sup>81</sup>. The upper surface of the filter was coated with 40  $\mu$ L of water-diluted extracellular matrix (ECM) gel from Engelbreth-Holm-Swarm murine sarcoma (final concentration 25  $\mu$ g/mL; Sigma-Aldrich, St. Louis, MO), and left to dehydrate overnight, and rehydrated 2 hours prior to cell seeding with 50  $\mu$ L of serum-free DMEM per transwell insert. Cells were grown to approximately 40% confluence under normal conditions, and transferred into reduced serum (2% FBS) medium for 32–34 hours prior to seeding. Cells were harvested, resuspended in serum-free DMEM, and  $2.5 \times 10^5$  cells in 100  $\mu$ L was added to the upper chamber (total 150  $\mu$ L of cell suspension per transwell, including 50  $\mu$ L of rehydration medium added earlier). To the lower chamber, 600  $\mu$ L of pharmacological treatment in DMEM supplemented with 10% serum (chemoattractant) was added, and cells were incubated for 24 hours at 37°C in 5% CO<sub>2</sub>. Non-migrated cells were scraped from the upper surface of the membrane with a cotton swab; migrated cells remaining on the bottom surface were counted after staining with crystal violet<sup>82</sup>.

**Statistical analyses.** Statistical analyses performed with GraphPad Prism 7.02 software involved one-way ANOVA and post-hoc Bonferroni tests. Statistically significant outcomes are represented as (\*) $p < 0.05$ , (\*\*)  $p < 0.01$ , (\*\*\*) $p < 0.001$ , or (\*\*\*\*) $p < 0.0001$ ; NS is not significant; other characters indicating significance (# and +) use the same pattern for defining  $p$  values. All data are presented as mean  $\pm$  standard error of the mean (SEM);  $n$  values for independent samples are indicated in italics above the  $x$ -axes in histogram figures.

## Data Availability

All data generated or analysed during this study are included in this published article (and its Supplementary Information files).

## References

1. Ferlay, J. *et al.* (Lyon, France: International Agency for Research on Cancer, 2013).
2. Chaffer, C. L. & Weinberg, R. A. A perspective on cancer cell metastasis. *Science* **331**, 1559–1564 (2011).
3. Mehlen, P. & Puisieux, A. Metastasis: a question of life or death. *Nature Reviews Cancer* **6**, 449–458 (2006).
4. Yoshida, T. *et al.* Expression of aquaporin-1 is a poor prognostic factor for stage II and III colon cancer. *Molecular and clinical oncology* **1**, 953–958 (2013).
5. Kang, B. W. *et al.* Expression of aquaporin-1, aquaporin-3, and aquaporin-5 correlates with nodal metastasis in colon cancer. *Oncology* **88**, 369–376 (2015).
6. Ishibashi, K., Hara, S. & Kondo, S. Aquaporin water channels in mammals. *Clinical and experimental nephrology* **13**, 107–117 (2009).
7. Saadoun, S., Papadopoulos, M. C., Davies, D. C., Bell, B. A. & Krishna, S. Increased aquaporin 1 water channel expression in human brain tumours. *Br J Cancer* **87**, 621–623 (2002).
8. Moon, C. *et al.* Involvement of aquaporins in colorectal carcinogenesis. *Oncogene* **22**, 6699–6703 (2003).
9. Mazal, P. R., Susani, M., Wrba, F. & Haitel, A. Diagnostic significance of aquaporin-1 in liver tumors. *Hum Pathol* **36**, 1226–1231 (2005).
10. Hoque, M. O. *et al.* Aquaporin 1 is overexpressed in lung cancer and stimulates NIH-3T3 cell proliferation and anchorage-independent growth. *Am J Pathol* **168**, 1345–1353 (2006).
11. Guan, B., Zhu, D., Dong, Z. & Yang, Z. Expression and distribution of aquaporin 1 in laryngeal carcinoma. *Lin Chuang Er Bi Yan Hou Tou Jing Wai Ke Za Zhi* **21**, 269–272 (2007).

12. De Ieso, M. L. & Yool, A. J. Mechanisms of Aquaporin-Facilitated Cancer Invasion and Metastasis. *Frontiers in Chemistry* **6**, 135 (2018).
13. Saadoun, S., Papadopoulos, M. C., Hara-Chikuma, M. & Verkman, A. S. Impairment of angiogenesis and cell migration by targeted aquaporin-1 gene disruption. *Nature* **434**, 786–792 (2005).
14. Hu, J. & Verkman, A. S. Increased migration and metastatic potential of tumor cells expressing aquaporin water channels. *FASEB J* **20**, 1892–1894 (2006).
15. Jiang, Y. Aquaporin-1 activity of plasma membrane affects HT20 colon cancer cell migration. *IUBMB Life* **61**, 1001–1009 (2009).
16. Papadopoulos, M., Saadoun, S. & Verkman, A. Aquaporins and cell migration. *Pflug Arch Eur J Phy* **456**, 693–700 (2008).
17. McCoy, E. & Sontheimer, H. Expression and function of water channels (aquaporins) in migrating malignant astrocytes. *Glia* **55**, 1034–1043 (2007).
18. Yool, A. J. & Campbell, E. M. Structure, function and translational relevance of aquaporin dual water and ion channels. *Mol Aspects Med* **33**, 443–561 (2012).
19. Yu, J., Yool, A. J., Schulten, K. & Tajkhorshid, E. Mechanism of gating and ion conductivity of a possible tetrameric pore in aquaporin-1. *Structure* **14**, 1411–1423 (2006).
20. Sui, H., Han, B.-G., Lee, J. K., Walian, P. & Jap, B. K. Structural basis of water-specific transport through the AQP1 water channel. *Nature* **414**, 872–878 (2001).
21. Anthony, T. L. *et al.* Cloned human aquaporin-1 is a cyclic GMP-gated ion channel. *Mol Pharmacol* **57**, 576–588 (2000).
22. Boassa, D. & Yool, A. J. Single amino acids in the carboxyl terminal domain of aquaporin-1 contribute to cGMP-dependent ion channel activation. *BMC Physiol* **3**, 12 (2003).
23. Zhang, W. *et al.* Aquaporin-1 channel function is positively regulated by protein kinase C. *J Biol Chem* **282**, 20933–20940 (2007).
24. Kourghi, M., De Ieso, M. L., Nourmohammadi, S., Pei, J. V. & Yool, A. J. Identification of loop D domain amino acids in the human Aquaporin-1 channel involved in activation of the ionic conductance and inhibition by AqB011. *Frontiers in chemistry* **6**, 142 (2018).
25. Saparov, S. M., Kozono, D., Rothe, U., Agre, P. & Pohl, P. Water and ion permeation of aquaporin-1 in planar lipid bilayers. Major differences in structural determinants and stoichiometry. *J Biol Chem* **276**, 31515–31520 (2001).
26. Tsunoda, S. P., Wiesner, B., Lorenz, D., Rosenthal, W. & Pohl, P. Aquaporin-1, nothing but a water channel. *J Biol Chem* **279**, 11364–11367 (2004).
27. Campbell, E. M., Birdsell, D. N. & Yool, A. J. The activity of human aquaporin 1 as a cGMP-gated cation channel is regulated by tyrosine phosphorylation in the carboxyl-terminal domain. *Mol Pharmacol* **81**, 97–105 (2012).
28. Yool, A. J. & Weinstein, A. M. New roles for old holes: Ion channel function in aquaporin-1. *News Physiological Sciences* **17**, 68–72 (2002).
29. Yool, A. J., Brokl, O. H., Pannabecker, T. L., Dantzer, W. H. & Stamer, W. D. Tetraethylammonium block of water flux in Aquaporin-1 channels expressed in kidney thin limbs of Henle's loop and a kidney-derived cell line. *BMC Physiol* **2**, 4 (2002).
30. Yool, A. J. *et al.* AqF026 is a pharmacologic agonist of the water channel aquaporin-1. *J Am Soc Nephrol* **24**, 1045–1052 (2013).
31. Schwab, A., Nechyporuk-Zloy, V., Fabian, A. & Stock, C. Cells move when ions and water flow. *Pflug Arch Eur J Phy* **453**, 421–432 (2007).
32. Boassa, D., Stamer, W. D. & Yool, A. J. Ion channel function of aquaporin-1 natively expressed in choroid plexus. *J Neurosci* **26**, 7811–7819 (2006).
33. Kourghi, M. *et al.* Divalent cations regulate the ion conductance properties of diverse classes of aquaporins. *International journal of molecular sciences* **18**, 2323 (2017).
34. Kourghi, M., Pei, J. V., De Ieso, M. L., Flynn, G. & Yool, A. J. Bumetanide Derivatives AqB007 and AqB011 Selectively Block the Aquaporin-1 Ion Channel Conductance and Slow Cancer Cell Migration. *Molecular pharmacology* **89**, 133–140 (2016).
35. Preston, G. M., Jung, J. S., Guggino, W. B. & Agre, P. The mercury-sensitive residue at cysteine 189 in the CHIP28 water channel. *J Biol Chem* **268**, 17–20 (1993).
36. Brooks, H. L., Regan, J. W. & Yool, A. J. Inhibition of aquaporin-1 water permeability by tetraethylammonium: involvement of the loop E pore region. *Mol Pharmacol* **57**, 1021–1026 (2000).
37. Detmers, F. J. *et al.* Quaternary ammonium compounds as water channel blockers. Specificity, potency, and site of action. *J Biol Chem* **281**, 14207–14214 (2006).
38. Niemietz, C. M. & Tyerman, S. D. New potent inhibitors of aquaporins: silver and gold compounds inhibit aquaporins of plant and human origin. *FEBS Lett* **531**, 443–447 (2002).
39. Migliati, E. *et al.* Inhibition of aquaporin-1 and aquaporin-4 water permeability by a derivative of the loop diuretic bumetanide acting at an internal pore-occluding binding site. *Mol Pharmacol* **76**, 105–112 (2009).
40. Pei, J. V. *et al.* Differential Inhibition of Water and Ion Channel Activities of Mammalian Aquaporin-1 by Two Structurally Related Bacopaside Compounds Derived from the Medicinal Plant *Bacopa monnieri*. *Mol Pharmacol* **90**, 496–507 (2016).
41. Klebe, S. *et al.* Blockade of aquaporin 1 inhibits proliferation, motility, and metastatic potential of mesothelioma *in vitro* but not in an *in vivo* model. *Disease markers* **2015** (2015).
42. Dorward, H. S. *et al.* Pharmacological blockade of aquaporin-1 water channel by AqB013 restricts migration and invasiveness of colon cancer cells and prevents endothelial tube formation *in vitro*. *Journal of Experimental & Clinical Cancer Research* **35**, 36 (2016).
43. Smith, E. *et al.* The Purified Extract from the Medicinal Plant *Bacopa monnieri*, Bacopaside II, Inhibits Growth of Colon Cancer Cells *In Vitro* by Inducing Cell Cycle Arrest and Apoptosis. *Cells* **7**, 81 (2018).
44. Monzani, E., Bazzotti, R., Perego, C. & La Porta, C. A. AQP1 is not only a water channel: it contributes to cell migration through Lin7/beta-catenin. *PLoS One* **4**, e6167 (2009).
45. Hayashi, S. *et al.* Involvement of aquaporin-1 in gastric epithelial cell migration during wound repair. *Biochem Biophys Res Commun* **386**, 483–487 (2009).
46. Wei, X. & Dong, J. Aquaporin 1 promotes the proliferation and migration of lung cancer cell *in vitro*. *Oncology reports* **34**, 1440–1448 (2015).
47. Cramer, L. P., Siebert, M. & Mitchison, T. J. Identification of novel graded polarity actin filament bundles in locomoting heart fibroblasts: implications for the generation of motile force. *The Journal of cell biology* **136**, 1287–1305 (1997).
48. Suraneni, P. *et al.* The Arp2/3 complex is required for lamellipodia extension and directional fibroblast cell migration. *The Journal of cell biology* **197**, 239–251 (2012).
49. Verkman, A. S. Knock-out models reveal new aquaporin functions. *Handb Exp Pharmacol*, 359–381 (2009).
50. Jung, H. J., Park, J.-Y., Jeon, H.-S. & Kwon, T.-H. Aquaporin-5: a marker protein for proliferation and migration of human breast cancer cells. *PLoS one* **6**, e28492 (2011).
51. Cao, X. C. *et al.* Aquaporin3 is required for FGF-2-induced migration of human breast cancers. *PLoS One* **8**, e56735 (2013).
52. Saadoun, S. *et al.* Involvement of aquaporin-4 in astroglial cell migration and glial scar formation. *Journal of cell science* **118**, 5691–5698 (2005).
53. Pollard, T. D. & Borisy, G. G. Cellular motility driven by assembly and disassembly of actin filaments. *Cell* **112**, 453–465 (2003).
54. Wang, Y.-L. Exchange of actin subunits at the leading edge of living fibroblasts: possible role of treadmilling. *The Journal of cell biology* **101**, 597–602 (1985).
55. Theriot, J. A. & Mitchison, T. J. Actin microfilament dynamics in locomoting cells. *Nature* **352**, 126–131 (1991).
56. Stroka, K. M. *et al.* Water permeation drives tumor cell migration in confined microenvironments. *Cell* **157**, 611–623 (2014).

57. Frede, J. *et al.* Ovarian cancer: Ion channel and aquaporin expression as novel targets of clinical potential. *Eur J Cancer* **49**, 2331–2344 (2013).
58. McCoy, E. S., Haas, B. R. & Sontheimer, H. Water permeability through aquaporin-4 is regulated by protein kinase C and becomes rate-limiting for glioma invasion. *Neuroscience* **168**, 971–981 (2010).
59. McFerrin, M. B. & Sontheimer, H. A role for ion channels in glioma cell invasion. *Neuron glia biology* **2**, 39–49 (2006).
60. Shan, T. *et al.* Impact of AQP-5 on the growth of colorectal cancer cells and the underlying mechanism. *International Journal of Clinical and Experimental Pathology* **11**, 58–67 (2018).
61. Shan, T., Cui, X., Li, W., Lin, W. & Li, Y. AQP5: a novel biomarker that predicts poor clinical outcome in colorectal cancer. *Oncology reports* **32**, 1564–1570 (2014).
62. Kang, S. K. *et al.* Role of human aquaporin 5 in colorectal carcinogenesis. *The American journal of pathology* **173**, 518–525 (2008).
63. Marinelli, R. A., Pham, L., Agre, P. & LaRusso, N. F. Secretin Promotes Osmotic Water Transport in Rat Cholangiocytes by Increasing Aquaporin-1 Water Channels in Plasma Membrane Evidence For a Secretin-Induced Vesicular Translocation of Aquaporin-1. *Journal of Biological Chemistry* **272**, 12984–12988 (1997).
64. Chakravarty, A. K. *et al.* Bacopaside I and II: two pseudogujubogenin glycosides from *Bacopa monniera*. *Phytochemistry* **58**, 553–556 (2001).
65. Mendanha, S. A., Moura, S. S., Anjos, J. L., Valadares, M. C. & Alonso, A. Toxicity of terpenes on fibroblast cells compared to their hemolytic potential and increase in erythrocyte membrane fluidity. *Toxicology in vitro* **27**, 323–329 (2013).
66. Mendanha, S. A. & Alonso, A. Effects of terpenes on fluidity and lipid extraction in phospholipid membranes. *Biophysical chemistry* **198**, 45–54 (2015).
67. Camargos, H. S. *et al.* Terpenes increase the lipid dynamics in the Leishmania plasma membrane at concentrations similar to their IC50 values. *PLoS One* **9**, e104429 (2014).
68. Zeisig, R., Koklič, T., Wiesner, B., Fichtner, I. & Sentjurč, M. Increase in fluidity in the membrane of MT3 breast cancer cells correlates with enhanced cell adhesion *in vitro* and increased lung metastasis in NOD/SCID mice. *Archives of biochemistry and biophysics* **459**, 98–106 (2007).
69. Zhao, W. *et al.* Candidate antimetastasis drugs suppress the metastatic capacity of breast cancer cells by reducing membrane fluidity. *Cancer research* **76**, 2037–2049 (2016).
70. Palethorpe, H. M. *et al.* The Aquaporin 1 Inhibitor Bacopaside II Reduces Endothelial Cell Migration and Tubulogenesis and Induces Apoptosis. *International journal of molecular sciences* **19**, 653 (2018).
71. Aguiar, S. & Borowski, T. Neuropharmacological review of the nootropic herb *Bacopa monnieri*. *Rejuvenation Res* **16**, 313–326 (2013).
72. Rohini, G. & Devi, C. S. *Bacopa monniera* extract induces apoptosis in murine sarcoma cells (S-180). *Phytother Res* **22**, 1595–1598 (2008).
73. Jacob, F. *et al.* Careful Selection of Reference Genes Is Required for Reliable Performance of RT-qPCR in Human Normal and Cancer Cell Lines. *Plos One* **8**, e59180 (2013).
74. Wardill, H. R. *et al.* A novel *in vitro* platform for the study of SN38-induced mucosal damage and the development of Toll-like receptor 4-targeted therapeutic options. *Experimental Biology and Medicine* **241**, 1386–1394 (2016).
75. Pei, J. V. *et al.* Lithium ‘Hot-spots’: Real-time Analysis of non-selective cation channel activity in migrating cancer cells. *Mol Pharmacol* (2019).
76. De Ieso, M. L. & Pei, J. V. An Accurate and Cost-Effective Alternative Method for Measuring Cell Migration with the Circular Wound Closure Assay. *Bioscience Reports* (2018).
77. Kam, Y., Guess, C., Estrada, L., Weidow, B. & Quaranta, V. A novel circular invasion assay mimics *in vivo* invasive behavior of cancer cell lines and distinguishes single-cell motility *in vitro*. *BMC cancer* **8**, 198 (2008).
78. Simpson, K. J. *et al.* Identification of genes that regulate epithelial cell migration using an siRNA screening approach. *Nature cell biology* **10**, 1027–1038 (2008).
79. Pei, J. V. *et al.* Development of a Photoswitchable Lithium-Sensitive Probe to Analyze Nonselective Cation Channel Activity in Migrating Cancer Cells. *Molecular Pharmacology* **95**, 573–583 (2019).
80. Schindelin, J. *et al.* Fiji: an open-source platform for biological-image analysis. *Nature methods* **9**, 676 (2012).
81. Nourmohammadi, S. *et al.* Effect of Compound Kushen Injection, a Natural Compound Mixture, and Its Identified Chemical Components on Migration and Invasion of Colon, Brain, and Breast Cancer Cell Lines. *Frontiers in Oncology* **9** (2019).
82. Shaw, L. M. Tumor cell invasion assays, In *Cell Migration* 97–105 (Springer, 2005).

## Acknowledgements

The authors thank Dr. Agatha Labrinidis and Dr. Jane Sibbons from Adelaide Microscopy for providing technical support with confocal microscopy and live cell imaging. Funding was provided by Australian Research Council (ARC) grant DP16112724, and scholarship support from the University of Adelaide; an Australian Postgraduate Award; The Florey Medical Research Foundation Jemima Lendrum Prize; and the Gerald Germer Honours Scholarship.

## Author Contributions

Experimental tools and methods (M.L.D., J.V.P., M.K., E.S., J.H., A.J.Y., S.N.). Research design (M.L.D., J.V.P., A.J.Y.). Data acquisition and analysis (M.L.D., J.V.P., S.N.). Interpretation of results (M.L.D., J.V.P., A.J.Y.). Preparation of manuscript text and figures (M.L.D., J.V.P., A.J.Y.). Review and discussion of the manuscript (all authors).

## Additional Information

**Supplementary information** accompanies this paper at <https://doi.org/10.1038/s41598-019-49045-9>.

**Competing Interests:** The authors declare no competing interests.

**Publisher’s note:** Springer Nature remains neutral with regard to jurisdictional claims in published maps and institutional affiliations.




**Open Access** This article is licensed under a Creative Commons Attribution 4.0 International License, which permits use, sharing, adaptation, distribution and reproduction in any medium or format, as long as you give appropriate credit to the original author(s) and the source, provide a link to the Creative Commons license, and indicate if changes were made. The images or other third party material in this article are included in the article's Creative Commons license, unless indicated otherwise in a credit line to the material. If material is not included in the article's Creative Commons license and your intended use is not permitted by statutory regulation or exceeds the permitted use, you will need to obtain permission directly from the copyright holder. To view a copy of this license, visit <http://creativecommons.org/licenses/by/4.0/>.

© The Author(s) 2019



# Development of a Photoswitchable Lithium-Sensitive Probe to Analyze Nonselective Cation Channel Activity in Migrating Cancer Cells<sup>§</sup>

Jinxin V. Pei, Sabrina Heng, Michael L. De Ieso, Georgina Sylvia, Mohamad Kourghi, Saeed Nourmohammadi, Andrew D. Abell, and  Andrea J. Yool

Adelaide Medical School, and the Institute for Photonics and Advanced Sensing (IPAS) (J.V.P., M.D.I., M.K., S.N., A.J.Y.) and ARC Centre of Excellence for Nanoscale BioPhotonics, IPAS, School of Physical Sciences (S.H., G.S., A.D.A.), University of Adelaide, Adelaide, South Australia, Australia

Received December 3, 2018; accepted March 5, 2019

## ABSTRACT

This is the first work to use a newly designed Li<sup>+</sup>-selective photoswitchable probe Sabrina Heng Lithium (SHL) in living colon cancer cells to noninvasively monitor cation channel activity in real time by the appearance of lithium hot spots detected by confocal microscopy. Punctate Li<sup>+</sup> hot spots are clustered in the lamellipodial leading edges of HT29 human colon cancer cells and are colocalized with aquaporin-1 (AQP1) channels. AQP1 is a dual water and cyclic-nucleotide-gated cation channel located in lamellipodia and is essential for rapid cell migration in a subset of aggressive cancers. Both the Li<sup>+</sup> hot spots and cell migration are blocked in HT29 cells by the AQP1 ion channel antagonist AqB011. In contrast, Li<sup>+</sup> hot spots are not evident in a poorly migrating colon cancer cell line, SW620, which lacks comparable membrane expression of

AQP1. Knockdown of AQP1 by RNA interference in HT29 cells significantly impairs Li<sup>+</sup> hot spot activity. The SHL probe loaded in living cells shows signature chemical properties of ionic selectivity and reversibility. Dynamic properties of the Li<sup>+</sup> hot spots, turning on and off, are confirmed by time-lapse imaging. SHL is a powerful tool for evaluating cation channel function in living cells in real time, with particular promise for studies of motile cells or interlinked networks not easily analyzed by electrophysiological methods. The ability to reset SHL by photoswitching allows monitoring of dynamic signals over time. Future applications of the Li<sup>+</sup> probe could include high-throughput optical screening for discovering new classes of channels, or finding new pharmacological modulators for nonselective cation channels.

## Introduction

Cell migration is central to critical processes of repair, regeneration, immune protection, development, and maintenance of multicellular organisms, and in disease conditions such as cancer metastasis (Friedl and Wolf, 2003; Papadopoulos et al., 2008; Olson and Sahai, 2009; Petrie et al., 2009; Krummel et al., 2016). In addition to regulating fluid balance (Agre et al., 1993; King et al., 2004), some aquaporins facilitate rapid cell migration. For example, aquaporin-1 (AQP1) enhances the mobility of some of the most motile cells, such as T cells,

fibroblasts, cancers, and amoebae (Pei et al., 2016a). While the exact mechanisms have yet to be determined, we do know that elevated expression of AQP1 is apparent at the leading edges of lamellipodia in these classes of migrating cells. Genetic knockdown of AQP1 expression can impair cell migration significantly (Hu and Verkman, 2006; McCoy and Sontheimer, 2007), whereas reintroduction of AQP1 but not other channels, such as AQP4, can restore motility (McCoy and Sontheimer, 2007). A major difference is that AQP1, but not AQP4, can function as a nonselective monovalent cation channel gated by cGMP, as well as a water channel (Anthony et al., 2000; Boassa and Yool, 2003). Dissecting the role of AQP1 ion channels in cell migration would advance our knowledge of basic mechanisms that enhance motility in cancer, stem cells, and regenerating tissues, and identify possible targets for intervention, such as in cancer metastasis.

Here, we demonstrate that a newly designed reversible lithium sensor Sabrina Heng Lithium (SHL) can be used to monitor cation channel activity in living cells, and we demonstrate proof of principle using a metastatic colon cancer cell line (HT29) that relies on high levels of AQP1 expression for rapid migration capability (Dorward et al., 2016) as compared with a

This work was supported by the Australian Research Council [Grants DP160104641 and DP190101745]. Sensor development was supported by the Centre for Nanoscale BioPhotonics, with funding from the Australian Research Council [Grant CE140100003].

Part of this work was presented at the 2018 Biophysics Conference, and the abstract was published in the following Biophysical Journal conference proceedings: Pei JV, Heng S, De Ieso M, Sylvia G, Kourghi M, Abell AD, and Yool AJ (2018) Real-Time Imaging of Lithium 'Hot-Spots': An Analysis of Ion Conductance in Aquaporin-1 using Novel Photo-Switchable Sensor. *Biophys J* 114:360a DOI: 10.1016/j.bpj.2017.11.1999.

<https://doi.org/10.1124/mol.118.115428>.

<sup>§</sup> This article has supplemental material available at molpharm.aspetjournals.org.

**ABBREVIATIONS:** AQP1, aquaporin-1; DMEM, Dulbecco's modified Eagle's medium; Em, emission; Ex, excitation; MC, merocyanine; PBS, phosphate-buffered saline; PCR, polymerase chain reaction; RFU, relative fluorescence unit; RT, room temperature; SHL, Sabrina Heng Lithium; siRNA, small interfering RNA; SP, spiropryan; TEA, tetraethylammonium.

relatively sedentary colon cancer line (SW620), which lacks high AQP1 expression (Smith et al., 2018). SHL was designed to be selective for a low-abundance monovalent ion,  $\text{Li}^+$ , over  $\text{Na}^+$  and  $\text{K}^+$ . AQP1 ion channels have properties that make them an excellent choice for this study; once activated, they show long open times (with open bursts lasting hundreds of milliseconds), a high single-channel conductance (150 pS in physiologic salines), and high permeability to monovalent cations  $\text{Na}^+$ ,  $\text{K}^+$ , and  $\text{Cs}^+$  (Anthony et al., 2000). Work here shows the AQP1 ion channel is also permeable to  $\text{Li}^+$  and, thus, can be hypothesized to enable  $\text{Li}^+$  ion influx, which could be detected by the SHL probe. The exciting finding that launched this study was the observation that the punctate SHL signals are clustered in the lamellipodia of migrating cancer cells. Subsequent confirmation that SHL detects AQP1-mediated  $\text{Li}^+$  entry took advantage of the selective AQP1 ion channel inhibitor (AqB011), cation-substituted extracellular salines, and molecular knockdown of AQP1 to show that  $\text{Li}^+$  entry into the cells and the punctate hot spot signals depended on the presence of ion-conducting AQP1 channels.

Results here show that activation of the sensor intracellularly is dependent on transport of extracellular  $\text{Li}^+$  into the cell. Since the SHL probe is membrane-permeable, it is expected to be uniformly distributed through the cell; the presence of discrete points of fluorescent signal (“hot spots”) implies locations of increased lithium entry. Selective inhibition of AQP1 with AqB011 and knockdown of AQP1 with small interfering RNA show that the  $\text{Li}^+$  transport occurs through AQP1 channels. These results provide the first evidence of hot spots that colocalize with nonselective monovalent cation channels, as confirmed by properties of pharmacological sensitivity, ion selectivity, and levels of expression. These data illustrate the selectivity and applicability of the SHL probe as a powerful biologic tool and add further support to the idea that the ion channel function of AQP1 is an intriguing target for new strategies to manage AQP1-expressing cancers.

## Materials and Methods

**Oocyte Expression and Electrophysiology.** Two electrode voltage clamp recordings were used to determine the ability of  $\text{Li}^+$  to carry current in AQP1-expressing oocytes. Oocyte preparation and cRNA injection were performed as detailed in previous studies (Kourghi et al., 2016; Pei et al., 2016b). In brief, with a protocol approved by the University of Adelaide Animal Ethics Committee (M2018-016) in accord with Australian National Guidelines, partial ovariectomy of anesthetized adult *Xenopus laevis* female frogs was used to obtain lobes of unfertilized oocytes. Oocytes were separated from follicular coats with collagenase, rinsed in  $\text{Ca}^{2+}$ -free isotonic  $\text{Na}^+$  saline, and incubated in frog Ringer’s saline at 16–18°C. Selected oocytes were injected with 30–50 nl of sterile water with and without 1 ng of cRNA from cloned human Aquaporin-1 (NM\_198098), linearized, and transcribed in vitro as per published methods. Oocytes without AQP1 cRNA served as non-AQP-expressing controls. Recordings were performed at room temperature in standard isotonic  $\text{Na}^+$  saline or in  $\text{Li}^+$ -substituted isotonic saline containing either 100 mM NaCl or 100 mM LiCl, and 2 mM KCl, 4.5 mM  $\text{MgCl}_2$ , and 5 mM HEPES, pH 7.3. Capillary glass electrodes (1–3 M $\Omega$ ; 1 M KCl) were used for recordings. cGMP was applied to the bath saline at a final concentration of 10–20  $\mu\text{M}$  using the membrane-permeable cGMP analog [Rpl]-8-[para-chlorophenylthio]-cGMP (Sigma-Aldrich, Castle Hill, NSW, Australia). Ion conductances were determined by linear fits of current amplitudes as a function of voltage, applied by a step protocol from +60 to –110 mV from a –40-mV holding

potential (Kourghi et al., 2016; Pei et al., 2016b). Ionic conductance values were monitored over 25 minutes after the bath application of cGMP to allow sufficient time to achieve maximal response. Recordings were done using a GeneClamp amplifier and pClamp 9.0 software (Molecular Devices, Sunnyvale, CA).

**Cancer Cell Cultures and Confocal Imaging.** HT29 and SW620 colorectal cancer cell lines (American Type Culture Collection, Manassas, VA) were cultured in Dulbecco’s modified Eagle’s medium (DMEM) supplemented with 10% fetal bovine serum (v/v), penicillin and streptomycin (100 U/ml each), and 1 $\times$  glutaMAX (Life Technologies, Scoresby, VIC, Australia), referred to as complete DMEM. Cultures were maintained in 5%  $\text{CO}_2$  at 37°C. Cells were seeded on eight-well uncoated Ibidi  $\mu$ -Slides (Ibidi, Munich, Germany) at a density of  $1.0 \times 10^5$  cells/ml and allowed 24 hours to settle.

All imaging experiments were performed in a darkroom. Prior to imaging, cells were incubated with 50  $\mu\text{M}$  SHL sensor for 2 hours, then washed twice with warm phosphate-buffered saline. For the AqB011-treated group, cells were then incubated with 20 to 80  $\mu\text{M}$  AqB011 for 2 hours or with vehicle (0.1% dimethylsulfoxide). All cells were stained with 0.5 mg/ml of Hoechst 33258 for 20 minutes. Either  $\text{Li}^+$  saline (137 mM LiCl, 3.5 mM KCl, 0.68 mM  $\text{KH}_2\text{PO}_4$ , 5 mM HEPES, 10 mM glucose, and 4.4 mM  $\text{MgSO}_4$ ) or tetraethylammonium ( $\text{TEA}^+$ ) saline (with 137 mM TEA Cl substituted for LiCl and all other components identical to those in  $\text{Li}^+$  saline) was used for the imaging. The  $\mu$ -Slide was mounted on a Leica TCS SP5 laser-scanning confocal microscope (Leica, Wetzlar, Germany) with the 63 $\times$  objective selected. To detect the signal emitted by the SHL sensor, the following excitation (Ex)/emission (Em) setting was used: Ex = 513 nm/Em = 550 nm–700 nm. For visualizing Hoechst 33258 staining, the following setting was used: Ex = 405 nm/Em = 425–500 nm.

**Small Interfering RNA Transfection.** HT29 cells were cultured in six-well plates or eight-well uncoated Ibidi  $\mu$ -Slides in complete DMEM medium to reach 30% confluency prior to transfection. Transfection with Lipofectamine 2000 (11668019; Life Technologies) used 50 nM of either Ambion Silencer Select AQP1 siRNA (4390824; Life Technologies) or Ambion Silencer Select Negative Control #1 siRNA (4390843; Life Technologies), together with 50 nM Dharmacon siGLO Green Transfection Indicator (D-001630-01-05; Millennium Science, Mulgrave, VIC, Australia). Cells were incubated in 5%  $\text{CO}_2$  at 37°C for 48 hours prior to confocal imaging or real-time polymerase chain reaction (PCR) analyses. For signals emitted by siGLO Green, the setting Ex = 496 nm/Em = 506 nm–606 nm was used.

**Quantitative Reverse-Transcription Polymerase Chain Reaction.** At 48 hours post-transfection, cells were harvested from six-well plates, and RNA was extracted using Invitrogen PureLink RNA Mini Kit (1876897; Life Technologies) according to the manufacturer’s protocol. RNA was quantified in Take3 Micro-Volume Plates with a Synergy 2 plate reader (BioTek, Winooski, VT). RNA (1  $\mu\text{g}$ ) was reverse transcribed using the QuantiNOVA Reverse Transcription kit (205413; Qiagen, Chadstone Centre, VIC, Australia). Quantitative reverse-transcription polymerase chain reactions of the reference sequence ribosomal protein S13 (RPS13) and AQP1 were performed using SYBR Select Master Mix (4472908; Life Technologies) in triplicate using the Rotorgene 6000 (Qiagen). Primers used for AQP1 were as follows: forward primer, AGTCACTTCCCAAGATCTGC; reverse primer, CAGGTGGGTCCCTTTCTTTCA.

**Immunohistochemistry.** Cells were cultured in eight-well Ibidi  $\mu$ -Slides to achieve 50% confluency prior to the experiment. Cells were rinsed with phosphate-buffered saline (PBS), fixed in 4% paraformaldehyde for 20 minutes at room temperature (RT), and washed four times in PBS (5-minute washes at RT) on a rocker. Cells were permeabilized with 0.1% PBS Tween for 5 minutes, washed three times with PBS at RT for 5 minutes on a rocker, and then blocked with 10% goat serum in PBS (GS/PBS) for 40 minutes at RT on a rocker. Incubation with the rabbit anti-AQP1 antibody (ab15080; Abcam, VIC, Australia) in 0.1% GS/PBS lasted 2 hours at RT. The cells were then washed three times in PBS (7 minutes; RT) on a rocker and incubated with AlexaFluor 488-conjugated goat anti-rabbit antibody

(ab150077; Abcam) diluted in 0.1% GS/PBS (35 minutes; RT, in the dark). After washing three times in PBS (7 minutes; RT) on a rocker, cells were incubated with Hoechst 33258 (Sigma-Aldrich) for 5 minutes in the dark. The cells were rinsed with PBS twice and mounted using Hydromount mounting medium (Sigma-Aldrich).

**In Cell Photoswitching Experiment.** The plate was mounted on a microscope with an overhanging UV lamp and table light. The first image was taken after the plate had been exposed to white light for 10 minutes (OFF1). The second image was taken after subsequent UV (632 nm) light exposure for 10 minutes (ON1). Over the next 10 minutes, images were captured every 2 minutes during white light exposure, ending with the seventh image (OFF2). The final image was taken after 10-minute incubation in total darkness (ON2). Fluorescent intensities were quantified using ImageJ software (National Institutes of Health, Bethesda, MD).

**Chemical Synthesis and Characterization.** Details for the synthesis of SHL are reported as Supplemental Materials (Supplemental Synthesis Experiment and Supplemental Scheme 1). The characterization of SHL is provided as Supplemental Materials (Supplemental Spectroscopic Experiments), which show the absorbance spectrum (Supplemental Fig. 1), Job's plot analysis of binding stoichiometry (Supplemental Fig. 2), photoswitching properties (Supplemental Fig. 3), metal ion titration tests (Supplemental Fig. 4), and results for excitation to emission to absorbance integration (Supplemental Fig. 5).

**Statistics.** Differences were analyzed for significance using one-way analysis of variance for multiple comparisons where relevant and post hoc analyses by Student's unpaired *t* test unless otherwise indicated.

Results are reported as  $P < 0.001$  (\*\*\*) and  $P < 0.0001$  (\*\*\*\*); *n* values are indicated above the *x*-axis (*n*) in histograms.

## Results

**Design and Characterization of the Reversible Lithium Sensor SHL.** The sensor described here (see Fig. 1A for SHL structure) contains a photochromic spiropyran that can be reversibly switched between a nonfluorescent spiropyran isomer (SP) and a charge-delocalized fluorescent merocyanine isomer (MC) when interacting with an appropriate metal ion (Rivera-Fuentes et al., 2015), such as  $\text{Li}^+$  (Fig. 1A). The ability to switch between the two states is advantageous for visualizing  $\text{Li}^+$  transport into cells. SHL shows enhanced fluorescence when complexed to  $\text{Li}^+$  (MC- $\text{Li}^+$  complex in Fig. 1A) while maintaining low background fluorescence in the absence of the ion (SP isomer in Fig. 1A). This sensor characteristic is desirable for visualizing ion binding with confocal microscopy and is predicted to yield better resolution than conventional fluorescent probes due to its enhanced signal-to-background ratio (Kolmakov et al., 2010; Klajn, 2014). A critical characteristic of the SHL sensor is its selectivity for  $\text{Li}^+$  over other biologically abundant ions. We showed that incorporation of suitable ionophores on the spiropyran nucleus provided selective binding of defined ions (Heng et al., 2017). Here, we incorporated a 1-aza-15-crown-5 substituent at

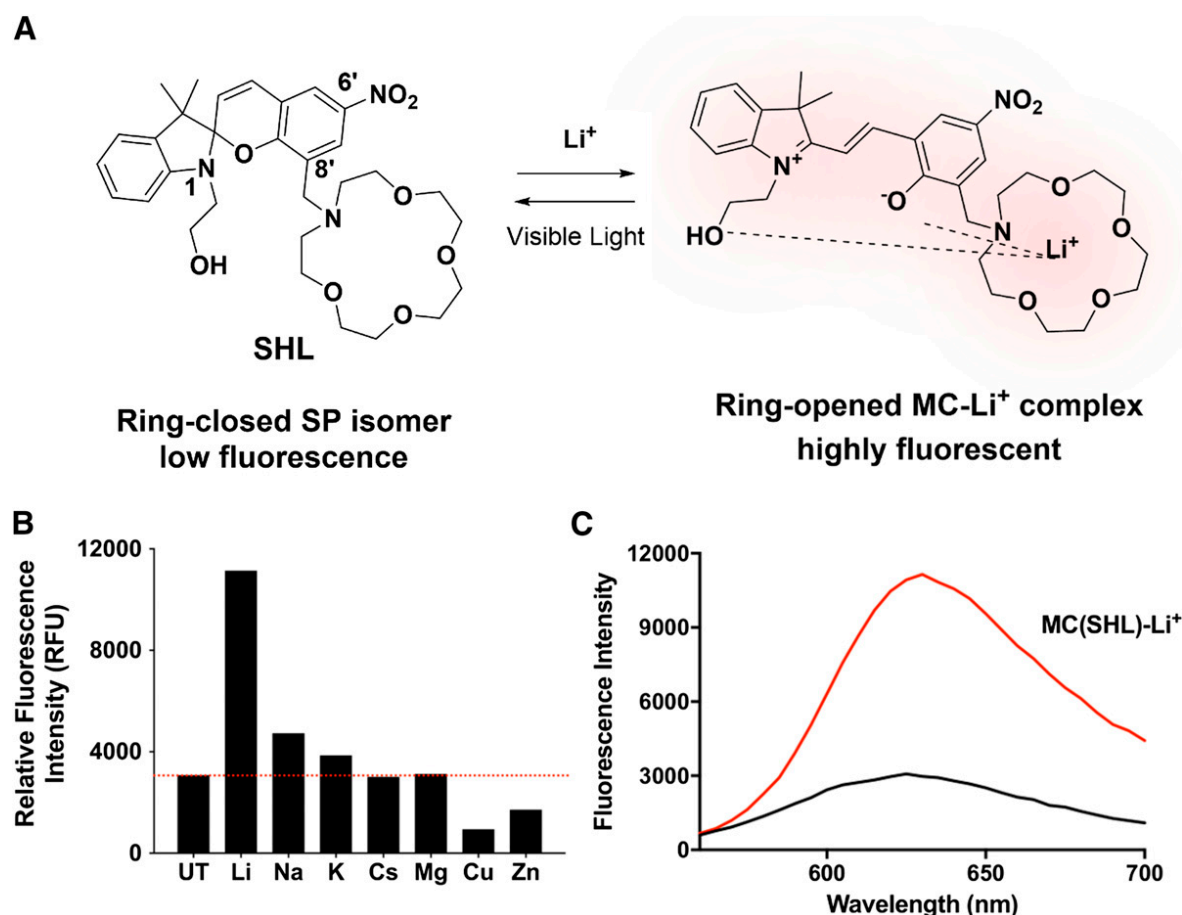


**Fig. 1.** Properties of the lithium sensor SHL. (A) Structures of the SP and merocyanine-lithium complexes of the sensor SHL [MC(SHL)- $\text{Li}^+$ ] and reversible binding of  $\text{Li}^+$ . The ring-closed spiropyran has lower fluorescence than the open merocyanine. (B) Fluorescence intensities of SHL (50  $\mu\text{M}$ ) in the presence of  $\text{Li}^+$  or other biologically relevant metal ions. Excitation wavelength = 532 nm; emission wavelength = 625 nm. (C) Fluorescence spectra of SHL in water (50  $\mu\text{M}$ ). Black spectrum, SHL with no added  $\text{Li}^+$ ; red spectrum, SHL with  $\text{Li}^+$  (100  $\mu\text{M}$ ).

C8 and a hydroxyethyl substituent at N1 to impart selectivity for  $\text{Li}^+$  (Fig. 1A). Finally, we incorporated an  $\text{NO}_2$  substituent at C6 of the benzopyran ring as an electron-withdrawing group at that position, known to stabilize the ring-opened MC form, thus favoring ion binding. Details on the synthesis of SHL are reported in the synthesis section of the Supplemental Information. In brief, the  $\text{Li}^+$  sensor was prepared from 1-aza-15-crown-5 and 1-(2-hydroxyethyl)-2,3,3-trimethyl-3H-indol-1-ium to give SHL with an overall yield of 20% using a modification to existing methodology (Heng et al., 2013; Stubing et al., 2016).

The addition of excess  $\text{Li}^+$  (100  $\mu\text{M}$ ) to SHL (50  $\mu\text{M}$ ) gave rise to strong fluorescence ( $\lambda_{\text{ex}} = 532 \text{ nm}$ ) at approximately  $\lambda_{\text{em}} = 635 \text{ nm}$ , as shown in Fig. 1C, which is consistent with the formation of the MC(SHL)- $\text{Li}^+$  complex as expected based on our sensor design. Importantly, the red fluorescence represents an emission bandwidth that is distinct from the blue nuclear stain (Hoechst 33258) and green AQP1 immunofluorescence signals. Additional spectroscopic properties of SHL, such as absorbance, detection limits, photoswitching, and

quantum yields, are detailed in the Supplemental Note section. The selectivity of SHL for  $\text{Li}^+$  over other biologically relevant ions was confirmed through ion binding assays with the addition of excess ions ( $\text{Li}^+$ ,  $\text{Na}^+$ ,  $\text{K}^+$ ,  $\text{Cs}^+$ ,  $\text{Mg}^{2+}$ ,  $\text{Mn}^{2+}$ ,  $\text{Cu}^{2+}$ , or  $\text{Zn}^{2+}$ ). Results in Fig. 1B show that SHL had the highest affinity for  $\text{Li}^+$  and relatively little response to similar monovalent ions, such as  $\text{Na}^+$  and  $\text{K}^+$ . The red-emitting properties and selectivity of SHL for  $\text{Li}^+$  demonstrated that the emission observed in the cell was not due to autofluorescence or interaction of the sensor with other endogenous ions; the signal was specific to the MC(SHL)- $\text{Li}^+$  complex.

**The AQP1 Cation Channel Is Permeable to  $\text{Li}^+$  and Blocked by AqB011.** AQP1-expressing and non-AQP control *Xenopus* oocytes were recorded by two-electrode voltage clamp in isotonic saline with 137 mM  $\text{Li}^+$  substituted for standard physiologic  $\text{Na}^+$ . Ion currents in isotonic  $\text{Li}^+$  saline (Fig. 2A) were measured for human AQP1-expressing *Xenopus* oocytes and nonexpressing control oocytes before (“initial”) and after treatment with a membrane-permeable analog of

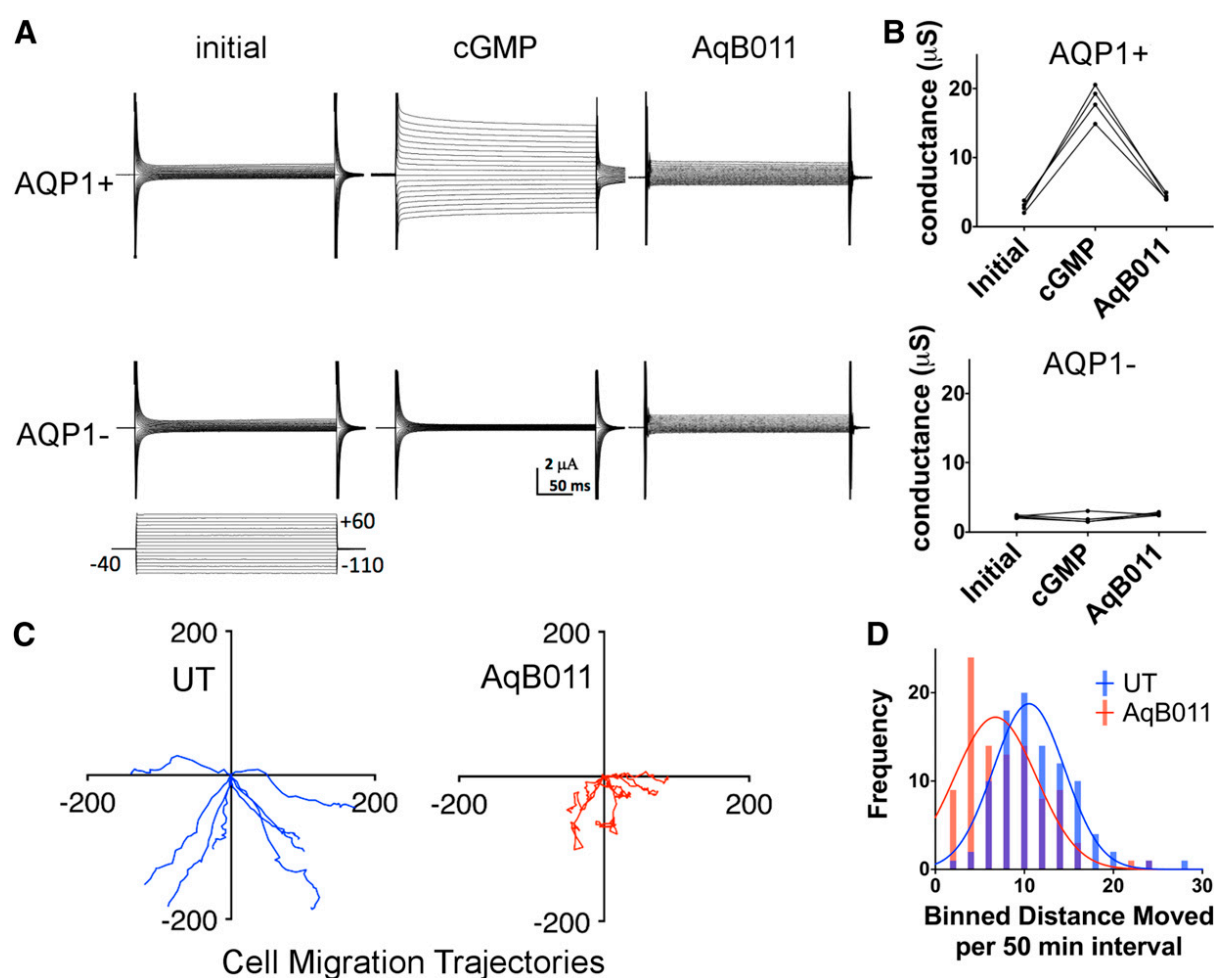


**Fig. 2.** AQP1 ion channels are permeable to  $\text{Li}^+$  and blocked by the pharmacological agent AqB011, which also impairs migration in an AQP1-expressing cancer cell line. (A) Two-electrode voltage clamp recordings in  $\text{Li}^+$  isotonic saline of human AQP1-expressing (AQP1+) and nonexpressing control (AQP1-) *Xenopus* oocytes. After initial recordings (initial), ionic conductance responses were activated in AQP1+ but not AQP1- oocytes by 25 minutes after application of CPT-cGMP (cGMP). Post incubation in AqB011 (30  $\mu\text{M}$ ; 2 hours), the AQP1 conductance was unresponsive to the second application of cGMP (AqB011). (B) Trend plots illustrate responses for AQP+ oocytes measured before (initial) and after the first application of chlorophenylthio-cGMP (cGMP) and after the second application of CPT-cGMP following 2-hour incubation in saline with AqB011. Ion conductance responses were not observed in AQP1 control oocytes. (C) Migration trajectories for individual HT29 cells were monitored by live cell imaging at 50-minute intervals over 24 hours with (AqB011) and without AqB011 (UT) (80  $\mu\text{M}$ ).  $n = 8$  cells per treatment. (D) Compiled Gaussian distributions of individual cell distances moved per 50-minute interval and illustration of impaired rates of migration in the AqB011-treated HT29 cells (mean  $\pm$  S.E.M. was  $5.69 \pm 0.54 \mu\text{m/h}$  with AqB011 and  $8.83 \pm 0.22 \mu\text{m/h}$  with AqB011;  $n = 8$  per treatment group). UT, untreated.

cGMP (chlorophenylthio-cGMP; see *Materials and Methods* for details), demonstrating  $\text{Li}^+$  permeability of the ion conductance in AQP1-expressing oocytes and not in control oocytes. Oocytes were then incubated 2 hours in  $30 \mu\text{M}$  AqB011 and tested for reactivation by cGMP (“AqB011”) in  $\text{Li}^+$  saline. Results (Fig. 2B) showed that approximately 90% of the cGMP-induced current in AQP1-expressing oocytes was successfully blocked by AqB011, whereas control oocytes (AQP1 $^-$ ) lacked appreciable cGMP-activated current responses and showed no effect of the AqB011 inhibitor.

**AqB011 Blocks Migration in AQP1-Expressing HT29 Colon Cancer Cells.** Live-cell imaging was used to map the trajectories of cultured HT29 cells (Fig. 2C) to quantify migration rates in the presence and absence of the AQP1 ion channel blocker AqB011. Histogram summaries of the distances moved by individual cells per unit time interval show that the Gaussian distribution was substantially shifted to shorter distances in the presence of the AQP1 inhibitor (Fig. 2D), demonstrating that block of the ion channel activity impaired cell migration.

**$\text{Li}^+$  Entry through Hot Spots in AQP1-Expressing HT29 Cells.** The ability of SHL to detect  $\text{Li}^+$  in live cells was

investigated using confocal microscopy. HT29 colon cancer cells are known to have high AQP1 expression (Pei et al., 2016b) and were chosen as a useful model for testing cellular imaging of  $\text{Li}^+$  permeation through nonselective cation channels. SHL ( $50 \mu\text{M}$  in physiologic saline) was incubated with the HT29 cells for 2 hours prior to imaging to allow loading of SHL into the cells. The cells were counterstained with Hoechst 33258 to label nuclei.

Illumination with green laser light activated the MC(SHL)- $\text{Li}^+$  complex, which resulted in a red fluorescence signal characteristic of this chemical interaction (Fig. 3A, ON1). Exposure of the cells to continuous white light for 10 minutes progressively shifted the signal to a low level of fluorescence, consistent with the expected photoswitching from the fluorescent MC(SHL)- $\text{Li}^+$  complex to the nonfluorescent SP isomer. After prolonged white light illumination, the probe was reset to a responsive state by 10-minute recovery in darkness, which allowed reactivation of the probe signal (ON2). Fluorescence intensity decreased as a single-phase decay function over time when cells were illuminated with standard white light (Fig. 3B), as illustrated by images taken at 2-minute intervals. The normalized signal intensity decreased from 100 relative

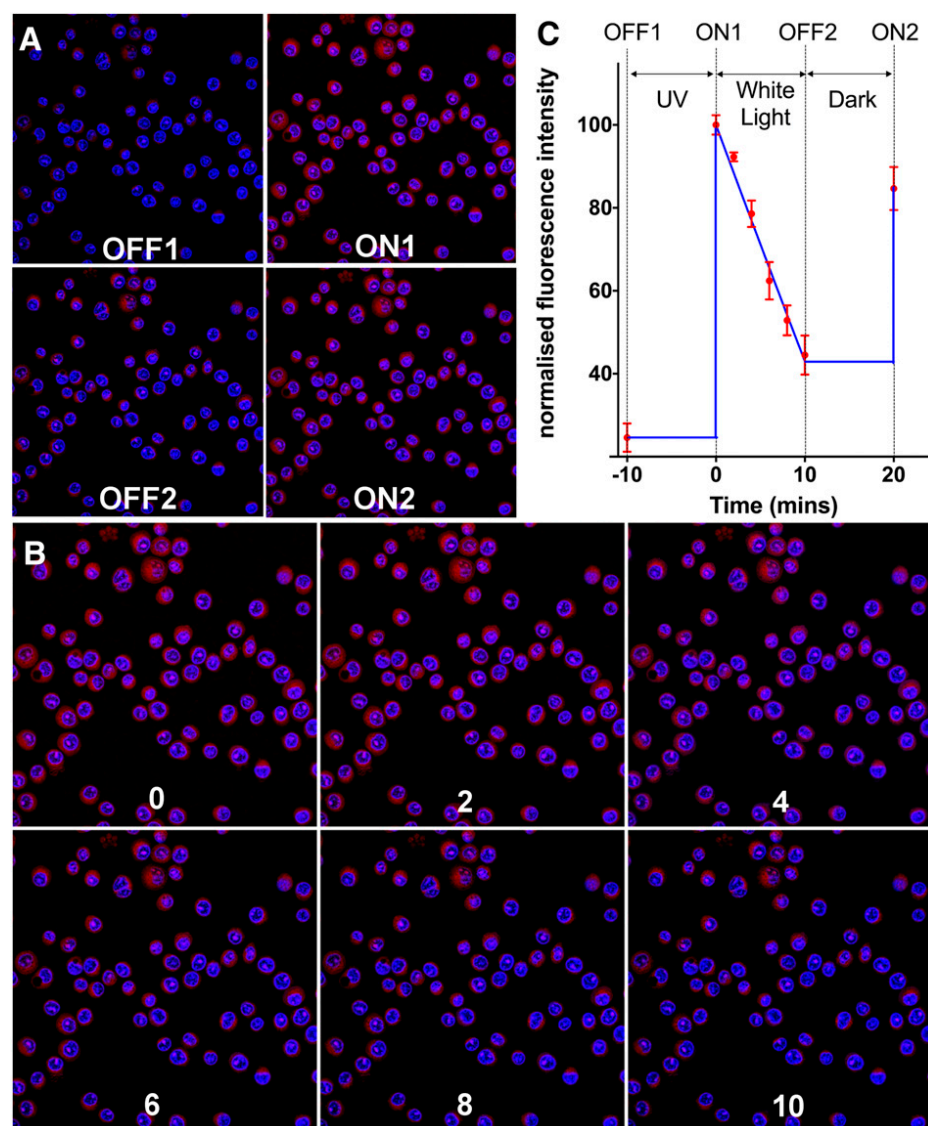


**Fig. 3.** Confocal time series for SHL signals in HT29 cells. (A) HT29 cells were incubated with  $50 \mu\text{M}$  SHL for 2 hours prior to imaging. Cell nuclei were labeled with Hoechst 33258 (blue). Four distinctive states of the sensor during the photoswitch cycles are illustrated. Cells were first illuminated under visible light radiation for 10 minutes to convert the majority of the sensor back to nonfluorescent SP isomer (OFF1). Then, cells were illuminated under UV light for 10 minutes to convert SP isomer to fluorescent MC(SHL)- $\text{Li}^+$  complex (ON1), followed by exposure under white light for 10 minutes with measurement taken every 2 minutes (OFF2). Finally, cells were incubated in the dark for 10 minutes to allow the formation of the MC isomer and the binding of  $\text{Li}^+$  to form the MC(SHL)- $\text{Li}^+$  complex (OFF2). (B) Ten-minute white light illumination was applied to cells after ON1 state; images were taken every 2 minutes as illustrated. Red SHL signals gradually faded with time. (C) Red fluorescent signals were measured for individual cells in the field of view, and values were normalized to ON1 state. Data are the mean  $\pm$  S.E.M.; the  $n$  value is 43. A single-phase decay function was fitted to values between ON1 (100%) and OFF2 (44.51%) states; the half-life was determined to be 4.13 minutes, with a  $\tau$  value estimated at 5.95 minutes. After 10-minute incubation in the dark, sensors converted back to the MC isomer, and the normalized intensity increased from 44.51% (OFF2) to 84.65% (ON2).

fluorescence units (RFUs) to 44.51 RFUs after 10 minutes of visible light radiation (Fig. 3C). Under these experimental conditions, the half-life was determined to be 4.13 minutes with a  $\tau$  value estimated at 5.95 minutes. Recovery in darkness for 10 minutes allowed the formation of the MC isomer. The binding of  $\text{Li}^+$  regenerated the MC(SHL)- $\text{Li}^+$  complex at a normalized intensity of 84.65 RFUs (Fig. 3C; ON2). Repeated cycles of photoswitching performed on the same cells gave reproducible changes in fluorescence, demonstrating the ability of SHL to photoswitch reversibly in living cells. This innovation defines a new probe for monitoring changes in intracellular  $\text{Li}^+$  in a biologic sample over time without loss of sensitivity imposed by photobleaching of a sensor. The photoswitching property allows repeated comparisons of function across multiple experimental treatments and provides additional advantages for biologic assays in which sample availability can be limited.

Distinctive punctate signals, referred to here as lithium "hot spots," were observed in HT29 cells when imaged in  $\text{Li}^+$ -containing saline (Fig. 4A, 1). A loss of hot spot events was observed after treatment with the AQP1 ion channel antagonist AqB011 (20  $\mu\text{M}$  for 2 hours), after which only a faint background fluorescence was observed (Fig. 4A, 2). The removal of  $\text{Li}^+$  from the extracellular saline by equimolar substitution with the  $\text{TEA}^+$  ion also caused a loss of hot spots (Fig. 4A, 3), showing that the observed events resulted from  $\text{Li}^+$  ion entry. In saline with  $\text{TEA}^+$ , application of the blocker AqB011 had no additional effect on hot spot activity (Fig. 4A, 4). The fluorescent signal for the entire cell was reduced 2-fold in HT29 cells when  $\text{Li}^+$  entry was compromised by pharmacological block of the ion channel with AqB011 or by removal of extracellular  $\text{Li}^+$  ion via replacement with other cations as chloride salts (Fig. 4B). Collectively, these data confirmed that the bright punctate  $\text{Li}^+$  signals depended on the presence of extracellular  $\text{Li}^+$  and the presence of functional AQP1 ion channels, and ruled out the possibility that hot spots were indirectly due to nonspecific interactions with other intracellular cations or entry of  $\text{Li}^+$  through other cation pathways. The most parsimonious interpretation is that the lithium hot spots represent  $\text{Li}^+$  entry across the plasma membrane through AQP1 cation channels.

Knockdown of AQP1 expression with small interfering RNA (siRNA) resulted in a dramatic loss of red  $\text{Li}^+$  hot spots, specifically in transfected HT29 cells (labeled green with cotransfected siGLO transfection indicator) and not in nontransfected cells in the same culture plate (Fig. 4C). The fluorescence intensity of signals from the SHL  $\text{Li}^+$  probe (Fig. 4D) and the levels of AQP1 transcript assessed by quantitative PCR (Fig. 4E) both were reduced significantly with AQP1-siRNA treatment, but not with control scrambled siRNA treatment. These data confirm that in HT29 cells, the appearance of  $\text{Li}^+$  hot spots requires the expression of AQP1 channels.

**$\text{Li}^+$  Hot Spots Were Not Observed in SW620 Cells Lacking High Levels of AQP1 Expression.** The role of AQP1 ion channels in mediating the lithium hot spot events was tested by comparison with another colon cancer cell line (SW620) which is similar to HT29 in having an adherent epithelial phenotype (Fogh et al., 1977) but different in that rates of migration are slower. Levels of AQP1 expression were approximately 2.6-fold lower in SW620 than in HT29 cells (Fig. 5, A and B); this finding is further supported by the reverse-transcription PCR data (Fig. 5C). HT29 cells and

SW620 cells were preincubated in SHL for 2 hours, transferred into  $\text{Li}^+$ -substituted saline, and imaged. Results show that the lithium hot spots are more abundant and brighter in HT29 cells (Fig. 5D, 1–3) than in SW620 cells (Fig. 5D, 4–6). In migrating HT29 cells, lithium hot spots are concentrated in leading edges (Fig. 5D, 2 and 3) in contrast to the uniform distribution seen in nonmigrating cells (Fig. 5D, 1). This observation is consistent with the known clustering of AQP1 channels in the leading edges of specific classes of cells during migration (McCoy and Sontheimer, 2007), where these channels are proposed to facilitate fluid movements needed for volume changes during extension, and possibly to compensate for changes in osmotic pressure associated with actin polymerization and depolymerization (Hu and Verkman, 2006).

AQP1 expression and localization were determined by immunofluorescent imaging using confocal microscopy. AQP1 protein was immunolabeled with anti-AQP1 primary antibody and green fluorescent AlexaFluor 488 secondary antibody and visualized by 488-nm laser excitation. HT29 cells demonstrated high AQP1 signal intensities as compared with SW620 cells (Fig. 6, A and B). Comparison with SW620 cells confirmed that a reduced abundance of lithium hot spots correlated with lower levels of AQP1 expression. In combination, results here based on pharmacology, ion substitution, and a comparison of cell lines with different levels of AQP1 expression provide evidence that the lithium hot spots measured by the novel probe SHL mark the locations of active AQP1 ion channels.

**Lithium Hot Spots Are Colocalized with AQP1 Channels in HT29 Cells.** The spatial correlation between the locations of the lithium hot spots and AQP1 channels was assessed using confocal microscopy. Signal intensities using Z-stack compiled images were measured as a function of distance across the cell diameter (indicated by straight lines crossing the cell centers; two cross-sections per cell). Signals were plotted as a function of X-Y distance to quantify the correspondence between the SHL  $\text{Li}^+$  fluorescence intensity [red channel; MC(SHL)- $\text{Li}^+$  complex] and the AQP1 protein signal intensity (green channel; immunofluorescence). Results in Fig. 6C show that the two fluorescence signals were strongly colocalized in HT29 cells (with superimposed red and green signals represented as yellow), yielding RFUs ranging from 50 to 200 that were consistent with data shown in Fig. 5A. The spatial profiles of the red and green signals across the cell diameter are illustrated by plots of signal intensity (Fig. 6D).  $\text{Li}^+$  and AQP1 signals in HT29 cells were strongly correlated, with  $R^2$  values ranging 0.61 to 0.68. In contrast, SW620 cells (Fig. 6D) showed low signal intensities and poor spatial correlation, with signal values mainly at 0–50 RFUs and  $R^2$  values ranging from 0.06 to 0.09. This work opens new avenues for the potential real-time visualization of cation channel function and the localization of active channel domains in living cells, and provides additional insight into the relevance of cation channels such as AQP1 in dynamic cellular responses, such as migration.

**Lithium Hot Spots Are Dynamic When Imaged in HT29 Cells.** The ability of SHL to detect dynamic  $\text{Li}^+$  entry through AQP1 was tested using a 300-second time-lapse video of an SHL-loaded cell directly after perfusion with  $\text{Li}^+$ -substituted extracellular saline. The intensity of  $\text{Li}^+$  hot spots increased during the first half of the recording, then cycled between increasing and decreasing signal intensities during the second half (Fig. 7). The montage shows a time series for a  $2 \times 3\text{-}\mu\text{m}$  field of view (rectangle), illustrating the dynamic fluorescence

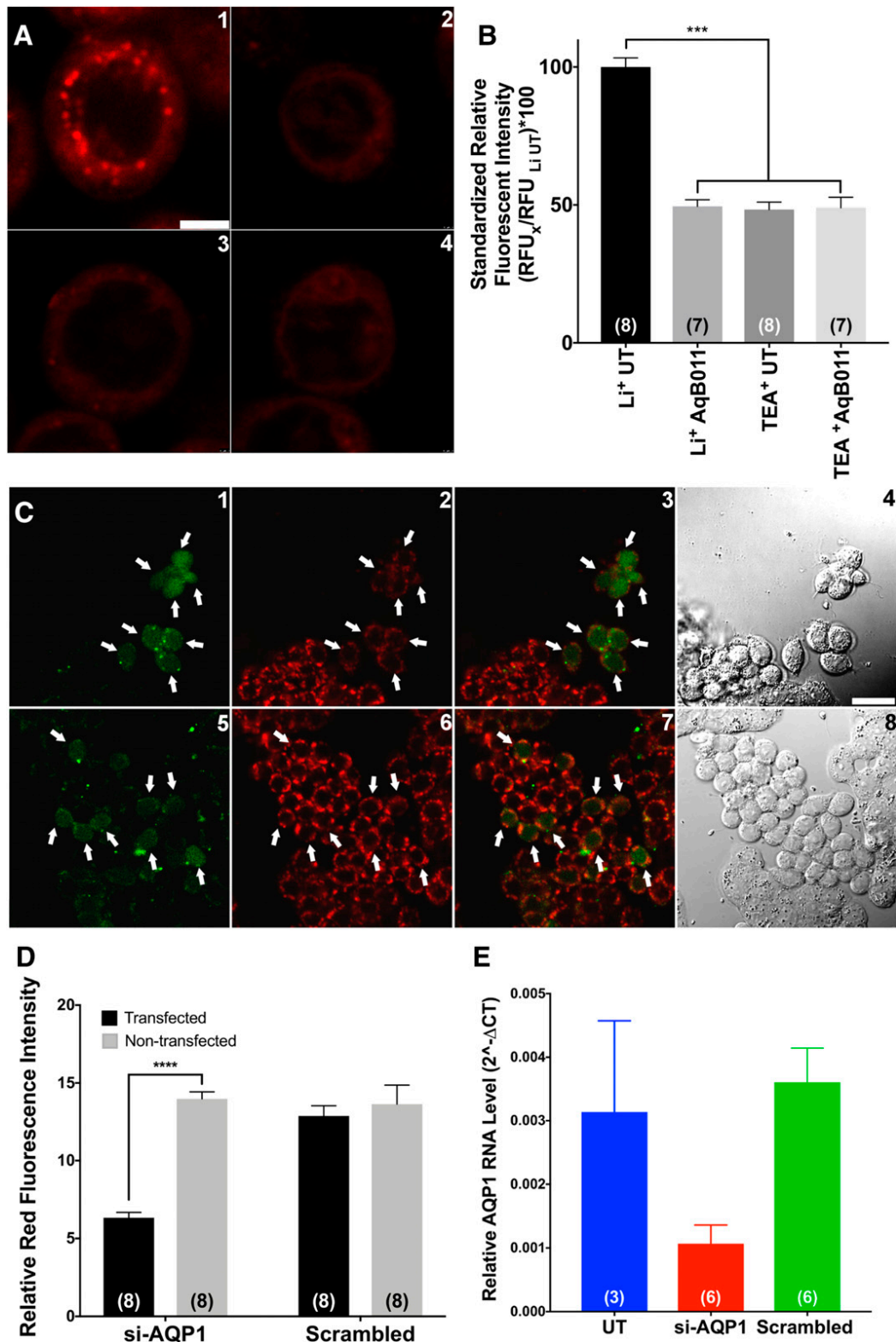


**Fig. 4.** Lithium hot spot signals depend on functional AQP1 channels. (A) Distinctive punctate Li<sup>+</sup> hot spots were observed in HT29 cells imaged in Li<sup>+</sup>-substituted extracellular saline (1). In cells that were pretreated with 20 μM AqB011 for 2 hours, Li<sup>+</sup> hot spots were not observed (2). Similar losses of hot spot events were observed after the removal of Li<sup>+</sup> from the extracellular saline by equimolar substitution of TEA<sup>+</sup> (3). Pretreatment with 20 μM AqB011 (2 hours) caused no further change in the signal in the absence of extracellular Li<sup>+</sup> (4). (B) Li<sup>+</sup>-selective fluorescent signals were quantified by measuring red fluorescence intensities of individual cells. Intensities were normalized to those of HT29 cells imaged in Li<sup>+</sup> saline. Li<sup>+</sup> entry was significantly compromised by pharmacological block (AqB011) or removal of Li<sup>+</sup> ion from the saline by equimolar replacement with other cations, such as TEA<sup>+</sup>. Significant differences were analyzed by comparing the Li<sup>+</sup> AqB011, TEA<sup>+</sup> UT, and TEA<sup>+</sup> AqB011 groups to the Li<sup>+</sup> UT group (see *Materials and Methods* for details). (C) HT29 cells were transfected with either siRNA targeting AQP1 (si-AQP1, upper panels) or scrambled siRNA (scrambled, lower panels) before confocal imaging. Cells were preincubated in transfection indicator siGLO Green (green, 1 and 5) and SHL (red, 2 and 6). Stacked images of both green and red channels are illustrated in 3 and 7, and bright field images are illustrated in 4 and 8. Li<sup>+</sup> signals were impaired in cells successfully transfected with AQP1 siRNA (cells with green nucleus, 3) but not in cells transfected with scrambled siRNA (cells with green nucleus, 7). (D) Li<sup>+</sup>-selective

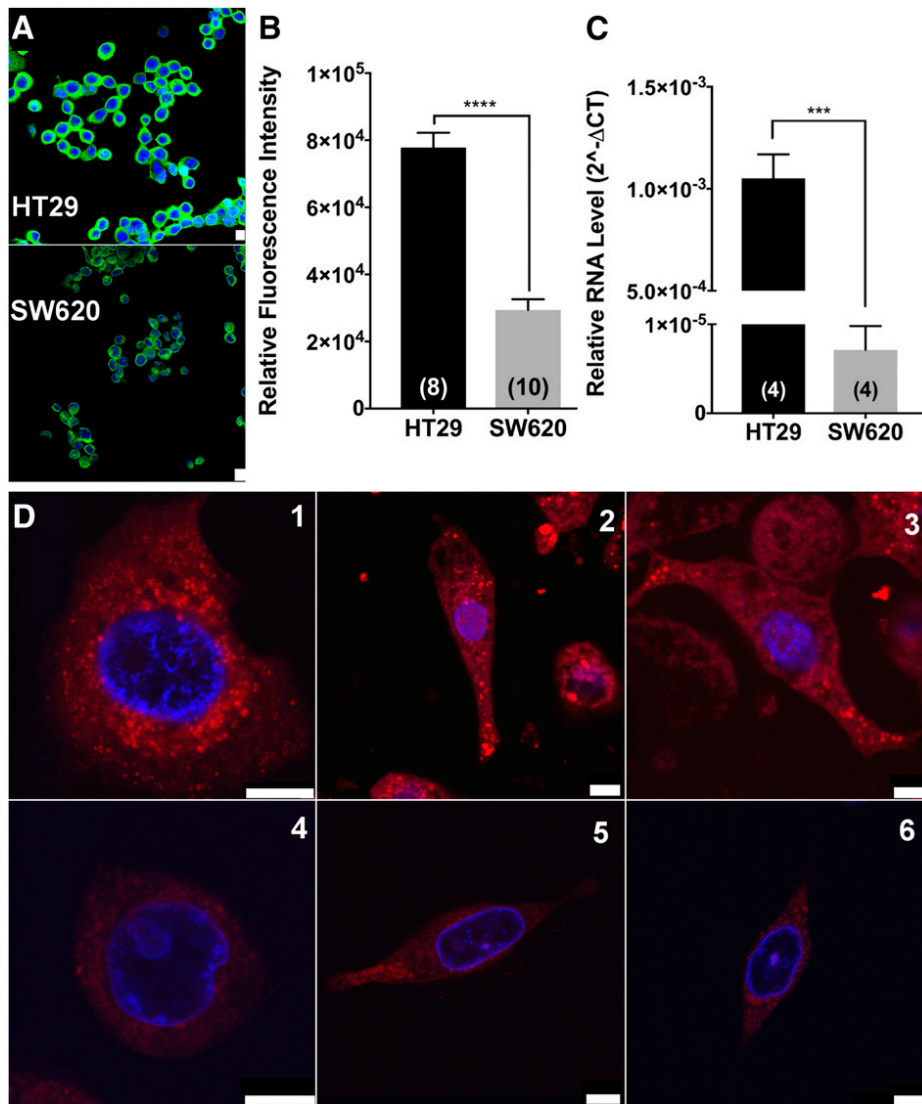


**Fig. 5.** Characterization of lithium hot spots in AQP1-expressing and AQP1-deficient cells. (A) Cells were labeled with Hoechst nuclear stain (blue) and anti-AQP1 antibody (tagged with fluorescent secondary antibody; green). (B) Anti-AQP1 immunofluorescence intensities for HT29 cells were approximately 2.6-fold higher than in SW620 cells. (C) AQP1 RNA levels measured by reverse-transcription quantitative PCR were more than 100-fold lower in SW620 cells as compared with HT29 cells. (D) HT29 and SW620 cells were loaded with SHL for 2 hours prior to imaging. A strong Li<sup>+</sup> signal was observed in all HT29 cells (1, 2, 3) as compared with the minimal Li<sup>+</sup> signals observed in SW620 cells (4, 5, 6). In nonmigrating HT29 cells, Li<sup>+</sup> hot spots appeared as widely distributed across the cell (1). In migrating HT29 cells, Li<sup>+</sup> hot spots were concentrated at leading edges of the cells (2, 3). White scale bars indicate 5 μm. Significant differences were analyzed by unpaired *t* test and are reported as *P* < 0.001 (\*\*\*) (see *Materials and Methods* for details).

emission properties. A movie depicting Li<sup>+</sup> hot spot activity in HT29 cells in real time is available as Supplemental Material (Supplemental Video).

## Discussion

Work with confocal imaging presented here is the first to demonstrate the use of a new Li<sup>+</sup>-selective photoswitchable probe as a tool for monitoring nonselective cation entry in living cells, with AQP1 ion channels of migrating cancer cells selected as a model for illustrating feasibility and potential significance. Nonselective monovalent cation channel activity was monitored with the probe SHL, which is selective for Li<sup>+</sup>. Lithium hot spots were abundant in HT29 colon cancer cells expressing high levels of AQP1 and rare in SW620 colon cancer cells which have comparatively little AQP1. The spatial

localization of Li<sup>+</sup> hot spots at the leading edges of HT29 cells was an exciting observation, fitting the predicted location of AQP1 ion channels. Future studies characterizing the dynamic temporal and spatial properties of ion fluxes in migrating cells at higher resolution will be of interest.

The initial proposal that AQP1 works as a nonselective cation channel in addition to its known role as a water channel (Yool et al., 1996) generated controversy (Agre et al., 1997; Tsunoda et al., 2004). Subsequent analyses confirmed the capacity of AQP1 to function as a dual water and ion channel, showing the ion channel activity was gated directed by intracellular cGMP and indirectly regulated by intracellular signaling cascades including tyrosine phosphorylation (Anthony et al., 2000; Saparov et al., 2001; Boassa and Yool, 2003; Campbell et al., 2012), but left unclear the physiologic relevance of the dual water and ion channel function (Saparov et al., 2001). Recent work has since

fluorescent signals were quantified by measuring red fluorescent intensities of individual cells that were either transfected (green nucleus signal) or nontransfected (no nucleus signal). Li<sup>+</sup> entry was significantly impaired in cells with AQP1 knockdown. Significant differences were analyzed by one-way ANOVA with post hoc Bonferroni tests and are reported as *P* < 0.0001 (\*\*\*\*). (E) AQP1 RNA levels were quantified by using reverse-transcription PCR. AQP1 RNA levels were lowered in cells transfected with siRNA targeting AQP1 compared with either cells without transfection (UT) or cells with scrambled siRNA transfection (scrambled). UT, untreated.



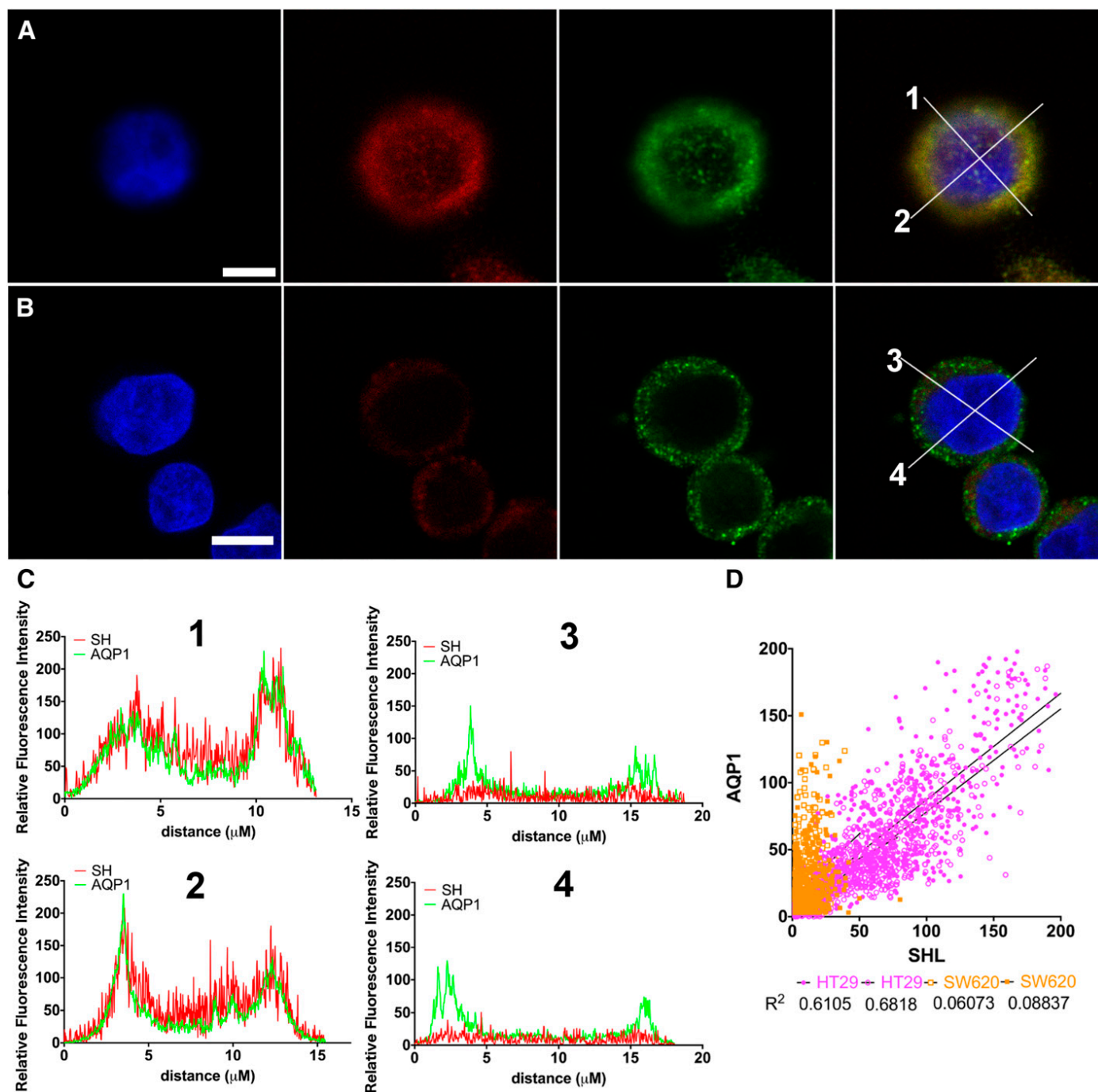


**Fig. 6.** Quantitative confocal analyses of the colocalization of AQP1 and  $\text{Li}^+$  hot spots. HT29 cells (A) and SW620 cells (B) were preincubated with SHL (red) and then fixed and labeled with AQP1 primary antibody and AlexaFluor-488-conjugated secondary antibody (green). Nuclei were stained with Hoechst (blue). Both the  $\text{Li}^+$  and AQP1 signals were at higher intensities in HT29 cells than in SW620 cells. In the far-right panels, all three signal bandwidth images are combined, with colocalized red and green signals seen as yellow. Fluorescence signals from the MC(SHL)- $\text{Li}^+$  complex and AQP1 were strongly localized in HT29 cells but not in SW620 cells. (C) Two cross-sections through cell centers were selected (labeled 1 and 2 for HT29, 3 and 4 for SW620). The red  $\text{Li}^+$  and green AQP1 signal intensities in the cross-sectional lines were plotted as a function of X-Y distance across the cell. HT29 cells showed robust levels and a strong correlation between  $\text{Li}^+$  and AQP1 signal intensities, which was not seen in SW620 cells. (D) Linear regression analyses quantified the correlation between  $\text{Li}^+$  signal and AQP1 signal intensities in HT29 cells (pink) and SW620 cells (orange) for data from (C).  $R^2$  values calculated using GraphPad Prism 7 were 0.61 and 0.68 for HT29 cell cross sections, and 0.06 and 0.09 for SW620 cells.

demonstrated that the AQP1 ion conductance is essential for rapid cell movement in a subset of cancer cells which show high metastasis or invasiveness (Kourghi et al., 2016; Pei et al., 2016b), demonstrating a functional role for the AQP1 ion channel.

AQP1 channels are not the only pathway for  $\text{Li}^+$  transport across cell membranes.  $\text{Li}^+$  is also conducted through

voltage-gated  $\text{Na}^+$  channels (Hille, 1972; Richelson, 1977; Timmer and Sands, 1999) and the  $\text{Na}^+$ -proton exchanger (Lenox et al., 1998). Some of the  $\text{Li}^+$  signal described here could involve additional channels or transporters. However, the alternative hypothesis that the lithium signal observed in HT29 cancer cells is due entirely to mechanisms unrelated to

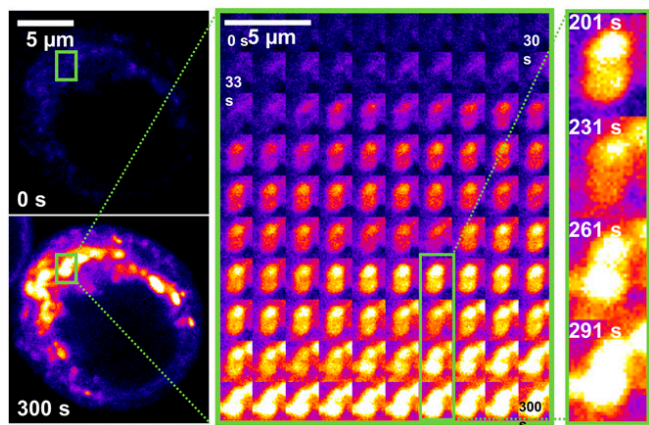


**Fig. 7.** Dynamic properties of  $\text{Li}^+$  hot spots illustrating ON/OFF SHL probe transitions in a living HT29 cell. HT29 cells preloaded with SHL were imaged for 100 frames at 3-second intervals. Extracellular saline was replaced with  $\text{Li}^+$  saline at time 0. Multiple  $\text{Li}^+$  hot spots were activated, as illustrated in the left panels at time 0 and 300 seconds. Images were cropped to show higher magnification views of two discrete  $\text{Li}^+$  hot spots (middle panel) as a time-lapse montage, illustrating the independent ON/OFF/ON transitions of the hot spots (inset, right).

AQP1 seems unlikely for several reasons. First, results here show that pharmacological inhibition with the AQP1 ion channel blocker AqB011 significantly diminished the  $\text{Li}^+$  signal to a level similar to the response observed in cells imaged in saline with  $\text{TEA}^+$  (which does not bind to SHL). Other AQP modulators in the library of bumetanide derivatives that include AqB011 have been shown to be selective for specific AQP classes without off-target effects on other signaling and transport mechanisms (Migliati et al., 2009; Yool et al., 2013). Second, the punctate  $\text{Li}^+$  signal pattern was not evident in SW620 cells that have low levels of AQP1 expression but otherwise express various channels and transporters required for basic cellular function and low-level motility. Third, the colocalization of AQP1 expression and  $\text{Li}^+$  signals showed a robust correlation.

Since SHL passively diffuses across the membrane, it should achieve a reasonably uniform distribution on the cytoplasmic side. Punctate  $\text{Li}^+$  hot spots indicate local areas of  $\text{Li}^+$  entry and accumulation. As shown using the oocyte expression system, AQP1 ion channels mediate  $\text{Li}^+$  influx. In combination with results of pharmacological block and siRNA knockdown, data here support the interpretation that the interaction of  $\text{Li}^+$  with SHL resulting in hot spots occurs in the vicinity of active AQP1 ion channels. The remaining intracellular SHL throughout areas without substantial  $\text{Li}^+$  influx would remain predominantly in the nonfluorescent form, consistent with the low-level background fluorescence.

The increased incidence of hot spots in cellular protrusions was consistent with work from others indicating that AQP1 is localized at the leading edges in migrating cells (McCoy and Sontheimer, 2007). The slow temporal resolution used here for image capture was sufficient to illustrate the dynamic property of the  $\text{Li}^+$  hot spots, which turned on and off over time (as shown in Fig. 7). The observed on/off dynamics of SHL in AQP1-expressing cells was limited by our confocal microscopy setup to a minimal image acquisition rate of 3 seconds per frame; optimization will be needed to enable better evaluations of channel kinetics. Our focus on AQP1 for testing the SHL probe may have benefitted from the usually slow gating properties of the AQP1 ion channel, which once

opened, shows long bursts persisting for hundreds of milliseconds and sets of bursts lasting for seconds (Anthony et al., 2000).

Evidence that AQP1 is not just a water channel but also functions as a monovalent cation channel contributes to our understanding of the diverse mechanisms that govern cell migration. Looking ahead to translational applications, we propose that the lithium sensor will be useful for investigating cation channel function in many types of living cells, including sensory cells, immune cells, cancer cells, and more. The AQP1 ion channel itself is an attractive candidate for development of new therapeutics, and the  $\text{Li}^+$  sensor SHL could be a powerful tool in high-throughput screening for new pharmacological agents that might ultimately help manage metastasis in aggressive AQP1-dependent cancers.

#### Acknowledgments

The authors acknowledge Dr. Xiaozhou Zhang for useful discussions, and Dr. Agatha Labrinidis and Dr. Jane Sibbons at Adelaide Microscopy for training and access to core microscopy facilities.

#### Authorship Contributions

*Participated in research design:* Pei, Heng, Abell, Yool.

*Conducted experiments:* Pei, Heng, De Ieso, Sylvia, Kourghi, Nourmohammadi.

*Contributed new reagents or analytic tools:* Pei, Heng, Abell.

*Performed data analysis:* Pei, Heng, De Ieso, Sylvia, Kourghi, Nourmohammadi, Yool.

*Wrote or contributed to the writing of the manuscript:* Pei, Heng, De Ieso, Sylvia, Kourghi, Nourmohammadi, Abell, Yool.

#### References

- Agre P, Lee MD, Devidas S, and Guggino WB (1997) Aquaporins and ion conductance. *Science* **275**:1490, author reply 1492.
- Agre P, Preston GM, Smith BL, Jung JS, Raina S, Moon C, Guggino WB, and Nielsen S (1993) Aquaporin CHIP: the archetypal molecular water channel. *Am J Physiol* **265**:F463–F476.
- Anthony TL, Brooks HL, Boassa D, Leonov S, Yanochko GM, Regan JW, and Yool AJ (2000) Cloned human aquaporin-1 is a cyclic GMP-gated ion channel. *Mol Pharmacol* **57**:576–588.
- Boassa D and Yool AJ (2003) Single amino acids in the carboxyl terminal domain of aquaporin-1 contribute to cGMP-dependent ion channel activation. *BMC Physiol* **3**:12.
- Campbell EM, Birdsall DN, and Yool AJ (2012) The activity of human aquaporin 1 as a cGMP-gated cation channel is regulated by tyrosine phosphorylation in the carboxyl-terminal domain. *Mol Pharmacol* **81**:97–105.
- Dorward HS, Du A, Bruhn MA, Wrin J, Pei JV, Evdokiou A, Price TJ, Yool AJ, and Hardingham JE (2016) Pharmacological blockade of aquaporin-1 water channel by AqB013 restricts migration and invasiveness of colon cancer cells and prevents endothelial tube formation in vitro. *J Exp Clin Cancer Res* **35**:36.
- Fogh J, Fogh JM, and Orfeo T (1977) One hundred and twenty-seven cultured human tumor cell lines producing tumors in nude mice. *J Natl Cancer Inst* **59**:221–226.
- Friedl P and Wolf K (2003) Tumour-cell invasion and migration: diversity and escape mechanisms. *Nat Rev Cancer* **3**:362–374.
- Heng S, Mak AM, Kostecki R, Zhang X, Pei J, Stubing DB, Ebendorff-Heidepriem H, and Abell AD (2017) Photoswitchable calcium sensor: 'On'-'Off' sensing in cells or with microstructured optical fibers. *Sens Actuators B Chem* **252**:965–972.
- Heng S, Nguyen M, Kostecki R, Monro TM, and Abell AD (2013) Nanoliter-scale, regenerable ion sensor: sensing with a surface functionalized microstructured optical fiber. *RSC Adv* **3**:8308–8317.
- Hille B (1972) The permeability of the sodium channel to metal cations in myelinated nerve. *J Gen Physiol* **59**:637–658.
- Hu J and Verkman AS (2006) Increased migration and metastatic potential of tumor cells expressing aquaporin water channels. *FASEB J* **20**:1892–1894.
- King LS, Kozono D, and Agre P (2004) From structure to disease: the evolving tale of aquaporin biology. *Nat Rev Mol Cell Biol* **5**:687–698.
- Klajn R (2014) Spiropyran-based dynamic materials. *Chem Soc Rev* **43**:148–184.
- Kolmakov K, Belov VN, Bierwagen J, Ringemann C, Müller V, Eggeling C, and Hell SW (2010) Red-emitting rhodamine dyes for fluorescence microscopy and nanoscopy. *Chemistry* **16**:158–166.
- Kourghi M, Pei JV, De Ieso ML, Flynn G, and Yool AJ (2016) Bumetanide derivatives AqB007 and AqB011 selectively block the aquaporin-1 ion channel conductance and slow cancer cell migration. *Mol Pharmacol* **89**:133–140.
- Krummel MF, Bartumeus F, and Gérard A (2016) T cell migration, search strategies and mechanisms. *Nat Rev Immunol* **16**:193–201.
- Lenox RH, McNamara RK, Papke RL, and Manji HK (1998) Neurobiology of lithium: an update. *J Clin Psychiatry* **59** (Suppl 6):37–47.
- McCoy E and Sontheimer H (2007) Expression and function of water channels (aquaporins) in migrating malignant astrocytes. *Glia* **55**:1034–1043.

- Migliati E, Meurice N, DuBois P, Fang JS, Somasekharan S, Beckett E, Flynn G, and Yool AJ (2009) Inhibition of aquaporin-1 and aquaporin-4 water permeability by a derivative of the loop diuretic bumetanide acting at an internal pore-occluding binding site. *Mol Pharmacol* **76**:105–112.
- Olson MF and Sahai E (2009) The actin cytoskeleton in cancer cell motility. *Clin Exp Metastasis* **26**:273–287.
- Papadopoulos MC, Saadoun S, and Verkman AS (2008) Aquaporins and cell migration. *Pflügers Arch* **456**:693–700.
- Pei JV, Burton JL, Kourghi M, De Ieso ML, and Yool AJ (2016a) Drug discovery and therapeutic targets for pharmacological modulators of aquaporin channels, in *Aquaporins in Health and Disease: New Molecular Targets for Drug Discovery* (Soveral G, Casinin A, and Nielsen S eds) pp 275–297, CRC Press, Oxfordshire, UK.
- Pei JV, Kourghi M, De Ieso ML, Campbell EM, Dorward HS, Hardingham JE, and Yool AJ (2016b) Differential inhibition of water and ion channel activities of mammalian aquaporin-1 by two structurally related bacopaside compounds derived from the medicinal plant bacopa monnieri. *Mol Pharmacol* **90**:496–507.
- Petrie RJ, Doyle AD, and Yamada KM (2009) Random versus directionally persistent cell migration. *Nat Rev Mol Cell Biol* **10**:538–549.
- Richelson E (1977) Lithium ion entry through the sodium channel of cultured mouse neuroblastoma cells: a biochemical study. *Science* **196**:1001–1002.
- Rivera-Fuentes P, Wrobel AT, Zastrow ML, Khan M, Georgiou J, Luyben TT, Roder JC, Okamoto K, and Lippard SJ (2015) A far-red emitting probe for unambiguous detection of mobile zinc in acidic vesicles and deep tissue. *Chem Sci (Camb)* **6**:1944–1948.
- Saparov SM, Kozono D, Rothe U, Agre P, and Pohl P (2001) Water and ion permeation of aquaporin-1 in planar lipid bilayers. Major differences in structural determinants and stoichiometry. *J Biol Chem* **276**:31515–31520.
- Smith E, Palethorpe HM, Tomita Y, Pei JV, Townsend AR, Price TJ, Young JP, Yool AJ, and Hardingham JE (2018) The purified extract from the medicinal plant *Bacopa monnieri*, bacopaside II, inhibits growth of colon cancer cells in vitro by inducing cell cycle arrest and apoptosis. *Cells* **7**.
- Stubing DB, Heng S, and Abell AD (2016) Crowned spiropyran fluoroionophores with a carboxyl moiety for the selective detection of lithium ions. *Org Biomol Chem* **14**:3752–3757.
- Timmer RT and Sands JM (1999) Lithium intoxication. *J Am Soc Nephrol* **10**:666–674.
- Tsunoda SP, Wiesner B, Lorenz D, Rosenthal W, and Pohl P (2004) Aquaporin-1, nothing but a water channel. *J Biol Chem* **279**:11364–11367.
- Yool AJ, Morelle J, Cnops Y, Verbavatz JM, Campbell EM, Beckett EA, Booker GW, Flynn G, and Devuyt O (2013) AqF026 is a pharmacologic agonist of the water channel aquaporin-1. *J Am Soc Nephrol* **24**:1045–1052.
- Yool AJ, Stamer WD, and Regan JW (1996) Forskolin stimulation of water and cation permeability in aquaporin 1 water channels. *Science* **273**:1216–1218.

---

**Address correspondence to:** Andrea J. Yool, Adelaide Medical School, Helen Mayo South, Frome Road, University of Adelaide, Adelaide 5005 Australia. E-mail: andrea.yool@adelaide.edu.au

---



# Identification of Loop D Domain Amino Acids in the Human Aquaporin-1 Channel Involved in Activation of the Ionic Conductance and Inhibition by AqB011

Mohamad Kourghi, Michael L. De Ieso, Saeed Nourmohammadi, Jinxin V. Pei and Andrea J. Yool\*

Aquaporin Physiology and Drug Discovery Program, Adelaide Medical School, University of Adelaide, Adelaide, SA, Australia

## OPEN ACCESS

### Edited by:

Graça Soveral,  
Universidade de Lisboa, Portugal

### Reviewed by:

Eric Beitz,  
Christian-Albrechts-Universität zu Kiel,  
Germany  
Oscar Moran,  
Istituto di Biofisica (CNR), Italy

### \*Correspondence:

Andrea J. Yool  
andrea.yool@adelaide.edu.au

### Specialty section:

This article was submitted to  
Chemical Biology,  
a section of the journal  
Frontiers in Chemistry

Received: 15 February 2018

Accepted: 12 April 2018

Published: 27 April 2018

### Citation:

Kourghi M, De Ieso ML,  
Nourmohammadi S, Pei JV and  
Yool AJ (2018) Identification of Loop D  
Domain Amino Acids in the Human  
Aquaporin-1 Channel Involved in  
Activation of the Ionic Conductance  
and Inhibition by AqB011.  
Front. Chem. 6:142.  
doi: 10.3389/fchem.2018.00142

Aquaporins are integral proteins that facilitate the transmembrane transport of water and small solutes. In addition to enabling water flux, mammalian Aquaporin-1 (AQP1) channels activated by cyclic GMP can carry non-selective monovalent cation currents, selectively blocked by arylsulfonamide compounds AqB007 (IC<sub>50</sub> 170 μM) and AqB011 (IC<sub>50</sub> 14 μM). *In silico* models suggested that ligand docking might involve the cytoplasmic loop D (between AQP1 transmembrane domains 4 and 5), but the predicted site of interaction remained to be tested. Work here shows that mutagenesis of two conserved arginine residues in loop D slowed the activation of the AQP1 ion conductance and impaired the sensitivity of the channel to block by AqB011. Substitution of residues in loop D with proline showed effects on ion conductance amplitude that varied with position, suggesting that the structural conformation of loop D is important for AQP1 channel gating. Human AQP1 wild type, AQP1 mutant channels with alanines substituted for two arginines (R159A+R160A), and mutants with proline substituted for single residues threonine (T157P), aspartate (D158P), arginine (R159P, R160P), or glycine (G165P) were expressed in *Xenopus laevis* oocytes. Conductance responses were analyzed by two-electrode voltage clamp. Optical osmotic swelling assays and confocal microscopy were used to confirm mutant and wild type AQP1-expressing oocytes were expressed in the plasma membrane. After application of membrane-permeable cGMP, R159A+R160A channels had a significantly slower rate of activation as compared with wild type, consistent with impaired gating. AQP1 R159A+R160A channels showed no significant block by AqB011 at 50 μM, in contrast to the wild type channel which was blocked effectively. T157P, D158P, and R160P mutations had impaired activation compared to wild type; R159P showed no significant effect; and G165P appeared to augment the conductance amplitude. These findings provide evidence for the role of the loop D as a gating domain for AQP1 ion channels, and identify the likely site of interaction of AqB011 in the proximal loop D sequence.

**Keywords:** major intrinsic protein, MIP, AQP1, water channel, non-selective cation channel, cyclic GMP, arylsulfonamide

## INTRODUCTION

Aquaporins (AQPs) are a diverse family of channels for water and solutes, classified as major intrinsic proteins (MIPs) (Benga et al., 1986; Agre et al., 1993; Reizer et al., 1993). In mammals, classes of AQPs are differentially expressed in endothelial, epithelial and other cell types, and comprise key components of mechanisms for fluid homeostasis in single cells, barrier tissues, and organs (Nielsen et al., 1993; Boassa and Yool, 2005; Hachez and Chaumont, 2010). Some classes of aquaporin channels have been found shown to transport molecules other than water across the cell membrane, including glycerol, ammonia, urea, protons, as well as CO<sub>2</sub> and O<sub>2</sub> gases (Madeira et al., 2014; Kitchen et al., 2015), and ions (Yool, 2007; Yool and Campbell, 2012).

Aquaporin ion channel functions have been described for multiple members of the MIP family. Recent work has shown that a plant aquaporin channel (AtPIP2;1) serves as a non-selective cation channel that is sensitive to Ca<sup>2+</sup> and pH (Byrt et al., 2016), addressing a mystery regarding the molecular basis of a Ca<sup>2+</sup>-inhibited leak current known to be involved in environmental stress responses of roots (Demidchik and Tester, 2002). The insect aquaporin Big Brain (BIB) channel in *Drosophila* (Yanochko and Yool, 2002) and mammalian lens MIP (AQP0) have been characterized as ion channels (Zampighi et al., 1985; Ehring et al., 1990); their importance of these channels is evident from the consequences of genetic knockouts resulting in impaired nervous system development (Rao et al., 1992) and cataract formation (Berry et al., 2000), respectively. However the precise roles of their ion channel activities in cell signaling and development remain to be determined.

Controversy on the role of AQP1 as an ion channel, first proposed in 1996 (Yool et al., 1996), stemmed from a paradigm which stated AQP1 was nothing but a water channel (Tsunoda et al., 2004). An extensive body of work published since has shown: (i) AQP1 is a dual water and cation channel with a unitary conductance of 150 pS under physiological conditions, permeable to Na<sup>+</sup>, K<sup>+</sup>, and Cs<sup>+</sup>, and gated by the binding of cGMP at the intracellular loop D domain (Anthony et al., 2000; Yu et al., 2006). (ii) AQP1 carries water through the individual intra-subunit pores, whereas cations pass through the central pore of the tetramer (Yu et al., 2006; Campbell et al., 2012). (iii) Single channel activity of natively expressed AQP1 is selectively lost after small interfering knockdown of AQP1 expression (Boassa et al., 2006). (iv) The availability of AQP1 to be activated as an ion channel is regulated by tyrosine kinase phosphorylation of the carboxyl terminal domain (Campbell et al., 2012). (v) AQP1 ion channel properties are altered by site-directed mutagenesis of the central pore domain, which changes the cationic selectivity of the current, and creates a gain-of-function blocking site by Hg<sup>2+</sup> via introduction of a cysteine residue at the extracellular side (Campbell et al., 2012). (vi) Mutations of the carboxyl terminal domain of hAQP1 alter the efficacy of cGMP in activating the ionic conductance (Boassa and Yool, 2003). (vii) Molecular dynamic simulations confirmed it was theoretically feasible to move Na<sup>+</sup> ions through the AQP1 central pore and identified the

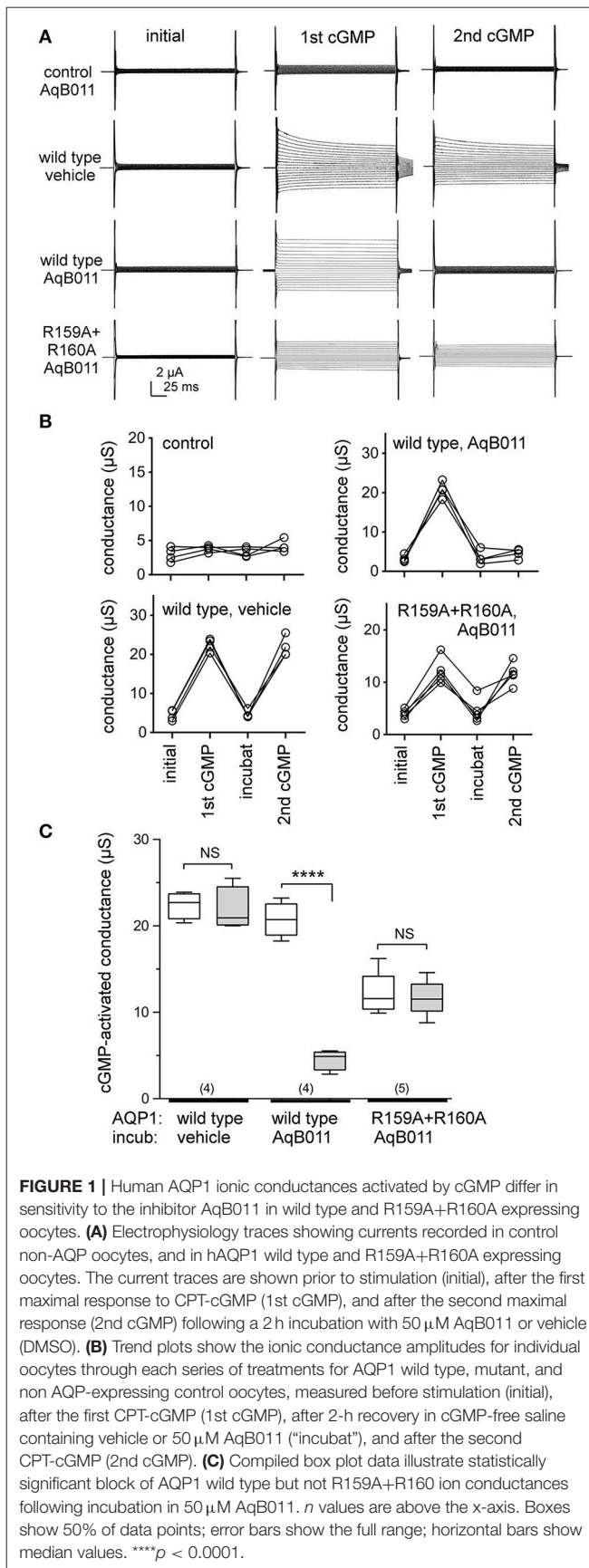
cytoplasmic loop D domain as involved in gating of the ion channel; mutation of key loop D residues impaired ion channel activation without preventing water channel activity (Yu et al., 2006).

The ability to change specific ion channel properties of activation, ion selectivity, and block using site-directed mutations of the AQP1 amino acid sequence have provided convincing evidence that AQP1 directly mediates the observed ionic current (Anthony et al., 2000; Boassa and Yool, 2003; Yu et al., 2006; Campbell et al., 2012). The alternative suggestion that responses were due to unidentified native ion channels translocated into the membrane along with AQP1 was ruled out by these studies, which showed that the altered ion channel functions associated with mutations of AQP1 did not prevent normal assembly and plasma membrane expression of AQP1 channels as evidenced by immunolabeling, western blot, and measures of osmotic water permeability.

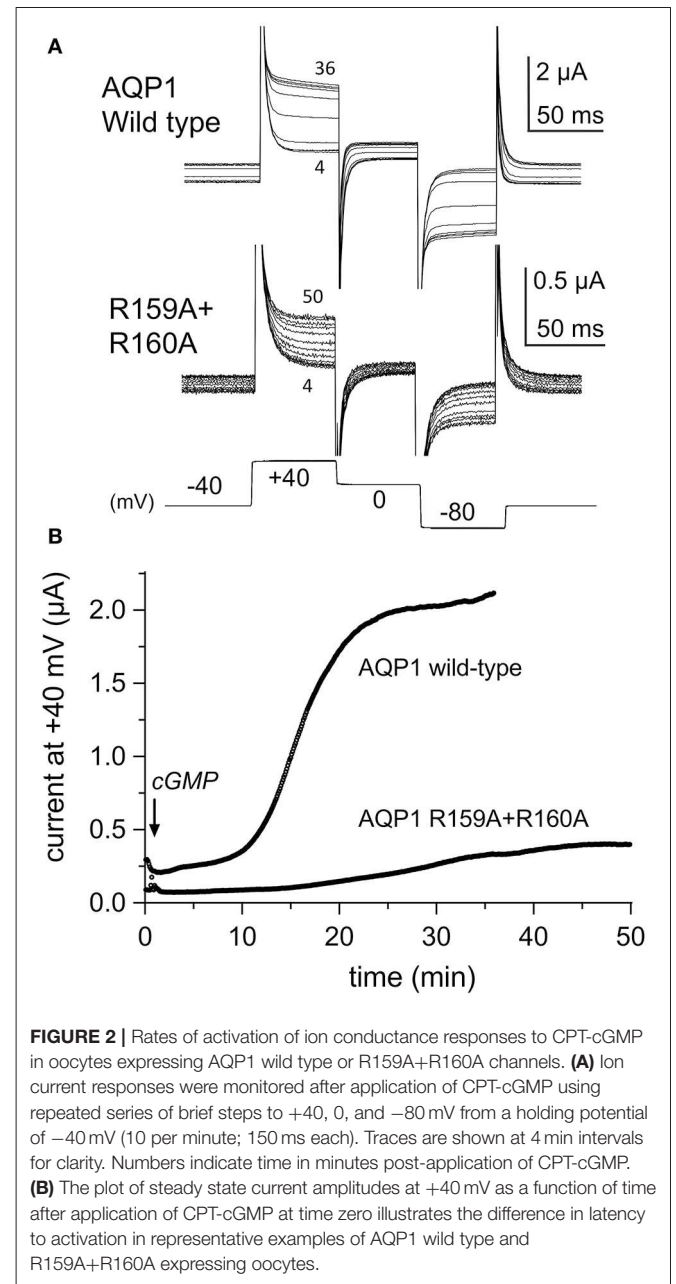
While the ion channel function of AQP1 was confirmed independently by other groups (Saparov et al., 2001; Zhang et al., 2007), the physiological relevance of AQP1 ion channel function remained uncertain, given the low proportion of ion conducting channels observed in reconstituted membrane assays. Mathematical modeling tested the premise, assuming only a tiny fraction of AQP1 acted as ion channels, and showed the predicted effects were sufficient for a meaningful impact on net transport in epithelial cells (Yool and Weinstein, 2002). Interestingly the relative amplitudes of ion currents and water fluxes for mammalian AQP6, also thought to be a dual water and ion channel (Yasui et al., 1999), were similar to those of AQP1, suggesting AQP6 similarly has a low proportion of functioning ion channels within the total population. Although high densities of water channels might be needed to move substantial fluid volumes, the apparently low ratios for aquaporins reinforce a basic concept in the ion channel field; relatively few charge-selective ion channels are needed to alter transmembrane voltage gradients (Hille, 2001).

With development of the first selective AQP1 ion channel inhibitor AqB011 (Kourghi et al., 2016), the question of the physiological function of the AQP1 ion channel could be directly addressed. Kourghi and colleagues showed AqB011 selectively inhibited migration in AQP1-expressing cancer cell lines, but not in those without AQP1, demonstrating that the AQP1 ion conductance can serve an essential role in cellular functions such as migration. Of the pharmacological inhibitors of AQP1 ion channel identified thus far, AqB011 is the most potent (IC<sub>50</sub> 14 μM). Osmotic water fluxes in hAQP1-expressing oocytes were not altered by 200 μM AqB011, indicating the block is selective for AQP1 ion channel activity. Molecular docking models suggested loop D domain as a candidate binding site for the AqB011 (Kourghi et al., 2016), but the prediction remained to be tested.

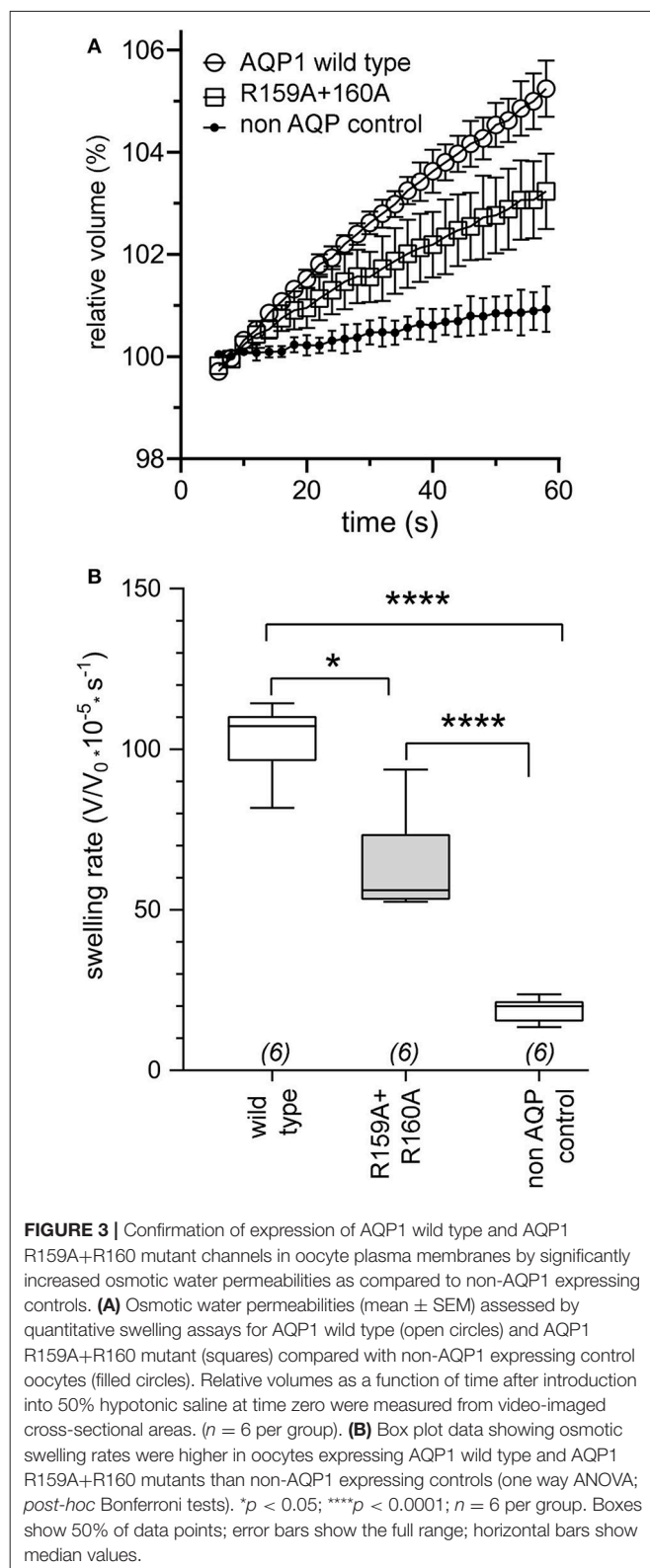
The role of AQP1 loop D residues in ion conductance activation and in mediating block by AqB011 was tested here using site-directed mutations of amino acids. Conserved arginine residues at positions 159 and 160 in human AQP1 were mutated to alanines. As compared with wild type, the cGMP-mediated activation of the AQP1 ionic conductance



response was significantly slower in R159A+R160A channels, the maximal amplitude of the activated current in the mutant construct was reduced as compared to wild type, and the mutant was insensitive to the inhibitor AqB011. Human AQP1 mutant constructs in which proline was substituted for conserved single residues threonine (T157P), aspartate (D158P), arginine (R159P, R160P), and glycine (G165P) showed differential effects on conductance activation depending on position, which suggested the conformation of loop D is important for AQP1 ion channel gating. Proline enables tight bends in peptide structures (Vanhoof et al., 1995). These results support the role of conserved loop D residues in AQP1 ion channel activation and inhibition



by AqB011, and provide further support for the concept that loop D is a gating domain for the AQP1 central ion pore.



## MATERIALS AND METHODS

### Oocyte Preparation and Injection

Unfertilized oocytes were harvested by partial ovariectomy from anesthetized *Xenopus laevis* frogs following national guidelines (Australian Code of Practice for the Care and Use of Animals for Scientific Purposes), and approved by the University of Adelaide Animal Ethics Committee (approval # M2013-167). Oocytes were defolliculated with collagenase (type 1A, 1 mg/ml; Sigma-Aldrich, St. Louis, MO) in the presence of trypsin inhibitor (0.05 mg/ml; Sigma-Aldrich, St. Louis, MO) for 1 to 1.5 h in OR-2 saline (96 mM NaCl, 2 mM KCl, 5 mM MgCl<sub>2</sub>, penicillin 100 units/ml, streptomycin 0.1 mg/ml, and 5 mM HEPES; pH 7.6). Oocytes were then washed 4 times with OR-2 saline at  $\sim 10$  min intervals, and kept at 16–18°C in isotonic Frog Ringers saline [96 mM NaCl, 2 mM KCl, 5 mM MgCl<sub>2</sub>, 0.6 mM CaCl<sub>2</sub>, 5 mM HEPES buffer, horse serum (5%; Sigma-Aldrich, St. Louis, MO), penicillin 100 units/ml streptomycin 0.1 mg/ml, and tetracycline 0.5 mg/ml, pH 7.6]. Oocytes were injected with 50 nl of water (control oocytes), or 50 nl of water containing 1 ng of AQP1 wild type cRNA, or 2 ng of AQP1 mutant cRNAs. Oocytes were then transferred to sterile dishes containing Frog Ringers saline and incubated at 16–18°C for 48 h or more to allow time for protein expression. Isotonic Na<sup>+</sup> saline used for electrophysiology and osmotic swelling assays contained (in mM): NaCl 96 mM, KCl 2 mM, MgCl<sub>2</sub> 5 mM, CaCl<sub>2</sub> 0.6 mM, and HEPES 5 mM, pH 7.3, without antibiotics or serum.

### Site Directed Mutagenesis of AQP1

Site-directed mutations were generated in human AQP1 cDNA in the *Xenopus* expression vector (pXBGev), using the QuikChange site-directed mutagenesis kit (Agilent Technologies, Forest Hills, VIC, Australia) with custom-synthesized primers as described previously (Yu et al., 2006). The correct sequences of the constructs were confirmed by replicate DNA sequencing of the full-length cDNA constructs. Wild-type AQP1 and mutant cDNAs were linearized using BamHI and transcribed with T3 RNA polymerase using the mMessage mMachine kit (Ambion, Austin, TX).

### Osmotic Swelling Assays and Confocal Microscopy

Swelling assays or confocal microscopy were used to confirm AQP1 wild type and mutant channels were expressed in oocyte plasma membranes. Swelling assays were performed in 50% hypotonic saline (isotonic Na<sup>+</sup> saline diluted with equal volume of water). Prior to swelling assays the control (non-AQP expressing), AQP1 wild type and AQP1 mutant expressing oocytes were rinsed in isotonic saline (without horse serum or antibiotics) for 10 min. Rates of swelling were imaged using a grayscale camera (Cohu, San Diego, CA) fixed on a dissecting microscope (Olympus SZ-PT; Olympus, Macquarie Park, Australia), and images were captured at 0.5 Hz using Image J software from National Institutes of Health (<http://rsbweb.nih.gov/ij/>). Swelling rates were determined from slope values of linear regression fits of relative volume as a function of time using Prism (GraphPad Software Inc., San

Diego, CA). For confocal microscopy, oocytes were fixed in 4% paraformaldehyde, permeabilized with 0.1% Triton X-100, and incubated with rabbit polyclonal anti-AQP1 antibody (provided by WD Stamer; Duke University, USA) diluted in buffered solution with 300 mM NaCl, 30 mM Na citrate, 1% bovine serum albumin, 0.05% TritonX-100, and 0.02% sodium azide. After secondary labeling with FITC-conjugated goat anti-rat antibody, preparations were imaged with a Leica (Nussloch, Germany) TCS-4D laser scanning confocal microscope.

## Electrophysiological Recordings

Two-electrode voltage clamp recordings were performed at room temperature in standard isotonic Na<sup>+</sup> saline using a GeneClamp amplifier and Clampex 9.0 software (pClamp 9.0 Molecular Devices, Sunnyvale, CA, USA). Data were filtered at 2 kHz and stored to hard disk for analysis. Capillary glass pipettes (~1 MΩ) were filled with 1 M KCl. Initial conductance values were determined from current-voltage relationships measured prior to cGMP stimulation, by application of the nitric oxide donor sodium nitroprusside (SNP) at a final concentration of 7.5 mM, or by application of membrane permeable CPT-cGMP(8-(4-chlorophenylthio)-guanosine-3',5'-cyclic monophosphate) at a final concentration of 10 μM, as per published methods (Boassa and Yool, 2003; Campbell et al., 2012). From a holding potential of -40, voltage steps from +60 to -110 mV were applied to measure conductance. Repeated steps to +40 mV at 6 s intervals were used to monitor changes in ion current responses as a function of time after application of an activator or inhibitor.

For the studies of pharmacological inhibition by AqB011, after recording the conductance for the first response to CPT-cGMP, oocytes were transferred into isotonic Na<sup>+</sup> saline with either AqB011 or vehicle for 2 h. Incubation allowed recovery to initial conductance levels as well as time for AqB011 to cross the membrane to reach its intracellular site of action, as described previously (Kourghi et al., 2016). Recovery from block was very slow, taking hours after removal of the agent from the extracellular medium. Oocytes were then re-evaluated for responsiveness to a second application of CPT-cGMP to test for inhibition post-incubation without AqB011 present. AqB011 was synthesized by G Flynn (SpaceFill Enterprises LLC, Bozeman Montana USA) with preparation methods and chemical structure as previously published (Kourghi et al., 2016). AqB011 was prepared as a 1000x stock solution in the vehicle dimethylsulfoxide (DMSO) and diluted in recording saline to the final concentration; vehicle control saline was made with the equivalent amount of DMSO (0.1% V/V). Box plot histograms show 50% of data (boxes), the full range of data (error bars), and the median value (horizontal bar).

## RESULTS

### Reduced Sensitivity to Block by AqB011 in AQP1 R159A+R160A Channels

Voltage clamp recordings showed that application of extracellular CPT-cGMP activated ionic conductance responses in human AQP1 wild type and R159A+R160A mutant

GenBank ID	amino acid sequence	Genus; Common name
AAH22486.1	154 ATD <b>RRRR</b> DLGG <b>SAP</b> LAIGLSVALGH	180 <i>Homo</i> ; Human
AAH07125.1	154 ATD <b>RRRR</b> DLGG <b>SAP</b> LAIGLSVALGH	180 <i>Mus</i> ; Mouse
AAB46624.1	154 ATD <b>RRRR</b> DLGG <b>SAP</b> LAIGLSVALGH	180 <i>Rattus</i> ; Rat
XP_014989258.1	154 ATD <b>RRRR</b> DLGG <b>SAP</b> LAIGLSVALGH	180 <i>Macaca</i> ; Rhesus macaque
XP_012496173.1	154 ATD <b>RRRR</b> DLGG <b>SAP</b> LAIGLSVALGH	180 <i>Propithecus</i> ; Crowned sifaka
XP_012330551.1	154 ATD <b>RRRR</b> DLGG <b>SAP</b> LAIGLSVALGH	180 <i>Aotus</i> ; Night monkey
XP_008583141.1	154 ATD <b>RRRR</b> DLGG <b>SAP</b> LAIGLSVALGH	180 <i>Galeopterus</i> ; Malayan flying lemur
XP_005319226.1	154 ATD <b>RRRR</b> DLGG <b>SAP</b> LAIGLSVALGH	180 <i>Ictidomys</i> ; Thirteen lined ground squirrel
XP_022439712.1	156 ATD <b>RRRR</b> DLGG <b>SAP</b> LAIGLSVALGH	182 <i>Delphinapteru</i> ; Beluga whale
XP_010969922.1	156 ATD <b>RRRR</b> DL <b>SGSG</b> PLAIGLSVALGH	182 <i>Camelus</i> ; Bactrian camel
XP_005981267.1	156 ATD <b>RRRR</b> DL <b>GGSG</b> PLAIG <b>FS</b> VALGH	182 <i>Pantholops</i> ; Tibetan antelope
NP_777127.1	156 ATD <b>RRRR</b> DL <b>GGSG</b> PLAIG <b>FS</b> VALGH	182 <i>Bos</i> ; Cow
CAD92027.1	148 ATD <b>KRRR</b> D <b>VT</b> GSAPLAIGLSVALGH	173 <i>Anguilla</i> ; European eel
BAC82110.1	148 ATD <b>KRRR</b> D <b>VT</b> GSAPLAIGLSVALGH	173 <i>Anguilla</i> ; Japanese eel
ASW16810.1	144 ATD <b>KRRR</b> D <b>VAGS</b> APLAIGLSVALGH	169 <i>Coilia</i> ; Grenadier anchovy
AIL02123.1	144 ATD <b>KRRR</b> D <b>VT</b> GSAPLAIGLSVALGH	169 <i>Alosa</i> ; Alewife (herring)
NP_996942.1	145 ATD <b>KRRR</b> D <b>VSGS</b> APLAIGLSV <b>CL</b> GH	171 <i>Danio</i> ; Zebrafish
XP_020322871.1	147 <b>AV</b> D <b>KRRR</b> D <b>IT</b> GSAPLAIGLSVALGH	172 <i>Oncorhynchus</i> ; Coho salmon
XP_013996040.1	147 <b>AV</b> D <b>KRRR</b> D <b>VT</b> GSAPLAIGLSVALGH	172 <i>Salmo</i> ; Atlantic salmon
XP_007242700.2	148 <b>AA</b> T <b>D</b> K <b>RRR</b> D <b>VMGS</b> VPLAIGLSVALGH	174 <i>Astyanax</i> ; Blind cavefish
XP_016109136.1	146 ATD <b>KRRR</b> D <b>VT</b> GSAPLAIGLSV <b>CL</b> GH	171 <i>Sinocyclocheilus</i> ; Golden line fish
XP_015474877.1	156 ATD <b>RRRR</b> <b>NDVSGS</b> APLAIGLSVALGH	182 <i>Parus</i> ; Great tit
KQK77783.1	156 ATD <b>RRRR</b> <b>NDVSGS</b> APLAIGLSVALGH	182 <i>Amazona</i> ; Blue-fronted parrot
XP_013808479.1	156 ATD <b>RRRR</b> <b>NDVSGS</b> APLAIGLSVALGH	182 <i>Apteryx</i> ; Brown kiwi
XP_009878414.1	156 ATD <b>RRRR</b> <b>NDVSGS</b> APLAIGLSVALGH	182 <i>Charadrius</i> ; Killdeer (plover)

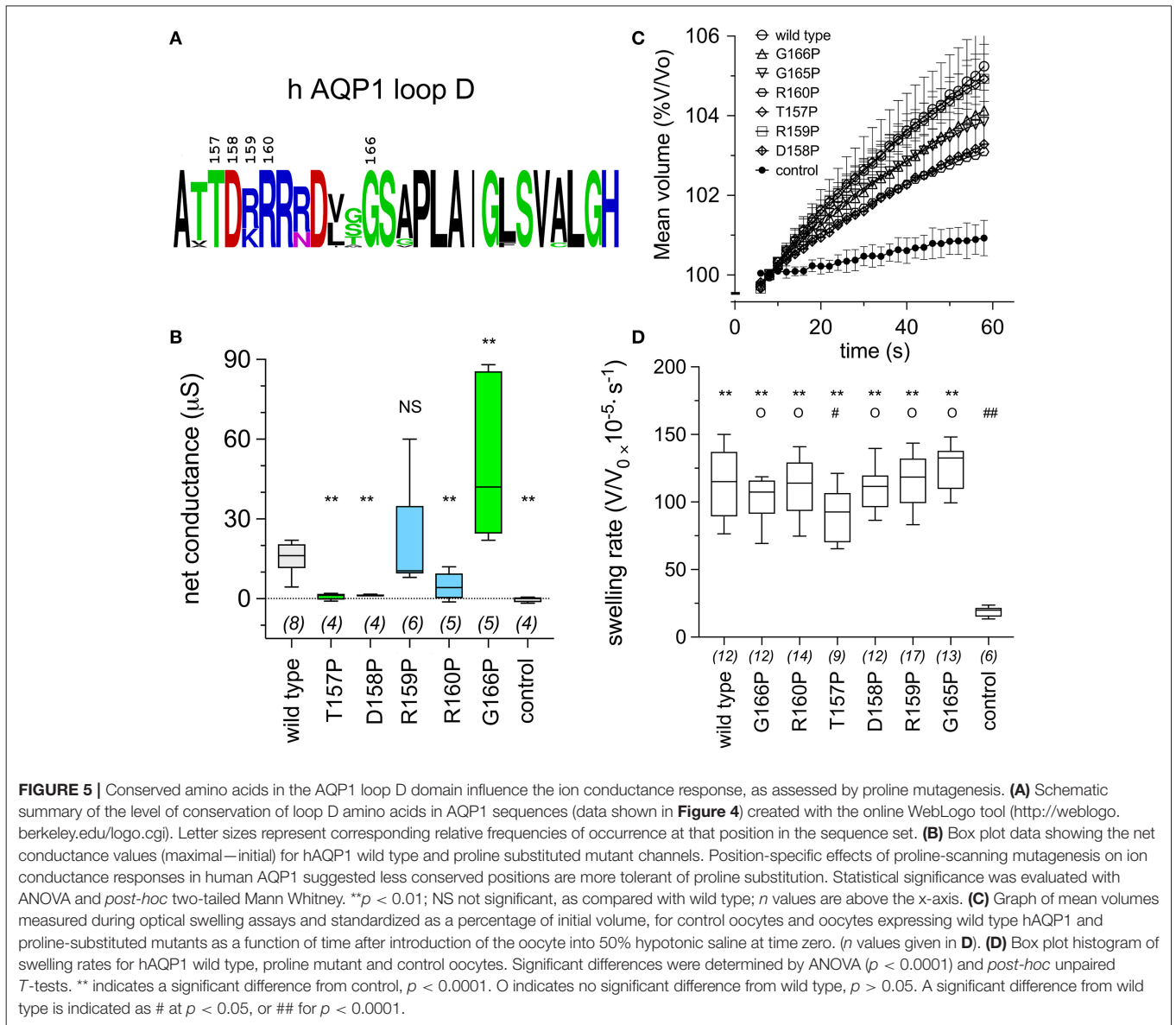
**FIGURE 4 |** Amino acid sequence alignment for the loop D and flanking domains of AQP1 channels from diverse classes of vertebrates (mammals, fish, and birds). Amino acid sequences downloaded from the National Center for Biotechnology Information (NCBI) Protein database ([www.ncbi.nlm.nih.gov/protein](http://www.ncbi.nlm.nih.gov/protein)) were aligned using the NCBI BlastP online application ([blast.ncbi.nlm.nih.gov](http://blast.ncbi.nlm.nih.gov)) for multiple sequences. Residues in black are identical with the query sequence *Homo sapiens* AQP1. Variations in sequence are highlighted in red.



expressing oocytes (**Figure 1A**). Initial recordings measured before the application of CPT-cGMP showed uniformly low currents, comparable to those of non-AQP control oocytes. The ionic conductance increased after application of CPT-cGMP in AQP1 wild type and R159A+R160A expressing oocytes, but in not non-AQP control oocytes. After recording the first response, oocytes were transferred into isotonic  $\text{Na}^+$  saline with  $50 \mu\text{M}$  AqB011 or vehicle. **Figure 1B** shows trend plots of the conductance responses of individual oocytes through each series of treatments. After 2 h incubation, the ionic conductance responses recovered to initial levels, and a second application of CPT-cGMP was used to assess the level of reactivation of current (**Figures 1A,B**). CPT-cGMP activated currents were not observed in non-AQP expressing control oocytes. **Figure 1C** shows compiled box plot data for the ionic conductance values for human AQP1 wild type and R159A+R160A mutants. AQP1

wild type currents were strongly blocked after incubation in AqB011 but not after incubation with vehicle. The amplitude of maximal activation was lower in R159A+R160A mutant-expressing oocytes than wild type, and the R159A+R160A conductance was not sensitive to block by AqB011.

The recovery of the AQP1 wild type and mutant currents to baseline levels during the incubation period demonstrated that the responses were reversible, thus not due to oocyte damage or leak. Complete reactivation of wild type ionic conductance response to the second application of CPT-cGMP (after incubation in saline with vehicle) demonstrated that prior activation did not impair responsiveness of the AQP1-expressing oocytes to subsequent stimulation. AQP1 wild type-expressing oocytes incubated in saline with AqB011 were not re-activated by a second application of CPT-cGMP, confirming inhibition of the ion current as described previously



(Kourghi et al., 2016). In contrast, the AQP1 R159A+R160A mutant channels showed no change in the second response to CPT-cGMP after incubation with or without AqB011, showing that sensitivity to the inhibitor was eliminated by the altered loop D sequence. The insensitivity of the R159A+R160A current furthermore demonstrated that the observed pharmacological block of wild type current by AqB011 cannot readily be ascribed to off-target effects on native oocyte channels or transporters, confirming the specificity of action of the antagonist compound.

### Increased Latency to Activation for AQP1 R159A+R160A Channels

The conductance responses of wild type and R159A+R160A mutant channels differed in rates of activation after application of CPT-cGMP. Oocytes expressing AQP1 wild type activated more rapidly and reached a higher maximal current amplitude that did those expressing AQP1 R159A+R160A channels (Figure 2A). In wild type, the maximal response was reached by ~20–30 min after application of CPT-cGMP, whereas 50–60 min was needed

for R159A+R160A expressing oocytes (Figure 2B). The latency to the onset of activation was considerably slower for the mutant construct. The long latency for R159A+R160A was consistent with prior work which reported no appreciable activation of the R159A+R160A mutant channels when assessed over a short time frame (within 8 min after application of the nitric oxide donor, sodium nitroprusside, which was used to stimulate endogenous oocyte cGMP production, and successfully activated AQP1 wild type ion currents) (Yu et al., 2006).

### Osmotic Water Permeability of AQP1 Wild Type and R159A+R160A Expressing Oocytes

Osmotic water permeability data (Figure 3A) confirmed successful expression of wild type and R159A+R160A mutant AQP1 channels in oocyte plasma membranes. The water channel activities of AQP1 wild type and R159A+R160A expressing oocytes were both significantly greater than those of non-AQP1 expressing control oocytes (Figure 3B), confirming that both AQP1 channel types were expressed, assembled, and trafficked to the plasma membrane of oocytes. Expression levels for the R159A+R160A mutant channels estimated by osmotic water permeability were ~10% lower than wild type; however the mean conductance response in the arginine double mutant (Figure 1C) was half that of wild type, consistent with impairment of channel activation.

### Effects of Proline Mutagenesis of the Loop D Amino Acid Sequence

Proline substituted mutant channels showed significant differences in response amplitudes that correlated with the degree of conservation of the amino acid residue in the loop D sequence. Sequence alignments for loop D and flanking domains illustrate the high level of identity for amino acids in AQP1 gene coding sequences from a diverse array of vertebrates, including mammals, fish, and birds (Figure 4). Net conductances, measured from amplitudes of the ionic conductance response, were calculated as the difference between the initial level and the final amplitude after SNP-mediated cGMP stimulation (Figure 5). Wild type AQP1 channels showed activation in response to SNP stimulation (Figure 5B) that was comparable in amplitude to that seen after application of CPT-cGMP (Figure 1). Control non-AQP-expressing oocytes showed no appreciable response. However, significantly impaired responses were seen for oocytes expressing AQP1 T157P, D158P, and R160P mutant channels (Figure 5B). T157, D158, and R160 residues exhibit complete identity across AQP1 sequences from diverse animals (Figure 5A). In contrast, AQP1 R159P expressing oocytes showed no significant difference from AQP1 wild type, which could fit with the observation that slightly more variation in amino acid sequence appears to be tolerated at that position. Interestingly, a significant difference also was observed for mutation to proline at the highly conserved G166, but the result was to promote rather than inhibit the activation of the conductance response as compared to wild type. The expression of functional channels in the oocyte membrane was confirmed

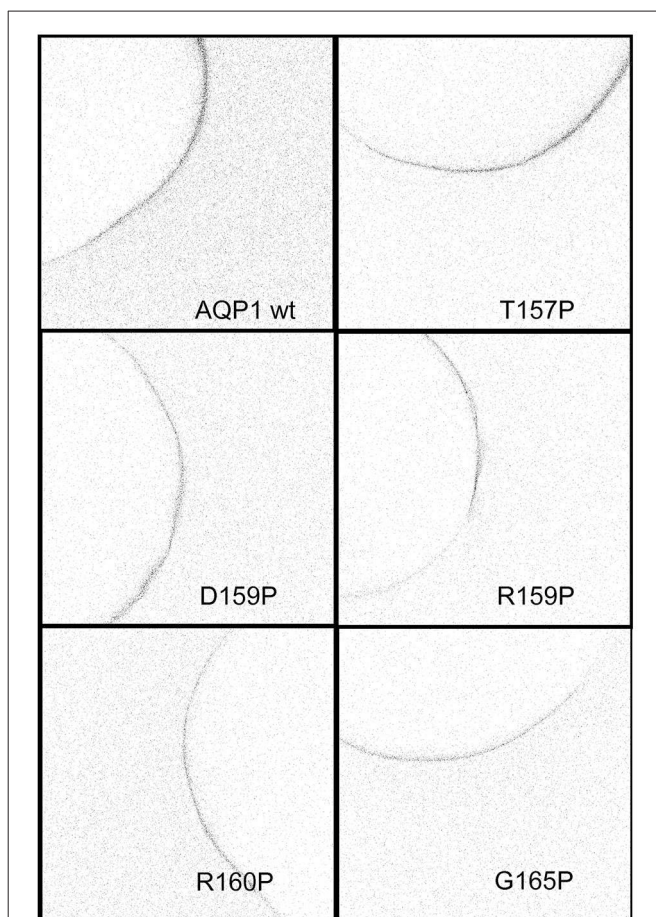


**FIGURE 6** | Confocal images of anti-AQP1 immunolabeled oocytes expressing wild type and proline substituted mutant channels confirmed protein expression in the oocyte plasma membrane. See Methods for details.

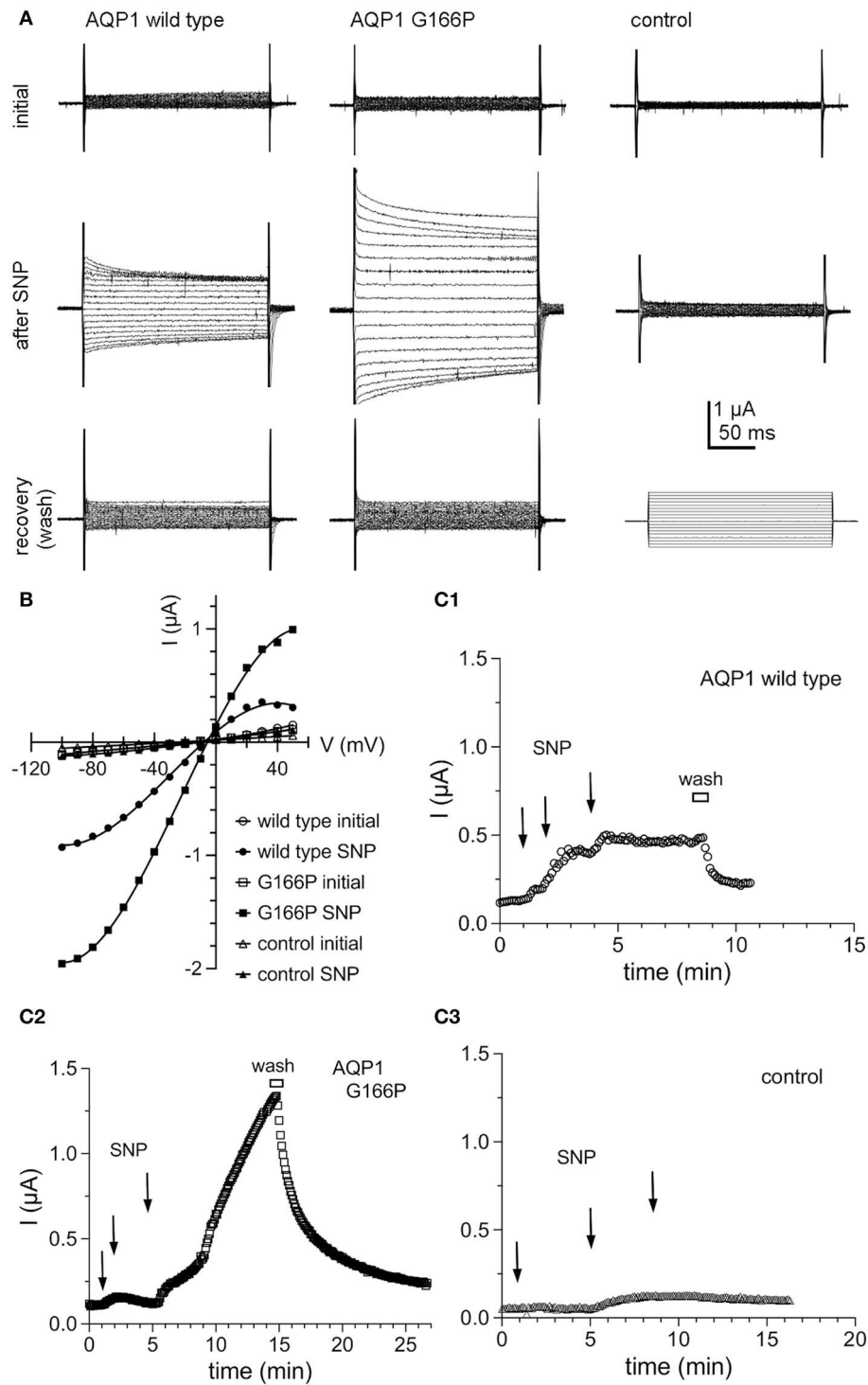


**FIGURE 7 |** Ion conductance responses of oocytes expressing human AQP1 wild type and G166P channels. **(A)** Currents recorded from wild type (left), G166P (middle), and non-AQP expressing control oocytes (right) by two-electrode voltage clamp before (initial) and after stimulation of intracellular cyclic GMP by application of the nitric oxide donor, sodium nitroprusside at a final concentration of 7.5 mM (after SNP). Perfusion of fresh bath saline without SNP (wash) promoted rapid recovery. **(B)** Current voltage relationships for the traces shown in **(A)**. **(C)** Steady state current amplitudes at +40 mV monitored as a function of time after three sequential applications of SNP (2.5 mM each) at times indicated by arrows, and after perfusion of bath saline without SNP (wash) shown by the horizontal bar, for wild type **(C1)**, G166P **(C2)**, and control **(C3)** oocytes. Data are from the same oocytes as shown in **(A)**.

by the demonstration of high osmotic water permeabilities for all the proline mutant constructs that were significantly greater than that of the non-AQP-expressing controls (Figures 5C,D). Confocal images of oocytes expressing AQP1 wild type and proline mutant channels confirmed that the constructs were expressed in the oocyte plasma membrane (Figure 6).

The conductance properties of AQP1 G166P-expressing oocytes, as compared with wild type and non-AQP control oocytes, are summarized in Figure 7. The ion conductance responses of AQP1 wild type and G166P-expressing oocytes showed an increase in amplitude but not in apparent kinetics (Figure 7A), reversal potential (Figure 7B), latency to activation, or reversibility of the responses after bath washout with fresh saline to remove SNP (Figure 7C). Control oocytes showed negligible responses to SNP (Figures 7A,B).

## DISCUSSION

The aim of this study was to evaluate a candidate binding site for the AQP1 ion channel antagonist AqB011 suggested from prior *in silico* modeling, and to test the role of the intracellular loop D domain in AQP1 ion channel activation. Discovery of pharmacological tools for AQPs has been an area of keen interest for many years (Huber et al., 2012). As illustrated by the

diagram in Figure 8, AQP1 ion channels are proposed to conduct solutes and water through pharmacologically distinct pathways (Saparov et al., 2001; Yool et al., 2002), with water transport mediated through the individual pores of the subunits (Jung et al., 1994), and ion transport proposed to be mediated by the central pore of the tetramer following activation by intracellular cGMP (Anthony et al., 2000; Yool and Weinstein, 2002; Campbell et al., 2012). The water channel function of hAQP1 is modulated by antagonists such as mercurial compounds (Preston et al., 1993); gold and silver compounds (Niemietz and Tyerman, 2002); the arylsulfonamide AqB013 (Migliati et al., 2009); medicinal herb compounds bacopasides I and II (Pei et al., 2016); aromatic carboxylic acid blockers referred to as CPD 1, 2, and 3 (Seeliger et al., 2013); and by agonist compounds such as AqF026 (Yool et al., 2013). Other inhibitors include TGN-020 for AQP4 (Igarashi et al., 2011), and gold-bipyridyl compounds for AQP3 (Martins et al., 2013; Graziani et al., 2017). The human AQP1 ion channel is pharmacologically distinct from the water pore, supporting the involvement of a separate pathway for ions through the central pore of the tetramer (Figure 8). The AQP1 ion pore is blocked by  $\text{Cd}^{2+}$  (Boassa et al., 2006), other divalent cations (Kourghi et al., 2017b), and arylsulfonamide compounds AqB007 and AqB011 (Kourghi et al., 2016).

AqB011 inhibits the human AQP1 ion current but not the water flux, and slows the migration of AQP1-expressing human colon cancer cells (Kourghi et al., 2016). Molecular docking studies suggested that AqB011 might interact with a conserved arginine residues located on loop D domain of AQP1, a region that has been suggested to be involved in gating of the central pore of the AQP1 channel (Yu et al., 2006). The role of the conserved loop D domain was tested using a mutant construct of the AQP1 channel in which the positively charged arginine residues in positions 159 and 160 of the human AQP1 amino acid sequence were replaced with alanine. The mutation R159A+R160A did not prevent the channel from being expressed on the membrane of oocytes, as demonstrated by measured osmotic water permeability. The hAQP1 R159A+R160A channel had previously been thought to be non-functional as an ion channel (Yu et al., 2006). However, work here showed the R159A+R160A ion conductance was activated by CPT-cGMP albeit at a significantly slower rate, to a lower maximal amplitude, and with a longer latency than for AQP wild type channels, which would have made it difficult to detect in protocols used previously. Nonetheless the residual ion channel function in the R159A+R160A mutant was significantly greater than in non-AQP controls and was sufficient to allow evaluation of a possible difference in sensitivity to block by AqB011.

The ion conductance in wild type AQP1 expressing oocytes was significantly inhibited by AqB011, confirming prior work (Kourghi et al., 2016). In contrast, AqB011 had no effect on the ion conductance response in R159A+R160A expressing oocytes. These results provide evidence that AqB011 is acting directly on the AQP1 channel, and not indirectly through hypothetical native oocyte channels or transporters associated with AQP1 proteins. The plant AQP AtPIP2;1 is a dual ion and water channel which also is insensitive to AqB011 (Kourghi et al., 2017b).

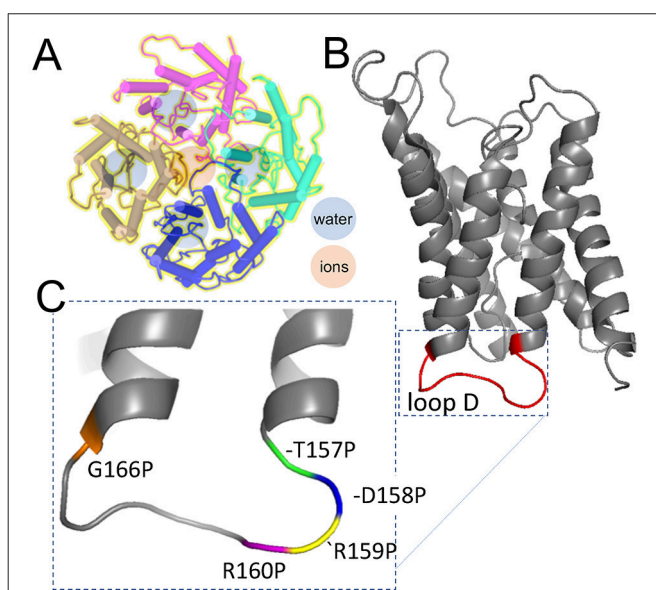


**FIGURE 8 |** Schematic diagrams illustrating the separate pathways proposed to mediate water and ion transport in the AQP1 tetrameric channel, and the position of the mutations tested in the loop D domain by proline mutagenesis. **(A)** AQP1 channels assemble as homomeric tetramers in the membrane bilayer. Water pores (blue) are located in each subunit; cations are thought to permeate via the central pore at the four-fold axis of symmetry in the channel (rose). **(B)** Loop D is a cytoplasmic loop between the 4 and 5th transmembrane domains in each subunit; loops D in the tetramer surround the central pore. **(C)** Amino acid residues in loop D tested by mutation to proline. Structural data used to create the diagrams were downloaded from the NCBI Structure database ([www.ncbi.nlm.nih.gov/structure/](http://www.ncbi.nlm.nih.gov/structure/)), for PDB ID 1IH5 human AQP1 (Ren et al., 2001); and PDB 1JN4 bovine AQP1 (Sui et al., 2001).

AtPIP2;1 has many amino acid sequence differences as compared to AQP1, but these include the absence of the poly-arginine series in loop D. Together these data suggest that selective pharmacological targeting of different classes of aquaporin ion channels will be possible, as structure-activity data for active agents continues to accrue, and discovery of new agents expands the tools available for evaluating physiological roles of dual water and ion channels in the MIP family.

Proline scanning mutagenesis was used here to assess the role of the loop D domain in activation of the AQP1 ion conductance. Scanning mutagenesis is a method for analyzing the functional roles of amino acid residues in proteins by systematic replacement with another amino acid, such as alanine, cysteine, or proline (Cunningham and Wells, 1989; Kürz et al., 1995; Patel et al., 2013). Alanine is compact, lacking a bulky side group, and preserves 3D structure without influencing electrostatic characteristics (Cunningham and Wells, 1989). Alternatively, conformational structure can be deliberately altered by substituting residues with proline, which is distinctive in having the nitrogen atom covalently bound in a 5-membered ring, which impairs formation of intermolecular hydrogen bonds (Williams and Deber, 1991), and introduces “kinks” in secondary structure (Barlow and Thornton, 1988; Woolfson and Williams, 1990; Sankararamakrishnan and Vishveshwara, 1992). Proline scanning mutagenesis has been used to investigate gating mechanisms of ion channels such as the inward rectifier and transient receptor potential (TRP) channels (Sadja et al., 2001; Jin et al., 2002). Sadja et al. (2001) showed proline substitution in the second transmembrane domain of G-protein-coupled inwardly rectifying potassium channels shifted the channels into an active conformation, suggesting the site for G $\beta\gamma$  mediated gating. Dong et al. (2009) showed proline substitutions in the fifth transmembrane domain of TRPML1

ion channels locked the channels in an active state, which similarly allowed definition of the site of cation conductance gating. Proline scanning mutagenesis used here showed that the AQP1 cation channel is sensitive to mutations capable of altering the structure of the loop D domain, with both down- and upregulation of channel activity observed depending on the location of the mutation in the conserved amino acid sequence (Figure 8).

In sum, results here support the hypothesis that interaction of the inhibitor AqB011 depends on the structure of the loop D domain of the AQP1 channel, and that this domain is important for AQP1 ion channel gating. Aquaporin channels are more than simple pathways for the passive flux of water and glycerol. As a group they are increasingly being found to include highly specialized, regulated, multifunctional channels with diverse roles across the kingdoms of life (Gomes et al., 2009; Kourghi et al., 2017a). Results here contribute to understanding the structural basis for gating and pharmacological block of the human AQP1 ion channel, and add further evidence supporting the role of the central pore as the pathway for ion flux in human AQP1.

## AUTHOR CONTRIBUTIONS

MK, JP, and AY: Participated in the research design. MK, SN, JP, and AY: Conducted experiments and performed data analysis. MK, MD, and AY: Wrote the manuscript. MK, MD, SN, JP, and AY: Reviewed and edited the manuscript.

## FUNDING

Funding support for this research was provided by the Australian Research Council, grant DP160104641.

## REFERENCES

- Agre, P., Preston, G. M., Smith, B. L., Jung, J. S., Raina, S., Moon, C., et al. (1993). Aquaporin CHIP: the archetypal molecular water channel. *Am. J. Physiol.* 265, F463–F476. doi: 10.1152/ajprenal.1993.265.4.F463
- Anthony, T. L., Brooks, H. L., Boassa, D., Leonov, S., Yanocho, G. M., Regan, J. W., et al. (2000). Cloned human aquaporin-1 is a cyclic GMP-gated ion channel. *Mol. Pharmacol.* 57, 576–588. doi: 10.1124/mol.57.3.576
- Barlow, D. J., and Thornton, J. M. (1988). Helix geometry in proteins. *J. Mol. Biol.* 201, 601–619. doi: 10.1016/0022-2836(88)90641-9
- Benga, G., Popescu, O., Pop, V. I., and Holmes, R. P. (1986). p-(Chloromercuri)benzenesulfonate binding by membrane proteins and the inhibition of water transport in human erythrocytes. *Biochemistry* 25, 1535–1538. doi: 10.1021/bi00355a011
- Berry, V., Francis, P., Kaushal, S., Moore, A., and Bhattacharya, S. (2000). Missense mutations in MIP underlie autosomal dominant ‘polymorphic’ and lamellar cataracts linked to 12q. *Nat. Genet.* 25, 15–17. doi: 10.1038/75538
- Boassa, D., Stamer, W. D., and Yool, A. J. (2006). Ion channel function of aquaporin-1 natively expressed in choroid plexus. *J. Neurosci.* 26, 7811–7819. doi: 10.1523/JNEUROSCI.0525-06.2006
- Boassa, D., and Yool, A. J. (2003). Single amino acids in the carboxyl terminal domain of aquaporin-1 contribute to cGMP-dependent ion channel activation. *BMC Physiol.* 3:12. doi: 10.1186/1472-6793-3-12
- Boassa, D., and Yool, A. J. (2005). Physiological roles of aquaporins in the choroid plexus. *Curr. Top. Dev. Biol.* 67, 181–206. doi: 10.1016/S0070-2153(05)67005-6
- Byrt, C. S., Zhao, M., Kourghi, M., Bose, J., Henderson, S. W., Qiu, J., et al. (2016). Non-selective cation channel activity of aquaporin AtPIP2;1 regulated by Ca<sup>2+</sup> and pH. *Plant Cell Environ.* 40, 802–815. doi: 10.1111/pce.12832
- Campbell, E. M., Birdsell, D. N., and Yool, A. J. (2012). The activity of human aquaporin 1 as a cGMP-gated cation channel is regulated by tyrosine phosphorylation in the carboxyl-terminal domain. *Mol. Pharmacol.* 81, 97–105. doi: 10.1124/mol.111.073692
- Cunningham, B. C., and Wells, J. A. (1989). High-resolution epitope mapping of hGH-receptor interactions by alanine-scanning mutagenesis. *Science* 244, 1081–1085. doi: 10.1126/science.2471267
- Demidchik, V., and Tester, M. (2002). Sodium fluxes through nonselective cation channels in the plasma membrane of protoplasts from Arabidopsis roots. *Plant Physiol.* 128, 379–387. doi: 10.1104/pp.010524
- Dong, X.-P., Wang, X., Shen, D., Chen, S., Liu, M., Wang, Y., et al. (2009). Activating mutations of the TRPML1 channel revealed by proline-scanning mutagenesis. *J. Biol. Chem.* 284, 32040–32052. doi: 10.1074/jbc.M109.037184
- Ehring, G. R., Zampighi, G., Horwitz, J., Bok, D., and Hall, J. E. (1990). Properties of channels reconstituted from the major intrinsic protein of lens fiber membranes. *J. Gen. Physiol.* 96, 631–664. doi: 10.1085/jgp.96.3.631
- Gomes, D., Agasse, A., Thiébaud, P., Delrot, S., Gerós, H., and Chaumont, F. (2009). Aquaporins are multifunctional water and solute transporters highly divergent in living organisms. *Biochim. Biophys. Acta* 1788, 1213–1228. doi: 10.1016/j.bbame.2009.03.009

- Graziani, V., Marrone, A., Re, N., Coletti, C., Platts, J. A., and Casini, A. (2017). A multi-level theoretical study to disclose the binding mechanisms of gold(III)-bipyridyl compounds as selective aquaglyceroporin inhibitors. *Chemistry* 23, 13802–13813. doi: 10.1002/chem.201703092
- Hachez, C., and Chaumont, F. (2010). Aquaporins: a family of highly regulated multifunctional channels. *Adv. Exp. Med. Biol.* 679, 1–17. doi: 10.1007/978-1-4419-6315-4\_1
- Hille, B. (2001). *Ion Channels of Excitable Membranes, 3rd Edn.* Sunderland MA: Sinauer Associates Inc.
- Huber, V. J., Tsujita, M., and Nakada, T. (2012). Aquaporins in drug discovery and pharmacotherapy. *Mol. Aspects Med.* 33, 691–703. doi: 10.1016/j.mam.2012.01.002
- Igarashi, H., Huber, V. J., Tsujita, M., and Nakada, T. (2011). Pretreatment with a novel aquaporin 4 inhibitor, TGN-020, significantly reduces ischemic cerebral edema. *Neurosci. Sci.* 32, 113–116. doi: 10.1007/s10072-010-0431-1
- Jin, T., Peng, L., Mirshahi, T., Rohacs, T., Chan, K. W., Sanchez, R., et al. (2002). The  $\beta\gamma$  subunits of G proteins gate a  $K^+$  channel by pivoted bending of a transmembrane segment. *Mol. Cell* 10, 469–481. doi: 10.1016/S1097-2765(02)00659-7
- Jung, J. S., Preston, G. M., Smith, B. L., Guggino, W. B., and Agre, P. (1994). Molecular structure of the water channel through aquaporin CHIP. The hourglass model. *J. Biol. Chem.* 269, 14648–14654.
- Kitchen, P., Day, R. E., Salman, M. M., Conner, M. T., Bill, R. M., and Conner, A. C. (2015). Beyond water homeostasis: diverse functional roles of mammalian aquaporins. *Biochim. Biophys. Acta* 1850, 2410–2421. doi: 10.1016/j.bbagen.2015.08.023
- Kourghi, M., Pei, J. V., De Ieso, M. L., Flynn, G., and Yool, A. J. (2016). Bumetanide derivatives AqB007 and AqB011 selectively block the aquaporin-1 ion channel conductance and slow cancer cell migration. *Mol. Pharmacol.* 89, 133–140. doi: 10.1124/mol.115.101618
- Kourghi, M., Pei, J. V., De Ieso, M. L., Nourmohammadi, S., Chow, P. H., and Yool, A. J. (2017a). Fundamental structural and functional properties of Aquaporin ion channels found across the kingdoms of life. *Clin. Exp. Pharmacol. Physiol.* 45, 401–409. doi: 10.1111/1440-1681
- Kourghi, M., Pei, J. V., Qiu, J., Mcgaughey, S., Tyerman, S. D., Byrt, C. S., et al. (2017b). Divalent cations regulate the ion conductance properties of diverse classes of aquaporins. *Int. J. Mol. Sci.* 18:E2323. doi: 10.3390/ijms18112323
- Kürz, L. L., Zühlke, R. D., Zhang, H.-J., and Joho, R. H. (1995). Side-chain accessibilities in the pore of a  $K^+$  channel probed by sulfhydryl-specific reagents after cysteine-scanning mutagenesis. *Biophys. J.* 68, 900–905. doi: 10.1016/S0006-3495(95)80266-3
- Madeira, A., Moura, T. F., and Soveral, G. (2014). Aquaglyceroporins: implications in adipose biology and obesity. *Cell Mol. Life Sci.* 72, 759–771. doi: 10.1007/s00018-014-1773-2
- Martins, A. P., Ciancetta, A., De Almeida, A., Marrone, A., Re, N., Soveral, G., et al. (2013). Aquaporin inhibition by gold(III) compounds: new insights. *ChemMedChem* 8, 1086–1092. doi: 10.1002/cmdc.201300107
- Migliati, E., Meurice, N., Dubois, P., Fang, J. S., Somasekharan, S., Beckett, E., et al. (2009). Inhibition of aquaporin-1 and aquaporin-4 water permeability by a derivative of the loop diuretic bumetanide acting at an internal pore-occluding binding site. *Mol. Pharmacol.* 76, 105–112. doi: 10.1124/mol.108.053744
- Nielsen, S., Smith, B. L., Christensen, E. I., and Agre, P. (1993). Distribution of the aquaporin CHIP in secretory and absorptive epithelia and capillary endothelia. *Proc. Natl. Acad. Sci. U.S.A.* 90, 7275–7279. doi: 10.1073/pnas.90.15.7275
- Niemietz, C. M., and Tyerman, S. D. (2002). New potent inhibitors of aquaporins: silver and gold compounds inhibit aquaporins of plant and human origin. *FEBS Lett.* 531, 443–447. doi: 10.1016/S0014-5793(02)03581-0
- Patel, N., Exell, J. C., Jardine, E., Ombler, B., Finger, L. D., Ciani, B., et al. (2013). Proline scanning mutagenesis reveals a role for the flap endonuclease-1 helical cap in substrate unpairing. *J. Biol. Chem.* 288, 34239–34248. doi: 10.1074/jbc.M113.509489
- Pei, J. V., Kourghi, M., De Ieso, M. L., Campbell, E. M., Dorward, H. S., Hardingham, J. E., et al. (2016). Differential inhibition of water and ion channel activities of mammalian aquaporin-1 by two structurally related bacopaside compounds derived from the medicinal plant *Bacopa monnieri*. *Mol. Pharmacol.* 90, 496–507. doi: 10.1124/mol.116.105882
- Preston, G. M., Jung, J. S., Guggino, W. B., and Agre, P. (1993). The mercury-sensitive residue at cysteine 189 in the CHIP28 water channel. *J. Biol. Chem.* 268, 17–20.
- Rao, Y., Bodmer, R., Jan, L. Y., and Jan, Y. N. (1992). The big brain gene of *Drosophila* functions to control the number of neuronal precursors in the peripheral nervous system. *Development* 116, 31–40.
- Reizer, J., Reizer, A., and Saier, M. H. Jr. (1993). The MIP family of integral membrane channel proteins: sequence comparisons, evolutionary relationships, reconstructed pathway of evolution, and proposed functional differentiation of the two repeated halves of the proteins. *Crit. Rev. Biochem. Mol. Biol.* 28, 235–257. doi: 10.3109/10409239309086796
- Ren, G., Reddy, V. S., Cheng, A., Melnyk, P., and Mitra, A. K. (2001). Visualization of a water-selective pore by electron crystallography in vitreous ice. *Proc. Natl. Acad. Sci. U.S.A.* 98, 1398–1403. doi: 10.1073/pnas.98.4.1398
- Sadja, R., Smadja, K., Alagem, N., and Reuveny, E. (2001). Coupling  $G\beta\gamma$ -dependent activation to channel opening via pore elements in inwardly rectifying potassium channels. *Neuron* 29, 669–680. doi: 10.1016/S0896-6273(01)00242-2
- Sankararamakrishnan, R., and Vishveshwara, S. (1992). Geometry of proline-containing alpha-helices in proteins. *Chem. Biol. Drug Des.* 39, 356–363. doi: 10.1111/j.1399-3011.1992.tb01595.x
- Saparov, S. M., Kozono, D., Rothe, U., Agre, P., and Pohl, P. (2001). Water and ion permeation of aquaporin-1 in planar lipid bilayers. Major differences in structural determinants and stoichiometry. *J. Biol. Chem.* 276, 31515–31520. doi: 10.1074/jbc.M104267200
- Seeliger, D., Zapater, C., Krenc, D., Haddoub, R., Flitsch, S., Beitz, E., et al. (2013). Discovery of novel human aquaporin-1 blockers. *ACS Chem. Biol.* 8, 249–256. doi: 10.1021/cb300153z
- Sui, H., Han, B.-G., Lee, J. K., Walian, P., and Jap, B. K. (2001). Structural basis of water-specific transport through the AQP1 water channel. *Nature* 414, 872–878. doi: 10.1038/414872a
- Tsunoda, S. P., Wiesner, B., Lorenz, D., Rosenthal, W., and Pohl, P. (2004). Aquaporin-1, nothing but a water channel. *J. Biol. Chem.* 279, 11364–11367. doi: 10.1074/jbc.M310881200
- Vanhoof, G., Goossens, F., Demeester, I., Hendriks, D., and Scharpé, S. (1995). Proline motifs in peptides and their biological processing. *FASEB J.* 9, 736–744. doi: 10.1096/fasebj.9.9.7601338
- Williams, K. A., and Deber, C. M. (1991). Proline residues in transmembrane helices: structural or dynamic role? *Biochemistry* 30, 8919–8923.
- Woolfson, D. N., and Williams, D. H. (1990). The influence of proline residues on  $\alpha$ -helical structure. *FEBS Lett.* 277, 185–188. doi: 10.1016/0014-5793(90)80839-B
- Yanochko, G. M., and Yool, A. J. (2002). Regulated cationic channel function in *Xenopus* oocytes expressing *Drosophila* big brain. *J. Neurosci.* 22, 2530–2540. doi: 10.1523/JNEUROSCI.22-07-02530.2002
- Yasui, M., Hazama, A., Kwon, T. H., Nielsen, S., Guggino, W. B., and Agre, P. (1999). Rapid gating and anion permeability of an intracellular aquaporin. *Nature* 402, 184–187. doi: 10.1038/46045
- Yool, A. J. (2007). Aquaporins: multiple roles in the central nervous system. *Neuroscientist* 13, 470–485. doi: 10.1177/1073858407303081
- Yool, A. J., Brokl, O. H., Pannabecker, T. L., Dantzer, W. H., and Stamer, W. D. (2002). Tetraethylammonium block of water flux in Aquaporin-1 channels expressed in kidney thin limbs of Henle's loop and a kidney-derived cell line. *BMC Physiol.* 2:4. doi: 10.1186/1472-6793-2-4
- Yool, A. J., and Campbell, E. M. (2012). Structure, function and translational relevance of aquaporin dual water and ion channels. *Mol. Aspects Med.* 33, 443–561. doi: 10.1016/j.mam.2012.02.001
- Yool, A. J., Morelle, J., Cnops, Y., Verbavatz, J. M., Campbell, E. M., Beckett, E. A., et al. (2013). AqF026 is a pharmacologic agonist of the water channel aquaporin-1. *J. Am. Soc. Nephrol.* 24, 1045–1052. doi: 10.1681/ASN.2012.080869
- Yool, A. J., Stamer, W. D., and Regan, J. W. (1996). Forskolin stimulation of water and cation permeability in aquaporin-1 water channels. *Science* 273, 1216–1218. doi: 10.1126/science.273.5279.1216
- Yool, A. J., and Weinstein, A. M. (2002). New roles for old holes: ion channel function in aquaporin-1. *News Physiol. Sci.* 17, 68–72. doi: 10.1152/nips.01372.2001

- Yu, J., Yool, A. J., Schulten, K., and Tajkhorshid, E. (2006). Mechanism of gating and ion conductivity of a possible tetrameric pore in aquaporin-1. *Structure* 14, 1411–1423. doi: 10.1016/j.str.2006.07.006
- Zampighi, G. A., Hall, J. E., and Kreman, M. (1985). Purified lens junctional protein forms channels in planar lipid films. *Proc. Natl. Acad. Sci. U.S.A.* 82, 8468–8472. doi: 10.1073/pnas.82.24.8468
- Zhang, W., Zitron, E., Hömme, M., Kihm, L., Morath, C., Scherer, D., et al. (2007). Aquaporin-1 channel function is positively regulated by protein kinase C. *J. Biol. Chem.* 282, 20933–20940. doi: 10.1074/jbc.M703858200

**Conflict of Interest Statement:** The authors declare that the research was conducted in the absence of any commercial or financial relationships that could be construed as a potential conflict of interest.

*Copyright* © 2018 Kourghi, De Ieso, Nourmohammadi, Pei and Yool. This is an open-access article distributed under the terms of the Creative Commons Attribution License (CC BY). The use, distribution or reproduction in other forums is permitted, provided the original author(s) and the copyright owner are credited and that the original publication in this journal is cited, in accordance with accepted academic practice. No use, distribution or reproduction is permitted which does not comply with these terms.